SAKARYA ÜNİVERSİTESİ

FEN BİLİMLERİ ENSTİTÜSÜ DERGİSİ

Sakarya University Journal of Science (SAUJS)

SAKARYA ÜNİVERSİTESİ

e-issn: 2147-835X

SAÜ Fen Bil Der/SAUJS

Cilt/Volume: 25

Sayı/Issue: 2

Nisan/April 2021

SAKARYA ÜNİVERSİTESİ FEN BİLİMLERİ ENSTİTÜSÜ DERGİSİ
(SAKARYA UNIVERSITY JOURNAL OF SCIENCE)
İÇİNDEKİLER/CONTENTS
Cilt/Volume: 25 – No/Issue: 2 (NİSAN/APRIL-2021)

RESEARCH ARTICLES

Sakarya Üniversitesi Fen Bilimleri Enstitüsü Dergisi
(Sakarya University Journal of Science)
Cilt/Volume: 25 No/ Issue: 2 Nisan/April 2021
Editör Kurulu/Editorial Boards

Editor-in-Chief

Editors

Editorial Board

Guest Editor

English Language Editor

SAKARYA ÜNİVERSİTESİ
FEN BİLİMLERİ ENSTİTÜSÜ DERGİSİ

Sakarya University Journal of Science
SAUJS

e-ISSN 2147-835X | Period Bimonthly | Founded: 1997 | Publisher Sakarya University |
http://www.saujs.sakarya.edu.tr/en/

Title: Mineralogical And Gemological Characteristics Of Metaophiolite Hosted Corundum (Malatya-Türkiye)

Authors: İlkay KAYDU AKBUDAK, Meltem GÜRBÜZ, Zeynel BAŞIBÜYÜK, Murat HATİPOĞLU, Ayten ÖZTÜFEKÇİ ÖNAL, Fikret İŞLER

Recieved: 2019-11-07 14:16:10

Accepted: 2020-10-28 09:26:42

Article Type: Research Article

Volume: 25
Issue: 2
Month: April
Year: 2021
Pages: 288-296

How to cite
İlkay KAYDU AKBUDAK, Meltem GÜRBÜZ, Zeynel BAŞIBÜYÜK, Murat HATİPOĞLU, Ayten ÖZTÜFEKÇİ ÖNAL, Fikret İŞLER; (2021), Mineralogical And Gemological Characteristics Of Metaophiolite Hosted Corundum (Malatya-Türkiye). Sakarya University Journal of Science, 25(2), 288-296, DOI: https://doi.org/10.16984/saufenbilder.644002
Access link
http://www.saujs.sakarya.edu.tr/en/pub/issue/60672/644002

Sakarya University Journal of Science 25(2), 288-296, 2021

Mineralogical And Gemological Characteristics Of Metaophiolite Hosted Corundum (Malatya-Türkiye)

İlkay KAYDU AKBUDAK[1], Meltem GÜRBÜZ[2], Zeynel BAŞIBÜYÜK[1,*], Murat HATİPOĞLU[3], Ayten ÖZTÜFEKÇİ ÖNAL[4], Fikret İŞLER[5]

Abstract

The corundum is found in the rocks of the Berit metaophiolite in Eastern Anatolia, near Doğanşehir a province of Malatya. Metaophiolitic rocks consist mainly of garnet metagabbro, granulite, amphibolite, mylonitic amphibolite, garnet amphibolite, amphibole schist, pyroxenite, mylonitic pyroxenite, orthopyroxenite, harzburgite, serpentinized dunite and diorite units. Corundum occurrences are mostly found in pyroxenites, amphibolites, peridotites and granulites. Their colors change in range between reddish pink, pink and light pink. They are usually in structure of translucent, vitreous and sometimes cracked. They are seen scattered or clustered together inside the rocks in which they are found. The size of their crystals ranges from 0.5 cm to 10 cm and their euhedral crystals are observed in pseudohexagonal form. As a result of the petrographic examinations, it was observed that pyroxene, amphibole, garnet and plagioclase minerals accompanied with the corundum. The samples of the rocks containing the corundum has qualifications which will be as an object of gemstone and ornament by means of cutting and shining. Large specimens of corundum can be processed alone. Samples, being as scattered and small granules inside the rock can be processed together with the host rock. In the processed samples, it was obtained patterns like the samples of corundum with zoisite which were in great demand in the world gemstone market.

Keywords: mineralogy, gemology, corundum, gemstone, Malatya

[*]Corresponding author: zbasibuyuk@ahievran.edu.tr

[1]Kırşehir Ahi Evran University, Faculty of Engineering and Architecture, Geology Engineering Department, 40100, Kırşehir. E-Mail: i.akbudak@ahievran.edu.tr; zbasibuyuk@ahievran.edu.tr ORCID: https://orcid.org/0000-0003-0884-5991; https://orcid.org/0000-0003-2845-148X

[2]Mersin University, School of Jewelry Technology and Design, Çiftlikköy, 33343, Mersin
E-Mail: mgurbuz@mersin.edu.tr ORCID: https://orcid.org/0000-0003-2501-0697

[3]Dokuz Eylül University, İzmir Vocational School, Jewelery and Jewelry Design Program 35380, İzmir E-Mail: murat.hatipoglu@deu.edu.tr ORCID: https://orcid.org/0000-0002-4345-9052

[4]Munzur University, Faculty of Engineering, 62000, Tunceli E-Mail: aytenoztufekci@gmail.com ORCID: https://orcid.org/0000-0003-2185-4884

[5]Çukurova University, Faculty of Engineering and Architecture, Balcalı, 01330, Adana E-Mail: fisler@cu.edu.tr ORCID: https://orcid.org/0000-0002-5989-9618

1. INTRODUCTION

The jewellery and tools made from gemstones [1, 2] have been important place in human life since centuries. Today, the demand for the jewellery and decoration stuff, made from natural minerals and rocks in different colors and transparency, which are resistant to atmospheric conditions, continues incremantally. The chemical formula of the corundum is Al_2O_3 and may contain impurities like iron, chromium, etc. [3, 4, 5, 6]. The corundum group is formed with ruby and sapphire [7, 8, 9, 10]. The chemical and physical properties of these two gem varieties belonging to the corundum group, which are defined in different colors, are similar; solely, the amount and variety the elements in which they contain have difference. The pure corundum is colorless and possess the high hardness (9) and specific weight (3,94 - 4,02) due to tight packing and strong bonding of the atoms, despite the presence of two light elements like aluminum and oxygen in its composition [7, 11]. When corundum has rutile inclusions, if they are cut and polished they show the asterism feature (star appearance). The high hardness makes this mineral usable as an abrasive. The reason of red color of the ruby is that the small amount of chromium substitute the aluminum, which is in its crystalline structure. The small amount of iron together with chromium gives brownish red color. The color of blue sapphire depends on the presence of a small amount of iron and titanium [12,13]. Foreign materials can sometimes be found at a rate of 10% or more, in which case a stone becomes cloudish color and loses its aesthetic value [14,15]. Corundum is a secondary mineral found commonly in some metamorphic rocks such as marble, mica-schist, and gneiss [16]. It occurs in regional and thermal metamorphosed bauxite deposits. The corundum in large-size occur in the pegmatites found together with nepheline syenites. In the world, it has been found in Myanmar (Burma), Cambodia, Thailand, Sri Lanka (Ceylon), India (Kashmir) and Australia. Ordinary corundum was found in South Africa and USA [17].

The extracting of valuable gemstone formations in Turkey and putting forth whether they are economical by determining mineralogical-petrographic and gemological features of them are important for contributing to regional economy. The corundum in the study area is pinkish mauve colored and multi-fractured and cracked [18]. For this reason, while the corundum crystals are not transparent, but the color tone in the processed samples and the pattern beauty created by the side rocks indicate that they can be used in jewellery production.

2. GEOLOGY

There are units having different age, tectonic location and rock types in the Southeastern Anatolia Region and its surroundings which are included in the study area. Southeastern Anatolian orogenic belt consists of three sections from south to north which are Arabic Platform, Accretionary Prism Zone and Nap zone [19, 20, 21] (Figure 1). The Arabic Platform consists of sedimentary units most of which have been deposited from the Early Cambrian to Mid-Miocene and are marine sediments [19, 20]. The accretionary prism zone is bounded by Arabic platform from the south and nap zone from the north and consists of tectonic slices containing various rock units in the range of Late Cretaceous-Mid-Miocene period [19, 20]. In the Nap zone consisting of two large tectonic units, sub-nap consists of ophiolitic rock assemblages underwent metamorphism and the mineral group which is exposed in the southern boundary of the study area, and the upper nap consists of the Southeast Anatolian metamorphic massifs [19, 20].

The oldest unit in the study area is the Malatya Metamorphics which is composed of various schists with Paleozoic-Mesozoic ages, recrystallized limestone and marbles (Figure 2). The Malatya Metamorphics overlay all of the Early-Middle Eocene aged units in the study area with tectonic contact. The Berite metaophiolite, which contains the ultramafic garnet, mafic cumulates, gabbro, amphibolite and volcanics, and cut by acidic intrusions, belonging to Early-Middle Eocene aged Doğanşehir Granitoid, overlays the Middle Eocene aged mine complex, which contains diabase, andesite and dacite

dykes, micritic, nummulitic limestone blocks and basic volcanics, with tectonic contact [19, 20, 22, 23, 24, 25, 26, 27, 28, 29, 30]

The Middle Eocene aged Suludere Formation unconformably overlies the Granitoid of Doğanşehir and the Berite Metaophiolite. All these units are overlaid unconformably by the Plio-Quaternary aged Beylerderesi formation and the Quaternary alluviums. The corundum formations are in the pyroxenites, amphibolites, peridotites and granulites belonging to the Berite Metaophiolite.

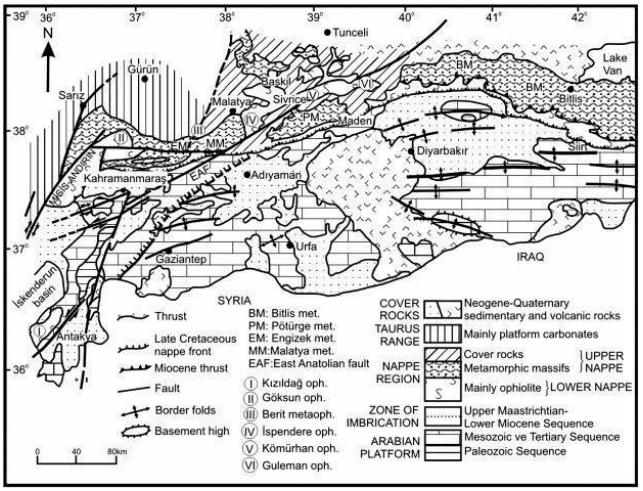

Figure 1 Regional geological map of the study area [19, 20, 21]

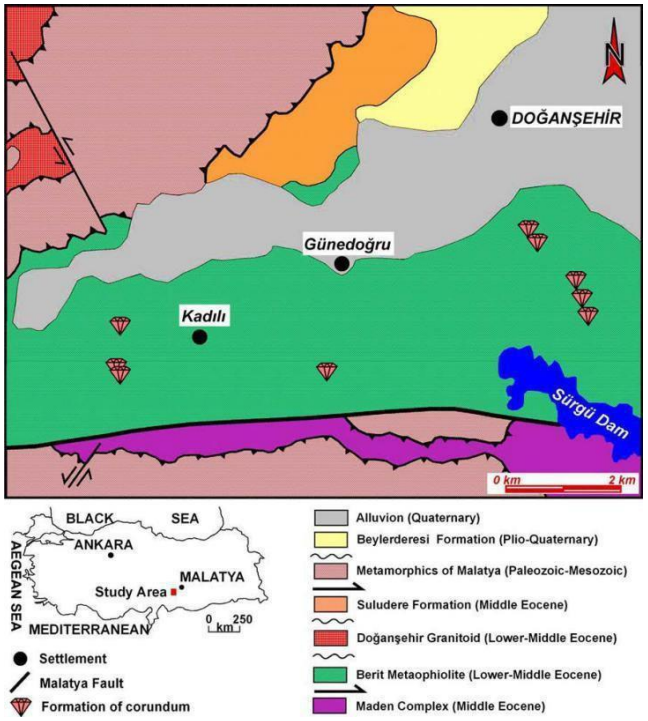

Figure 2 Geological map of the study area [24, 30]

3. METHOD

Eighty samples were taken with the purpose of determining the corundum distribution and its paragenetic relations and also its, geological, geochemical and mineralogical characteristics, in study area. XRD analyzes were performed in the Rigaku RadB-DMAX II Computer Controlled X-Ray Diffractometer at the XRD Analysis Laboratory of Mersin University in order to determine the mineralogical compositions of the samples. In the thin section laboratory of the Çukurova University Geological Engineering Department, thin sections were prepared from the corundum and side rock samples taken from the area and mineralogical determinations were made by examining them under polarizing microscope. Thin sections were prepared from the samples taken from the area and electron microprobe (EPMA) analyzes were carried out at Hacettepe University Geological Engineering. In addition, cabochon (curved) cutting techniques were applied to the corundum samples, which were taken from the area by using diamond coating saws, sinter diamond abrasive discs and polishing machine, and the gemstone workings were carried out with the aim of being used for the jewellery.

4. RESULTS

4.1. Macroscopic Examinations

The corundum, bearing gemstone features, is seen together with the pyroxenites, amphibolites, granulites and peridotites, which belong to Berite Metaophiolite in the study area [31, 32, 33, 34]. The rocks containing corundum in the area were observed as protrusions due to their hardness. However, these rocks are over-altered and have a very fragile structure. The colors of the corundum change in range between reddish pink, pink and light pink (Figure 3a). They are usually translucent, vitreous and sometimes cracked. They are seen scattered or clustered together

inside the rocks in which they are found. (Figure 3b). The size of their crystals ranges from 0.5 cm to 10 cm and their euhedral crystals are observed in pseudohexagonal form (Figure 3b). The extend of the metaophiolite containing corundum in the study area is more than 10 square kilometer. The corundum content in the metaophiolite is also very rich so as to be operated economically. The region was licensed for corundum, and will go into production in an early date.

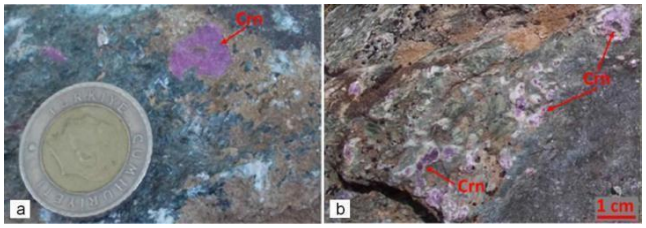

Figure 3 Reddish pink colored corundum mineral in amphibolites (a) and pyroxenites (b) belonging to Berit Metaophiolite

The Berite metaophiolite was metamorphosed at the lower limit of the granulite facies and the eclogite facies at pressures of 3.2-17.5 kbar and temperature range of 690-941°C [30]. This temperature and pressure overlap with the pressure and temperature values required for ruby crystallization [35, 36, 37, 38, 39, 40]. The corundum minerals in the study area are thought to have formed by having been exposed to high temperature high pressure metamorphism in the subduction zone of aluminium rich minerals as omphacite, plagioclase.

4.2. Mineralogy

XRD (Figure 4), thin section and electron microprobe analyses were performed on the corundum that is found in the study area. In the thin section, corundum is usually observed as anhedral and large granules reaching 5 millimeters. They are distinguished from other minerals by their high reliefs and refractive index. They have a very cracked structure and contain weak cleavages, mutually intersecting in partly (Figure 5). It shows a colorless and pinkish pleocroism in single nicol while, it has gray and yellow greyish in color in crossed polarized light (Figure 6). In the electron microprobe image, it was observed that the corundum minerals contain a bi-directional cleavage which is not apparent (Figure 7).

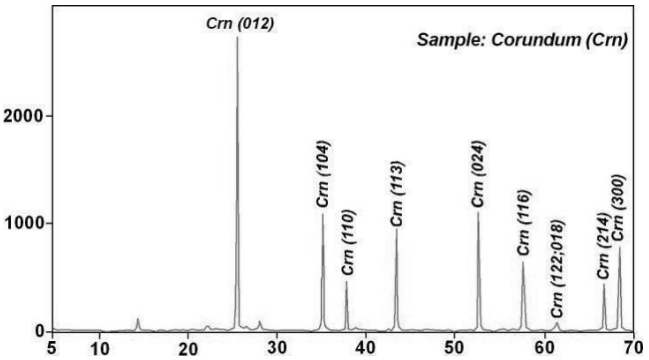

Figure 4 Result of XRD analys of corundum.

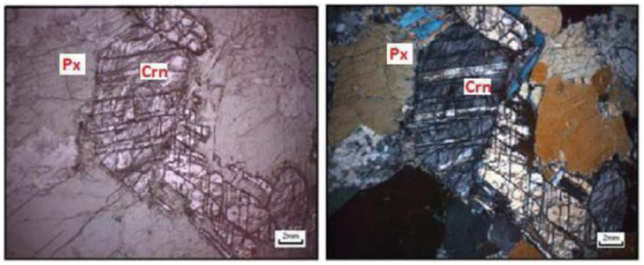

Figure 5 Bi-directional weak cleavage in the corundum in the pyroxenites (Px: Pyroxene, Crn: Corundum, a: Single nichol, b: Double nichol).

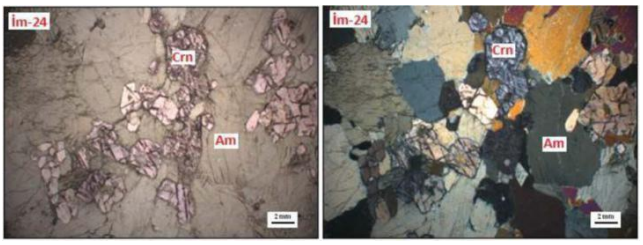

Figure 6 Abundantly cracked fine-grained pinkish-colored corundum minerals in amphibolites (Am: Amphibole, Crn: Corundum, a: Single nichole, b: Double nichole).

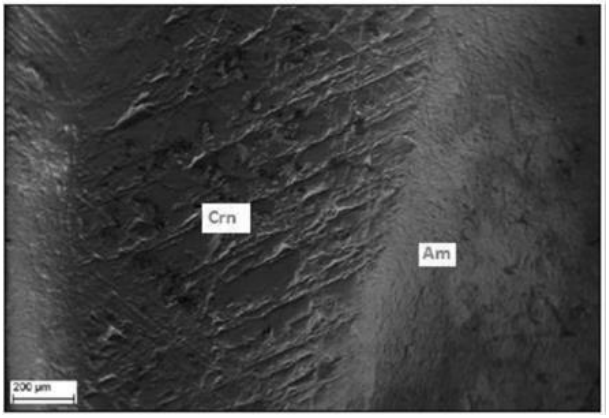

Figure 7 Electron microprobe image of the bi-directional weak cleavages observed in the corundum mineral of Kl-1 no. (Crn: Corundum, Am: Amphibole)

4.3. Geochemistry

As a result of the electron microprobe analysis of the corundum minerals in the amphibolite and pyroxenites in the study area it was determined that the corundum samples in the amphibolite contain 98.17% of Al_2O_3 and the corundum samples in the pyroxenit contain 97.13%of Al_2O_3. There are a few quantity of SiO_2, Na_2O, MgO, MnO and FeO as impurities in the corundum (Table 1). However, unlike pyroxenites, impurity of MnO were determined instead of FeO impurity in the corundum inside amphibolites.

Table 1
Chemical composition of corundum

	IM-24 (Amphiolite)	KL-1 (Pyroxenite)
SiO_2	0.818	1.856
Al_2O_3	98.169	97.133
FeO	0.003	0.106
Na_2O	0.513	0.570
MgO	0.276	0.333
K_2O	0.058	0.001
CaO	0.001	0.001
TiO_2	0.001	0.001
MnO	0.162	0.001

4.4. Gemology

The reddish pink, pink, and light pink corundum (Figure 8a) in the study area are often observed as anhedral scattered clusters and locally pseudohexagonal crystals. Examples of corundum are usually translucent, vitreous and sometimes cracked. The size of the crystals varies from 0.5 cm to 10 cm (Figure 8a-b). Because of their high hardness, it was encountered the corundum about 3 cm in diameter in separated way from other minerals in the area. Some of the samples containing corundum mineral were cut and polished to be used for gemstone and gemstone objects (Figure 8c-d). Large-size corundum samples were processed individually, while small-grain and scattered samples containing corundum mineral were processed with the side rock (Figure 8c-d). In this way, images similar to the samples of corundum with zoisite (Game, 1955), (Figure 8c-d).

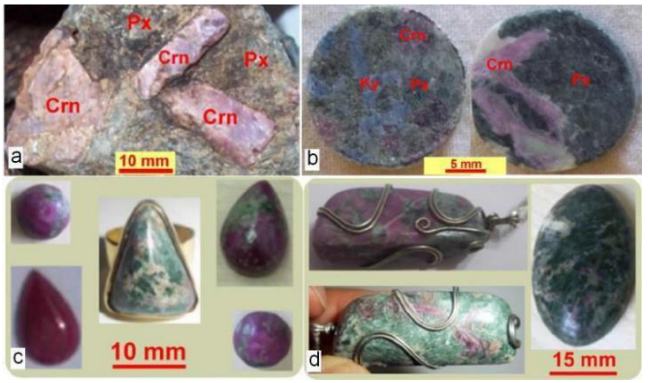

Figure 8 a: Pink colored prismatic corundum; b: Blue colored kyanite and pink colored corundum observed with green colored pyroxenes; c-d: Pyroxenes and corundum as gemstones (Crn: Corundum, Px: Pyroxene, Ky: Kyanite).

In the examination area, kyanite which is blue, transparent and glassy shine, accompany the corundum minerals, in places. The kyanite, in length of up to 1 cm and width of up to 0.5 cm are found as scattered in the pyroxenites. (Figure 9b).

5. CONCLUSION

The corundum, bearing gemstone features, is found within the pyroxenites, amphibolites, granulites and peridotites, which belong to Berite Metaophiolite in the study area [32]. The corundum is observed in reddish pink, pink

and light pink colors, glassy or cloudy shine, cracked and translucent. The dimensions of the crystals range from 0.5 cm to 10 cm, and the euhedal crystals are observed in pseudohexagonal form. In the thin-cut, the corundum usually have an anhedral and very cracked structure and contain weak cleavages intersecting bi-directional with each other, in partly. The reason for this fractured texture in corundum is thought to be due to the tectonism in the region.

As a result of the electron microprobe analysis of the corundum minerals it was determined that 98.17% of the corundum sample in the amphibolite and 97.13% of the corundum sample in the pyroxenit contain Al_2O_3. There are a few quantity of SiO_2, Na_2O, MgO, MnO and FeO as impurities in the corundum minerals, and unlike pyroxenites, impurity of MnO were determined instead of FeO impurity in the corundum mineral inside amphibolites.

Large-size corundum samples were processed individually, while small-grain and scattered samples containing corundum were processed with the wall rock, in the area. In the samples, machined at the result of flat cutting, images similar to the samples of corundum with zoisite [41], which have great demand in the World Gemstone Market, appeared.

Acknowledgments

The authors would like to thank the Çukurova University Scientific Research Projects Coordination Unit for contributing to the financial portion of the project.

Funding

This project studies were supported by Çukurova University Scientific Research Projects Coordination Unit. Project numbers were MMF2011D9

The Declaration of Conflict of Interest/ Common Interest

No conflict of interest or common interest has been declared by the authors.

Authors' Contribution

This study is the part of PhD thesis of İlkay KAYDU. Fikret İŞLER, Ayten ÖZTÜFEKÇİ ÖNAL, Meltem GÜRBÜZ, Zeynel BAŞIBÜYÜK and Murat HATİPOĞLU had a great contribution in providing support for the study, field studies, analyzing the rocks and minerals, interpreting the findings.

The Declaration of Ethics Committee Approval

The authors declare that this document does not require an ethics committee approval or any special permission.

The Declaration of Research and Publication Ethics

The authors of the paper declare that they comply with the scientific, ethical and quotation rules of SAUJS in all processes of the article and that they do not make any falsification on the data collected. In addition, they declare that Sakarya University Journal of Science and its editorial board have no responsibility for any ethical violations that may be encountered, and that this study has not been evaluated in any academic publication environment other than Sakarya University Journal of Science.

REFERENCES

[1] J.C. Hurlbut and G.S. Switzer, “ Gemology,” A Wiley-İnterscience Publication, Jhon Wiley & Sons, USA, 137-139, 1979.

[2] M. Hatipoğlu, M.S. Kırıkoğlu, H.B. Buzlu, Y. Kibici a nd C. Helvacı, “ Türkiye’deki süstaşlarının endüstriyel hammaddeler içerisindeki önemi.” 64 Uluslararası katılımlı Türkiye Jeoloji Kurultayı (25-29 Nisan) Bildiri Özleri Kitabı, Ankara, 203-204 (in Turkish), 2011.

[3] F. Forestier and B. Lasnier, “Découverte de niveaux d'amphibolite à pargasite,

anorthite,corindon et sapphirine dans les chistes cristallins de la vallée du Haut Allier Existencedu faciès granulite dans le Massif Central Francais," Contributions to Mineralogy and Petrology, 23, 194–235, 1969.

[4] R.W. Hughes, "Corundum," Northants, UK, Butterworth-Heinemann, 314 p, 1990.

[5] V. Garnier, G. Giuliani, H. Maluski, D. Ohnenstetter, T.P. Trong, V.H. Quang, L.P. Van, T.V. Van and D. Schwarz, " A Ar–Ar Age in phlogopites from marble-hosted ruby deposits in Northern Vietnam: Evidence for Cenozoic Ruby Formation,Virginie," Chemical Geology, 188, 33– 49, 2002.

[6] G. Giuliani, J. Dubessy, D. Banks, H.Q. Vinh, T. Lhomme, J. Pironon, V. Garnier, P.T. Trinh, P.V. Long, D. Ohnenstette a nd D. Schwarz, " CO2–H2S–COS–S8–AlO(OH)- Bearing Fuid Inclusions In Ruby From Marble-Hosted Deposits in Luc Yen area, North Vietnam," Chemical Geology, 194, 167–185, 2003.

[7] I.A. Mumme, " The World of Sapphires. Mumme Publications," Victoria, Australia, 11-12, 1988.

[8] R.W. Hughes, "Ruby & Sapphire," Boulder, CO, RWH Publishing, 512 p, 1997.

[9] C. Simonet, "Géologie des gisements de saphir et de rubis-L'exemple de la John Saul Ruby Mine, Mangare, Kenya," Unpublished Ph.D. thesis, University of Nantes, France, 349 p, 2000.

[10] R.W. Hughes, W. Manorotkul, a nd E.B. Hughes, "Ruby & Sapphire," Lotus Publishing, Bangkok, 816 p, 2017.

[11] M. Çelik a nd N. Karakaya, " Sistematik Mineraloji," Bizim Büro Basımevi, Konya. 71-72, 274-276 (in Turkish), 1998.

[12] C. Simonet, J.L. Paquette, C. Pin, B. Lasnier and E. Fritsch, " The Dusi (Garba Tula) Sapphire Deposit, Central Kenya — a Unique Pan-African Corundum-Bearing Monzonite," Journal of African Earth Sciences, 38, 401–410, 2004.

[13] C. Simonet, E. Fritsch a nd B. Lasnier, "Classification of Gem Corundum Deposits Aimed Towards Gem Exploration," Ore Geology Reviews, 34, 127–133, 2008.

[14] D. J. Content, "Ruby, Sapphire & Spinel," Brepols Publishers, Turnhout, Belgium, 2 vol., VIII+452 p, 2016.

[15] J.F. Halford-Watkins, "The Book of Ruby & Sapphire (Ed. R.W. Hughes)," RWH Publishing, 434 p, 2012.

[16] W. Ranson, J. Garihan a nd K. Ulmer, " Metamorphic reactions in ruby-corundum amphibolite from the Chunky Gal Mountain mafic-ultramafic complex, Clay County, North Carolina," Abstracts with Programs, Geological Society of America 24, 265, 1992.

[17] R. Webster, "Gems. Their Sources, Descriptions and Identification," Archon Books, London, 54-75, 1970.

[18] M. Hatipoğlu, R. Şanal a nd C. Helvacı, " İşlenmiş doğal ve yapay yakutlardaki (kırmızı korundum) tanımsal özelliklerinin immersiyonoskop ve FT-IR kullanılarak gemolojik incelemesi," 69. Uluslararası katılımlı Türkiye Jeoloji Kurultayı (11-15 Nisan) Bildiri Özleri Kitabı, Ankara, 314-315 (in Turkish), 2016.

[19] Y. Yılmaz, " New evidence and model on the evoluation of the southeast Anatolian Orogen," Geological Society of America Bulletin, 105, 251-71, 1993.

[20] Y. Yılmaz, E. Yiğitbaş a nd Ş.C. Genç, "Ophiolitic and metamorphic

assemblages of southeast Anatolia and their significance in the geological evolution of the orogenic belt," Tectonics, 12, 1280-1297, 1993.

[21] O. Parlak, T. Rızaoğlu, U. Bağcı, F. Karaoğlan a nd V. Höck, "Tectonic significance of the geochemistry and petrology of ophiolites in southeast Anatolia, Turkey," Tectonophysics, 473(1), 173-187, 2009.

[22] M. Yıldırım and Y. Yılmaz, "Güneydoğu Anadolu Orojenik Kuşağının Ekaylı Zonu," TPJD Bülteni, C:3/I, 57-73 (in Turkish), 1991.

[23] Ş. C. Genç, E. Yiğitbaş a nd Y. Yılmaz, "Berit Metaofiyolitinin Jeolojisi," A. Suat Erk Jeoloji Sempozyumu, bildiriler, 37-52 (in Turkish), 1993.

[24] A. Önal, "Polat-Beğre (Doğanşehir) Çevresindeki Magmatik Kayaçların Petrografik ve Petrolojik Özellikleri," Doktora Tezi, Fırat Üniversitesi Fen Bilimleri Enstitüsü, Elazığ, 159 p. (in Turkish), 1995.

[25] A. Önal and A.F. Bingöl, " Geochemical Characterisation and Petrogenesis of the Polat Granitoid in Eastern Taurus Belt, Turkey," Journal Geological Society of India, 56, 235-251, 2000.

[26] A. Önal and M. Beyarslan, "Doğanşehir (Malatya) Civarındaki Ofiyolitik Kayaçların Jeolojik ve Petrografik Özellikleri," S.Ü .Müh. Fak Derg., 16, 2, 67-75 (in Turkish), 2001.

[27] A. Uygun and E. Solakoğlu, "Pütürge (Malatya) Masifindeki Pirofillit Yataklarının Jeolojisi ve Kökeni," MTA Dergisi, 123-124, 13-19 (inTurkish), 2002.

[28] F. Karaoğlan, "Günedoğru-Beğre (Doğanşehir-Malatya) Arasında Yüzeyleyen Tektonomagmatik Birimlerin Petrografisi ve Jeokimyası," Yüksek Lisans Tezi, Çukuruova Üniversitesi, Fen Bilimleri Enstitüsü, Adana, 120 p. (in Turkish), 2005.

[29] O. Parlak, "Geodynamic significance of granitoid magmatism in the southeast Anatolian Orogen: Geochemical and geochronological evidence from Göksun-Afşin (Kahramanmaraş, Turkey) Region," International Journal of Earth Sciences, 95, 609- 627, 2006.

[30] F. Karaoğlan, O. Parlak, A. Robertson, M. Thöni, U. Klötzli, F. Koller and A.I. Okay, " Evidence of Eocene high-temperature/ high-pressure metamorphism of ophiolitic rocks and granitoid intrusion related to Neotethyan subduction processes (Doğanşehir area, SE Anatolia)," Geological Society, London, Special Publications 372, 249-272, 2013.

[31] A.M. Ay, M. Hatipoğlu, H. Günel, S. Kılınçarslan a nd T. Velioğlu, "Doğanşehir (Malatya) yakut oluşumlarının yayılımının tespiti ve oluşum kökenine ait yaklaşımlar," 66 Uluslararası katılımlı Türkiye Jeoloji Kurultayı (1-5 Nisan) Bildiri Özleri Kitabı, Ankara, 222-223 (in Turkish), 2013.

[32] İ. Kaydu, " Malatya ve Çevresindeki Süstaşı Oluşumlarının Mineralojik, Jeokimyasal İncelemesi Ve Gemolojik Özellikleri," Doktora Tezi, Çukurova Üniversitesi, Fen Bilimleri Enstitüsü, Adana, 135 p. (in Turkish), 2014.

[33] T. Velioğlu and Y.K. Kadıoğlu, "Yakut oluşumları ile ilgili kaya grupları: Doğu Anadolu, Türkiye," Değerli ve Yarı değerli Taşlar Çalıştayı (9-10 Aralık), Bildiri Özleri Kitabı, Istanbul, 119-125 (in Turkish), 2015.

[34] H. Günel, K. Sözeri, E. Duran, H. Gençoğlu, E. Sarıfakıoğlu, T. Velioğlu a nd N. Çevik, "Ekinözü (Kahramanmaraş) bölgesindeki korund

oluşumları ve süstaşı olarak kullanılabilirlikleri," 70. Uluslararası katılımlı Türkiye Jeoloji Kurultayı (10-14 Nisan) Bildiri Özleri Kitabı, Ankara, 124-125 (in Turkish), 2017.

[35] A. Mercierl, M. Rakotondrazafy a nd B. Ravolomiandrinarivo, " Ruby mineralization in Southwest Madagascar," Gondwana Research, 2, 3, 433-438, 1999.

[36] A. Mercierl, P. Debat a nd J.M. Saul, " Exotic origin of the Ruby Deposits of the Mangari area in SE Kenya," Ore Geology Reviews, 14, 83–104, 1999.

[37] V. Garnier, G. Giuliani, D. Ohnenstetter, A.E. Fallick, J. Dubessy, D. Banks, H.Q. Vinh, T. Lhomme, H. Maluski, A. Pêcher, K.A. Bakhsh, P.V. Long, P.T. Trinh a nd D. Schwarz, "Marble-hosted ruby deposits from Central and Southeast Asia: Towards a new genetic model," Ore Geology Reviews, 34, 169–191, 2008.

[38] I. Graham, L. Sutherland, K. Zaw, V. Nechaev a nd A. Khanchuk, "Advances İn Our Understanding Of The Gem Corundum Deposits Of The West Pacific Continental Margins İntraplate Basaltic Fields," Ore Geology Reviews, 34, 200–215, 2008.

[39] A.F.M. Rakotondrazafy, G. Giuliani, D. Ohnenstetter, A.E. Fallick, S. Rakotosamizanany, A. Andriamamonjy, T. Ralantoarison, M. Razanatseheno, Y. Offant, V. Garnier, H. Maluski, C. Dunaigre, D. Schwarz and V. Ratrimo, "Gem corundum deposits of Madagascar: A review," Ore Geology Reviews, 34, 134-154, 2008.

[40] T.F. Yui, K. Zaw and C.M. Wu, " A Preliminary stable isotope study on Mogok Ruby, Myanmar," Ore Geology Reviews, 34, 192–199, 2008.

[41] P. Game, "Zoisite amphibolite with corundum from Tanganyika," Mineralogical Magazine 30, 456–466, 1955.

SAKARYA ÜNİVERSİTESİ
FEN BİLİMLERİ ENSTİTÜSÜ DERGİSİ

Sakarya University Journal of Science
SAUJS

e-ISSN 2147-835X | Period Bimonthly | Founded: 1997 | Publisher Sakarya University |
http://www.saujs.sakarya.edu.tr/en/

Title: Theoretical Investigation Of Coverage Effects Of CO Adsorption On Cu(100) Surface

Authors: M. Oluş ÖZBEK

Recieved: 2020-09-16 00:00:00

Accepted: 2021-01-18 00:00:00

Article Type: Research Article

Volume: 25
Issue: 2
Month: April
Year: 2021
Pages: 297-307

How to cite
M. Oluş ÖZBEK; (2021), Theoretical Investigation Of Coverage Effects Of CO Adsorption On Cu(100) Surface. Sakarya University Journal of Science, 25(2), 297-307, DOI: https://doi.org/10.16984/saufenbilder.795798
Access link
http://www.saujs.sakarya.edu.tr/en/pub/issue/60672/795798

Sakarya University Journal of Science 25(2), 297-307, 2021

Theoretical Investigation Of Coverage Effects Of CO Adsorption On Cu(100) Surface

M. Oluş ÖZBEK [*1]

Abstract

This work investigates the CO adsorption on the metallic Cu(100) surface using periodic DFT computations. CO adsorption was studied at varying coverages from 1/16 ML to 1/1 ML for a combination of adsorption positions (4-fold, bridge and top). The results showed that adsorption energies are coverage dependent, however, not enough to identify the adsorption site and coverage. However, C-O stretching frequencies are almost unique for studied coverage and adsorption positions. CO adsorption energy changes between -250 kJ/mol to +21 kJ/mol; similarly, the vibrations' range in the 1702 cm^{-1} to 2110 cm^{-1} interval, within the studied coverage and adsorption positions. Nevertheless, under the saturation coverage ($\theta_{CO} \approx 0.55$ML) the preferable adsorption site is the on-top position identified with a C-O stretching frequency around ~2100 cm^{-1} and with ~117 kJ/mol adsorption energy.

Keywords: DFT, Carbon monoxide, Copper, adsorption, vibration.

1. INTRODUCTION

The interactions of carbon monoxide (CO) with copper is of importance for heterogeneous catalysis. The non-dissociative adsorption of CO on copper based catalysis is the key point for several reactions where CO is converted to CO_2, H_2 and/or methanol (CH_3OH) [1, 2] . Owing to the industrial and financial aspects of these reactions CO+Cu systems have been of interest for decades. Especially low index surfaces (100), (110) and (111) of metallic copper, which are stable with low surface energies [3], as well as stepped surfaces [4, 5] and copper doped structures [6, 7] were commonly investigated for CO interactions. Among these, literature is especially rich for Cu(111) surface due to its higher stability [1, 8].

For the (100) surface, published literature dates back to early 1970's [9], however, not as rich. Since then, the authors inspected the different aspects of CO interactions including adsorption energy, geometry, electronic effects, and so on [1, 3-6, 9-25].

Older studies on the polycrystalline copper [26, 27] did not produce conclusive results and reported adsorption energies varying between 38 – 70 kJ/mol without relating to a definite coverage or adsorption position. Later studies (experimental and computational) showed that the

[*]Corresponding author: oluş.ozbek@gtu.edu.tr
[1]Gebze Technical University, Faculty of Engineering, Chemical Engineering Dept., 41400, Gebze, Kocaeli.
E-Mail: oluş.ozbek@gtu.edu.tr
ORCID: https://orcid.org/0000-0001-5188-680

CO prefers to adsorb on-top (1-fold, linear) positions [16, 21, 22] with a coverage dependent adsorption energy between ~40 kJ/mol to ~80 kJ/mol [9, 24, 25], ~0.57ML being the saturation coverage [5, 17, 23], after which CO-CO interactions became repulsive. Similarly, CO vibration bands measured in the 2100 cm^{-1} region were assigned to the on-top CO adsorption on Cu(100) terraces, here again, varying between 2064 cm^{-1} to 2120 cm^{-1} with coverage [2, 5, 10, 17-19, 24, 28-32].

Nonetheless, within our knowledge a complete set of adsorption related data for the Cu/Cu(100) system does not exist in the published literature. Although parts of the data set are available in different reports, comparing these different data sets is mostly unhealthy, and sometimes impossible because of the experimental studies conducted under different conditions and setups, or computational studies carried out using different settings, software and methodologies. Especially, data for the low coverage, beyond the saturation coverage, and most importantly site-specific data are not available. For this reason this work aims to supply a complete data set through uniform and standardized computations for better understanding and comparison of CO interactions with the metallic Cu(100) surface.

2. COMPUTATIONAL DETAILS

The periodic DFT simulations were performed using the Quantum Espresso package [33]. Perdew–Burke–Ernzerhof (PBE) functional is used for the exchange-correlation energy. Norm conserving (NC) projector augmented wave (PAW) sets are used to describe the ionic core pseudopotential. Upon optimizing the Cu crystal structure, 5-layer p(1x1), p(2x2), p(3x3), p(3x1) and p(4x4) Cu(100) slabs were prepared with a minimum of 15 Å vacuum heights. During the simulations, the bottom 2 layers of the surface slabs were kept frozen while the top 3 layers and the interacting CO molecule(s) were relaxed. The Brillouin zone sampling was done with automatically generated Monkhorst–Pack k-points using 2x2x1, 3x3x1, 4x4x1, 3x8x1 and 8x8x1 meshes for p(4x4), p(3x3), p(2x2), p(3x1) and p(1x1) slabs, respectively. The gas phase CO molecule was modeled using a single gamma point, where the periodic molecules were separated with a minimum of 10 Å vacuum distances in all Cartesian Coordinates. The cut-off energies used in every simulation for the wavefunctions and the charge densities were 50 Ry and 350 Ry, respectively. All the results presented were obtained by relaxing the structures until the net force acting on the ions was Fnet < 0.001 Ry/Bohr. Necessary dipole corrections due to the asymmetric usage of slabs were included.

The adsorption energies of the CO molecules were calculated as the difference between the DFT energies of the products (CO adsorbed structure) and the sum of the reactants (clean Cu(100) surface + CO(g)).

$$\Delta E_{ads} = E_{CO/Cu(100)} - (E_{CO(g)} + E_{Cu(100)})$$

The work function (ϕ) is calculated as the difference between the Fermi energy (E_F) of the structure and the electrostatic potential (Ψ) of the vacuum.

$$\Phi = \Psi - E_F$$

The vibrational frequencies of adsorbed surface species were obtained by calculating the Hessian matrix. During the frequency computations symmetry was excluded explicitly. The frequencies of the surface ions were excluded basing on the frozen phonon approximation. The frequency plots were obtained using the vibrational band data and the corresponding intensities as produced by the software.

3. RESULTS AND DISCUSSION

The FCC Cu crystal structure was optimized with a lattice parameter of 3.643 Å, which is in good agreement (Δ=1.2%) with the experimentally reported value of 3.597 Å [34]. Figure 1 shows the top view of the Cu(100) slabs and the studied adsorption positions.

At this point it should be noted that the c(2x2) structure that was reported [10, 11, 17, 18, 21, 23] to form around 0.5 ML coverage with CO on-top positions was not modeled within this work in order not to break the continuity of the coverage

dependent data; as well as not to limit the study to on-top sites.

Adsorption energies (E_{ads}), CO stretching frequencies (ν_{CO}), bond distances (|C-O| and |C-Cu|), work function (ϕ) and Bader-charge data (calculated but not included within) were produced for a wide range of coverage (θ_{CO}) and combinations of adsorption positions. When producing the complete set of data both homogenous and non-homogenous distributions (or combinations) of adsorption positions were studied. However, it was observed that the combination of different positions (such as 4-fold + 2-fold) did not have a major effect on the site-specific absorption data. For this reason, only the homogeneous combinations (such as 4-fold + 4-fold) of absorption positions were selected (Figure 2 and Table 1) and presented below.

Table 1 and Figure 3 show that the exothermicity of the CO adsorption decreases with the increasing coverage. The change is almost linear for the θ_{CO} > 0.2 ML. Below this value a major difference was not observed between the adsorption energies of the 4-fold, bridge (2-fold) and the top (1-fold) positions. However, the differences become more pronounced at higher coverage. The most exothermic adsorptions belong to the on-top positions followed by the bridge and 4-fold positions, respectively. This finding is in line with the previous reports [16, 21, 22]. Although the trend and the preferred adsorption site agrees with the experimental data, previous studies reported E_{ads} changing between ~80 kJ/mol at low coverage (< 0.2 ML) to ~50 kJ/mol around saturation coverage (~0.55 ML) [5, 9, 17, 23-25, 35]. The computed value of 135 kJ/mol (for 0.22 ML) and ~90 kJ/mol (for 0.50 ML) appear to be overestimated. However, this kind of a mismatch is expected considering the temperature-pressure gap between the experiments and the DFT simulations (0 K, 0 bar). On the other hand, reported Cu-C and C-O bond lengths of 1.90 ± 0.1 Å and 1.15 ± 0.1 Å [11, 35, 36], are in perfect agreement with the produced data, especially with on-top adsorption at θ_{CO} = 0.50 ML, where most of the previous experimental data is produced.

Unlike many other adsorption systems [37], for the CO/Cu(100) system, adsorption site cannot be identified based on the adsorption energy alone. However, CO stretching bands show clear differences with the adsorption sites.

Figure 4 and Figure 5 show that the CO vibrations have a strong position dependency that creates a major distinction to identify the adsorption site. The coverage dependent shifts of the vibrational bands do not affect the positional distinction. The means of simulated CO stretching bands appear at 1766 cm^{-1} for 4-fold, 1927 cm^{-1} for 2-fold and 2043 cm^{-1} for 1-fold adsorptions. Previous works on CO/Cu system(s) assign the bands measured around 2100 cm-1 to CO at on-top positions on Cu(100) terraces [2, 5, 10, 17-19, 24, 28-32]. These reported values vary between 2064 cm^{-1} to 2120 cm^{-1}, mainly with the CO dosing. The calculated vibrational data for 1-fold adsorption agrees quite well with these reports both with mean value and the range. Furthermore, the readily available data in this work relates the frequencies and its changes to the corresponding CO coverage. For the CO adsorption on the bridge sites IR bands between 1800 cm^{-1} and 1900 cm^{-1} were expected, but not observed in previous works [17]. Nonetheless, the frequency data corresponding to the CO adsorption on bridge positions agrees with this range, nonetheless, being wider.

When Figure 4 and Figure 5 are compared, it can be seen that the frequency is also coverage dependent. Figure 5 shows different intensities and bifurcated band. Both depend on the number of CO molecules adsorbed on the specific simulation. The non-interacting CO molecules produced similar bands that increase the intensities. However, the bifurcations may shed a light to a different phenomenon. Experimental works reported shoulders in the vibrational spectra that shift or diminish with the coverage [2, 5, 18, 21, 24, 32]. Two explanations given for this phenomenon are i) the dipole effects, and ii) adsorption of CO on different sites. The diversity of the data produced within this work may clarify this point. The intersecting regions in Figure 5 may appear to support the second idea, where the logical choice would be combination of on-top

and bridge sites based on the adsorption energies. However, a deeper investigation shows that the matching frequencies of on-top and bridge positions belong to different surface coverages, which weakens the second idea. Furthermore, the simulations carried out using two different adsorption sites at various coverages (namely on-top and bridge sites) did not produce the shoulders as observed in previous works. On the other hand, Figure 5 shows that when more than one CO molecule exists on the surface the measured bands may bifurcate even for the same adsorption sites due to dipole interactions [24]. The simulations produced splits within the range of ~30 cm^{-1}, depending on the surface coverage. This agrees with the shoulders separated by ~10-20 cm^{-1} in the experimental works.

The calculated work function changes can be seen in Table 1 and Figure 6. The work function measurements are rather limited in the previous works [17, 23] and the reports vary. However, the common point is the increase in the work function with the coverage. Here again literature data is only available up to saturation coverage (~0.55 ML), without adsorption site distinctions. The work function increases for all the adsorption positions, which agrees with the previous reports, on-top adsorptions causing the highest changes.

4. CONCLUSION

CO interactions with the Cu(100) surface were investigated using periodic DFT computations. Adsorption energies, CO stretching frequencies, bond distances, work function and Bader-charge data were produced for a variety of CO coverage (0.0625 ML to 1.0 ML) and adsorption positions (4-fold, bridge and top) to fill in the gaps of missing data and uncertainties of the previous experimental works. The results showed that simultaneous existence of CO in two or more different adsorption sites did not have a major effect on the site-specific data. Although adsorption energies are coverage and site dependent, identification of adsorption position and coverage is not always possible basing on the adsorption energy alone. On the other hand, the CO stretching frequencies are almost unique for each coverage and adsorption site. The data produced for the on-top adsorption agrees well with the previous experimental works, in addition, introduces the possibility of adsorption in bridge positions at low coverages. The splitting of the stretching bands around 0.5 ML are caused by the dipole effects rather than the CO resting in two different sites.

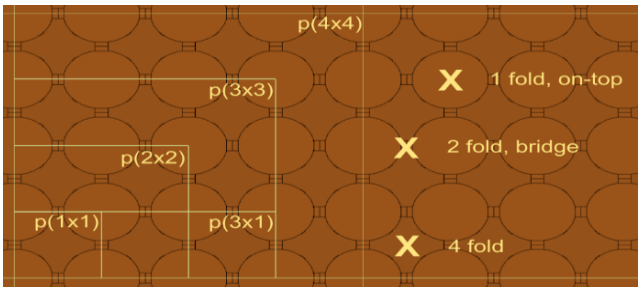

Figure 1 Top views of the a) p(1x1), p(2x2), p(3x3), p(3x1) and p(4x4) slabs, and b) CO adsorption positions. The darker shades represent the lower Cu layers. (Cu: orange)

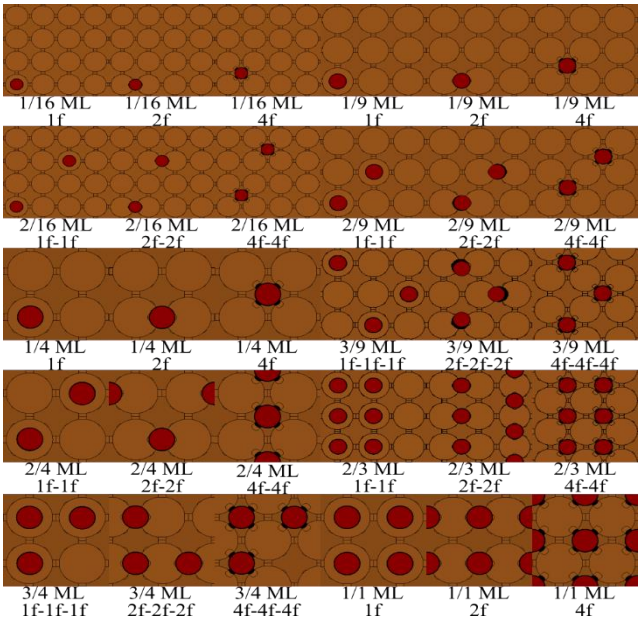

Figure 2 Top views of the CO adsorption geometries at given coverage and positions.

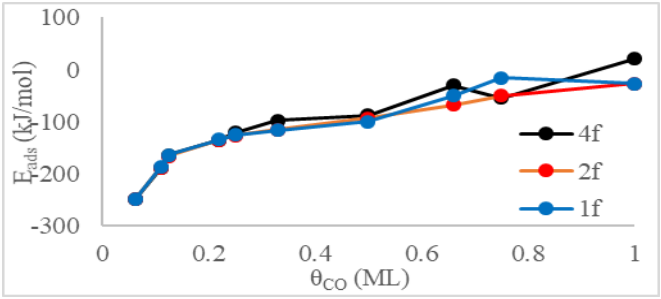

Figure 3 Adsorption energy of CO at varying coverage and adsorption positions.

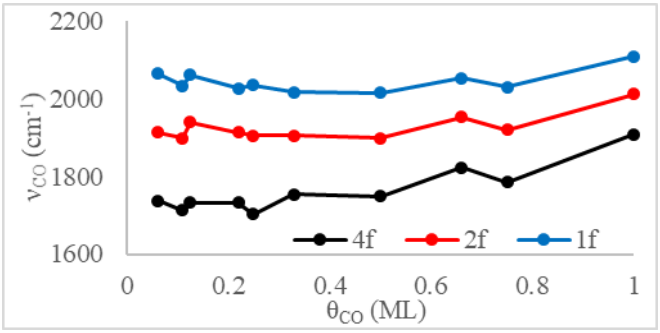

Figure 4 C-O stretching frequencies at given coverage and positions. Average value is plotted for the cases where more than one CO molecule is adsorbed.

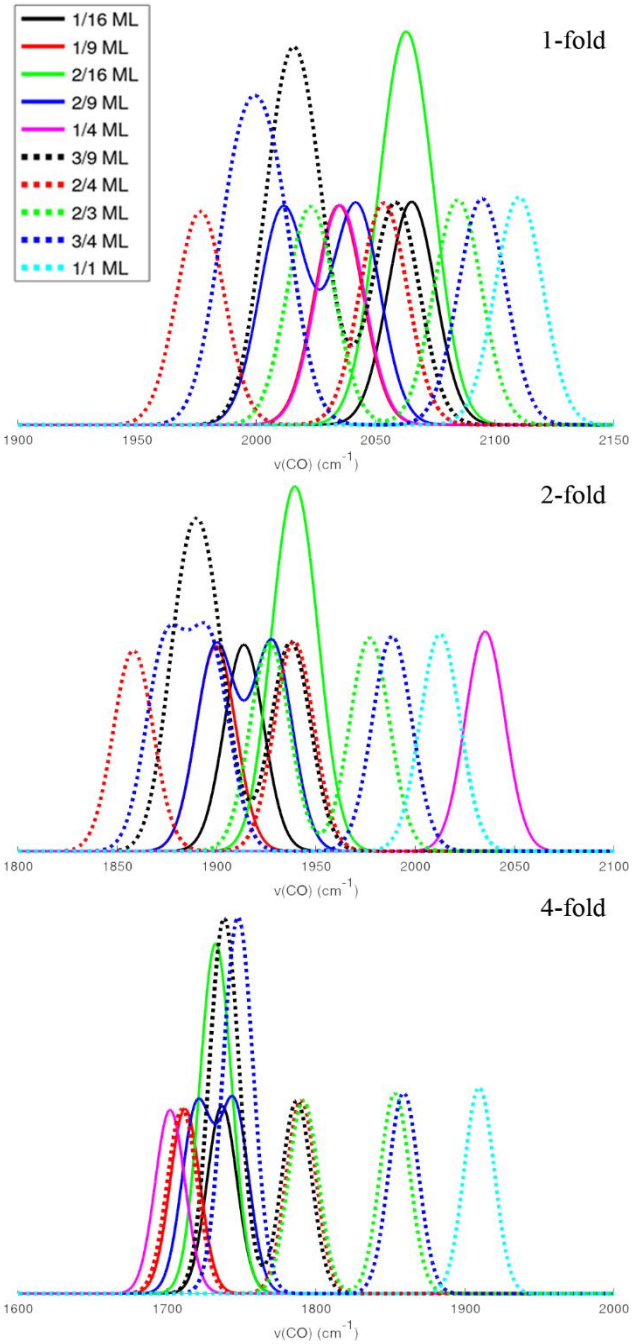

Figure 5 simulated vibrational spectrum of the CO adsorbed on Cu(110) surface at various coverage and adsorption positions.

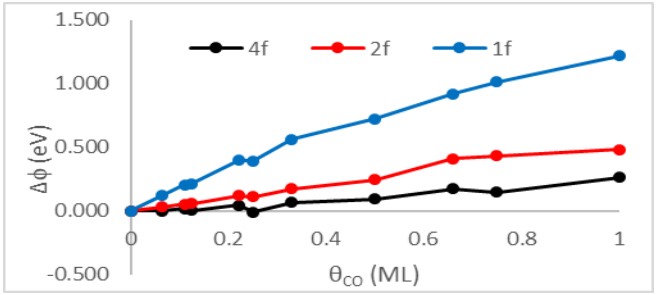

Figure 6 Changes in the work function for CO adsorption on Cu(100) at various coverage and adsorption positions.

Table 1
Adsorption energy (E_{ads}, kJ/mol), C-O stretching frequency (ν_{CO}, cm^{-1}), C-O and C-Cu bonds distances (Å), and change in work function ($\Delta\phi$, eV) for the studied coverage (θ_{CO}, ML) and positions.

θ_{CO}	Site	E_{ads}	ν_{CO}	|C-O|	|C-Cu|	$\Delta\phi$
1/16	4 fold	-249	1737	1.197	2.141	0.000
(0.0625)	2 fold	-250	1914	1.170	1.983	0.029
	1 fold	-249	2064	1.154	1.847	0.121
1/9	4 fold	-190	1712	1.198	2.138	0.015
(0.1111)	2 fold	-189	1899	1.170	1.980	0.053
	1 fold	-187	2034	1.154	1.842	0.204
2/16	4 fold	-164	1729	1.197	2.144	0.003
(0.1250)			1736	1.197	2.138	
	2 fold	-166	1934	1.170	1.981	0.059
			1945	1.170	1.981	
	1 fold	-165	2057	1.154	1.842	0.212
			2067	1.154	1.844	
2/9	4 fold	-135	1720	1.195	2.127	0.044
(0.2222)			1745	1.195	2.166	
	2 fold	-135	1899	1.169	1.985	0.120
			1928	1.169	1.982	
	1 fold	-134	2011	1.154	1.840	0.396
			2042	1.154	1.840	
1/4	4 fold	-121	1702	1.195	2.138	-0.012
(0.2500)	2 fold	-127	1905	1.169	1.981	0.111
	1 fold	-125	2035	1.154	1.841	0.394
3/9	4 fold	-97	1738	1.190	2.138	0.069
(0.3333)			1739	1.192	2.162	
			1787	1.190	2.138	
	2 fold	-115	1883	1.170	1.991	0.172
			1896	1.170	1.991	
			1938	1.167	2.008	
	1 fold	-116	2010	1.155	1.841	0.563
			2021	1.155	1.838	
			2059	1.155	1.838	
2/4	4 fold	-87	1710	1.188	2.174	0.094
(0.5000)			1789	1.188	2.179	
	2 fold	-93	1858	1.168	1.992	0.244
			1939	1.168	1.992	
	1 fold	-100	1976	1.155	1.840	0.722
			2054	1.155	1.840	
2/3	4 fold	-15	1792	1.179	2.144	0.174
(0.6666)			1853	1.181	2.183	
	2 fold	-68	1928	1.166	1.986	0.409
			1979	1.165	1.980	
	1 fold	-50	2023	1.153	1.851	0.919
			2084	1.153	1.851	
3/4	4 fold	-16	1747	1.180	2.197	0.148
(0.750)			1748	1.179	2.183	
			1859	1.180	2.202	
	2 fold	-51	1874	1.164	1.982	0.432
			1896	1.167	1.994	
			1988	1.164	1.982	
	1 fold	-55	1992	1.153	1.851	1.014
			2006	1.154	1.851	
			2094	1.153	1.851	
1/1	4 fold	21	1909	1.174	2.207	0.264
(1.0000)	2 fold	-26	2012	1.163	1.981	0.479
	1 fold	-27	2110	1.152	1.857	1.218

a) Average Eads is reported when more than one CO molecules are adsorbed. b) Average bond lengths are reported for 2-fold and 4-fold positions. c) The X and Y positions of these geometries were kept frozen to prevent shifting into other positions.

Acknowledgements

The DFT computations reported in this paper were performed at TUBITAK ULAKBIM, High Performance and Grid Computing Center (TRUBA resources).

Funding

This Project did not receive any financial funding.

The Declaration of Conflict of Interest/ Common Interest

No conflict of interest or common interest has been declared by the authors.

Authors' Contribution

The author solemly performed the computations and wrote the manuscript.

The Declaration of Ethics Committee Approval

The author declare that this document does not require an ethics committee approval or any special permission.

The Declaration of Research and Publication Ethics

The authors of the paper declare that they comply with the scientific, ethical and quotation rules of SAUJS in all processes of the article and that they do not make any falsification on the data collected. In addition, they declare that Sakarya University Journal of Science and its editorial board have no responsibility for any ethical violations that may be encountered, and that this study has not been evaluated in any academic publication environment other than Sakarya University Journal of Science.

REFERENCES

[1] B. Eren *et al.*, "Activation of Cu(111) surface by decomposition into nanoclusters driven by CO adsorption," *Science*, vol. 351, no. 6272, pp. 475-478, 2016, doi: 10.1126/science.aad8868.

[2] A. M. Bradshaw and J. Pritchard, "Infrared Spectra of Carbon Monoxide Chemisorbed on Metal Films: A Comparative Study of Copper, Silver, Gold, Iron, Cobalt and Nickel," *Proceedings of the Royal Society of London. Series A, Mathematical and Physical Sciences*, vol. 316, no. 1525, pp. 169-183, 1970. [Online]. Available: www.jstor.org/stable/77710.

[3] Q. Jiang, H. M. Lu, and M. Zhao, "Modelling of surface energies of elemental crystals," *Journal of Physics: Condensed Matter*, vol. 16, no. 4, pp. 521-530, 2004/01/16 2004, doi: 10.1088/0953-8984/16/4/001.

[4] X. Liu *et al.*, "pH effects on the electrochemical reduction of CO(2) towards C_2 products on stepped copper," *Nature Communications*, vol. 10, no. 1, p. 32, 2019/01/03 2019, doi: 10.1038/s41467-018-07970-9.

[5] E. Borguet and H. L. Dai, "Site-specific properties and dynamical dipole coupling of CO molecules adsorbed on a vicinal Cu(100) surface," *The Journal of Chemical Physics*, vol. 101, no. 10, pp. 9080-9095, 1994, doi: 10.1063/1.468038.

[6] H. Yamashita, M. Matsuoka, K. Tsuji, Y. Shioya, M. Anpo, and M. Che, "In-Situ XAFS, Photoluminescence, and IR Investigations of Copper Ions Included within Various Kinds of Zeolites. Structure of Cu(I) Ions and Their Interaction with CO Molecules," *The Journal of Physical Chemistry*, vol. 100, no. 1, pp. 397-402, 1996/01/01 1996, doi: 10.1021/jp952666z.

[7] B. Ipek *et al.*, "Formation of [Cu2O2]2+ and [Cu_2O]2+ toward C–H Bond Activation in Cu-SSZ-13 and Cu-SSZ-39," *ACS Catalysis*, vol. 7, no. 7, pp. 4291-4303, 2017/07/07 2017, doi: 10.1021/acscatal.6b03005.

[8] X. Liu, J. Xiao, H. Peng, X. Hong, K. Chan, and J. K. Nørskov, "Understanding trends in electrochemical carbon dioxide reduction

rates," *Nature Communications*, vol. 8, no. 1, p. 15438, 2017/05/22 2017, doi: 10.1038/ncomms15438.

[9] R. W. Joyner, C. S. McKee, and M. W. Roberts, "The adsorption of carbon monoxide on Cu(001): LEED and Auger emission studies," *Surface Science*, vol. 26, no. 1, pp. 303-309, 1971/06/01/ 1971, doi: https://doi.org/10.1016/0039-6028(71)90129-4.

[10] S. Andersson, "Vibrational excitations and structure of CO chemisorbed on Cu(100)," *Surface Science*, vol. 89, no. 1, pp. 477-485, 1979/01/01/ 1979, doi: https://doi.org/10.1016/0039-6028(79)90632-0.

[11] S. Andersson and J. B. Pendry, "Structure of CO Adsorbed on Cu(100) and Ni(100)," *Physical Review Letters*, vol. 43, no. 5, pp. 363-366, 07/30/ 1979, doi: 10.1103/PhysRevLett.43.363.

[12] A. O. Elnabawy, J. Schumann, P. Bothra, A. Cao, and J. K. Nørskov, "The Challenge of CO Hydrogenation to Methanol: Fundamental Limitations Imposed by Linear Scaling Relations," *Topics in Catalysis*, vol. 63, no. 7, pp. 635-648, 2020/08/01 2020, doi: 10.1007/s11244-020-01283-2.

[13] B. Eren, Z. Liu, D. Stacchiola, G. A. Somorjai, and M. Salmeron, "Structural Changes of Cu(110) and Cu(110)-(2 × 1)-O Surfaces under Carbon Monoxide in the Torr Pressure Range Studied with Scanning Tunneling Microscopy and Infrared Reflection Absorption Spectroscopy," *The Journal of Physical Chemistry C*, vol. 120, no. 15, pp. 8227-8231, 2016/04/21 2016, doi: 10.1021/acs.jpcc.6b02143.

[14] F. H. P. M. Habraken, C. M. A. M. Mesters, and G. A. Bootsma, "The adsorption and incorporation of oxygen on Cu(100) and its reaction with carbon monoxide; comparison with Cu(111) and Cu(110)," *Surface Science*, vol. 97, no. 1, pp. 264-282, 1980/07/01/ 1980, doi: https://doi.org/10.1016/0039-6028(80)90118-1.

[15] K. Hermann, P. S. Bagus, and C. J. Nelin, "Size dependence of surface cluster models: CO adsorbed on Cu(100)," *Physical Review B*, vol. 35, no. 18, pp. 9467-9473, 06/15/ 1987, doi: 10.1103/PhysRevB.35.9467.

[16] B. N. J. Persson and M. Persson, "Vibrational lifetime for CO adsorbed on Cu(100)," *Solid State Communications*, vol. 36, no. 2, pp. 175-179, 1980/10/01/ 1980, doi: https://doi.org/10.1016/0038-1098(80)90677-8.

[17] J. Pritchard, "On the structure of CO adlayers on Cu(100) and Cu(111)," *Surface Science*, vol. 79, no. 1, pp. 231-244, 1979/01/01/ 1979, doi: https://doi.org/10.1016/0039-6028(79)90039-6.

[18] M. Roiaz, L. Falivene, C. Rameshan, L. Cavallo, S. M. Kozlov, and G. Rupprechter, "Roughening of Copper (100) at Elevated CO Pressure: Cu Adatom and Cluster Formation Enable CO Dissociation," *The Journal of Physical Chemistry C*, vol. 123, no. 13, pp. 8112-8121, 2019/04/04 2019, doi: 10.1021/acs.jpcc.8b07668.

[19] R. Ryberg, "Carbon monoxide adsorbed on Cu(100) Studied by infrared spectroscopy," *Surface Science*, vol. 114, no. 2, pp. 627-641, 1982/02/01/ 1982, doi: https://doi.org/10.1016/0039-6028(82)90710-5.

[20] R. B. Sandberg, J. H. Montoya, K. Chan, and J. K. Nørskov, "CO-CO coupling on Cu facets: Coverage, strain and field effects," *Surface Science*, vol. 654, pp. 56-62, 2016/12/01/ 2016, doi: https://doi.org/10.1016/j.susc.2016.08.006.

[21] A. Sandell, P. Bennich, A. Nilsson, B. Hernnäs, O. Björneholm, and N. Mårtensson, "Chemisorption of CO on Cu(100), Ag(110) and Au(110)," *Surface*

Science, vol. 310, no. 1, pp. 16-26, 1994/05/01/ 1994, doi: https://doi.org/10.1016/0039-6028(94)91366-8.

[22] C. Somerton, C. F. McConville, D. P. Woodruff, D. E. Grider, and N. V. Richardson, "Valence band photoemission study of the coadsorption of CO and K on Cu{100}," *Surface Science,* vol. 138, no. 1, pp. 31-39, 1984/03/01/ 1984, doi: https://doi.org/10.1016/0039-6028(84)90493-X.

[23] J. C. Tracy, "Structural Influences on Adsorption Energy. III. CO on Cu(100)," *The Journal of Chemical Physics,* vol. 56, no. 6, pp. 2748-2754, 1972, doi: 10.1063/1.1677603.

[24] C. M. Truong, J. Rodriguez, and D. W. Goodman, "CO adsorption isotherms on Cu(100) at elevated pressures and temperatures using infrared reflection absorption spectroscopy," *Surface Science,* vol. 271, no. 3, pp. L385-L391, 1992/01/01/ 1992, doi: https://doi.org/10.1016/0039-6028(92)90896-E.

[25] S. Vollmer, G. Witte, and C. Wöll, "Determination of Site Specific Adsorption Energies of CO on Copper," *Catalysis Letters,* vol. 77, no. 1, pp. 97-101, 2001/11/01 2001, doi: 10.1023/A:1012755616064.

[26] B. M. W. Trapnell and C. N. Hinshelwood, "The activities of evaporated metal films in gas chemisorption," *Proceedings of the Royal Society of London. Series A. Mathematical and Physical Sciences,* vol. 218, no. 1135, pp. 566-577, 1953, doi: doi:10.1098/rspa.1953.0125.

[27] R. M. Dell, F. S. Stone, and P. F. Tiley, "The adsorption of oxygen and other gases on copper," *Transactions of the Faraday Society,* 10.1039/TF9534900195 vol. 49, no. 0, pp. 195-201, 1953, doi: 10.1039/TF9534900195.

[28] R. P. Eischens and W. A. Pliskin, "The Infrared Spectra of Adsorbed Molecules," in *Advances in Catalysis*, vol. 10, D. D. Eley, W. G. Frankenburg, V. I. Komarewsky, and P. B. Weisz Eds.: Academic Press, 1958, pp. 1-56.

[29] A. W. Smith and J. M. Quets, "Adsorption of carbon monoxide on copper: Infrared absorption spectra and thermodesorption," *Journal of Catalysis,* vol. 4, no. 2, pp. 163-171, 1965/04/01/ 1965, doi: https://doi.org/10.1016/0021-9517(65)90007-2.

[30] A. M. Bradshaw, J. Pritchard, and M. L. Sims, "Reflection spectroscopy of chemisorbed carbon monoxide under ultrahigh vacuum conditions," *Chemical Communications (London),* 10.1039/C19680001519 no. 23, pp. 1519-1520, 1968, doi: 10.1039/C19680001519.

[31] J. Pritchard, "Surface-potential study of the chemisorption of hydrogen and carbon monoxide on evaporated copper and gold films," *Transactions of the Faraday Society,* 10.1039/TF9635900437 vol. 59, no. 0, pp. 437-452, 1963, doi: 10.1039/TF9635900437.

[32] T. Wadayama, H. Yoshida, S. Oda, and N. Todoroki, "Infrared Reflection Absorption Study for Carbon Monoxide Adsorption on Chromium Deposited Cu(100) Surfaces," *MATERIALS TRANSACTIONS,* vol. 50, no. 4, pp. 819-824, 2009, doi: 10.2320/matertrans.MRA2008442.

[33] P. Giannozzi *et al.*, "QUANTUM ESPRESSO: a modular and open-source software project for quantum simulations of materials," *Journal of Physics: Condensed Matter,* vol. 21, no. 39, p. 395502, 2009/09/01 2009, doi: 10.1088/0953-8984/21/39/395502.

[34] W. P. Davey, "Precision Measurements of the Lattice Constants of Twelve Common Metals," *Physical Review,* vol. 25, no. 6, pp.

753-761, 06/01/ 1925, doi: 10.1103/PhysRev.25.753.

[35] K. M. Gameel, I. M. Sharafeldin, A. U. Abourayya, A. H. Biby, and N. K. Allam, "Unveiling CO adsorption on Cu surfaces: new insights from molecular orbital principles," *Physical Chemistry Chemical Physics,* 10.1039/C8CP04253E vol. 20, no. 40, pp. 25892-25900, 2018, doi: 10.1039/C8CP04253E.

[36] A. W. Robinson, D. P. Woodruff, J. S. Somers, A. L. D. Kilcoyne, D. E. Ricken, and A. M. Bradshaw, "Photoelectron diffraction study of the local adsorption site in the Cu(110)(2 × 3)-N structure," *Surface Science,* vol. 237, no. 1, pp. 99-107, 1990/11/01/ 1990, doi: https://doi.org/10.1016/0039-6028(90)90522-A.

[37] M. O. Ozbek, I. Onal, and R. A. van Santen, "Effect of Surface and Oxygen Coverage on Ethylene Epoxidation," *Topics in Catalysis*, vol. 55, no. 11, pp. 710-717, 2012/08/01 2012, doi: 10.1007/s11244-012-9870-7.

SAKARYA ÜNİVERSİTESİ
FEN BİLİMLERİ ENSTİTÜSÜ DERGİSİ

Sakarya University Journal of Science
SAUJS

e-ISSN 2147-835X | Period Bimonthly | Founded: 1997 | Publisher Sakarya University |
http://www.saujs.sakarya.edu.tr/en/

Title: A New Fuzzy Approach for Analyzing the Smartness of Cities: Case Study for Turke

Authors: Melike ERDOĞAN

Recieved: 2020-09-24 00:00:00

Accepted: 2021-01-21 00:00:00

Article Type: Research Article

Volume: 25
Issue: 2
Month: April
Year: 2021
Pages: 308-325

How to cite
Melike ERDOĞAN; (2021), A New Fuzzy Approach for Analyzing the Smartness of Cities: Case Study for Turke. Sakarya University Journal of Science, 25(2), 308-325, DOI: https://doi.org/10.16984/saufenbilder.799469
Access link
http://www.saujs.sakarya.edu.tr/en/pub/issue/60672/799469

Sakarya University Journal of Science 25(2), 308-325, 2021

A New Fuzzy Approach for Analyzing the Smartness of Cities: Case Study for Turkey

Melike Erdoğan*[1]

Abstract

Smart cities, developed as alternative to classical urbanism, are areas where information and communication technologies are used to make places more livable, sustainable and efficient. If a city offers solutions to problems related to governance, people, economy, mobility, environment and living issues, it can be defined as "smart city". The smartness of cities can be measured on these six basic axes. By analyzing the smartness of cities, evaluations can be made on the quality of life, health, public safety, environment and services. Hereby, appropriate measures can be taken against problems and strategies can be developed to increase the smartness of cities. This paper proposes a new decision making analysis to evaluate and compare the smartness of cities. For this aim, we considered the cities which are the candidates to be smart areas in Turkey. At this point, we applied multi-criteria decision-making (MCDM) analysis to evaluate criteria and alternatives in the decision process. We also utilized from fuzzy logic to model the uncertainty in the best way. Furthermore, we applied extended version of ordinary fuzzy sets which is named spherical fuzzy sets for the first time with QUALIFLEX method. Thus, one of the most comprehensive qualitative analyses ever made in the evaluation of smart cities is revealed and the usability of spherical fuzzy sets by MCDM methods is demonstrated. In addition, a sensitivity analysis was used to examine the robustness of the proposed method. As a result, a novel fuzzy decision-making approach has been proposed in the evaluation of smart cities.

Keywords: decision making, QUALIFLEX, smartness of cities, spherical fuzzy sets

1. INTRODUCTION

The smart city is a concept model with many "smart" sub-elements using technological developments to improve the living conditions of citizens. In recent years, the concept of the smart city has appeared as an area where expectations and calculations about social futures are made [1]. Because it is predicted that 70% of the world's population will reside in urban areas by 2050 and cities exhibit complex dynamics and require new solutions, the "smart city" model, which aims to deal with these problems, is becoming more and more important [2]. Since the demand of the high-density city population for energy, transportation, water supply, buildings and public spaces is higher, cities have to be “smarter” in the presence of the mentioned problems [3]. The idea behind

*Corresponding author: melikeerdogan@duzce.edu.tr
[1]Düzce University, Department of Industrial Engineering, Düzce, Turkey
ORCID: https://orcid.org/0000-0003-0329-8562

the smart city is not only that a city's physical infrastructures and donations characterize an urban area and its functions, but it is also not easy to describe as information communication and social infrastructure. [4]. A smart city is a subject that is frequently handled both in practice and academia because of its potential to refer to several negative effects of rapid urbanization, industrialization and consumerism practices [5]. Because of different disciplines and sectoral perspectives, consensus on the definition of smart city could still not be built [5]. The definition of smart city is expanding and changing, recently this concept has been used in the same sense as information technology cities [6]. The smart city is the place that effectively uses strategic planning methods and innovative answers to improve the quality of life of their public, including ecological, cultural, political, institutional, social and economic components [5].

Besides many definitions of smart city concept, if a city applies solutions based on communication and information technologies to problems in six dimensions such as mobility, people, environmental, governance, quality of life and basic services and economy, it is regarded as "smart" [6-7]. With these axes, a smart city is much more than a digital city where attention is particularly focused on information and communication technology elements to enable data and information connectivity and exchange in an urban environment [4]. Considering these axes, the smart city is not only evaluated for the automation of services, buildings, traffic systems, it is also evaluated on behalf of undertakings to monitor, understand, analyze and plan the city in order to improve efficiency, equality and quality of life for citizens [7]. For a city to be considered a smart city, it should include initiatives and projects in its development plans [6]. The smartness measurement of cities is connected to the quality of life, health, public safety, disaster management, environmental aspects and services [8]. It is necessary to measure the smartness of cities in order to take appropriate actions in developing smartness features. The smartness of the cities can be measured with indicators under these six axes. Thus, many goals can be achieved, such as preparing action plans for smart cities, developing strategies, or comparing the smartness of cities. Using these six basic axes related to smart cities, studies on comparing the smartness of the cities were carried out. However, most of the studies are only based on qualitative analysis. The survey is one of the most used approaches in this sense. One of the approaches that allow the opportunity to examine and analyze these six axes together in evaluating and comparing the smartness of the cities is to use multi-criteria decision-making methods (MCDM). MDCM is an approach that aims to determine the most appropriate alternative or ranking of the alternatives in the decision environment where multiple, contradictory and interactive criteria exist. When trying to make a satisfactory decision with ambiguous and incomplete data, indecision, the presence of linguistic variables and multi-criteria, a decision maker should apply to MCDM methods under fuzzy environment [9]. The fuzzy set theory proposed by Zadeh [10] is one of the most effective ways to deal with vagueness and uncertainty [11]. In literature, MCDM methods which are classified as traditional and fuzzy are frequently used for the ranking of alternatives in decision problems. However traditional MCDM methods are insufficient in addressing linguistic uncertainty. Therefore MCDM methods are applied with fuzzy sets to consider the linguistic uncertainty better [12]. In most real-life MCDM problems, linguistic expressions are used to evaluate alternatives based on specified criteria, since the available information tends to be ambiguous, subjective or imprecise [13]. In the evaluation of the smartness of cities, situations such as the fact that there are conflicting criteria that cannot be measured numerically, and besides, situations, where alternatives are desired to be ranked in the presence of these criteria, make the problem a fuzzy MCDM problem. Based on all these, we have adopted the fuzzy MCDM approach in the evaluation and comparison of the smartness of cities in this paper. For this aim, we applied an extended version of the ordinary fuzzy sets which is named spherical fuzzy sets for the first time with QUALIFLEX MCDM method. This study fills an important gap in the literature, as it is one of the most detailed studies in the field of application area and the first time QUALIFLEX method are applied under spherical

fuzzy environment. Thus, one of the most comprehensive quantitative analyses ever made in the evaluation of smart cities are revealed and the usability of spherical fuzzy sets by MCDM methods are demonstrated. For this reason, we believe that this paper is a prominent study for researchers and practitioners who are working on the implementation of MCDM methods within the framework of extended fuzzy sets in the specified area.

The rest of the paper is organized as follows. Section 2 presents the relevant literature on the problem and solution methodology that we adopted. Section 3 describes the proposed methodology. Section 4 contains the application for the evaluation of the smartness of cities in Turkey with the proposed methodology. Section 5 shows the results of the sensitivity analysis for the real case study. Finally, conclusions and future suggestions are presented in Section 6.

2. LITERATURE REVIEW

Many studies can be seen in the literature on the concept of smart city and the analysis of the smartness of the cities. Most of them carried out using questionnaires in the smartness analysis of cities. In a significant number of studies, six axes which are governance, people, economy, mobility, environment, and living were also taken into consideration in the evaluation of the smartness for the cities. Prominent studies in evaluating the smartness of the cities can be summarized as follows. Yigitcanlar and Kamruzzaman [5] aimed to incorporate a causal link between urban smartness and new ways of working, for instance working from home, and discover whether changes in urban smartness have remodeled the way residents go to work. Calderón et al. [6] prepared a survey to explain the current state of smartness and perceived readiness of Latin American Cities. Carli et al. [7] offered a two-dimensional study to classify the performance indicators of a smart city in determining technologies that can be adopted for the smart measurement and monitoring of a smart city. McKenna [14] analyzed the multidimensionality of smart cities by looking at relationships and interdependencies by associating the dimensions of smartness. Marsal-Llacuna [15] presented a set of indicators that serve to measure the newly accepted international definition in smart cities, and this set of indicators be used to measure the smartness of the city of Girona, Spain. Ahvenniemi and Huovila [16] showed a new perspective to discussions on various city concepts by investigating how smartness and sustainability are displayed in the city strategies of the six cities of Finland using content analysis. Hajduk [17] examined the diversity of smartness of European cities based on International Standards 37120 Norms on sustainable development of communities. Lima et al. [18] explored the main rules of the Brazilian City Statue, which have significant potential for having smarter and more sustainable Brazilian cities, and used a survey to prioritize the sixteen directives of the City Statue. Baykurt and Raetzsch [1] studied what smartness has done in the field by examining how media visions expected in policy decisions and local practices have been interpreted and acted upon since the early 2000s. Bernardino et al. [3] analyzed to what extent the heritage of European Capitals of Culture increased the smartness of cities and applied a qualitative method based on semi-structured interviews and desk research to evaluate its impact on the dimensions of the smart city. Axelsson and Granath [19] aimed to establish a structure that considers stakeholders and smartness dimensions in city planning and was applied to investigate the complexity of city planning on the development of a city area where a new planning method was applied in Sweden. Al-Nasrawi et al. [20] explored what smartness is and the method of assessment to apprehend the performance of the smart sustainable cities concept and pointed out that the smartness of cities is not limited to the application of smart solutions that meet the needs of citizens. Dall'O et al. [21] proposed a method for assessing smartness through indicators applicable to small and medium-sized cities, complying with the ISO 37120 standard and inspired by environmental indicators used in the EU's Sustainable Energy Action Plan. El Khayat and Fashal [22] dealt with the problems of how to place smart city components internally and how smart cities are placed relative to each other and their publics with

the tools of optimization and Geographic Information Systems. Corsini et al. [23] evaluated economic and socio-demographic variables and smart city characteristics of 63 European cities using factor analysis and as a result of the study, they showed that there is no correlation between the city size and the smart city features, between economic wealth and smart city features.

Spherical fuzzy sets, which are an extension of the ordinary fuzzy sets adopted in this paper, were proposed by Kutlu Gündoğdu and Kahraman [24]. Since it is a newly developed method, there are only limited studies in the literature. Kutlu Gündoğdu and Kahraman [25] introduced accuracy functions; arithmetic and aggregation operations for spherical fuzzy sets with interval values, and then used the interval-valued spherical fuzzy TOPSIS method for selecting 3D printers. Kahraman et al. [26] applied spherical fuzzy MCDM approach for the selection process of debt collection firms in Turkey. Boltürk [27] handled the Automated Storage and Retrieval Systems technology selection problem by applying spherical fuzzy TOPSIS and neutrosophic fuzzy TOPSIS methods. Kutlu Gündoğdu and Kahraman [28] presented spherical fuzzy AHP method to show the applicability and validity of a problem of renewable energy location selection. Barukab et al. [29] developed the TOPSIS method under global fuzzy clusters when both the weight of the decision-makers and the criteria were not fully known and made an illustrative example for the robot selection problem. Kutlu Gündoğdu and Kahraman [30] applied the VIKOR method to the warehouse location selection problem by extending it under spherical fuzzy sets. Liu et al. [31] extended the MABAC (Multi-Attributive Border Approximation area Comparison) and TODIM (Interactive and Multi-Criteria Decision Making Portuguese abbreviation) methods into the linguistic spherical fuzzy environment for the evaluation of shared bicycles in China. Kutlu Gündoğdu and Kahraman [32] identified spherical fuzzy distances based on the parameters of membership, nonmembership and hesitancy and developed spherical fuzzy CODAS (COmbine Distance Based Assessment) method, demonstrating applicability in an illustrative example. Kahraman et al. [33] adopted the spherical fuzzy TOPSIS method in developing a quality house approach in comparing firms. Kutlu Gündoğdu [34] extended the MULTIMOORA method with spherical fuzzy numbers and used neutrosophic MULTIMOORA and intuitionistic fuzzy TOPSIS methods in the study where they exemplified the solution of the method. Yang et al. [35] developed the spherical normal fuzzy Bonferroni average operator and the weighted Bonferroni average operator and created an MCDM approach based on spherical normal fuzzy information and the proposed operators. They used the proposed approach to confirm the applicability in the antivirus mask selection problem according to the COVID-19 pandemic. Unlike all these studies, we have expanded the QUALIFLEX method for the first time with spherical fuzzy numbers. Besides, a comprehensive decision-making approach is proposed for the first time using extended fuzzy sets means that it is analyzed with a much more detailed decision-making approach among other the smart city assessment studies examined. Therefore, we believe that this study is a prominent paper in terms of both the adopted method and application area.

3. PROPOSED METHODOLOGY

In this section, the methodology that we proposed in the evaluation of the smartness of the cities is explained in the following subsections. Firstly, information about spherical fuzzy numbers was given, then the spherical fuzzy QUALIFLEX method developed in this study was introduced.

3.1. Spherical Fuzzy Sets

Spherical fuzzy sets are defined by three parameters membership, non-membership and hesitancy parameters (μ, ϑ, π). In spherical fuzzy sets, while the squared sum of membership, non-membership and hesitancy parameters can be between 0 and 1, each of them can be defined between 0 and 1 independently to satisfy that their squared sum is at most equal to 1 [24], [36], [37].

In this section, the definition of spherical fuzzy sets and summarize spherical distance

measurement, arithmetic operations, aggregation operators and defuzzification operations are explained [24], [26], [38].

Definition 1. A spherical fuzzy set $\tilde{A}_s$ of the universe of discourse *U* is given by

$$\tilde{A}_s = \left\{ \left\langle u, (\mu_{\tilde{A}_s}(u), \vartheta_{\tilde{A}_s}(u), \pi_{\tilde{A}_s}(u)) \mid u \in U \right\rangle \right\} \quad (1)$$

where

$$\mu_{\tilde{A}_s} : U \to [0,1], \quad \vartheta_{\tilde{A}_s} : U \to [0,1], \quad \pi_{\tilde{A}_s} : U \to [0,1],$$

and

$$0 \le \mu_{\tilde{A}_s}^2 + \vartheta_{\tilde{A}_s}^2 + \pi_{\tilde{A}_s}^2 \le 1 \qquad \forall u \in U \quad (2)$$

For each u, the numbers $\mu_{\tilde{A}_s}^2, \vartheta_{\tilde{A}_s}^2$ and $\pi_{\tilde{A}_s}^2$ are the degree of membership, nonmembership and hesitancy of *u* to $\tilde{A}_s$, respectively [24], [25], [28], [30], [32].

Definition 2. Basic Operators

Union;

$$\tilde{A}_s \cup \tilde{B}_s = \left\{ \max\{\mu_{\tilde{A}_s}, \mu_{\tilde{B}_s}\}, \min\{\vartheta_{\tilde{A}_s}, \vartheta_{\tilde{B}_s}\}, \left\{ \min\left(1 - \left((\max\{\mu_{\tilde{A}_s}, \mu_{\tilde{B}_s}\})^2 + (\min\{\vartheta_{\tilde{A}_s}, \vartheta_{\tilde{B}_s}\})^2\right)\right)^{1/2}, \max\left\{\pi_{\tilde{A}_s}, \pi_{\tilde{B}_s}\right\} \right\} \right\} \quad (3)$$

Intersection;

$$\tilde{A}_s \cap \tilde{B}_s = \left\{ \min\{\mu_{\tilde{A}_s}, \mu_{\tilde{B}_s}\}, \max\{\vartheta_{\tilde{A}_s}, \vartheta_{\tilde{B}_s}\}, \max\left\{ \left(1 - \left((\min\{\mu_{\tilde{A}_s}, \mu_{\tilde{B}_s}\})^2 + (\max\{\vartheta_{\tilde{A}_s}, \vartheta_{\tilde{B}_s}\})^2\right)\right)^{1/2}, \min\left\{\pi_{\tilde{A}_s}, \pi_{\tilde{B}_s}\right\} \right\} \right\} \quad (4)$$

Addition;

$$\tilde{A}_s \oplus \tilde{B}_s = \left\{ \left(\mu_{\tilde{A}_s}^2 + \mu_{\tilde{B}_s}^2 - \mu_{\tilde{A}_s}^2 \mu_{\tilde{B}_s}^2\right)^{1/2}, \upsilon_{\tilde{A}_s}\upsilon_{\tilde{B}_s}, \left(\left(1-\mu_{\tilde{B}_s}^2\right)\pi_{\tilde{A}_s}^2 + \left(1-\mu_{\tilde{A}_s}^2\right)\pi_{\tilde{B}_s}^2 - \pi_{\tilde{A}_s}^2\pi_{\tilde{B}_s}^2\right)^{1/2} \right\} \quad (5)$$

Multiplication;

$$\tilde{A}_s \otimes \tilde{B}_s = \left\{ \mu_{\tilde{A}_s}\mu_{\tilde{B}_s}, \left(\upsilon_{\tilde{A}_s}^2 + \upsilon_{\tilde{B}_s}^2 - \upsilon_{\tilde{A}_s}^2\upsilon_{\tilde{B}_s}^2\right)^{1/2}, \left(\left(1-\upsilon_{\tilde{B}_s}^2\right)\pi_{\tilde{A}_s}^2 + \left(1-\upsilon_{\tilde{A}_s}^2\right)\pi_{\tilde{B}_s}^2 - \pi_{\tilde{A}_s}^2\pi_{\tilde{B}_s}^2\right)^{1/2} \right\} \quad (6)$$

Multiplication by a scalar; $\lambda > 0$

$$\lambda.\tilde{A}_s = \left\{ \left(1-\left(1-\mu_{\tilde{A}_s}^2\right)^{\lambda}\right)^{1/2}, \upsilon_{\tilde{A}_s}^{\lambda}, \left(\left(1-\mu_{\tilde{A}_s}^2\right)^{\lambda} - \left(1-\mu_{\tilde{A}_s}^2-\pi_{\tilde{A}_s}^2\right)^{\lambda}\right)^{1/2} \right\} \quad (7)$$

λ. Power of $\tilde{A}_s$; λ > 0

$$\tilde{A}_S^{\lambda} = \left\{ \mu_{\tilde{A}_s}^{\lambda}, \left(1-\left(1-\upsilon_{\tilde{A}_s}^2\right)^{\lambda}\right)^{1/2}, \left(\left(1-\upsilon_{\tilde{A}_s}^2\right)^{\lambda} - \left(1-\upsilon_{\tilde{A}_s}^2-\pi_{\tilde{A}_s}^2\right)^{\lambda}\right)^{1/2} \right\} \quad (8)$$

Definition 3. For these spherical fuzzy sets $\tilde{A}_s = (\mu_{\tilde{A}_s}, \upsilon_{\tilde{A}_s}, \pi_{\tilde{A}_s})$ and $\tilde{B}_s = (\mu_{\tilde{B}_s}, \upsilon_{\tilde{B}_s}, \pi_{\tilde{B}_s})$, the followings are valid under the condition $\lambda, \lambda_1, \lambda_2 > 0$.

i. $\tilde{A}_s \oplus \tilde{B}_s = \tilde{B}_s \oplus \tilde{A}_s$ (9)

ii. $\tilde{A}_s \otimes \tilde{B}_s = \tilde{B}_s \otimes \tilde{A}_s$ (10)

iii. $\lambda(\tilde{A}_s \oplus \tilde{B}_s) = \lambda\tilde{A}_s \oplus \lambda\tilde{B}_s$ (11)

iv. $\lambda_1\tilde{A}_s \oplus \lambda_2\tilde{A}_s = (\lambda_1 + \lambda_2)\tilde{A}_s$ (12)

v. $(\tilde{A}_s \otimes \tilde{B}_s)^{\lambda} = \tilde{A}_s^{\lambda} \otimes \tilde{B}_s^{\lambda}$ (13)

vi. $\tilde{A}_s^{\lambda_1} \otimes \tilde{A}_s^{\lambda_2} = \tilde{A}_s^{\lambda_1+\lambda_2}$ (14)

Definition 4. Spherical Weighted Arithmetic Mean (SWAM) with respect to, $w=(w_1,w_2,..,w_n);\ \ w_i\in[0,1];\ \sum_{i=1}^{n} w_i=1,$ SWAM is defined as;

$$SWAM_w(\tilde{A}_{s_1},\tilde{A}_{s_2},...,\tilde{A}_{s_n})=w_1\tilde{A}_{s_1}+w_2\tilde{A}_{s_2}+.....+w_n\tilde{A}_{s_n}$$
$$=\left\{\left[1-\prod_{i=1}^{n}(1-\mu_{\tilde{A}_S}^2)^{w_i}\right]^{1/2},\right.$$
$$\left.\prod_{i=1}^{n}\upsilon_{\tilde{A}_S}^{w_i},\left[\prod_{i=1}^{n}(1-\mu_{\tilde{A}_S}^2)^{w_i}-\prod_{i=1}^{n}(1-\mu_{\tilde{A}_S}^2-\pi_{\tilde{A}_S}^2)^{w_i}\right]^{1/2}\right\} \quad (15)$$

Definition 5. Spherical Weighted Geometric Mean (SWGM) with respect to, $w=(w_1,w_2,..,w_n);\ \ w_i\in[0,1];\ \sum_{i=1}^{n} w_i=1,$ SWGM is defined as;

$$SWGM_w(\tilde{A}_{s_1},\tilde{A}_{s_2},...,\tilde{A}_{s_n})=\tilde{A}_{s_1}^{w_1}+\tilde{A}_{s_1}^{w_2}+.....+\tilde{A}_{s_n}^{w_n}$$
$$=\left\{\prod_{i=1}^{n}\mu_{\tilde{A}_{S_i}}^{w_i},\left[1-\prod_{i=1}^{n}(1-\upsilon_{\tilde{A}_{S_i}}^2)^{w_i}\right]^{1/2},\right.$$
$$\left.\left[\prod_{i=1}^{n}(1-\upsilon_{\tilde{A}_{S_i}}^2)^{w_i}-\prod_{i=1}^{n}(1-\upsilon_{\tilde{A}_{S_i}}^2-\pi_{\tilde{A}_{S_i}}^2)^{w_i}\right]^{1/2}\right\} \quad (16)$$

3.2. Spherical Fuzzy QUALIFLEX

The qualitative flexible multiple (QUALIFLEX) ranking method is the generalization of Jacquet-Lagreze's permutation approach and is beneficial in decision analysis due to its flexibility regarding cardinal and ordinal information [39]. The approach was firstly introduced by Paelinck in 1975 [40]. It analyzes all possible permutations of the alternatives based on the results of the whole criteria [41]. As decision-making environments often involve uncertainty, one of the most frequently used approaches to address uncertainty in the process is to use fuzzy logic. In particular, the solution of almost all MCDM problems has been expanded with fuzzy logic to provide more realistic results recently. At this point, the QUALIFLEX method has found application with ordinary fuzzy sets and extended fuzzy sets in MCDM problems in different areas. For example, interval-valued intuitionistic fuzzy QUALIFLEX approach with a likelihood-based comparison method is suggested to select most appropriate bridge construction [42], interval type-2 fuzzy sets for QUALIFLEX method applied in a medical decision-making problem [39], a Fine - Kinney occupational risk assessment approach with type-2 fuzzy QUALIFLEX approach is implemented in the chrome plating unit [46], type-2 QUALIFLEX method is used to estimate carbon emissions [48], regret theory and QUALIFLEX under a 2-dimensional vague linguistic variable is suggested for sustainable supplier selection [49], the Gray Group QUALIFLEX method is applied in the project management case [53], the multiple criteria hierarchy process and QUALIFLEX methodology is combined to be suitable for interaction modeling between criteria using the concept of the bipolar Choquet integral [54], QUALIFLEX method is integrated with the ORESTE model to evaluate the performance of green mines in uncertain hesitant conditions [55], probabilistic linguistic QUALIFLEX method is suggested for group decision-making problems in which the evaluation information of alternatives is expressed in hesitant fuzzy sets and the weights are partly known [56], QUALIFLEX is adopted in determining the performance efficiency of existing ballast water treatment system used on ships under interval type-2 fuzzy environment [57] and QUALIFLEX is employed in handling multiple evaluation criteria with heterogeneity [58]. Unlike all these studies, we have extended the QUALIFLEX outranking method with spherical fuzzy sets for the first time in this study.

The QUALIFLEX method based on spherical fuzzy numbers has been presented as follows [39-40], [43], [57], [59]:

Step 1: Formulate the decision-making problem in which the evaluation criteria $X=\{x_1,x_2,....x_n\}$ and feasible alternatives $A=\{A_1,A_2,...A_m\}$.

Step 2. Select appropriate linguistic variables and translation standards for conversion into spherical fuzzy numbers for the importance weights of criteria and the linguistic ratings for the alternatives with respect to each criterion. The linguistic scale that we apply to spherical fuzzy QUALIFLEX method is in Table 1 [30].

Table 1
Spherical fuzzy numbers for linguistic terms

Linguistic Terms	**(μ, Ʊ, π)**
Absolutely More Importance (AMI)	(0.9,0.1,0.1)
Very High Importance (VHI)	(0.8,0.2,0.2)
High Importance (HI)	(0.7,0.3,0.3)
Slightly More Importance (SMI)	(0.6,0.4,0.4)
Equally Importance (EI)	(0.5,0.5,0.5)
Slightly Low Importance (SLI)	(0.4,0.6,0.4)
Low Importance (LI)	(0.3,0.7,0.3)
Very Low Importance (VLI)	(0.2,0.8,0.2)
Absolutely Low Importance (ALI)	(0.1,0.9,0.1)

Step 3. The linguistic evaluation of criteria and alternatives with respect to each criterion that best represents the importance of the criteria and the alternative evaluation, respectively, is provided by experts.

Step 4. The linguistic evaluation is converted to the spherical fuzzy numbers to obtain the rating A_{ij} of the alternative A_i on the criterion x_j and the importance weight w_j of the criterion x_j which satisfies $0 \le w_j \le 1$ and $\sum_{j=1}^{n} w_j = 1$ for each expert. Denote the evaluation values of alternatives $A_i \ (i = 1,2,....m)$ with respect to the criterion $x_j \ (j = 1,2,...n)$ by $x_j(\tilde{A}_i) = (\mu_{ij}, \upsilon_{ij}, \pi_{ij})$ and $\tilde{D} = (x_j(\tilde{A}_i)_{mxn}$ is a spherical fuzzy decision matrix. For an MCDM problem with spherical fuzzy sets, the decision matrix $\tilde{D} = (x_j(\tilde{A}_i)_{mxn}$ should be constructed as in Equation (Eq.) (17) and the importance of criteria vector W as in Eq (18).

$$\tilde{D} = (x_j(\tilde{A}_i)_{mxn} = \begin{pmatrix} (\mu_{11},\upsilon_{11},\pi_{11}) & (\mu_{11},\upsilon_{11},\pi_{11}) & \dots & (\mu_{1n},\upsilon_{1n},\pi_{1n}) \\ (\mu_{21},\upsilon_{21},\pi_{21}) & (\mu_{11},\upsilon_{11},\pi_{11}) & \dots & (\mu_{2n},\upsilon_{2n},\pi_{2n}) \\ \vdots & \vdots & \vdots & \vdots \\ (\mu_{m1},\upsilon_{m1},\pi_{m1}) & (\mu_{m2},\upsilon_{m2},\pi_{m2}) & \dots & (\mu_{mn},\upsilon_{mn},\pi_{mn}) \end{pmatrix} \quad (17)$$

$$\tilde{W}_j = (\tilde{w}_1, \tilde{w}_2, ...\tilde{w}_n) \quad (18)$$

Step 5. The judgments of each decision-maker/expert for criteria-alternative evaluations and criteria weights are aggregated using Spherical Weighted Arithmetic Mean (SWAM) operators that are given in Definitions (4).

Step 6. Calculate the score index for the aggregated decision matrix and criteria vector as in Eq. (19) and Eq. (20), respectively. Then normalize the criteria weights as in Eq. (21).

$$Score(x_j(\tilde{A}_i)) = (2\mu_{ij} - \pi_{ij})^2 - (\upsilon_{ij} - \pi_{ij})^2 \quad (19)$$

$$Score(\tilde{w}_j) = (2\mu_{ij} - \pi_{ij})^2 - (\upsilon_{ij} - \pi_{ij})^2 \quad (20)$$

$$\bar{w}_j = \frac{Score(\tilde{w}_j)}{\sum_{j=1}^{n} Score(\tilde{w}_j)} \quad (21)$$

Step 7. List all of the possible *m*! permutations of the *m* alternatives that must be tested. Let $P_l = (l = 1,2,...,m!)$ denote the *l*th permutation. Assume that the alternative $\tilde{A}_\alpha$ has a higher score index than or equal to $\tilde{A}_\beta$. Given the alternative set *A* with *m* alternatives, *m*! permutations of the ranking of the alternatives exist. Let *Pl* denote the *l*th permutation:

$P_l = (..,\tilde{A}_\alpha,...,\tilde{A}_\beta,...)$, for *l=1,2,…,m!*

The evaluation values of $\tilde{A}_\alpha$ and $\tilde{A}_\beta$ with respect to each criterion $x_j \in X$ are

$$\tilde{A}_{\alpha j} = (\mu_{\tilde{A}_{\alpha j}}, \nu_{\tilde{A}_{\alpha j}}, \pi_{\tilde{A}_{\alpha j}})$$

$$\tilde{A}_{\beta j} = (\mu_{\tilde{A}_{\beta j}}, \nu_{\tilde{A}_{\beta j}}, \pi_{\tilde{A}_{\beta j}})$$

The score index values for $\tilde{A}_{\alpha j}$ and $\tilde{A}_{\beta j}$ is taking into consideration to rank the corresponding alternatives.

Step 8. The score index based approach is used to identify the concordance/discordance index. The concordance/discordance index, $I_j^l(\tilde{A}_\alpha, \tilde{A}_\beta)$, for each pair of alternatives, $(\tilde{A}_\alpha, \tilde{A}_\beta)$, $\tilde{A}_\alpha, \tilde{A}_\beta \in A$, at the level of preorder, according to the criterion $xj \in X$ and the ranking corresponding to the lth permutation, is as follows:

$$I_j^l(\tilde{A}_\alpha, \tilde{A}_\beta) = \begin{cases} 1 & \textit{if there is concordance} \\ 0 & \textit{if there is aequo} \\ -1 & \textit{if there is discordance} \end{cases} \quad (22)$$

There are concordance, ex aequo, and discordance if $I_j^l(\tilde{A}_\alpha, \tilde{A}_\beta) > 0, I_j^l(\tilde{A}_\alpha, \tilde{A}_\beta) = 0$, and $I_j^l(\tilde{A}_\alpha, \tilde{A}_\beta) < 0$, respectively. Moreover, the concordance/discordance index I_j^l, between the preorder according to the criterion xj and the ranking corresponding to the lth permutation, is:

$$I_j^l = \sum_{\tilde{A}_\alpha, \tilde{A}_\beta \in \tilde{A}} I_j^l(\tilde{A}_\alpha, \tilde{A}_\beta) \quad (23)$$

Step 9. The weighted concordance and discordance index is calculated for each pair of alternatives in mth permutation as following:

$$I^l(\tilde{A}_\alpha, \tilde{A}_\beta) = \sum_{j=1}^{n} I_j^l(\tilde{A}_\alpha, \tilde{A}_\beta).\bar{w}_j \quad (24)$$

Step 10. The comprehensive concordance and discordance index I^l is calculated using Equation (25).

$$I^l = \sum_{\tilde{A}_\alpha, \tilde{A}_\beta \in \tilde{A}} \sum_{j=1}^{n} I_j^l(\tilde{A}_\alpha, \tilde{A}_\beta).\bar{w}_j \quad (25)$$

The permutation with the maximal I^l value is the optimal ranking order of the alternatives.

4. REAL CASE ANALYSIS

A new fuzzy MCDM approach has been proposed to evaluate the smartness of the municipalities which are Istanbul Metropolitan Municipality, Karaman Municipality, Osmaniye Municipality, Karadeniz Ereğli Municipality and Antalya Metropolitan Municipality. They are the candidate smart cities in Turkey determined by Ministry of Environment and Urbanization and involved in studies on the smart city concept. For this purpose, the relevant literature has been reviewed to determine which criteria can be taken into consideration in the smartness comparison of these municipalities. As a result of this research, it is determined that six main axes which are governance, people, economy, mobility, environment, and living can be used to evaluate the smartness of the cities as the criteria. For this reason, smart city alternatives determined by 2020-2023 National Smart Cities Strategy and Action Plan for Turkey [60] published by the Ministry of Environment and Urbanization were evaluated on governance, people, economy, mobility, environment, and living axes and the smartness levels for the determined municipalities were tried to be ranked. In order to calculate the criteria weights and criteria-alternative scores, assessments were get from three decision makers (experts) who previously worked on smart city concept. Then, the evaluations received from the experts were converted into spherical fuzzy numbers with the linguistic scale in Table 1 and the steps of the proposed method were initiated. In this decision making process, Expert-1's weight is 0.2, Expert-2's weight is 0.35 and finally Expert-3's weight is 0.45 by level of their expertise. Table 2 shows the evaluations for criteria weights while Table 3 shows the criteria – alternatives evaluations for each expert.

Table 2
Evaluations for criteria weights by experts

Criteria / Expert	***Expert-1***	***Expert-2***	***Expert-3***
C1: Governance	SMI	SLI	SMI
C2: People	SLI	LI	EI
C3: Economy	HI	SLI	SMI
C4: Mobility	EI	SMI	HI
C5: Environment	SLI	SLI	EI

C6: Living	SMI	EI	SLI

Table 3
Criteria – alternative evaluations by experts

Expert-1			***Criteria***			
Alternatives	Gover	Pe	Eco	Mo	Enviro	Liv
Istanbul	SLI	HI	SMI	HI	SLI	S
Karaman	SMI	LI	SLI	EI	SLI	SL
Osmaniye	SLI	SL	SMI	SLI	SMI	HI
Karadeniz Ereğli	EI	HI	SLI	SMI	HI	SL
Antalya	HI	V	SMI	SMI	HI	S
Expert-2			***Criteria***			
Alternatives	Gover	Pe	Eco	Mo	Enviro	Liv
Istanbul	SMI	HI	SLI	SMI	SLI	SL
Karaman	SMI	LI	SMI	EI	SMI	S
Osmaniye	SLI	SL	SLI	SLI	SMI	S
Karadeniz Ereğli	EI	HI	SLI	SLI	HI	LI
Antalya	HI	EI	SMI	SMI	EI	S
Expert- 3			***Criteria***			
Alternatives	Gover	Pe	Eco	Mo	Enviro	Liv
Istanbul	EI	HI	SMI	HI	SLI	S
Karaman	SLI	LI	SLI	EI	SLI	SL
Osmaniye	SMI	S	EI	SLI	SMI	HI
Karadeniz Ereğli	EI	HI	SLI	SMI	HI	SL
Antalya	HI	V	SMI	EI	SLI	EI

After obtaining evaluations from the experts regarding the criteria weights and criteria - alternative scores, and converting into spherical fuzzy sets using the linguistic variables in Table 1, evaluations were aggregated using the SWAM operator presented in Definition (4). The aggregated evaluations for weights of criteria and criteria – alternative scores were respectively presented in Table 4 and Table 5.

Table 4
Aggregated criteria weights

Criteria	Weight (μ,Ʊ,π)
Governance	(0.544,0.461,0.402)
People	(0.423,0.583,0.434)
Economy	(0.572,0.435,0.380)
Mobility	(0.635,0.367,0.375)
Environment	(0.449,0.553,0.454)
Living	(0.485,0.519,0.442)

Table 5
Aggregated criteria – alternative scores

Criteria /Alternative	Governance			People		
	μ	Ʊ	π	μ	Ʊ	π
A1: Istanbul Metropolitan Municipality	0.524	0.480	0.449	0.700	0.300	0.300
A2: Karaman Municipality	0.526	0.480	0.402	0.300	0.700	0.300
A3: Osmaniye Municipality	0.507	0.500	0.402	0.507	0.500	0.402
A4: Karadeniz Ereğli Municipality	0.500	0.500	0.500	0.700	0.300	0.300
A5: Antalya Metropolitan Municipality	0.700	0.300	0.300	0.731	0.276	0.302
Criteria /Alternative	**Economy**			**Mobility**		
	μ	Ʊ	π	μ	Ʊ	π
A1: Istanbul Metropolitan Municipality	0.544	0.461	0.402	0.669	0.332	0.335
A2: Karaman Municipality	0.486	0.521	0.402	0.500	0.500	0.500
A3: Osmaniye Municipality	0.494	0.510	0.451	0.400	0.600	0.400
A4: Karadeniz Ereğli Municipality	0.400	0.600	0.400	0.544	0.461	0.402
A5: Antalya Metropolitan Municipality	0.600	0.400	0.400	0.559	0.442	0.445
Criteria /Alternative	**Environment**			**Living**		
	μ	Ʊ	π	μ	Ʊ	π
A1:Istanbul Metropolitan Municipality	0.400	0.600	0.400	0.544	0.461	0.402
A2: Karaman Municipality	0.486	0.521	0.402	0.486	0.521	0.402
A3: Osmaniye Municipality	0.600	0.400	0.400	0.669	0.332	0.335
A4: Karadeniz Ereğli Municipality	0.700	0.300	0.300	0.369	0.633	0.371
A5: Antalya Metropolitan Municipality	0.519	0.490	0.420	0.559	0.442	0.445

After the evaluations from experts are aggregated, the score indexes for both criteria-alternative evaluations and criteria weights are calculated as in Eq. (19) and Eq. (20). Score indexes calculated for weights are normalized as in Eq. (21). All possible permutations of the rankings of the five smart cities are enumerated and discordance and concordance indexes are determined which reflects the concordance and discordance of ranks and evaluation preorder for each couple of alternatives of permutations. In this way, for each permutation, 5! (120) matrices are created with the concordance and discordance index calculated. Then, weighted concordance and discordance index are calculated for each alternative pair in *m.* permutation. Table 6 shows the concordance, ex aequo, and discordance matrix for each pair of alternatives in Permutation -1 (P1).

The detailed concordance and discordance index I^l is calculated using Eq. (25) for all permutations. Table 7 shows the concordance and discordance index values for each permutation.

Table 6
The concordance, ex aequo, and discordance matrix for Permutation-1

P1:	**A1>A2>A3>A4>A5**										
	I(A1,A2)	I(A1,A3)	I(A1,A4)	I(A1,A5)	I(A2,A3)	I(A2,A4)	I(A2,A5)	I(A3,A4)	I(A3,A5)	I(A4,A5)	Total
C1	1	1	0	-1	-1	-1	-1	-1	-1	-1	-5
C2	1	1	1	-1	1	1	-1	1	-1	-1	2
C3	1	1	1	1	1	-1	-1	-1	-1	1	2
C4	1	1	1	1	1	-1	-1	-1	-1	1	2
C5	-1	-1	-1	-1	-1	-1	-1	-1	1	1	-6
C6	1	-1	1	1	-1	1	-1	1	1	-1	2
										I^1 :	0.248219

Table 7
The comprehensive concordance and discordance index for each permutation

Permutation	Index Value	Permutation	Index Value	Permutation	Index Value	Permutation	Index Value
P1:A1>A2>A3>A4>A5	0.248219	**P31: A2>A3>A1>A4>A5**	-2.94171	**P61: A3>A4>A1>A2>A5**	-1.68359	**P91: A4>A5>A3>A1>A2**	2.306055
P2: A1>A2>A3>A5>A4	-0.51912	**P32: A2>A3>A1>A5>A4**	-3.70905	**P62: A3>A4>A1>A5>A2**	0.316411	**P92: A4>A5>A3>A2>A1**	0.519121
P3: A1>A2>A4>A3>A5	1.642034	**P33: A2>A3>A4>A1>A5**	-4.34989	**P63: A3>A4>A2>A1>A5**	-3.47052	**P93: A4>A5>A1>A3>A2**	3.709055
P4: A1>A2>A4>A5>A3	3.176073	**P34: A2>A3>A4>A5>A1**	-5.2881	**P64: A3>A4>A2>A5>A1**	-4.40873	**P94: A4>A5>A1>A2>A3**	4.354541
P5: A1>A2>A5>A4>A3	2.408732	**P35: A2>A3>A5>A4>A1**	-6.05544	**P65: A3>A4>A5>A2>A1**	-2.40873	**P95: A4>A5>A2>A1>A3**	2.567607
P6: A1>A2>A5>A3>A4	0.883878	**P36: A2>A3>A5>A1>A4**	-4.64726	**P66: A3>A4>A5>A1>A2**	-0.6218	**P96: A4>A5>A2>A3>A1**	1.164607
P7: A1>A3>A2>A4>A5	-0.39727	**P37: A2>A5>A4>A3>A1**	-3.12759	**P67: A3>A5>A1>A4>A2**	0.019038	**P97: A5>A2>A3>A4>A1**	-2.65244
P8: A1>A3>A2>A5>A4	-1.16461	**P38: A2>A4>A3>A5>A1**	-3.76325	**P68: A3>A5>A1>A2>A4**	-1.50582	**P98: A5>A2>A3>A1>A4**	-1.24426
P9: A1>A3>A4>A2>A5	1.127588	**P39: A2>A4>A1>A3>A5**	-1.42204	**P69: A3>A5>A4>A1>A2**	-1.38914	**P99: A5>A2>A4>A3>A1**	-1.12759
P10: A1>A3>A4>A5>A2	3.127588	**P40: A2>A4>A1>A5>A3**	-0.01904	**P70: A3>A5>A4>A2>A1**	-3.17607	**P100: A5>A2>A4>A1>A3**	0.275412
P11: A1>A3>A5>A4>A2	2.360247	**P41: A2>A4>A5>A1>A3**	-0.95725	**P71: A3>A5>A2>A4>A1**	-4.70093	**P101: A5>A2>A1>A4>A3**	1.683589
P12: A1>A3>A5>A2>A4	0.835393	**P42: A2>A4>A5>A3>A1**	-2.36025	**P72: A3>A5>A2>A1>A4**	-3.29275	**P102: A5>A2>A1>A3>A4**	0.158735
P13: A1>A4>A3>A2>A5	2.652442	**P43: A2>A5>A3>A4>A1**	-4.65244	**P73: A4>A2>A3>A1>A5**	-1.30018	**P103: A5>A3>A2>A4>A1**	-3.29793
P14: A1>A4>A3>A5>A2	4.652442	**P44: A2>A5>A3>A1>A4**	-3.24426	**P74: A4>A2>A3>A5>A1**	-2.23839	**P104: A5>A3>A2>A1>A4**	-1.88975
P15: A1>A4>A2>A3>A5	3.297928	**P45: A2>A5>A4>A3>A1**	-3.12759	**P75: A4>A2>A1>A3>A5**	0.102816	**P105: A5>A3>A4>A2>A1**	-1.77307
P16: A1>A4>A2>A5>A3	4.700927	**P46: A2>A5>A4>A1>A3**	-1.72459	**P76: A4>A2>A1>A5>A3**	1.505816	**P106: A5>A3>A4>A1>A2**	0.01386
P17: A1>A4>A5>A2>A3	6.700927	**P47: A2>A5>A1>A4>A3**	-0.31641	**P77: A4>A2>A5>A1>A3**	0.567607	**P107: A5>A3>A1>A4>A2**	1.422038
P18: A1>A4>A5>A3>A2	6.055441	**P48: A2>A5>A1>A3>A4**	-1.84127	**P78: A4>A2>A5>A3>A1**	-0.83539	**P108: A5>A3>A1>A2>A4**	-0.10282
P19: A1>A5>A3>A4>A2	3.763246	**P49: A3>A2>A1>A4>A5**	-3.5872	**P79: A4>A3>A2>A1>A5**	-1.94567	**P109: A5>A4>A3>A2>A1**	-0.24822
P20: A1>A5>A3>A2>A4	2.238392	**P50: A3>A2>A1>A5>A4**	-4.35454	**P80: A4>A3>A2>A5>A1**	-2.88388	**P110: A5>A4>A3>A1>A2**	1.538715
P21: A1>A5>A4>A3>A2	5.288101	**P51: A3>A2>A4>A1>A5**	-4.99538	**P81: A4>A3>A1>A2>A5**	-0.15873	**P111: A5>A4>A2>A3>A1**	0.397267
P22: A1>A5>A4>A2>A3	5.933587	**P52: A3>A2>A4>A5>A1**	-5.93359	**P82: A4>A3>A1>A5>A2**	1.841265	**P112: A5>A4>A2>A1>A3**	1.800266
P23: A1>A5>A2>A4>A3	4.408732	**P53: A3>A2>A5>A4>A1**	-6.70093	**P83: A4>A3>A5>A1>A2**	0.903056	**P113: A5>A4>A1>A2>A3**	3.5872
P24: A1>A5>A2>A3>A4	2.883878	**P54: A3>A2>A5>A1>A4**	-5.29275	**P84: A4>A3>A5>A2>A1**	-0.88388	**P114: A5>A4>A1>A3>A2**	2.941714
P25: A2>A1>A3>A4>A5	-1.53871	**P55: A3>A1>A2>A4>A5**	-1.80027	**P85: A4>A1>A3>A2>A5**	1.244265	**P115: A5>A1>A3>A4>A2**	2.825037
P26: A2>A1>A3>A5>A4	-2.30606	**P56: A3>A1>A2>A5>A4**	-2.56761	**P86: A4>A1>A3>A5>A2**	3.244265	**P116: A5>A1>A3>A2>A4**	1.300183
P27: A2>A1>A4>A3>A5	-0.01386	**P57: A3>A1>A4>A2>A5**	-0.27541	**P87: A4>A1>A2>A3>A5**	1.88975	**P117: A5>A1>A4>A3>A2**	4.349891
P28: A2>A1>A4>A5>A3	1.389139	**P58: A3>A1>A4>A5>A2**	1.724588	**P88: A4>A1>A2>A5>A3**	3.29275	**P118: A5>A1>A4>A2>A3**	4.995377
P29: A2>A1>A5>A4>A3	0.621798	**P59: A3>A1>A5>A4>A2**	0.957247	**P89: A4>A1>A5>A2>A3**	5.29275	**P119: A5>A1>A2>A4>A3**	3.470523
P30: A2>A1>A5>A3>A4	-0.90306	**P60: A3>A4>A1>A2>A5**	-0.56761	**P90: A4>A1>A5>A3>A2**	4.647264	**P120: A5>A1>A2>A3>A4**	1.945669

After calculating the detailed indexes for all permutations, the permutation with the highest index value is investigated. When Table 7 is examined, it is seen that the permutation with the highest index value is the 17th permutation, "A1> A4> A5> A2> A3". In other words, Istanbul, which is the first alternative – A1, is placed in the first rank in evaluating the smartness of the cities. The second smartest city was found as "Karadeniz Ereğli". The third alternative is Antalya; Karaman takes fourth place and Osmaniye alternative takes the last place. Istanbul is a pioneer city in smart city applications. Intelligent systems are used in many areas such as water management, disaster and emergency management, health, tourism, or security throughout the city. For this reason, it is not surprising that it appears as the "smartest" city in the country. Under favour of the city's plans and breakthroughs in these mentioned directions, Karadeniz Ereğli Municipality has been identified as the second smartest city. The last alternative ranked is the city of Osmaniye. It is seen that it lags behind other alternatives in the planning and implementation of smart systems in the city. At this point, considering the criteria included in the proposed decision problem, Osmaniye can become competitive with other alternatives as a result of making strides in smart systems and instilling the concept of smart into the city.

5. Sensitivity Analysis

We applied sensitivity analysis to understand the robustness of the results obtained from the proposed approach and to monitor the results that change according to criteria weights. Thus, it has been investigated whether flexible recommendations can be developed to take into account the changing conditions in the decision-making process. For this purpose, different scenarios were created by increasing the weight of one criterion higher than others, respectively, keeping the others small and constant, and thus the effect of the criterion on the decision-making process was examined. Each of the six different criteria weighted 0.8 in one scenario, while the other criteria weights were kept constant at 0.04.

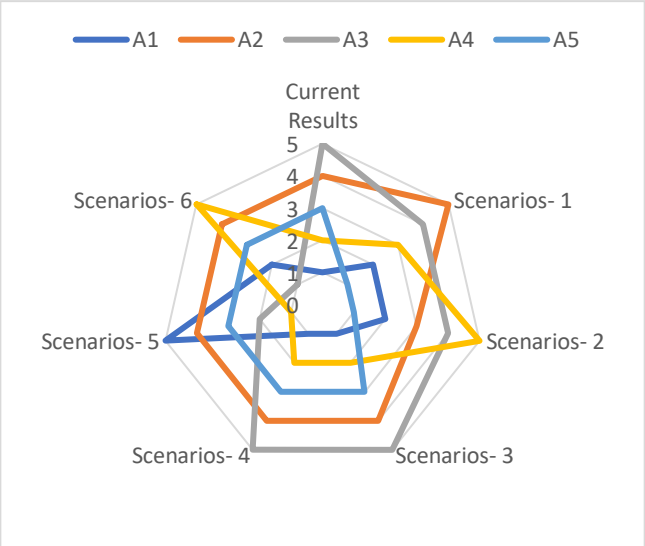

Figure 1: Sensitivity results

According to the sensitivity analysis results, two of the six scenarios (scenarios 3 and 4) gave the same ranking as the current situation. These are scenarios where the weights of the third and fourth criteria are increased. At this point, it can be argued that the third and fourth criteria weights do not have a significant effect on the result of fuzzy MCDM analysis. In scenarios 1 and 2, the A5 alternative was in the first place, in scenario 5 the A4 alternative and in scenario 6, the A3 alternative was found in the first place. Except for the 3rd and 4th scenarios, the Istanbul alternative, which is currently determined in the first place, is determined in the 2nd place in scenarios 1,2 and 6. That is, even if the criteria weights change, the alternative found in the first place in the current situation is taken place near the top. As a result of this sensitivity analysis, it can be said that the proposed approach is affected by different criteria weights parameters, but the results are robust.

6. Conclusions and Future Suggestions

The smart city is a place that effectively uses strategic planning methods and innovative responses to enhance the quality of life, including ecological, social, cultural, institutional and economic factors. A city is considered "smart" if it applies solutions based on information and communication technologies to problems in governance, people, economy, mobility, environment and life. Some scientific approaches have been developed to measure the smartness of

a city. Among these approaches, MCDM, which can evaluate many qualitative and quantitative criteria at the same time, becomes prominent. MCDM approaches are generally used in the framework of fuzzy logic when uncertainty is present in decision-making processes. In order to better reflect the uncertainty in the decision-making problem, extended versions instead of ordinary fuzzy sets are adopted. The independent designation of the parameters of membership with broader domains creates a new perspective on the problem of determining the smartness of the cities with using spherical fuzzy sets.

In this paper, the evaluation of smartness of the cities was carried out with the use of spherical fuzzy sets for the first time. In addition, QUALIFLEX, which is an effective MCDM method, was applied for the first time with spherical fuzzy sets and thus an important gap in the literature was also filled with this application. A smartness analysis for the five cities in Turkey which are determined as the smart city candidates by the Ministry of Environment and Urbanization is conducted and İstanbul was found to be the smartest city in Turkey. In addition, as a result of the sensitivity analysis, changes in the results were examined under different criteria weights. In the current situation, the alternative of Istanbul, which was determined in the first place, was also in the first place in different scenarios and the robustness of the proposed approach was revealed. In addition, as a result of the sensitivity analysis, changes in the results were examined according to the different criteria weights. The alternative of Istanbul, which was determined in the first place in the current situation, was also in the first place in some different scenarios in sensitivity analysis and the robustness of the proposed approach was revealed with this analysis. With this paper, the use of spherical fuzzy sets with MCDM approaches has been implemented under a method that has not been used before, and therefore an important contribution has been made to the literature in fuzzy MCDM area.

In future studies that we suggest, different MCDM methods can be employed to make a comparative analysis or different fuzzy sets extensions can be used.

The Declaration of Conflict of Interest/ Common Interest

No conflict of interest or common interest has been declared by the authors.

The Declaration of Ethics Committee Approval

The authors declare that this document does not require an ethics committee approval or any special permission.

The Declaration of Research and Publication Ethics

The authors of the paper declare that they comply with the scientific, ethical and quotation rules of SAUJS in all processes of the article and that they do not make any falsification on the data collected. In addition, they declare that Sakarya University Journal of Science and its editorial board have no responsibility for any ethical violations that may be encountered, and that this study has not been evaluated in any academic publication environment other than Sakarya University Journal of Science.

REFERENCES

[1] B. Baykurt and C. Raetzsch, "What smartness does in the smart city: From visions to policy," *Converg. Int. J. Res. into New Media Technol.*, p. 135485652091340, Mar. 2020.

[2] J. R. Gil-Garcia, T. A. Pardo, and T. Nam, "A Comprehensive View of the 21st Century City: Smartness as Technologies and Innovation in Urban Contexts," in *Public Administration and Information Technology*, vol. 11, Springer, 2016, pp. 1–19.

[3] S. Bernardino, J. Freitas Santos, and J. Cadima Ribeiro, "The legacy of European Capitals of Culture to the 'smartness' of

cities: The case of Guimarães 2012," *J. Conv. Event Tour.*, vol. 19, no. 2, pp. 138–166, Mar. 2018.

[4] B. Murgante and G. Borruso, "Cities and smartness: A critical analysis of opportunities and risks," in *Lecture Notes in Computer Science (including subseries Lecture Notes in Artificial Intelligence and Lecture Notes in Bioinformatics)*, 2013, vol. 7973 LNCS, no. PART 3, pp. 630–642.

[5] T. Yigitcanlar and M. Kamruzzaman, "Smart Cities and Mobility: Does the Smartness of Australian Cities Lead to Sustainable Commuting Patterns?," *J. Urban Technol.*, vol. 26, no. 2, pp. 21–46, Apr. 2019.

[6] M. Calderon, G. Lopez, and G. Marin, "Smartness and technical readiness of Latin American Cities: A critical assessment," *IEEE Access*, vol. 6, pp. 56839–56850, 2018.

[7] R. Carli, M. Dotoli, R. Pellegrino, and L. Ranieri, "Measuring and managing the smartness of cities: A framework for classifying performance indicators," in *Proceedings - 2013 IEEE International Conference on Systems, Man, and Cybernetics, SMC 2013*, 2013, pp. 1288–1293.

[8] S. H. Alsamhi, O. Ma, M. S. Ansari, and F. A. Almalki, "Survey on collaborative smart drones and internet of things for improving smartness of smart cities," *IEEE Access*, vol. 7. Institute of Electrical and Electronics Engineers Inc., pp. 128125–128152, 2019.

[9] C. Kahraman, "Multi-criteria decision making methods and fuzzy sets," in *Springer Optimization and Its Applications*, vol. 16, Springer International Publishing, 2008, pp. 1–18.

[10] L. A. Zadeh, "Fuzzy sets," *Inf. Control*, vol. 8, no. 3, pp. 338–353, Jun. 1965.

[11] Z. Eslaminasab and A. Hamzehee, "Determining appropriate weight for criteria in multi criteria group decision making problems using an Lp model and similarity measure," 2019.

[12] İ. Kaya, M. Çolak, and F. Terzi, "A comprehensive review of fuzzy multi criteria decision making methodologies for energy policy making," *Energy Strategy Reviews*, vol. 24. Elsevier Ltd, pp. 207–228, 01-Apr-2019.

[13] E. Afful-Dadzie, Z. K. Oplatková, and L. A. Beltran Prieto, "Comparative State-of-the-Art Survey of Classical Fuzzy Set and Intuitionistic Fuzzy Sets in Multi-Criteria Decision Making," *Int. J. Fuzzy Syst.*, vol. 19, no. 3, pp. 726–738, Jun. 2017.

[14] H. P. McKenna, "Human-smart environment interactions in smart cities: Exploring dimensionalities of smartness," *Futur. Internet*, vol. 12, no. 5, p. 79, May 2020.

[15] M. L. Marsal-Llacuna, "Measuring the standardized definition of 'smart city': A proposal on global metrics to set the terms of reference for urban 'smartness,'" *Lect. Notes Comput. Sci. (including Subser. Lect. Notes Artif. Intell. Lect. Notes Bioinformatics)*, vol. 9156, pp. 593–611, 2015.

[16] H. Ahvenniemi and A. Huovila, "How do cities promote urban sustainability and smartness? An evaluation of the city strategies of six largest Finnish cities," *Environ. Dev. Sustain.*, pp. 1–27, May 2020.

[17] S. Hajduk, "The smartness profile of selected European cities in urban management – A comparison analysis," *J. Bus. Econ. Manag.*, vol. 19, no. 6, pp. 797–812, Dec. 2018.

[18] E. G. Lima *et al.*, "Smart and Sustainable Cities: The Main Guidelines of City Statute for Increasing the Intelligence of Brazilian

Cities," *Sustainability*, vol. 12, no. 3, p. 1025, Jan. 2020.

[19] K. Axelsson and M. Granath, "Stakeholders' stake and relation to smartness in smart city development: Insights from a Swedish city planning project," *Gov. Inf. Q.*, vol. 35, no. 4, pp. 693–702, Oct. 2018.

[20] S. Al-Nasrawi, A. El-Zaart, and C. Adams, "Assessing smartness of smart sustainable cities: A comparative analysis," in *2017 Sensors Networks Smart and Emerging Technologies, SENSET 2017*, 2017, vol. 2017-January, pp. 1–4.

[21] G. Dall'O, E. Bruni, A. Panza, L. Sarto, and F. Khayatian, "Evaluation of cities' smartness by means of indicators for small and medium cities and communities: A methodology for Northern Italy," *Sustain. Cities Soc.*, vol. 34, pp. 193–202, Oct. 2017.

[22] G. A. El Khayat and N. A. Fashal, "Inter and intra cities smartness: A survey on location problems and gis tools," in *Handbook of Research on Geographic Information Systems Applications and Advancements*, IGI Global, 2016, pp. 295–320.

[23] F. Corsini, F. Rizzi, and M. Frey, "Analysing smartness in European cities: a factor analysis based on resource efficiency, transportation and ICT," *Int. J. Glob. Environ. Issues*, vol. 15, no. 3, pp. 235–254, 2016.

[24] F. K. Gündoğdu and C. Kahraman, "Spherical fuzzy sets and spherical fuzzy TOPSIS method," *J. Intell. Fuzzy Syst.*, vol. 36, no. 1, pp. 337–352, Jan. 2019.

[25] F. Kutlu Gündoğdu and C. Kahraman, "A novel fuzzy TOPSIS method using emerging interval-valued spherical fuzzy sets," *Eng. Appl. Artif. Intell.*, vol. 85, pp. 307–323, Oct. 2019.

[26] C. Kahraman, S. C. Onar, and B. Oztaysi, "Performance measurement of debt collection firms using spherical fuzzy aggregation operators," in *Advances in Intelligent Systems and Computing*, 2020, vol. 1029, pp. 506–514.

[27] E. Boltürk, "AS/RS technology selection using spherical fuzzy TOPSIS and neutrosophic TOPSIS," in *Advances in Intelligent Systems and Computing*, 2020, vol. 1029, pp. 969–976.

[28] F. Kutlu Gündoğdu and C. Kahraman, "A novel spherical fuzzy analytic hierarchy process and its renewable energy application," *Soft Comput.*, vol. 24, no. 6, pp. 4607–4621, Mar. 2020.

[29] O. Barukab, S. Abdullah, S. Ashraf, M. Arif, and S. A. Khan, "A new approach to fuzzy TOPSIS method based on entropy measure under spherical fuzzy information," *Entropy*, vol. 21, no. 12, Dec. 2019.

[30] F. Kutlu Gündoğdu and C. Kahraman, "A novel VIKOR method using spherical fuzzy sets and its application to warehouse site selection," *J. Intell. Fuzzy Syst.*, vol. 37, no. 1, pp. 1197–1211, 2019.

[31] P. Liu, B. Zhu, P. Wang, and M. Shen, "An approach based on linguistic spherical fuzzy sets for public evaluation of shared bicycles in China," *Eng. Appl. Artif. Intell.*, vol. 87, Jan. 2020.

[32] F. K. Gündoğdu and C. Kahraman, "Extension of codas with spherical fuzzy sets," *J. Mult. Log. Soft Comput.*, vol. 33, no. 4–5, pp. 481–505, 2019.

[33] C. Kahraman, F. K. Gündoğdu, A. Karaşan, and E. Boltürk, "Advanced Fuzzy Sets and Multicriteria Decision Making on Product Development," in *Studies in Systems, Decision and Control*, vol. 279, Springer, 2020, pp. 283–302.

[34] F. Kutlu Gündoğdu, "A spherical fuzzy

extension of MULTIMOORA method," *J. Intell. Fuzzy Syst.*, vol. 38, no. 1, pp. 963–978, 2020.

[35] Z. Yang, X. Li, H. Garg, and M. Qi, "Decision support algorithm for selecting an antivirus mask over COVID-19 pandemic under spherical normal fuzzy environment," *Int. J. Environ. Res. Public Health*, vol. 17, no. 10, May 2020.

[36] K. T. Atanassov, "Intuitionistic fuzzy sets," *Fuzzy Sets Syst.*, vol. 20, no. 1, pp. 87–96, Aug. 1986.

[37] R. R. Yager and A. M. Abbasov, "Pythagorean membership grades, complex numbers, and decision making," *Int. J. Intell. Syst.*, vol. 28, no. 5, pp. 436–452, May 2013.

[38] F. Kutlu Gündoğdu and C. Kahraman, "A novel VIKOR method using spherical fuzzy sets and its application to warehouse site selection," *J. Intell. Fuzzy Syst.*, vol. 37, no. 1, pp. 1197–1211, Jan. 2019.

[39] T. Y. Chen, C. H. Chang, and J. F. Rachel Lu, "The extended QUALIFLEX method for multiple criteria decision analysis based on interval type-2 fuzzy sets and applications to medical decision making," *Eur. J. Oper. Res.*, vol. 226, no. 3, pp. 615–625, May 2013.

[40] J. H. P. Paelinck, "Qualiflex: A flexible multiple-criteria method," *Econ. Lett.*, vol. 1, no. 3, pp. 193–197, Jan. 1978.

[41] T. Y. Chen, "Data construction process and qualiflex-based method for multiple-criteria group decision making with interval-valued intuitionistic fuzzy sets," *Int. J. Inf. Technol. Decis. Mak.*, vol. 12, no. 3, pp. 425–467, May 2013.

[42] T. Y. Chen, "Interval-valued intuitionistic fuzzy QUALIFLEX method with a likelihood-based comparison approach for multiple criteria decision analysis," *Inf. Sci. (Ny).*, vol. 261, pp. 149–169, Mar. 2014.

[43] Z. Zhang, "Multi-criteria decision-making using interval-valued hesitant fuzzy QUALIFLEX methods based on a likelihood-based comparison approach."

[44] Y. Liang, J. Qin, L. Martínez, and J. Liu, "A heterogeneous QUALIFLEX method with criteria interaction for multi-criteria group decision making," *Inf. Sci. (Ny).*, vol. 512, pp. 1481–1502, Feb. 2020.

[45] J. Li and J. qiang Wang, "An Extended QUALIFLEX Method Under Probability Hesitant Fuzzy Environment for Selecting Green Suppliers," *Int. J. Fuzzy Syst.*, vol. 19, no. 6, pp. 1866–1879, Dec. 2017.

[46] M. Gul, S. Mete, F. Serin, and E. Celik, "Fine–kinney-based occupational risk assessment using interval type-2 fuzzy qualiflex," in *Studies in Fuzziness and Soft Computing*, vol. 398, Springer Science and Business Media Deutschland GmbH, 2021, pp. 135–149.

[47] A. Zare, M. Malakoutikhah, and M. Alimohammadlou, "Selecting lighting system based on workers' cognitive performance using fuzzy best–worst method and QUALIFLEX," *Cogn. Technol. Work*, vol. 22, no. 3, pp. 641–652, Aug. 2020.

[48] C. Zhou, D. Liu, P. Zhou, J. Luo, S. Yuksel, and H. Dincer, "Hybrid predictive decision-making approach to emission reduction policies for sustainable energy industry," *Energies*, vol. 13, no. 9, May 2020.

[49] L. Liu, Z. Bin, B. Shi, and W. Cao, "Sustainable supplier selection based on regret theory and QUALIFLEX method," *Int. J. Comput. Intell. Syst.*, vol. 13, no. 1, pp. 1120–1133, 2020.

[50] X. F. Ding, L. X. Zhu, M. S. Lu, Q. Wang, and Y. Q. Feng, "A Novel Linguistic Z - Number QUALIFLEX Method and Its

Application to Large Group Emergency Decision Making," *Sci. Program.*, vol. 2020, 2020.

[51] X. Tian, Z. Xu, X. Wang, J. Gu, and F. E. Alsaadi, "Decision Models to Find a Promising Start-Up Firm with Qualiflex under Probabilistic Linguistic Circumstance," *Int. J. Inf. Technol. Decis. Mak.*, vol. 18, no. 4, pp. 1379–1402, Jul. 2019.

[52] D. Banerjee, D. Guha, and F. Kouchakinejad, "Ranking alternatives using QUALIFLEX method by computing all spanning trees from pairwise judgements," in *Advances in Intelligent Systems and Computing*, 2019, vol. 816, pp. 235–247.

[53] A. Mahmoudi, S. A. Javed, Z. Zhang, and X. Deng, "Grey Group QUALIFLEX Method: Application in Project Management," in *Proceedings of IEEE 14th International Conference on Intelligent Systems and Knowledge Engineering, ISKE 2019*, 2019, pp. 189–195.

[54] D. Banerjee, B. Dutta, D. Guha, and L. Martínez, "SMAA-QUALIFLEX methodology to handle multicriteria decision-making problems based on q-rung fuzzy set with hierarchical structure of criteria using bipolar Choquet integral," *Int. J. Intell. Syst.*, vol. 35, no. 3, pp. 401–431, Mar. 2020.

[55] W. Liang, B. Dai, G. Zhao, and H. Wu, "Assessing the performance of green mines via a hesitant fuzzy ORESTE-QUALIFLEX method," *Mathematics*, vol. 7, no. 9, Sep. 2019.

[56] X. Feng, Q. Liu, and C. Wei, "Probabilistic linguistic QUALIFLEX approach with possibility degree comparison," *J. Intell. Fuzzy Syst.*, vol. 36, no. 1, pp. 719–730, 2019.

[57] H. Demirel, E. Akyuz, E. Celik, and F. Alarcin, "Ships and Offshore Structures An interval type-2 fuzzy QUALIFLEX approach to measure performance effectiveness of ballast water treatment (BWT) system on-board ship An interval type-2 fuzzy QUALIFLEX approach to measure performance effectiveness of ballast water treatment (BWT) system on-board ship," 2018.

[58] S. Song, H. Zhou, and W. Song, "Sustainable shelter-site selection under uncertainty: A rough QUALIFLEX method," *Comput. Ind. Eng.*, vol. 128, pp. 371–386, Feb. 2019.

[59] A. Alinezhad and N. Esfandiari, "Sensitivity Analysis in the QUALIFLEX and VIKOR Methods," *J. Optim. Ind. Eng.*, vol. 10, pp. 29–34, 2012.

[60] Turkish Republic Ministry of Environment and Urbanization, "2020-2023 National Smart Cities Strategy and Action Plan," 2019.

SAKARYA ÜNİVERSİTESİ
FEN BİLİMLERİ ENSTİTÜSÜ DERGİSİ

Sakarya University Journal of Science
SAUJS

e-ISSN 2147-835X | Period Bimonthly | Founded: 1997 | Publisher Sakarya University |
http://www.saujs.sakarya.edu.tr/en/

Title: Investigation of Hazelnut Husk Combustion by using A Novel Non-linear Kinetic Model through Thermogravimetric Analysis

Authors: Senem SEZER, Uğur ÖZVEREN,

Recieved: 2020-10-16 00:00:00

Accepted: 2021-01-26 00:00:00

Article Type: Research Article

Volume: 25
Issue: 2
Month: April
Year: 2021
Pages: 326-338

How to cite
Senem SEZER, Uğur ÖZVEREN, ; (2021), Investigation of Hazelnut Husk Combustion by using A Novel Non-linear Kinetic Model through Thermogravimetric Analysis. Sakarya University Journal of Science, 25(2), 326-338, DOI: https://doi.org/10.16984/saufenbilder.811684
Access link
http://www.saujs.sakarya.edu.tr/en/pub/issue/60672/811684

Sakarya University Journal of Science 25(2), 326-338, 2021

Investigation of Hazelnut Husk Combustion by using A Novel Non-linear Kinetic Model through Thermogravimetric Analysis

Senem SEZER[1], Uğur ÖZVEREN*[1]

Abstract

Considering economic and environmental issues, boosting renewable energy source is the main subject to fulfill energy demand in these days. Biomass as natural and abundant energy source can be typically used to produce electricity, fuels and heat applying thermochemical conversion processes such as combustion, pyrolysis or gasification. Biomass combustion is the most common process to produce electricity and useful heat in Turkey and all over the world. The aim of this study is to investigate the considerable influence of heating rates on combustion characteristics and kinetics employing a new developed non-linear kinetic model for hazelnut husk samples through thermogravimetric analysis. Furthermore, this work comprehensively assesses the variations in the reactivity of hazelnut husk combustion, expressed from thermogravimetric curves. The non-linear kinetic model developed in this study integrates the various kinetic pathway to estimate the major controlling parameter of combustion reactivity, its activation energy, pre-exponential factor and reaction order. According to comparison of results from the non-linear kinetic model for volatile combustion and fixed carbon combustion, correlation coefficients (R^2) for both models are higher than 0.9985. These results proved the non-linear regression model for kinetic pathways in combustion reactivity worked properly to estimate thermal decomposition behavior.

Keywords: thermogravimetric analysis (TGA), combustion, kinetic analysis, non-linear regression, biomass

1. INTRODUCTION

The upsurge of environmental issues and energy crisis has been increased the attention of energy study about the sustainability and efficiency [1]. Energy production using the renewable energy source has become critical to sufficiently reduce consequence of greenhouse gas emissions and air pollution [2]. Turkey's energy demand has been increasing rapidly in last years consequence of growing population and industry. Thus, by using the renewable energy source instead of fossil fuels which are the primary energy source in Turkey has been getting importance day by day [3]. Biomass has the critical advantage in terms of its abundant reserves and being carbon neutral material [4]. Turkey offers a broad potential of biomass particularly as agricultural wastes. There is diversity on the biomass characteristics depending on the agricultural crops grown

* Corresponding author: ugur.ozveren@marmara.edu.tr
[1] Marmara University, Faculty of Engineering, Chemical Engineering Department, 34722, İstanbul.
E-Mail: senemsezer@marun.edu.tr; ugur.ozveren@marmara.edu.tr
ORCID: http://orcid.org/0000-0002-1732-4840; http://orcid.org/0000-0002-3790-0606.

naturally in different regions [3]. Black Sea region is the responsible of hazelnut production as highest amount in the worldwide that corresponds to 75% [5]. As follows, this amount of production accompanies with enormous quantity of hazelnut waste. Considering the hazelnut wastes such as husk and shell, they can be used in production of energy and valuable chemicals as a feedstock [6]. Thermochemical conversion of biomass to gas or liquid fuels is a good alternative instead of fossil fuels for outstanding contribution to renewable energy generation [7]. Innovative technologies of biomass conversion process like combustion, pyrolysis and gasification play a key role for the concept of biomass to energy [8]. Higher volatile content and lower ignition temperature of biomass improve the performance of conversion process [9]. Combustion process cleaves the chemical bonds of fuel and generates series of reaction presence of air or oxygen under the heat [10]. Combustion may be seen the most feasible and conventional way to utilize biomass as a renewable energy source [11-13]. In order to carefully evaluate combustion performance, it is important to recognize the chemical and physical characteristics of biomass. Thermogravimetric analysis (TGA) is typically used to investigate thermal decomposition characteristics of solid materials based on weight change at the determined heating rate as a function of time constant or temperature. TGA is a simple and fast method, which explains why it is commonly used in many studies [14, 15].

Knowledge about the combustion characteristics of biomass is important to conduct effective combustion process. Thermal behavior of the biomass samples should be known to develop and optimize the combustion processes. TGA describes the combustion profile at the different heating rates and obtained results can be used to calculate kinetic parameters for combustion reactions[16, 17]. Several studies have been carried out with TGA to reveal the thermogravimetric and kinetic characteristics of biomass combustion [18-21]. The calculation of kinetic parameters such as activation energy (Ea), pre-exponential factor and reaction order are very complex and needs to employ appropriate methods for successive reactions. K. Jayaraman used the Arrhenius and Coats & Redfern methods to investigate the kinetics of coal-biomass blends[22]. Another methods which are Ozawa-Flynn-Wall [23-25], Kissinger–Akahira–Sunose (KAS) [26], Friedman [27-29] have been used to calculate kinetic parameters for different applications in the literature. These methods can calculate kinetic parameters with some assumption and using equation constants that cause some deficiency to achieve kinetic parameters. Unlike the other methods, iteration can be conducted for non-linear regression analysis for confident prediction of the kinetic parameters. It has advantage to represent the multistep and complex reactions with good accuracy because there is no restriction related to complexity of the possible reactions [30]. However, only iterative procedures can be employed for estimation of the kinetic parameters non-linear regression method represents the multistep and complex reactions with good accuracy [31, 32].

The purpose of this work is investigation of the combustion characteristic of hazelnut husk as the agricultural waste. Experiments for TGA were properly conducted, and results were discussed considering the peak and burn-out temperature values, total mass changes at the three different heating rates. New developed non-linear regression model has been applied to achieve the combustion kinetics of hazelnut shell and determine the kinetic parameters.

2. MATERIALS AND METHODS

2.1. Material Selection and Characterization

This study focusses on to specify combustion mechanism and kinetics of hazelnut husk. Selection of hazelnut husk maintains the great importance because Turkey is the leading area for production [33, 34]. Thus, residues of the hazelnut can be obtained plenty amount as agricultural waste from Black Sea and northwest of Marmara Regions in Turkey [35]. The sample used in this work was collected from local growers from northwest of Marmara Regions in Turkey and

prepared at Marmara University. First, size of biomass sample was reduced using by IKA M20 Universal Mill Sample, then it was grinded and sieved under 250 μm. The proximate and ultimate analyze of hazelnut husk were conducted according to ASTM D3172 and D3176 test methods and results are presented in Table 1.

Table 1

Proximate and ultimate analysis results of the hazelnut husk

	Hazelnut Husk
Moisture (wt %)	3.96
Fixed Carbon (wt %)	22.89
Volatile Matter (wt %)	64.45
Ash (wt %)	8.70
C (wt %)	39.75
H (wt %)	5.06
O (wt %)	52.30
N (wt %)	0.82
S (wt %)	2.07

The proximate analysis were carried out via "NETZSCH 409 PC" thermogravimetric analysis device. Ultimate analysis results were performed in Advanced Technologies Application and Research Center, Hacettepe University by using LECO brand Truspec micro elemental analyzer. Results show that hazelnut husk sample compositions for ultimate and proximate analyses within the range for biomass. Ash content of agricultural wastes commonly varies between 0.5% and 10% [13].

2.2. TGA Experiments

Scope of this work, TGA method has been used to determine combustion characteristics of hazelnut husk. TGA was applied using STA409 device, made by NETZSCH GmbH, Germany, it can be seen in the Figure 1. Before staring the experiment, approximately 10 mg sample was put into a ceramic crucible (Al_2O_3) for each experiment. Then, sample was heated from ambient temperature (25°C) to 800 °C under 21% O_2 and 79% Ar atmosphere and the total gas flow was set to 100 mL/min. At the same experimental conditions, this study has been conducted at the heating rate of 10, 20, and 40 °C/min.

Figure 1 STA409 NETZSCH GmbH, Germany

The weight loss of the sample was continuously monitored and recorded versus of temperature and time via STA409 software. Weight losses are calculated based on weight loss rate and DTG curve peaks. The ignition and burnout temperature values are important parameters to define combustion characteristics of fuel and they are determined based on TG/DTG curves. When the no weight loss rate at the starting of combustion that is defined as ignition temperature, moreover, if the no weight loss rate at the end of the combustion it can be defined as burnout temperature.

2.3. Combustion Index

Combustion index is used as a comprehensive analysis of the combustion characteristics of different fuels, which is described by using Eq. (1) [36].

$$S = DTG_{max} \times DTG_{mean}/(T_i^2 \times T_b) \quad (1)$$

The value of S indicates the insensitivity of combustion and the reactivity of fuels in combustion. T_i in Eq. 1 can be calculated based on a TG curve by using ignition temperature. T_b is determined by using burnout temperature. DTG_{mean} and DTG_{max} refer the average weight

loss rate and maximum weight loss rate respectively.

2.4. Kinetic Analysis

Kinetic study is one of the important methods used to evaluate effect of operating parameters on the combustion reactivity. Kinetic analysis of hazelnut shell combustion process was studied in detail in this section. The kinetic parameters were obtained selecting the most probable kinetic model for the thermal breakdown in the Netzsch Thermokinetics-3 software. Non-linear regression analysis has been applied to find kinetic parameters of the combustion process based on the TGA results of experiments. Using initial values of linear regression, non-linear regression started from reaction mechanism (2). Then, nonlinear regressions were performed for reaction mechanisms (3) until reaching desired correlation coefficient R^2 value using by the data sets collected from experiments at three heating rates. For solving the reaction (3) and optimizing kinetic parameters, calculations of Ea, pre-exponential factor and reaction orders were conducted considering the iteration range at the evaluation range between 0.0005-0.9995.

$A - 1 \rightarrow B$ with s reaction code (2)

$A - 1 \rightarrow B - 2 \rightarrow C$ with d;f reaction code (3)

For the three reaction mechanisms; A is the initial reactants, B is the intermediate product and C is the final crosslinked product. Reaction mechanism (3) named as d;f stated the two-steps consecutive reactions and 2 and 3 indicate the reaction steps. TGA curves for each heating rate were divided into two stages to evaluate combustion kinetics more accurately for volatile matter and fixed carbon combustion for each scan. Parameters in the Table 2 are optimized to obtain the results of each experiments.

Table 2
Definition of kinetic parameters in a two-step successive reaction A→ B→C

Parameter	Description
log(A1/s^{-1}), log(A2/s^{-1})	Logarithm of the pre-exponential factors for step 1 and 2
E1/kJ.mol^{-1}, E2/kJ.mol^{-1}	Activation energies for step 1 and 2
n^{th} order 1 and 2	Reaction order (step 1 and 2)
FollReact. 1	Share of step 1 (total mass loss)
Mass Loss 1/%	Total mass loss (scan 1)
Mass Loss 2/%	Total mass loss (scan 2)
Mass Loss 3/%	Total mass loss (scan 3)

Parameters derived from calculations and experiments are compared and simulation run is ended when the R^2 value reaches to success. Initial and optimum values and standard deviations of parameters are recorded at the end of the simulation.

3. RESULTS

3.1. TG/DTG Analysis

The combustion characteristics of hazelnut shell has been obtained from TG/TG results, which can be seen in Figure 3. The main combustion parameters such as ignition and burnout temperature values and mass changes at the different points were derived from the TG/DTG curves for heating rates 10 °C/min, 20 °C/min, 40°C/min. Two main stages which are volatile and fixed carbon combustions can be observed in the combustion processes of hazelnut shell as seen in Figure 3.

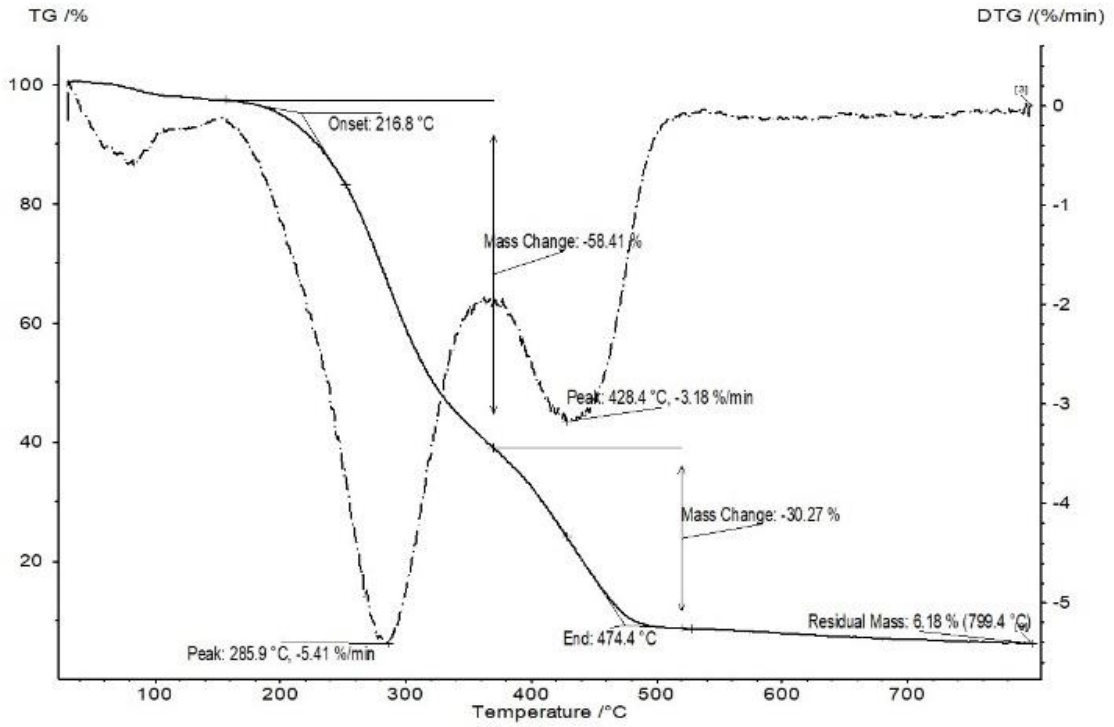
TG /%
DTG /(%/min)
Onset: 216.8 °C
Mass Change: -58.41 %
Peak: 428.4 °C, -3.18 %/min
Mass Change: -30.27 %
Residual Mass: 6.18 % (799.4 °C)
Peak: 285.9 °C, -5.41 %/min
End: 474.4 °C
Temperature /°C

(a)

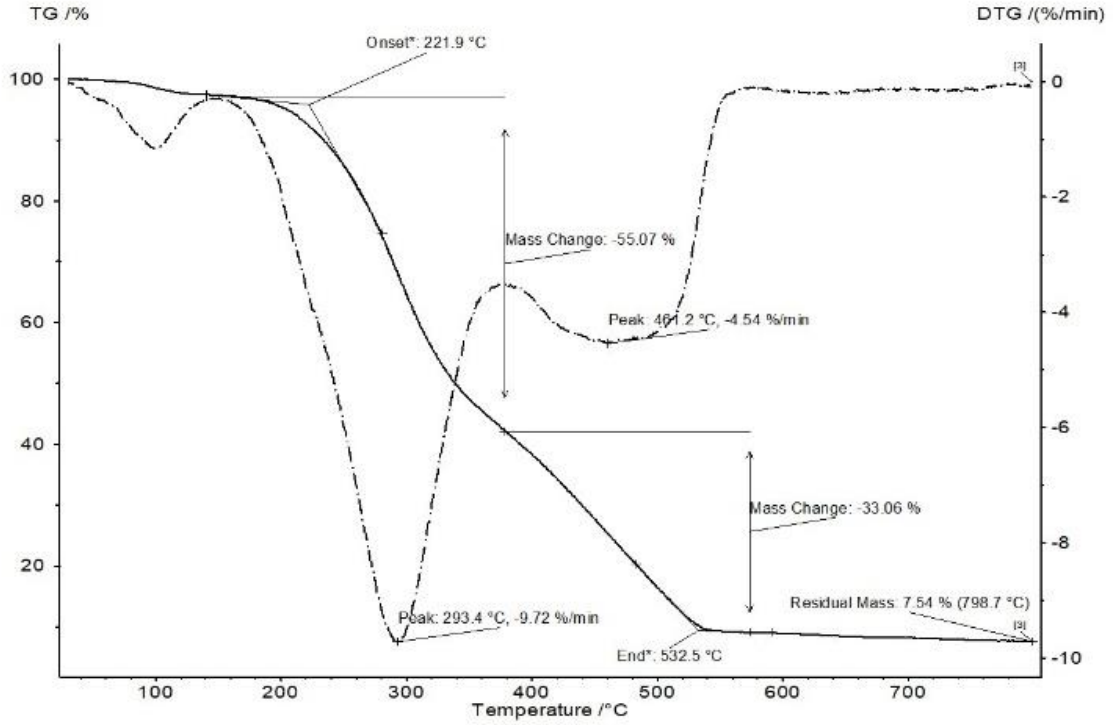
TG /%
DTG /(%/min)
Onset*: 221.9 °C
Mass Change: -55.07 %
Peak: 461.2 °C, -4.54 %/min
Mass Change: -33.06 %
Residual Mass: 7.54 % (798.7 °C)
Peak: 293.4 °C, -9.72 %/min
End*: 532.5 °C
Temperature /°C

(b)

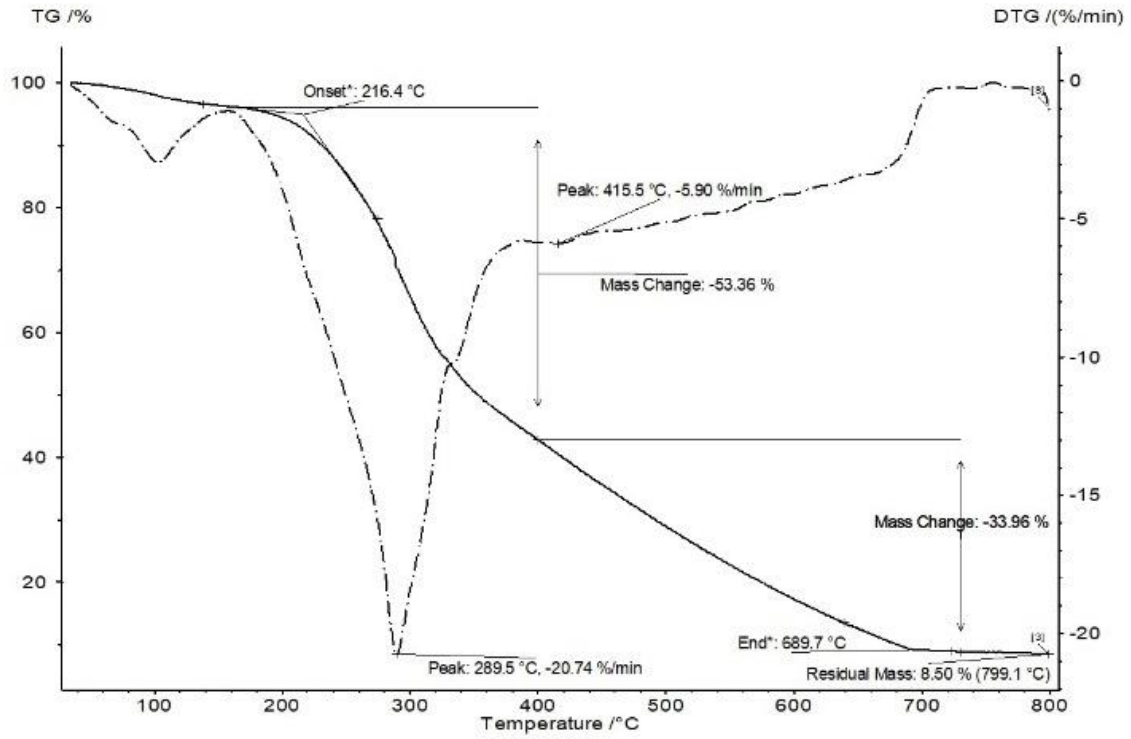

(c)

Figure 2 TG/DTG analysis of hazelnut shell combustion at the heating rates (a) 10 °C/min, (b) 20 °C/min, (c) 40 °C/min.

In the Figure 3a, combustion reaction was conducted at the heating rate 10°C/min. Ignition temperature was recorded 216.8 °C and mass change rate reached the maximum value 5.41 %/min at the peak temperature 285.9 °C in the volatile combustion zone, the temperature varies between 150 °C and 370 °C. In the fixed carbon combustion zone, burnout temperature was saved 474.4 °C and mass change rate was obtained 3.18 %/min at the peak temperature 428.4 °C. Total mass loss values were recorded 58.41% and 30.27% for first and second stages separately, moreover residual mass was determined 6.18% when the mass change rate is being constant at the temperature 799.4 °C. According to mass loss in the first and second stages, it is obvious that mass loss in the volatile combustion zone is higher and faster than fixed carbon combustion zone because hemicellulose and cellulose thermally decompose in the volatile zone together [37].

TG/DTG analysis of hazelnut shell at the heating rate 20 °C/min is shown in the Figure 3b. Ignition and burnout temperature values were determined 221.9 °C and 532.5 °C. In the first stage, mass loss was recorded 55.07% and maximum value of mass change rate has been seen 9.72 %/min at the peak temperature 293.4 °C.

Mass loss in the second stage and residual mass at the end of the combustion were obtained 33.06% and 7.54 % respectively. Maximum mass change rate of the second stage were obtained at the peak temperature 461.2 °C. Compared to DTG curves at the heating rates 10 °C/min and 20 °C/min, it is seen that peak value of the mass change rate at the heating rate 20 °C/min is not as sharp as at the heating rate 10 °C/min, in the second stage. Furthermore, temperature ranges of the each stages were expanded, for instance, in the first stage of combustion at the heating rate 10 °C/min is in the range between 150 °C and 370 °C whereas same stage at the heating rate 20 °C/min is in the range between 140 °C and 380 °C. As seen in the Figure 3a and 3b, increase of heating rate caused the shifting of decomposition peaks to higher temperature because of the shorter residence time and bad thermal conductivity. These results show the good consistency with the literature studies [27, 38].

Besides, Figure 3c. displays the thermal decomposition of hazelnut shell when the heating rate is the fastest of this study. Unlike the other two heating rates, only one peak is seen clearly in the DTG curve at the heating rate 40 °C/min. Ignition and burnout temperature values are 216.4 °C and 689.7 °C and peak temperature values for first and second stages are 289.5 °C and 415.5 °C respectively.

Total mass loss has been found 53.36% and maximum mass change rate was obtained 20.74 %/min for the first stage. Even the peak point cannot be seen in the second stage, mass change rate was determined 5.90 %/min and total mass loss was recorded 33.96% in the second stage. In accordance with the experimental conditions of combustion, hemicellulose, cellulose and lignin in the content of biomass sample can be decomposed at the different temperature. TG/DTG results prove that peak temperature values for the first stage where the hemicellulose and cellulose decomposition generally take place in here are different for each heating rates in Figure 3. Researchers have studied about the biomass structure since many years and their results show that hemicellulose and cellulose content of biomass are higher than lignin content [37, 39, 40]. Consequently, total mass losses in the second stage are higher than in the second stage for each experiment regardless of heating rates because the thermal decomposition of hemicellulose and cellulose occurs in the first stage and hemicellulose and lignin decomposition occurs in the second stage as mentioned above. Residual mass amounts are shown in the Fig 3. for each experiment, it displays that increasing heating rate caused the bad thermal conductivity and was increased the residual mass amounts.

3.2. Combustion Index

Based on the Eq. 1, combustion index (S) has been calculated for the all heating rates which are studying in this work. Calculation results and performance parameters of combustion are presented in the Table 3.

Table 3
Combustion Index Calculation Results at Different Heating Rates for Hazelnut Husk

	Heating Rate (°C/min)		
	10	**20**	**30**
T_i (°C)	216.8	221.9	216.4
T_b (°C)	474.4	532.5	689.7
DTGmax (%/min)	-5.41	-9.72	-20.74
DTGmean (%/min)	-2.32	-4.04	-6.18
S	6.99E-08	1.99E-07	5.55E-07

As seen in the above Table 3, increase of heating rate influenced the ignition and burnout temperature values. Their effects on the combustion characteristics has been increased the combustion index values. The higher heating rate was decreased the residence time, but it was increased the amount of decomposed fuel per unit time. Thus reactivity of fuels in combustion increased with increases of heating rate [22].

3.3. Non-Linear Regression Analysis

Comparison of experimental and calculated TGA results are presented in Figure 4. for the different heating rates. Stage 1 and 2 which are represented volatile and fixed carbon combustion zones were evaluated separately and results were discussed based on regression coefficient R^2.

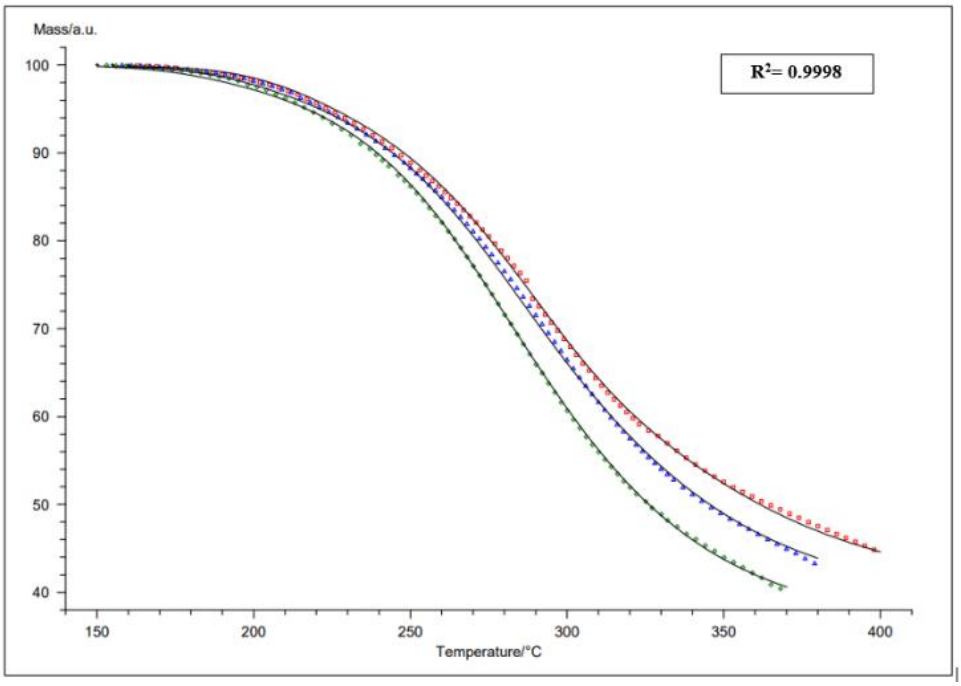

(a)

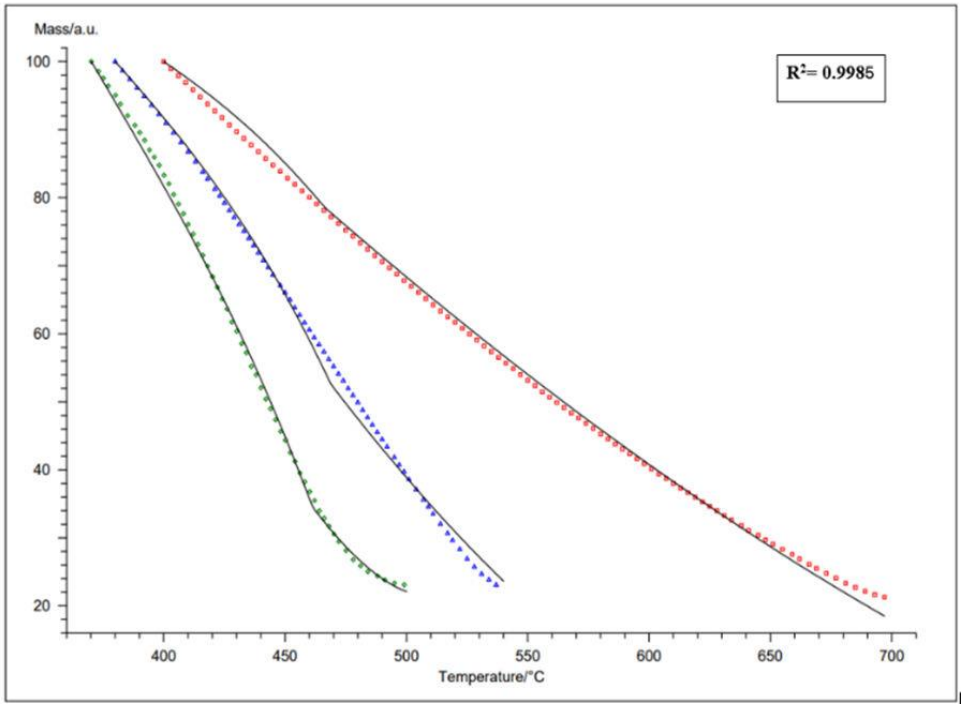

(b)

Figure 4 Comparison of experimental and calculated TGA curves for the hazelnut combustion (a) zone 1 and (b) zone 2 (green, blue and red lines represent 10°C/min, 20 °C/min, 40°C/min heating rates respectively)

In the first stage is shown in Figure 4a, hemicellulose and cellulose combustion has been executed using by two-step reaction mechanism ($A-1 \rightarrow B-2 \rightarrow C$). The correlation coefficient (R^2) of 0.9998 support that this mechanism was represented volatile combustion zone for each heating rate successfully. The two-step reaction mechanism was used for the second stage as well as for the first stage. Figure 4b illustrates of the credibility of the reaction

mechanism for hemicellulose and lignin decomposition process. It is clear from the curves at the different heating rates and R^2 =0.9985 that the experimental and non-linear model results are very similar. As seen in Figure 4 (a) and (b), the non-linear regression model displayed the great performance based on R^2 values.

3.4. Kinetic Parameters

Kinetic parameters of combustion process are presented after conducting non-linear regression analysis. R^2 values were found in the satisfactory limits for each stage, thus the kinetic parameters were proved to be correct. Kinetic parameters were listed in the Table 4 and 5 for volatile and fixed carbon combustion zones separately.

Table 4
Kinetic Parameters for Volatile Combustion Zone

Parameters	Optimum Value
log(A1/s^{-1})	10.3736
E1/kJ.mol^{-1},	135.6839
React. ord.1	2.6841
log(A2/s^{-1})	6.9187
E2/kJ.mol^{-1}	67.7445
React. ord.2	1.2508
FollReact. 1	80.4621
Mass Loss 1/%	-58.0000
Mass Loss 2/%	-60.0000
Mass Loss 3/%	-63.0000

According to results presented in Table 4 activation energies (E1 and E2) for two step reaction were found 135.68 kJ.mol^{-1} and 67.74 kJ.mol^{-1} respectively. Reaction orders were determined 2.68 for reaction step 1 and 1.25 for reaction step 2. Pre-exponential factor for each reaction step and total mass losses at the different heating rates are also presented in Table 4.

Table 5
Kinetic Parameters for Fixed Carbon Combustion Zone

Parameters	Optimum Value
log(A1/s^{-1})	-1.4534
E1/kJ.mol^{-1},	14.3585
React. Ord.1	0.5913
log(A2/s^{-1})	13.0922
E2/kJ.mol^{-1}	210.9523
React. Ord.2	0.5471
FollReact. 1	0.6436
Mass Loss 1/%	-33.3044
Mass Loss 2/%	-32.2621
Mass Loss 3/%	-29.4685

In the Table 5, kinetic parameters are listed for two step reaction mechanism that is occurred in the fixed carbon combustion zone. Activation energies were found 14.3585 kJ.mol^{-1} and 210.9523 kJ.mol^{-1} for reaction step 1 and 2 respectively. Reaction orders were determined 0.59 for reaction step 1 and 0.54 for reaction step 2. Based on the values in Table 4 and 5 and selected reaction mechanisms for each stage showed good results when compared with experimental data. Kinetic study results also showed good agreement with proximate analysis results presented in Table 1. Total mass losses in the first stage (58%, 60%, 63%) for each heating rate are higher than in the second stage (33.30%, 32.26%, 29.47%) because volatile content of hazelnut husk is higher than fixed carbon content.

4. CONCLUSIONS

The experiments of hazelnut husk combustion were conducted at three different heating rates and combustion characteristics were determined using by TGA. Combustion behavior and kinetic analysis of hazelnut husk were presented and discussed in this study. Results showed thermal decomposition characteristics of hazelnut husk have been affected changing of heating rate. TGA

results were evaluated considering two main parts then the ignition and burnout temperature values and total mass changes were recorded for each heating rate. Results displayed a good consistency with literature in terms of mass losses which is greater in the volatile combustion zone than fixed carbon combustion zone. Combustion index is a criterion to show reactivity of hazelnut husk increased with enhancing of heating rate. Ea, reaction orders and pre-exponential factors were estimated for two stages by non-linear regression method. According to comparison of TGA curves for experimental and calculated data sets, R^2 values were found 0.9998 and 0.9985 for volatile and fixed carbon combustion zones respectively. R^2 values proved that the new developed non-linear model worked properly to estimate thermal decomposition behavior and calculate kinetic parameters of combustion process. This study will be a good reference for biomass combustion plants and other industrial applications of hazelnut husk that currently use or will be used in the future.

Acknowledgments

The authors would like to thank the Marmara University Scientific Research Projects Commission (BAP) for contributing to the financial portion of the project.

Funding

This project studies were supported by Marmara University Scientific Research Projects Commission. Project numbers were FEN-C-YLP-250919-0272

The Declaration of Conflict of Interest/ Common Interest

No conflict of interest or common interest has been declared by the authors.

Authors' Contribution

The authors contributed equally to the study.

The Declaration of Ethics Committee Approval

This study does not require ethics committee permission or any special permission.

The Declaration of Research and Publication Ethics

The authors of the paper declare that they comply with the scientific, ethical and quotation rules of SAUJS in all processes of the paper and that they do not make any falsification on the data collected. In addition, they declare that Sakarya University Journal of Science and its editorial board have no responsibility for any ethical violations that may be encountered, and that this study has not been evaluated in any academic publication environment other than Sakarya University Journal of Science.

REFERENCES

[1] B. Rijal, S. H. Gautam, and L. LeBel, "The impact of forest disturbances on residual biomass supply: A long-term forest level analysis," *Journal of Cleaner Production*, vol. 248, p. 119278, 2020.

[2] S. de Oliveira Junior, *Exergy: production, cost and renewability*. Springer Science & Business Media, 2012.

[3] L. Rincon, M. Puri, A. Kojakovic, and I. Maltsoglou, "The contribution of sustainable bioenergy to renewable electricity generation in Turkey: Evidence based policy from an integrated energy and agriculture approach," *Energy Policy*, vol. 130, pp. 69-88, 2019.

[4] H. S. Kambo and A. Dutta, "Comparative evaluation of torrefaction and hydrothermal carbonization of lignocellulosic biomass for the production of solid biofuel," *Energy conversion and management*, vol. 105, pp. 746-755, 2015.

[5] S. Brand, R. F. Susanti, S. K. Kim, H.-s. Lee, J. Kim, and B.-I. Sang, "Supercritical ethanol as an enhanced medium for lignocellulosic biomass liquefaction: Influence of physical process parameters," *Energy*, vol. 59, pp. 173-182, 2013.

[6] E. Demirkaya, O. Dal, and A. Yüksel, "Liquefaction of waste hazelnut shell by using sub-and supercritical solvents as a reaction medium," *The Journal of Supercritical Fluids*, vol. 150, pp. 11-20, 2019.

[7] M. Phanphanich and S. Mani, "Impact of torrefaction on the grindability and fuel characteristics of forest biomass," *Bioresource technology*, vol. 102, no. 2, pp. 1246-1253, 2011.

[8] S. Sadaka, H. Liechty, M. Pelkki, and M. Blazier, "Pyrolysis and combustion kinetics of raw and carbonized cottonwood and switchgrass agroforests," *BioResources*, vol. 10, no. 3, pp. 4498-4518, 2015.

[9] Q. Li *et al.*, "Gaseous ammonia emissions from coal and biomass combustion in household stoves with different combustion efficiencies," *Environmental Science & Technology Letters*, vol. 3, no. 3, pp. 98-103, 2016.

[10] A. Demirbas, "Political, economic and environmental impacts of biofuels: A review," *Applied energy*, vol. 86, pp. S108-S117, 2009.

[11] M. Morin, S. Pécate, and M. Hémati, "Kinetic study of biomass char combustion in a low temperature fluidized bed reactor," *Chemical Engineering Journal*, vol. 331, pp. 265-277, 2018.

[12] J. Chen, L. Mu, J. Cai, H. Yin, X. Song, and A. Li, "Thermal characteristics and kinetics of refining and chemicals wastewater, lignite and their blends during combustion," *Energy Conversion and Management*, vol. 100, pp. 201-211, 2015.

[13] A. Demirbas, "Combustion characteristics of different biomass fuels," *Progress in energy and combustion science*, vol. 30, no. 2, pp. 219-230, 2004.

[14] Q.-V. Bach, K.-Q. Tran, Ø. Skreiberg, and T. T. Trinh, "Effects of wet torrefaction on pyrolysis of woody biomass fuels," *Energy*, vol. 88, pp. 443-456, 2015.

[15] B. Ru, S. Wang, G. Dai, and L. Zhang, "Effect of torrefaction on biomass physicochemical characteristics and the resulting pyrolysis behavior," *Energy & Fuels*, vol. 29, no. 9, pp. 5865-5874, 2015.

[16] A. Toptas, Y. Yildirim, G. Duman, and J. Yanik, "Combustion behavior of different kinds of torrefied biomass and their blends with lignite," *Bioresource technology*, vol. 177, pp. 328-336, 2015.

[17] X. Peng, X. Ma, and Z. Xu, "Thermogravimetric analysis of co-combustion between microalgae and textile dyeing sludge," *Bioresource Technology*, vol. 180, pp. 288-295, 2015.

[18] W. Cao, J. Li, and L. Lue, "Study on the ignition behavior and kinetics of combustion of biomass," *Energy Procedia*, vol. 142, pp. 136-141, 2017.

[19] H. H. Sait, A. Hussain, A. A. Salema, and F. N. Ani, "Pyrolysis and combustion kinetics of date palm biomass using thermogravimetric analysis," *Bioresource Technology*, vol. 118, pp. 382-389, 2012.

[20] M. V. Gil, D. Casal, C. Pevida, J. Pis, and F. Rubiera, "Thermal behaviour and kinetics of coal/biomass blends during co-combustion," *Bioresource Technology*, vol. 101, no. 14, pp. 5601-5608, 2010.

[21] A. Álvarez, C. Pizarro, R. García, J. Bueno, and A. Lavín, "Determination of kinetic parameters for biomass combustion," *Bioresource technology*, vol. 216, pp. 36-43, 2016.

[22] K. Jayaraman, M. V. Kök, and I. Gökalp, "Combustion mechanism and model free kinetics of different origin coal samples: Thermal analysis approach," *Energy*, p. 117905, 2020.

[23] R. Junga, W. Knauer, P. Niemiec, and M. Tańczuk, "Experimental tests of co-combustion of laying hens manure with coal by using thermogravimetric analysis," *Renewable Energy*, vol. 111, pp. 245-255, 2017.

[24] T. Ozawa, "A new method of analyzing thermogravimetric data," *Bulletin of the chemical society of Japan*, vol. 38, no. 11, pp. 1881-1886, 1965.

[25] J. H. Flynn and L. A. Wall, "General treatment of the thermogravimetry of polymers," *Journal of Research of the National Bureau of Standards. Section A, Physics and Chemistry*, vol. 70, no. 6, p. 487, 1966.

[26] T. Akahira and T. Sunose, "Method of determining activation deterioration constant of electrical insulating materials," *Res Rep Chiba Inst Technol (Sci Technol)*, vol. 16, no. 1971, pp. 22-31, 1971.

[27] R. Barzegar, A. Yozgatligil, H. Olgun, and A. T. Atimtay, "TGA and kinetic study of different torrefaction conditions of wood biomass under air and oxy-fuel combustion atmospheres," *Journal of the Energy Institute*, vol. 93, no. 3, pp. 889-898, 2020.

[28] H. L. Friedman, "Kinetics of thermal degradation of char-forming plastics from thermogravimetry. Application to a phenolic plastic," in *Journal of polymer science part C: polymer symposia*, 1964, vol. 6, no. 1: Wiley Online Library, pp. 183-195.

[29] U. Özveren, "Theoretical and experimental investigation of biomass and coal gasification," 2013.

[30] K. Chrissafis, "Kinetics of thermal degradation of polymers," *Journal of Thermal Analysis and Calorimetry*, vol. 95, no. 1, pp. 273-283, 2009.

[31] J. Opfermann, "Kinetic analysis using multivariate non-linear regression. I. Basic concepts," *Journal of thermal analysis and calorimetry*, vol. 60, no. 2, pp. 641-658, 2000.

[32] N. Tudorachi and F. Mustata, "Curing and thermal degradation of diglycidyl ether of bisphenol A epoxy resin crosslinked with natural hydroxy acids as environmentally friendly hardeners," *Arabian Journal of Chemistry*, vol. 13, no. 1, pp. 671-682, 2020.

[33] H. Şenol, "Biogas potential of hazelnut shells and hazelnut wastes in Giresun City," *Biotechnology Reports*, vol. 24, p. e00361, 2019.

[34] S. Karata *et al.*, "Examination of modern and traditional applications in hazelnut production," in *IX International Congress on Hazelnut 1226*, 2017, pp. 329-332.

[35] A. Sezer, F. S. Dolar, S. J. Lucas, Ç. Köse, and E. Gümüş, "First report of the recently introduced, destructive powdery mildew Erysiphe corylacearum on hazelnut in Turkey," *Phytoparasitica*, vol. 45, no. 4, pp. 577-581, 2017.

[36] S. Niu, M. Chen, Y. Li, and T. Lu, "Combustion characteristics of municipal sewage sludge with different initial moisture contents," *Journal of Thermal Analysis and Calorimetry*, vol. 129, no. 2, pp. 1189-1199, 2017.

[37] C. Di Blasi, "Modeling chemical and physical processes of wood and biomass pyrolysis," *Progress in energy and combustion science*, vol. 34, no. 1, pp. 47-90, 2008.

[38] I. Mian *et al.*, "Combustion kinetics and mechanism of biomass pellet," *Energy,* p. 117909, 2020.

[39] L. Burhenne, J. Messmer, T. Aicher, and M.-P. Laborie, "The effect of the biomass components lignin, cellulose and hemicellulose on TGA and fixed bed pyrolysis," *Journal of Analytical and Applied Pyrolysis,* vol. 101, pp. 177-184, 2013.

[40] S. D. Stefanidis, K. G. Kalogiannis, E. F. Iliopoulou, C. M. Michailof, P. A. Pilavachi, and A. A. Lappas, "A study of lignocellulosic biomass pyrolysis via the pyrolysis of cellulose, hemicellulose and lignin," *Journal of analytical and applied pyrolysis*, vol. 105, pp. 143-150, 2014.

SAKARYA ÜNİVERSİTESİ
FEN BİLİMLERİ ENSTİTÜSÜ DERGİSİ

Sakarya University Journal of Science
SAUJS

e-ISSN 2147-835X | Period Bimonthly | Founded: 1997 | Publisher Sakarya University |
http://www.saujs.sakarya.edu.tr/en/

Title: DNA Interactions, Mutagenic, Anti-Mutagenic And Antimicrobial Activities of (E)-2-((3,5-Bis(Trifluoromethyl)Phenylimino)Methyl)-4,6-Dimethoxyphenol

Authors: Nuray YILDIRIM, Neslihan DEMİR

Recieved: 2020-09-17 17:06:32

Accepted: 2021-01-27 19:08:39

Article Type: Research Article

Volume: 25
Issue: 2
Month: April
Year: 2021
Pages: 339-348

How to cite
Nuray YILDIRIM, Neslihan DEMİR; (2021), DNA Interactions, Mutagenic, Anti-Mutagenic And Antimicrobial Activities of (E)-2-((3,5-Bis(Trifluoromethyl)Phenylimino)Methyl)-4,6-Dimethoxyphenol. Sakarya University Journal of Science, 25(2), 339-348, DOI: https://doi.org/10.16984/saufenbilder.793776
Access link
http://www.saujs.sakarya.edu.tr/en/pub/issue/60672/793776

Sakarya University Journal of Science 25(2), 339-348, 2021

DNA Interactions, Mutagenic, Anti-Mutagenic And Antimicrobial Activities of (E)-2-((3,5-Bis(Trifluoromethyl)Phenylimino)Methyl)-4,6-Dimethoxyphenol

Nuray YILDRIM[*1], Neslihan DEMİR[2]

Abstract

Small molecules that interact with DNA are known to be effective as anticancer and antimicrobial agents. Therefore it is significant to search for new molecules interacting with DNA as potential new therapeutic agents. In this study, we aimed to investigate interactions of novel fluorine substituted imine compound with DNA, (E)-2-((3,5-bis(trifluoromethyl) phenylimino)methyl)-4,6-dimethoxyphenol, and investigate its biological activities. DNA interactions of the compound were investigated by UV-Vis absorption spectroscopy and gel electrophoresis. The results demonstrated that the compound binds to DNA via intercalation. Agarose gel electrophoresis experiments showed that the compound does not cleave pBR322 plasmid DNA hydrolytically or oxidatively. Furthermore, mutagenic, anti-mutagenic, and antimicrobial activities of the compound were studied by Ames and broth microdilution test, respectively. The compound showed mutagenic activity on both TA98 and TA100 strains. Also, the antimutagenic activity was observed in TA100 strain of *S. typhimurium*. It demonstrated antimicrobial activity against the microorganisms tested in the concentration range of 16-64 µg/µL. The results show that the compound intercalates with DNA and has promising biological activities.

Keywords: DNA binding, DNA cleavage, mutagenicity, antimicrobial activity

1. INTRODUCTION

DNA is the main target for many drugs including anticancer drugs and antibiotics since DNA codes the genetic information to carry out replication and transcription in the cells. Small molecules interacting with DNA were reported as effective anticancer, antiviral, and antibiotic agents [1-2]. Cisplatin is the first inorganic antineoplastic drug, which was used in modern medicine to treat several cancers [3]. However, due to the adverse side effects and high toxicity, its effectiveness is limited so, there is a necessity for developing more effective, less toxic anticancer drugs [4]–[6]. Today, many antitumors, antiviral, and antibiotics that are used clinically show their effects by binding to DNA, such as netropsin, mithramycin, etc. [7]. Therefore, it is significant

[*]Corresponding author: nurayyildirim@comu.edu.tr
[1]Çanakkale Onsekiz Mart University, Vocational School of Health Services, 17100, Çanakkale
ORCID: https://orcid.org/0000-0002-4807-5357
[2]Çanakkale Onsekiz Mart University, Faculty of Arts And Sciences, 17100, Çanakkale
E-Mail: neslihandemir@comu.edu.tr
ORCID: https://orcid.org/0000-0002-2347-8344

to search novel molecules for developing more effective anticancer drugs [2].

During the last decade, there has been an increasing focus on the small molecule-DNA binding studies, because many drugs perform their antitumor effects via binding to DNA consequently inhibiting the replication process and resulting in growth inhibition and death of the cells [8]. Developing new drugs that target the DNA requires an understanding of how these molecules interact with DNA [9]. Small molecules non-covalently bind to DNA via three binding modes: groove binding, intercalation, and electrostatic interactions. Intercalation, and groove-binding are the most effective binding modes leading to cell degradation [10-11].

Imine compounds are an important class of compounds and have many applications in medicine and pharmaceutical fields as antibacterial, antifungal, and chemotherapeutic agents [12-14]. Fluorine substitution is a widely used strategy for developing drugs that can change the conformation, membrane permeability, and electrical charge of a ligand [15]. Keeping the view the facts mentioned, we decided to study a novel fluorine substituted imine compound, (E)-2-((3,5-bis(trifluoromethyl) phenylimino)methyl)-4,6-dimethoxyphenol, which we predicted to have useful biological activities. For this purpose, we studied DNA binding properties of the compound by UV-Vis spectroscopy and DNA cleavage activity with gel electrophoresis techniques. Furthermore, mutagenic, antimutagenic, and antimicrobial activities were investigated by the Ames and broth microdilution tests, respectively.

2. MATERIALS AND METHODS

2.1. Materials

All chemicals and reagents were obtained commercially and prepared as instructed by the manufacturer. The ^{1}H and ^{13}C NMR spectra were recorded on a Bruker AVANCE- 500 spectrometer operating at 400 and 101,6 MHz. Infrared absorption spectra were obtained from a Perkin Elmer BX II spectrometer in KBr discs and were reported in cm-1units. The UV-VIS spectra were measured using a SHIMADZU 1800 series spectrometer. Elementary analyses were performed on a Vario EL III CHNS elemental analyzer. Melting points were measured with an Electro Thermal IA 9100 apparatus using a capillary tube. 3,5-Dimethoxysalicylaldehyde, 3,5-bis(triflouromethyl)aniline, calf thymus DNA (CT-DNA), ethidium bromide, Mueller Hinton Broth, RPMI 1640 were purchased from Sigma-Aldrich. pBR322 supercoiled plasmid DNA and EcoRI enzyme were purchased from Thermo Fisher Scientific.

DNA stock solution was prepared by the manufacturer's instructions and stored at 4 ˚C for up to ten days. To determine the purity and concentration of the CT-DNA, UV absorbance was measured at 260 nm and 280 nm. A_{260}/A_{280} gave a ratio of 1.8-1.9 demonstrating that DNA was free of protein. The molar concentration of the DNA was calculated from its absorption intensity at 260 nm with a molar extinction coefficient of 6600 $M^{-1}cm^{-1}$ [16].

2.2. Synthesis of 2-((3,5-bis(trifluoromethyl) phenylimino)methyl)-4,6-dimethoxyphenol

3,5-Dimethoxysalicylaldehyde (0.396 g, $2.18x10^{-3}$ mol) was added to EtOH (100 mL) solution of 3,5-bis(triflouromethyl)aniline (0.499 g, $2.18x10^{-3}$ mol). The mixture was stirred and refluxed for 1 h. Compound was obtained from the evaporation of EtOH (Fig. 1). It was crystallized from $CHCl_3$:n-hexane (3:2) as a yellow crystal, mp 125 °C, 0.73 g (85%) yield. Found: C, 51.85; H, 3.31; N, 3.56. Calc. For $C_{17}H_{13}F_6NO_3$; C, 51,90; H, 3.30; N, 3.56 %. IR(KBr, cm^{-1}); νO-H; 3435 m, νAr-H; 3051 w, νC-H; 2980-2940-2848 m, νC=N; 1631 s, νC=C; 1601-1571-1517 s, νC-N; 1474 s, νC-O; 1371 s, νC-O-C; 1180-1170-1100 s. ^{1}H-NMR (DMSO); δ ppm, 10.03 (s, 1H, Ar-O<u>H</u>); 9.03 (s, 1H, Ar-C<u>H</u>=N-); 8.10-6.09 (m, 7H, Ar-<u>H</u>); 3,81 and 3,79 (s, 3H and 3H, OCH_3). ^{13}C-NMR (DMSO); δ ppm, 119.79 (s, 1C, <u>C</u>1); 162.13 (s, 1C, <u>C</u>2); 165.25 (s, 1C, <u>C</u>3); 103.33 (s, 1C, <u>C</u>4); 166.60 (s, 1C, <u>C</u>5); 106.38 (s, 1C, <u>C</u>6); 168.03 (s, 1C, -<u>C</u>7); 161.38 (s, 1C, <u>C</u>8); 125.32 (s, 2C, <u>C</u>9); 150.50 (s, 2C, <u>C</u>10); 122.57 (s, 1C,

C11); 130.63 (s, 2C, C14); 94.29 (s, 1C, C15); 91.38 (s, 1C, C16).

2.3. DNA Binding

The UV-Vis absorption spectra titrations were investigated to study the binding affinity between DNA and ligand in 5 mM Tris-HCl, 50 mM NaCl buffer (pH 7.2) at room temperature. 1.6 mL solutions of the ligand ($4x10^{-5}$ M) and the blank were added into quartz cuvettes. One aliquot of the CT-DNA solution (5.25 mM) was added to each cuvette. To eliminate the absorbance of DNA itself, it was also added to the blank. In each step, the ligand-DNA solution was incubated for 5 min at room temperature.

2.4. Cleavage Activity

DNA cleavage experiments were studied by agarose gel electrophoresis [17]. pBR322 supercoiled plasmid DNA (0.1 μg μL^{-1}) treated with the various concentrations of the ligand (25-400 μM) in the presence or absence of H_2O_2 in Tris –HCl buffer (10 μM, pH 7.2) and incubated for 3 h at 37 °C. H_2O_2 was used as an oxidizing agent to investigate oxidative cleavage activity. Then, loading buffer was added to reaction mixture and run on 1% agarose gel in TBE (Tris-Boric acid- EDTA, pH 8.0) buffer at 60 Volt for an hour. Bands were visualized by UV light.

2.5. Mutagenic Activity and Antimutagenic Activity

Potential mutagenic and antimutagenic activities of the compound were studied with the Ames/*Salmonella* test system using the standard plate incorporation method [18]. The experiments were carried out with *Salmonella typhimurium* TA98 (for frame-shift mutagens) and TA100 (for base-substitution mutagens) strains in the absence of S9 metabolic activation [18-19]. In mutagenicity assay, 0.1 mL of each bacterial culture and 0.5 mL of sodium phosphate buffer (0.2 M, pH 7.4) were mixed with 2 mL of top agar which contained different concentrations of the compound. This mixture was then poured onto minimal agar plates (MGA). After the incubation of the plates for 48 h at 37 ºC, the revertant bacterial colonies (his^+) were counted on each plate. In the antimutagenic activity assay, the standard mutagens were also added to the mixture before pouring onto MGA.

During the mutagenicity and antimutagenicity studies, as parallel to the study, the positive, negative, and spontaneous controls were used. The standard mutagens 4-nitro-*o*-phenylenediamine (NPD) for TA98 strain and sodium azide (SA) for TA100 were used as positive controls, Dimethyl suphoxide (DMSO) was used for both strains as negative control.

A compound was considered mutagenic when the two-fold increase was detected in the revertant colonies as compared to negative control [19]. The antimutagenic activity was calculated according to the rate of inhibition using the given formula:

$$\text{Inhibition rate (\%)} = (A-B/A-C) \times 100 \quad (1)$$

Where A is the number of revertant colonies in the plate containing mutagen, B is the number of revertant colonies in the presence of mutagen and compound/plate, C is the number of spontaneous colonies/plate.

The antimutagenic effect was considered moderate when the inhibition rate was 25–40% and strong when it was more than 40%. Inhibitory rate less than 25% was considered as not antimutagenic [20-22].

2.6. Antimicrobial Activity

To determine antimicrobial activities of the compound against bacterial and fungal strains; *Bacillus subtilis* ATCC 6633, *Staphylococcus aureus* ATCC 25923, *Escherichia coli* ATCC 25922, *Enterococcus faecalis* ATCC 29212, *Pseudomonas aeruginosa* ATCC 254992, *Escherichia coli* ATCC 35218, *Bacillus cereus* NRRL B-3711, *Proteus vulgaris* ATCC 13315, *Candida albicans* ATCC 60193, and *Candida tropicalis* ATCC 13803 referance strains were used. Minimal inhibitory concentration (MIC) of the compound was determined using the broth microdilution method according to procedures

and principles of the Clinical Laboratory Standards Institute [23].

Gentamicin and Fluconazole were used as positive controls. The compound stock solution was prepared with DMSO which was tested against the microorganisms and showed no effect. 100 µL of Mueller Hinton Broth for bacteria and RPMI 1640 medium for fungi were added in 96-well microplates. Two-fold dilutions of compounds and reference drugs were distributed into the wells (256-0.5 µg/mL). Inoculum suspensions of the bacteria and fungi strains were prepared and adjusted to 0.5 McFarland turbidity and 100 µL of inoculum were added to the wells. After addition of inoculum, each well contained approximately 5 x 10^5 CFU/mL bacterial concentration in the final test. Then plates were incubated at 37 ˚C for 16-20 h for bacteria and 20-24 h for fungi. The lowest concentration of compound that prevented visible growth was evaluated as MIC.

3. RESULTS AND DISCUSSION

3.1. FT-IR, ^{1}H NMR and ^{13}C NMR Spectroscopic studies

The FT-IR, ^{1}H-NMR and ^{13}C-NMR data are given in synthesis for the compound. The OH, C=N, C-O and C-O-C vibration band are observed at 3435, 1631, 1371 and 1180-1170-1100 cm^{-1} of compound, respectively (Fig. 1). The ^{1}H-NMR data for the compound show that the tautomeric equilibrium favours the enol-imine in DMSO. The -OH and -CH=N- protons are observed at 10.03 and 9.03 ppm singlets for the compound. The phenyl protons of the compound gave multiplets at 8.10-6.09 ppm (Fig. 2). According to the ^{13}C-NMR spectra, the compound has 14 signals, showing that the structures in solution are symmetrical (Fig. 3).

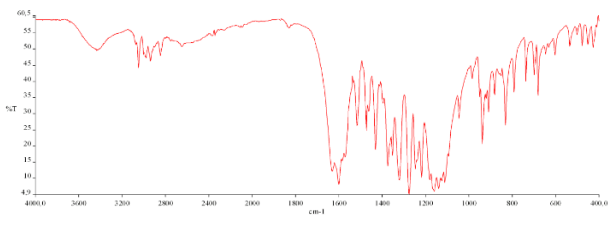

Figure 1 FT-IR spectrum of the compound

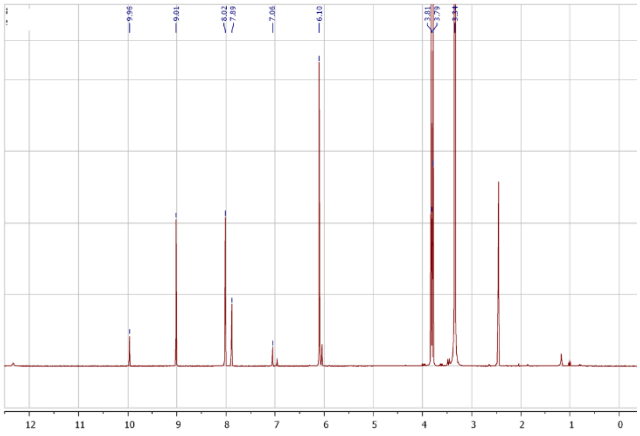

Figure 2 ^{1}H-NMR spectrum of the compound

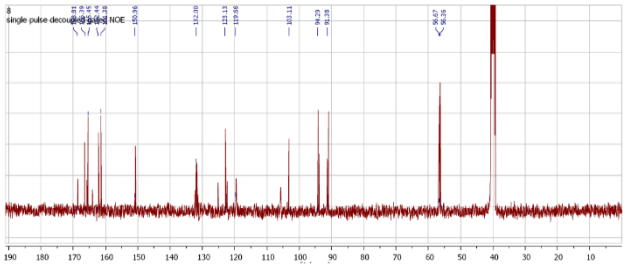

Figure 3 ^{13}C-NMR spectrum of the compound

3.2. DNA Binding

It is widely known that for many antitumor drugs DNA is a primary pharmacological target. Therefore, studying interactions between DNA and new compounds are important to discover new potential drugs and understand the mechanism of binding. Spectrophotometric titration is a widely used technique to investigate small molecule-DNA interactions and binding affinity of a molecule [24]. Thus, whether the compound (Fig. 4) has a binding ability to the CT-DNA was studied by UV spectra titrations. The absorption spectrum of the compound at 20 µM concentration, in the absence and presence of the CT-DNA, is shown in Fig. 5.

Binding of a small molecule to DNA usually causes changes in the absorbance and shift in the wavelength [24]. The compound as seen in Fig. 5 shows maximum absorbance in 353 nm and after

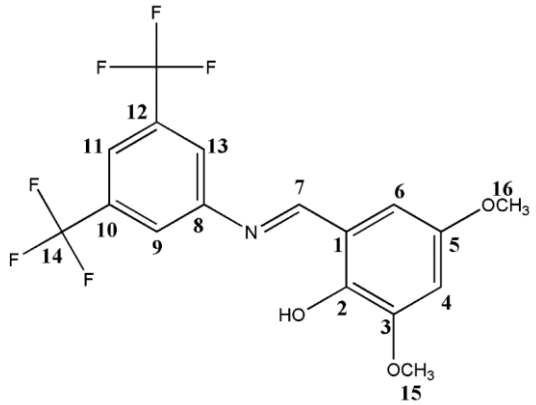

2-((3,5-Bis(trifluoromethyl)phenylimino)methyl)-4,6-dimethoxyphenol

Figure 4 Chemical formula of the compound

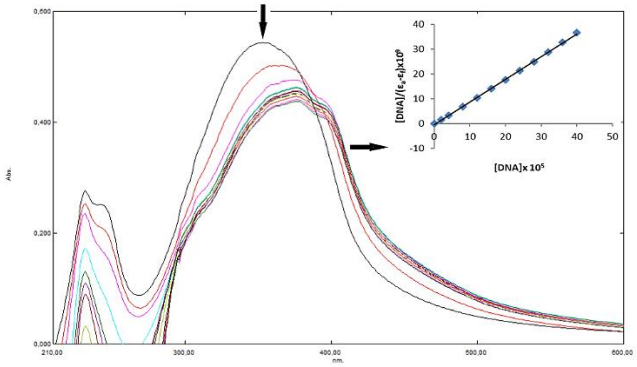

Figure 5. Absorption spectra of the compound in the absence and presence of increasing amounts of CT-DNA. Conditions: [DNA]/[Compound]=0-10 μM. Inset: Plot of [DNA]/(ε_a-ε_b) versus [DNA] for the titration of DNA with the compound.

the addition of increasing amounts of DNA, while compound concentration was fixed, its absorption spectra showed %8-19 hypochromic effect and 24 nm red-shift. Hypochromism and red-shift are associated with intercalation binding mode suggesting that there is a strong stacking interaction where an aromatic chromophore inserted between DNA base pairs [5]. After a ligand intercalates to the DNA, the π^* orbital of the intercalated ligands could pair up with π orbitals of the base pairs on the DNA, hence decreases the π-π^*transition energies [10], [25]. Therefore, the extend of the hypochromic effect is usually associated with the strength of intercalation [26]. This result shows that the compound binds to DNA via intercalation.

To determine DNA binding affinity, the intrinsic binding constant K_b was calculated by using the equation:

$$[DNA]/(\varepsilon_a-\varepsilon_b) = [DNA]/(\varepsilon_b-\varepsilon_f) + 1\ /K_b(\varepsilon_a-\varepsilon_b) \quad (2)$$

Where, K_b is the binding constant, [DNA] is the concentration of the DNA in base pairs, ε_a is apparent coefficient, ε_b is the extinction coefficient of the fully bound drug, ε_f extinction coefficient of the free drug [27]. By using this equation, the binding constant K_b was found $2{,}5x10^5$ M^{-1}. In the intercalation process, planar molecules insert between the base pairs of the DNA and change the helical structure, resulting in lengthening of the DNA. It is reported that even though this process needs a serious amount of free energy, with the favorable help of hydrogen bonding, hydrophobic, ionic, and van der Waals forces give rise to 10^5 to 10^{11} M^{-1} association constants [28-29]. Results of the experiment show that the binding constant of the compound indicates intercalation binding mode.

3.3. DNA Cleavage Activities

DNA cleavage activities of the compound were determined by agarose gel electrophoresis. When agarose gel electrophoresis conducted, supercoiled plasmid DNA migrates faster due to its size while nicked plasmid DNA migrates relatively slow. Linear form migrates between these two.

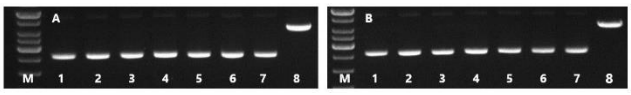

Figure 6. DNA cleavage activity of the compound. A. Hydrolytic cleavage B. Oxydative cleavage. M. Marker (1 Kb), 1. Supercoiled pBR322, 2-7. Supercoiled pBR322+ 5, 25, 50, 100, 200, 400 μM compound), 8. Positive control (linearized pBR322 using EcoRI enzyme).

The cleavage activity of the compound was studied by using supercoiled pBR322 plasmid DNA as a substrate in Tris-HCl buffer under physiological conditions. The compound was tested for hydrolytic and oxidative cleavage activities with concentrations in the range of 5-

400 μM and as shown in Fig. 6 no cleavage activity was observed.

3.4. Mutagenic and Antimutagenic Activities

As shown in the Table 1, there is almost a 2-fold increase in the number of revertants at the concentration of 50 and 500 ppm in compare to negative control (12±1.09) for TA98, and there is even more than 3-fold increase in the number of revertansts at the concentrations of 5, 50, and 500 ppm in compare to negative control (148±2.65) for TA100. Based on these findings, the compound shows mutagenic activity on both TA98 and TA100 strains.

Although DNA intercalators have a capacity to alter the genetic material of the cell and can result in a toxic effect, not all intercalators have a genotoxic effect. For toxicity, basic electrophilic or cationic functional groups are often necessary [29-31].

The compound did not have antimutagenic activity on strain TA98 (< 25% inhibition) but had antimutagenic activity on strain TA100. The moderate antimutagenic activity was observed at 0.5 and 5 ppm/plate concentrations (25-40% inhibition) The strongest antimutagenic activity was observed at 50 and 500 ppm/plate concentration (>40% inhibition) against *S. typhimurium* TA100 strain (Table 2).

Table 1
Mutagenicity assay results of the compound for *S. typhimurium* TA98 and TA100 strains

Sample/ Standard		Concent-ration (ppm)	His^+ Revertant Number of Colony /Plate	
			TA98	TA100
			Mean±SE	Mean±SE
Positive Control	**NPD**	10^{-2}	770±5.06	
	SA	10^{-3}		1043±5.41
Compound		0.5	13±0.05	61±1.11
		5	15±0.06	638±9.67
		50	21±0.14	647±8.55
		500	23±0.08	572±6.23
Negative Control		DMSO	12±1.09	148±2.65
Spontaneous Control			33±2.16	124±5.89

* NPD: 4-nitro-*o*-phenylenediamine, SA: Sodium azide, DMSO: Dimethyl sulphoxide

Table 2
Antimutagenicity assay results of the compound for *S. typhimurium* TA98 and TA100 strains

Treatment		Concentration (ppm)	His^+ Revertant Number of Colony /Plate			
			TA98	% Inhibition	TA100	% Inhibition
			Mean±SE		Mean ±SE	
Positive Control	**NPD**	10^{-2}	774±7.49			
	SA	10^{-3}			1006±18.48	
Compound		0.5	712±8.63	8.29	706±10.74	33.71
		5	678±9.21	12.83	638±9.67	36.58
		50	652±5.77	16.31	647±8.55	40.33
		500	724±6.46	6.68	572±6.23	48.76
Negative Control		DMSO	12±1.05		140±6.53	
Spontaneous Control			26±3.01		116±5.89	

* NPD: 4-nitro-*o*-phenylenediamine, SA: Sodium azide, DMSO: Dimethyl sulphoxide

Table 3
MIC (μg/μL) of the compound

Microorganisms	Compound (μg/ μL)	Gentamicin (μg/ μL)	Fluconazole (μg/ μL)
Staphylococcus aureus ATCC 25923	64	8	-
Enterococcus faecalis ATCC 29212	64	8	-
Bacillus cereus NRRL B-3711	64	1	-

Bacillus subtilis ATCC 6633	32	1	-
Escherichia coli ATCC 25922	32	0.125	-
Escherichia coli ATCC 35218	64	0.125	-
Pseudomonas aeruginosa ATCC 254992	32	0.125	-
Proteus vulgaris ATCC 13315	32	1	-
Candida albicans ATCC 60198	16	-	0.125
Candida tropicalis ATCC 13803	32	-	1

3.5. Antimicrobial Activities

Antibacterial and antifungal activities of the compound were screened using the broth microdilution method according to the procedures of CLSI [23]. The lowest concentration of the compound that inhibits the visible growth of the microorganisms was recorded as MICs. Average data from the three replicated experiments are presented in Table 3. The compound inhibited the growth of the tested microorganisms and showed antibacterial and antifungal activity with the MIC values in the range of 32-64 μg/μL and 16-32 μg/μL, respectively. However, the compound was less effective compared to reference drugs gentamicin and fluconazole.

The compound demonstrated similar antibacterial and antifungal effect against the tested bacteria and fungi. Among the tested microorganisms the compound was the most effective against *C. albicans* with the MIC value of 16 μg/μL.

4. CONCLUSION

The most encouraging ways to develop more effective drugs is to research new molecular structures that present more effective antitumor activities. Therefore, many scientists have been driven to look for new molecules with better biological activities.

In this paper, we studied the DNA binding properties of novel fluorine substituted imine compound, (E)-2-((3,5-bis(trifluoromethyl) phenylimino)methyl)-4,6-dimethoxyphenol. In addition, cleavage activity, mutagenicity, antimutagenicity, and antimicrobial activity of the compound were also investigated. The compound displayed intercalative binding to CT-DNA with the $K_b = 2.5x10^5$ M^{-1}. The observed value of binding constant K_b shows that the compound is strongly bound with CT-DNA. Although, it is lower than the classical intercalators like ethidium bromide ($7x10^7$ M^{-1}), it is comperable to other intercalators such as propidium ($3.1x10^5$ M^{-1}), DAPI ($1.2x10^5$ M^{-1}) [32-33]. Cleavage experiments using pBR322 supercoiled plasmid DNA showed that the compound does not have cleavage activity. Although DNA intercalators have the ability to alter the DNA, not all intercalators have cleavage activity. Many anticancer drugs initiate their extended damage to the DNA by their cleavage activity which eventually leads cells to apoptosis and cell death. However, even without the cleavage activity, intercalation alters the DNA structure and this prevents DNA replication and transcription by interfering with the action of topoisomerases [34]. The compound showed mutagenic activity on both TA98 and TA100 strains. The compound demonstrated antimutagenic activity only on TA100 strain. Intercalation in DNA can alter the helical structure of the DNA in the cell and this may lead to triggering the activity of the DNA repairing mechanisms which can explain antimutagenic activity of the compound [35]. The compound showed antimicrobial activity against tested microorganisms in the concentration range of 16-64 μg/μL.

The results show that the compound has promising biological activities that may have potential practical applications. Further studies are needed to investigate its potential pharmacological properties such as topoisomerase inhibition, DNA footprinting for sequence specisifity and citotoxicity assay to determine its activity on human cells. The results obtained from this study will be useful in understanding the molecular intercalation mechanism and in designing its potential biological and pharmacological effects in the future.

Acknowledgements

We are grateful to Assoc.Prof. Dr. Mustafa Yıldız in Çanakkale Onsekiz Mart University, Faculty of Arts And Sciences, Chemistry department for providing the compound that used in this research.

Funding

This study is supported by Çanakkale Onsekiz Mart University, Scientific Research Project Committee (ÇOMÜ BAP), Project number: FBA-2017-1125.

Conflict of Interest

There is no conflict of interest in this study.

Authors Contributon

N.Y: Writing the article, general literature review, experimental section of DNA binding and antimicrobial activities, general data analysis, discussion of all experimental results, and conclusions.

N.D: Experimental section of mutagenic and antimutagenic activities, data analysis, discussion of results and conclusions.

Ethics Committee Approval

This paper does not require ethics committee permission or any special permission.

Research And Publication Ethics

In the writing process of this study, international scientific, ethical and citation rules were followed, and no falsification was made on the collected data. Sakarya University Journal of Science and its editorial board have no responsibility for all ethical violations. All responsibility belongs to the responsible author and this study has not been evaluated in any academic publication environment other than Sakarya University Journal of Science.

REFERENCES

[1] A. Rabbani-Chadegani, S. Keyvani-Ghamsari, and N. Zarkar, "Spectroscopic studies of dactinomycin and vinorelbine binding to deoxyribonucleic acid and chromatin," *Spectrochim. Acta - Part A Mol. Biomol. Spectrosc.*, vol. 84, no. 1, pp. 62–67, 2011.

[2] N. Li, Y. Ma, C. Yang, L. Guo, and X. Yang, "Interaction of anticancer drug mitoxantrone with DNA analyzed by electrochemical and spectroscopic methods," *Biophys. Chem.*, vol. 116, no. 3, pp. 199–205, 2005.

[3] S. Ghosh, "Cisplatin: The first metal based anticancer drug," *Bioorganic Chemistry*, vol. 88. p. 102925, 2019.

[4] S. M. Pradeepa, H. S. Bhojya Naik, B. Vinay Kumar, K. Indira Priyadarsini, A. Barik, and S. Jayakumar, "Synthesis and characterization of cobalt(II), nickel(II) and copper(II)-based potential photosensitizers: Evaluation of their DNA binding profile, cleavage and photocytotoxicity," *Inorganica Chim. Acta*, vol. 428, pp. 138–146, 2015.

[5] B. L. Fei *et al.*, "Effects of copper ions on DNA binding and cytotoxic activity of a chiral salicylidene Schiff base," *J. Photochem. Photobiol. B Biol.*, vol. 132, pp. 36–44, 2014.

[6] R. Gust, W. Beck, G. Jaouen, and H. Schönenberger, "Optimization of cisplatin for the treatment of hormone dependent tumoral diseases. Part 1: Use of steroidal ligands," *Coordination Chemistry Reviews*, vol. 253, no. 21–22. pp. 2742–2759, 2009.

[7] K. Dhara, P. Roy, J. Ratha, M. Manassero, and P. Banerjee, "Synthesis, crystal structure, magnetic property and DNA cleavage activity of a new terephthalate-bridged tetranuclear copper(II) complex," *Polyhedron*, vol. 26, no. 15, pp. 4509–

4517, 2007.

[8] Y. L. Æ. Z. Yang, "Crystal structures , antioxidation and DNA binding properties of Yb (III) complexes with Schiff-base ligands derived from 8-hydroxyquinoline-2-carbaldehyde and four aroylhydrazines," *Biometals*, pp. 733–751, 2009.

[9] B. dui Wang, Z. Y. Yang, and T. rong Li, "Synthesis, characterization, and DNA-binding properties of the Ln(III) complexes with 6-hydroxy chromone-3-carbaldehyde-(2′-hydroxy) benzoyl hydrazone," *Bioorganic Med. Chem.*, vol. 14, no. 17, pp. 6012–6021, 2006.

[10] Z. C. Liu *et al.*, "Crystal structures, DNA-binding and cytotoxic activities studies of Cu(II) complexes with 2-oxo-quinoline-3-carbaldehyde Schiff-bases," *Eur. J. Med. Chem.*, vol. 45, no. 11, pp. 5353–5361, 2010.

[11] G. Zhang, S. Shuang, C. Dong, D. Liu, and M. M. F. Choi, "Investigation on DNA assembly to neutral red-cyclodextrin complex by molecular spectroscopy," *J. Photochem. Photobiol. B Biol.*, vol. 74, no. 2004, pp. 127–134, 2004.

[12] X. Qiao *et al.*, "Study on potential antitumor mechanism of a novel Schiff Base copper(II) complex: Synthesis, crystal structure, DNA binding, cytotoxicity and apoptosis induction activity," *J. Inorg. Biochem.*, vol. 105, no. 5, pp. 728–737, 2011.

[13] S. Dhar, P. A. N. Reddy, M. Nethaji, S. Mahadevan, M. K. Saha, and A. R. Chakravarty, "Effect of Steric Encumbrance of Tris(3-phenylpyrazolyl)borate on the Structure and Properties of Ternary Copper(II) Complexes Having N,N-Donor Heterocyclic Bases Complexes of formulation [Cu(Tp Ph)(L)](ClO 4) (1−4), where Tp," vol. 41, no. 2002, pp. 3469–3476, 2002.

[14] D. K. Chand *et al.*, "Affinity and Nuclease Activity of Macrocyclic Polyamines and Their CuII Complexes," *Chem. – A Eur. J.*, vol. 6, no. 21, pp. 4001–4008, 2000.

[15] B. E. Smart, "Fluorine substituent effects (on bioactivity)," in *Journal of Fluorine Chemistry*, vol. 109, no. 1, pp. 3–11, 2001.

[16] T. C. Jenkins, "Optical Absorbance and Fluorescence Techniques for Measuring DNA–Drug Interactions," in *Drug-DNA Interaction Protocols*, New Jersey: Humana Press, pp. 195–218, 1997.

[17] V. C. da Silveira, J. S. Luz, C. C. Oliveira, I. Graziani, M. R. Ciriolo, and A. M. da C. Ferreira, "Double-strand DNA cleavage induced by oxindole-Schiff base copper(II) complexes with potential antitumor activity," *J. Inorg. Biochem.*, vol. 102, no. 2008, pp. 1090–1103, 2008.

[18] D. M. Maron and B. N. Ames, "Revised methods for the Salmonella mutagenicity test," *Mutation Research/Environmental Mutagenesis and Related Subjects*, vol. 113, no. 3–4. Elsevier, pp. 173–215, 1983.

[19] K. Mortelmans and E. Zeiger, "The Ames Salmonella/microsome mutagenicity assay," *Mutat. Res. - Fundam. Mol. Mech. Mutagen.*, vol. 455, no. 1–2, pp. 29–60, 2000.

[20] Y. Ikken, P. Morales, A. Martínez, M. L. Marín, A. I. Haza, and M. I. Cambero, "Antimutagenic effect of fruit and vegetable ethanolic extracts against N-nitrosamines evaluated by the Ames test," *J. Agric. Food Chem.*, vol. 47, no. 8, pp. 3257–3264, 1999.

[21] P. S. Negi, G. K. Jayaprakasha, and B. S. Jena, "Antioxidant and antimutagenic activities of pomegranate peel extracts," *Food Chem.*, vol. 80, no. 3, pp. 393–397, 2003.

[22] C. E. Hong and S. Y. Lyu, "Genotoxicity detection of five medicinal plants in

Nigeria," *J. Toxicol. Sci.*, vol. 36, no. 1, pp. 87–93, 2011.

[23] Clinical and Laboratory Standards Institute, "Clinical and Laboratory Standards Institute," Wane, Pennsylvania: Clinical and Laboratory Satandards Institute, pp. 604–604, 2019.

[24] G. J. Chen *et al.*, "Synthesis, DNA binding, photo-induced DNA cleavage, cytotoxicity and apoptosis studies of copper(II) complexes," *J. Inorg. Biochem.*, vol. 105, no. 2, pp. 119–126, 2011.

[25] A. M. Pyle, J. P. Rehmann, R. Meshoyrer, N. J. Turro, J. K. Barton, and C. V Kumar, "Mixed-Ligand complexes of ruthenium(II): Factors governing binding to DNA," *J. Am. Chem. Soc.*, vol. 111, no. 8, pp. 3051–3058, 1989.

[26] N. Vamsikrishna, M. P. Kumar, G. Ramesh, N. Ganji, S. Daravath, and Shivaraj, "DNA interactions and biocidal activity of metal complexes of benzothiazole Schiff bases: synthesis, characterization and validation," *J. Chem. Sci.*, vol. 129, no. 5, pp. 609–622, 2017.

[27] R. Prabhakaran *et al.*, "DNA binding, antioxidant, cytotoxicity (MTT, lactate dehydrogenase, NO), and cellular uptake studies of structurally different nickel(II) thiosemicarbazone complexes: Synthesis, spectroscopy, electrochemistry, and X-ray crystallography," *J. Biol. Inorg. Chem.*, vol. 18, no. 2, pp. 233–247, 2013.

[28] J. B. Chaires, "Energetics of drug-DNA interactions," *Biopolymers*, vol. 44, no. 3, pp. 201–215, 1997.

[29] R. Palchaudhuri and P. J. Hergenrother, "DNA as a target for anticancer compounds: methods to determine the mode of binding and the mechanism of action," *Curr. Opin. Biotechnol.*, vol. 18, no. 6, pp. 497–503, 2007.

[30] R. D. Snyder, J. McNulty, G. Zairov, D. E. Ewing, and L. B. Hendry, "The influence of N-dialkyl and other cationic substituents on DNA intercalation and genotoxicity," *Mutat. Res. - Fundam. Mol. Mech. Mutagen.*, vol. 578, no. 1–2, pp. 88–99, 2005.

[31] R. D. Snyder, "Assessment of atypical DNA intercalating agents in biological and in silico systems," *Mutat. Res. - Fundam. Mol. Mech. Mutagen.*, vol. 623, no. 1–2, pp. 72–82, 2007.

[32] L. Subha, C. Balakrishnan, S. Thalamuthu, and M. A. Neelakantan, "Mixed ligand Cu(II) complexes containing o-vanillin-L-tryptophan Schiff base and heterocyclic nitrogen bases: Synthesis, structural characterization, and biological properties," *J. Coord. Chem.*, vol. 68, no. 6, pp. 1021–1039, 2015.

[33] L. Strekowski and B. Wilson, "Noncovalent interactions with DNA: An overview," *Mutat. Res. - Fundam. Mol. Mech. Mutagen.*, vol. 623, no. 1–2, pp. 3–13, 2007.

[34] H. S. B. N. Sangeetha Gowda K.R., Blessy Baby Mathew, C.N. Sudhamani, "Mechanism of DNA Binding and Cleavage, Biomedicine and Biotechnology," *Biomed. Biotechnol.*, vol. Vol. 2 No., no. 1, pp. 1–9, 2014.

[35] E. Buraka *et al.*, "DNA-binding studies of AV-153, an antimutagenic and DNA repair-stimulating derivative of 1,4-dihydropiridine," *Chem. Biol. Interact.*, vol. 220, no. 2014, pp. 200–207, 2014.

SAKARYA ÜNİVERSİTESİ
FEN BİLİMLERİ ENSTİTÜSÜ DERGİSİ

Sakarya University Journal of Science
SAUJS

e-ISSN 2147-835X | Period Bimonthly | Founded: 1997 | Publisher Sakarya University |
http://www.saujs.sakarya.edu.tr/en/

Title: Fiber Bragg Grating Sensor Interrogation Using Tunable Erbium-Doped Fiber Ring Laser Source

Authors: Şerif Ali SADIK, Fırat Ertaç DURAK, Ahmet ALTUNCU

Recieved: 2020-09-02 14:01:42

Accepted: 2021-02-01 00:10:12

Article Type: Research Article

Volume: 25
Issue: 2
Month: April
Year: 2021
Pages: 349-356

How to cite
Şerif Ali SADIK, Fırat Ertaç DURAK, Ahmet ALTUNCU; (2021), Fiber Bragg Grating Sensor Interrogation Using Tunable Erbium-Doped Fiber Ring Laser Source. Sakarya University Journal of Science, 25(2), 349-356, DOI:
https://doi.org/10.16984/saufenbilder.789433
Access link
http://www.saujs.sakarya.edu.tr/en/pub/issue/60672/789433

Sakarya University Journal of Science 25(2), 349-356, 2021

Fiber Bragg Grating Sensor Interrogation Using Tunable Erbium-Doped Fiber Ring Laser Source

Şerif Ali SADIK*[1], Fırat Ertaç DURAK[1], Ahmet ALTUNCU[1]

Abstract

Fiber Bragg gratings (FBG) are ideal sensors for temperature, strain or vibration sensing applications with their advantages over conventional electronics sensor systems. In this paper, two different FBG sensor interrogation schemes based on broadband ASE source and tunable EDFRL source are demonstrated and compared. With both interrogator configurations, the response of the FBG sensor to temperature change is found to be linear and the sensitivities are measured as 11 pm/°C and 10.5 pm/°C, respectively. The experimental results have revealed that the optical power reflected from the FBG sensor is almost 20 dB higher with tunable EDFRL source than broadband ASE source. Thus, an interrogation method with tunable EDFRL can be suitable for remote, quasi-distributed sensor applications requiring high output power and OSNR.

Keywords: Fiber Bragg grating, broadband ASE source, tunable erbium doped fiber ring laser source, optical sensor interrogation

1. INTRODUCTION

Optical fiber based sensor systems have been studied extensively with their advantages of compactness, stability, durability, immunity to electromagnetic interference, high multiplexing capacity and suitability for remote sensing [1–7]. Among these studies, fiber Bragg grating (FBG) sensors have attracted great attention with its unique capabilities. In addition to advantages mentioned above, FBGs have the benefits of low-cost, wavelength coded linear response, quasi-distributed and embedded sensing ability [1,8]. With quasi-distribution several FBGs can be multiplexed in wavelength and/or time domain on a single optical fiber link to acquire responses from same or different parameters (e.g. temperature, strain, vibration etc.) and interrogated with a single system [8–14].

Since the response of a FBG to a measured quantity is a shift at the peak wavelength, the amount of the wavelength shift must be observed to quantify the sensor response. There are two main types of optical sources presented in the literature used for FBG based sensor interrogators. First group consist of broadband

*Corresponding author: serifali.sadik@dpu.edu.tr
[1]Kütahya Dumlupınar University, Faculty of Engineering, Electrical and Electronics Engineering Department, 43100, Kütahya, Turkey.
E-Mail: serifali.sadik@dpu.edu.tr; firat.durak@dpu.edu.tr; altuncu@dpu.edu.tr
ORCID: https://orcid.org/0000-0003-2883-1431; https://orcid.org/0000-0002-4278-6561; https://orcid.org/0000-0002-3753-9515

optical sources, such as amplified spontaneous emission (ASE) source, which is commonly used [4,7,15–17], or superluminescence light emitting diodes (sLED) [18-20]. An interrogator with a broadband light source is easy to install and has a compact structure. However, the ASE source has low output power and optical signal to noise ratio (OSNR). Thus, the maximum distance for long range quasi-distributed sensing may be limited. Also sLEDs have comparatively narrower spectral bandwidth which is usually some tens of nanometers, that limits the multiplexed sensor count [1,15,20].

The second group of optical sources for FBG sensor interrogator is based on tunable laser sources (TLS) [3,8,21–23]. The tunable laser sources offer wider spectral range, higher output power and OSNR which enable long distance remote sensing [14,21–23]. Among these, tunable erbium doped fiber ring lasers (EDFRL) are widely used for optical fiber sensor interrogation systems[1,24,25]. They offer many advantages such as high output power, high OSNR, wide tuning range, narrow linewidth and high stability [26,27]. These advantages may also moderately be offered by the bulk type solid state TLSs. However, EDFRLs have also more advantages over a bulk type tunable laser system which are a better beam quality, easy heat dissipation, compact in-line device, no need for bulk type optics, easy and low coupling loss to an output fiber, coupling a higher pumping power to the laser cavity and consequently low cost [28]. Therefore, EDRFLs have recently become a very promising and economical solution for FBG based and non-FBG based sensor interrogation systems.

In this work, we have realized FBG sensor interrogation with both a broadband ASE light source and a tunable EDFRL. In the experiments, firstly a broadband ASE signal obtained using a C-EDFA was used as the broadband light source and we have analyzed the spectral response of the FBG sensor to temperature variation as the measured physical quantity. Later, a tunable EDFRL was used as an FBG based temperature sensor interrogator. The results obtained for both interrogation schemes were compared and discussed. This paper is organized as follows. In Section 2, the experimental setup is introduced. Section 3 presents the experimental results. Finally, the results are discussed in the Section 4.

2. EXPERIMENTAL SETUP

The experimental setup of the FBG temperature sensor interrogator with a broadband ASE source is shown in Figure 1(a). For the broadband ASE source design, a laser diode operating at 976 nm with a pump power of 120 mW was used as the forward pump laser source. An EDF (LIEKKI Er30-4/125) with length of 3 m was used as the active medium. The broadband ASE signal generated in C-EDFA is shown in Figure 2. It can be seen from Figure 2 that the ASE signal source has low output power (< -15 dBm) and a limited bandwidth in C band (1525-1575 nm). Also, the power level is not constant in the entire C band.

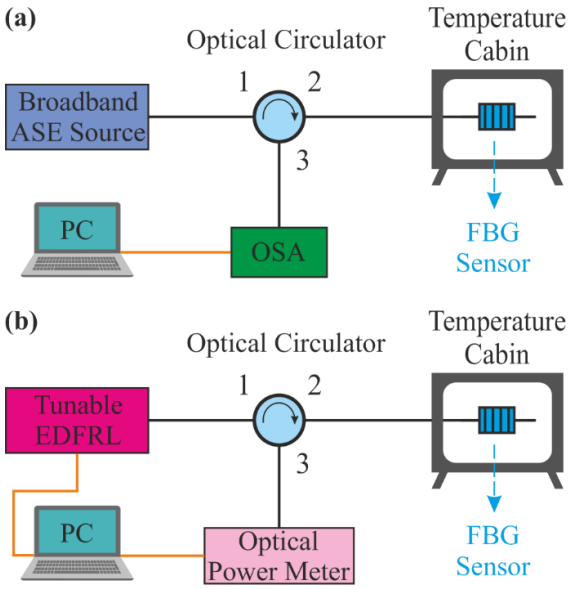

Figure 1 Experimental setup of FBG temperature sensor interrogator (a) with broadband ASE source (b) Tunable EDFRL source.

Figure 1(b) shows the FBG interrogation system with a tunable EDFRL. The tunable EDFRL source was designed, characterized and optimized for wideband operation between 1525 nm-1605 nm in a previous work [26]. The measured output power spectra of the tunable EDFRL used in this study is shown in Figure 3. One can see from Figure 3 that the tunable EDFRL used has 60 nm

(1525-1585 nm) (-3dB) tuning range and ~5.5 dBm output power in entire tuning range.

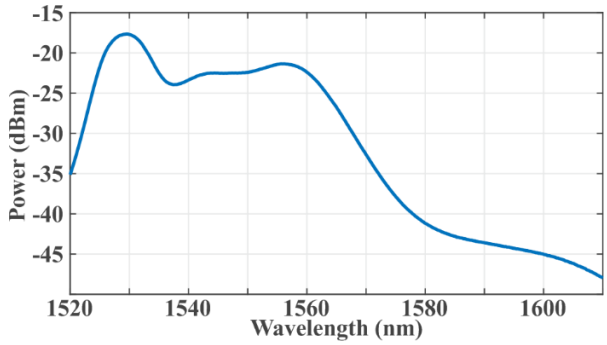

Figure 2 The output spectrum of the broadband ASE signal generated in C-EDFA.

In both configurations, the source signal (broadband ASE signal or narrow linewidth tunable EDFRL output signal) was directed to an FBG temperature sensor through a wideband optical circulator (1520-1625 nm). The center wavelength of the FBG temperature sensor is 1533.45 nm at room temperature, the reflectivity of FBG is 95% and and its 3-dB bandwith is 0.1 nm. The FBG sensor was placed inside a climatic test cabinet (NUVE TK120). The reflected signal was observed with an optical spectrum analyser (OSA, Antritsu MS9710B) and the acquired sensor data were processed and stored on a computer.

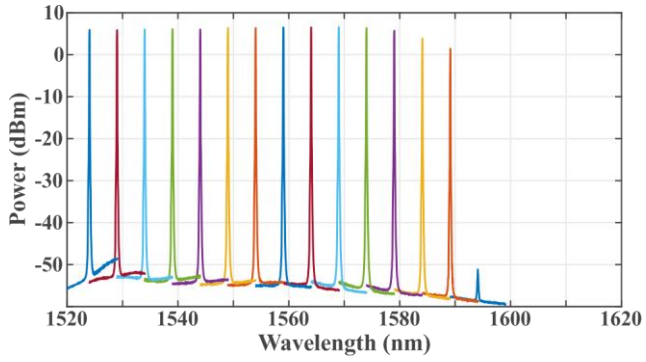

Figure 3 The output spectra of tunable EDFRL.

3. EXPERIMENTAL RESULTS

Using the measurement setups presented, we have measured the response of the FBG sensor to temperature variation. The temperature inside the climatic test cabinet was increased from 0°C to 40°C. At each measurement step, the temperature of the cabinet was kept constant for 15 minutes to achieve a uniform stabilized temperature distribution in the cabinet.

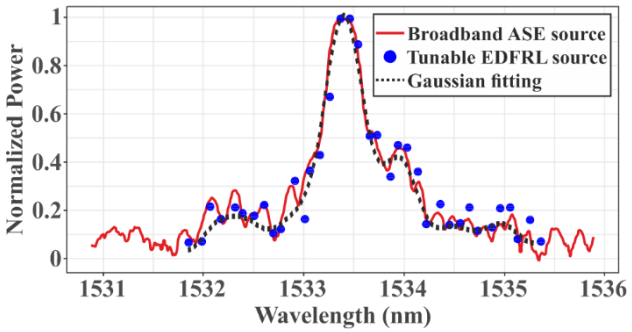

Figure 4 Measured reflection spectrum of the FBG sensor at room temperature (25°C) with a broadband ASE source and a narrow linewidth tunable EDFRL source as interrogator and Gaussian fitting curve of the points.

Firstly, the reflection spectrum of the FBG sensor was measured at room temperature (25°C). In Figure 4 solid red line shows the reflection spectrum obtained with broadband ASE source and the blue dots shows the discrete measurement points taken with 0.1 nm steps from reflection spectrum with narrow linewidth tunable EDFRL source. Also, the dashed black line shows the Gaussian fitting curve of the points obtained by the EDRFL interrogation system. Studies have shown that Gaussian fitting method is a precise peak detection method with a low detection error for the detection of FBG sensor peak reflection wavelength [29], [30]. It can be clearly seen from Figure 4 that, the reflection spectrum of the FBG sensor can be reconstructed from the peak points of discrete reflection spectra obtained with narrow linewidth tunable EDFRL source and Gaussian fitting algorithm. Also, one may increase the spectral resolution of discrete points to obtain a more precise reflection spectrum of FBG sensor.

3.1. Interrogation with a broadband ASE source

At the first measurement, we have employed an FBG temperature sensor interrogation system with a broadband ASE source which has been used for temperature sensing.

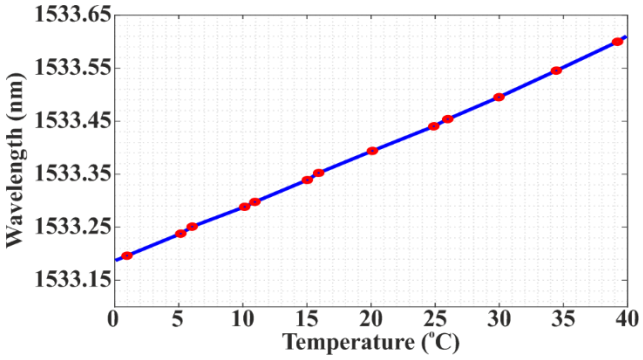

Figure 5 Linear response of the FBG sensor to temperature variation from 0°C to 40°C with broadband ASE source interrogator.

The shift at the center wavelength of the FBG sensor for varying temperature values from 0°C to 40°C is shown in Figure 5. The wavelength shift shows a linear response to temperature variation and the sensitivity of the FBG sensor was obtained as 11 pm/°C.

3.2. Interrogation with a narrow linewidth tunable EDFRL source

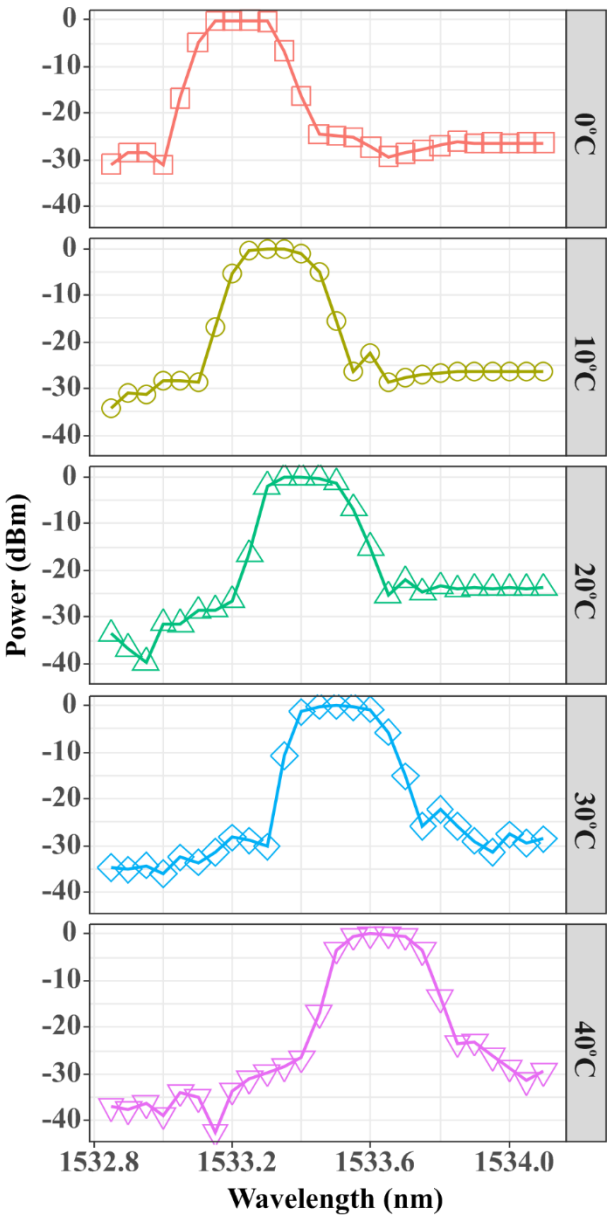

Figure 6 Reflection spectra of the FBG temperature sensor for different temperature values. Here, the interrogator is a narrow linewidth tunable EDFRL source.

As a second type of FBG temperature sensor interrogator, a narrow linewidth tunable EDFL source was utilized. The wavelength of the tunable EDFRL source was tuned from 1532.85 to 1534.10 with 0.05 nm steps and the reflection spectrum of the FBG temperature sensor was reconstructed from the peak powers of the reflections measured at each step.

Figure 6 shows the reconstructed spectra of the FBG temperature sensor for temperature values from 0°C to 40°C. It can be seen from the Figure 6 that, the peak wavelength of the reflection spectrum shifts towards to longer wavelengths as the temperature in the cabinet increases.

The linear relationship between the center reflection wavelength of the FBG sensor and the temperature is shown in Figure 7. It can be seen that, the wavelength shift response of the FBG sensor to temperature variation is linear and the experimental sensitivity is found to be 10.5 pm/°C. Our experimental sensitivity results for both interrogator schemes are highly consistent with the results given in the literature [3,31].

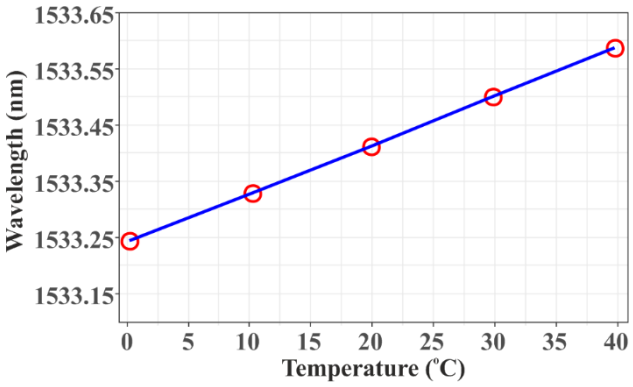

Figure 7 Linear response of the FBG sensor to temperature variation from 0°C to 40°C with tunable EDFRL interrogator.

4. CONCLUSION

In this work, the applications of a broadband ASE source and a narrow linewidth tunable EDFRL source as a FBG temperature sensor interrogator were demonstrated. From 0°C to 40°C, a positive linear response of the FBG sensor to temperature increase was successfully obtained with both interrogator configurations. The sensitivity of the FBG sensor is found to be 11 pm/°C and 10.5 pm/°C with broadband ASE source and narrow linewidth tunable EDFRL source interrogators, respectively.

With the broadband ASE source, the reflected optical power from the FBG temperature sensor was relatively low (~ -20 dBm) and its spectrum is not flat compared with the tunable EDFRL source. Therefore, a narrow linewidth tunable EDFRL source interrogator may be preferred to a broadband ASE source interrogator as it can support long range and multipoint quasi-distributed sensing systems due to its high output power, flat tuning spectrum and high OSNR. In addition, tunable EDFRL source interrogator has low cost advantageous due to lack of an expensive OSA or a wideband spectrometer in the system.

Further studies will be focused on multi-point, quasi-distributed sensing with FBG sensors using a narrow linewidth tunable EDFRL source interrogator. Also, further studies will be conducted in order to achieve simultaneous temperature and strain sensing with WDM and/or TDM techniques using narrow linewidth tunable EDFRL interrogator.

Acknowledgements

The authors would like to thank the Kütahya Dumlupınar University Scientific Research Projects Commission (BAP) for contributing to the financial portion of the project. The experiments were carried out in the laboratories of the Photonic Technologies Research and Application Center of Kutahya Dumlupınar University.

Funding

This work was financially supported by the Scientific Research Projects of Kütahya Dumlupinar University, project number 2017/43.

The Declaration of Conflict of Interest/ Common Interest

No conflict of interest or common interest has been declared by the authors.

Authors' Contribution

This study was the Ph.D. thesis of Şerif Ali SADIK, and the idea of the studies belongs to supervisor that is Ahmet ALTUNCU. Fırat Ertaç DURAK had a great contribution in providing support for the experiments.

The Declaration of Ethics Committee Approval

The authors declare that this document does not require an ethics committee approval or any special permission.

The Declaration of Research and Publication Ethics

The authors of the paper declare that they comply with the scientific, ethical and quotation rules of SAUJS in all processes of the article and that they do not make any falsification on the data collected. In addition, they declare that Sakarya University Journal of Science and its editorial board have no responsibility for any ethical violations that may be encountered, and that this study has not been evaluated in any academic publication environment other than Sakarya University Journal of Science.

REFERENCES

[1] Z. Fu, D. Yang, W. Ye, J. Kong, and Y. Shen, "Widely tunable compact erbium-doped fiber ring laser for fiber-optic sensing applications," *Opt. Laser Technol.*, vol. 41, no. 4, pp. 392–396, 2009.

[2] W. W. Morey, G. Meltz, and W. H. Glenn, "Fiber Optic Bragg Grating Sensors," in *Proceedings 1169, Fiber Optic and Laser Sensors VII*, 1990, vol. 1169, pp. 1110–1169.

[3] Y. Wang, J. Gong, B. Dong, D. Y. Wang, T. J. Shillig, and A. Wang, "A Large Serial Time-Division Multiplexed Fiber Bragg Grating Sensor Network," *Journal of Lightwave Technology*, vol. 30, no. 17. pp. 2751–2756, 2012.

[4] T. Vella *et al.*, "Full-spectrum interrogation of fiber Bragg gratings at 100 kHz for detection of impact loading," *Meas. Sci. Technol.*, vol. 21, no. 9, p. 94009, 2010.

[5] H. Tsuda, "Fiber Bragg grating vibration-sensing system, insensitive to Bragg wavelength and employing fiber ring laser," *Opt. Lett.*, vol. 35, no. 14, pp. 2349–2351, 2010.

[6] S. Sugavanam, A. A. Gbadebo, M. Kamalian-Kopae, and A. Majumdar, "A Compressed Sensing Approach to Fibre Bragg Interrogation," in *2019 Conference on Lasers and Electro-Optics Europe & European Quantum Electronics Conference (CLEO/Europe-EQEC)*, 2019, p. 1.

[7] Z. Luo, H. Wen, H. Guo, and M. Yang, "A time- and wavelength-division multiplexing sensor network with ultra-weak fiber Bragg gratings.," *Opt. Express*, vol. 21, no. 19, pp. 22799–22807, Sep. 2013.

[8] K. Yuksel and D. Pala, "Analytical investigation of a novel interrogation approach of fiber Bragg grating sensors using Optical Frequency Domain Reflectometry," *Opt. Lasers Eng.*, vol. 81, pp. 119–124, Jun. 2016.

[9] T. A. Berkoff, M. A. Davis, D. G. Bellemore, A. D. Kersey, G. M. Williams, and M. A. Putnam, "Hybrid time- and wavelength-division multiplexed fiber Bragg grating sensor array," 1995, vol. 2444, pp. 2444–2447.

[10] C. Crunelle, M. Wuilpart, C. Caucheteur, and P. Mégret, "Original interrogation system for quasi-distributed FBG-based temperature sensor with fast demodulation technique," *Sensors Actuators A Phys.*, vol. 150, no. 2, pp. 192–198, Mar. 2009.

[11] D. J. Cooper, T. Coroy, and P. W. Smith, "Time-division multiplexing of large serial fiber-optic Bragg grating sensor arrays," *Appl. Opt.*, vol. 40, no. 16, p. 2643—2654, 2001.

[12] S. Werzinger, S. Bergdolt, R. Engelbrecht, T. Thiel, and B. Schmauss, "Quasi-Distributed Fiber Bragg Grating Sensing Using Stepped Incoherent Optical Frequency Domain Reflectometry," *J. Light. Technol.*, vol. 34, no. 22, pp. 5270–

5277, 2016.

[13] S. Kirpiksiz and M. Yücel, "Düzgün Olmayan Yapılarda Fiber Bragg Izgara Sensör Tasarımı ve Uygulaması," *J. Polytech.*, pp. 1–1, May 2020.

[14] M. Burunkaya and M. Yucel, "Measurement and Control of an Incubator Temperature by Using Conventional Methods and Fiber Bragg Grating (FBG) Based Temperature Sensors," *J. Med. Syst.*, vol. 44, no. 10, p. 178, 2020.

[15] H. Y. Fu, H. L. Liu, W. H. Chung, and H. Y. Tam, "A Novel Fiber Bragg Grating Sensor Configuration for Long-Distance Quasi-Distributed Measurement," *IEEE Sens. J.*, vol. 8, no. 9, pp. 1598–1602, 2008.

[16] A. Hegyi, P. Kiesel, and A. Raghavan, "Time- and Wavelength-Multiplexed Wavelength Shift Detection for High-Resolution, Low-Cost Distributed Fiber-Optic Sensing," *J. Light. Technol.*, vol. 35, no. 19, pp. 4234–4241, 2017.

[17] G. R. Kirikera, O. Balogun, and S. Krishnaswamy, "Adaptive Fiber Bragg Grating Sensor Network for Structural Health Monitoring: Applications to Impact Monitoring," *Struct. Heal. Monit.*, vol. 10, no. 1, pp. 5–16, Apr. 2010.

[18] Y. Dai, Y. Liu, J. Leng, G. Deng, and A. Asundi, "A novel time-division multiplexing fiber Bragg grating sensor interrogator for structural health monitoring," *Opt. Lasers Eng.*, vol. 47, no. 10, pp. 1028–1033, 2009.

[19] H. K. Kim, W. Shin, and T. J. Ahn, "UV sensor based on photomechanically functional polymer-coated FBG," *IEEE Photonics Technol. Lett.*, vol. 22, no. 19, pp. 1404–1406, 2010.

[20] L. Yan, Z. Wu, Z. Zhang, W. Pan, B. Luo, and P. Wang, "High-Speed FBG-Based Fiber Sensor Networks for Semidistributed Strain Measurements," *IEEE Photonics J.*, vol. 5, no. 2, p. 7200507, 2013.

[21] Y. Wang, J. Gong, D. Y. Wang, B. Dong, W. Bi, and A. Wang, "A quasi-distributed sensing network with time-division-multiplexed fiber bragg gratings," *IEEE Photonics Technol. Lett.*, vol. 23, no. 2, pp. 70–72, 2011.

[22] T. Saitoh, K. Nakamura, Y. Takahashi, H. Iida, Y. Iki, and K. Miyagi, "Ultra-long-distance (230 km) FBG sensor system," in *19th International Conference on Optical Fibre Sensors*, 2008, vol. 7004, p. 70046C.

[23] M. Fernandez-Vallejo, S. Rota-Rodrigo, and M. Lopez-Amo, "Remote (250 km) fiber Bragg grating multiplexing system," *Sensors*, vol. 11, no. 9, pp. 8711–8720, 2011.

[24] S. H. Yun, D. J. Richardson, and B. Y. Kim, "Interrogation of fiber grating sensor arrays with a wavelength-swept fiber laser," *Opt. Lett.*, vol. 23, no. 11, pp. 843–845, 1998.

[25] Y. Wang, Y. Cui, and B. Yun, "A fiber Bragg grating sensor system for simultaneously static and dynamic measurements with a wavelength-swept fiber laser," *IEEE Photonics Technol. Lett.*, vol. 18, no. 14, pp. 1539–1541, 2006.

[26] S. A. Sadik, F. E. Durak, and A. Altuncu, "Spectral Characterization of an Erbium-Doped Fiber Ring Laser for Wideband Operation," in *2018 Advances in Wireless and Optical Communications (RTUWO)*, 2018, pp. 130–133.

[27] S. A. Sadik, F. E. Durak, and A. Altuncu, "Widely tunable erbium doped fiber ring laser based on loop and double-pass EDFA design," *Opt. Laser Technol.*, vol. 124, Apr. 2020.

[28] A. Bellemare, "Continuous-wave silica-based erbium-doped fibre lasers," *Prog. Quantum Electron.*, vol. 27, no. 4, pp. 211–266, Jan. 2003.

[29] Y. Li, Y. Xie, and G. Yao, "Comparison of Peak Searching Algorithms for Wavelength Demodulation in Fiber Bragg Grating Sensors," in *2010 2nd International Conference on Information Engineering and Computer Science*, 2010, pp. 1–4.

[30] M. Yücel and N. F. Öztürk, "FBG Algılama Sistemlerinde Gaussian Uyarlama Yöntemi ile Merkez Dalgaboyunun Belirlenmesi," *J. Polytech.*, vol. 24, no. 1, pp. 63–68, Feb. 2020.

[31] R. M. Liu, D. K. Liang, and A. Asundi, "Small diameter fiber Bragg gratings and applications," *Measurement*, vol. 46, no. 9, pp. 3440–3448, 2013.

SAKARYA ÜNİVERSİTESİ
FEN BİLİMLERİ ENSTİTÜSÜ DERGİSİ

Sakarya University Journal of Science
SAUJS

e-ISSN 2147-835X | Period Bimonthly | Founded: 1997 | Publisher Sakarya University |
http://www.saujs.sakarya.edu.tr/en/

Title: Parameter Optimization of Frequency Selective Surfaces Made of Composite Materials

Authors: Abdullah Oğuz KIZILÇAY

Recieved: 2020-10-28 00:00:00

Accepted: 2021-02-03 00:00:00

Article Type: Research Article

Volume: 25
Issue: 2
Month: April
Year: 2021
Pages: 357-363

How to cite
Abdullah Oğuz KIZILÇAY; (2021), Parameter Optimization of Frequency Selective Surfaces Made of Composite Materials. Sakarya University Journal of Science, 25(2), 357-363, DOI: https://doi.org/10.16984/saufenbilder.817605
Access link
http://www.saujs.sakarya.edu.tr/en/pub/issue/60672/817605

Sakarya University Journal of Science 25(2), 357-363, 2021

Parameter Optimization of Frequency Selective Surfaces Made of Composite Materials

Abdullah Oğuz KIZILÇAY*[1]

Abstract

Debye model is used for approximating the frequency dependent complex effective permittivity of the composite structures in filter and shielding applications at microwave frequencies. In Debye model, desired shielding effectiveness (SE) is obtained by determining the Debye parameters using trial and error method. But this may result in wasting time or not converging to an optimum solution. In this work to overcome this problem Debye parameters were optimized by using Differential Evolution (DE) algorithm. A Maxwell Garnett (MG) mixing rule was applied to these optimized parameters to obtain frequency selective surface (FSS) parameters. 12dB shielding threshold was chosen between 0.05 – 5GHz frequency range. In accordance with the obtained parameters of FSS, a structure was designed in CST simulation software and simulations had been conducted to obtain SE results. It was seen that the results obtained from analytical computations agree with those obtained from simulations.

Keywords: Frequency selective surface, Debye model, composite material, differential evolution algorithm

1. INTRODUCTION

Composite structures which include conductive inclusions such as carbon rods, spheres have become widely used materials in electromagnetic (EM) shielding problems. Filters, integrated

optical microwave guides, thin films, memory devices, new generation antennas, radar absorbing materials can be counted as application areas where composite structure are used [1-6]. Covering such a wide usage area makes researchers more involved in this subject.

Currently, many composite shield materials are designed with random parameters and numerically analyzed with software like CST, HFSS, FEKO and etc [7-8]. The obtained results are checked whether they meet expectations, before production process is initiated. However, these commercial simulation programs conducted with trial error method do not bring success and

*Corresponding author: oguzkizilcay@yyu.edu.tr
[1]Van Yuzuncu Yil University, Engineering Faculty, Electrical and Electronics Engineering Department, 65080, Van, Turkey , E-Mail: oguzkizilcay@yyu.edu.tr
ORCID: https://orcid.org/0000-0002-7607-0924

they also waste time. Fortunately, heuristic algorithms have a special place as an alternative way of overcoming similar problems.

One of the simplest optimization heuristic algorithms is Differential Evolution algorithm [9]. It was derived from genetic algorithm which can be come across widely in literature. Compared to its counterparts, DE algorithm is relatively easy to apply on problems. In this work, since there were few parameters to be optimized, DE was used.

The main principle of DE is to find local minimum or local maximum value of cost function. Thus, it would be easy to find maximum shielding with given Debye parameters. However, the main feature of FSS is to shield waves in specific frequency band. Because of that, in our case algorithm will converge to desired shielding effectiveness in 0.5 - 5GHz frequency range.

In literature, design parameters of shield materials developed by using Debye model are determined by trial error method. Also, researchers investigating different mathematical approaches did not make use of optimization method either. Seager [3] in his work produce FSS by sewing fiber on fabric. Mannaa and Aldhaheri [5] proposed FSS design aiming to shield GSM 900 and 1800 MHz frequencies. Ghosh et. al. [10] derived transmission line model for their FSS design. Kiermier and Biebl [6] also developed a transmission line model and calculated cutoff frequencies. They aimed to shield GSM and WLAN frequencies. Wang et al. [4] computed the shielding effectiveness of homogenous composite materials with cylindrical inclusions by FDTD method. They observed frequency selective attributes of composite materials. Nisanci et. al. [11] in their work analyzed the effect of physical and electrical parameters of composite structure on shielding efficiency. The common point of all these studies is that produced FSS models were developed by trial and error method. Therefore, literature lacks analytical or optimized solution in designing FSS structure. This work will be promising in optimizing the parameters needed in FSS design.

Within the scope of the study firstly the boundaries of Debye parameters and of physical parameters of material were defined. After, optimum values were selected from inside the boundaries by DE algorithm. These values were put into MG equations to get physical dimensions of FSS model. Proposed FSS was tested with numerical method FDDT widely used in solving EM problems.

2. MATERIALS AND METHODS

Dielectric materials or composite materials with dielectric properties have low reflection loss and considerably absorption loss [12-14]. The dielectric of the material directly affects its conductivity, the impedance of the environment and thus the propagation of the EM wave. One of the models that associate this relation with the shielding effect is Debye model.

2.1. Debye Parameters in SE calculation

Dielectric varies depending on frequency [15]. The dielectric of the composite material according to the single-term Debye model is defined as

$$\varepsilon_D = \varepsilon_\infty + \frac{\varepsilon_s - \varepsilon_\infty}{1 + j\omega\tau} \quad (1)$$

$$\tau = \frac{1+\sqrt{2}}{2\pi F_{Low}} \quad (2)$$

where ε_s is the static relative permittivity, ε_∞ is the relative high-frequency limit permittivity, τ is the relaxation time, F_{Low} is the lowest boundary and ε_D is the complex frequency dependent relative permittivity of the equivalent homogeneous material described by the single-term Debye model [16-17]. In shielding problems ε_D determines the impedance of the material.

$$Z_m = Z_0/\sqrt{\varepsilon_D} \quad (3)$$

where Z_m is the impedance of the material. Reflection and transmission at the boundaries in depends on the impedance of the material.

$$R_1 = \frac{Z_m - Z_n}{Z_m + Z_n} \quad (4)$$

$$R_2 = \frac{Z_0 - Z_m}{Z_0 + Z_m} \quad (5)$$

$$T_1 = \frac{2Z_m}{Z_m + Z_0} \quad (6)$$

$$T_2 = \frac{2Z_0}{Z_m + Z_0} \quad (7)$$

where $R_{1,2}$ and $T_{1,2}$ are reflection and transmission coefficients respectively.

Total transmittance depends on reflection coefficients $R_{1,2}$ and transmission coefficients $T_{1,2}$. These quantities are defined as [1],[17-18].

$$T = \frac{T_1 T_2 e^{-\gamma_m W}}{1 + R_1 R_2 e^{-2\gamma_m W}} \quad (8)$$

$$\gamma_m = j\omega\sqrt{\mu_0 \varepsilon_0}\sqrt{\varepsilon_D} \quad (9)$$

where γ_m is the propagation constant. And the relation between SE with transmittance is as follows.

$$SE = -20\log(|T|) \quad (10)$$

As can be seen from Equation 2-9, ε_D in the Debye model can be used to determine the SE value. Therefore, it is possible to find the desired SE value by changing the value of ε_D.

Debye parameters and physical properties of FSS describe the flatness and the strength of SE. b_∞ is the parameter that determines the flatness of SE. This parameter is defined as

$$b_\infty = \frac{(\varepsilon_s - \varepsilon_\infty)W}{2 \cdot c_0 \cdot \tau\sqrt{\varepsilon_\infty}} \quad (11)$$

where b_∞ is dependent on ε_s , ε_∞ and W values which will be involved in optimization processes. $b \in [0.8 - 1.6]$ ensures the flatness of shielding line [16] above the threshold between the F_{Low} and F_{High} which were set to 0.5GHz and 5GHz respectively.

2.2. Differential Evolution Algorithm

The algorithm has the following steps: Initialization, Mutation, Recombination, Selection and Termination [9], [21].

2.2.1. Initialization

In this stage constant values are defined as:
Number of individuals, $NP \geq 4$
Crossover ratio, $CR \in [0\ 1]$
Mutation factor, $F \in [0\ 2]$
Generation number, G

2.2.2. Mutation

First, target individual is selected. Then 3 random distinct individuals inside population $x_{r_1,G}$, $x_{r_2,G}$ and $x_{r_3,G}$ are selected so that $r_1 \neq r_2 \neq r_3 \neq target$.

Create a trial individual by adding weighted difference of 2 randomly selected individuals to third one.

$$V = x_{r_1} + F \cdot \left(x_{r_2} - x_{r_3}\right) \quad (12)$$

2.2.3. Recombination

The values of parameters inside trial individual are replaced with the value of corresponding parameter inside target individual with probability CR.

$$u_{j,i,G+1} = \begin{cases} u_{j,i,G+1} & if\ rand_{j,i} \leq CR \ \ or \ \ j = I_{rand} \\ x_{j,i,G} & if\ rand_{j,i} > CR \ \ and \ \ j \neq I_{rand} \end{cases} \quad (13)$$

where $i = 1,2,\dots,NP; j = 1,2,\dots,D;$ $rand_{j,i} \sim U[0\ 1]$ and I_{rand} is a random integer from in $[1,2,\dots,D]$. D is the solution's dimension.

2.2.4. Selection

The calculated cost value of target individual is compared with the one of trial vector V. A vector with better cost value is admitted to the next generation.

2.2.5. Termination

The algorithm terminates when the defined generation number is reached or stopping criteria is met.

2.3. Optimizing Parameters

The main purpose of the optimization is to obtain the physical properties of the shielding material. Additionally, final output must be available in the market or can be produced by use of composites. Therefore, computations must be carried out regarding these cases. For this, boundaries of Debye parameters were chosen specifically.

In order to start the algorithm several configurations must be done. Accordingly, width $W \in [1\ \ 4]mm$, dielectric constant $\varepsilon_\infty \in [1\ 100]$ and Debye parameter $\varepsilon_s \in [1000\ \ 4000]$ was set [16] and DE algorithm parameters were initialized. The pseudocode of the algorithm is given in the Appendix.

As it is seen from the pseudocode the algorithm converges to the solution in iteration T. A variable T was assigned as 20, which was adequate to find the solution. A case of failure may be faced with if only desired shielding is unattainable because of narrow boundaries of Debye parameters. In this case, desired shielding should be lowered or Debye parameters boundaries should be widened. After, algorithm may be initiated from the beginning.

Population size was determined as 20 and they filled with random numbers not exceeding boundaries. Inside iteration, a random target individual was chosen among individuals in population. Once a target individual was chosen it was exposed to mutation and recombination which resulted in new individual called trial vector. Afterwards the fitness of trial vector was evaluated at frequency F_{Low}. The fitness results included SE and b values. If newly found SE was greater than desired SE, then trial vector is reevaluated and SE was checked whether it was greater than desired SE for whole frequency range from F_{Low} to F_{High}. In case of failure, code would run from the beginning of current loop and another target would be chosen for further operations. However, in case of success and if variable b fitted in its defined boundaries then the code will print results and terminate.

3. RESULTS AND DISCUSSION

As a result of code run, Debye parameters were found as $\varepsilon_\infty = 11.056$, $\varepsilon_s = 3826$, $W = 3.97mm$. The host permittivity was chosen as $\varepsilon_e = 11.5$ that is close to permittivity of inclusion. It was determined with accordance of availability of this material. Other physical parameters of shield material was found by evaluating Debye parameters in Maxwell Garnet equations [22-23]. As a result of computation, physical parameters of material were found as $s = W/4$, conductivity $\sigma = 103.93\,S/m$, length $l = 177.7mm$ and radius $r = 0.46mm$. Figure 1a shows physical dimensions of every single inclusion.

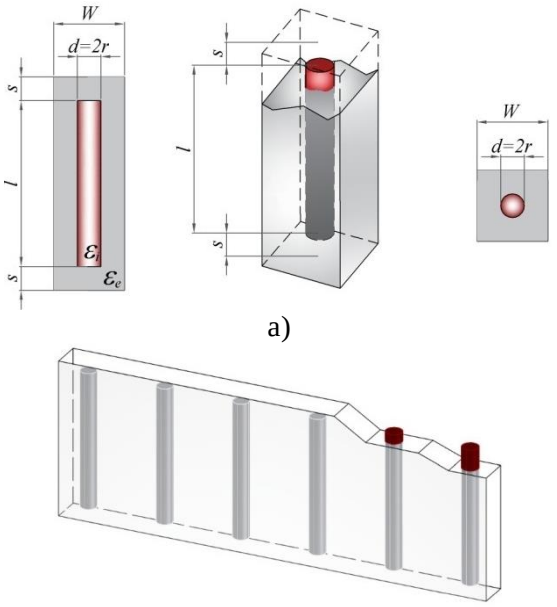

a)

b)

Figure 1. a) Cylindrical inclusion and its extent, b) 3D shielding material

Obtained physical parameters indicated low conductive dielectric material. 3D FSS (Figure 1b) was designed in CST simulation software [24], where electric field polarized plane wave excitation was used. Electric field probe was placed behind the shielding material. After setting other physical parameters, simulation was started (Figure 2).

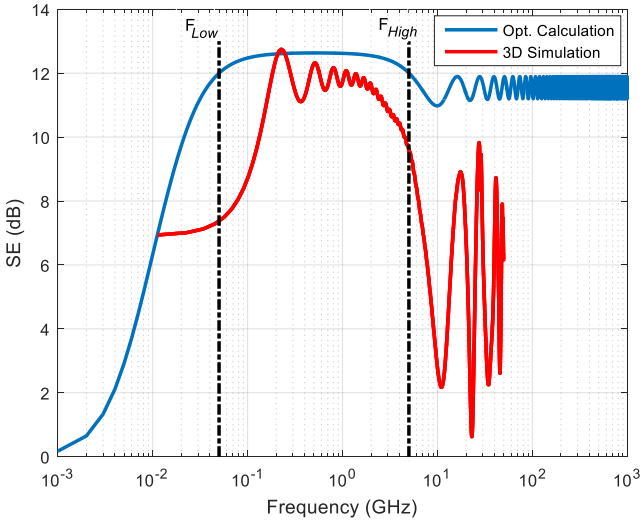

Figure 2. Comparison of Debye model with CST simulation

Debye parameters were evaluated in Eq. 1-10 and obtained SE values were simulated as in Figure 2. It is obvious that SE above threshold is quite flat. This is also guaranteed by value b which was found as 0.98.

In the Figure a red line indicates the simulation result whereas blue line indicates the optimized calculation. As it is seen from Figure, between F_{Low} and F_{High}, CST simulation results are similar to those obtained by analytical computation.

4. CONCLUSION

In this work, despite traditional trial and error method, Debye parameters were optimized with the help of Differential Evolution algorithm and obtained in a much faster and precise way. Afterwards, in order to obtain physical parameters of FSS, these parameters were evaluated in Maxwell Garnett solutions. Then, a shield was modeled and simulated in CST Studio software which analysis EM interference problems with FDTD method. The SE results from proposed work and simulation was compared. It was seen that they nearly overlapped between F_{Low} and F_{High}. It can be concluded that, the performance of thought shield model can be predicted before production. This will save time and ease the computation process.

Appendix

A pseudocode given below is referred in section 2.3. It describes an implementation of DE algorithm on Debye parameters.

initialize algorithm, define Debye parameters and set their boundaries
for (iteration from 1 to T)
  for (target from 1 to population)
    determine target
    follow mutation and recombination steps
    evaluate trial vector fitness at F_{Low}
    if ($SE \geq desiredSE$)
      target = trial
      for (frequencies from F_{Low} to F_{High})
        evaluate trial vector fitness at F
        if($SE < desiredSE$)
          set flag
          break loop
        end
      end
      if(not set flag && $b \in [0.8 - 1.6]$)
        set foundFlag
        break loop
      end
    end
  end
  if(foundFlag)
    break loop
  end
end
print target

Funding

The author(s) has no received any financial support for the research, authorship or publication of this study.

The Declaration of Conflict of Interest/Common Interest

No conflict of interest or common interest has been declared by the authors.

Authors' Contribution

The authors contributed equally to the study

The Declaration of Ethics Committee Approval

This study does not require ethics committee permission or any special permission

The Declaration of Research and Publication Ethics

The authors of the paper declare that they comply with the scientific, ethical and quotation rules of SAUJS in all processes of the paper and that they do not make any falsification on the data collected. In addition, they declare that Sakarya University Journal of Science and its editorial board have no responsibility for any ethical violations that may be encountered, and that this study has not been evaluated in any academic publication environment other than Sakarya University Journal of Science.

REFERENCES

[1] B. Kanberoğlu, M. H. Nisanci, A. Ş. Demirkıran. "Electromagnetic characterization of ceramic material produced with natural zeolite", Materials Science in Semiconductor Processing, Vol.38, pp.352, 2015.

[2] M. H. Nisanci, F. De Paulis, D. Di Febo, and A. Orlandi, "Synthesis of composite materials with conductive aligned cylindrical inclusions," *Prog. Electromagn. Res. Symp.*, no. May 2015, pp. 646–649, 2012.

[3] R. D. Seager, A. Chauraya, J. Bowman, M. Broughton, and N. Nimkulrat, "Fabrication of fabric based Frequency Selective Surfaces (FSS)," *8th Eur. Conf. Antennas Propagation, EuCAP 2014*, no. September 2017, pp. 1978–1980, 2014.

[4] J. Wang, B. Zhou, L. Shi, C. Gao, and B. Chen, "Analyzing the electromagnetic performances of composite materials with the FDTD method," *IEEE Trans. Antennas Propag.*, vol. 61, no. 5, pp. 2646–2654, 2013.

[5] Y. Mannaa and R. W. Aldhaheri, "New dual-band frequency selective surface for GSM shielding in secure-electromagnatic buildings using square loop fractal configurations," *Mediterr. Microw. Symp.*, pp. 1–4, 2017.

[6] W. Kiermeier and E. Biebl, "New dual-band frequency selective surfaces for GSM frequency shielding," *Proc. 37th Eur. Microw. Conf. EUMC*, no. October, pp. 222–225, 2007.

[7] S. Kovar, J. Valouch, H. Urbancokova, M. Adamek, and V. Mach, "Simulation of Shielding Effectiveness of Materials Using CST Studio," *Wseas Trans. Commun.*, vol. 16, pp. 131–136, 2017.

[8] E. Delihasanlar and A. H. Yuzer, "Wearable Textile Fabric Based 3D Metamaterials Absorber in X-Band," vol. 35, no. 2, pp. 230–236, 2020.

[9] R. Storn and K. Price, "Differential Evolution - A Simple and Efficient Heuristic for Global Optimization over Continuous Spaces," *J. Glob. Optim.*, vol. 11, pp. 341–359, 1997.

[10] S. Ghosh and S. Lim, "Fluidically reconfigurable multifunctional frequency-selective surface with miniaturization Characteristic," *IEEE Trans. Microw. Theory Tech.*, vol. 66, no. 8, pp. 3857–3865, 2018.

[11] M. H. Nisanci, F. De Paulis, D. Di Febo, and A. Orlandi, "Sensitivity analysis of electromagnetic transmission, reflection and absorption coefficients for biphasic composite structures," *IEEE Int. Symp. Electromagn. Compat.*, vol. 0, pp. 438–443, 2014.

[12] D.D.L. Chung, "Materials for Electromagnetic Interference Shielding," *J. Mater. Eng. Perform.*, vol. 9, no. 3, pp. 350–354, 2000.

[13] Y. Akinay and A. O. Kizilcay,

"Computation and modeling of microwave absorbing CuO/graphene nanocomposites" *Polym. Compos.*, vol. 41, no. 1, pp. 227–232, 2020.

[14] S. Kashi, R. K. Gupta, T. Baum, N. Kao, and S. N. Bhattacharya, "Dielectric properties and electromagnetic interference shielding effectiveness of graphene-based biodegradable nanocomposites," *Mater. Des.*, vol. 109, no. February 2018, pp. 68–78, 2016.

[15] E. Delihasanlar and A. H. Yuzer, "Simulation modelling and calculation of dielectric permittivity of Opuntia at 1.7–2.6 GHz," *J. Microw. Power Electromagn. Energy*, vol. 51, no. 2, pp. 150–158, 2017.

[16] F. De Paulis, M. H. Nisanci, A. Orlandi, M. Y. Koledintseva, and J. L. Drewniak, "Design of homogeneous and composite materials from shielding effectiveness specifications," *IEEE Trans. Electromagn. Compat.*, vol. 56, no. 2, pp. 343–351, 2014.

[17] C. D. Erbaş and S. Kent, "Ekranlama Verimliliği Karakteristiği Baz Alinarak Madde Sentezlenmesi İçin Analitik Bir Yaklaşim," *Uludağ Univ. J. Fac. Eng.*, vol. 22, no. 1, pp. 95–95, 2017.

[18] N. N. Rao, *Elements of Engineering Electromagnetics*, Fifth Ed. Upper Saddle River, NJ: Prentice-Hall, Inc, 2000.

[19] L. Jebaraj, C. Venkatesan, I. Soubache, and C. C. A. Rajan, "Application of differential evolution algorithm in static and dynamic economic or emission dispatch problem: A review," *Renew. Sustain. Energy Rev.*, vol. 77, no. March 2020, pp. 1206–1220, 2017.

[20] H. Lei, L. Li, and C. H. Wu, "Evolutionary model selection and parameter estimation for protein-protein interaction network based on differential evolution algorithm," *IEEE/ACM Trans. Comput. Biol. Bioinforma.*, vol. 12, no. 3, pp. 622–631, 2015.

[21] D. Karaboğa and S. Ökdem, "A simple and global optimization algorithm for engineering problems: Differential evolution algorithm," *Turkish J. Electr. Eng. Comput. Sci.*, vol. 12, no. 1, pp. 53–60, 2004.

[22] A. . De Paulis, Francesco; Nisanci, M. Hilmi; Koledintseva, M.Y.;Drewniak, J.L.; Orlandi, "Derivation of Homogeneous Permittivity of Cal Inclusions for Causal Electromagnetic," vol. 37, no. July 2011, pp. 205–235, 2012.

[23] D. Micheli, A. Vricella, R. Pastore, and M. Marchetti, "Synthesis and electromagnetic characterization of frequency selective radar absorbing materials using carbon nanopowders," *Carbon N. Y.*, vol. 77, pp. 756–774, 2014.

[24] Computer Simulation Technology, CST Studio Suite 2019, Available: http://www.cst.com/

SAKARYA ÜNİVERSİTESİ
FEN BİLİMLERİ ENSTİTÜSÜ DERGİSİ

Sakarya University Journal of Science
SAUJS

e-ISSN 2147-835X | Period Bimonthly | Founded: 1997 | Publisher Sakarya University |
http://www.saujs.sakarya.edu.tr/en/

Title: Synthesis and Characterization of Dimeric Thio-Schiff Bases by Nano Cerium Oxide and Examination of Their Antimicrobial Activities

Authors: Aslıhan DALMAZ, Sefa DURMUŞ, Gorkem DULGER, Başaran DÜLGER

Recieved: 2020-05-15 15:05:54

Accepted: 2021-02-04 21:30:27

Article Type: Research Article

Volume: 25
Issue: 2
Month: April
Year: 2021
Pages: 364-378

How to cite
Aslıhan DALMAZ, Sefa DURMUŞ, Gorkem DULGER, Başaran DÜLGER; (2021), Synthesis and Characterization of Dimeric Thio-Schiff Bases by Nano Cerium Oxide and Examination of Their Antimicrobial Activities. Sakarya University Journal of Science, 25(2), 364-378, DOI: https://doi.org/10.16984/saufenbilder.737671
Access link
http://www.saujs.sakarya.edu.tr/en/pub/issue/60672/737671

Sakarya University Journal of Science 25(2), 364-378, 2021

Synthesis and Characterization of Dimeric Thio-Schiff Bases by Nano Cerium Oxide and Examination of Their Antimicrobial Activities

Aslıhan DALMAZ*[1], Sefa DURMUŞ[1], Gorkem DULGER[1], Başaran DÜLGER[1]

Abstract

In this work, firstly, CeO_2 nanoparticles, which can be used as catalysts in many reactions, were synthesized by preparing aqueous solution of cerium(III) nitrate hexahydrate in basic medium. In the second step, the synthesis of dimeric thio Schiff bases was carried out using two different methods. Effect of catalyst on some parameters such as reaction time and yield of product were investigated. The antimicrobial activities of the ligands have been screened in vitro against the organisms *Acinetobacter baumannii*, *Escherichia coli*, *Klebsiella pneumoniae* (Gram negative bacteria), *Staphylococcus aureus*, *Staphylococcus epidermidis*, *Enterococcus faecalis*, *Bacillus cereus* (Gram positive bacteria) and *Candida albicans*, *C. tropicalis*, *C. guilliermondii*, *C. glabrata* by Disc Diffusion and Microdilution methods. At the same time, antimicrobial activities of ligands were compared to standard antibiotics (Cefotaxime, Amoxicillin/clavulanic acid, Posacanazole, Nystatin and Gentamicin). Generally, the results obtained in this research showed that all tested ligands exhibited more effect towards Gram positive bacteria and *Candida* species as compared to standard antibiotics.

Keywords: Anti-bacterial, Anti-candidal, Ceria, Disulphide-Schiff bases, Nano-catalyst

1. INTRODUCTION

One of the materials that has remarkable applications in the fields of catalysis, photochemistry and materials science is cerium oxide (CeO_2). [1,2]. Ceria has the ability to undergo a simple conversion between "IV" and "III" formal oxidation states. [3]. The reactions of various ligands containing metal ions and disulfide groups can be found in the literature. In the advancing years, disulphide have been important compounds in terms of both synthetic and biological [4,5]. Besides, different types of Schiff bases have been studied due to their remarkable aspects [6,7]. Moreover, these compounds exhibit antibacterial and antifungal

* Corresponding Author: aslihandalmaz91@gmail.com
[1] Duzce University, Faculty of Medicine, Department of Natural and Herbal Products/Cosmetic Products, Duzce.
E-Mail: aslihandalmaz91@gmail.com, ORCID: https://orcid.org/ 0000-0002-1691-2616,
E-Mail:sefadurmus@duzce.edu.tr, ORCID: https://orcid.org/0000-0001-6974-513X
E-Mail:gorkemdulger@duzce.edu.tr, ORCID: https://orcid.org/0000-0002-1506-1549
E-Mail:basarandulger@duzce.edu.tr, ORCID: https://orcid.org/0000-0002-3184-2652

activity as well as their photochromic properties. [8-11]. In recent years, antibiotic resistance has become a major problem. The World Health Organization (WHO) has said that the spread of deadly superbugs is now a reality. Bugs have developed and have become resistant to antibiotics and other drugs [12,13]. Therefore, in recent years, all scientists have been searching for new antibiotics.

In our study, thio-Schiff bases were synthesized both without catalyst and catalyst (with CeO_2 nanoparticles) through reaction of the 2,2'-diaminodiphenyl disulfide amine compound with various aldehydes having different substituent groups. The structures of thio-Schiff bases obtained were characterized by various spectroscopic methods. In addition, we have studied antibacterial and anti-Candidal activities of thio-Schiff bases. The antimicrobial activities of compound have been screened in vitro against the human pathogens by disc diffusion methods.

2. MATERIALS AND METHODS

2.1. General

The morphology and crystal specialties of synthesized CeO_2 nanocatalyst were characterized. Ligands structures were illustrated by Fourier Transform Infrared Spectroscopy (FTIR), Nuclear Magnetic Resonance Spectroscopy (NMR) and Mass Spectroscopy (MS). Melting points were defined with the Stuart apparatus. FTIR results were recorded by Perkin Elmer spectrometer. The average of the wave numbers was taken in the spectrum range of 550-4000 cm^{-1}. The ^1H NMR spectra were recorded $CDCl_3$ on a Bruker spectrometer λ-400 MHz. The ^{13}C NMR spectra were recorded in $CDCl_3$ and DMSO-d_6 on Bruker spectrometer operating at 101 MHz. All chemical shifts were reported in δ (ppm) using TMS as an internal standard. Mass spectra were obtained in a AB SCIEX 4000 Q-TRAP LC-MS/MS instrument. Elemental analyses were carried out a Thermo Scientific Flash 2000.

The compounds 2-aminothiophenol, benzaldehyde, 2-thiophen carbaldehyde, 3-methyl-2-thiophen carbaldehyde, 5-methyl-2-thiophen carbaldehyde, sodium hydroxide and solvents were purchased from Merck(Germany), and cerium(III) nitrate hexahydrate, *o*-tolualdehyde, *p*-tolualdehyde were purchased from Acros (Acros Organics NJ, USA), and 2-hydroxy-1-naphthaldehyde was purchased from Sigma-Aldrich (Germany), and CeO_2 nanoparticles were prepared according to previous literatures [13].

2.2. Chemistry

Synthesis of 2,2'-diaminodiphenyl disulfide was carried out by exposure to 2-aminothiophenol oxidation **(1)** (method B). Ligands were synthesized according to previous studies [14,15]. It has been observed that the (-S-CH_2-CH_2-S-) disulfide compounds containing two atoms of carbon-carbon ethane between two sulfur atoms have been synthesized in previous studies [16-18]. But, in this study, nano-CeO_2 catalyst (method A) was used in the synthesis of dimeric thio-Schiff bases as a new method, different from the previous study.

*2,2'-disulfanediyldianiline **(2)***

Shiny yellow solid (EtOH), mp 90–92 °C. IR (ATR): ν_{max} 3375, 1471, 744, cm^{-1}. ^{1}HNMR (400 MHz, $CDCl_3$, δ): 7.19 – 7.07 (m, 2H), 6.66 (dd, 1H,*J* = 8.5, 1.3 Hz), 6.56 (td, 1H, *J* = 7.5, 1.2 Hz), 4.31 (s, 2H). ^{13}C NMR (101 MHz, $CDCl_3$,δ): 148.7, 136.9, 131.7, 118.8, 118.2, 115. MS (*m/z)*: 249.3 $[M+H]^+$. Combustion analysis for $C_{12}H_{12}N_2S_2$: Calculated. C 58.03, H 4.87, N 11.28, S 25.82; found C 58.01, H4.69, N 11.14, S 26.16.

*(NZ,N'Z)-2,2'-disulfanediylbis(N-benzylidene aniline) **(3)***

Light yellow solid (EtOH), mp 133 °C. IR (ATR) ν_{max} 1617, 1459, 761, 556 cm^{-1}. ^1H NMR (400 MHz, $CDCl_3$, δ): 8.47 (s, 1H), 7.99 – 7.96 (m, 2H), 7.66 (dd, 1H, *J* = 7.7, 1.5 Hz), 7.48 (d, 1H, *J* = 1.8 Hz), 7.17 (dd, 1H, *J* = 7.4, 1.6 Hz), 7.14 (dd, 1H, *J* = 7.6, 1.6 Hz), 7.02 (d, 1H, *J* = 1.5 Hz). ^{13}C NMR (101 MHz, $CDCl_3$,δ): 160.05, 148.96, 135.99, 132.06, 131.76, 129.16, 128.86, 126.96,

126.02, 117.26. MS (*m/z)*: 425.5 $[M+H]^+$. Combustion analysis for $C_{26}H_{20}N_2S_2$: Calculated. C 73.55, H 4.75, N 6.60, S 15.10; found C 73.71, H 4.59, N 6.47, S 15.23.

3,3'-((1Z,1'Z)-((disulfanediylbis(2,1-phenylene)) bis(azanylylidene))bis(methanylylidene))bis(nap hthalen-2-ol) ***(4)***

Bright orange solid (EtOH), mp 210 °C. IR (ATR)ν_{max} 1610, 1462, 1278, 747, 556 cm^{-1}. ^1H NMR (400 MHz, $CDCl_3$, δ): 14.94 (s, 1H), 9.43 (s, 1H), 8.17 (d, 1H, *J* = 8.5 Hz), 7.87 (d, 1H, *J* = 9.0 Hz), 7.79 (d, 1H, *J* = 7.8 Hz), 7.71 (dd, 1H, *J* = 7.7, 1.0 Hz), 7.55 (t, 1H, *J* = 7.2 Hz), 7.42 – 7.35 (m, 1H), 7.24 – 7.21 (m, 1H), 7.21 – 7.18 (m, 1H). ^{13}C NMR (101 MHz, DMSO-d_6,δ):164.8, 158.7, 145.1, 136.1, 132.6, 129.4, 128.9, 128.6, 128.0, 127.6, 127.4, 127.2, 123.7, 120.8, 119.9, 119.0, 109.4. MS (*m/z)*: 557.53 $[M+H]^+$. Combustion analysis for $C_{34}H_{24}N_2O_2S_2$: Calculated. C 73.35, H 4.35, N 5.03, O 5.75, S 11.52; found C73.17, H4.44, N 5.12,O 5.66, S 11.61.

(NZ,N'Z)-2,2'-disulfanediylbis(N-(thiophen-2-ylmethylene)aniline) ***(5a)***

Light brown solid (EtOH), mp 166 °C. IR (ATR) ν_{max} 1604, 1459, 749, 575 cm^{-1}. ^1H NMR (400 MHz, $CDCl_3$,δ): 8.55 (s, 1H), 7.65 (dd, 1H, *J* = 7.7, 1.5 Hz), 7.53 (d, 1H, *J* = 5.0 Hz), 7.51 (d, 1H, *J* = 3.6 Hz), 7.15 (dd, 2H, *J* = 7.4, 1.7 Hz), 7.12 (dd, 1H, *J* = 3.4, 1.4 Hz), 7.01 (dd, 1H, *J* = 7.4, 1.6 Hz). ^{13}C NMR (101 MHz, $CDCl_3$,δ):152.75, 148.48, 142.78, 132.57, 132.16, 131.22, 127.80, 126.91, 126.19, 117.30. MS (*m/z)*: 437.2 $[M+H]^+$. Combustion analysis for $C_{22}H_{16}N_2S_4$: Calculated. C 60.52, H 3.69, N 6.42, S 29.37; found C 60.39, H 3.82, N 6.35, S 29.44.

(NZ,N'Z)-2,2'-disulfanediylbis(N-((3-methylthio phen-2-yl)methylene)aniline) ***(5b)***

Shiny yellow solid (EtOH), mp 165 °C. IR (ATR) ν_{max} 2872, 1607, 1454, 751, 569 cm^{-1}. ^1H NMR (400 MHz, $CDCl_3$,δ): 8.60 (s, 1H), 7.65 (dd, 1H, *J* = 7.7, 1.4 Hz), 7.25 (dd, 2H, *J* = 10.9, 9.8 Hz), 7.20 (dd, 1H, *J* = 6.0, 1.6 Hz), 7.18 – 7.12 (m, 1H), 6.86 (t, 1H, *J* = 7.5 Hz), 2.33 (s, 3H). ^{13}C NMR (101 MHz, $CDCl_3$, δ):163.01, 159.49, 134.72, 131.62, 130.36, 127.64, 127.53, 126.52, 118.78, 118.45, 117.61, 15.68. MS (*m/z)*: 465.1 $[M+H]^+$. Combustion analysis for $C_{24}H_{20}N_2S_4$: Calculated. C 62.03, H 4.34, N 6.03, S 27.60; found C 62.11, H 4.26, N 6.13, S 27.50.

(NZ,N'Z)-2,2'-disulfanediylbis(N-((5-methylthio phen-2-yl)methylene)aniline) ***(5c)***

Shiny yellow solid (EtOH), mp 194 °C. IR (ATR)ν_{max} 2872,1608, 1454, 751, 569cm^{-1}. ^1H NMR (400 MHz, $CDCl_3$,δ): 8.47 (s, 1H), 7.64 (dd, 1H, *J* = 7.7, 1.5 Hz), 7.32 (d, 1H, *J* = 3.6 Hz), 7.16 (td, 1H, *J* = 7.4, 1.5 Hz), 7.11 (td, 1H, *J* = 7.5, 1.5 Hz), 7.01 (dd, 1H, *J* = 7.5, 1.4 Hz), 6.81 (dd, 1H, *J* = 3.5, 0.8 Hz), 2.56 (s, 3H). ^{13}C NMR (101 MHz, $CDCl_3$, δ): 152.61, 148.61, 146.94, 140.76, 133.12, 132.10, 126.72, 126.61, 126.34, 125. 98, 117.19, 16.07. MS (*m/z)*: 465.1 $[M+H]^+$. Combustion analysis for $C_{24}H_{20}N_2S_4$: Calculated. C 62.03, H 4.34, N 6.03, S 27.60; found C 62.09, H 4.28, N 6.08, S 27.55.

(NZ,N'Z)-2,2'-disulfanediylbis(N-(2-methyl

benzylidene)aniline) ***(6a)***

Shiny, light-colored yellow solid (EtOH), mp 141-145 °C. IR (ATR) ν_{max} 2891, 1615, 1457, 754, 573cm^{-1}. ^1H NMR (400 MHz, $CDCl_3$,δ):8.76 (s, 1H), 8.13 (dd, 1H, *J* = 7.6, 1.4 Hz), 7.67 (dd, 1H, *J* = 7.8, 1.4 Hz), 7.40 – 7.35 (m, 1H), 7.32 (t, 1H, *J* = 6.9 Hz), 7.23 (dd, 1H, *J* = 9.2, 4.7 Hz), 7.19 (dd, 1H, *J* = 7.5, 1.5 Hz), 7.14 (td, 1H, *J* = 7.6, 1.5 Hz), 7.03 (dd, 1H, *J* = 7.6, 1.4 Hz), 2.66 (s, 3H). ^{13}C NMR (101 MHz, $CDCl_3$,δ): 159.25, 149.58, 139.08, 133.93, 132.04, 131.30, 131.21, 129.21, 126.95, 126.80, 126.41, 126.00, 117.26, 19.99. MS (*m/z)*: 453.3 $[M+H]^+$. Combustion analysis for $C_{28}H_{24}N_2S_2$: Calculated. C 74.30, H 5.34, N 6.19, S 14.17; found C 74.19, H 5.45, N 6.14, S 14.22.

(NZ,N'Z)-2,2'-disulfanediylbis(N-(4-methyl benzylidene)aniline) ***(6b)***

Shiny, light-colored yellow solid (EtOH), mp158-160°C. IR (ATR) ν_{max}2915, 1623, 1460, 753, 573cm^{-1}. ^1H NMR (400 MHz, $CDCl_3$, δ): 8.41 (s, 1H), 7.85 (d, 2H, *J* = 8.1 Hz), 7.65 (d, 1H, *J*= 7.8 Hz), 7.15 (dd, 1H, *J* =7.5, 1.5 Hz), 7.12 (dd, 1H, *J* = 7.6, 1.5 Hz), 7.01 (dd, 1H, *J* = 7.5, 1.4 Hz),

2.39 (s, 3H). ^{13}C NMR (101 MHz, $CDCl_3$, δ): 160.00, 158.20, 140.70, 138.00, 133.40, 130.70, 129.10, 127.50, 126.00, 117.10, 21.30. MS (*m/z)*: 453.3 $[M+H]^+$. Combustion analysis for $C_{28}H_{24}N_2S_2$: Calculated. C 74.30, H 5.34, N 6.19, S 14.17; found C 74.22, H 5.42, N 6.12, S 14.24.

2.3. Antimicrobial Screening

Test microorganisms

The *in vitro* antimicrobial studies were carried out with three Gram-negative bacteria (*Acinetobacter baumannii, Escherichia coli, Klebsiella pneumoniae*), four Gram positive bacteria (*Staphylococcus aureus, Staphylococcus epidermidis, Enterococcus faecalis, Bacillus cereus*) and four Candida species (*Candida albicans, C. tropicalis, C. guilliermondii, C. glabrata*) obtained from the Microbiology Research Laboratory of the Duzce University Department of Biology.

Disk diffusion method

In this study, test microorganisms isolated from patients admitted to Düzce University Medical Faculty Hospital were used. Antimicrobial susceptibility testing was performed using the disc diffusion method according to the protocol applied by CLSI (Clinical and Laboratory Standards Institute) [19,20]. For this purpose, sterilized antibiotic discs (6 mm) were used. Fresh stock solutions (30 μgL^{-1}) prepared from DMSO (dimethyl sulfoxide) of ligands (**2-6b**) were used. To eliminate the solvent effect on bacterial and fungal growth, a control test was performed with DMSO-assisted test medium containing the same procedures as the ligands. All test bacteria in the study were incubated for 24 hours at 30-35 °C in Brain Heart Infusion Water (BH). Inoculums containing $1.5x10^8$ cfu/mL bacterial cells or yeast cells were spread on Mueller Hinton Agar plates (1 mL inoculums for each plate). The discs were impregnated with 50 µL of each ligands solution. Discs were placed on agar. Incubated for bacteria and yeast at 35 °C (24 hours) and 25 °C (72 hours), respectively. Concurrently, the antibacterial and anti-candidal activities of ligands **2-6b** were compared to standard antibiotics. Cefotaxime and Amoxicillin/clavulanic acid for antibacterial activity were tested against the pathogenic bacteria and Posaconazole was tested against pathogenic yeasts. All experiments were repeated three times. Average values were recorded as the last reading.

Dilution method

Based on the procedure started out in the Clinical Microbial Handbook. Following the procedure in this Handbook, a clinical micro-dilution was prepared and a screening for antibacterial and antifungal activities was performed [21]. All bacteria were incubated and activated by inoculation for 24 hours at 30 °C, yeasts were incubated in Malt Extract for 48 hours. The ligands were dissolved in DMSO (2 $mgmL^{-1}$) and diluted using carefully adjusted Mueller Hinton Broth (Oxoid). Twice-fold serial concentrations of ligands were preferred to result MIC between 200 and 1.56$mgmL^{-1}$. Cultures were grown at 37 °C (20 h). The final inoculation (inoculums) was about 106 cfu mL^{-1}. Test cultures were incubated at 37 °C (24 h). The lowest concentrations of antimicrobial agents that result in complete inhibition of the micro-organisms were represented as MIC ($mgmL^{-1}$). In each case triplicate tests were performed. The results were expressed as means.

3. RESULTS AND DISCUSSION

3.1. Chemistry

As starting material **(2)** 2,2'-disulfanediyldianiline was selected to synthesize disulphide containing thio-Schiff bases. The synthesis of thio-Schiff bases **(3-6b)** were carried out by reacting ligand **2** with several different aldehydes called benzaldehyde, 2-hydroxy-1-naphthaldehyde, 2-thiophen carbaldehyde, 3-methyl-2-thiophen carbaldehyde, 5-methyl-2-thiophen carbaldehyde, 3-methyl benzaldehyde, 5-methyl benzaldehyde, respectively. At the same time, the syntheses of these thio-Schiff bases were carried out in two ways using no catalyst and using CeO_2 nanocatalyst. The methods used to obtain the targeted ligands are shown in (Figure 1 and 2). In the reaction performed in the presence

of nanocatalyst, it was determined that the reaction rate and efficiency increased. (Table 1).

In the determination of structures of the ligands, the vibrational spectra of the ligands synthesized with the literature data were compared [22]. Some of the thio-Schiff base ligands in this work have been functional groups such as -NH_2, -OH, -CH_3. The groups -CH_3 in the structures of ligands **(5b-5c)** and **(6a-6b)** are in different positions. The characteristic peaks of $\nu(CH_3)$ in the methyl group are seen in the range of 2915-2872 cm^{-1}. Also, the sharp stretching vibrations of group ν(C=N) which is the basis of Schiff bases, are observed in the range of 1623-1604 cm^{-1} [22].

Specific peaks of $\nu(C\text{-}C_{Ar})$, $\nu(C\text{-}O_{Ar})$, ν(C-S) and ν(S-S) are observed in the range of 1471-1457, 1278, 761-744, 575-556 cm^{-1}, respectively. It is seen that the vibration values change depending on the presence of different groups such as -CH_3, -OH, -NH_2 in the structures of the ligands and the increase of the aromatics. In addition to having sharp peaks, there are differences in the intensity of functional groups depending on their ortho and para orientation. ^{1}H NMR spectra of the ligands synthesized were recorded using DMSO-d_6, $CDCl_3$ solvents, and the peaks of these solvents were determined as 7.25 and 2.51 ppm. When the ^{1}H NMR spectra of synthesized ligands are examined, there are some specific proton signals that are noted. From these, the signals of the azomethine (H-C = N) proton were observed as a proton singlet in the range of 8.41-9.43 ppm [23,24]. The protons of the hydroxy and methyl groups in the structure of some ligands were found as a singlet with chemical shifts of 14.94 ppm and 2.33-2.66 ppm, respectively. The protons belonging to the aromatic ring were observed as dublets, triplets and multiplets between 8.17 and 6.56 ppm. When the ^{13}C NMR spectra of the ligands synthesized were examined, it was found that the aromatic carbons were in the region of 110.02-159.49 ppm depending on the substituent groups [22,25]. It was also found that the carbon atoms bound to the azomethine group were found in the region 152.61-163.01 ppm, and the methyl group carbons were found in the region 15.68-21.30 ppm.

Although all the compounds were obtained with high efficiency in both methods, the yields were increased highly with nanocatalyst method, and the reaction time for several hours decreased to the minute. The authenticities of (**2-6b**) ligands were checked with mixing TLC, melting point and NMR spectrum values.

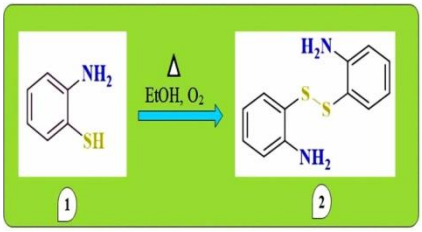

Figure 1 Demonstration of compound 2 synthesis

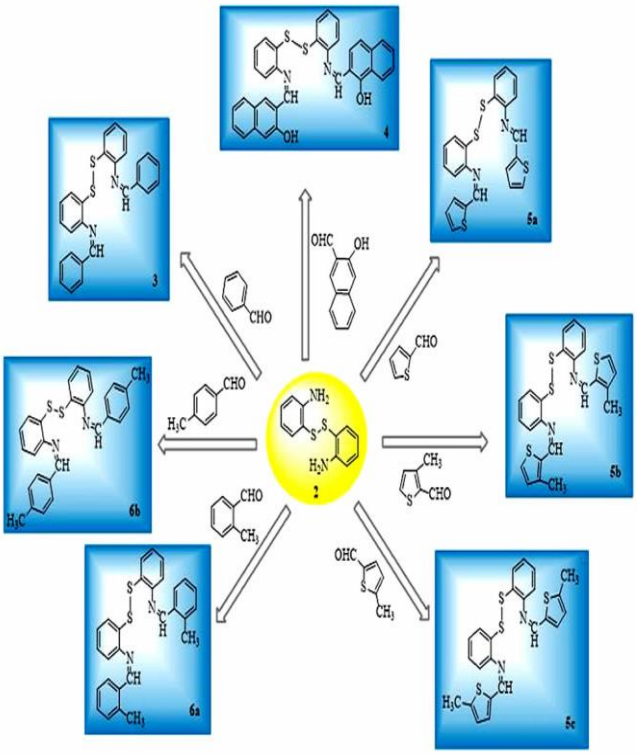

Figure 2 Synthesis of disulphide Schiff base ligand derivatives

Table 1 Structures of synthesized disulphide-Schiff base ligands and reaction parameters (synthesis time, yield)

Entry	Structure	Yield (%) Method (A)	Yield (%) Method (B)	Time (min.) Method (A)	Time (h.) Method (B)	Entry	Structure	Yield (%) Method (A)	Yield (%) Method (B)	Time (min.) Method (A)	Time (h.) Method (B)
2	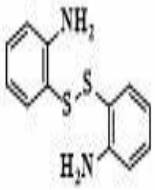	-	75	-	9	5b	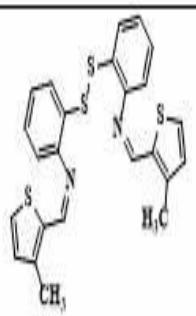	94	85	15	6
3	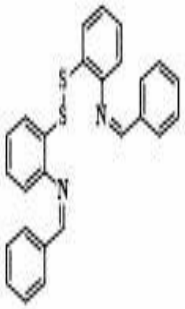	88	65	15	6	5c	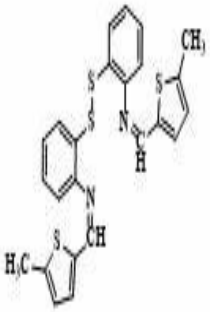	97	80	15	6
4	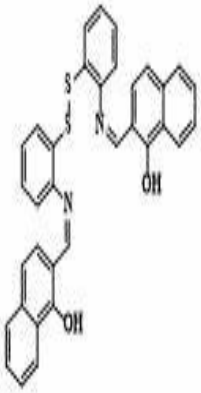	98	87	15	4	6a	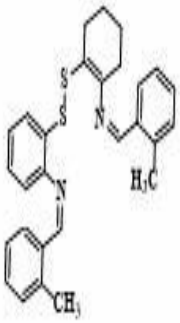	95	80	15	5
5a	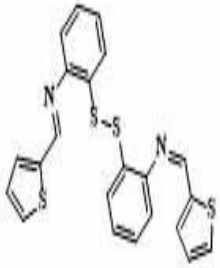	92	84	15	17	6b	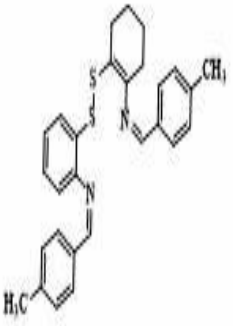	98	86	15	6

3.2. Biological Activity

Antibacterial and anti-Candidal screening

The results for in vitro antibacterial and anti-Candidal activities of ligands together with the inhibition zone values and MIC values of standard drugs are summarized in (Table 2-3 and Figure 3-6). Researchers have been reported that aromatic substituent at different positions in some Schiff compounds show different electronic characteristics and biological activity [12].

The ligands **2-6b** were tested against Gram negative bacteria (*A. baumannii*, *E. coli* and *K. pneumaniae*) and Gram positive bacteria (*S. aureus, S. epidermidis, E. faecalis* and *B. cereus*) at concentrations 30 μg/mL. Generally, the disc diffusion results showed that all tested ligands exhibited more effect towards Gram positive bacteria than Gram negative bacteria (Table 2). Ligand **2** was found to be more effective than all ligands (**3**, **4**, **5a**, **5b**, **5c**, **6a**, **6b**) and standard antibiotics (CTX30, AMC30). In a previous study, researchers reported that the compound 2,2'-disulfanedidyldianiline, which contains sulfur and nitrogen [25], has a toxic effect on bacteria [8]. Similarly, it was determined that the compound obtained in our study showed antimicrobial activity against bacteria and yeast. Ligand **3**, **5a** and **5c** have shown a strong antibacterial effect than those of the standard antibiotics CTX30 and AMC30 against *S. epidermidis* and *E. faecalis*. Antibacterial effects of ligand **5a** and **5b** are equivalent to AMC30 against *E. faecalis*. In addition, ligand **4**, **5a** and **5 c**are more potent to CTX30 against *B. cereus*. Ligand **5a** has no effect against *A. baumannii*. It has significant activity against *E. coli* and *K. pneumaniae* as compared to CTX30 but it has low effect against the same bacteria as compared to AMC30. Ligand **6a** and **6b** have a low effect against *A. baumannii* than those of AMC30 and this effect higher than those of CTX30. The same ligands were also found to be more effective against other tested bacteria as compared to CTX30. But these ligands have been less effective than AMC30 against all test bacteria.

For instance, ligand **2** showed high activity against all Gram negative bacteria (1.56 $mgmL^{-1}$), than did the reference Gentamycin on the same bacteria and Gram positive bacteria such as *S. epidermidis* and *E. faecalis* (1.56 $mgmL^{-1}$). Against Gram-positive bacteria *Staphylococcus aureus* and *B. cereus,* ligand **2** has shown a potential antibacterial activity (3.13 $mgmL^{-1}$), as compared to standard antibiotic Gentamycin. Besides, ligand **3** (3.13 $mgmL^{-1}$), **4** (6.25 $mgmL^{-1}$), **5a** (6.25 $mgmL^{-1}$) have more potent effects than those of the standard reference antibiotic Gentamycin against *S. epidermidis*, while ligand **3**, **4**, **5a**, **5b** and **5c** equivalent to Gentamycin effects (6.25 $mgmL^{-1}$). Notably, Ligand **6a** and **6b** (3.13 $mgmL^{-1}$) have shown a strong antibacterial activity as compared to Gentamycin (6.25 $mgmL^{-1}$). Similarly, the same ligand shows a superior antifungal activity against *C. Guilliermondii* (0.78 $mgmL^{-1}$) than occurred with the reference Nystatin (Table 3). Against *C. albicans* and *C. tropicalis* (1.56 $mgmL^{-1}$), *C. Glabrata* (3.13 $mgmL^{-1}$), ligand **2** is equivalent to the reference antifungal antibiotic Nystatin. The other ligands were far below than the reference antifungal antibiotics.

Presence of a strong electron donor methyl group attached to the benzene ring is thought to increase both antibacterial [27] and anti-Candidal activity. It has been determined that groups with para position have antibacterial effect against *S. aureus* [13]. In our study, thio-Schiff bases (**5b**, **5c**, **6a**, **6b**) containing methyl groups have been para position and ortho position are showed same effect with standard antibiotic against *S. aureus*. [28].

According to the anti-Candidal activity results, ligand **2** show improved anti-Candidal activity compared to the other test ligands on all test yeast, particularly against *C. guilliermondii*. This ligand exhibit about the same antifungal activity against *C. tropicalis* and *C. albicans*. Other test ligands tested in this study were compared to Posaconazole (PCZ 5 μg) under the experimental conditions given. Interestingly, it is either very weakly effective or has no effect on Candida species.

Table 2 The in vitro antibacterial and anti-Candidal activity of ligands **2-6b**

	Inhibition zones (mm)*										
Microorganisms	**Ligands**								**Antibiotics**		
(Gram negative bacteria)	**2**	**3**	**4**	**5a**	**5b**	**5c**	**6a**	**6b**	**CTX30**	**AMC30**	**PCZ5**
Acinetobacter baumannii	20.0	11.0	7.0	6.0	8.0	7.0	9.0	9.0	7.0	11.0	-
Escherichia coli	20.0	8.0	10.0	7.0	7.0	7.0	10.0	9.0	6.0	13.0	-
Klebsiella pneumaniae	21.0	13.0	11.0	10.0	8.0	9.0	7.0	6.0	6.0	13.0	-
(Gram positive bacteria)											
Staphylococcus aureus	17.0	12.0	7.0	9.0	10.0	9.0	8.0	7.0	8.0	10.0	-
Staphylococcus epidermidis	28.0	19.0	17.0	18.0	15.0	13.0	10.0	12.0	15.0	17.0	-
Enterococcus faecalis	25.0	17.0	17.0	18.0	18.0	19.0	17.0	16.0	18.0	18.0	-
Bacillus cereus	21.0	12.0	15.0	13.0	15.0	16.0	6.0	9.0	14.0	18.0	-
***(Candida* species)**											
Candida tropicalis	20.0	6.0	8.0	8.0	8.0	7.0	6.0	6.0	-	-	12.0
Candida guilliermondii	25.0	10.0	8.0	7.0	6.0	9.0	10.0	10.0	-	-	13.0
Candida albicans	20.0	10.0	9.0	10.0	7.0	10.0	9.0	9.0	-	-	20.0
Candida glabrata	17.0	11.0	6.0	7.0	7.0	10.0	11.0	8.0	-	-	19.0

CTX30: Cefotaxime 30 µg; AMC30: Amoxicillin/clavulanicacid 30 µg; PCZ5: Posacanazole 5 µg

(*): The figures on the scale show the inhibition diameters.

Table 3 The i*n vitro* antimicrobial activity (MIC, mgmL^{-1}) of the of ligands **2-6b**

Microorganism	**Ligands**								**Antibiotics**	
(Gram negative bacteria)	**2**	**3**	**4**	**5a**	**5b**	**5c**	**6a**	**6b**	**GEN**	**NYS**
Acinetobacter baumannii	1.56	25.0	25.0	25.0	25.0	25.0	25.0	25.0	6.25	-
Escherichia coli	1.56	25.0	25.0	25.0	25.0	25.0	12.5	25.0	6.25	-
Klebsiella pneumaniae	1.56	12.5	25.0	25.0	25.0	25.0	25.0	25.0	6.25	-
(Gram positive bacteria)										
Staphylococcus aureus	3.13	12.5	25.0	25.0	25.0	25.0	25.0	25.0	25.0	-
Staphylococcus epidermidis	1.56	3.13	6.25	6.25	12.5	25.0	25.0	25.0	12.5	-
Enterococcus faecalis	1.56	6.25	6.25	6.25	6.25	6.25	3.13	3.13	6.25	-
Bacillus cereus	3.13	25.0	12.5	25.0	12.5	12.5	25.0	25.0	6.25	-
***Candida* species**										
Candida tropicalis	1.56	25.0	25.0	25.0	25.0	25.0	25.0	25.0	-	1.56
Candida guilliermondii	0.78	25.0	25.0	25.0	25.0	25.0	25.0	25.0	-	3.13
Candida albicans	1.56	25.0	25.0	25.0	25.0	25.0	25.0	25.0	-	1.56
Candida glabrata	3.13	25.0	25.0	25.0	25.0	25.0	25.0	25.0	-	3.13

GEN: Gentamycin; NYS: Nystatin

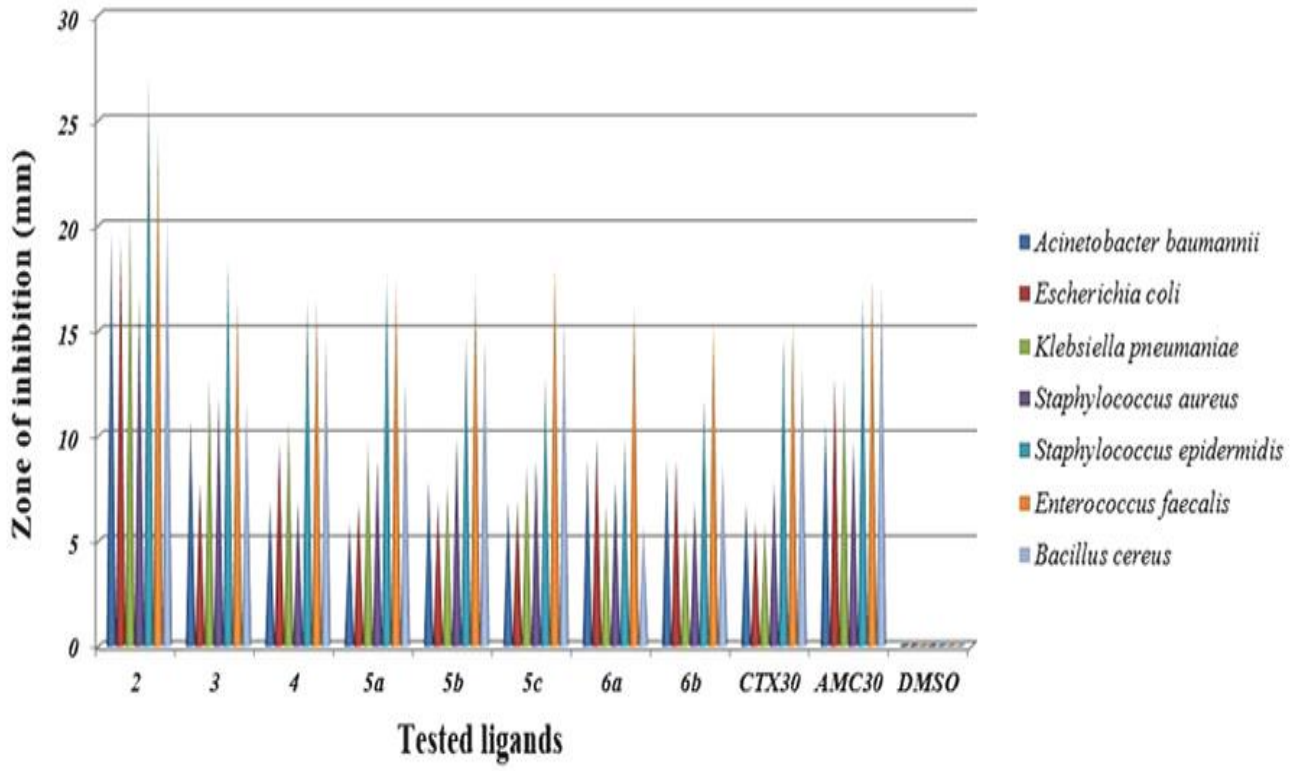

Figure 3 The *in vitro* antibacterial activity of ligands **(2-6b)**

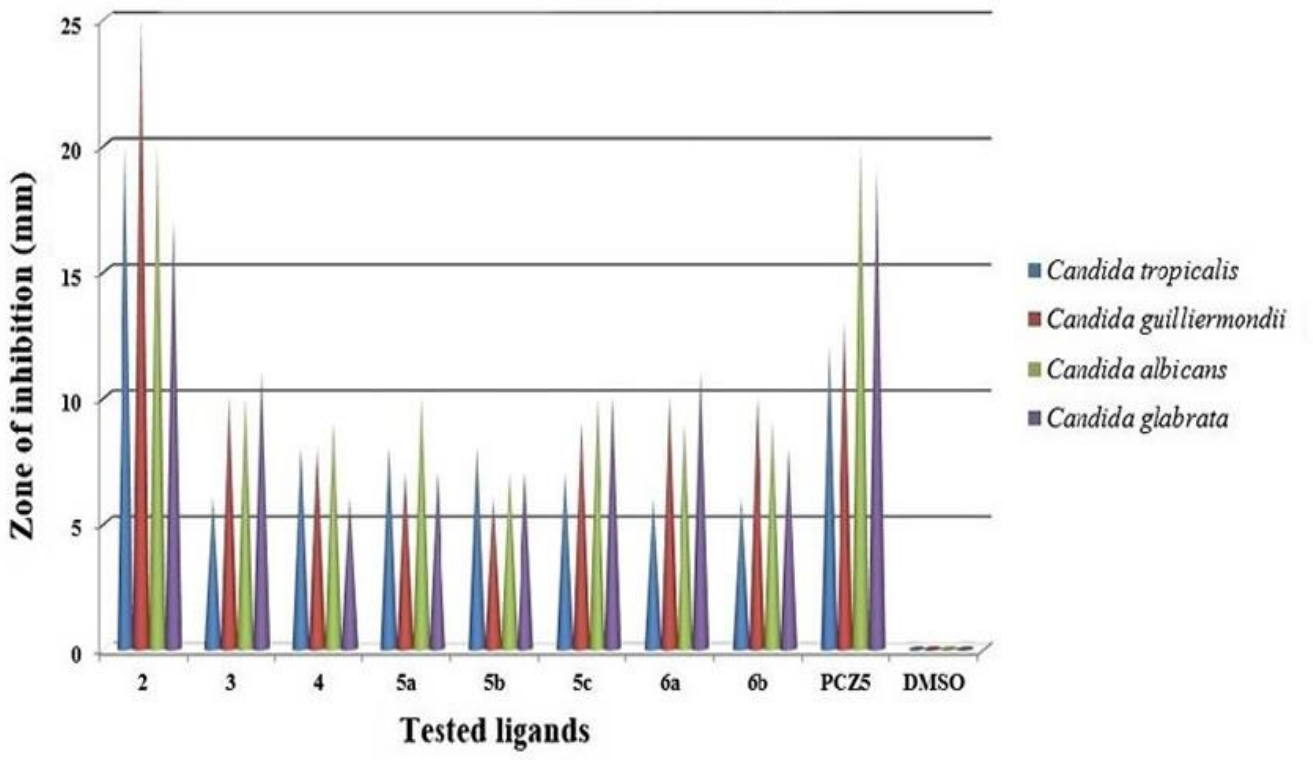

Figure 4 The *in vitro* anti-Candidal activity of ligands **(2-6b)**

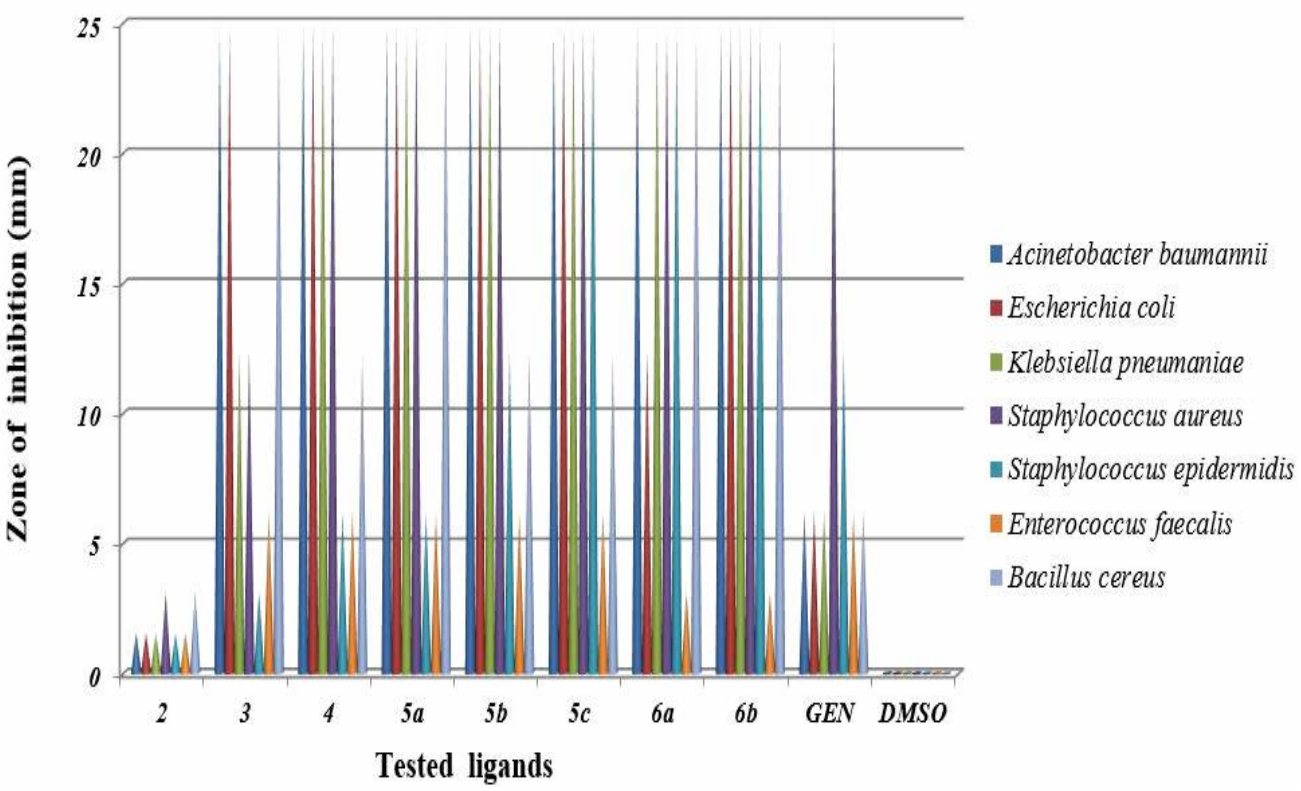

Figure 5 The *in vitro* antibacterial activity (MIC, $mgmL^{-1}$) of ligands **(2-6b)**

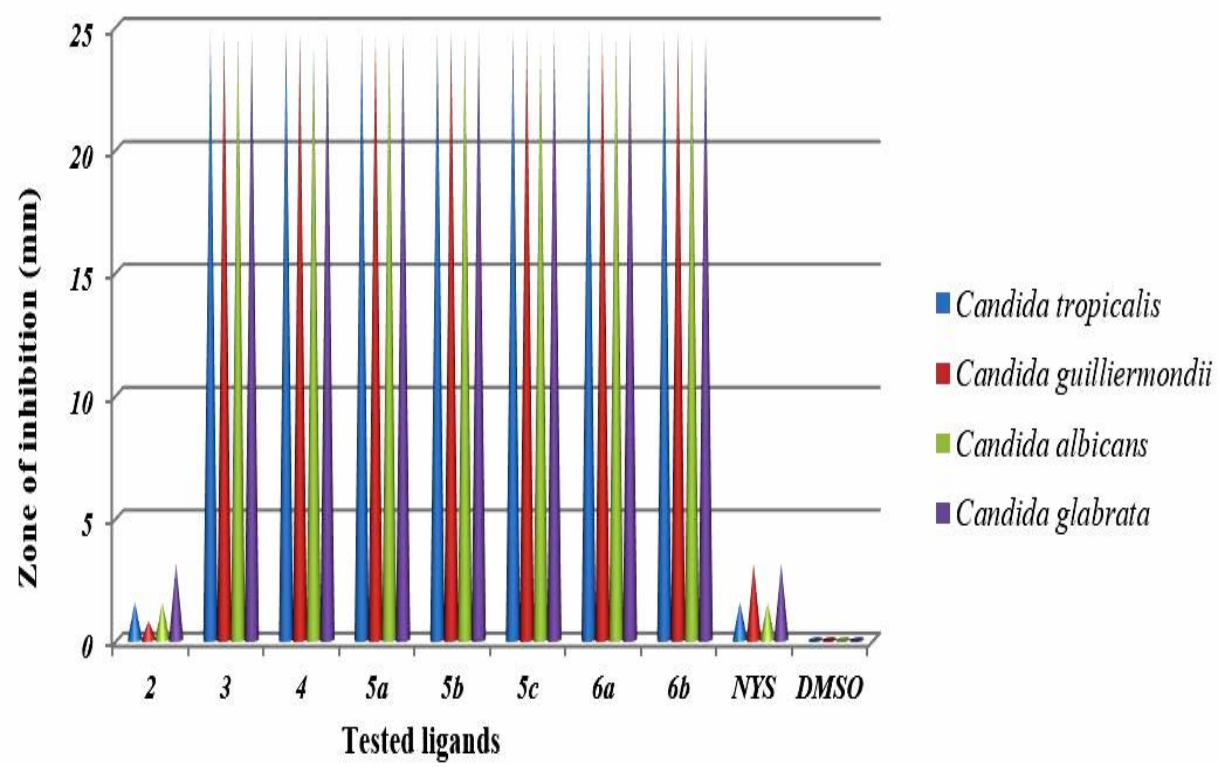

Figure 6 The *in vitro* anti-Candidal activity (MIC, $mgmL^{-1}$) of ligands **(2-6b)**

4. CONCLUSIONS

In short, a dimeric amine and seven dimeric thio-Schiff bases were successfully obtained by two different methods (without catalyst and using CeO_2 nanocatalyst). In addition, the catalytic effect of the prepared CeO_2 nanocatalyst on the synthesis of dimeric thio-Schiff bases was investigated in this work and found to be an efficient and reversible catalyst. Additively, we were studied antibacterial and anti-Candidal activities of dimeric thio-Schiff bases. At the same time, antimicrobial activities of ligands **2-6b** were compared to standard antibiotics. Overall, ligand **2** was found to be more efficient than other all ligands (**3**, **4**, **5a**, **5b**, **5c**, **6a**, **6b**) and standard antibiotics (CTX30, AMC30, PCZ5). The short reaction time of the second process, being environmentally friendly, non-hazardous, reusability of the catalyst, ease of preparation and applicability to a wide variety of ligands make this method preferable. The results of our study showed that dimeric thio-Schiff bases will be useful when producing new and different metabolites. The ligands exhibiting especially antimicrobial activity against Gram positive bacteria and *Candida* species could result in the discovery of novel antibacterial and antifungal agents, showing demonstrating broad spectrum activities. This study may help in the discovery of new chemical class antibiotics used in the treatment of infectious diseases in future pharmacological investigations.

Acknowledgements

The authors would like to thank the Duzce University Scientific Research Projects Commission (BAP) for contributing to the financial portion of the project.

Funding

This research was supported by Duzce University Scientific Research Fund (BAP) (Project No: 2014-05-03-259 and 2015-05-03-354).

The Declaration of Conflict of Interest/ Common Interest

No conflict of interest or common interest has been declared by the authors.

Authors' Contribution

Aslıhan DALMAZ and Görkem DÜLGER conceived and designed the experiments, analyzed and interpreted data and performed experiments; Sefa DURMUŞ and Başaran DÜLGER conceived and designed the experiments, analyzed and interpreted data, revised the manuscript. All authors discussed the results and contributed to the final manuscript.

The Declaration of Ethics Committee Approval

The authors declare that this document does not require an ethics committee approval or any special permission.

The Declaration of Research and Publication Ethics

The authors of the paper declare that they comply with the scientific, ethical and quotation rules of SAUJS in all processes of the article and that they do not make any falsification on the data collected. In addition, they declare that Sakarya University Journal of Science and its editorial board have no responsibility for any ethical violations that may be encountered, and that this study has not been evaluated in any academic publication environment other than Sakarya University Journal of Science.

REFERENCES

[1] K. Schermanz, "Catalysis by ceria and related materials," World Scientific, London, Chapter I, 2002.

[2] A. M. Thompson, "Oxides of the Rare Earths," John Wiley & Sons, New York, 1978.

[3] J. D. McCullough and K. N. Trueblood, "The crystal structure of baddeleyite (monoclinic

ZrO_2),” Acta Crystallographica, vol. 12, pp. 507-511, 1959.

[4] B. Schmidt, S. Lindman, W. Tong, G. Lindeberg, A. Gogoll, Z. Lai, M. Sohtell, “Design, Synthesis, and Biological Activities of Four Angiotensin II Receptor Ligands with γ-Turn Mimetics Replacing Amino Acid Residues 3−5,” Journal of Medicinal Chemistry, vol. 40, pp. 903-919, 1997.

[5] B. D. Palmer, G. W Rewcastle, A. M. Thompson, M. Boyd, H. H. Showalter, A.D. Sercel, W. A. Denny, **“**Tyrosine Kinase Inhibitors. 4. Structure-Activity Relationships among N- and 3-Substituted 2,2'-Dithiobis(1H-indoles) for in vitro Inhibition of Receptor and Nonreceptor Protein Tyrosine Kinases,” Journal of Medicinal Chemistry, vol. 38, pp. 58-67, 1995.

[6] S. Murtaza, A. Abbas, K. Iftikhar, S. Shamim, M.S. Akhtar, Z. Razzaq, K. Naseem, A.M. Elgorban, “Synthesis, biological activities and docking studies of novel 2,4-dihydroxybenzaldehyde based Schiff base,” Medicinal Chemistry Research, vol. 25, pp. 2860-2871, 2016.

[7] P. Khatkar, S. Asija and N. Singh, “Synthesis, spektral studies and in vitro antimicrobial activity of soma new Di/Triorganotin (IV) complexes of Schiff base derived from 2-benzoylpyridine,” Journal of the Serbian Chemical Society, vol. 82, pp. 13–23, 2017.

[8] M. G. Bhowon, S. Jhaumeer-Laulloo, N. Soukhee, A. Allibacus, V. Shiboo, “Synthesis, catalytic and antibacterial activity of 2-aminophenyldisulphide,” Journal of Coordination Chemistry, vol. 60, pp. 1335-1343, 2007.

[9] G. G. Mohamed, M. M. Omar and A.M. Hindy, “Metal Complexes of Schiff Bases: Preparation, Characterization, and Biological Activity,” Turkish Journal of Chemistry, vol. 30, pp. 361-382, 2006.

[10] S. C. C. Oliveira, C. K. Z. Andrade, R. M. Varela, J. M. G. Molinillo, F. A. Macías, “Phytotoxicity Study of Ortho-Disubstituted Disulfides and Their Acyl Derivatives,” American Chemical Society Omega, vol. 4, pp. 2362−2368, 2019.

[11] F. N. Moghadam, M. Amirnasr, K. Eskandari, S. Meghdadia, “A new disulfide Schiff base as versatile “OFF-ON-OFF” fluorescent colorimetric chemosensor for sequential detection of CN^- and Fe^{3+} ions: Combined experimental and theoretical studies,” Royal Society of Chemistry, vol. 1, pp. 1-3, 2019.

[12] S. M. A. Hamour, A. O'bichere, J. L. Peters, P. J. McDonald, “Patient perceptions of MRSA,” Annals of the Royal College of Surgeons of England, vol. 85, pp. 123-125, 2003.

[13] Y. Narain, S. Jhaumeer-Laulloo, and M. G. Bhowon, “Structure-activity relationship of Schiff base derivatives of bis (aminophenyl) disulfide and p-vanillin as antimicrobial agents,” International Journal of Biological and Chemical Science, vol. 4, pp. 69-74, 2010.

[14] S. Durmus, A. Dalmaz, M. Ozdincer, S. Sivrikaya, “Preparation of Lanthanide Oxide Nanoparticles: An efficient catalyst for the synthesis of dimeric disulphide Schiff Bases,” CBU Journal of Science, vol. 13, pp. 25, 2017.

[15] Saima, A. G. Lavekar, R. Kumar, A. K. Sinha, “Bovine serum albumin triggered waste-free aerobic oxidative coupling of thiols into disulphides on water: An extended synthesis of bioactive dithiobis (phenylene) bis (benzylideneimine) via sequential oxidative coupling–condensation reactions in one pot from

aminothiophenol and benzaldehyde," Journal of Molecular Catalysis B: Enzymatic, vol. 116, pp. 113-123, 2015.

[16] S. Chandra and R. Kumar, "Synthesis and spectral studies on mononuclear complexes of chromium(III) and manganese(II) with 12-membered tetradentate N2O2, N2S2 and N4 donor macrocyclic ligands," Transition Metal Chemistry, vol. 29, pp. 269, 2004.

[17] S. Sarkar and K. Dey, "Synthesis and Spectroscopic Characterization of Some Transition Metal complexes of a new hexadentate $N_2S_2O_2$ Schiff Base Ligand," Spectrochimica Acta Part A: Molecular and Biomolecular Spectroscopy, vol. 62, pp. 383-393, 2005.

[18] M. Rasouli, M. Morshedi, M. Amirnasr, M. Z. S. Alexandra, R. Randall, "Synthesis, Crystal Structure and Electrochemical Properties of Cu(I) Coordination Polymers with Two New $NS)_2$ Schiff-base Ligands Containing Long Flexible Spacers," Journal of Coordination Chemistry, vol. 66, pp. 1974-1984, 2013.

[19] Clinical and Laboratory Standards Institute (CLSI), reference method for broth dilution antifungal susceptibility testing of yeasts, approved standard – third edition. CLSI document M27-A3; Wayne, PA 2008.

[20] Clinical and Laboratory Standards Institute, methods for dilution antimicrobial susceptibility tests for bacteria that grow aerobically, approved standard –ninth edition. CLSI document M07-A9; Wayne, PA 2012.

[21] R. N. Jones, A. L. Barry, T. L. Gaven, J. A. Washington, E. H. Lennette, A. Balows, "Antibacterial Activities of Ciprofloxacin, Norfloxacin, Oxolinic Acid, Cinoxacin, and Nalidixic Acid," Antimicrobial Agents and Chemotherapy, vol. 25, p. 972-977, 1984,.

[22] M. G. Bhowon, S. Jhaumeer-Laulloo and M. Dowlut, "Synthesis, catalytic and characterization of bis(2-aminophenyl) disulphide imine derivatives and their ruthenium complexes," Transition Metal Chemistry, vol. 30, pp. 35-39, 2005.

[23] E. Labisbal, A. Blas, J. A .García-Vázquez, J. Romero, M. L. Durán, A. Sousa, "The synthesis of tin(IV) complexes of 2-(2-mercaptophenyl)-imino-phenols by the electrochemical cleavage of a disulphide bond: The crystal structure of bis{2-(2-mercaptophenyl)imino-4,6-dimethoxy-phenoxy}tin(IV)," Polyhedron, vol. 11, pp. 227-233, 1992.

[24] E. Labisbal, J. A. García-Vázquez, C. Gómez, A. Macias, J. Romero, A. Sousa, U. Englert, D. E. Fenton, "The synthesis of zinc(II) complexes of 2-(2-mercaptophenyl)-imino-phenol by electrochemical cleavage of a disulfide bond: the crystal structure of {(2,2'-bipyridine)[2-(2-mercaptophenyl)imino-phenoxy]}zinc(II)," Inorganic Chimica Acta, vol. 203, pp. 671-, 1993.

[25] M. Behpour, S. M. Ghoreishi, N. Mohammadi, N. Soltani, M. Salavati-Niasari, "Investigation of some Schiff base compounds containing disulfide bond as HCl corrosion inhibitors for mild steel," Corrosion Science, vol. 52, pp. 4046-4057, 2010.

[26] C. Praveen, K. H. Kumar, D. Muralidharan, P. T. Perumal, "Oxidative cyclization of thiophenolic and phenolic Schiff's bases promoted by PCC: a new oxidant for 2-substituted benzothiazoles and benzoxazoles," Tetrahedron**,** vol. 64, pp. 2369-2374, 2008.

[27] S. Bharti, M. Choudhary, B. Mohan, S. P. Rawat, S. R. Sharma, K. Ahmad, "Syntheses, spectroscopic, characterization, SOD-like properties and antibacterial activities of dimer copper (II) and nickel(II) complexes based on imine ligands containing 2-aminothiophenol moiety: X-ray crystal structure determination of disulfide Schiff Bases," Journal of Molecular Structure, vol.1164, pp. 137-154, 2018.

[28] A. Goszczyńska, H. Kwiecień, K. Fijałkowski, "Synthesis and antibacterial activity of Schiff bases and amines derived from alkyl 2-(2-formyl-4-nitrophenoxy) alkanoates," Medicinal Chemistry Research, vol. 24, pp. 3561-3577, 2015.

SAKARYA ÜNİVERSİTESİ
FEN BİLİMLERİ ENSTİTÜSÜ DERGİSİ

Sakarya University Journal of Science
SAUJS

e-ISSN 2147-835X | Period Bimonthly | Founded: 1997 | Publisher Sakarya University |
http://www.saujs.sakarya.edu.tr/en/

Title: Rodent Species of Sarıkum Nature Protection Area

Authors: Pınar ÇAM İCİK

Recieved: 2020-10-28 00:00:00

Accepted: 2021-02-08 00:00:00

Article Type: Research Article

Volume: 25
Issue: 2
Month: April
Year: 2021
Pages: 379-388

How to cite
Pınar ÇAM İCİK; (2021), Rodent Species of Sarıkum Nature Protection Area. Sakarya University Journal of Science, 25(2), 379-388, DOI: https://doi.org/10.16984/saufenbilder.817534
Access link
http://www.saujs.sakarya.edu.tr/en/pub/issue/60672/817534

Sakarya University Journal of Science 25(2), 379-388, 2021

Rodent Species of Sarıkum Nature Protection Area

Pınar ÇAM İCİK*[1]

Abstract

Sarıkum Nature Protection area, located in the west of Sinop Province with the registration of 'nature protection area' and declaration of 'grade 1 natural site area', has a wide variety of ecosystems in which lake, swamp, dune, terrestrial forest and floodplain forestland ecosystems change within short distances. The fact that the region has different life alternatives is very important in diversifying wildlife species. With this study, the rodent species that have distributed in the Sarıkum Nature Protection Area have been identified. Field works were carried out between September 2018 and November 2019. Most of the small mammals belonging to order of Rodentia were caught by live catch traps and identified. After the species identification the specimens in the traps were let out to the region which they were captured. In Sarıkum Nature Protection Area, a total of ten different rodent species belonging to 3 families, Sciuridae, Cricetidae and Muridae, have been identified. One species, *Sciurus anomalus*, which was one of the Sciuridae family species, could be directly observed. Remaining 9 rodent species were detected by using live catch traps. The most frequently caught rodent species among all was *Apodemus mystacinus* from Muridae family, with a percentage of 23%. The habitat type, where the largest number of rodent species were obtained and observed, were mixed plants and shrub land areas. All of the rodent species identified in Sarıkum Nature Protection Area were in LC (wide spread, low risk) category of IUCN (International Union for Conservation of Nature and Natural Resources). Identification of rodent species in Sarıkum Nature Protection Area contribute to mammalian biodiversity at the regional level and will enable species-based approach in subsequent studies.

Keywords: Sarıkum, Sinop, Rodents, Rodentia

INTRODUCTION

Sarıkum Nature Protection Area is an area of 785 hectares within the borders of Sarıkum village on Sinop- Ayancık state highway and 20 km from Sinop province. This area has been classified as a "Nature Protection Area" due to the fact that it contains many ecosystems such as sea, coastal, dune, lake, wetland and forest ecosystems and because of the rich biological variety and resource values in these ecosystems. Sarıkum Nature Protection Area has both a Nature Protection Area (NPA) registry and a site notice [1].

When compared with other nature protection areas in our country, Sarıkum NPA is very

* Corresponding Author: pinarcam@sinop.edu.tr
[1] Sinop University, Faculty of Arts and Science, Sinop, Turkey, ORCID: https://orcid.org/0000-0002-0714-3536

different from the others due to its distinct sand topography despite being located in the region with the highest rainfall. Sarıkum Nature Protection Area is in the list of Important Bird Areas (IBA) and there is a bird watching tower in the area [2]. Sarıkum NPA has not been declared as a Ramsar site, although it is an "international wetland" according to the Ramsar Convention criteria, since it is on bird migration routes and it provides breeding and sheltering areas for many different types of bird [3]. Sarıkum Lake and wetland within Sarıkum NPA is one of the most important areas in terms of biological diversity and it is one of the important bird watching areas in the Black Sea Region [4].

Sarıkum Lake and wetland has been formed on the coastal plain between the mountains and the coastline. There are flatlands surrounded by forests in places on the upper parts of the mountains behind the coastal area which is not too wide. There is only one village settlement called Sarıkum village in Sarıkum Nature Protection Area. This is a village of the central district of Sinop province. The 4 km long Sarıkum beach is the longest and the unique natural beach in Sinop. The depth of Sarıkum Lake is between 0.5 and 1 m. The water of this lake has high salinity since it mixes with sea water. Sarıkum lagoon has an area that can be described as a "desert", which keeps its mobility with northwest winds and which is occupied by coastal dunes. The forest areas around the lake consist of flooded forests formed by broad-leaved trees such as beech, oak and hornbeam. Also there are *Pinus maritima* forests which were later created artificially in the region [5]. Quaternary deposits are common in the West and South of Sarıkum Nature Protection Area which is located in the fourth degree earthquake zone. Plio-quaternary deposits consisting of yellow sands have also been effective in naming the area as 'Sarıkum (yellow sand) facies' in geology maps [6]. Figure 1 shows the map with the geographical location of Sarıkum Nature Protection Area.

Rodentia are represented in Turkey with a total of 9 families as Sciuridae, Castoridae, Dipodidae, Muridae, Gerbilidae, Spalacidae, Gliridae, Hystricidae and Myocastoridae, and 30 genera [7].

Figure 1 Sarıkum Lake Geographical Location

A total of 5 habitats were determined in which rodent species lived by evaluating the study of Yiğit *et al.* [8]: 1) Semi-arid steppes and plains, 2) Wetlands, 3) Mixed forest and bushes, 4) Coniferous forest, 5) Rocky and stony areas. It has been noted that the habitat type in which grain agriculture is generally carried out is semi-arid steppes and plains and that a large number of rodents are obtained from the areas where this habitat type is dominant [8]. Altough Çam and Ölmez (2015) [9] studied the mammal fauna of Sinop province, rodent fauna and the population density of the species in Sarıkum Nature Protection Area have not been evaluated in detail. Also, small mammal species from the specific regions of Sinop province were used for taxonomic studies [10-11], [12]. The mammal fauna in these regions have been specified by a Biodiversity Research within the scope of Sarıkum Lake and Aksaz-Karagöl Wetland Sub-Basins [5] Some observations about the mammal fauna were also presented in the Wildlife Potential and Evaluation report of Ayancık Forest Management Directorate [13]. Some of the mammals distributed in Sinop province have also been listed in the provincial environmental status report of Sinop province [2].

The aim of this study was to identify the rodent species distributed in Sarıkum NPA and contributed to taxonomic and ecological studies in this area.

2. MATERIALS AND METHODS

For the identification of rodent species in Sarıkum Nature Protection Area, field studies were carried out in a period of 15 months between 2018 and 2019. In the field studies, first the stations were determined, and then observation and trapping studies were conducted. Garmin Etrex 10 GPS (Global Positioning System was used to record Geographical latitude-longitude of the central regions of the stations). In the identification of the species belonging to Rodentia, species-specific nest entrances on the ground were primarily evaluated. Live traps were placed in areas where nests were frequent: above ground, in forests, in dense vegetation and on the border lines of cultivated agricultural land. Both metal and wire traps were preferred to increase species-based preference

Metal traps are based on the system of closing when the animal enters, depending on the pedal system inside the trap. Wire traps, on the other hand, allow the animal to be caught with the closure of the hook by getting free. While the bait was left on the pedal part of the metal trap, it was fixed on the hook attached to the lid inside the trap in wire traps (Figure 2). Metal and wire traps were prepared by leaving peanut butter on bread. The traps were left with open lid on the stations determined in Sarıkum NPA when it was about to get dark. Metal traps can roll depending on wind and other outside influences or they can close before the animal gets in during the day. For this reason, the metal traps left in the field with a stone or a piece of branch on them. In the field studies conducted within the context of this study, a total of 45 traps (35 of them were metal and 10 of them were wire) were used. The traps, which were equally distributed in the land, were collected just after sunrise in the early hours of the next day. Trap collection process was carried out with great care. When it was realized that the lid of the trap was closed, it was opened slowly to take a clear image of the animal which was possibly inside. Sometimes we did not take a photo but observed the specimen. Only for some individuals with small body, there was a chance to take photo when the animal was inside the trap. After the traps were controlled, the species information and the station that they were caught were recorded. Later, the captured animals were released.

Within the context of this study, 72784983-488.04-115954 numbered research permit was taken from the Ministry of Forest and Water Management General Directorate of Nature Protection and National Parks for all field studies to be carried out in Sarıkum Nature Protection Area. In addition, this study was approved with 22.05.2018 dated and 2018/01 numbered decision of Sinop University Rectorate Animal Experiments Local Ethics Committee.

Figure 2 a. Baits placed on the pedal of the metal trap b. Baits placed on the hook of the wire trap

Table 1
Rodent species found in Sarıkum NPA, Turkish/English nomenclature, families and IUCN threat categories

Family	Species	Turkish/English nomenclature	IUCN threat category
Sciuridae	*Sciurus anomalus*	Anadolu sincabı/ Caucasian squirrel	LC
Cricetidae	*Microtus levis*	Çayır tarla faresi/ East European vole	LC
Cricetidae	*Microtus subterraneus*	Avrupa çam Sıçanı/ European pine vole	LC
Muridae	*Apodemus flavicollis*	Sarı boyunlu orman faresi/ Yellow necked field mouse	LC
Muridae	*Apodemus mystacinus*	Kaya Faresi/Eastern broad-toothed field mouse	LC
Muridae	*Mus domesticus*	Ev faresi/ House mouse	LC
Muridae	*Mus macedonicus*	Sarı ev faresi, kısa kuyruklu ev faresi/ Macedonian mouse	LC
Muridae	*Rattus rattus*	Sıçan, Keme/ House rat	LC
Muridae	*Rattus norvegicus*	Göçmen Sıçan/ Brown rat	LC
Cricetidae	*Myodes glareolus*	Kırmızı sırtlı Fare, Kırmızı Fare/ Bank Vole	LC

3. RESULTS

Table 1 shows the species, families, Turkish/English nomenclature and IUCN threat categories of rodents found during field studies in Sarıkum Nature Protection Area.

A total of 10 species belonging to Sciuridae, Cricetidae and Muridae families were found in Sarıkum NPA. These species were systematically classified by Corbet [14], Wilson and Reeder [15] and Kryštufek and Vohralík [16]. All of the species except *Sciurus anomalus* (Anatolian squirrel) were identified with trapping method. https://www.iucnredlist.org/ [17] web site was used for IUCN threat categories.

Class: MAMMALIA

Order: RODENTIA

Family: SCIURIDAE Hemprich, 1820

Subfamily: SCIURINAE Hemprich, 1820

Genus: *SCIURUS* Linnaeus, 1758

Sciurus anomalus Gueldenstaedt, 1785 (Caucasian Squirrel) (Direct Observation)

It was observed especially from April to September in the afforested area and open forest areas in Sarıkum NPA. It was observed that the specimens preferred feeding in shrubby areas with mixed plants.

Family: CRICETIDAE G. Fischer, 1817

Subfamily: ARVICOLINAE Gray, 1821

Genus: *MICROTUS* Schrank, 1798

Microtus levis Miller, 1908 (East European Vole) (Trapping)

It was often caught from the border lines of cultivated agricultural land in Sarıkum NPA. It was trapped in shrubby areas with mixed plants though few.

Family: CRICETIDAE G. Fischer, 1817

Subfamily: ARVICOLINAE Gray, 1821

Genus: *MICROTUS* Schrank, 1798

Microtus subterraneus (de Sélys Longchamps, 1836) (European Pine Vole) (Trapping)

It was found in traps set in cultivated agricultural land, although not as much as *Microtus levis. It was caught* in a low level in shrubby areas with mixed plants. It was trapped in the parts of flooded forest areas opening to road.

Family: MURIDAE Illiger, 1815

Subfamily: MURINAE Illiger, 1815

Genus: *APODEMUS* Kaup, 1829

Apodemus flavicollis (Melchior, 1834) (Yellow-Necked Field Mouse) (Trapping)

It was obtained from traps set up in terrestrial forest areas, forested areas and dense shrubs. It was the most common species found in trap in the stations, but less number. It was caught from 4 of the 8 stations with 3 different habitat types.

Family: MURIDAE Illiger, 1815

Subfamily: MURINAE Illiger, 1815

Genus: *APODEMUS* Kaup, 1829

Apodemus mystacinus (Danford and Alston, 1877) (Eastern Broad-Toothed Field Mouse) (Trapping)

It is the most common rodent species caught by trap. It was caught from shrubby areas with mixed plants, and from the entrances of forested areas.

Family: MURIDAE Illiger, 1815

Subfamily: MURINAE Illiger, 1815

Genus: *MUS* Linnaeus, 1758

Mus domesticus Schwarz & Schwarz, 1943 (House Mouse) (Trapping)

It was caught outside barns, coops, houses and garages, and the outside of buildings used as warehouse in Sarıkum village in Sarıkum NPA. It was trapped in an open area surrounded by mixed plants on one side used as dump.

Family: MURIDAE Illiger, 1815

Subfamily: MURINAE Illiger, 1815

Genus: *MUS* Linnaeus, 1758

Mus macedonicus Petrov & Ružić, 1983 (Macedonian Mouse) (Trapping)

It was trapped in an area surrounded by mixed plants on one side and used as dump, around buildings used as warehouse close to Sarıkum village.

Family: MURIDAE Illiger, 1815

Subfamily: MURINAE Illiger, 1815

Genus: *RATTUS* Fischer, 1803

Rattus rattus (Linnaeus, 1758) (House Rat) (Trapping)

It was trapped in areas close to Sarıkum village. It was not found in forested areas. It was found on trap in an area surrounded by plants on one side and used as dump.

Family: MURIDAE Illiger, 1815

Subfamily: MURINAE Illiger, 1815

Genus: *RATTUS* Fischer, 1803

Rattus norvegicus (Berkenhout, 1769) (Brown Rat) (Trapping)

It was caught in traps outside houses in Sarıkum village. It was not found in open area and forest area.

Family: CRICETIDAE G. Fischer, 1817

Subfamily: ARVICOLINAE Gray, 1821

Genus: *MYODES* Pallas, 1811

Myodes glareolus (Schreber, 1780) (Bank Vole) (Trapping)

It was found frequently in traps set in shrubby areas. It was found in open areas in forest, although lesser relatively.

Traps were set up in 18 of 20 field studies carried out in Sarıkum Nature Protection Area. During the field studies, a total of 635 traps were left in the field and rodent species were found in 307 of these. The remaining number constituted the traps in which animals did not enter or those which closed on their own. On some days, on reaching the field to collect the traps, it was realized that the places of the traps had changed. Based on the traces on the ground, it was found that large mammal species had dragged the traps and caused a few traps to become unusable. It was found many times that species which were not members of Rodentia also were caught in traps.

In all of the field studies, in traps, *Microtus levis* species was found 37 times, *Microtus subterraneus* species was found 34 times, *Apodemus flavicollis* species was found 45 times, *Apodemus mystacinus* species was found 71 times, *Mus domesticus* species was found 26 times, *Mus macedonicus* species was found 22 times, *Rattus rattus* species was found 17 times, *Rattus norvegicus* species was found 12 times, and *Myodes glareolus* species was found 43 times. Figure 3 shows the graph created according to the percentages of rodent species caught with traps during the field studies carried out in Sarıkum Nature Protection Area. *Sciurus anomalus* species, which was seen frequently in forest areas and dense bushy areas during field studies, was excluded in this graph. The most caught species in the field was *Apodemus mystacinus* from Muridae family with a rate of 23%. The second most caught species was *Apodemus flavicollis,* another species of the same genus, with a rate of 15%. *Rattus rattus* and *Rattus norvegicus* species obtained from Sarıkum village settlement area (station number 3) were the least captured species. The reason of this avoiding of *Rattus* species being trapped due to their slightly larger body.

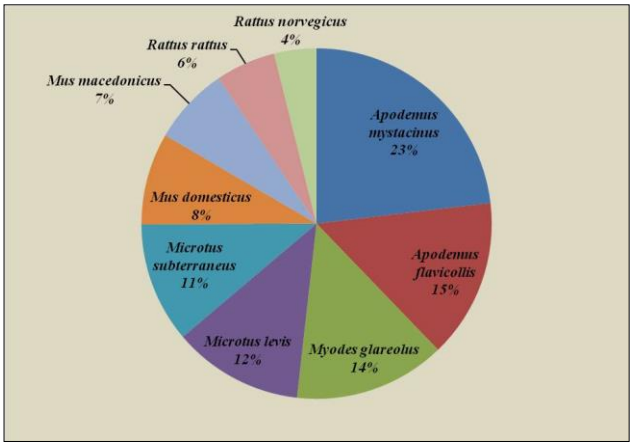

Figure 3 The chart created according to the rodent species' percentage of being caught in a trap

Figure 4 shows images of *Sciurus anomalus* (Caucasian squirrel) species observed frequently which were not caught in trap but which were often observed in forest habitats. Figures 5-7 show images of rodent species which were caught in traps and which were photographed.


Figure 4 *Sciurus anomalus* (Caucasian Squirrel) observed in Sarıkum NPA (Photo by: İdris Ölmez)


Figure 5 *Apodemus mystacinus* caught with a trap in Sarıkum NPA

(Eastern Broad-Toothed Field Mouse)

Figure 6 *Apodemus flavicollis* caught with a trap in Sarıkum NPAYellow-Necked Field Mouse)

Figure 7 *Myodes glareolus* (Bank Vole) caught with a trap in Sarıkum NPA

In trapping studies carried out in Sarıkum NPA, another small mammal frequently trapped was *Crocidura suaveolens* species (Figure 8). This species is known as garden rats with a pointed rose and belongs to order Eulipotyphla. *Crocidura suaveolens* is a species with a wide distribution.

All of the trappings in Sarıkum Nature Protection were planned by taking habitat types and different environments into consideration. Table 2 shows whether the species trapped and observed in Sarıkum NPA existed in different habitats were represented by stations.

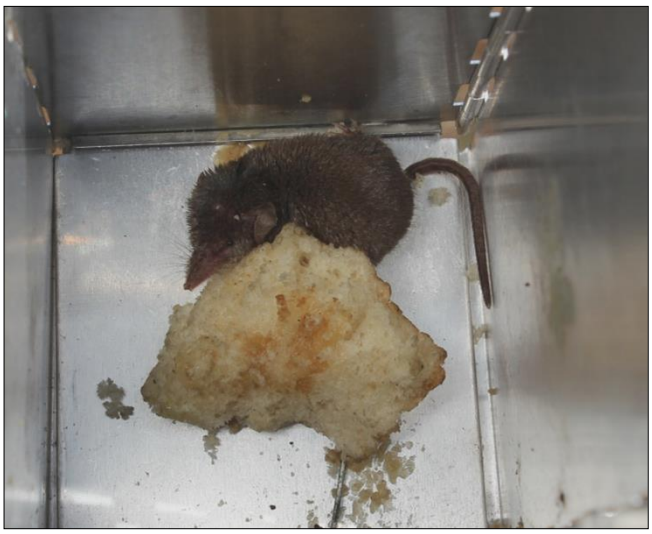

Figure 8 Small mammal *Crocidura suaveolens* (Lesser Shrew) which is not a rodent, but which is frequently trapped

Table 2
Availability of species identified in Sarıkum NPA according to habitats
(+: caught/observed in the related habitat; -not caught/not observed in the related habitat)

	Cultivated agricultural fields, edges of fields	Flooded forest	Sarıkum village settlement area	Dune fields	Terrestrial forest areas	Mixed plants and shrubs	Afforested areas (Coniferous forest)
Sciurus anomalus	-	-	-	-	+	+	+
Microtus levis	+	-	-	-	-	+	-
Microtus subterraneus	+	+	-	-	-	+	-
Apodemus flavicollis	-	-	-	-	+	+	+
Apodemus mystacinus	-	-	-	-	+	+	-
Mus domesticus	-	-	+	-	-	+	-
Mus macedonicus	-	-	+	-	-	+	-
Rattus rattus	-	-	+	-	-	+	-
Rattus norvegicus	-	-	+	-	-	-	-
Myodes glareolus	-	-	-	-	+	+	-

The only settlement area within Sarıkum Nature Protection Area is Sarıkum Village of the central district. A small interview was held with the residents of this village. In this interview, I asked them whether they had to deal or not with rodent species they came across within Sarıkum NPA borders at home or in their fields, and whether they used any rodenticide for rodent species. Almost all of the residents in the village remarked that they fed cats in their homes or garden to fight mouse and rat species. They also told that the number of rodent species increased significantly if they did not feed cats in their garden. Most of the residents in the village complained about *Martes foina* (rock marten) rather than rodent species. They said that *Martes foina* got in their coops frequently and killed the chicken, chicks, geese and ducks they fed. Another species they complained about was *Crocidura suaveolens*, one of the Eulipotyphla order, which the people called the pig rat. They told that *C. suaveolens* got in their homes, cut their cables, and that they caught this species in their barns and coops. They remarked that they fought with the *Rattus* species they did not want to see in their homes or around their homes by using sticky traps. They asserted that they did not use any chemicals or rodenticides while fighting rodent species in their agricultural areas.

4. DISCUSSION and CONCLUSIONS

Although the species identified in Sarıkum Nature Protection Area were consistent with the rodent species in the study by Çam and Ölmez [9] which was evaluated the mammal fauna in Sinop province, *Dryomys nitedula* (forest dormouse) was not found in field studies conducted within the scope of this study. The habitats in this study were exactly consistent with a study which evaluated the habitats of rodents in Turkey and their effects on agricultural areas [8]. The habitats including the largest number of species contained mixed plants and shrubs. For example, it was observed that the study area including Sinop province where the *Myodes glareolus* (bank vole) samples were collected in a study which allozyme variations were evaluated [12], was terrestrial forestry areas and shrubs with mixed plants with a rate of 14% in Sarıkum NPA. In addition, I found *Crocidura suaveolens* specimens, a species which was evaluated in a study about distribution of it [10], in Gerze district of Sinop and from the banks of Karasu Stream. Although a large number of the same species were observed in the capture studies carried out within the scope of this study, it was excluded from the evaluation because it was not included in Rodentia.

The dune zones of Sarıkum Nature Protection Area was very different namely that Rodent species weren't observed or trapped in this zone. The possible reason for this result may be that the nutrients in the dune areas cannot supply the food needs of the rodents. All rodent species were caught/observed in Sarıkum NPA were in the IUCN red list under LC (Least Concern), wide distribution, low risk category [17].

In conclusion, this study reveals valuable results in many aspects: (1) this was the first study which Rodentia species in or around Sarıkum Nature Protection Area were observed and/or captured; (2) Rodent species which were identified in Sarıkum Nature Protection Area constituted about 15% of the 65 rodent species distributed in Turkey. Considering that Sarıkum NPA is a 785 hectare area, this rate indicates moderate species richness for Rodentia mammals. To define the wild animals in Sarıkum NPA, which was declared as a Nature Protection Area and site, will increase the ecological importance of the region.

(3) During the field studies within the context of this study, I interviewed Sarıkum village villagers about the rodent species in this region. The residents of Sarıkum village will contribute to the prevention of unconscious struggle with rodents by knowing the rodent species living around them.

(4) The present study is also important in terms of providing a basis for molecular studies to protect the gene resources of Sinop province.

Sarıkum Lake, which is one of the ecological values of Sinop province, and its surroundings are visited by many nature lovers and bird watchers.

In my opinion, precautions should be increased to protect the area from anthropogenic effects and to prevent holiday makers using the beach in summer from harming the nature of Sarıkum NPA. Warning signs in the area should be increased. Entrances and exits to the area should be controlled more strictly.

Funding

This study was funded by Sinop University Scientific Research Projects Coordinatorship, with the project number FEF-1901-18-24.

The Declaration of Conflict of Interest/ Common Interest

No conflict of interest or common interest has been declared by the author.

The Declaration of Ethics Committee Approval

The author declare that this study was approved with the 22.05.2018 dated and 2018/01 numbered decision of Sinop University Rectorate Animal Experiments Local Ethics Committee.

The Declaration of Research and Publication Ethics

The author of the paper declare that she complies with the scientific, ethical and quotation rules of SAUJS in all processes of the paper and that she does not make any falsification on the data collected. In addition, she declares that Sakarya University Journal of Science and its editorial board have no responsibility for any ethical violations that may be encountered, and that this study has not been evaluated in any academic publication environment other than Sakarya University Journal of Science.

REFERENCES

[1] Sinop Doğa Turizmi Master Planı. 2013. T.C. Orman ve Su İşleri Bakanlığı, Doğa Koruma ve Milli Parklar Genel Müdürlüğü. 10. Bölge Müdürlüğü, Sinop.

[2] Sinop İli 2017 Yılı Çevre Durum Raporu.2018. T.C. Çevre ve Şehircilik Bakanlığı. T.C. Sinop Valiliği. Çevre ve Şehircilik İl Müdürlüğü

[3] T.C. Tarım ve Orman Bakanlığı 10. Bölge Müdürlüğü Resmi web sitesi http://bolge10.ormansu.gov.tr/10bolge/AnaSayfa/Korunan_Alanlarimiz/Tabiatikorumaalanlari/SarikumTKA.aspx?sflang=tr (last access: 20.09.2020)

[4] Akpınar, E. ve Bulut, Y. 2010. Ülkemizde Alternatif Turizm Bir Dalı Olan Ekoturizmi Çeşitlerinin Bölgelere Göre Dağılımı ve Uygulama Alanları. III. Ulusal Karadeniz Ormancılık Kongresi, 20-22 Mayıs 2010. Cilt IV, s.1575-1594.

[5] Sarıkum Gölü ve Aksaz- Karagöl Sulak Alanı Sulak Alan Alt Havzaları Biyolojik Çeşitlilik Araştırma Alt Projesi. T.C. Orman ve Su İşleri Bakanlığı Doğa Koruma ve Milli Parklar Genel Müdürlüğü. Hassas Alanlar Dairesi Başkanlığı Sulak Alanlar Şube Müdürlüğü. X. Bölge Müdürlüğü. Sinop İl Şube Müdürlüğü.

[6] Yılmaz, C. 2005. Sarıkum Gölü Ekosistemi (Sinop). TURQUA – Türkiye Kuvaterner Sempozyumu V, (02–03 Haziran 2005), Bildiriler Kitabı, (Editörler: O. Tüysüz - M.K. Erturaç), İstanbul Teknik Üniversitesi, Avrasya Yerbilimleri Enstitüsü Yayını, (219-226), İstanbul.

[7] Yiğit, N., Çolak, E., Sözen, M. ve Karataş, A., 2006. Rodents of Türkiye (Türkiye Kemiricileri), 1-114. Meteksan A.Ş. Ankara.

[8] Yiğit, N., Çolak, E., Sözen, M. ve Özkurt, Ş. 1999. Türkiye Kemiricilerinin (Mammalia: Rodentia) Habitatları ve Tarım Alanları Üzerine Etkileri. Gazi Üniversitesi Fen Bilimleri Enstitüsü Dergisi. 12 (4): 885-905.

[9] Çam, P. ve Ölmez, İ. 2015. Sinop İli Memeli Hayvan Faunasının Değerlendirilmesi. Iğdır Üniversitesi Fen Bilimleri Enstitüsü Dergisi. 5(3): 9-16.

[10] Kefelioğlu, H. and Tez, C. 1999. The Distribution Problem of *Crocidura russula* (Hermann, 1780) (Mammalia: Insectivora) in Turkey. Tr. J. Of Zoology. 23: 247-251.

[11] Çolak, E. and Kıvanç, E. 1991. Distribution and Taxonomic Status of Genus *Clethrionomys* Tilesius, 1850 (Mammalia: Rodentia) in North Anatolia. Commun. Fac. Sci. Univ. Ankara Series C. 9:1-16.

[12] Çolak, R., Kandemir İ, Karacan Olgun, G., Kankılıç, T., Çolak, E., Yiğit, N. and Özkurt, Ö. Ş., 2013. Allozyme variation in bank vole, *Myodes glareolus* (Mammalia: Rodentia) in Northern Anatolia. Biochemical Systematics and Ecology, 50: 304-309.

[13] Küçük, Ö. 2012. Ayancık Orman İşletme Müdürlüğü'nün Yaban Hayatı Potansiyeli ve Değerlendirilmesi. Kastamonu Üniversitesi Orman Fakültesi.

[14] Corbet, G.B. 1978. The Mammals of the Palaearctic Region Taxonomic Review, British Museum (Nat.Hist.) Cornell Univ. Pres, London & Ithaca.

[15] Wilson, D. E. and Reeder, D-A.M. 1993. Mammal species of the world. A taxonomic and geographic reference. 2nd edition. Smitsonian Institution Press, Washington, 1-56098-217-9.

[16] Kryštufek, B., Vohralík, V. and Janžekovič, F. 2009. Mammals of Turkey and Cyprus: Rodentia II: Cricetinae, Muridae, Spalacidae, Calomyscidae, Capromydae, Hystricidae, Castoridae. Univerza na Primorskem, Znanstveno –raziskovalno središče, Založba Annales.

[17] International Union for Conservation of Nature official website https://www.iucnredlist.org/ (last access 08.10.2020)

SAKARYA ÜNİVERSİTESİ
FEN BİLİMLERİ ENSTİTÜSÜ DERGİSİ

Sakarya University Journal of Science
SAUJS

e-ISSN 2147-835X | Period Bimonthly | Founded: 1997 | Publisher Sakarya University |
http://www.saujs.sakarya.edu.tr/en/

Title: Modified Sumudu Transform and Its Properties

Authors: Uğur DURAN

Recieved: 2020-11-12 00:00:00

Accepted: 2021-02-08 00:00:00

Article Type: Research Article

Volume: 25
Issue: 2
Month: April
Year: 2021
Pages: 389-396

How to cite
Uğur DURAN; (2021), Modified Sumudu Transform and Its Properties. Sakarya University Journal of Science, 25(2), 389-396, DOI: https://doi.org/10.16984/saufenbilder.825180
Access link
http://www.saujs.sakarya.edu.tr/en/pub/issue/60672/825180

Sakarya University Journal of Science 25(2), 389-396, 2021

Modified Sumudu Transform and Its Properties

Uğur DURAN*[1]

Abstract

Saif et al. (J. Math. Comput. Sci. 21 (2020) 127-135) considered modified Laplace transform and developed some of their certain properties and relations. Motivated by this work, in this paper, we define modified Sumudu transform and investigate many properties and relations including modified Sumudu transforms of the power function, sine, cosine, hyperbolic sine, hyperbolic cosine, exponential function, and function derivatives. Moreover, we attain two shifting properties and a scale preserving theorem for the modified Sumudu transform. We give modified inverse Sumudu transform and investigate some relations and examples. Furthermore, we show that the modified Sumudu transform is the theoretical dual transform to the modified Laplace transform.

Keywords: Gamma function, Sumudu transform, Laplace transform, convolution

1. INTRODUCTION

Throughout this paper, the symbols $\mathbb{C}$, $\mathbb{R}$, $\mathbb{Z}$, $\mathbb{N}$ and $\mathbb{N}_0$ are referred to the set of all complex numbers, the set of all real numbers, the set of all integers, the set of all-natural numbers, and the set of all non-negative integers, respectively.

Integral transforms have been played a key role to solve the differential or integrodifferential equations *cf*. [1-12]. One of the most useful integral transforms is the Laplace transform, for f being a function defined for $t \geq 0$, defined by

$$F(s) = \left(f(t) \right) = \int_0^\infty e^{-st} f(t) dt, \tag{1.1}$$

provided that the integral converges. It has powerful applications, not only in applied mathematics but also in other branches of science such as astronomy, engineering, physics, etc., *cf* [5-9]. Also, diverse integral transforms such as Sumudu, Fourier, Elzaki, and M -transforms have been considered, and their properties and applications have been examined in detail by many scientists, *cf*. [1-12] and see also the references cited therein. The Laplace transform is the theoretical dual transform of the Sumudu transform which is introduced by Watugula [10], given by

* Corresponding Author: mtdrnugur@gmail.com & ugur.duran@iste.edu.tr
[1]Iskenderun Technical University, Faculty of Engineering and Natural Sciences, Department of the Basic Concepts of Engineering, TR-31200 Hatay, Turkey
ORCID: https://orcid.org/0000-0002-5717-1199

$$G(u)=\mathbf{S}\left[f(t)\right]=\int_0^{\infty}e^{-t}f(ut)\,dt$$

$$=\frac{1}{u}\int_0^{\infty}e^{-\frac{t}{u}}f(t)\,dt,\ u\in(-\tau_1,\tau_2),\qquad(1.2)$$

over the set of functions

$$A=\left\{f(t)\middle|\exists M,\tau_1,\tau_2>0,\left|f(t)\right|<Me^{\frac{|t|}{\tau_j}},\ \text{if } t\in(-1)^j\times[0,\infty)\right\}.$$

Several applications of Sumudu transform have been investigated and studied by many physicists and mathematicians, *cf.* [1-4, 6, 10-12]. For instance, Watagula [11] defined two variables Sumudu transform and provided an example solving partial differential equations with known initial conditions. Weerakoon [12] attained the Sumudu transform of partial derivatives and proved its applicability demonstrated utilizing three different partial differential equations. Kilicman et al. [6] studied some properties of the Sumudu transform and relationship between Sumudu and Laplace transforms, and then gave an application of the double Sumudu transform to solve the wave equation in one dimension having singularity at initial conditions. Asiru [1] provided Sumudu transform of several special functions and derived some applications with Abel's integral equation, an integrodifferential equation, a dynamic system with delayed time signals and a differential dynamic system. Belgacem et al. [2] developed fundamental properties including scale and unit-preserving properties of Sumudu transform and proved a solution to an integral production-depreciation problem. Belgacem [3] analyzed deeper Sumudu properties and connections. Belgacem et al. [4] generalized all existing Sumudu integration, differentiation, and Sumudu shifting theorems and convolution theorems. In this study, we introduce modified Sumudu transform and investigate many properties and relations including modified Sumudu transforms of the power function, sine, cosine, hyperbolic sine, hyperbolic cosine, exponential function, and function derivatives. Moreover, we obtain two shifting properties and a scale preserving theorem for the modified Sumudu transform. We provide modified inverse Sumudu transform and derive some relations and examples. Furthermore, we show that modified Sumudu transform is the theoretical dual transform to modified Laplace transform. Lastly, we give duality between the modified Laplace transform and the modified Sumudu transform.

The Sumudu transformation satisfies the following operational properties, *cf.* [2,4]:

$\mathbf{S}[1]=1$	$\mathbf{S}[\sin(at)]=\frac{au}{1+u^2a^2}$
$\mathbf{S}[t]=u$	$\mathbf{S}[\cos(at)]=\frac{1}{1+u^2a^2}$
$\mathbf{S}[t^n]=n!u^n$	$\mathbf{S}[\sinh(at)]=\frac{au}{1+u^2a^2}$
$\mathbf{S}[e^{at}]=\frac{1}{1-ua}$	$\mathbf{S}[\cosh(at)]=\frac{1}{1+u^2a^2}$
$\mathbf{S}[f(at)]=G(au)$	$\mathbf{S}[e^{at}f(t)]=\frac{1}{1-au}G\left(\frac{u}{1-au}\right)$

Let $f(t),g(t)\in A$ be Sumudu transforms $M(u)$ and $N(u)$, respectively. Then the Sumudu transform of the convolution of f and g is given by

$$\mathbf{S}\left[(f*g)(t)\right]=uM(u)N(u),\qquad(1.4)$$

where the convolution integral is given by (*cf.* [2,4])

$$(f*g)(t)=\int_0^t g(x)f(t-x)\,dx\qquad(1.5)$$

for $f(t)$ and $g(t)$ are piece-wise continuous and of exponential order.

The gamma function is defined by the following improper integral (*cf.* [5-9]):

$$\Gamma(s)=\int_0^{\infty}e^{-t}t^{s-1}dt,\qquad(1.6)$$

where s is a complex number with $Re(s)>0$. The gamma function satisfies the following relations

$$\Gamma(s+1)=s\Gamma(s)\text{and}\,\Gamma(n+1)=n!$$

for n being a non-negative integer.

2. MODIFIED SUMUDU TRANSFORM

In [9], the modified Laplace transform of a function $f(t)$ which is peace-wise continuous and of exponential order is considered as follows

$$L_a\left(f(t)\right)=F(s;a)=\int_0^{\infty}a^{-st}f(t)dt, \quad (2.1)$$

where $Re(s)>0$ and $a\in(0,\infty)\setminus\{1\}$. Note that upon setting $a=e$, modified Laplace transform reduces to usual Laplace transform in (1.1). Then the authors gave several basic properties of modified Laplace transform and provided connections with different functions in [9].

Motivated by the above, we define modified Sumudu transform as follows.

Definition 1 Let $a\in(0,\infty)\setminus\{1\}$ and

$$A_a=\left\{f(t)\middle|\exists M,\tau_1,\tau_2>0 \text{ such that } |f(t)|<Ma^{1/\tau_j}(|t|), \text{if } t\in(-1)^j\times[0,\infty)\right\}. \quad (2.2)$$

Then, for $f(t)\in A_a$, we define modified Sumudu transform by the following improper integral:

$$\mathcal{G}_a(u)=\mathcal{S}_a\left[f(t)\right]=\frac{1}{u}\int_0^{\infty}a^{\frac{-s}{u}}f(t)dt, u\in(-\tau_1,\tau_2). \quad (2.3)$$

We note that

$$\mathcal{S}_e\left[f(t)\right]:=\mathbf{S}\left[f(t)\right].$$

Let $f(t),g(t)\in A_a$ and $\gamma,\omega\in\mathbb{R}$. The modified Sumudu transformation is a linear transform, namely

$$\begin{aligned}\mathcal{S}_a\left[\gamma f(t)+\omega g(t)\right]&=\frac{1}{u}\int_0^{\infty}a^{\frac{-t}{u}}\left[\gamma f(t)+\omega g(t)\right]dt\\&=\frac{\gamma}{u}\int_0^{\infty}a^{\frac{-t}{u}}f(t)dt+\frac{\omega}{u}\int_0^{\infty}a^{\frac{-t}{u}}g(t)dt\\&=\gamma\mathcal{S}_a\left[f(t)\right]+\omega\mathcal{S}_a\left[g(t)\right].\end{aligned}$$

By Definition 1, for $f(t)=1,$ we observe that

$$\begin{aligned}\mathcal{S}_a[1]&=\frac{1}{u}\int_0^{\infty}a^{\frac{-t}{u}}dt=\lim_{R\to\infty}\frac{1}{u}\int_0^{R}e^{-\frac{t}{u}\log a}dt\\&=\frac{1}{u}\lim_{R\to\infty}\left.\frac{e^{-\frac{t}{u}\log a}}{-\frac{1}{u}\log a}\right|_0^{R}=\lim_{R\to\infty}\left(\frac{e^{-\frac{R}{u}\log a}}{-\frac{1}{u}\log a}+\frac{1}{\log a}\right)\\&=\frac{1}{\log a},\quad\frac{\log a}{u}>0\end{aligned}$$

and for $f(t)=t$ with $\frac{\log a}{u}>0$,

$$\begin{aligned}\mathcal{S}_a[t]&=\frac{1}{u}\int_0^{\infty}ta^{\frac{-t}{u}}dt=\lim_{R\to\infty}\left(\left.-\frac{ta^{\frac{-t}{u}}}{\log a}\right|_0^{R}+\frac{1}{\log a}\int_0^{R}a^{\frac{-t}{u}}\right)dt\\&=-\lim_{R\to\infty}\left.\frac{u}{(\log a)^2}a^{\frac{-t}{u}}\right|_0^{R}dt=\frac{u}{(\log a)^2},\end{aligned}$$

which gives the following theorem.

Theorem 1 We have

$$\mathcal{S}_a[1]=\frac{1}{\log a},\quad\frac{\log a}{u}>0 \quad (2.4)$$

and

$$\mathcal{S}_a[t]=\frac{u}{(\log a)^2},\quad\frac{\log a}{u}>0. \quad (2.5)$$

By Definition 1, for $f(t)=t^n$ with $n\in\mathbb{N}$ and $\frac{\log a}{u}>0,$ we observe that

$$\begin{aligned}\mathcal{S}_a\left[t^n\right]&=\frac{1}{u}\int_0^{\infty}t^na^{\frac{-t}{u}}dt=\frac{n}{\log a}\int_0^{\infty}t^{n-1}a^{\frac{-t}{u}}dt\\&=\frac{n(n-1)}{(\log a)^2}u\int_0^{\infty}t^{n-2}a^{\frac{-t}{u}}dt=\ldots\\&=\frac{n!u^{n-1}}{(\log a)^n}\int_0^{\infty}a^{\frac{-t}{u}}dt=\frac{n!u^n}{(\log a)^{n+1}}\end{aligned}$$

and for $f(t)=e^{bt}$,

$$\begin{aligned}\mathcal{S}_a\left[e^{bt}\right]&=\frac{1}{u}\int_0^{\infty}e^{bt}a^{\frac{-t}{u}}dt\\&=\frac{1}{u}\int_0^{\infty}e^{t\left(b-\frac{\log a}{u}\right)}dt=\frac{1}{u}\lim_{R\to\infty}\left.\frac{e^{t\left(b-\frac{\log a}{u}\right)}}{b-\frac{\log a}{u}}\right|_0^{R}\\&=\frac{1}{u}\lim_{R\to\infty}\left(\frac{e^{t\left(b-\frac{\log a}{u}\right)}}{b-\frac{\log a}{u}}-\frac{1}{b-\frac{\log a}{u}}\right)\\&=\frac{1}{\log a-bu},\quad b<\frac{\log a}{u},\end{aligned}$$

which provides the following theorem.

Theorem 2 Let $n \in \mathbb{N}$. We have

$$\mathcal{S}_a\left[t^n\right] = \frac{n!u^n}{\left(\log a\right)^{n+1}}, \quad 0 < \frac{\log a}{u} \tag{2.6}$$

and

$$\mathcal{S}_a\left[e^{bt}\right] = \frac{1}{\log a - bu}, \quad b < \frac{\log a}{u}. \tag{2.7}$$

From Definition 1 and using formula (2.7), we have

$$\begin{aligned}\mathcal{S}_a\left[\sin\left(bt\right)\right] &= \mathcal{S}_a\left[\frac{e^{ibt}-e^{-ibt}}{2i}\right] \\ &= \frac{1}{2i}\left(\mathcal{S}_a\left[e^{ibt}\right]-\mathcal{S}_a\left[e^{-ibt}\right]\right) \\ &= \frac{1}{2i}\left(\frac{1}{\log a - ibu}-\frac{1}{\log a + ibu}\right) \\ &= \frac{bu}{\left(\log a\right)^2 + b^2u^2}\end{aligned}$$

and

$$\begin{aligned}\mathcal{S}_a\left[\cos\left(bt\right)\right] &= \mathcal{S}_a\left[\frac{e^{ibt}+e^{-ibt}}{2}\right] \\ &= \frac{1}{2}\left(\mathcal{S}_a\left[e^{-ibt}\right]+\mathcal{S}_a\left[e^{-ibt}\right]\right) \\ &= \frac{1}{2}\left(\frac{1}{\log a - ibu}+\frac{1}{\log a - ibu}\right) \\ &= \frac{\log a}{\left(\log a\right)^2 + b^2u^2},\end{aligned}$$

where $i = \sqrt{-1}$. Thus we give the following theorem.

Theorem 3 We have

$$\mathcal{S}_a\left[\sin(bt)\right] = \frac{bu}{(\log a)^2 + b^2u^2} \text{ and } \mathcal{S}_a\left[\cos(bt)\right] = \frac{\log a}{(\log a)^2 + b^2u^2}. \tag{2.8}$$

By Definition 1, and utilizing formula (2.7), we derive

$$\mathcal{S}_a\left[\sinh\left(bt\right)\right] = \mathcal{S}_a\left[\frac{e^{bt}-e^{-bt}}{2}\right] = \frac{bu}{\left(\log a\right)^2 - b^2u^2}$$

and

$$\mathcal{S}_a\left[\cosh\left(bt\right)\right] = \mathcal{S}_a\left[\frac{e^{bt}+e^{-bt}}{2}\right] = \frac{\log a}{\left(\log a\right)^2 - b^2u^2}.$$

Therefore, we give the following theorem.

Theorem 4 We have

$$\mathcal{S}_a\left[\sinh(bt)\right] = \frac{bu}{(\log a)^2 - b^2u^2} \text{ and } \mathcal{S}_a\left[\cosh(bt)\right] = \frac{\log a}{(\log a)^2 - b^2u^2}. \tag{2.9}$$

By Definition 1 and (1.6), for $b \in \mathbb{R}$ with $b > -1$, we derive

$$\begin{aligned}\mathcal{S}_a\left[t^b\right] &= \frac{1}{u}\int_0^\infty t^b a^{\frac{-t}{u}}dt = \frac{u^{b-1}}{\left(\log a\right)^b}\int_0^\infty\left(\frac{t\log a}{u}\right)^b e^{\frac{-t}{u}\log a}dt \\ &= \frac{u^b}{\left(\log a\right)^{b+1}}\int_0^\infty t^b e^{-t}dt = \frac{u^b}{\left(\log a\right)^{b+1}}\Gamma\left(b+1\right).\end{aligned}$$

Thus we give the following theorem.

Theorem 5 The following

$$\mathcal{S}_a\left[t^b\right] = \frac{u^b}{\left(\log a\right)^{b+1}}\Gamma\left(b+1\right)$$

is valid for $b \in \mathbb{R}$ with $b > -1$.

We now investigate some formulas for modified Sumudu transform of derivatives of functions.

By Definition 1, for $\frac{\log a}{u} > 0$, we see that

$$\mathcal{S}_a\left[f'(t)\right] = \frac{1}{u}\int_0^\infty f'(t)a^{\frac{-t}{u}}dt = \frac{1}{u}\left(\log a\mathcal{G}_a(u) - f(0)\right). \tag{2.10}$$

By means of (2.10), we acquire

$$\begin{aligned}\mathcal{S}_a\left[f^{(2)}(t)\right] &= \frac{1}{u}\int_0^\infty f^{(2)}(t)a^{\frac{-t}{u}}dt \\ &= \frac{1}{u^2}\left(\left(\log a\right)^2\mathcal{G}_a(u) - \log a f(0) - uf'(0)\right).\end{aligned}$$

Continuing this process, we get

$$\mathcal{S}_a\left[f^{(n)}(t)\right] = \frac{\left(\log a\right)^n}{u^n}\mathcal{G}_a(u) - \frac{1}{u^n}\sum_{i=0}^{n-1}\left(\log a\right)^{n-i-1}u^i f^{(i)}(0). \tag{2.11}$$

By (2.11), we provide the following theorem.

Theorem 6 The following modified Sumudu transform

$$\mathcal{S}_a\left[f^{(n)}(t)\right] = \frac{\left(\log a\right)^n}{u^n}\mathcal{G}_a(u) - \frac{1}{u^n}\sum_{i=0}^{n-1}\left(\log a\right)^{n-i-1}u^i f^{(i)}(0). \tag{2.12}$$

is valid for $n\in\mathbb{N}$ and $\frac{\log a}{u}>0$.

By Definition 1, for $u\in(-\tau_1,\tau_2)$, we observe that

$$\frac{d}{du}\mathcal{G}_a(u)=-\frac{1}{u^2}\int_0^\infty a^{\frac{-t}{u}}f(t)dt+\frac{\log a}{u^3}\int_0^\infty a^{\frac{-t}{u}}tf(t)dt$$
$$=-\frac{1}{u}\mathcal{G}_a(u)+\frac{\log a}{u^2}\mathcal{S}_a\left[tf(t)\right],$$

$$\frac{d^2}{du^2}\mathcal{G}_a(u)=\frac{d}{du}\left(-\frac{1}{u}\mathcal{G}_a(u)+\frac{\log a}{u^2}\mathcal{S}_a\left[tf(t)\right]\right)$$
$$=\frac{1}{u^2}\mathcal{G}_a(u)-\frac{1}{u}\left(-\frac{1}{u}\mathcal{G}_a(u)+\frac{\log a}{u^2}\mathcal{S}_a\left[tf(t)\right]\right)-\frac{2}{u^3}\mathcal{S}_a\left[tf(t)\right]$$
$$+\frac{1}{u^2}\left(-\frac{1}{u}\mathcal{S}_a\left[tf(t)\right]+\frac{\log a}{u^2}\mathcal{S}_a\left[t^2f(t)\right]\right)$$
$$=\frac{2}{u^2}\mathcal{G}_a(u)-\frac{3+\log a}{u^3}\mathcal{S}_a\left[tf(t)\right]+\frac{\log a}{u^4}\mathcal{S}_a\left[t^2f(t)\right].$$

and

$$\frac{d^3}{du^3}\mathcal{G}_a(u)=\frac{d}{du}\left(\frac{2}{u^2}\mathcal{G}_a(u)-\frac{3+\log a}{u^3}\mathcal{S}_a\left[tf(t)\right]+\frac{\log a}{u^4}\mathcal{S}_a\left[t^2f(t)\right]\right)$$
$$=-\frac{6}{u^3}\mathcal{G}_a(u)+\frac{12+6\log a}{u^4}\mathcal{S}_a\left[tf(t)\right]$$

$$-\frac{(\log a)^2+4\log a}{u^5}\mathcal{S}_a\left[t^2f(t)\right]+\frac{(\log a)^2}{u^6}\mathcal{S}_a\left[t^3f(t)\right].$$

Therefore, we give the following theorem.

Theorem 7 For $u\in(-\tau_1,\tau_2)$ and $\frac{\log a}{u}>0$, we have

$$\frac{d}{du}\mathcal{G}_a(u)=-\frac{1}{u}\mathcal{G}_a(u)+\frac{\log a}{u^2}\mathcal{S}_a\left[tf(t)\right]$$
$$\frac{d^2}{du^2}\mathcal{G}_a(u)=\frac{2}{u^2}\mathcal{G}_a(u)-\frac{3+\log a}{u^3}\mathcal{S}_a\left[tf(t)\right]+\frac{\log a}{u^4}\mathcal{S}_a\left[t^2f(t)\right]$$

and

$$\frac{d^3}{du^3}\mathcal{G}_a(u)=-\frac{6}{u^3}\mathcal{G}_a(u)+\frac{12+6\log a}{u^4}\mathcal{S}_a\left[tf(t)\right]$$
$$-\frac{(\log a)^2+4\log a}{u^5}\mathcal{S}_a\left[t^2f(t)\right]+\frac{(\log a)^2}{u^6}\mathcal{S}_a\left[t^3f(t)\right].$$

From Definition 1, we observe that

$$\mathcal{S}_a\left[f(bt)\right]=\frac{1}{u}\int_0^\infty f(bt)a^{\frac{-t}{u}}dt=\frac{1}{u}\int_0^\infty f(bt)a^{\frac{-bt}{bu}}dt$$

and setting $\omega=bt$, then

$$\mathcal{S}_a\left[f(bt)\right]=\frac{1}{bu}\int_0^\infty f(\omega)a^{\frac{-\omega}{bu}}d\omega=\mathcal{G}_a(bu).$$

Thereby, we give the following theorem.

Theorem 8 The following

$$\mathcal{S}_a\left[f(bt)\right]=G_a(bu) \tag{2.13}$$

holds.

Let $\delta(t-c)$ be unit step function given the below:

$$\delta(t-c)=\{.0,\ x<c,1,\ x\geq c.$$

Then, we get

$$\mathcal{S}_a\left[\delta(t-c)\right]=\frac{1}{u}\int_0^c 0a^{\frac{-t}{u}}dt+\frac{1}{u}\int_c^\infty a^{\frac{-t}{u}}dt=\frac{a^{\frac{-c}{u}}}{\log a},\ \frac{\log a}{u}>0.$$

By Definition 1, for $\mathcal{S}_a\left[f(t)\right]=G_a(u)$, we observe

$$\mathcal{S}_a\left[a^{bt}f(t)\right]=\frac{1}{u}\int_0^c a^{-\left(\frac{1-bu}{u}\right)t}f(t)dt=G_a\left(\frac{u}{1-bu}\right)$$

and

$$\mathcal{S}_a\left[f(t-c)\delta(t-c)\right]=\frac{1}{u}\int_c^\infty a^{\frac{-t}{u}}f(t-c)dt$$
$$=\frac{1}{u}\int_0^\infty a^{\frac{-t+c}{u}}f(t)dt=a^{-\frac{c}{u}}\mathcal{S}_a\left[f(t)\right].$$

Hence, two shifting properties of modified Sumudu transform are given by the following theorem.

Theorem 9 Let $\mathcal{S}_a\left[f(t)\right]=G_a(u)$. Each of the following properties

$$\mathcal{S}_a\left[a^{bt}f(t)\right]=G_a\left(\frac{u}{1-bu}\right)$$ (The first shifting property)

and

$$\mathcal{S}_a\left[f(t-c)\delta(t-c)\right]=a^{-\frac{c}{u}}\mathcal{S}_a\left[f(t)\right]$$ (The second shifting property)

holds for $\frac{\log a}{u}>0$.

By (1.5), it can be readily shown that the set of all modified Sumudu transformable functions form a commutative semigroup with respect to the convolution operator $*$.
By Definition 1 and (1.5), we attain

$$\mathcal{S}_a\left[(f*g)(t)\right]=\frac{1}{u}\int_0^\infty a^{\frac{-t}{u}}(f*g)(t)\,dt$$
$$=\frac{1}{u}\int_0^\infty a^{\frac{-t}{u}}\left(\int_0^t g(\omega)\,f(t-\omega)\,d\omega\right)dt.$$

Setting $t-\omega=\gamma$ yields $dt=d\gamma$, and we have

$$\mathcal{S}_a\left[(f*g)(t)\right]=\frac{1}{u}\int_0^\infty\int_0^\infty a^{\frac{-\gamma+\omega}{u}}g(\omega)\,f(\gamma)\,d\omega d\gamma$$
$$=u\left(\frac{1}{u}\int_0^\infty a^{\frac{-\omega}{u}}f(\omega)\,d\omega\right)\left(\frac{1}{u}\int_0^\infty a^{\frac{-\gamma}{u}}g(\gamma)\,d\gamma\right)$$
$$=u\mathcal{S}_a\left[f(t)\right]\mathcal{S}_a\left[g(t)\right].$$

Thus, we give the following theorem.

Theorem 10 For $f(t)$ and $g(t)$ being piece-wise continuous and of exponential order functions on $[0,\infty]$, let $\mathcal{S}_a\left[f(t)\right]=G_a(u)$ and $\mathcal{S}_a\left[g(t)\right]=H_a(u)$. Modified Sumudu transform of the convolution is as follows:

$$\mathcal{S}_a\left[(f*g)(t)\right]=uG_a(u)H_a(u).$$

3. FURTHER REMARKS

By (1.1) and (1.2), the Sumudu transform is the theoretical dual transform to the Laplace transform given below (*cf.* [2,4])

$$G(u)=\frac{F(1/u)}{u}\ \text{and}\ F(s)=\frac{G(1/s)}{s}.\quad(3.1)$$

Using (2.1) and (2.3), for $f(t)\in A_a$ and $-\tau_1<u<\tau_2$, we observe that

$$G_a(u)=\mathcal{S}_a\left[f(t)\right]=\frac{1}{u}\int_0^\infty a^{\frac{-t}{u}}f(t)\,dt=\frac{1}{u}F\left(\frac{1}{u};a\right)\quad(3.2)$$

and

$$F(s;a)=L_a\left(f(t)\right)=\frac{1}{s}\frac{1}{\frac{1}{s}}\int_0^\infty a^{-st}f(t)\,dt=\frac{1}{s}G_a\left(\frac{1}{s}\right)\quad(3.3)$$

which are the modified version of the duality in (3.1). Therefore, the relations (3.2) and (3.3) between the modified Sumudu transform and the modified Laplace transform means to acquire one from the other when needed. For example, since $L_a\left(\sinh(bt)\right)=\dfrac{b}{s^2(\log a)^2-b^2}$, recall from Theorem 4, we have

$$F(s;a)=\frac{1}{s}\frac{b(1/s)}{(\log a)^2-(1/s)^2b^2}=\frac{1}{s}G_a\left(\frac{1}{s}\right).$$

Hence, we can say from (3.2) and (3.3) that the modified Sumudu transform is the theoretical dual transform to the modified Laplace transform. We now introduce modified inverse Sumudu transform of a function $f(t)$ as follows:

$$f(t)=\mathcal{S}_a^{-1}\left[G_a(u)\right]=\frac{1}{2\pi i}\int_{\gamma-i\infty}^{\gamma+i\infty}a^{ut}G_a(u)\,du,\quad(\gamma>0).\quad(3.4)$$

It can be readily seen that modified inverse Sumudu transform is a linear transform, namely, for $\beta,\omega\in\mathbb{R}$,

$$\mathcal{S}_a^{-1}\left[\beta G_a(u)+\omega H_a(u)\right]$$
$$=\beta\mathcal{S}_a^{-1}\left[G_a(u)\right]+\omega\mathcal{S}_a^{-1}\left[H_a(u)\right]=\beta f(t)+\omega g(t),$$

where $\mathcal{S}_a\left[f(t)\right]=G_a(u)$ and $\mathcal{S}_a\left[g(t)\right]=H_a(u)$.

From (3.4) and Theorem 10, we get

$$\mathcal{S}_a^{-1}\left[G_a(u)H_a(u)\right]=\frac{1}{u}(f*g)(t).$$

Some examples of the modified inverse Sumudu transform are stated below.

$$\mathcal{S}_a^{-1}\left[\frac{1}{\log a}\right]=1\quad\text{by (2.4)}$$

$$\mathcal{S}_a^{-1}\left[u^n\right]=\frac{(\log a)^{n+1}t^n}{n!}\quad\text{by (2.5)}$$

$$\mathcal{S}_a^{-1}\left[\frac{1}{\log a-bu}\right]=e^{bt}\quad\text{by (2.7)}$$

$$\mathcal{S}_a^{-1}\left[\frac{u}{(\log a)^2+b^2u^2}\right]=\frac{\sin(bt)}{b}\quad\text{by (2.8)}$$

$$\mathcal{S}_a^{-1}\left[\frac{1}{(\log a)^2+b^2u^2}\right]=\frac{\cos(bt)}{\log a}\quad\text{by (2.8)}$$

$$\mathcal{S}_a^{-1}\left[\frac{u}{(\log a)^2-b^2u^2}\right]=\frac{\sinh(bt)}{b}\quad\text{by (2.9)}$$

$$\mathcal{S}_a^{-1}\left[\frac{1}{(\log a)^2 - b^2u^2}\right] = \frac{\cos h(bt)}{\log a} \quad \text{by (2.9).}$$

4. CONCLUSIONS

Saif et al. [9] defined the modified Laplace transform as follows:

$$L_a\left(f(t)\right) = F(s;a) = \int_0^\infty a^{-st} f(t)\,dt,$$

if the integral converges. Several properties and interesting formulas for modified Laplace transform were investigated in [9]. Inspired by this study, in this paper, we have considered modified Sumudu transform by the following improper integral:

$$G_a(u) = \mathcal{S}_a\left[f(t)\right] = \frac{1}{u}\int_0^\infty a^{\frac{-t}{u}} f(t)\,dt,$$

$$u \in (-\tau_1, \tau_2) \text{ and } a \in (0,\infty)/\{0\}$$

for

$$f(t) \in A_\lambda = \left\{ f(t) \middle| \exists M, \tau_1, \tau_2 > 0 \text{ such that } |f(t)| < Ma^{1/\tau_j}(|t|), \text{if } t \in (-1)^j \times [0,\infty) \right\}.$$

Then, we have given many properties and relations covering modified Sumudu transforms of the power function, sine, cosine, hyperbolic sine, hyperbolic cosine, exponential function, and function derivatives. We also attained two shifting properties and a scale preserving theorem for the modified Sumudu transform. Moreover, we have provided modified inverse Sumudu transform and developed some relations and examples. Furthermore, we have shown that the modified Sumudu transform is the theoretical dual transform to the modified Laplace transform.

Funding

The author has no received any financial support for the research, authorship or publication of this study.

The Declaration of Ethics Committee Approval

The author declares that this document does not require an ethics committee approval or any special permission.

The Declaration of Conflict of Interest/Common Interest

No conflict of interest or common interest has been declared by the author.

The Declaration of Research And Publication Ethics

The author of the paper declares that he complies with the scientific, ethical and quotation rules of SAUJS in all processes of the article and that he does not make any falsification on the data collected. In addition, he declares that Sakarya University Journal of Science and its editorial board have no responsibility for any ethical violations that may be encountered, and that this study has not been evaluated in any academic publication environment other than Sakarya University Journal of Science.

REFERENCES

[1] M. U. Asiru, "Further properties of the Sumudu transform and its applications," International Journal of Mathematical Education in Science and Technology, vol. 33, no.3, pp. 441-449, 2002.

[2] F. B. M. Belgacem, A. A. Karaballi, and S. L. Kalla, "Analytical investigations of the Sumudu transform and applications to integral production equations," Mathematical Problems in Engineering, vol. 2003, no.3, pp. 103-118, 2003.

[3] F. B. M. Belgacem, "Introducing and analysing deeper Sumudu properties," Nonlinear Studies, vol. 13, no.1, pp. 23-41, 2006.

[4] F. B. M. Belgacem, Karaballi, A. A. "Sumudu transform fundamental properties investigations and applications," International Journal of Stochastic Analysis, article id 91083, pp. 1-23, 2016.

[5] L. Debnath, "Integral Transforms and Their Applications," CRC Press, Florida, 1995.

[6] A. Kilicman, H. E. Gadian, "On the application of Laplace and Sumudu

transforms," Journal of The Franklin Institute, vol. 347, pp. 848-862, 2010.

[7] A. D. Poularikas, "The Transforms and Applications Handbook, The Electrical Engineering Handbook Series" CRC Press, Florida, 1996.

[8] R. Saadeh, A. Qazza, A. Burqan, "A New Integral Transform: ARA Transform and Its Properties and Applications," Symmetry, vol. 12, article no.925, 2020.

[9] M. Saif, F. Khan, K. S. Nisar, S. Araci, "Modified Laplace transform and its properties," Journal of Mathematics and Computer Science, vol. 21, no.2, pp. 127-135, 2020.

[10] G. K. Watugula, "Sumudu transform: A new integral transform to solve differential equations and control engineering problems," International Journal of Mathematical Education in Science and Technology, vol. 24, pp. 35-43, 1993.

[11] G. K. Watagula, "The Sumudu transform for functions of two variables," Mathematical Engineering in Industry, vol. 8, no.4, pp. 293-302, 2002.

[12] S. Weerakoon, "Application of Sumudu transform to partial differential equations," International Journal of Mathematical Education in Science and Technology, vol. 25, no.2, pp. 277-283, 1994.

SAKARYA ÜNİVERSİTESİ
FEN BİLİMLERİ ENSTİTÜSÜ DERGİSİ

Sakarya University Journal of Science
SAUJS

e-ISSN 2147-835X | Period Bimonthly | Founded: 1997 | Publisher Sakarya University |
http://www.saujs.sakarya.edu.tr/en/

Title: A Review of Genetic Programming Popular Techniques, Fundamental Aspects, Software Tools and Applications

Authors: Davut ARI, Barış Baykant ALAGÖZ

Recieved: 2020-09-10 16:32:01

Accepted: 2021-02-15 23:00:48

Article Type: Research Article

Volume: 25
Issue: 2
Month: April
Year: 2021
Pages: 397-416

How to cite
Davut ARI, Barış Baykant ALAGÖZ; (2021), A Review of Genetic Programming Popular Techniques, Fundamental Aspects, Software Tools and Applications. Sakarya University Journal of Science, 25(2), 397-416, DOI: https://doi.org/10.16984/saufenbilder.793333
Access link
http://www.saujs.sakarya.edu.tr/en/pub/issue/60672/793333

Sakarya University Journal of Science 25(2), 397-416, 2021

A Review of Genetic Programming: Popular Techniques, Fundamental Aspects, Software Tools and Applications

Davut ARI[*1], Barış Baykant ALAGÖZ[2]

Abstract

Genetic Programming (GP) is one of the evolutionary computation (EC) methods followed with great interest by many researchers. When GP first appeared, it has become a popular computational intelligence method because of its successful applications and its potentials to find effective solutions for difficult practical problems of many different disciplines. With the use of GP in a wide variety of areas, numerous variants of GP methods have emerged to provide more effective solutions for computation problems of diverse application fields. Therefore, GP has a very rich literature that is progressively growing. Many GP software tools developed along with process of GP algorithms. There is a need for an inclusive survey of GP literature from the beginning to today of GP in order to reveal the role of GP in the computational intelligence field. This survey study aims to provide an overview of the growing GP literature in a systematic way. The researchers, who need to implement GP methods, can gain insight of potentials in GP methods, their essential drawbacks and prevalent superiorities. Accordingly, taxonomy of GP methods is given by a systematic review of popular GP methods. In this manner, GP methods are analyzed according to two main categories, which consider the discrepancies in their program (chromosome) representation styles and their methodologies. Besides, GP applications in diverse problems are summarized. This literature survey is especially useful for new researchers to gain the required broad perspective before implementing a GP method in their problems.

Keywords: Genetic programming, gp types, gp applications, gp software

1. INTRODUCTION

GP is an EC type that allows computers to automatically formulate the solution of problems without making an assumption for the problem solution formulation [1-2]. Since the first appearance of the GP idea, it has been used to solve different analysis and modeling problems in different fields by using genetic coding techniques.

While spreading of the standard GP interdisciplinary domains, the researchers observed that computation capabilities of the standard GP cannot be sufficient for very hard

[*]Corresponding author: dari@beu.edu.tr
[1]Bitlis Eren University, Faculty of Engineering and Architecture, Computer Engineering Department,13100,Bitlis.
ORCID: https://orcid.org/ 0000-0001-6439-7957
[2]İnönü University, Faculty of Engineering, Computer Engineering Department,44280, Malatya.
E-Mail: baykant.alagoz@inonu.edu.tr.
ORCID: https://orcid.org/ 0000-0001-5238-6433

computational problems in different disciplines [3-5]. This becomes a central motivation for development of more advanced GP algorithms, and enhanced GP variants have been proposed to solve the difficult problems encountered in applications. Researchers mostly concentrated their research effort on improvements of representation formats of GP programs (individuals of the population).

Looking at the literature, it is seen that GP has been widely preferred in the problems that need symbolic regression for data modeling [6]. Accordingly, GP applications come out in many different disciplines such as classification problems[7], production scheduling [8], climate change analysis [9], energy and energy saving [10-12] besides educational technologies [13], urbanization [14], building [15], hydrology [16], medicine[17]. Additionally, GP has widely utilized in many computer sciences problems such as in computer vision[18], image processing [19], signal processing [20], artificial neural network design [21]. Moreover, GP methods were used in the field of evolutionary hardware [22] and circuit design [23]. One can find many application of GP in the field of economy e.g. finance [24] and trading [25] problems.

The use of GP methods in many disciplines and fields, not limited to the above-mentioned fields, shows that it is a popular and versatile calculation intelligence method.

This paper aims to review GP literature to gain a perfective on progress of GP algorithms, foundations of GP structures, popular GP trends and software tools without need of a deep knowledge of GP. For this reason, this study covers the introduction of GP essentials, review of popular methods and practices, and providing recent aspects on the latest developments on GP methodologies. Becoming a popular computing tool led the GP have a rich literature. The current study surveys the GP literature without complicating the topic by giving the deepened technical details of GP algorithms and tools.

Organization of the paper is as follows: Section 2 presents comparative introduction of fundamental GP methods. In Section 3, the taxonomy of GP methods is provided in two major branches that classify GP approaches according to discrepancies in their representation formats and their methodological differences. Section 4 presents an overview on considerable GP applications. Section 5 introduces the software tools that were developed and used by researchers.

2. GENETIC PROGRAMMING AND THE NATURE OF PROBLEMS TO APPLY

GP can be seen as a special EC method in which the individuals, also known as programs or chromosomes, in the population are basically represented in the form of computer programs. In GP, a computer program expresses a population individual that can be a candidate solution to a problem. As shown in Figure 1, in GP, the population of the programs, namely individuals, is generated randomly, as in other evolutionary computation methods [2]. Then, each candidate program (individual) created is tested for compatibility according to its ability to solve the problem. In the next stages, high-fitting computer programs are selected subjected to evolutionary processes such as crossover and mutation, thus enabling them to become more appropriate programs for the solution in the next generation. These evolution processes are repeated until the GP termination criteria are met.

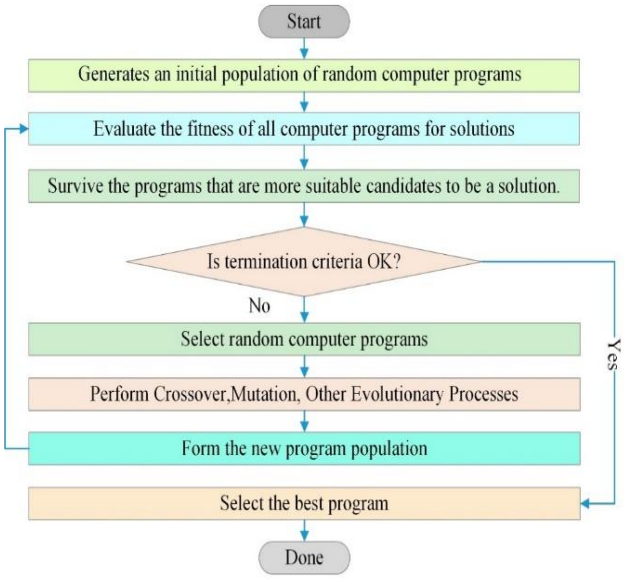

Figure 1 The basic algorithm of Genetic Programming

The program, which has the best solution according to the needs of the targeted problem, continues to exist in time. Hence, it is the best fitting solution to the problem, which are able to maintain its existence until the termination criterion of the GP algorithm is met [26]. This property is known as elitism in evolutionary computation. The GP methods use elitist evolution strategies in order to reach better individuals and they commonly transfer individuals with higher fitness values to the next generations. It can contribute to reducing bloat problems of GP methods [27]. The main difference of the standard GP compared to Genetic Algorithm (GA) is that the program representation of GP can be variable-length instead of being the fixed-length representations such as bits, real numbers, and symbols in the GA [8], [26].

The GP method may be appropriate to use, especially if the interrelationships between the relevant variables in the problem are not known or poorly understood, or in case of a doubt that known relationship among the parameters may be wrong [28]. In other words, when the mathematical model is not known or valid, GP can provide acceptable solutions via model exploration and provide its best-fit solution to the problem.

In addition, if there are large amounts of data, which requires in-depth analysis, classification, and clustering on the computer, the GP can yield satisfactory results. The main reason for this advantage comes from the fact that individuals representing candidate solutions in GP are more flexible and adaptable than other metaheuristic methods.

3. POPULAR GENETIC PROGRAMMING APPROACHES

In the historical development of the GP, a tree-based structure was initially used by Koza [1]. In this review study, the most frequently used GP methods in the literature are introduced briefly and the works, devoted for introduction and analysis of the GP methods. These efforts help researchers to have an overview on a wide range of GP studies, and in case of need for deepened knowledge, they can easily reach the related papers that are considered in the scope of this study. For taxonomical organization of the literature knowledge, the hierarchy of GP methods is build in two main branches that are formed regarding the program representation formats and methodological differences.

3.1 Genetic Programming Types According to Program Representation Format

The most commonly used program representation formats of GP in the literature are tree, linear and graphical representations. For instance, one can consider standard GP [1] for tree-based representation, Cartesian Genetic Programming (CGP) [29] for graphical representation, and Linear Genetic Programming (LGP) [30] for linear representation.

3.1.1 Tree-Based Genetic Programming

The tree-based GP is the first and the most widely used representation format [1]. Hence, this type of representation is called the standard GP in the literature. Mainly, programs in software development processes composed of reusable program parts such as sub-functions, functions, and classes in the form of repeated steps. In

contrast, in tree-based GP, population individuals are usually expressed by syntax trees rather than lines of code [2], [28].

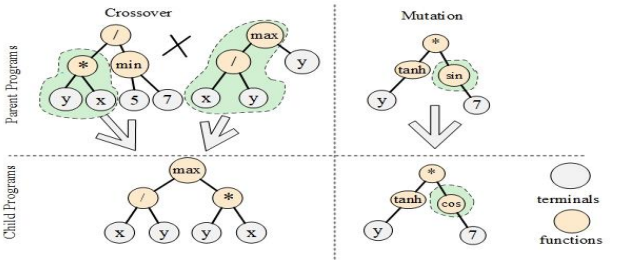

Figure 2 Standard (Tree-based) GP structure and its evolution steps

Figure 2 shows the tree-based GP structure and its evolution steps. For example, the tree representation of the program *x*y/min(5,7)* is processed in the evolutionary operation part of the figure. The variables and constants {*x, y, 5, 7*} in the program are called terminals in the leaves of the tree, while the arithmetic operations {*, / , min()} are called functions that are represented on internal nodes. In tree-based GP, program representations, namely candidate solutions, are formed by the placement of terminals and functions on nodes of a tree graph.

3.1.2 Cartesian Genetic Programming

Cartesian Genetic Programming(CGP) [31] was first added to the literature by Miller in 1999. It was adopted as an innovative genetic programming type in the early 2000s [29]. As shown in Figure 3, programs in CGP are directly represented by grid graphics. This graphics consist of a two-dimensional grid of computation nodes. The term *"cartesian"* also takes its name from this grid arrangement of entities. Genes that make up the genotype (individual representations) in CGP are integers representing where a node receives its data at inputs, the actions on the data are performed at the node. The output data appears at the output of nodes for processing of the following nodes [32-33].

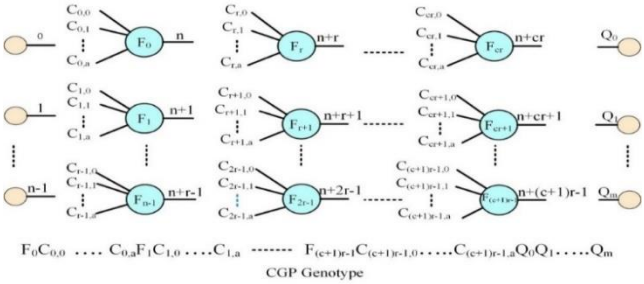

Figure 3 CGP graphic representation form [32]

Unlike the tree representations, CGP can represent individuals with a graphical drawing, the solutions can have multiple outputs, and the nodes can be used repeatedly within the repeating structures. In particular, it is a popular and easily adaptable representation method for the solution of many problems. Also CGP is an appropriate method of GP to represent many computational process such as equations, state machines, neural networks, algorithms, and electronic circuits [33].

As it can be seen in Figure 3, the CGP allows the internal calculations to reuse of data, as the outputs of the nodes in the graph can be reused multiple times. This property has attracted the attention of researchers working in the field of evolutionary computing and genetic programming since the CGP first appeared.

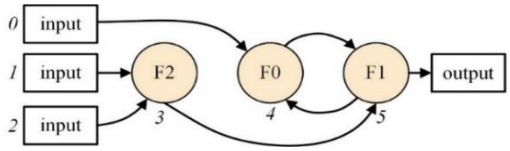

Figure 4 Recurrent CGP[34] chromosome structure

In order to overcome the difficulties encountered in engineering problems, CGP types that have many different features have been proposed in the literature. Figure 4 shows the Recurrent CGP [35], which is a type of CGP that allows the creation of repetitive/circular charts. Since the focus of this review article is not a comprehensive elaboration of all CGP variants, for further details on CGP variants, readers can consider some articles that focus on the CGP methods in literature [32], [36].

3.1.3 Linear Genetic Programming

Linear Genetic programming (LGP) is another GP variant, which differs in the program representation format. The individuals(programs)

of LGP are represented by a linear code structure, as shown in Figure 5(b). The main difference between LGP and the tree-based GP is that instead of using a tree graph representation of the programs, it consists of a set of instructions, which are analogous to the machine codes in the register [30], [37].

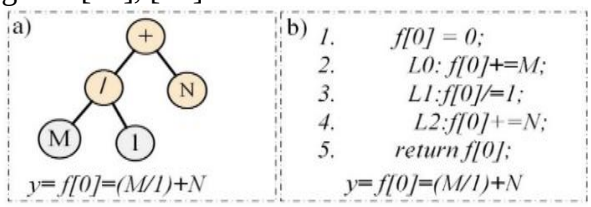

Figure 5 a) Standard GP, b) Linear GP [37-38]

In Figure 5, f[0] represents temporary program variables while *L*'s represent command lines. Here, LGP has a structure that allows the variable to take different values in each command line. Each command structure contains an operator, an array of functions, and a return value [39].Since the LGP can be represented very similar to the programming languages, it can be more effective to synthesize computer programs than the standard GP [40-41].

3.1.4 Stack-based Genetic Programming

Stack-based Genetic Programming (SBGP) is another variant of GP, which was proposed by Perkis [42]. The representation format of SBGP consists of programs as lists of nodes of functions or terminals that receive their inputs from a stack and place their outputs on a stack [43]. It is a less preferred representation format compared to other representation formats.

3.2 GP Types According to Their Methodological Differences

Since the standard GP encounters technical complications (e.g. bloating, growing complexity) in solution of difficult problems, in addition to the progresses based on new representation formats in the literature, many different GP variants have also been proposed to improve performance of GPs by performing methodological enhancements on GP methods.

3.2.1 Strongly-typed GP

Strongly-typed Genetic Programming (STGP) [44], is an improved type of the standard GP by using data type restrictions. STPG is similar to standard GP, but the programs have a structure in which each node has different data types.

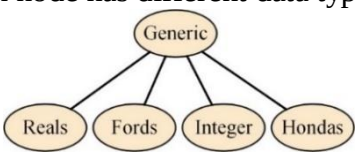

Figure 6 Strongly-typed GP [44]

As shown in Figure 6, the data types of functions and terminals need to be specified in STGP and therefore the population is only constructed with syntactically correct decomposed trees, which significantly reduces the search area[45]. Without data type limitation in the program nodes of the standard GP, the GP may cause processing numerous combinations of trees. In contrast, in STGP, the characteristics of each node are predetermined.

3.2.2 Multi-Gene GP

Multi-Gene Genetic Programming (MGGP) [46] can be accounted as a multi-gene form of the standard GP [1]. The classic symbolic regression problems employ the standard GP to evolve a population of programs that are represented in the form of single tree. Therefore, each of the trees represents a mathematical formulation that is a candidate solution of the regression problem. In contrast, MGGP benefits from a mathematical formulation that is a weighted linear combination of the outputs from a number of GP trees [47]. MGGP was suggested in the study of solving a complicated symbolic regression problem [46]. MGGP can be accounted as a powerful GP variant that effectively accumulates the abilities of standard GP solutions to empower prediction skills of regression model [47]. Therefore, it is very suitable to solve regression and modeling problems.

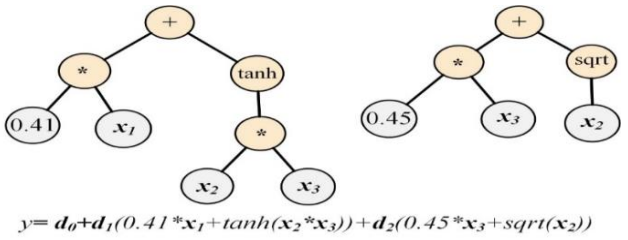

Figure 7 Multi-gene symbolic model [48]

When compared to the standard GP, the depth of the tree representation of genes can remain relatively shallow in MGGP, and it is can contribute to the relief of the bloating problem. The typical multiple gene models are shown in Figure 7. This model results in a mathematical formulation of an output variable based on weighted sum of two tree expressions of three input variables (x_1, x_2, and x_3). Such a formulation of MGGP have been shown to be more efficient than the standard GP in nonlinear problems [53-54].

3.2.3 Multi-objective GP

Standard GP is usually optimized for a single objective, and it has a single fitness function [50], [51]. Standard GP is insufficient in multi-objective optimization tasks. In a multi-objective optimization (MOGP) problem, problem-solution is optimized with respect to the multiple goals or objective functions [2].

A disadvantage of using a single objective in the optimization process of the GP is that the evolutional solution models can become extremely complex. Therefore, the two main objectives of MOGP are devised for minimizing complexity while maximizing fitness value [51].

3.2.4 Gene Expression Programming

In Gene Expression Programming (GEP), the genome or chromosome consists of one or more expression trees (ET) of linear, symbolic, fixed lengths consisting of one or more genes [52]. GEP is one of the most frequently used GP types in many different fields. GEP genes consist of a *head* and *tail*. Despite the fact that the head contains symbols representing functions (elements from the *F* function set) and terminals (elements from the *T* terminal set), the tail contains only the terminals. If we express, for a problem, t is the length of the tail, h is the length of the head, n is the number of arguments, the relationship between these variables is expressed by the following equation(1).

$$t = h\,(n\text{-}1) + 1 \text{ [52]}(1)$$

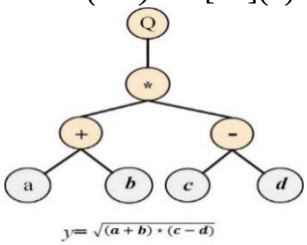

Figure 8 A sample GEP tree [52]

The program representation shown in Figure 8 is actually the phenotype of GEP individuals, the genotype can easily produced from the phenotype as follows:

01234567
Q*+-abcd

GEP selects population individuals by using one or more genetic operators according to their fitness, and it provides a variety of genetic variations [52]. In GEP, the individuals consist of strings of fixed length structure which are expressed as nonlinear entities of different sizes and shapes such as expression trees [52]. GEP allows solution of high complexity problems on personal computers [52] because GEP has rather simple genetic operations that minimize the need for powerful hardware for evolutionary computing [53][54].

3.2.5 Grammar Guided GP

Grammar Guided Genetic Programming (GGGP or G3P) [55-56] is a variant of the original GP. Grammar-guided GP is also known as grammar-based GP in the literature. Grammar provides many benefits to GP. Undoubtedly the most important benefit is that it can be used as a restriction tool on a flexible search space [57].

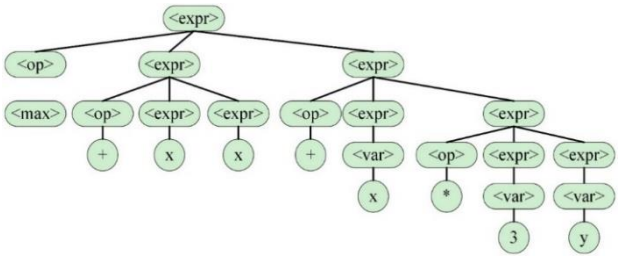

Figure 9 Grammar-based tree[58]

Grammar-based formulations are the basic representation structures of computer science[57]. They are widely used to express constraints in general areas by limiting the expressions that can be used. The individuals of GGGP can use both linear and tree representation methods. In Figure 9, an example of grammar-based tree representation is illustrated.

3.2.6 Grammar Evolution (GE)

As a sub-type of GGGP, the GE [59] is a GP method that performs evolutionary processes in variable-length binary strings instead of real programs. GE perform a mapping technic for create programs in any language using binary strings to creating rules in a Backus-Naur Format (BNF) grammar. This approach is to obtain a syntactically suitable expression from a binary string, which can then be evaluated with a fitness model [59].

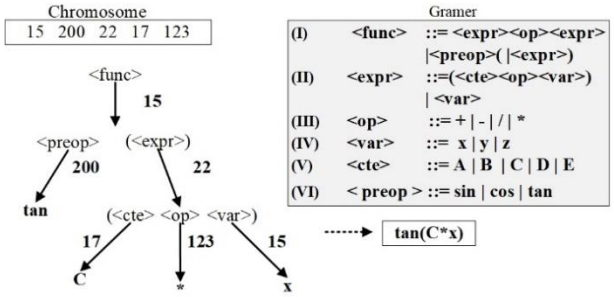

Figure 10 Performing a sample decoding in GE [60]

The purpose and main cycle are basically the same as standard GP, but they differ in the way that solutions are created and updated [61]. Figure 10 shows an example of decoding with GE. If you want to solve a problem with GE, the first thing to do is to define an appropriate grammar, which is usually done using the Backus-Naur form (BNF). Thus, it is an important step as it defines the search space for the solution of the problem and calculation expressions (individuals) will be place in this search space [62].

3.2.7 Geometric Semantic Genetic Programming

Geometric Semantic Genetic Programming (GSGP) [63] is one of the recently proposed GP types. GSGP establishes a semantic field that uses semantics of possible solutions and benefits from different distance metrics in order to measure the suitability of GP individuals for the solution. There are several methods for defining the semantics of the population program. Depending on the properties of the distance metrics, the semantic field can have different conical forms. The GSGP searches for the solution in the semantic space of the programs. In this way, it facilitates searching in the solution space [64].

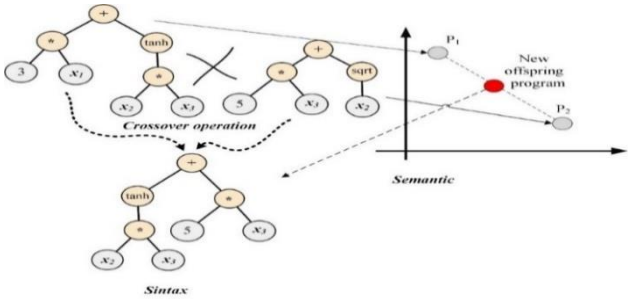

Figure 11 Geometric semantic crossover[65]

Geometric semantic operators change the programs to generate new programs in a semantic space [66]. Figure 11 shows an example of a geometric semantic crossover operation in the semantic space. Before the crossover operation, each individual has its own position in the semantic space. After the crossover operation, a semantic point (value) corresponding to the newly formed offspring program is assigned. Similarly, in the mutation process, a relevant semantic operation of the program individuals is performed, and the geometric semantic values are assigned according to the suitability of new programs [65].

3.3 Some Popular GP Types

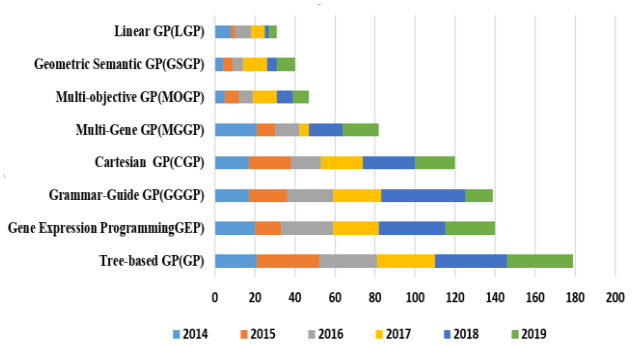

Figure 12 GP variants between 2014 and 2019

It can be useful to illustrate yearly publication distributions of the popular GP types to reveal emerging trends among GP types compares

yearly publication rates in the years between 2014 and 2019. Although the tree-based GP is trendy even though it is shortcomings mentioned in Section 2, one can observe that the GEP, GGGP, and Cartesian GP variants also have a frequent use in the publications. The main reason for the widespread use of these GP types is their easy applicability and delivery of many software tools and documents related to these GP types.

4. APPLICATION FIELDS OF GENETIC PROGRAMMING

This section surveys the recent application fields of the GP methods and considerable application articles in these fields. The analysis of application trends is especially useful for new researchers who need to explore application domains of GP algorithms. In order to keep the reviewed articles at a reasonable extend, instead of explaining all GP applications, we summarized the study collections that were intensified into the specific application fields.

Symbolic regression: Symbolic regression is a topic at the intersection of applied mathematics and computer science, which investigate approaches to produce the best symbolic mathematical expression that describes the model of the existing relationships between a well-known set of independent variables and the associated values of dependent variables [67]. Mechanisms of GP methods well suit for characteristics of symbolic regression problems, and it has been used intensely in this area [64], [68]–[70].

Artificial Neural Network (ANN) design: A corporation of Artificial Neural Network (ANN) and Evolutionary Algorithm (EA) is a branch of machine learning, which was named as NeuroEvolution (NE) [71], [72]. There are many studies [21], [72]–[74] that use CGP in the optimization of ANN's topology and networks. In this fashion, hybrid approaches [75] based on collaboration of GP and ANNs have been proposed. Meanwhile, there is a CGP type, namely Recurrent CGP (RCGP) [34], particularly developed for ANNs.

Computer vision: GP algorithms have been utilized in computer vision applications e.g. recognition of human motion [18], improving the performance of the histogram of oriented gradients (HOG) algorithm for human detection problems [76], in robotics[77], human movement modeling [78], improving edge detection in images [79] and in the pattern recognition problems [80] etc.

Circuit Design and Evolvable hardware: Evolutionary Hardware (EHW) is a design approach that uses a reconfigurable hardware structure to develop a circuit that performs a specific function. Hardware can be designed automatically by using GP algorithms without the need for a circuit designer [22]. Due to convenience of program representations to express hardware, the CGP method is employed extensively in circuit design works. As a consequence, the GP has been widely utilized in EHW studies [22], [81], [82] Besides, the GP is frequently used in digital circuit design tasks [23], [83]–[85].

Scheduling: The Scheduling is a process that deals with the allocation of limited resources by serving for the given times. It has been utilized in many production and service industries [86]. The GP has been frequently used in many timing problems such as dynamic job shop scheduling(JSS) [8], [87] production scheduling [88], action scheduling [89] scheduling in heterogeneous network [90], [91]

Environmental, natural disasters and agriculture: GP methods have used especially for data modeling and forecasting in many areas such as carbon emission [92], monitoring of volcanoes [93], earthquake prediction [94], atmosphere studies [95], airflow measurement [96], modeling rainwater quality [97], analysis of agricultural yield response [98], reservoir operations and irrigation [9].

Classification: The relevance of the selected features is one of the important factors that can affect the classification performance. The appropriate feature selection increases distinguishability between classes. However, in some real-world classification applications, there may not be enough information about the available features [99]. GP has been used to explore effective features in classification problems [7], [94], [99] and associative classification [100].

Urbanization and Building: The energy management and infrastructure planning problems can require high complexity computational models. To produce feasible solutions for efficiency and sustainability concerns, effective computational intelligence methods are needed to overcome such model complexity. Therefore, GP algorithms have found applications these problems such as energy efficiency in buildings [11], [101], the ground and soil analyzes [15], [102], urban transportation and infrastructure planning [14], [103]

Financing, trade, and economy: The financial market introduces very complex, nonstationary and chaotic data models. To overcome this challenge, GP methods have been implemented and successful results have been reported. One can see GP applications in finance, commerce, and economy problems, for examples supply selection [104], investment management [105]–[107], market analysis [108], financial security [24], stock analysis and management [109-110] etc.

Image processing: Digital imaging technologies and image processing are used in various fields, e.g. medical applications, meteorology, geology, and biology etc. These images may contain noise and requires a preprocessing task [111]. Researchers from image processing field have used the GP methods in image processing studies such as in noise suppression [111-112], image reconstruction [113], feature extraction[114], image classification [115] etc.

Signal processing: GP algorithms has been utilized in the classification of EEG signals [116], which is a very important task in the diagnosis of several diseases and disorders such as epileptic seizures [117], sleep disorders [141]. One may also see GP employments in processing of other medical signals such as classification of electrocardiography (ECG) signals [20], [118], which are the medical signals that are used to diagnose heart problems. The another signal processing application of GP is related to audio signal processing for instance audio signal reconstruction application [119].

Education: With beginning of Industry 4.0, artificial intelligence techniques will be used more frequently in order to reduce the workload of teachers and to provide student-friendly solutions in education systems. Nowadays, online intelligent learning systems are capable of automated assessment of learning activities, and therefore computational intelligence begins to play an important role in education [120]. In this fashion, GP methods have been performed in student performance prediction [13], [121-122].

Hydrology: Hydrology is a branch of water science that widely needs predictions models. GP was widely used in hydrology applications such as precipitation prediction and measurement [123], Rainfall-Runoff modeling [124-125] groundwater quality prediction [126], evapotranspiration estimation [127] etc. A comprehensive review study focuses on GP applications in the field of hydrology [128].

Medicine, Biology and Bioinformatics: GP methods have found a wide application in the medical, biology and bioinformatics fields, particularly for diagnosis, classification, prediction and modeling purposes. For examples, analysis and modeling of blood chemicals [17], [129] such as glucose-dynamics models that are vital for diabetes diseases, data mining in medicine[37] for analyses in asthma and allergy epidemiology [58], predictions of pharmacokinetic parameters [130], and diabetes mellitus [131], and automatic diagnosis of Parkinson disease [132] are some of the applications.

Time Series Prediction: Time series used in many fields such as statistics and econometrics. GP methods are used in time series prediction studies [133-137]

Energy: Nowadays, due to a growing demand for energy all over the globe, it is great importance to improve energy efficiency and reliability by providing more efficient use of energy resources, optimal energy generation and demand balance, consumption prediction, and reduction of energy lost etc. GP methods has been used in energy field such as energy consumption prediction analysis [138-139], energy demand estimation [60], biomass energy analysis [140], risk analysis in nuclear energy systems [141], flexibility analysis in waste-to-energy systems [142] etc.

5. SOFTWARE TOOLS FOR GENETIC PROGRAMMING

This section introduces available software tools that were developed for GP applications.

DEAP: DEAP [143] is an advanced Python-based, open-source evolutionary computing software tool, where target problems can be quickly adapted and tested.

GPLEARN: Gplearn [144] is an open-source Python-based GP library. It uses a tree-based representation format. The Gplearn tool is quite suitable for symbolic regression problems.

GELAB: GELAB is an open-source Matlab[145] library [146] The application of the GGGP types to problems can be conducted by using GELAB in the Matlab environment.

CGP4Matlab: CGP4Matlab [147] is another open-source software tool that enables developing CGP applications in Matlab environment. CGP4Matlab was developed especially for signal processing and image processing problems [148].

GPTIPS 2: GPTIPS [149] is also an open-source Matlab GP software development tool. Many articles [150-152] used this software tool, and this indicates the interest of researchers to implement this tool in their works. Also, the GPTIPS tool was used for symbolic regression problems [153].

PonyGE2: PonyGE2 [154-155] is a open-source software tool that offers a development environment in Python language. This tool includes grammar-based types of GP.

GeneXproTools: GeneXproTools [156] is a desktop commercial software that enables analysis with various data model. This professional software was developed for specialists with knowledge of statistics, mathematics, machine learning or programming. It includes GEP type and it is used in emotion classification study [157] and in soil temperature analysis [158].

GEP4J: GEP4J [159] is an open source Java library. It allows developing GEP applications in Java environment.

PyGEP: PyGEP [160] is an open-source Python library. It allows GEP applications in Python.

JGEP: JGEP [161] is another open-source Java library where GEP applications can be developed.

EpochX: EpochX [162] is an open-source GP software development package. It has a Java framework that is specially developed to analyze evolutionary automated programming. EpochX is licensed under the GNU LGPL version 3 license.

Karoo GP: Karoo GP [163] is a GP open-source software package written in Python. With this tool, both symbolic regression and classification studies can be carried out easily. Karoo GP is a scalable platform with multicore and the TensorFlow support [164], which may facilitate working with real-world data. Karo GP is licensed under the MIT license.

GISMO: GISMO [165] is a software package for open source, multipurpose GP studies with parallel computing capability [166-167].

KNIME: KNIME [168-169] is a cross-platform for data analysis, reporting and integration platforms. In addition, data processing and visualization operations in the form of new modules or nodes can be performed by KNIME. KNIME is available in commercial and free versions. Researchers can access free versions and contribute to improvements [170].

GSGP-C++:GSGP-C++ 2.0 [171] is an open source C ++ GP development library. It supports GSGP [172-173].

GPLAB:GPLAB [174] a software package for developing GP applications in Matlab environment. It has been claimed by the study that the GP bloating problem can be controlled in GPLAB [175].

6. SOME RECENT REVIEW WORKS ON GENETIC PROGRAMING

Several review type works related with applications of the genetic programming have been presented. A framework of product scheduling and the related works have been explained in [8]. The role of genetic programming in the empirical modeling has been surveyed[176]. An interpretation of the term of ”emergence” according to genetic programming was discussed and related works was mentioned in [177]. A review of the semantic methods in the genetic programming has been presented in [178]. Survey works for use of GP in the specific fields were also provided; for instance, in the water resource engineering [128], the energy efficiency [179], and civil engineering [180]. Some survey works addressed specific GP approaches such as

grammar-based Genetic programming [26], gene expression programming [181]. However, a general review of GP domain, which presents an outlook for the growing GP literature in a systematic way, is limited [28]. This review study aims to provide a general view for the GP field from beginning to the recent developments for new researchers who decide to implement GP methods in their applications.

7. CONCLUSIONS

This review article reveals the fact that GP topic has turned into a fast growing interdisciplinary field, where the powerful and flexible computation potential of GP algorithms has been utilized for the solution of wide-range of real world problems in many disciplines. Therefore GP literature has been widely expanded and still expanding with new types of GPs so that the standard GP can not sufficiently respond such diversity in problem types and their difficulty levels. As problems are getting harder and the need for progressing GP algorithms keeps on.

The current paper also highlights yearly publication trends of GP variants from 2014 and 2019 and the application fields that GP utilization has been intensified. These efforts give a clue for recent trends in GP algorithms and their spreading fields of application. In addition, a detailed list of GP software development tools has been mentioned for researchers who step into GP world. Many developers of the GP software tool aim to provide user-friendly tools that can be used not only by those who are experts in software but also those who do not have programming knowledge. In addition, thanks to the increasing computation power in the today's computers and high-performance processors, GP algorithms can run faster than before. This progress allows implementation of GP algorithm in more complicated and complex real world problems as an effective computational intelligence tools.

This literature survey also aims to be a good starting point for new researchers who want to start working on GP algorithms. Thus, the paper provides an overview to the field of GP and its development stages.

One can conclude that, according to the increase in the number of recent works of GP taken into consideration, GP will continue its progress as a strong branch of computational intelligence by increasing its popularity in the future applications. It is very expectable that by adding additions to the basic features of GP, emergence of fresh GP types with superior computing abilities, which can give better results in much more complex and complicated problems, will be a continuing trend.

Funding

The authors received no financial support for the research, authorship or publication of this study.

The Declaration of Conflict of Interest/ Common Interest

No conflict of interest or common interest has been declared by the authors.

Authors' Contribution

All authors have contributed in experimental study and writing of the manuscript equally.

The Declaration of Ethics Committee Approval

The authors declare that this document does not require an ethics committee approval or any special permission.

The Declaration of Research and Publication Ethics

The authors of the paper declare that they comply with the scientific, ethical and quotation rules of SAUJS in all processes of the article and that they do not make any falsification on the data collected. In addition, they declare that Sakarya University Journal of Science and its editorial board have no responsibility for any ethical violations that may be encountered, and that this study has not been evaluated in any academic publication environment other than Sakarya University Journal of Science.

REFERENCES

[1] J. R. Koza, 'Genetic programming: on the programming of computers by means of natural selection', MIT press.,1992.

[2] R. Poli, W. B. Langdon, and N. F. McPhee, 'A Field Guide to Genetic Programing', no. March,Lulu Enterprises, UK Ltd, 2008.

[3] M. Amir Haeri, M. M. Ebadzadeh, and G. Folino, 'Statistical genetic programming for symbolic regression', Appl. Soft Comput., vol. 60, ,pp. 447–469, 2017.

[4] M. O'Neill, L. Vanneschi, S. Gustafson, and W. Banzhaf, 'Open issues in Genetic Programming', Genet. Program. Evolvable Mach., vol. 11, no. 3–4, ,pp. 339–363, 2010.

[5] A. Cano and S. Ventura, 'GPU-parallel subtree interpreter for genetic programming', Proceedings of the 2014 conference on Genetic and evolutionary computation - GECCO '14, no. July, New York, New York, USA,ACM Press,pp. 887–894, 2014.

[6] L. F. Dal Piccol Sotto and V. V. De Melo, 'Investigation of linear genetic programming techniques for symbolic regression', Proc. - 2014 Brazilian Conf. Intell. Syst. BRACIS 2014, ,pp. 146–151, 2014.

[7] B. Tran, B. Xue, and M. Zhang, 'Genetic programming for feature construction and selection in classification on high-dimensional data', Memetic Comput., vol. 8, no. 1, ,pp. 3–15, 2016.

[8] S. Nguyen, Y. Mei, and M. Zhang, 'Genetic programming for production scheduling: a survey with a unified framework', Complex Intell. Syst., vol. 3, no. 1, ,pp. 41–66, 2017.

[9] P.-S. Ashofteh, O. B. Haddad, and H. A. Loáiciga, 'Evaluation of Climatic-Change Impacts on Multiobjective Reservoir Operation with Multiobjective Genetic Programming', J. Water Resour. Plan. Manag., vol. 141, no. 11, ,p. 04015030, 2015.

[10] M. Castelli, L. Trujillo, L. Vanneschi, and A. Popovič, 'Prediction of energy performance of residential buildings: A genetic programming approach', Energy Build., vol. 102, ,pp. 67–74, 2015.

[11] A. Tahmassebi and A. H. Gandomi, 'Building energy consumption forecast using multi-objective genetic programming', Measurement, vol. 118, no. January, ,pp. 164–171, 2018.

[12] S. H. A. Kaboli, A. Fallahpour, J. Selvaraj, and N. A. Rahim, 'Long-term electrical energy consumption formulating and forecasting via optimized gene expression programming', Energy, vol. 126, ,pp. 144–164, 2017.

[13] A. Zafra and S. Ventura, 'Multi-instance genetic programming for predicting student performance in web based educational environments', Appl. Soft Comput., vol. 12, no. 8, ,pp. 2693–2706, 2012.

[14] A. K. Patnaik and P. K. Bhuyan, 'Application of genetic programming clustering in defining LOS criteria of urban street in Indian context', Travel Behav. Soc., vol. 3, ,pp. 38–50, 2016.

[15] A. Keshavarz and M. Mehramiri, 'New Gene Expression Programming models for normalized shear modulus and damping ratio of sands', Eng. Appl. Artif. Intell., vol. 45, ,pp. 464–472, 2015.

[16] M. Shoaib, A. Y. Shamseldin, B. W. Melville, and M. M. Khan, 'Runoff forecasting using hybrid Wavelet Gene Expression Programming (WGEP) approach', J. Hydrol., vol. 527, ,pp. 326–344, 2015.

[17] I. De Falco, A. Della Cioppa, T. Koutny, M. Krcma, U. Scafuri, and E. Tarantino, 'Genetic Programming-based induction of a glucose-dynamics model for telemedicine', J. Netw. Comput. Appl., vol. 119, no. December 2017, ,pp. 1–13, 2018.

[18] L. Liu, L. Shao, X. Li, and K. Lu, 'Learning Spatio-Temporal Representations for Action Recognition: A Genetic Programming Approach', IEEE Trans. Cybern., vol. 46, no. 1, ,pp. 158–170, 2016.

[19] L. Shao, L. Liu, and X. Li, 'Feature learning for image classification via multiobjective genetic programming', IEEE Trans. Neural Networks Learn. Syst., vol. 25, no. 7, ,pp. 1359–1371, 2014.

[20] M. Feli and F. Abdali-Mohammadi, 'A novel recursive backtracking genetic programming-based algorithm for 12-lead ECG compression', Signal, Image Video Process., vol. 13, no. 5, ,pp. 1029–1036, 2019.

[21] M. Suganuma, S. Shirakawa, and T. Nagao, 'A genetic programming approach to designing convolutional neural network architectures',

Proceedings of the Genetic and Evolutionary Computation Conference on - GECCO '17, New York, New York, USA,ACM Press,pp. 497–504, 2017.

[22] J. Mora, R. Salvador, and E. de la Torre, 'On the scalability of evolvable hardware architectures: comparison of systolic array and Cartesian genetic programming', vol. 20, no. 2,Springer US, 2019.

[23] M. Sikulova, G. Komjathy, and L. Sekanina, 'Towards compositional coevolution in evolutionary circuit design', IEEE SSCI 2014 - 2014 IEEE Symp. Ser. Comput. Intell. - IEEE ICES 2014 IEEE Int. Conf. Evolvable Syst. Proc., ,pp. 157–164, 2014.

[24] H. Li and M. L. Wong, 'Financial Fraud Detection by using Grammar-based Multi-objective Genetic Programming with ensemble learning', 2015 IEEE Congr. Evol. Comput. CEC 2015 - Proc., ,pp. 1113–1120, 2015.

[25] A. Fallahpour, E. U. Olugu, S. N. Musa, D. Khezrimotlagh, and K. Y. Wong, 'An integrated model for green supplier selection under fuzzy environment: application of data envelopment analysis and genetic programming approach', Neural Comput. Appl., vol. 27, no. 3, ,pp. 707–725, 2016.

[26] M. W. Khan and M. Alam, 'A survey of application: Genomics and genetic programming, a new frontier', Genomics, vol. 100, no. 2, ,pp. 65–71, 2012.

[27] R. Poli, N. F. McPhee, and L. Vanneschi, 'Elitism reduces bloat in genetic programming', GECCO'08 Proc. 10th Annu. Conf. Genet. Evol. Comput. 2008, ,pp. 1343–1344, 2008.

[28] R. Poli, W. B. Langdon, N. F. McPhee, and J. R. Koza, 'Genetic programming an introductory tutorial and a survey of techniques and applications', Tech Rep CES475, vol. 18, no. October 2007, ,pp. 1–112, 2007.

[29] P. T. J.F. Miller, 'Cartesian genetic programming', Proceedings of the European Conference on Genetic Programming, ,pp. 121–132, 2000.

[30] M. Brameier and W. Banzhaf, 'Evolving Teams of Predictors with Linear Genetic Programming', Genet. Program. Evolvable Mach., vol. 2, no. 4, ,pp. 381–407, 2001.

[31] J. F. Miller, 'An empirical study of the efficiency of learning boolean functions using a Cartesian Genetic Programming approach', Proc. Genet. Evol. Comput. Conf., vol. 2, ,pp. 1135--1142, 1999.

[32] J. F. Miller, 'Cartesian Genetic Programming', Berlin, Heidelberg,Springer Berlin Heidelberg,pp. 17–34, 2011.

[33] J. F. Miller, 'Cartesian genetic programming: its status and future', no. April,Springer US, 2019.

[34] A. J. Turner and J. F. Miller, 'Recurrent Cartesian Genetic Programming of Artificial Neural Networks', Genet. Program. Evolvable Mach., vol. 18, no. 2, ,pp. 185–212, 2017.

[35] A. J. Turner and J. F. Miller, 'Recurrent Cartesian Genetic Programming', ,pp. 476–486, 2014.

[36] A. Manazir and K. Raza, 'Recent developments in cartesian genetic programming and its variants', ACM Comput. Surv., vol. 51, no. 6, 2019.

[37] M. Brameier and W. Banzhaf, 'A comparison of linear genetic programming and neural networks in medical data mining', IEEE Trans. Evol. Comput., vol. 5, no. 1, ,pp. 17–26, 2001.

[38] H. Shavandi and S. Saeedi Ramyani, 'A linear genetic programming approach for the prediction of solar global radiation', Neural Comput. Appl., vol. 23, no. 3–4, ,pp. 1197–1204, 2013.

[39] T. Hu, J. L. Payne, W. Banzhaf, and J. H. Moore, Genetic Programming and Evolvable Machines, vol. 13, no. 3. ,pp. 305–337, ,pp. 305–337, 2012.

[40] W. Banzhaf, F. D. Francone, R. E. Keller, and P. Nordin., 'Genetic Programming: An Introduction.',San Francisco, CA,Morgan Kaufmann Publishers, 1998.

[41] A. Guven and O. Kisi, 'Monthly pan evaporation modeling using linear genetic programming', J. Hydrol., vol. 503, ,pp. 178–185, 2013.

[42] T. Perkis, 'Stack-based genetic programming', Proceedings of the First IEEE Conference on Evolutionary Computation. IEEE World Congress on Computational Intelligence, IEEE,pp. 148–153, 1994.

[43] D. S. P. Elko B. Tchernev, 'Control structures in linear and stack-based Genetic

Programming', Late Breaking Papers at the 2004 Genetic and Evolutionary Computation Conference, Seattle, Washington, USA., 2004.

[44] D. J. Montana, 'Strongly Typed Genetic Programming', Evol. Comput., vol. 3, no. 2, ,pp. 199–230, 1995.

[45] T. D. Haynes, D. A. Schoenefeld, and R. L. Wainwright, 'Type Inheritance in Strongly Typed Genetic Programming', 1996.

[46] G. W. Hinchliffe, M. P., Willis, M. J., Hiden, H., Tham, M. T., McKay, B., & Barton, 'Modelling chemical process systems using a multi-gene genetic programming algorithm', In Genetic Programming: Proceedings of the First Annual Conference, ,pp. 56–65, 1996.

[47] A. H. Gandomi and A. H. Alavi, 'A new multi-gene genetic programming approach to nonlinear system modeling. Part I: Materials and structural engineering problems', Neural Comput. Appl., vol. 21, no. 1, ,pp. 171–187, 2012.

[48] W. M. Searson DP, Leahy DE, 'GPTIPS: An Open Source Genetic Programming Toolbox For Multigene Symbolic Regression', International MultiConference of Engineers and Computer Scientists 2010 (IMECS), ,pp. 77–80, 2010.

[49] D. Searson, M. Willis, and G. Montague, 'Co-evolution of non-linear PLS model components', J. Chemom., vol. 21, no. 12, ,pp. 592–603, 2007.

[50] R. Dai, Y. Gao, S. Huang, F. Ning, and Z. Feng, 'Multi-objective Genetic Programming based Automatic Modulation Classification', 2019 IEEE Wireless Communications and Networking Conference (WCNC), vol. 2019-April, IEEE,pp. 1–6, 2019.

[51] A. H. Gandomi, S. Sajedi, B. Kiani, and Q. Huang, 'Genetic programming for experimental big data mining: A case study on concrete creep formulation', Autom. Constr., vol. 70, ,pp. 89–97, 2016.

[52] C. Ferreira, 'Gene Expression Programming: a New Adaptive Algorithm for Solving Problems', ,pp. 1–22, 2001.

[53] A. Ş. Şahin, E. Dikmen, and S. Şentürk, 'A gene expression programming approach for thermodynamic properties of working fluids used on Organic Rankine Cycle', Neural Comput. Appl., vol. 31, no. 8, ,pp. 3947–3955, 2019.

[54] C. Ferreira, 'Gene Expression Programming', vol. 21,Springer Berlin Heidelberg, 2006.

[55] Man Leung Wong and Kwong Sak Leung, 'Inducing logic programs with genetic algorithms: the Genetic Logic Programming System', IEEE Expert, vol. 10, no. 5, ,pp. 68–76, 1995.

[56] M. L. Wong and K. S. Leung, 'Evolutionary Program Induction Directed by Logic Grammars', Evol. Comput., vol. 5, no. 2, ,pp. 143–180, 1997.

[57] R. I. McKay, N. X. Hoai, P. A. Whigham, Y. Shan, and M. O'neill, 'Grammar-based Genetic programming: A survey', Genet. Program. Evolvable Mach., vol. 11, no. 3–4, ,pp. 365–396, 2010.

[58] R. V. Veiga, H. J. C. Barbosa, H. S. Bernardino, J. M. Freitas, C. A. Feitosa, S. M. A. Matos, N. M. Alcântara-Neves, and M. L. Barreto, 'Multiobjective grammar-based genetic programming applied to the study of asthma and allergy epidemiology', BMC Bioinformatics, vol. 19, no. 1, ,pp. 1–16, 2018.

[59] M. O'Neill and C. Ryan, 'Grammatical evolution', IEEE Trans. Evol. Comput., vol. 5, no. 4, ,pp. 349–358, 2001.

[60] J. M. Colmenar, J. I. Hidalgo, and S. Salcedo-Sanz, 'Automatic generation of models for energy demand estimation using Grammatical Evolution', Energy, vol. 164, ,pp. 183–193, 2018.

[61] C. Martín, D. Quintana, and P. Isasi, 'Evolution of trading strategies with flexible structures: A configuration comparison', Neurocomputing, vol. 331, ,pp. 242–262, 2019.

[62] I. Fajfar, Á. Bűrmen, and J. Puhan, 'Grammatical evolution as a hyper-heuristic to evolve deterministic real-valued optimization algorithms', vol. 19, no. 4,Springer US, 2018.

[63] A. Moraglio, K. Krawiec, and C. G. Johnson, 'Geometric Semantic Genetic Programming', Berlin,Springer, Berlin, Heidelberg,pp. 21–31, 2012.

[64] Q. Chen, B. Xue, and M. Zhang, 'Improving Generalization of Genetic Programming for Symbolic Regression with Angle-Driven Geometric Semantic Operators', IEEE Trans. Evol. Comput., vol. 23, no. 3, ,pp. 488–502,

2019.

[65] L. Vanneschi, M. Castelli, I. Goncalves, L. Manzoni, and S. Silva, 'Geometric semantic genetic programming for biomedical applications: A state of the art upgrade', 2017 IEEE Congr. Evol. Comput. CEC 2017 - Proc., ,pp. 177–184, 2017.

[66] J. P. Papa, G. H. Rosa, and L. P. Papa, 'A binary-constrained Geometric Semantic Genetic Programming for feature selection purposes', Pattern Recognit. Lett., vol. 100, ,pp. 59–66, 2017.

[67] F. Casadei, J. F. B. S. Martins, and G. L. Pappa, 'A multi-objective approach for symbolic regression with semantic genetic programming', Proc. - 2019 Brazilian Conf. Intell. Syst. BRACIS 2019, ,pp. 66–71, 2019.

[68] Z. Qu, Y. X. Chen, L. Liu, Y. Xie, and Q. Zhou, 'The Algorithm of Concrete Surface Crack Detection Based on the Genetic Programming and Percolation Model', IEEE Access, vol. 7, ,pp. 57592–57603, 2019.

[69] Y. Wang, N. Wagner, and J. M. Rondinelli, 'Symbolic regression in materials science', MRS Commun., vol. 9, no. 3, ,pp. 793–805, 2019.

[70] P. DIng, Q. Qian, H. Wang, and J. Yao, 'A Symbolic Regression Based Residual Useful Life Model for Slewing Bearings', IEEE Access, vol. 7, ,pp. 72076–72089, 2019.

[71] G. M. Khan, R. Arshad, and N. M. Khan, 'Efficient Prediction of Dynamic Tariff in Smart Grid Using CGP Evolved Artificial Neural Networks', 2017 16th IEEE International Conference on Machine Learning and Applications (ICMLA), vol. 2017-Decem, IEEE,pp. 493–498, 2017.

[72] J. M. Melo Neto, H. S. Bernardino, and H. J. C. Barbosa, 'Hybridization of Cartesian Genetic Programming and Differential Evolution for Generating Classifiers Based on Neural Networks', 2018 IEEE Congress on Evolutionary Computation (CEC), IEEE,pp. 1–8, 2018.

[73] R. Arshad, G. M. Khan, and S. A. Mahmud, 'Smart bandwidth management using a recurrent Neuro-Evolutionary technique', Proc. Int. Jt. Conf. Neural Networks, ,pp. 2240–2247, 2014.

[74] M. M. Khan, G. M. Khan, and J. F. Miller, 'Evolution of neural networks using Cartesian Genetic Programming', IEEE Congress on Evolutionary Computation, IEEE,pp. 1–8, 2010.

[75] M. Mazari and D. D. Rodriguez, 'Prediction of pavement roughness using a hybrid gene expression programming-neural network technique', J. Traffic Transp. Eng. (English Ed., vol. 3, no. 5, ,pp. 448–455, 2016.

[76] M. Wiglasz and L. Sekanina, 'Evolutionary approximation of gradient orientation module in HOG-based human detection system', 2017 IEEE Global Conference on Signal and Information Processing (GlobalSIP), vol. 2018-Janua, IEEE,pp. 1300–1304, 2017.

[77] J. Leitner, A. Forster, and J. Schmidhuber, 'Improving robot vision models for object detection through interaction', 2014 International Joint Conference on Neural Networks (IJCNN), IEEE,pp. 3355–3362, 2014.

[78] W. He, S. Hu, S. Li, J. Jin, and K. Li, 'Human Motion Model Construction Based on Gene Expression Programming', Springer Singapore,pp. 473–485, 2018.

[79] W. Fu, M. Johnston, and M. Zhang, 'Low-level feature extraction for edge detection using genetic programming', IEEE Trans. Cybern., vol. 44, no. 8, ,pp. 1459–1472, 2014.

[80] H. Al-Sahaf, M. Zhang, A. Al-Sahaf, and M. Johnston, 'Keypoints detection and feature extraction: A dynamic genetic programming approach for evolving rotation-invariant texture image descriptors', IEEE Trans. Evol. Comput., vol. 21, no. 6, ,pp. 825–844, 2017.

[81] J. Mora, A. Otero, E. De La Torre, and T. Riesgo, 'Fast and compact evolvable systolic arrays on dynamically reconfigurable FPGAs', 10th Int. Symp. Reconfigurable Commun. Syst. ReCoSoC 2015, ,pp. 1–7, 2015.

[82] Z. Vasicek, 'Bridging the Gap Between Evolvable Hardware and Industry Using Cartesian Genetic Programming', ,pp. 39–55, 2018.

[83] Z. Vasicek and L. Sekanina, 'Evolutionary design of approximate multipliers under different error metrics', 17th International Symposium on Design and Diagnostics of Electronic Circuits & Systems, IEEE,pp. 135–140, 2014.

[84] V. Mrazek and Z. Vasicek, 'Parallel optimization of transistor level circuits using cartesian genetic programming', Proceedings of the Genetic and Evolutionary Computation Conference Companion on - GECCO '17, New York, New York, USA,ACM Press,pp. 1849–1856, 2017.

[85] F. Castejón and E. J. Carmona, 'Automatic design of analog electronic circuits using grammatical evolution', Appl. Soft Comput., vol. 62, ,pp. 1003–1018, 2018.

[86] M. Đumić, D. Šišejković, R. Čorić, and D. Jakobović, 'Evolving priority rules for resource constrained project scheduling problem with genetic programming', Futur. Gener. Comput. Syst., vol. 86, ,pp. 211–221, 2018.

[87] J. Park, Y. Mei, S. Nguyen, G. Chen, and M. Zhang, 'An investigation of ensemble combination schemes for genetic programming based hyper-heuristic approaches to dynamic job shop scheduling', Appl. Soft Comput., vol. 63, ,pp. 72–86, 2018.

[88] M. Đurasević, D. Jakobović, and K. Knežević, 'Adaptive scheduling on unrelated machines with genetic programming', Appl. Soft Comput., vol. 48, ,pp. 419–430, 2016.

[89] M. A. Abud Kappel, 'Action scheduling optimization using cartesian genetic programming', Proc. - 2019 Brazilian Conf. Intell. Syst. BRACIS 2019, ,pp. 293–298, 2019.

[90] T. Dou, Y. Kaszubowski Lopes, P. Rockett, E. A. Hathway, and E. Saber, 'GPML: an XML-based standard for the interchange of genetic programming trees', Genet. Program. Evolvable Mach., no. 0123456789, 2019.

[91] T. Saber, D. Fagan, D. Lynch, S. Kucera, H. Claussen, and M. O'Neill, 'A Hierarchical Approach to Grammar-Guided Genetic Programming: The Case of Scheduling in Heterogeneous Networks', ,pp. 225–237, 2018.

[92] A. Garg, L. Gao, W. Li, S. Singh, X. Peng, X. Cui, Z. Fan, H. Singh, and C. M. M. Chin, 'Evolutionary framework design in formulation of decision support models for production emissions and net profit of firm: Implications on environmental concerns of supply chains', J. Clean. Prod., vol. 231, ,pp. 1136–1148, 2019.

[93] G. Khattak, M. S. Khan, G. M. Khan, F. Huenupan, and M. Curilem, 'Automatic Classification of seismic signals of the Chilean Llaima Volcano using Cartesian Genetic Programming based Artificial Neural Network', ,pp. 36 (6 .)-36 (6 .), 2017.

[94] K. M. Asim, A. Idris, T. Iqbal, and F. Martínez-Álvarez, 'Seismic indicators based earthquake predictor system using Genetic Programming and AdaBoost classification', Soil Dyn. Earthq. Eng., vol. 111, no. February, ,pp. 1–7, 2018.

[95] T. Zerenner, V. Venema, P. Friederichs, and C. Simmer, 'Downscaling near-surface atmospheric fields with multi-objective Genetic Programming', Environ. Model. Softw., vol. 84, ,pp. 85–98, 2016.

[96] M. Khandelwal, D. J. Armaghani, R. S. Faradonbeh, P. G. Ranjith, and S. Ghoraba, 'A new model based on gene expression programming to estimate air flow in a single rock joint', Environ. Earth Sci., vol. 75, no. 9, ,pp. 1–13, 2016.

[97] K. Zhang, A. Deletic, P. M. Bach, B. Shi, J. M. Hathaway, and D. T. McCarthy, 'Testing of new stormwater pollution build-up algorithms informed by a genetic programming approach', J. Environ. Manage., vol. 241, no. January, ,pp. 12–21, 2019.

[98] A. S. Kima, S. Traore, Y.-M. Wang, and W.-G. Chung, 'Multi-genes programing and local scale regression for analyzing rice yield response to climate factors using observed and downscaled data in Sahel', Agric. Water Manag., vol. 146, ,pp. 149–162, 2014.

[99] J. Ma and G. Teng, 'A hybrid multiple feature construction approach for classification using Genetic Programming', Appl. Soft Comput. J., vol. 80, ,pp. 687–699, 2019.

[100] F. Padillo, J. M. Luna, and S. Ventura, 'A Grammar-Guided Genetic Programing Algorithm for Associative Classification in Big Data', Cognit. Comput., vol. 11, no. 3, ,pp. 331–346, 2019.

[101] O. May Tzuc, I. Hernández-Pérez, E. V. Macias-Melo, A. Bassam, J. Xamán, and B. Cruz, 'Multi-gene genetic programming for predicting the heat gain of flat naturally ventilated roof using data from outdoor environmental monitoring', Measurement, vol. 138, ,pp. 106–117, 2019.

[102] A. Tahmasebi Poor, A. Barari, M. Behnia, and T. Najafi, 'Determination of the ultimate limit states of shallow foundations using gene expression programming (GEP) approach', Soils Found., vol. 55, no. 3, ,pp. 650–659, 2015.

[103] S. K. Beura and P. K. Bhuyan, 'Operational Analysis of Signalized Street Segments Using Multi-gene Genetic Programming and Functional Network Techniques', Arab. J. Sci. Eng., vol. 43, no. 10, ,pp. 5365–5386, 2018.

[104] A. Fallahpour, E. U. Olugu, S. N. Musa, D. Khezrimotlagh, and K. Y. Wong, 'An integrated model for green supplier selection under fuzzy environment: application of data envelopment analysis and genetic programming approach', Neural Comput. Appl., vol. 27, no. 3, ,pp. 707–725, 2016.

[105] H. H. Chen, C. B. Yang, and Y. H. Peng, 'The trading on the mutual funds by gene expression programming with Sortino ratio', Appl. Soft Comput. J., vol. 15, ,pp. 219–230, 2014.

[106] C. H. Lee, C. B. Yang, and H. H. Chen, 'Taiwan stock investment with gene expression programming', Procedia Comput. Sci., vol. 35, no. C, ,pp. 137–146, 2014.

[107] I. Contreras, J. I. Hidalgo, L. Nuñez-Letamendía, and J. M. Velasco, 'A meta-grammatical evolutionary process for portfolio selection and trading', Genet. Program. Evolvable Mach., vol. 18, no. 4, ,pp. 411–431, 2017.

[108] F. Hauser, J. Huber, and B. Kaempff, 'Costly Information in Markets with Heterogeneous Agents: A Model with Genetic Programming', Comput. Econ., vol. 46, no. 2, ,pp. 205–229, 2015.

[109] H. Qu and X. Li, 'Building Technical Trading System with Genetic Programming: A New Method to Test the Efficiency of Chinese Stock Markets', Comput. Econ., vol. 43, no. 3, ,pp. 301–311, 2014.

[110] B. Ghaddar, N. Sakr, and Y. Asiedu, 'Spare parts stocking analysis using genetic programming', Eur. J. Oper. Res., vol. 252, no. 1, ,pp. 136–144, 2016.

[111] A. Khmag, A. R. Ramli, S. A. R. Al-haddad, S. Yusoff, and N. H. Kamarudin, 'Denoising of natural images through robust wavelet thresholding and genetic programming', Vis. Comput., vol. 33, no. 9, ,pp. 1141–1154, 2017.

[112] S. G. Javed, A. Majid, and Y. S. Lee, 'Developing a bio-inspired multi-gene genetic programming based intelligent estimator to reduce speckle noise from ultrasound images', Multimed. Tools Appl., vol. 77, no. 12, ,pp. 15657–15675, 2018.

[113] M. Yamagiwa, E. Kikuchi, M. Uehara, M. Murakami, and M. Yoneyama, 'Reconstruction for Artificial Degraded Image Using Constructive Solid Geometry and Strongly Typed Genetic Programming', 2009 International Conference on Complex, Intelligent and Software Intensive Systems, IEEE,pp. 162–168, 2009.

[114] P. Thong-On and U. Watchareeruetai, 'Detection of fibrosis in liver biopsy images using multi-objective genetic programming', 2017 9th Int. Conf. Inf. Technol. Electr. Eng. ICITEE 2017, vol. 2018-Janua, ,pp. 1–6, 2017.

[115] M. Iqbal, B. Xue, H. Al-Sahaf, and M. Zhang, 'Cross-Domain Reuse of Extracted Knowledge in Genetic Programming for Image Classification', IEEE Trans. Evol. Comput., vol. 21, no. 4, ,pp. 569–587, 2017.

[116] Í. M. Miranda, C. Aranha, and M. Ladeira, 'Classification of EEG signals using genetic programming for feature construction', Proceedings of the Genetic and Evolutionary Computation Conference, New York, NY, USA,ACM,pp. 1275–1283, 2019.

[117] A. Bhardwaj, A. Tiwari, R. Krishna, and V. Varma, 'A novel genetic programming approach for epileptic seizure detection', Comput. Methods Programs Biomed., vol. 124, ,pp. 2–18, 2016.

[118] M. feli and F. Abdali-Mohammadi, '12 Lead Electrocardiography Signals Compression By a New Genetic Programming Based Mathematical Modeling Algorithm', Biomed. Signal Process. Control, vol. 54, ,p. 101596, 2019.

[119] N. M. Khan and G. M. Khan, 'Audio Signal Reconstruction Using Cartesian Genetic Programming Evolved Artificial Neural Network (CGPANN)', 2017 16th IEEE International Conference on Machine Learning and Applications (ICMLA), vol. 2018-Janua, IEEE,pp. 568–573, 2017.

[120] N. Pillay, 'The impact of genetic programming in education', Genet. Program. Evolvable Mach., no. October 2018, 2019.

[121] W. Xing, R. Guo, E. Petakovic, and S. Goggins, 'Participation-based student final performance prediction model through interpretable Genetic Programming: Integrating learning analytics, educational data mining and theory', Comput. Human Behav., vol. 47, ,pp. 168–181, 2015.

[122] Y. Li, C. Yuan, C. Zhang, S. Li, K. Sun, and X. Wang, 'A Novel Approximation Algorithm Based on Genetic Programming in Digital Learning Environment', 2015 International Conference of Educational Innovation through Technology (EITT), IEEE,pp. 33–36, 2015.

[123] S. Liu and H. Shi, 'A Recursive Approach to Long-Term Prediction of Monthly Precipitation Using Genetic Programming', Water Resour. Manag., vol. 33, no. 3, ,pp. 1103–1121, 2019.

[124] J. Chadalawada, V. Havlicek, and V. Babovic, 'A Genetic Programming Approach to System Identification of Rainfall-Runoff Models', Water Resour. Manag., vol. 31, no. 12, ,pp. 3975–3992, 2017.

[125] A. Danandeh Mehr and V. Nourani, 'Season Algorithm-Multigene Genetic Programming: A New Approach for Rainfall-Runoff Modelling', Water Resour. Manag., vol. 32, no. 8, ,pp. 2665–2679, 2018.

[126] A. Aryafar, V. Khosravi, H. Zarepourfard, and R. Rooki, 'Evolving genetic programming and other AI-based models for estimating groundwater quality parameters of the Khezri plain, Eastern Iran', Environ. Earth Sci., vol. 78, no. 3, ,pp. 1–13, 2019.

[127] J. Shiri, A. A. Sadraddini, A. H. Nazemi, O. Kisi, G. Landeras, A. Fakheri Fard, and P. Marti, 'Generalizability of Gene Expression Programming-based approaches for estimating daily reference evapotranspiration in coastal stations of Iran', J. Hydrol., vol. 508, ,pp. 1–11, 2014.

[128] A. Danandeh Mehr, V. Nourani, E. Kahya, B. Hrnjica, A. M. A. Sattar, and Z. M. Yaseen, 'Genetic programming in water resources engineering: A state-of-the-art review', J. Hydrol., vol. 566, no. September, ,pp. 643–667, 2018.

[129] J. I. Hidalgo, J. M. Colmenar, J. L. Risco-Martin, A. Cuesta-Infante, E. Maqueda, M. Botella, and J. A. Rubio, 'Modeling glycemia in humans by means of Grammatical Evolution', Appl. Soft Comput. J., vol. 20, ,pp. 40–53, 2014.

[130] L. Vanneschi, 'Improving genetic programming for the prediction of pharmacokinetic parameters', Memetic Comput., vol. 6, no. 4, ,pp. 255–262, 2014.

[131] M. B. Erdem, Z. Erdem, and S. Rahnamayan, 'Diabetes mellitus prediction using multi-objective genetic programming and majority voting', 14th Int. Conf. Comput. Sci. Educ. ICCSE 2019, no. Iccse, ,pp. 953–958, 2019.

[132] R. Senatore, A. Della Cioppa, and A. Marcelli, 'Automatic diagnosis of Parkinson disease through handwriting analysis: A cartesian genetic programming approach', Proc. - IEEE Symp. Comput. Med. Syst., vol. 2019-June, ,pp. 312–317, 2019.

[133] D. Moskowitz, 'Implementing the template method pattern in genetic programming for improved time series prediction', Genet. Program. Evolvable Mach., vol. 19, no. 1–2, ,pp. 271–299, 2018.

[134] A. Kattan, S. Fatima, and M. Arif, 'Time-series event-based prediction: An unsupervised learning framework based on genetic programming', Inf. Sci. (Ny)., vol. 301, ,pp. 99–123, 2015.

[135] M. Graff, H. J. Escalante, F. Ornelas-Tellez, and E. S. Tellez, 'Time series forecasting with genetic programming', Nat. Comput., vol. 16, no. 1, ,pp. 165–174, 2017.

[136] L. Yang, J. Zhang, X. Wu, Y. Zhang, and J. Li, 'A chaotic time series prediction model for speech signal encoding based on genetic programming', Appl. Soft Comput. J., vol. 38, ,pp. 754–761, 2016.

[137] F. Yang, M. Li, A. Huang, and J. Li, 'Forecasting time series with genetic programming based on least square method', J. Syst. Sci. Complex., vol. 27, no. 1, ,pp. 117–129, 2014.

[138] B. Barán, J. Paciello, V. Cañete, and N. Hernández, 'Estimating electrical energy consumption using Linear Genetic Programming', Proceedings of the The International Conference on Engineering & MIS 2015 - ICEMIS '15, New York, New York, USA,ACM Press,pp. 1–7, 2015.

[139] A. Garg, J. S. L. Lam, and L. Gao, 'Energy conservation in manufacturing operations:

Modelling the milling process by a new complexity-based evolutionary approach', J. Clean. Prod., vol. 108, ,pp. 34–45, 2015.

[140] I. Boumanchar, K. Charafeddine, Y. Chhiti, F. E. M'hamdi Alaoui, A. Sahibed-dine, F. Bentiss, C. Jama, and M. Bensitel, 'Biomass higher heating value prediction from ultimate analysis using multiple regression and genetic programming', Biomass Convers. Biorefinery, vol. 9, no. 3, ,pp. 499–509, 2019.

[141] V. H. C. Pinheiro and R. Schirru, 'Genetic programming applied to the identification of accidents of a PWR nuclear power plant', Ann. Nucl. Energy, vol. 124, ,pp. 335–341, 2019.

[142] J. Hu and W. Guo, 'Flexibility analysis in waste-to-energy systems based on decision rules and gene expression programming', Conf. Proc. - IEEE Int. Conf. Syst. Man Cybern., vol. 2019-Octob, ,pp. 988–993, 2019.

[143]'DEAP',https://deap.readthedocs.io/en/master/,accessed 6 February 2020.

[144]'GPLEARN',https://gplearn.readthedocs.io/en/stable/,accessed 6 February 2020.

[145]'Matlab',https://www.mathworks.com/,accessed 7 February 2020.

[146] 'GELAB: A Matlab ToolBox',https://github.com/adilraja/GELAB, accessed 7 February 2020.

[147] 'CGP4Matlab',https://github.com/tiagoinacio/CGP4Matlab,accessed 7 February 2020.

[148] R. Miragaia, G. Reis, F. Fernandéz, T. Inácio, and C. Grilo, 'CGP4Matlab - A Cartesian Genetic Programming MATLAB Toolbox for Audio and Image Processing', Applications of Evolutionary Computation April 4-6, 2018, Parma, Italy,Springer, Cham,pp. 455–471, 2018.

[149] 'GPTIPS 2',https://sites.google.com/site/gptips4matlab/home,accessed 7 February 2020.

[150] I. Pan and S. Das, 'When Darwin meets Lorenz: Evolving new chaotic attractors through genetic programming', Chaos, Solitons & Fractals, vol. 76, ,pp. 141–155, 2015.

[151] D. P. Searson, 'GPTIPS 2: An Open-Source Software Platform for Symbolic Data Mining', Cham,Springer International Publishing,pp. 551–573, 2015.

[152] P. K. Muduli, M. R. Das, S. K. Das, and S. Senapati, 'Lateral Load Capacity of Piles in Clay Using Genetic Programming and Multivariate Adaptive Regression Spline', Indian Geotech. J., vol. 45, no. 3, ,pp. 349–359, 2015.

[153] D. P. Searson, D. E. Leahy, and M. J. Willis, 'Predicting the Toxicity of Chemical Compounds Using GPTIPS: A Free Genetic Programming Toolbox for MATLAB', ,pp. 83–93, 2011.

[154]'PonyGE2',https://github.com/PonyGE/PonyGE2/,accessed 7 February 2020.

[155] M. Fenton, J. McDermott, D. Fagan, S. Forstenlechner, E. Hemberg, and M. O'Neill, 'PonyGE2: grammatical evolution in Python', Proceedings of the Genetic and Evolutionary Computation Conference Companion on - GECCO '17, New York, New York, USA,ACM Press,pp. 1194–1201, 2017.

[156]'GeneXproTools',https://www.gepsoft.com/,accessed 7 February 2020.

[157] Y. Sun, Z. Li, C. Tang, W. Zhou, and R. Jiang, 'An Evolving Neural Network for Authentic Emotion Classification', 2009 Fifth International Conference on Natural Computation, vol. 2, IEEE,pp. 109–113, 2009.

[158] S. Mehdizadeh, F. Fathian, M. J. S. Safari, and A. Khosravi, 'Developing novel hybrid models for estimation of daily soil temperature at various depths', Soil Tillage Res., vol. 197, ,p. 104513, 2020.

[159]'GEP4J',https://code.google.com/p/gep4j/,accessed 7 February 2020.

[160]'PyGEP',https://code.google.com/p/pygep/.,accessed 7 February 2020.

[161]'JGEP',https://sourceforge.net/projects/jgep/.,accessed 7 February 2020.

[162]'Epochx',https://www.epochx.org/,accessed 7 February 2020.

[163] 'Karoo GP',http://kstaats.github.io/karoo_gp/,accessed 7 February 2020.

[164]'Tensorflow',https://www.tensorflow.org/,accessed 7 February 2020.

[165]'GISMO',http://www0.cs.ucl.ac.uk/staff/W.Langdon/gismo/,accessed 8 February 2020.

[166] W. B. Langdon, 'Genetic Improvement of Software for Multiple Objectives', ,pp. 12–28, 2015.

[167] W. B. Langdon and M. Harman, 'Optimizing existing software with genetic programming', IEEE Trans. Evol. Comput., vol. 19, no. 1, ,pp. 118–135, 2015.

[168]'KNIME',https://www.knime.com/,accessed 8 February 2020.

[169] M. R. Berthold, N. Cebron, F. Dill, T. R. Gabriel, T. Kötter, T. Meinl, P. Ohl, K. Thiel, and B. Wiswedel, 'KNIME - the Konstanz information miner', ACM SIGKDD Explor. Newsl., vol. 11, no. 1, ,pp. 26–31, 2009.

[170] S. O'Hagan and D. B. Kell, 'Software review: the KNIME workflow environment and its applications in genetic programming and machine learning', Genet. Program. Evolvable Mach., vol. 16, no. 3, ,pp. 387–391, 2015.

[171] 'GSGP-C++ 2.0',http://gsgp.sourceforge.net/,accessed 8 February 2020.

[172] M. Castelli, S. Silva, and L. Vanneschi, 'A C++ framework for geometric semantic genetic programming', Genet. Program. Evolvable Mach., vol. 16, no. 1, ,pp. 73–81, 2015.

[173] M. Castelli and L. Manzoni, 'GSGP-C++ 2.0: A geometric semantic genetic programming framework', SoftwareX, vol. 10, ,p. 100313, 2019.

[174] 'GPLAB',http://gplab.sourceforge.net/,accessed 8 February 2020.

[175] S. Silva and J. Almeida, 'GPLAB-a genetic programming toolbox for MATLAB', Proc. Nord. MATLAB Conf., ,pp. 273–278, 2003.

[176] V. K. Dabhi and S. Chaudhary, 'Empirical modeling using genetic programming: a survey of issues and approaches', Nat. Comput., vol. 14, no. 2, ,pp. 303–330, 2015.

[177] W. Banzhaf, 'Genetic programming and emergence', Genet. Program. Evolvable Mach., vol. 15, no. 1, ,pp. 63–73, 2014.

[178] L. Vanneschi, M. Castelli, and S. Silva, 'A survey of semantic methods in genetic programming', Genet. Program. Evolvable Mach., vol. 15, no. 2, ,pp. 195–214, 2014.

[179] I. Costa-Carrapiço, R. Raslan, and J. N. González, 'A systematic review of genetic algorithm-based multi-objective optimisation for building retrofitting strategies towards energy efficiency', Energy Build., vol. 210, ,p. 109690, 2020.

[180] Q. Zhang, K. Barri, P. Jiao, H. Salehi, and A. H. Alavi, 'Genetic programming in civil engineering: advent, applications and future trends', Artif. Intell. Rev., 2020.

[181] J. Zhong, L. Feng, and Y.-S. Ong, 'Gene Expression Programming: A Survey', IEEE Comput. Intell. Mag., vol. 12, no. 3, ,pp. 54–72, 2017.

SAKARYA ÜNİVERSİTESİ
FEN BİLİMLERİ ENSTİTÜSÜ DERGİSİ

Sakarya University Journal of Science
SAUJS

e-ISSN 2147-835X | Period Bimonthly | Founded: 1997 | Publisher Sakarya University |
http://www.saujs.sakarya.edu.tr/en/

Title: A Comparative Study of Optimization Algorithms for Global Path Planning of Mobile Robots

Authors: Mustafa Yusuf YILDIRIM, Rüştü AKAY

Recieved: 2020-09-25 00:00:00

Accepted: 2021-02-22 00:00:00

Article Type: Research Article

Volume: 25
Issue: 2
Month: April
Year: 2021
Pages: 417-428

How to cite
Mustafa Yusuf YILDIRIM, Rüştü AKAY; (2021), A Comparative Study of Optimization Algorithms for Global Path Planning of Mobile Robots. Sakarya University Journal of Science, 25(2), 417-428, DOI: https://doi.org/10.16984/saufenbilder.800067
Access link
http://www.saujs.sakarya.edu.tr/en/pub/issue/60672/800067

Sakarya University Journal of Science 25(2), 417-428, 2021

A Comparative Study of Optimization Algorithms for Global Path Planning of Mobile Robots

Mustafa Yusuf YILDIRIM*[1], Rüştü AKAY[1]

Abstract

It is an essential issue for mobile robots to reach the target points with optimum cost which can be minimum duration or minimum fuel, depending on the problem. In this paper, it was aimed to develop a software for the optimal path planning of mobile robots in user-defined two-dimensional environments with static obstacles and to analyze the performance of some optimization algorithms for this problem using this software. The developed software is designed to create obstacles of different shapes and sizes in the work area and to find the shortest path for the robot using the selected optimization algorithm. Particle Swarm Optimization (PSO), Artificial Bee Colony (ABC) and Genetic Algorithm (GA) were implemented in the software. These algorithms have been tested for optimum path planning in four models with different problem sizes and different difficulty levels. When the results are evaluated, it is observed that the ABC algorithm gives better results than other algorithms in terms of the shortest distance. With this study, the use of optimization algorithms in real-time path planning of land mobile robots or unmanned aerial vehicles can be simulated.

Keywords: Mobile robot, path planning, cubic spline interpolation, optimization algorithms, simulation

1. INTRODUCTION

Path planning is performed for a mobile robot to determine the path it needs to track in order to reach its destination in an environment. With a successful planning system, mobile robots can access the desired point without any intervention. The primary purpose of optimization-based path planning for mobile robots is to find away from the start point to the target point without colliding any obstacles. Quality of the path affects all planning and the planned path should be feasible in terms of time and distance [1, 3-5].

In order for mobile robots to be used more efficiently, the distance between the start and target points must be covered in the shortest time and with the least cost without colliding the obstacles. For this purpose, many path planning algorithms have been developed for these robots [2]. Mobile robots reach the desired point most effectively with these algorithms [5].

*Corresponding author: myyildirim@erciyes.edu.tr
[1]Erciyes University, Faculty of Engineering, Mechatronics Engineering Department, 38039, Kayseri.
E-Mail: myyildirim@erciyes.edu.tr; akay@erciyes.edu.tr
ORCID: https://orcid.org/0000-0003-0302-8466; https://orcid.org/0000-0002-3585-3332

Some studies on the path planning for mobile robots in the literature can be explained as follows: Wang et al. firstly found the shortest path with the A Star algorithm and when they detected obstacles on this path, they reached the nearest safe point and optimized the path again with the PSO algorithm. [1]. Buniyamin et al. used an improved version of the Ant Colony Optimization algorithm for path planning [4]. Alajlan et al. used GA to solve the path planning problems in large-scale grid maps. [5]. Ajeil et al. used a hybridized PSO - Modified Frequency Bat algorithm for mobile robots in both static and dynamic conditions, minimizing the distance and fulfilling the path smoothness criteria. They also identified possible points that will be produced by a new Local Search algorithm integrated into this algorithm and converted into feasible solutions. [6]. Wang et al. developed a Multi-Objective PSO algorithm for path planning on rough terrain. They found that the proposed algorithm provides an advantage in obtaining Pareto optimal solutions. [7]. Zhang et al. developed a hybrid algorithm including Deep Learning, Ray Tracing, Waiting Rule, and Rapidly-Exploring Random Tree algorithms in known indoor environments. They compared the proposed algorithm with traditional and some intelligent algorithms in static and dynamic environments and proved their applicability. [8]. Dewang et al. developed the Adaptive PSO algorithm for the global path planning of mobile robots in environments with static obstacles. With this algorithm, the robot has reached the target point in a shorter time than the traditional PSO algorithm. [9]. Low et al. improved the performance of the Q-learning algorithm using the Flower Pollination algorithm because of the slow convergence rate of the Q-learning algorithm in the global path planning of mobile robots. With the proposed algorithm, the convergence of the Q-learning algorithm has been accelerated. [10]. Patle et al. developed The Matrix-Binary Codes based Genetic Algorithm for path planning of mobile robots in both static and dynamic conditions. They found that the proposed control mechanism is optimal in terms of path and time compared to other navigation controls. [11]. Das et al. developed a version of the PSO algorithm used with evolutionary operators for path planning of multi-robot systems in known and complex environments. They have observed that the proposed algorithm performs better compared to other algorithms. [12]. Saeed et al. developed the Boundary Node Method for global path planning of mobile robots in static environments, and they found that the proposed method produced better results compared with other methods. [13]. Nazarahari et al. developed Artificial Potential Field and Enhanced GA algorithms for path planning of multi-robot systems. They used the first to identify all suitable paths, and the second to find the optimum path. They observed that the developed algorithm system performs better compared to other algorithms. [14]. Saraswathi et al. developed a hybrid version of the Cuckoo-Search and Bat Algorithm algorithms for the global path planning of mobile robots. They used the proposed algorithm in the conditions that environmental factors are unknown and found that the proposed algorithm takes less time to reach the target point than other algorithms. [15]. Rosas et al. developed a membrane evolutionary artificial potential field for global path planning problem in both static and dynamic environments. They observed that the proposed approach performed better compared to other methods. [16]. Bayat et al. developed the Electrostatic potential field approach for the global path planning of mobile robots. They tested the proposed approach in static and dynamic environments and proved its applicability. [17]. Qu et al. developed a grey wolf optimizer algorithm with reinforcement learning for path planning. The proposed algorithm has been proven to be successful in complex environments. [18]. Patle et al. used the Firefly Algorithm for mobile robot navigation in environments where environmental conditions change. They found that the proposed study produced better results compared to other intelligent navigation approaches. [19]. Song et al. used the Compact Cuckoo Search algorithm for the 3D path planning, and proposed a new Parallel Communication Strategy. The proposed method produced better results compared to other algorithms. [20]. Elhoseny et al. developed a Bézier curve based approach that uses Modified Genetic Algorithm for global path planning in

dynamic environments. The proposed approach is efficient method regarding the energy consumption of the robot in harsh environments. [21]. Patle et al. increased the performance of the Fuzzy Logic algorithm alone using the Probability and Fuzzy Logic algorithm for robot navigation. They found that this study produced better results compared to other navigation approaches. [22]. Goel et al. used the Glow-worm Swarm Optimization algorithm for 3D path planning. The proposed method has provided high convergence speed and accuracy compared to other heuristic algorithms. [23]. Li et al. developed a navigation system with a sensor network using a novel Artificial Potential Field algorithm. This method is used in environments with dynamic conditions. The tests and simulations proved the accuracy of this system. [24].

Unlike the studies in the literature, in this paper, a MATLAB-based generalizable simulation interface where different optimization algorithms are applied for global path planning has been designed and the performances of these optimization algorithms are evaluated in terms of shortest path and algorithm running time. This software will contribute to the literature by guiding in simulating a desired environment in which a robot moves, determining the best performanced optimization algorithm and the optimum path for real-time applications. In addition, this interface is designed not only for the optimization algorithms used in this paper, but also to be easily integrated for other methods used for path planning in the literature.

The rest of paper is organized as follows: In the second section, the optimization algorithms used in this paper are briefly explained. In the third chapter, material and method are presented, and the fourth section shows the results of the simulation. The fifth part is dedicated the conclusion.

2. OPTIMIZATION ALGORITHMS

2.1. Particle Swarm Optimization

Particle swarm optimization algorithm is a swarm-based optimization algorithm developed by Eberhart and Kennedy in 1995 [25]. This algorithm was developed inspired by the social behaviours of birds and fishes. The algorithm is often used for numerical problems. The basic steps of the algorithm are shown in Algorithm 1.

Algorithm 1 The basic steps of the PSO algorithm [25]

1: Initialize the control parameters of algorithm
2: Generate initial positions and velocities of particles
3: **While (stopping criteria not met)**
4: Evaluate fitness values
5: Determine the current best position for all particles
6: Update the global best position
7: Update the velocity and position of all particles
8: **End while**
9: Return the best solution

In this algorithm, the initial positions of the particles are generated randomly. Generally, the initial velocities of the particles are zero. The fitness values of the randomly generated positions are calculated using the objective function. The best position of each particle so far ($x_{best,i}$) and the best position of the population (g_{best}) are determined by their fitness values.

Using these positions, the velocities of the particles are updated. Equation 1 shows the velocity update equation.

$$v_i(t+1) = v_i(t) + r_1.c_1.\left(x_{best,i} - x_i(t)\right) + r_2.c_2.\left(g_{best} - x_i(t)\right);\ \ i = 1, \dots, P \quad (1)$$

where $v_i(t+1)$ is the current velocity of the particle i, $v_i(t)$ is the old velocity of the particle i, $x_i(t)$ is the old position of the particle i, r_1 and r_2 are random numbers generated between (0, 1), c_1 and c_2 are learning coefficients, P is the number of particles (size of the population). Positions of the particles are updated using this updated velocity. Equation 2 shows the position update equation.

$$x_i(t+1) = x_i(t) + v_i(t+1) \quad (2)$$

where $x_i(t+1)$ the current position of the particle i. The best solution is stored in memory after velocity and position update, and the iterative

process continues until the stop criterion is met [26].

2.2. Artificial Bee Colony

Artificial bee colony algorithm is a swarm-based optimization algorithm developed by Karaboga in 2005 [25]. This algorithm has been developed by modeling bees' foraging behaviors. The basic steps of the algorithm are shown in Algorithm 2. In this algorithm, initial food sources are generated randomly using Equation 3.

Algorithm 2 The basic steps of the ABC algorithm [25]

1: Initialize the control parameters of algorithm
2: Generate initial population
3: **While (stopping criteria not met)**
4: Apply employee bee phase to generate new food sources
5: Calculation of probabilities according to the information from the employee bees.
6: Apply onlooker bee phase to generate new food sources
7: Abandonment of consumed resources and generating scout bees (scout bees phase)
8: **End while**
9: Return the best solution

$$x_{i,j} = x_j^{min} + rand(0,1)\,.\,\left(x_j^{max} - x_j^{min}\right);\quad i = 1,\dots,SN;\ j = 1,\dots,D \tag{3}$$

where is food source, SN is food source number, D is number of parameters to be optimized, x_j^{min} is the lower limit of the parameter j and x_j^{max} is the upper limit of the parameter j. Employed bees are dispatched to food sources. It determines the new food source adjacent to the source it works and evaluates its quality. The equations used at this stage are shown in Equations 4, 5 and 6.

$$v_{i,j} = x_{i,j} + \varphi_{i,j}.\left(x_{i,j} - x_{k,j}\right);\ k = 1,\dots,SN \tag{4}$$

$$v_{i,j} = \begin{cases} x_j^{min} & ;\ v_{i,j} < x_j^{min} \\ v_{i,j} & ;\ x_j^{max} < v_{i,j} < x_j^{max} \\ x_j^{max} & ;\ v_{i,j} > x_j^{max} \end{cases} \tag{5}$$

$$fit_i = \begin{cases} 1/(1+f_i) & ;\ f_i \geq 0 \\ 1 + abs(f_i) & ;\ f_i < 0 \end{cases};\ f_i = f\left(v_{i,j}\right) \tag{6}$$

where $v_{i,j}$ is a new food source, $\varphi_{i,j}$ is a random number generated between [-1, 1], $x_{k,j}$ is the food source randomly selected for the parameter j and fit_i is fitness value of the source $v_{i,j}$. The greedy selection process is applied according to this fitness value. If the new solution is better, replaces the old solution with this new solution. Otherwise, a counter is generated for the old solution, and this counter increases by one. By using fitness values, probabilities to be used by the onlookers in the selection are calculated as in Equation 7.

$$p_i = \frac{fit_i}{\sum_{j=1}^{SN} fit_j} \tag{7}$$

where p_i is the probability of selecting the source i. By using these values, a random number is generated in the range of [0, 1] according to the roulette wheel, and if the value p_i is greater than this random number, the scouts produce a new solution using Equation 4. If this new solution is better, replaces with the old solution with this new solution and the counter generated for the old solution is reset. Otherwise, the counter increases by one. At the end of the iteration, the counters are checked. The resources which their counters are above a certain threshold (limit) are abandoned, and a new food source is searched. The best solution is stored in memory, and the iterative process continues until the stop criterion is met [25].

2.3. Genetic Algorithm

The genetic algorithm is an evolutionary algorithm based on natural selection and genetic laws developed by Holland in 1975 [25]. The basic steps of the algorithm are shown in Algorithm 3. In this algorithm, the initial population is generated randomly and then, the fitness values of these solutions are calculated. The probability of survival of solutions is calculated based on their fitness values. By generating a random number, it is determined which solutions will survive. This process is called selection stage.

Parents are randomly selected from surviving solutions for crossover. A random number is generated, and if this number is smaller than the

crossover rate, the relevant parents are crossed to find new solutions. The crossover rate is usually chosen from 0.6 to 1. After crossover, each solution is subjected to mutation. Another random number is generated and if this number is smaller than the mutation rate, some bits of the relevant solution will change. The mutation rate is usually chosen from 0.001 to 0.1. The best solution is stored in memory, and the iterative process continues until the stop criterion is met [27].

Algorithm 3 The basic steps of the GA [25]

1: Initialize the control parameters of algorithm
2: Generate initial population
3: **While (stopping criteria not met)**
4: Calculation of fitness values
5: Selection Stage
6: Crossover Stage
7: Mutation Stage
8: **End while**
9: Return the best solution

3. MATERIAL AND METHODS

3.1. Simulation Software

The The simulation software was designed through the MATLAB GUI. The software shown in Figure 1 includes environment screen, convergence screen, model creation interface, model and algorithm selections, path planning parameters, and control parameters of algorithms.

On the environment screen, start and target points of the mobile robot, obstacles and planned optimum paths are shown. The environment screen has an area of 100 m2. The convergence screen shows the convergence graph of the algorithm used at the end of each global path planning. This graph represents the shortest distance in meters. In the model creation interface, obstacles are created in the form of circles, squares and equilateral triangles. Obstacles create using the mouse left click. In this paper, the radius of the circle, an edge length of the square and triangle are defined as sizes, and the size of each shape can be selected with a step length of 0.1 meters between [0.2, 2] meters. In path planning parameters, the start and target points of the robot and the number of parameters can be determined. In control parameters of algorithms, population size and the maximum number of iterations can be determined. Also, learning coefficients for PSO, the limit for ABC, crossover and mutation rates for GA can be used as inputs. In the selection of the model, there are four different models. When one of these models is selected, it is displayed on the environment screen. In the algorithm selection, one of GA [27], PSO [28] and ABC [29] algorithms is selected. The RUN button is used to run the path planning optimization, and the RESET button is used to initialize the system.

3.2. Problem Formulation

The optimum path of the mobile robot is planned with cubic spline interpolation in this paper. Some points are required for this purpose. The number of these points is expressed as the number of parameters (d). The solution is determined as the coordinates of these points. In each iteration, these points are transferred to an array with start and target points. This array is interpolated using the cubic spline function and q query points. The interpolated path contains n points and these points are expressed as P_i.

Figure 1 Simulation software developed in this paper

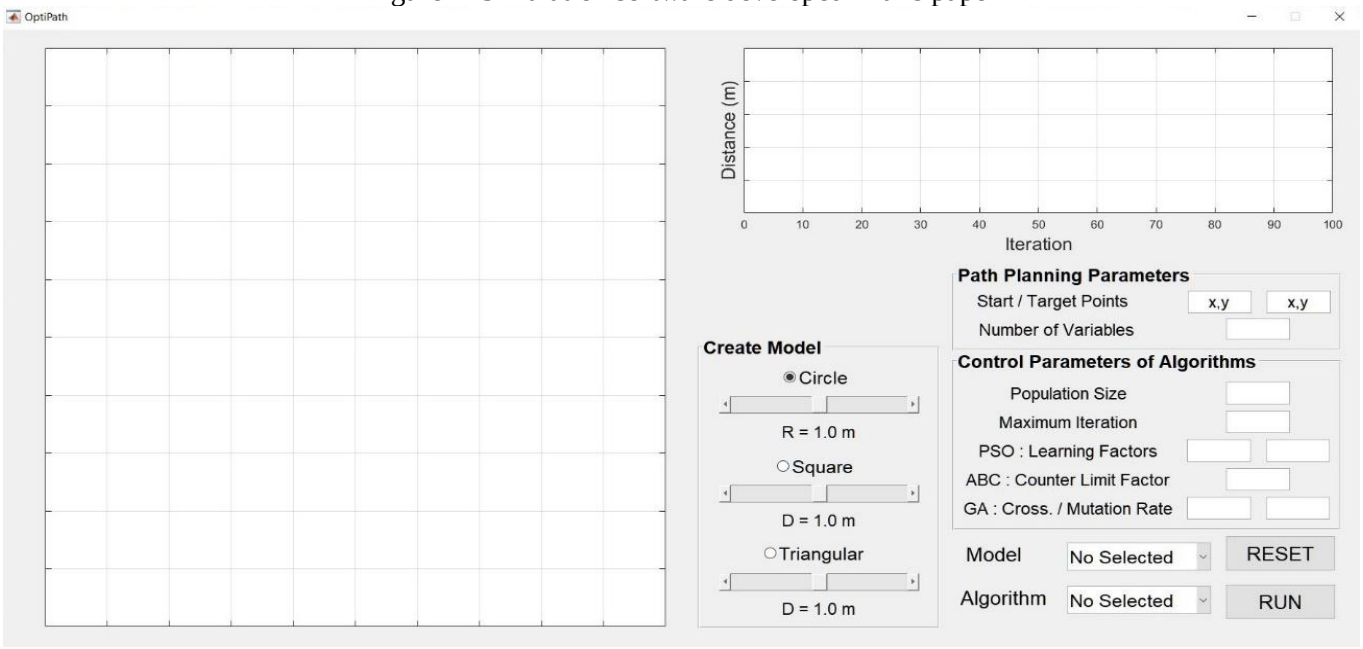

The objective function used in the paper is composed of two parts. The first calculates the length of the path, and the second calculates the feasible distance between the robot and obstacles. The objective function to be optimized is shown in Equation 8.

$$\min\ F(P_i, O_j) = L(P_i).\left[1 + \beta.V(P_i, O_j)\right];\quad i = 1, \dots, q;\ j = 1, \dots, o \tag{8}$$

where O_j is the location of obstacles, $L(P_i)$ is path length function, β is obstacle violation factor, $V(P_i, O_j)$ is violation function, o is the number of obstacles. Violation function is required to calculate the feasible distance between the robot and obstacles. The path length function is shown in Equation 9, and the violation function in Equation 10.

$$L(P_i) = \sum_{i=1}^{n-1} \sqrt{(P_{ix} - P_{(i+1)x})^2 + (P_{iy} - P_{(i+1)y})^2} \tag{9}$$

$$V(P_i, O_j) = \frac{1}{n}\sum_{i=1}^{o}\left[\sum_{j=1}^{n} \max\left(1 - \frac{\sqrt{(P_{ix} - O_{jx})^2 + (P_{iy} - O_{jy})^2}}{a_j}\right)\right] \tag{10}$$

where a_j is the radius if the obstacle j is circle, half the length of the diagonal if the obstacle j is square, and the height if the obstacle j is triangle [30].

4. ANALYSIS OF RESULTS

The simulation software was developed using the MATLAB 2019a programming language and was run in a computer of the Windows 10 operating system with an INTEL CORE i7 processor and 16 GB of RAM. In the software, the start point is symbolized by a square mark and the target point by a star mark. The shortest distance without obstacle is 14.142 meters. Limit values of the problem are determined as [0.5 9.5] for x and y. The obstacle violation factor β is 100, the query point for the cubic spline interpolation q is 100. In the ABC algorithm, the counter limit value changes according to population size and the number of parameters. In the GA algorithm, the selection process is carried out by the roulette wheel method, and the crossing process is performed by the one-point crossing method. The mutation process is carried out by the value coding method. Random numbers r_1 and r_2 in PSO algorithm, random number $\varphi_{i,j}$ in ABC algorithm, random numbers used for selection/crossover/mutation operations in the GA algorithm are generated differently in each iteration.

PSO, ABC and GA optimization algorithms have been applied in four different models in the software. The number of parameters was

determined as 2, 3, 4, 5, 6, and 8. Algorithms for each model and number of parameters were run with 30 runs. Control parameters of algorithms are shown in Table 1, the models in the software in Figure 2, parameters of obstacles in Table 2, the sample convergence graphs for each model and number of parameters in Figures 3, 4, 5 and 6, average shortest distances, average CPU times and success rates in problem solving (path planning with obstacle avoidance) in Table 3.

Table 1
Control parameters of algorithms [25, 27, 31]

Control Parameters	PSO	ABC	GA
Number of Iteration	100	100	100
Population Size (npop)	50	50	50
c_1 / c_2	2 / 2	-	-
Counter limit Value	-	(0.5).(npop).(d)	-
Crossover / Mutation Rates	-	-	0.98 / 0.1

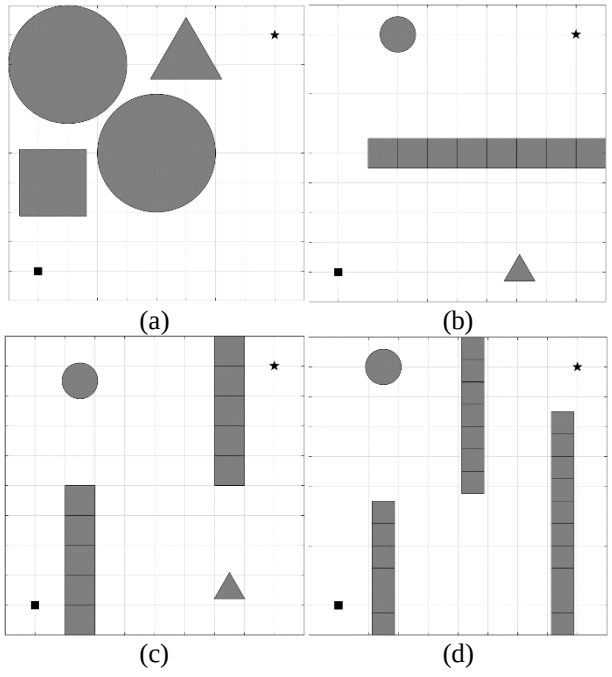

Figure 2 The models in the software:
(a) Model 1, (b) Model 2, (c) Model 3, (d) Model 4

Table 2
Parameters of obstacles: number (size (m))

Obstacle	Model 1	Model 2	Model 3	Model 4
Circle	2 (2)	1 (0.6)	1 (0.6)	1 (0.6)
Square	1 (2.25)	8 (1)	10 (1)	23(0.75)
Triangle	1 (2.4)	1 (1)	1 (1)	-

Considering the results, the fastest running algorithm was determined as GA according to the CPU times in Table 3. When the shortest distance values in the same table are examined, the ABC algorithm has shown the best performance in all models. Considering the convergence graphics of all models, although the convergences of the algorithms are close to each other in all models, it can be said that the ABC algorithm converges slightly faster than the other algorithms examined in this study for the best number of parameters calculated. When the success rates of problem solving are evaluated, the ABC algorithm has also performed best. However, it can be said that the problem solving ability of algorithms is weakened as the environment models become more difficult. Difficulty in problems causes algorithms to plan paths by ignoring obstacles.

When the success rate in Table 3 is examined, it is seen that the algorithms cannot solve the problem in some of 30 runs in difficult models. Besides, it is seen that the number of parameters in difficult models is effective in the success rate of problem solutions. In easy models such as Model 1, 2 and 3, the optimum number of parameters is 2, while in Model 4, which is a difficult model, the optimum number of parameters is 3. Apart from this, it is observed that the path with the shortest distance cannot be planned in cases where the number of parameters is higher. The sample paths found by the algorithms using the optimum number of parameters are shown in Figure 7.

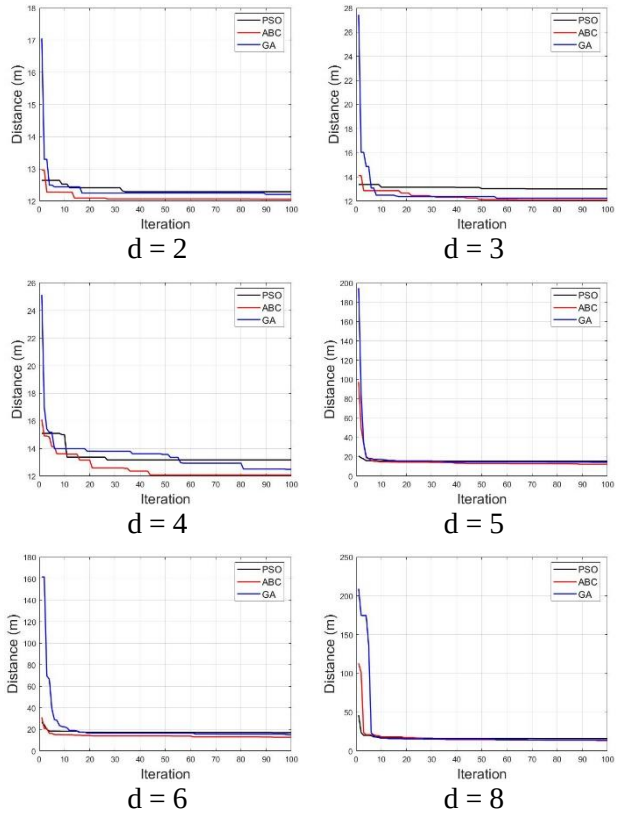

Figure 3 The sample convergence graphs for Model 1

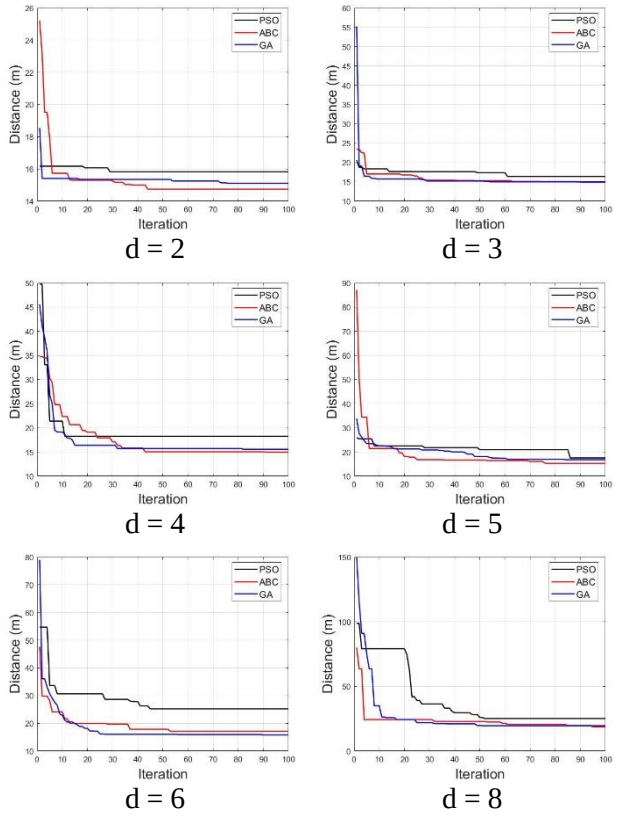

Figure 5 The sample convergence graphs for Model 3

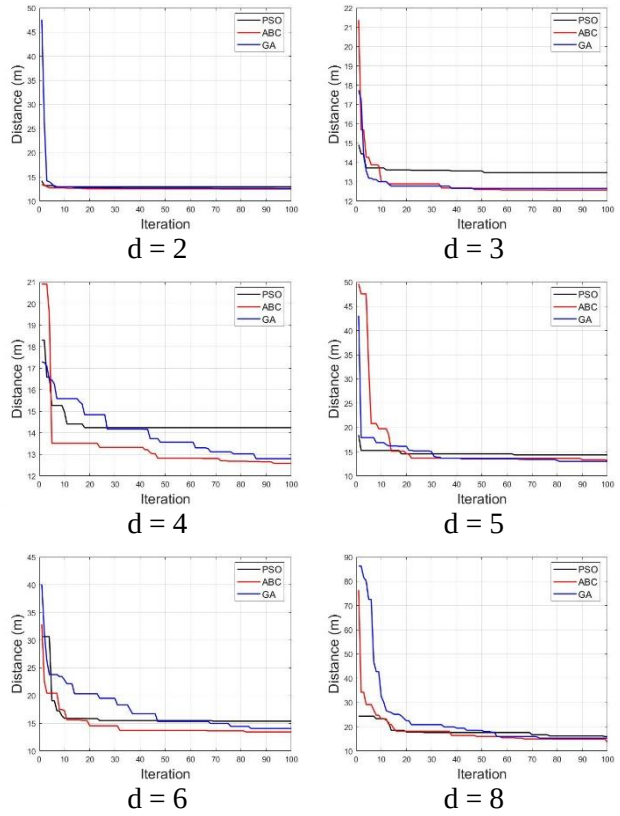

Figure 4 The sample convergence graphs for Model 2

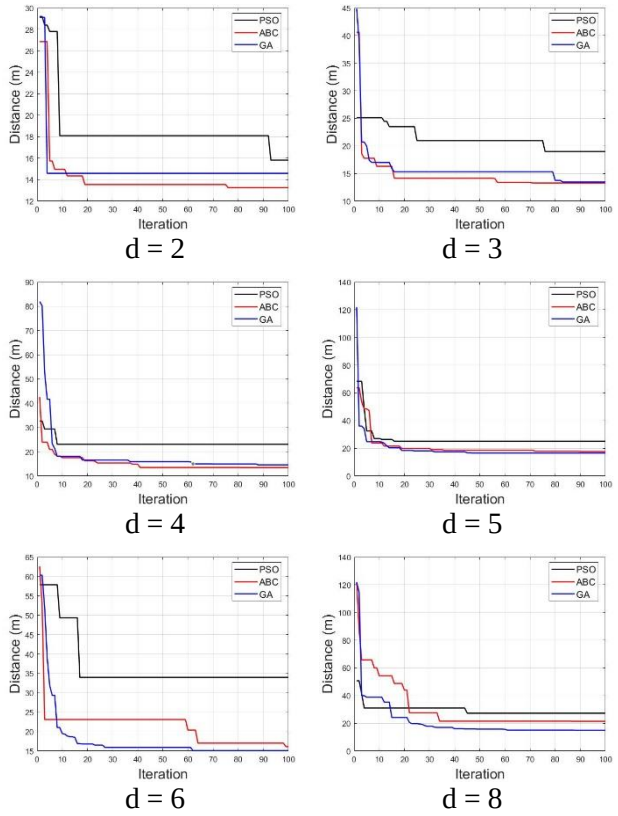

Figure 6 The sample convergence graphs for Model

Table 3
Average shortest distances, average CPU times and success rates in problem solving for each model and number of parameters (These results are average of 30 runs.)

d	Alg.	Model 1			Model 2			Model 3			Model 4		
		Shortest Distance (m)	**CPU Times (s)**	**Success Rate**	**Shortest Distance (m)**	**CPU Times (s)**	**Success Rate**	**Shortest Distance (m)**	**CPU Times (s)**	**Success Rate**	**Shortest Distance (m)**	**CPU Times (s)**	**Success Rate**
2	**PSO**	12.2516	13.0671	30/30	12.7961	13.0696	30/30	16.1726	13.9323	30/30	23.5283	16.3769	10/30
	ABC	**12.0513**	13.1331	**30/30**	**12.4981**	13.2297	**30/30**	**14.7748**	13.8110	**30/30**	14.8430	16.4044	30/30
	GA	12.1320	10.2890	30/30	12.5950	9.9604	30/30	15.1270	10.7339	30/30	19.4570	12.3910	23/30
3	**PSO**	12.8807	13.7011	30/30	13.3248	13.2030	30/30	18.6413	14.0377	25/30	20.4702	16.0140	13/30
	ABC	12.0766	13.4714	30/30	12.5489	13.2239	30/30	14.8989	14.0964	30/30	**13.4868**	16.2611	**30/30**
	GA	12.3257	10.4291	30/30	12.7055	9.8898	30/30	17.2975	10.7320	28/30	16.4833	12.9633	25/30
4	**PSO**	14.0715	13.7768	30/30	14.2845	13.2504	30/30	19.0725	15.0044	26/30	21.9463	16.5527	13/30
	ABC	12.1255	12.7223	30/30	12.6628	12.6753	30/30	15.0692	13.7729	30/30	14.3990	16.4541	30/30
	GA	12.6411	9.4862	30/30	13.0401	9.9745	30/30	17.4845	10.9125	27/30	17.9373	12.8952	20/30
5	**PSO**	15.1391	13.4782	30/30	15.4226	13.2664	29/30	20.7300	14.0262	25/30	23.5203	15.6928	11/30
	ABC	12.3318	13.4728	30/30	12.9595	13.1346	30/30	15.6299	14.1110	30/30	14.8681	16.2983	30/30
	GA	12.2479	10.4494	30/30	13.6584	10.0040	29/30	17.3574	10.8266	26/30	17.6135	12.8570	22/30
6	**PSO**	16.7272	13.8275	30/30	16.6338	13.3001	29/30	25.3959	14.0232	25/30	23.7252	16.4367	11/30
	ABC	12.7744	13.4735	30/30	13.5077	12.9580	30/30	16.3155	14.0974	30/30	16.2651	16.4173	28/30
	GA	13.5840	10.3748	30/30	14.2737	10.1366	29/30	18.8168	10.8185	25/30	19.4753	12.9667	13/30
8	**PSO**	18.1445	11.9220	30/30	18.8914	13.2407	26/30	29.2721	14.1039	27/30	28.1395	16.2067	6/30
	ABC	14.3306	11.5610	30/30	15.7884	13.0625	30/30	18.6938	13.7123	30/30	20.7455	16.5368	25/30
	GA	14.9606	9.1455	30/30	17.1932	10.0974	24/30	22.3556	10.2123	23/30	19.8974	12.9854	15/30

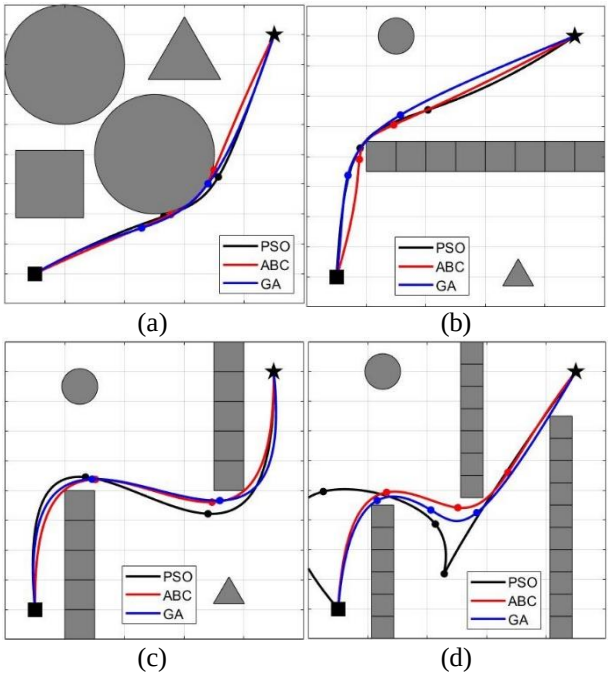

Figure 7 The sample paths found by the algorithms using the optimum number of parameters: (a) Model 1, (b) Model 2, (c) Model 3, (d) Model 4

5. CONCLUSION

In this paper, a software was developed for path planning of mobile robots in static environments, and the performances of different optimization algorithms were evaluated. Four model of different difficulty levels were used for the evaluation. As a result, while the fastest running algorithm is GA, the best performing algorithm is ABC. However, increasing the problem size (number of parameters in path planning) and making the models more difficult caused deterioration in problem solving abilities of these algorithms.

In future works, global paths can be planned for multi-robots in static environments, different approaches can be proposed to improve the performance of the algorithms, or global paths can be planned for single and multi-robots in the environments including static and dynamic obstacles.

The Declaration of Conflict of Interest/ Common Interest

No conflict of interest or common interest has been declared by the authors.

Authors' Contribution

Mustafa Yusuf YILDIRIM contributed to the conceptualization of this study, methodology, software, data improvement, visualization and writing a draft document. Rüştü AKAY contributed in supervision, methodology, reviewing and editing the draft document.

The Declaration of Ethics Committee Approval

The authors declare that this document does not require an ethics committee approval or any special permission.

The Declaration of Research and Publication Ethics

The authors of the paper declare that they comply with the scientific, ethical and quotation rules of SAUJS in all processes of the article and that they do not make any falsification on the data collected. In addition, they declare that Sakarya University Journal of Science and its editorial board have no responsibility for any ethical violations that may be encountered, and that this study has not been evaluated in any academic publication environment other than Sakarya University Journal of Science.

REFERENCES

[1] Y. Wang, F. Cai, and Y. Wang, “Dynamic Path Planning for Mobile Robot Based on Particle Swarm Optimization,” AIP Conference Proceedings 1864, 020024, pp. 1–4, 2017.

[2] M. E. Dere, “Optimum path planning for mobile robots,” MS Thesis, Konya Technical University, 2019.

[3] E. Bogar, “A Hybrid Optimization Method for Single and Multi-Objective Robot Path Planning Problem,” MS Thesis, Pamukkale University, 2016.

[4] N. Buniyamin, N. Sariff, W. A. J. Wan Ngah and Z. Mohamad, "Robot Global Path Planning Overview and A Variation of Ant Colony System Algorithm," International Journal of Mathematics and Computers in Simulation, vol. 1, no. 5, pp. 9–16, 2011.

[5] M. Alajlan, A. Koubaa, I. Chaari, H. Bennaceur and A. Ammar, "Global Path Planning for Mobile Robots in Large-Scale Grid Environments using Genetic Algorithms," International Conference on Individual and Collective Behaviors in Robotics (ICBR), pp. 1–8, 2013.

[6] F. H. Ajeil, I. K. Ibraheem, M. A. Sahib and A. J. Humaidi, "Multi-Objective Path Planning of an Autonomous Mobile Robot using Hybrid PSO-MFB Optimization Algorithm," Applied Soft Computing, vol. 89, 106076, pp. 1–13, 2020.

[7] B. Wang, S. Li, J. Guo and Q. Chen, "Car-Like Mobile Robot Path Planning in Rough Terrain using Multi-Objective Particle Swarm Optimization Algorithm," Neurocomputing, vol. 282, pp. 42–51, 2018.

[8] L. Zhang, Y. Zhang and Y. Li, "Path Planning for Indoor Mobile Robot Based on Deep Learning," Optics, vol. 219, 165096, pp. 1–17, 2020.

[9] H. S. Dewang, P. K. Mohanty and S. Kundu, "A Robust Path Planning for Mobile Robot using Smart Particle Swarm Optimization," Procedia Computer Science, vol. 133, pp. 290–297, 2018.

[10] E. S. Low, P. Ong and K. C. Cheah, "Solving The Optimal Path Planning of a Mobile Robot using Improved Q-Learning," Robotics and Autonomous Systems, vol. 115, pp. 143–161, 2019.

[11] B. K. Patle, D. R. K. Parhi, A. Jagadeesh and S. K. Kashyap, "Matrix-Binary Codes Based Genetic Algorithm for Path Planning of Mobile Robot," Computers & Electrical Engineering, vol. 67, pp. 708–728, 2018.

[12] P. K. Das and P. K. Jena, "Multi-Robot Path Planning using Improved Particle Swarm Optimization Algorithm through Novel Evolutionary Operators," Applied Soft Computing, vol. 92, 106312, pp. 1–24, 2020.

[13] R. A. Saeed, D. R. Recupero and P. Remagnino, "A Boundary Node Method for Path Planning of Mobile Robots," Robotics and Autonomous Systems, vol. 123, 103320, pp. 1–21, 2020.

[14] M. Nazarahari, E. Khanmirza and S. Doostie, "Multi-Objective Multi-Robot Path Planning in Continuous Environment using an Enhanced Genetic Algorithm," Expert Systems with Applications, vol. 115, pp. 106–120, 2019.

[15] M. Saraswathi, G. B. Murali and B. B. V. L. Deepak, "Optimal Path Planning of Mobile Robot using Hybrid Cuckoo Search-Bat Algorithm," Procedia Computer Science, vol. 133, pp. 510–517, 2018.

[16] U. O. Rosas, O. Montiel and R. Sepúlveda, "Mobile Robot Path Planning using Membrane Evolutionary Artificial Potential Field," Applied Soft Computing, vol. 77, pp. 236–251, 2019.

[17] F. Bayat, S. S. Najafinia and M. Aliyari, "Mobile Robots Path Planning: Electrostatic Potential Field Approach," Expert Systems with Applications, vol. 100, pp. 68–78, 2018.

[18] C. Qu, W. Gai, M. Zhong and J. Zhang, "A Novel Reinforcement Learning Based Grey Wolf Optimizer Algorithm for Unmanned Aerial Vehicles (Uavs) Path Planning," Applied Soft Computing, vol. 89, 106099, pp. 1–12, 2020.

[19] B. K. Patle, A. Pandey, A. Jagadeesh and D. R. Parhi, "Path Planning in Uncertain Environment by using Firefly Algorithm," Defence Technology, vol. 14, no. 6, pp. 691–701, 2018.

[20] P. C. Song, J. S. Pan and S. C. Chu, "A Parallel Compact Cuckoo Search Algorithm for Three-Dimensional Path Planning," Applied Soft Computing, vol. 94, 106443, pp. 1–16, 2020.

[21] M. Elhoseny, A. Tharwat and A. E. Hassanien, "Bezier Curve Based Path Planning in A Dynamic Field using Modified Genetic Algorithm," Journal of Computational Science, vol. 25, pp. 339–350, 2018.

[22] B. K. Patle, D. R. K. Parhi, A. Jagadeesh and S. K. Kashyap, "Application of Probability to Enhance the Performance of Fuzzy Based Mobile Robot Navigation," Applied Soft Computing, vol. 75, pp. 265–283, 2019.

[23] U. Goel, S. Varshney, A. Jain, S. Maheshwari and A. Shukla, "Three Dimensional Path Planning for UAVs in Dynamic Environment using Glow-Worm Swarm Optimization," Procedia Computer Science, vol. 133, pp. 230–239, 2018.

[24] H. Li and A. V. Savkin, "An Algorithm for Safe Navigation of Mobile Robots by a Sensor Network in Dynamic Cluttered Industrial Environments," Robotics and Computer-Integrated Manufacturing, vol. 54, pp. 65–82, 2018.

[25] D. Karaboga, "Artificial Intelligence Optimization Algorithms," Nobel Publishing, 2017.

[26] A. Ayari and S. Bouamama, "A New Multiple Robot Path Planning Algorithm: Dynamic Distributed Particle Swarm Optimization," Robotics and Biomimetics, vol. 4, no. 8, pp. 1–15, 2017.

[27] A. Altay, O. Ozkan and G. Kayakutlu, "Prediction of Aircraft Failure Times using Artificial Neural Networks and Genetic Algorithms," Journal of Aircraft, vol. 51, no. 1, pp. 47–53, 2014.

[28] M. K. Heris, Particle Swarm Optimization in MATLAB (URL: https://yarpiz.com/50/ypea102-particle-swarm-optimization), 2015.

[29] M. K. Heris, Artificial Bee Colony in MATLAB (URL: https://yarpiz.com/297/ypea114-artificial-bee-colony), 2015.

[30] E. Chołodowicz and D. Figurowski, "Mobile Robot Path Planning with Obstacle Avoidance using Particle Swarm Optimization," Pomiary Automatyka Robotyka, vol. 21, no. 3, pp. 59–68, 2017.

[31] Y. He, W. J. Ma and J. P. Zhang, "The Parameters Selection of PSO Algorithm Influencing on Performance of Fault Diagnosis," MATEC Web of Conferences 63-02019, pp. 1–5, 2016.

SAKARYA ÜNİVERSİTESİ
FEN BİLİMLERİ ENSTİTÜSÜ DERGİSİ

Sakarya University Journal of Science
SAUJS

e-ISSN 2147-835X | Period Bimonthly | Founded: 1997 | Publisher Sakarya University |
http://www.saujs.sakarya.edu.tr/en/

Title: Analytic Method for Vibration Analysis of Track Structure Induced by High-Speed Train

Authors: Mehmet Akif KOÇ

Recieved: 2020-11-08 00:00:00

Accepted: 2021-03-08 00:00:00

Article Type: Research Article

Volume: 25
Issue: 2
Month: April
Year: 2021
Pages: 429-438

How to cite
Mehmet Akif KOÇ; (2021), Analytic Method for Vibration Analysis of Track Structure Induced by High-Speed Train. Sakarya University Journal of Science, 25(2), 429-438, DOI: https://doi.org/10.16984/saufenbilder.823255
Access link
http://www.saujs.sakarya.edu.tr/en/pub/issue/60672/823255

Sakarya University Journal of Science 25(2), 429-438, 2021

Analytic Method for Vibration Analysis of Track Structure Induced by High-Speed Train

Mehmet Akif Koç*[1]

Abstract

Nowadays, the increase in heavy freight rail transport and high-speed train (HST) operations has encouraged scientists to investigate the dynamic response of rail structures under moving load using analytically and numerically computational methods. In this study, to analyse vibration of rail structure, the rail has been modelled as continuous Euler-Bernoulli elastic beam system. The effects of some basic parameters such as track foundation elasticity modulus, rail stiffness, wheel set axle load and rail critical velocity which affect rail vibrations, on vibrations were examined in detail by considering different track foundation properties. The vibration wave amplitude increases as the train speed approaches the rail infrastructure critical speed.

Keywords: HST, moving load, elastic foundation, continuous beam

1. INTRODUCTION

The increasing interest in high-speed rail transport in the last decade has led to more efforts to investigate the dynamic interaction between rail vehicle and rail structure. Studies on railway dynamics generally consist of models created to study rail vibrations. These rail models have been divided into two main categories in the literature: continuously supported rail beams and discrete supported rail beams [1]. In these models, rail, rail pads, fasteners, sleepers, ballast and ground are the components that define the value of the rail modulus.

The rail on the elastic foundation has been modelled according to Euler-Bernoulli beam theory in recent studies [2]. Euler-Bernoulli and Timoshenko beam theories are two most common used beam models in literature studies to research dynamic response of track effect of HST [2–5].

To investigate rail dynamic response, the first model is studied by Winkler in 1867. This model consist of a rail model which placed on the elastic foundation [6]. The elastic foundation of the rail track has been modelled as uniformly distributed linear spring to represent all rail components.

*Corresponding Author: makoc@subu.edu.tr
[1]Sakarya Applied Science University, Department of Mechatronics Engineering, Sakarya, Turkey. ORCID: https://orcid.org/0000-0001-7461-9795

Duffy [7] presented transient and steady state solutions of the Euler-Bernoulli beam with elastic foundation taking into moving mass inertial effect. Grassie and Cox [8] showed that the large stresses generated in the rail beam, which they analysed as a continuous support beam model, are related to low damping sleeper resonance. A study investigating effect of the rail pad stiffness upon sleeper stresses has been given by [9]. Consequently, it was proven that soft rail pad more isolate to vibration than hard pad and sleeper stresses measured soft rail pad is smaller than hard pad. Modern railway tracks are characterized by correctly placed and continuously welded rails and sleepers. In this technique, mechanical modelling of the railway track has been made very simple by considering railway track as two straight parallel beams supported by sleepers[10].Continuous supported rail models contains many dynamic behaviour parameter in order to have all properties of the railway tracks[11]. The discrete rail models are more appropriate because of conventional railway rails are discretely supported by rail pads and sleepers. Grassie *et al.* [12] investigated to railway track considering two different models with one continuous and the other incorporating the mass of sleepers in the frequency range from 50 to 1500 Hz. Hunt [13] modelled to rails on the railway as a pair of Euler-Bernoulli beams placed side by side on an elastic foundation.

Nowadays, it is very common technique to use computer programs in order to model, design and analyse any engineering structure. The computers present big advantages for scientist so as to model complex engineering problems and analyse due to having big capacity and presenting high performance processing. In previous studies [14,15] only one moving axle load is considered on the elastic structure for HST analysis. In this study, the mathematically model and computer simulation of the rail beam which modelled according to elastic beam theory and moving HST passing over the rail beam have been presented. The effect of some parameters such as rail stiffness, track ballast elasticity module, train wheelset load and HST's critical velocity upon rail displacement has been investigated in detail. In the context of this article, the mathematical formulation for physical model of the rail beam on the elastic foundation has been introduced in section 2. At the same time, in section 3, the effect of some parameters such as rail, elastic foundation and HST upon rail displacement has been investigated using some numerical examples considering different HST velocity and track foundation properties.

2. MATHEMATICAL FORMULATION

In this study, the physical model shown in Figures1a-b have been introduced to examine rail vibration effect of moving HST on the elastic track foundation. Figure 1a shows continuous elastic beam models for unloaded railway track superstructure. Similarly, Figure 1b presents rail beam effect of point moving load *P* with elastic foundation.

2.1. Analytic Formulation of Track Structure Considering Elastic Beam Model

The time dependent equation of motion for undamped continuous elastic rail beam given by Figure 1b has been derived as shown in Equation (1) using Hamilton principle considering moving on its single wheelset point load *F* [14,15].

$$EI\frac{\partial^4 w}{\partial x^4}+m\frac{\partial^2 w}{\partial t^2}+kw=-F\delta\left(x-vt\right) \qquad (1)$$

The parameters *E* and *I* in Equation (1) represent elasticity module of rail beam and inertial moment of the beam cross-section on the horizontal axis respectively. In addition to this, the parameter *w* represents displacement of the rail beam at any point *x* on location beam and at any time *t*. The parameters *m*, *k* and δ in Equation (1) equal to unit length mas of the rail beam, stiffness of the rail beam and Dirac-Delta function respectively. The constant movement velocity of the HST on the rail beam is represented by parameter *v*. The parameter *F* is the condensed wheelset load. To simplify Equation (1), following parameters are defined by Equation (2)

$$\varepsilon_1^2=\frac{m}{4EI},\qquad \varepsilon_2^4=\frac{k}{4EI} \qquad (2)$$

Equation (1) rearranged as follow using defining given by Equation (2).

$$\frac{\partial^4 w}{\partial x^4}+4\varepsilon_1^2\frac{\partial^2 w}{\partial t^2}+4\varepsilon_2^2 w=-\frac{F}{EI}\delta(x-vt) \tag{3}$$

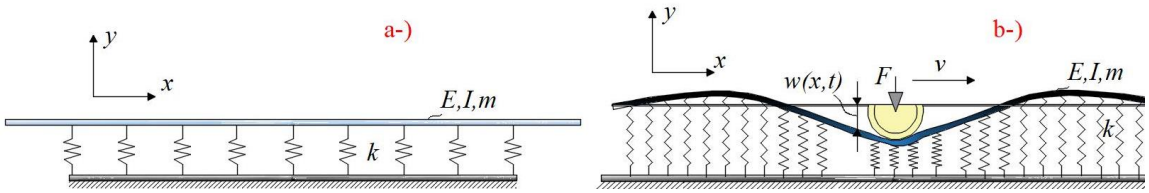

Figure 1 The track beam on elastic foundation, a-) without moving load, b-) with moving load.

$$w(x,t)=e^{\frac{j2\pi(x-ct)}{\lambda}} \tag{4}$$

The parameters λ and c in Equation (4) represent vibration wavelength and wave propagation velocity respectively. If Equation (4) rewritten in Equation (3), the following equation is obtained.

$$c=\frac{1}{2\varepsilon_1}\sqrt{\left[\frac{\lambda^2\varepsilon_2^4}{\pi^2}+\left(\frac{2\pi}{\lambda}\right)^2\right]} \tag{5}$$

When wavelength λ is equal to $\frac{\sqrt{2}\pi}{\varepsilon_2}$, the minimum wave propagation velocity is derived by Equation (6).

$$c_{\min}=\sqrt[4]{\frac{4kEI}{m^2}} \tag{6}$$

The parameter c_{min} in Equation (6) represents minimum wave propagation velocity or critical velocity of bending wave in track structure. The solution of the expression effect of wheelset load given by Equation (3) is $w(x-vt)$. Equation (3) is written as follows by defining $z=x-vt$.

$$\frac{\partial^4 w}{\partial x^4}+4\varepsilon_1^2\frac{\partial^2 w}{\partial t^2}+4\varepsilon_2^2 w=-\frac{F}{EI}\delta(z) \tag{7}$$

Characteristic equation for Equation (7) is

$$p^4+4\varepsilon_1^2 v^2 p^2+4\varepsilon_2^4=0 \tag{8}$$

The solution for the above characteristic equation is related to its coefficient. When $v<\varepsilon_2/\varepsilon_1$ If right side of the equality given by Equation (3) is equal to F=0, the homogeneous solution of the Equation (3) is as follows:

inequality satisfied, the solution of the equation is obtained as follows:

$$p=\pm\alpha\pm j\beta \tag{9}$$

The expressions in Equation (9) are given by Equation (10).

$$\alpha=\sqrt{\left(\varepsilon_2^2-v^2\varepsilon_1^2\right)},\qquad \beta=\sqrt{\left(\varepsilon_2^2+v^2\varepsilon_1^2\right)} \tag{10}$$

Then, the solution of the Equation (7) should be obtained by as follows:

$$\begin{aligned} w(z)=&e^{\alpha z}\left(D_1\cos\beta z+D_2\sin\beta z\right)+\\ &e^{-\alpha z}\left(D_3\cos\beta z+D_4\sin\beta z\right)+\varphi((z)) \end{aligned} \tag{11}$$

The parameter φ(z) in Equation (11) is related to the external moving load F on the rail beam. When z parameter is equal to z=0, in this situation x parameter is to be placed contact point between wheel and rail structure. The four unknown coefficients given by Equation (11) is obtained by following boundary conditions when parameter z is equal to z=0.

$$\begin{aligned} &w_1|_{z=0}=w_2|_{z=0},\quad \frac{\partial w_1}{\partial z}|_{z=0}=0,\\ &\frac{\partial w_2}{\partial z}|_{z=0}=0,\quad \mathrm{EI}\frac{\partial^3 w_1}{\partial z^3}|_{z=0}=\frac{F}{2} \end{aligned} \tag{12}$$

The solution of the Equation (7) given by following equation.

$$w(z) = -\frac{F}{8EI\alpha\varepsilon_2^2} e^{-\alpha|z|}\left(\cos\beta z + \frac{\alpha}{\beta}\sin\beta\,|z|\right) \qquad (13)$$

2.2. Dynamic Analysis of Tack Structure Under Multiple Moving Wheelset

When multiple moving wheelsets is on rail beam, the differential equation given by Equation (3) is derived by following equation.

$$\frac{\partial^4 w}{\partial x^4} + 4\varepsilon_1^2\frac{\partial^2 w}{\partial t^2} + 4\varepsilon_2^2 w = \ldots - \sum_{i=1}^{N} F_i\delta(x - a_i - vt) \qquad (14)$$

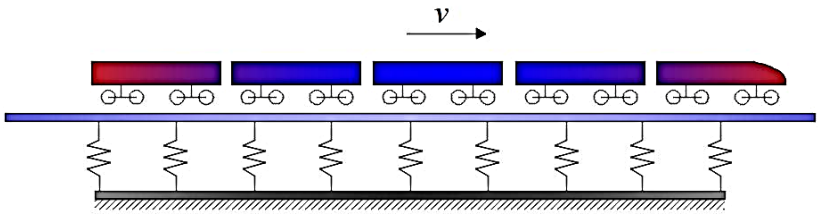

Figure 2 The computational model of a multiple wagon HST.

The parameter F_i in Equation (14) is *i*'th wheelset load, a_i is the distance between first wheelset and *i*'th wheelset, *N* is total number of wheelsets in HST. The solution of the Equation (14) is obtained by solution of undamped rail beam equation of motion effect of single moving wheelset load given by Equation (13) for each wheelset load separately. Then, these solutions are summed using superposition technique.

2.3. Track Equivalent Stiffness and Track Foundation Elasticity Modulus

The track equivalent stiffness parameter *k* and track foundation elasticity modulus E_s are related to each other. Heelis [16] proposed formulation given by Equation (15) for calculating track equivalent stiffness.

$$k = \frac{0.65E_s}{1-\nu_s^2}\sqrt[12]{\frac{E_s B^4}{EI}}, \qquad (15)$$

The parameters E_s, υ_s, *B* and *EI* in Equation (15) are track foundation elasticity modulus, poison ratio, sleeper length and rail flexural modulus respectively.

3. NUMERICAL EXAMPLES

In this section, dynamic response of rail beam effect of HST is analysed for different HST, track and foundation parameters. For the track foundation elasticity modulus E_s=50 MN/m^2 is named as "*Compacted clay*". The track equivalent stiffness for compacted clay is calculated as k=56.15 MN/m^2 considering poison ratio given in Table 1 υ_s=0.35 using Equation (15). The similar values are obtained as k=9.82 and 4.63 MN/m^2 for loam and soft subgrade respectively considering parameters given in Table 1.

Table 1.
The critical velocity of HST for different track foundation elasticity modulus.

Parameters	E_s (MN/m^2)	k (MN/m^2)	EI (MN/m^2)	m (kg/m)	B (m)	c_{min} (m/s)
Compacted clay	50	56.15	13.25	2735	2.5	141.24
Loam	10	9.82	13.25	2735	2.5	91.34
Soft subgrade	5	4.63	13.25	2735	2.5	75.7

As stated in Equation (6) before, the parameter track critical velocity varies depending on track equivalent stiffness, track unit length mass and rail flexural modulus. In this study, sleeper under rail and ballast masses were also taken into account when calculating the track unit length mass. Consequently, the rail unit length mass is calculated as m=2735 kg/m as shown in Table 1. Accordingly, the critical velocities are given by Table 1 for three different foundation properties.

3.1. Analysis of track vibration under a Moving Wheelset Load

In Figure 3a-c, track displacement caused by a wheelset moving on the track has been plotted for moving wheelset constant velocities v=50, 60, 70 m/s considering three different track foundation properties given in Table 1. In these analyses, the moving wheelset velocity is chosen maximum 70 m/s because of the smallest critical velocity value given in Table 1 is smaller than 75.7 m/s which indicated in Table1. Beside this, in these analyses, the constant load value of wheelset moving on the track beam is determined as F=170 kN. As shown in Figure 3a-c, maximum rail displacement for certain velocity is obtained in soft subgrade track foundation. Furthermore, the track displacement increases too as the wheelset velocity increases for certain foundation properties

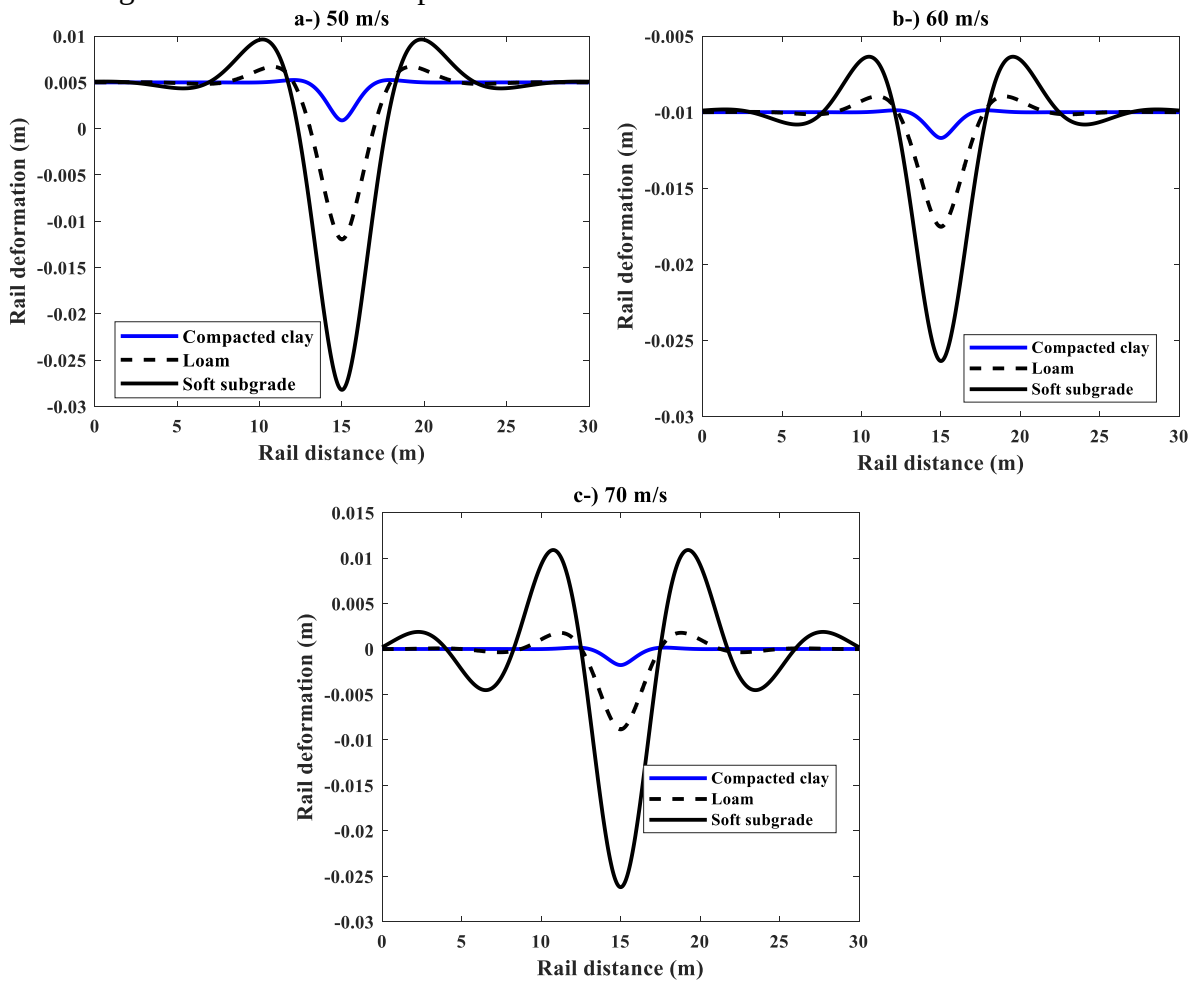

Figure 3 The track displacement for different track foundation and different single train wheelset load.

In Figure 4a-c, the effect of the wheelset velocity upon track displacement is figured out considering three different foundation properties given by Table 1 respectively. As a result of approaching of HST's velocity to rail critical velocity given in Table 1, the rail displacement is excessive increased.

3.2. The Track Transverse Vibration Effect of HST

In this section, the track vibration has been analysed under the influence of HST with multiple wheelsets for different train velocity, rail stiffness and track foundation elasticity modulus. Figure 5 shows axle distance for HST and wagon vehicles which used in analysis. In Figure 6a-c, track displacements have been investigated for three different HST's velocities (v=50, 60, 70 m/s) moving on the rail considering train wagon number N=5 and each wheelset axle load F=145 kN. As shown in figure, the maximum rail displacement is determined in soft subgrade track foundation properties given in Table 1 for multiple wheelsets load. Also, it is understood that the most important parameter affecting the rail critical velocity is track foundation elasticity modulus. The rail critical velocity is reduced as shown in Table 1, especially when the track has soft foundation. The critical velocity of soft subgrade foundation given by Table 1 can be easily exceeded by medium-speed train or HST. This case causes excessive vibrations on the rail beam. These vibrations affect riding comfort and riding safety negatively.

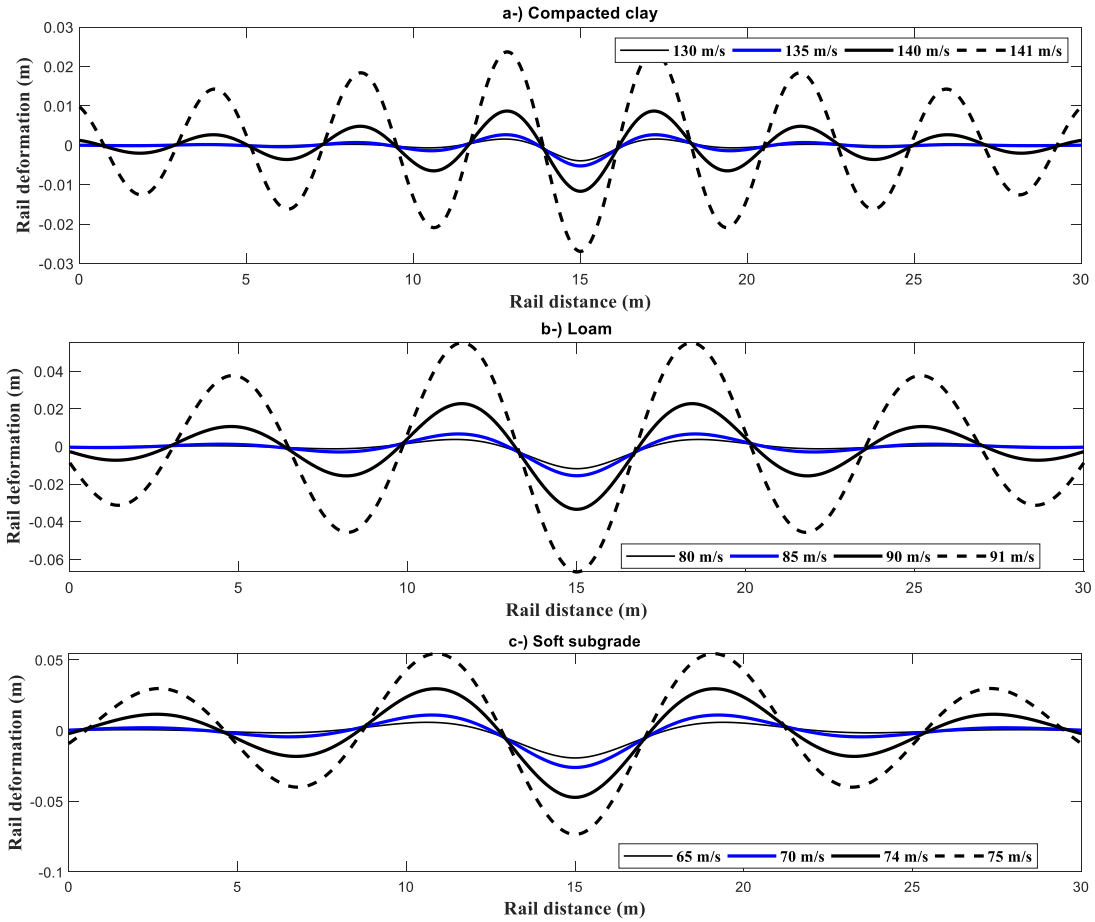

Figure 4 The track displacement for different HST velocity and track foundation.

The rail displacement is indicated for three different wheelset loads (F=100, 150, 200 kN) considering compacted clay given by Table 1 as shown in Figures 7a-c. The rail displacement is increased too as shown in figures as the wheelset load is increased. In these analyses, the number of HST's wagon is taken as N=4. In Figures 8a-c, the rail displacement has been analysed for three different rail flexural modulus considering compacted clay track foundation. As shown in figures, the rail displacement has been reduced as the rail flexural modulus is increased.

Moreover, it is understood that rail flexural modulus doesn't affect rail displacement as shown in Figures 8a-c when moving HST's velocity is smaller than rail critical velocity. But

the rail displacement is significantly reduced as rail flexural modulus is increased when HST's velocity approaches the rail critical velocity.

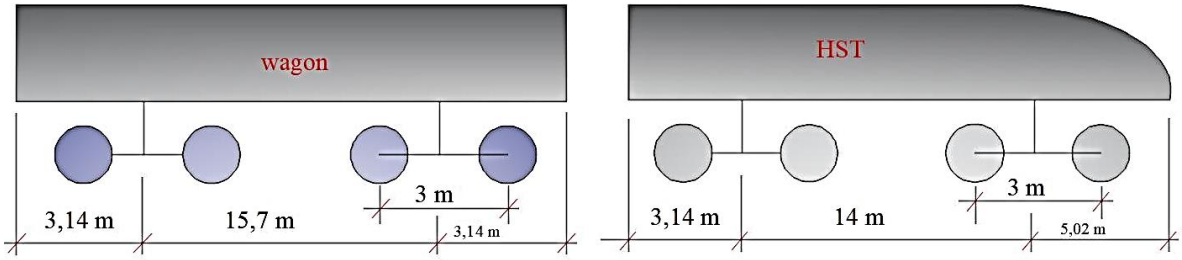

Figure 5. The computational model of a multiple wagon HST.

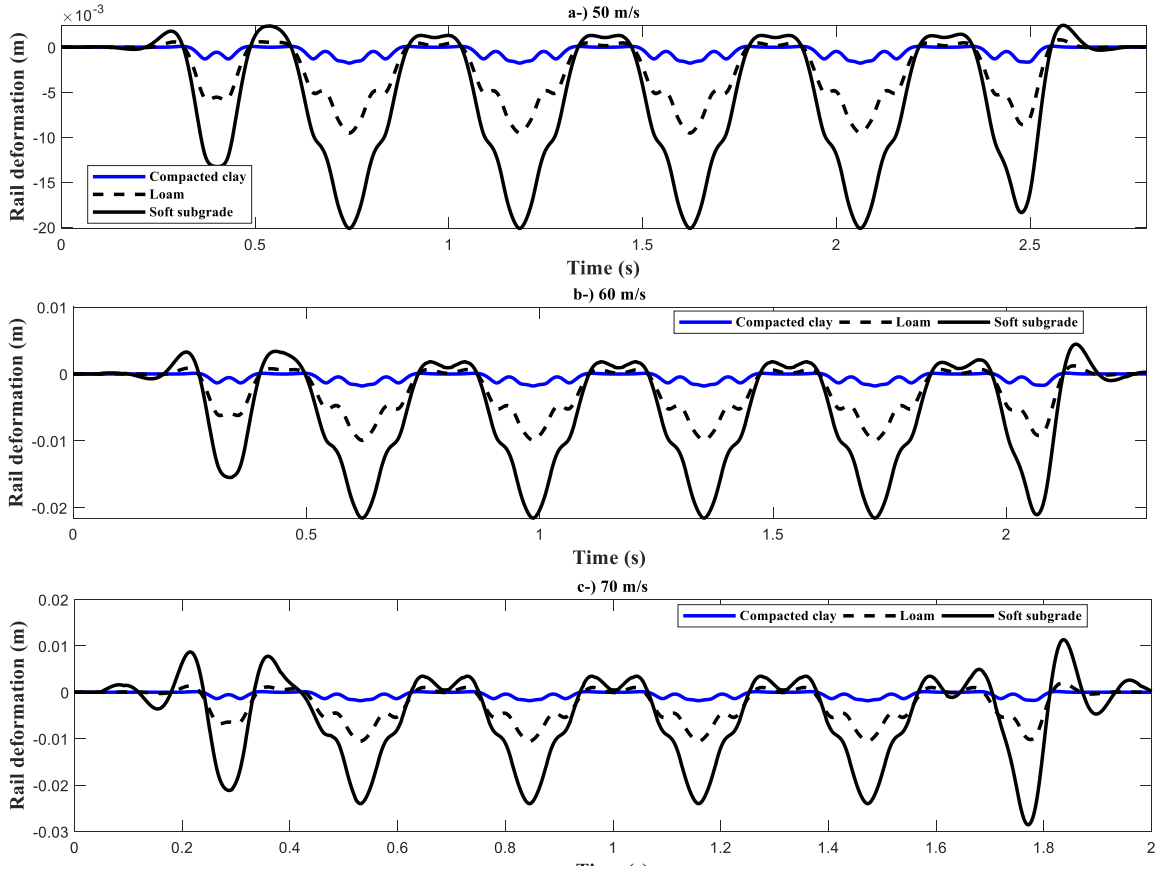

Figure 6 The track displacements considering various track foundation for the three different train velocities.

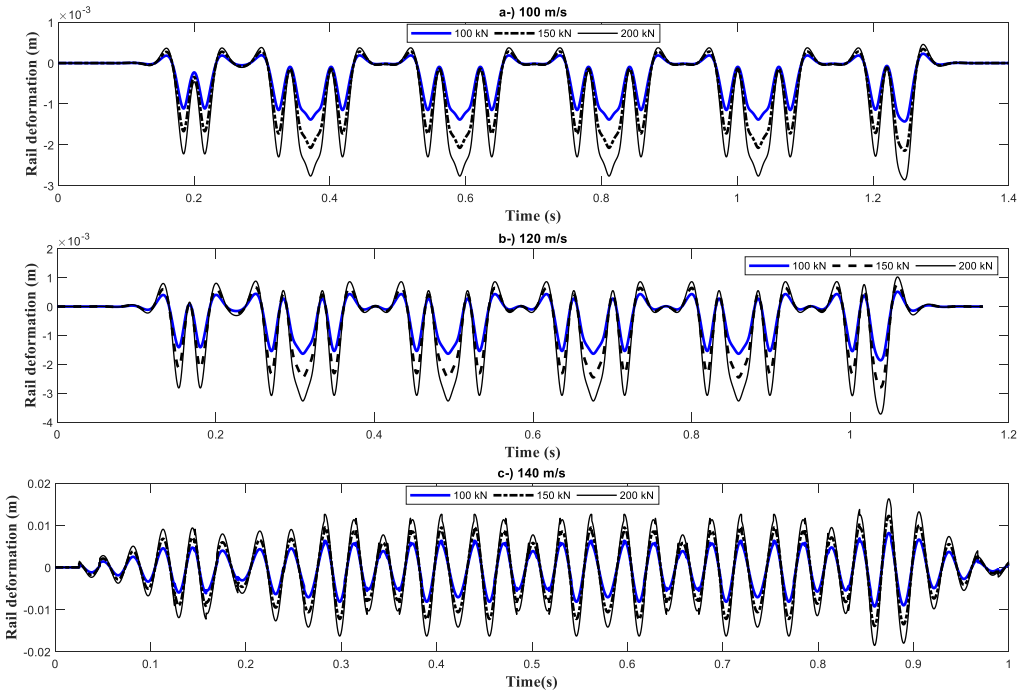

Figure 7 The track displacements considering various wheel load foundation for the three different train velocities.

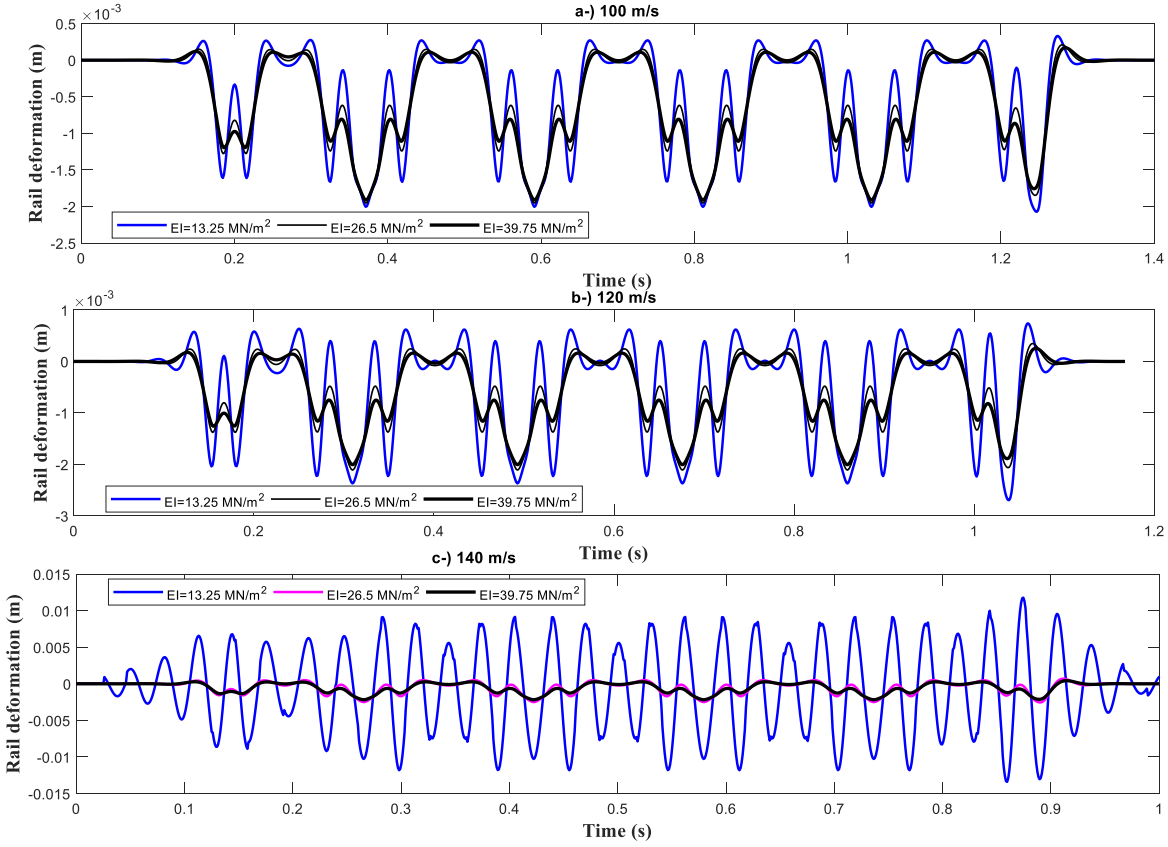

Figure 8 The track displacements considering various track foundation rigidity for the three different train velocities.

Figure 8 shows that rail stiffness has a great importance on the rail vibration waveform and its amplitude. When the rail stiffness is reduced, the waveform of vibration is multiple and vibration amplitude is large vice versa. Likewise, the rail stiffness is increased, the vibration wave number is reduced and vibration amplitude is decreased. This phenomenon is not clear when HST's velocity is very smaller than rail critical velocity as shown in figures. However, when the HST's velocity approaches the rail critical velocity, it is seen very clearly in Figure 8c. On the other hand, the vibration amplitude is increased too as the vibration wave frequency is raised. Consequently, this case causes liquefaction of ballast material under rail which would reduce the stability of the track foundation.

4. CONCLUSIONS

In this study, the rail which most important structure of railway transportation is modelled analytically according to elastic beam theory considering track foundation. Then, the effects of parameters such as ballast elasticity modulus, rail stiffness and rail critical velocity have been investigated in detail under influence of moving HST. Based on these computational results and considering three different track foundations, some conclusions are summarized as follows:

-The amplitude of the displacement on the rail beam is increased as the elasticity modulus of the ballast material is decreased.

-The rail displacement is gradually increased as the velocity of the HST moving on the rail beam approaches the rail critical velocity.

-As the wheelset axle load moving on the rail is increased, the rail displacement of the rail beam is increased too.

-The rail displacement is significantly decreased because of the rail flexural modulus is raised. This situation has been seen clearly especially HST's velocity approaches to rail critical velocity. The vibration wave amplitude increases as the train speed approaches the rail infrastructure critical speed.

Acknowledgments

The author would like to thank the reviewers for all useful and instructive comments on our manuscript.

Funding

The authors received no specific funding for this study.

The Declaration of Conflict of Interest/ Common Interest

The author received no specific funding for this study.

The Declaration of Ethics Committee Approval

The author declares that this document does not require an ethics committee approval or any special permission.

The Declaration of Research and Publication Ethics

The author of the paper declares that he complies with the scientific, ethical and quotation rules of SAUJS in all processes of the paper and that he does not make any falsification on the data collected. In addition, he declares that Sakarya University Journal of Science and its editorial board have no responsibility for any ethical violations that may be encountered, and that this study has not been evaluated in any academic publication environment other than Sakarya University Journal of Science.

REFERENCES

[1] S.L. Knothe, K.L; Grasssie, Modelling of railway track and vehicle/track interaction at high frequencies, Veh. Syst. Dyn. 22 (1993) 209–262.

[2] Z.P. Zeng, Z.W. Yu, Y.G. Zhao, W.T. Xu, L.K. Chen, P. Lou, Numerical simulation of vertical random vibration of train-slab track-bridge interaction system by PEM, Shock Vib. 2014 (2014).

doi:10.1155/2014/304219.

[3] Y.H. Chen, Y.H. Huang, C.T. Shih, Response of an infinite tomoshenko beam on a viscoelastic foundation to a harmonic moving load, J. Sound Vib. 241 (2001) 809–824. doi:10.1006/jsvi.2000.3333.

[4] B. Biondi, G. Muscolino, A. Sofi, A substructure approach for the dynamic analysis of train-track-bridge system, Comput. Struct. 83 (2005) 2271–2281. doi:10.1016/j.compstruc.2005.03.036.

[5] E. Celebi, G. Schmid, Investigation of ground vibrations induced by moving loads, Eng. Struct. 27 (2005) 1981–1998. doi:10.1016/j.engstruct.2005.05.011.

[6] M. Hetenyi, Beams on elastic foundation: Theory with applications in the fields of civil and mechanical engineering, University of Michigan Press, 1946.

[7] D.G. Duffy, The response of an infinite railroad track to a moving, vibrating mass, J. Appl. Mech. 57 (1990) 66–73.

[8] S.L. Grassie, S.J. Cox, The Dynamic Response of Railway Track With Flexible Sleepers to High Frequency Vertical Excitation, Proc. Inst. Mech. Eng. , Part I J. Syst. Control Eng. 198 (1984) 117–124. doi:10.1243/PIME.

[9] S. Iwnicki, Handbook of railway vehicle dynamics, 2006. doi:10.1201/9781420004892.

[10] A.P. De Man, Pin-pin resonance as a reference in determining ballasted railway track vibration behaviour, Heron. 45 (2000) 35–52.

[11] D.J. Thompson, Railway noise and vibration: mechanisms, modelling and means of control., Elsevier Science, Oxford, 2009.

[12] S.L. Grassie;, R.W. Gregory;, K.L. Johnson;, The dynamic response of railway track to high frequency vertical excitation., J. Mech. Eng. Sci. 24 (1982) 77–90.

[13] G.A. Hunt, Dynamic analysis of railway vehicle/track interaction forces, Loughborough University of Technology, 1986.

[14] W. Zhai, Vehicle – Track Coupled Dynamics, n.d.

[15] L. Fryba, Vibration solids and structures under moving loads, Thomas Telford House, 1999.

[16] M.E. Heelis, A.C. Collop, A.R. Dawson, D.N. Chapman, V.V. Krylov, Transient effects of high speed trains crossing soft soil, in: 12th Eur. Conf. Soil Mech. Geotechincal Eng., Amsterdam, 1999: pp. 1809–1814.

SAKARYA ÜNİVERSİTESİ
FEN BİLİMLERİ ENSTİTÜSÜ DERGİSİ

Sakarya University Journal of Science
SAUJS

e-ISSN 2147-835X | Period Bimonthly | Founded: 1997 | Publisher Sakarya University |
http://www.saujs.sakarya.edu.tr/en/

Title: Knowledge Discovery Using Clustering Methods in Medical Database: A Case Study for Reflux Disease

Authors: Yunus DOĞAN, Fatma RIDAOUI

Recieved: 2020-12-07 00:00:00

Accepted: 2021-03-13 12:52:00.995000

Article Type: Research Article

Volume: 25
Issue: 2
Month: April
Year: 2021
Pages: 439-452

How to cite
Yunus DOĞAN, Fatma RIDAOUI; (2021), Knowledge Discovery Using Clustering Methods in Medical Database: A Case Study for Reflux Disease. Sakarya University Journal of Science, 25(2), 439-452, DOI: https://doi.org/10.16984/saufenbilder.837209
Access link
http://www.saujs.sakarya.edu.tr/en/pub/issue/60672/837209

Sakarya University Journal of Science 25(2), 439-452, 2021

Knowledge Discovery Using Clustering Methods in Medicine: A Case Study for Reflux Disease

Yunus DOĞAN[*1], Fatma RIDAOUI[2]

Abstract

Digitalization spreads day by day around the world; thus, the amount of data collected is on the rise. An increasing amount of data leads us to use the data and get the advantage of it by using methods like Data mining. Data mining is used in several industries. Especially as medical data is essential to be understood, it is crucial to work on it. Reflux disease is a painful illness spreading around the world. Reflux is more common compared to formerly known numbers of patients. Even though reflux is not as fatal as cancer, it decreases the quality of life and makes many people suffer in their daily life. So, reflux is affecting mental health directly. If we can ease the process of diagnosis of reflux, we may provide a better quality of life for people. In this study, various data mining algorithms are applied, and it is seen from results that medical care can be improved by changing. Nowadays, artificial intelligence applications in the field of gastroenterology stand out in various sources in the literature. However, a large database required that is specific for Reflux disease to implement these applications is available only at the Reflux Research Center in Ege University in Turkey. By benefiting the Short Form36 and Quadrad12 questionnaire data in this database, 3,909 patients and many artificial intelligence algorithms were used to discover the hidden associations among responses in the quality of life of these patients. The algorithms used in the tests are Apriori, Frequent Pattern Growth, Density-Based Spatial Clustering of Applications with Noise, Self-Organizing Map, and KMeans. In the tests, it was observed that the most successful algorithm in terms of the structure of the data was KMeans, and a set of remarkable 27 rules according to the optimal Sum of Square Error value was obtained.

Keywords: Clustering, data mining, medical information systems, reflux disease

1. INTRODUCTION

Databases store important and viable data but they also store irrelevant and not useful data too. Knowledge discovery can be used for every size of data; however, it is meaningful and unavoidable to use for large data repositories. Understanding and interpreting the data gained more importance than just storing the data recently.

[*] Corresponding Author: yunus@cs.deu.edu.tr
[1] Dokuz Eylül University, ORCID: https://orcid.org/0000-0002-0353-5014
[2] Gebze Technical University, E-Mail: f.balci@gtu.edu.tr. ORCID: https://orcid.org/0000-0003-1653-1466

The study aims to export the hidden knowledge in the database that is collected in Ege University Reflux Center in Turkey. In other words, this study focuses to find rules about reflux disease, personality, and the quality of life. Especially in Turkey, such studies over huge medical data have not been performed before. The Reflux Center has collected and stored patients' data for years, and the number of patients is estimated at around 7,000. However, those data are not processed for the help of obtaining hidden outcomes such as what is the probability of a person being a reflux patient, etc.

Medical data is vital and sensitive, that is why it should be protected and used carefully for the sake of patient and healthcare. The Reflux Center has a huge amount of patient information that is not processed or interpreted. There is around 7,000 patient's information stored. This study aims to examine the relationship between data and clustering with the aid of analyzability, usability, and diagnostics.

Today, computer-based solutions have become compulsory and are seen in medicine, too. Current medical studies are on Data Mining [1], Artificial Intelligence (AI) [2], Machine Learning, and Deep Learning ranging from processing medical images on radiological data to early diagnosis issues [3, 4]. Examples of intelligent solutions for malignant diseases such as heart disease, cancer, and diabetes are also encountered [5, 6]. In these studies, more than 85,000 patients were analyzed to find confidential information; therefore, these studies could only be applied via data mining techniques. If it comes to the field of gastroenterology, it can be said that artificial intelligence studies have been handled to raise awareness in this regard all over the world [7-10]. In this study, the database in the Reflux Research Center has been used to discover the hidden outcomes in the quality of life of the patients by benefiting the Short Form (SF) 36 and Quadrad12 questionnaire data. The number of the patients is 3,909 and the algorithms used and tested are Apriori, Frequent Pattern (FP) Growth, Density-Based Spatial Clustering of Applications with Noise (DBSCAN), Self-Organizing Map (SOM), and KMeans.

Association rule mining algorithms are generally Apriori, FP-Growth, and their derivatives in the usages of the data mining applications in the literature. In this study, it has been observed that the response of SF36 and Quadrad12 questionnaires are unsuitable for Apriori and FP-Growth because the logic of the association rule mining algorithms is based on 0-1 or True-False structure. In other words, it means the selections in SF36 and Quadrad12 questionnaires do not have only the true or false values; Data needs a preprocessing for fuzzy selections. Nominal values can be used correctly. Thus, Apriori and FP-Growth algorithms have been tested, but the results have not been successful. As an alternative solution, clustering algorithms have been used to obtain the rules. The centroids of the clusters show the common characteristic of the cluster; by the means of this property, clustering algorithms have been preferred.

The contributions of this study are twofold. Firstly, a rule set has been obtained for the Reflux Disease peculiar to the Turkish population. Secondly, this study declares that clustering algorithms can be used for association rule mining problems for fuzzy data. The tests show that the conventional KMeans algorithm is more successful than the conventional association rule mining algorithms at discovering a rule set for the fuzzy data by evaluating the centroids as hidden characteristics of the bag of the data in the clusters.

In this paper, Section 2 mentions the related works; algorithms and methods are given in detail in Section 3; finally, results and their discussions are in Section 4, and Section 5 mentions the conclusion respectively.

2. RELATED WORKS

Data mining is a combination of a multidisciplinary area containing statistics subjects, database management systems, machine learning algorithms, visualization approaches, and artificial intelligence [11]. Data mining is used to provide preliminary information required for knowledge-driven and data-driven expert systems for the topics of study by exploring the

information in large datasets [12]. It is likely to discover knowledge based on data analysis from various perspectives with data mining; text mining, web mining, medical decision support systems, financial predictions, forecasting studies at all engineering fields, etc. can find application in a wide range of fields including subject titles [13]. In addition, data mining is part of the overall process for discovering information in databases, as the science and technology of data discovery to discover previously unknown patterns. In up-to-date information systems, large-scale knowledge in data warehouses also includes patterns to explore. The availability and abundance of this information make data mining very important and necessary [14]. In data mining, there are many techniques such as optimization algorithms, Association Rule Mining (Market Basket Analysis), supervised learning, and unsupervised learning algorithms. These techniques including Apriori, FP-Growth, Genetic Algorithms, Decision Trees, Deep Learning, Support Vector Machines, Clustering Algorithms, etc. are implemented to discover hidden knowledge that can guide the decisions at a sector and for processing knowledge received from various fields to provide information and for decision-making [15].

If medical studies are focused on; the aim of a study in 2009 [16] is to highlight a patient profile that lies with the association rules mining, underlining the groups of parts that often occur together in the 1919 group process. Moreover, the association rules are the determination of relationships and associations between the special values of the variables in large data sets. This approach enables to reveal patterns hidden in the big data sets of analysts and researchers [17]. Its usefulness, easy understanding, and revealing of all possible patterns are the strengths of the technique. But it has also a weakness that reveals all possibilities because decision-makers must overcome a large amount of knowledge to evaluate all these possibilities, which is difficult and time-consuming [18]. Nowadays, data collection has been accelerated with the information technologies used. This means more information and raises a challenge for physicians to analyze.

With the Association Rule Mining, evaluations are made mostly for the analysis of the consumption habits of the customers. Also, it supplies the identification of the products or product groups that tend to occur together in the purchasing processes [16]. In the Association Rules technique, algorithms such as Apriori and FP-Growth are used. These algorithms find rules based on validation values and use first-order logical representations. These values include different options such as class index, class verification threshold value, verification value, frequency threshold value, missing values and data, noise threshold value, number patterns, repeat patterns, ROC analysis, and output values [19]. Apriori is an inductive logic programming algorithm that looks for the highest values of the validation evaluation function. It explores the simplest different validation measures weighted with relative accuracy. A verification criterion shows the part of a rule's examples of the unexpected and expected counter. In the algorithm, two expected and observed probability values are calculated. Apriori extracts first-order rules and rules for association with other programs are used in mining tasks [20]. The Apriori algorithm has become a standard approach in mining association rules. It was first introduced by Agrawal and Srikant [21].

It can be seen in recent studies that new approaches have been developed for analysis in medical text data due to the inadequacy of the Apriori algorithm in terms of semantic relationship [22, 23]. In another current study, a novel association rule mining algorithm has been developed by combining a MapReduce distributed computing model and association rule [24].

3. METHODS AND THEIR COMPARISONS

Prior to data collection research, Non-Interventional Ethics Committee permission numbered 17-5.1/49 was granted and Ege University Clinical Researches Ethics Committee approval dated 08/09/2017 and numbered 70198063-050.06.04 were obtained.

In literature, a statistical study about SF36 and QoLRAD questionnaires, which is implemented by Hancerlioglu, et al., has been encountered. This study has detected important outcomes; however, these outcomes contain statistical results, and deep relations could not be discovered, because there has not been any data mining approach [25]. Conversely, in our study, data mining algorithms have been focused on.

At the beginning of the study, the data is not useful to explore the quality of life of the patients; therefore, the required steps have been done to make data ready to be mined. The steps can be summarized as the database preprocesses and the data mining process. The study aims to find hidden relationships and knowledge in the database with the help of data mining methods. Association rule mining, clustering algorithms are applied to data. Apriori and FP-Growth algorithms did not give expected results for the target dataset because of the existence of high density for the "No" response. The presence of no responses leads to the extraction of useless and meaningless relationships because the targeted output is to detect the hidden links between the "Yes" responses. Therefore, clustering algorithms have been implemented and examined. In Figure 1, 4 clusters are represented, and it means that 4 separate centroids as rules. This approach has been applied to clustering algorithms tested.

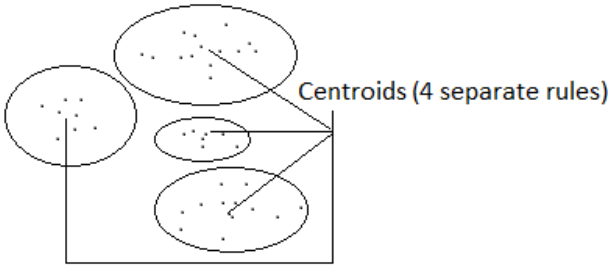

Figure 1 The match of centroids and rules

Quadrad12 and SF36 questionnaires have been stored separately and irregularly in the database. The database preprocessing has been basically done to prepare the dataset in the required structure. Before preprocessing the database, two questionnaires results were not a dataset structure where each column symbolizes a possible response and each row does a patient.

3.1. Quadrad12 and SF36 questionnaires

The questions of SF36 used in the study are given below:

- SF36_1 What can you tell about your health in general?
- SF36_2 If you compare your health with last year, how do you evaluate your health now, in general?
- SF36_3 The following items are related to your activities throughout the day. Does your health now restrict these activities? How much if it does?
- SF36_4 During the last 4 weeks, have you experienced any of the following problems with your work or other daily activities as a result of your physical health?
- SF36_5 During the last 4 weeks, have you experienced the following problems with your work or other daily activities as a result of your emotional problems (such as depression or anxiety)?
- SF36_6 During the last 4 weeks, how much did your physical health or emotional problems affect your social activities with your family, friends, or neighbors?
- SF36_7 How many pains have you had in the last 4 weeks?
- SF36_8 During the last 4 weeks, how much did your pain affect your normal work (both your housework and your out-of-home work)?
- SF36_9 The following questions are about how you feel during the last 4 weeks. For each question, please choose the best response to your feelings by considering the frequency of the last 4 weeks.
- SF36_10 How often did your physical health or emotional problems affect your social activities (such as visiting friends or relatives) during the last 4 weeks?
- SF36_11 How true or wrong are each statement below? Check the most appropriate for each statement.

As can be seen, while SF36 focuses on the health status of patients, Quadrad12 consists of questions having the aim of evaluating how much the complaints affect a patient's life. The

questions of Quadrad12 questionnaires are given below:

- Q12_1 How often did you feel tired or exhausted because of the pain/sour water coming from behind the chest during the last week or coming into your mouth / esophagus?
- Q12_2 During the past week, how often did you avoid leaning over the back of the breastbone or because of pain/sour water coming into your mouth/esophagus?
- Q12_3 During the last week how often you had to eat less than you used to eat, because of the blazing chest behind the breastbone or sucking water from your mouth/esophagus?
- Q12_4 During the past week, how often did the pain bruise from the back of the chest and/or bitter water into your mouth/esophagus prevent you from doing something with your family or friends?
- Q12_5 During the past week, how often did you feel tired or exhausted due to insomnia that is caused by the burning of the chest of the chest or bitter/sour water in your mouth/esophagus?
- Q12_6 During the last week, how did you wake up from the back of the chest and sneak from your mouth/esophagus/snuff/water?
- Q12_7 During the past week, how often did you feel very frustrated or impatient because of the burning of sour water on your back/esophagus during the last week?
- Q12_8 During the past week, how often did you find yourself awake and rested in the morning because of the painful or sour water coming from your chest/esophagus?
- Q12_9 During the past week, how often have you been worried or feared about your health because of complaining of bruising behind your breastbone or suffering/bitter water in your mouth/esophagus?
- Q12_10 During the past week, how often did you have to avoid certain foods and beverages because of the burning of the bones behind the breastbone or the bitter/sour water in your mouth/esophagus?
- Q12_11 During the past week, how often have you not been able to fulfill your daily activities (including jobs at home and outside the house) because of the burning of the chest behind the chest, or bitter/sour water in your mouth/esophagus?
- Q12_12 During the past week, how often have you not been able to fulfill your normal physical activities (including sports, full-time activities, and going out of the house) to the left because of the painful or sour water coming from your chest/esophagus?

3.2. Sub-operations in Methods

The data file formatted includes patients' information in each row and columns including the related titles of the responses. For example, in the first column and the first row, the first patient's response to the question about social security is represented. Each row for the same question includes the different kinds of social security such as "Social Security Institution", "Pension Fund", etc. Therefore, the format obtained was not able to use for data mining. The discretization method is used to turn them into the nominal form in the WEKA tool [26]. Thus, the "nominal to binary" method has been implemented in WEKA to obtain the dummy attributes. After all, the required binary matrix has been obtained. The final form of the dataset has contained 3,909 instances with 323 attributes as the binary matrix structure. Containing only binary values, the matrix has become useful for mining.

Figure 3 shows that firstly, patient responses are obtained in a view by joining the tables related to the questionnaire in the database. Secondly, the row-based database view is transformed into the column-based dataset by the "pivot" database queries; finally, nominal contents are converted into the binary attribute structure. Also, to discover hidden relationships, answer attributes with only one "1" in the data set were deleted and focused on attributes containing at least 2 "1". With this feature selection process, the number of attributes has been reduced by 12.

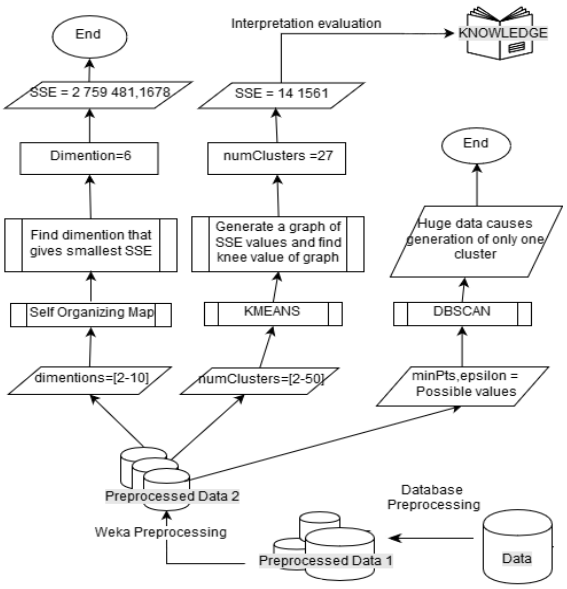

Figure 2 The entire process of the study

The next phase is to compare multiple algorithms to determine which algorithm has been giving better results. SOM is suitable as a clustering algorithm for the subject to determine rules and relationships among the instances.

Also, KMeans and DBSCAN algorithms are used to cluster data, too. In Figure 2, the entire process of the study has been figured as a flow chart. The comparisons have been accomplished with the help of the sum of squared error (SSE) for each applied algorithm. This error has been calculated with the formula in Eq. 1.

$$\mathrm{SSE} = \sum_{k=1}^{K} \sum_{i=1}^{I} (x_i - c_k)^2, \quad (1)$$

where K is the total number of clusters, l is the total number of instances and c is the current centroid.

KMeans is one of the popular unsupervised learning algorithms. The algorithm collects data that has many similarities around center points. After setting the number of clusters, each center allocates nearby data points. The algorithm is represented in Figure 5 as a pseudo-code. SSE values help the determination of the proper cluster number for the related dataset. For the study, after each cluster number between 2 and 50 observed, the pattern having 27 clusters has been decided to be used according to the SSE values given in Table 1.

The tests of KMeans clustering have been applied as KMeans++ version in WEKA 3.9 tool because of its accuracy advantage [27]. In tests, the significant parameter, "numClusters" has been changed between 2 and 50 to find which number of clusters makes the best pattern.

SSE values lead to compare the results of each number of clusters applied. Figure 4 shows the distribution of the SSE values to evaluate the optimum K number.

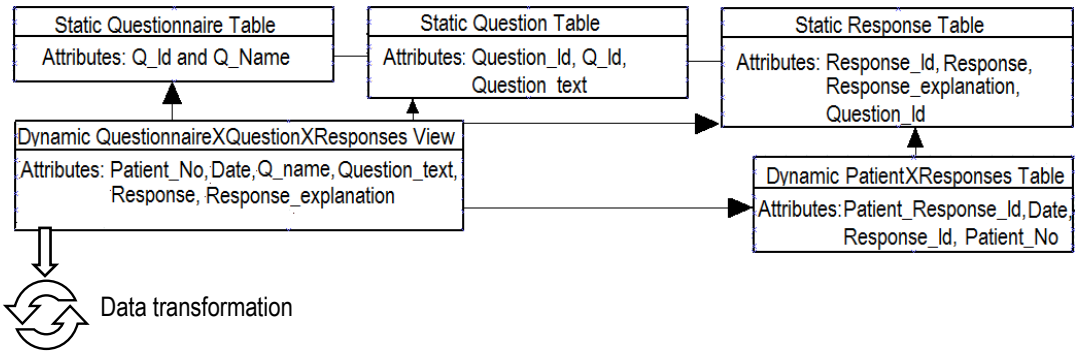

Patient	q1r1	q1r2	q2r1	q2r2	q2r3	q2r4	q3r1	q3r2	q4r1	q4r2	q4r3	q5r1	….
1	0	0	0	1	0	0	0	1	0	1	0	1	….
2	1	1	0	1	1	1	1	1	0	1	0	0	….
….	….	….	…..	….	….	….	….	….	….	….			….
3,909	1	0	1	0	0	0	1	1	1	0	1	0	….

Figure 3 Data transformation phases (q: question, r: response)

Table 1
SSE values for each cluster number

# of clusters	SSE	# of clusters	SSE
2	163003	27	141561
3	159846	28	141699
4	156112	29	141388
5	157383	30	141268
6	153617	31	140737
7	151553	32	140585
8	151044	33	140662
9	148529	34	140070
10	148672	35	139711
11	147512	36	139166
12	148082	37	139030
13	146555	38	139105
14	146379	39	138803
15	146145	40	138788
16	146018	41	138399
17	144917	42	138579
18	144671	43	138182
19	144535	44	137808
21	143390	45	138154
22	143067	46	137586
23	142674	47	137482
24	142588	48	137545
25	142042	49	137482
26	141842	50	137199

As can be seen in Figure 4, as cluster numbers increase, the SSE value is decreasing. It can be determined that increasing cluster numbers cause more accumulation and it decreases SSE value. Therefore, that elbow point [28] of the graph is significant to us which is 27 in the study. The SSE value obtained with 27 clusters has been compared to other algorithms' SSE values to choose the proper one. To detect 27 rules from this study, this pattern has been used.

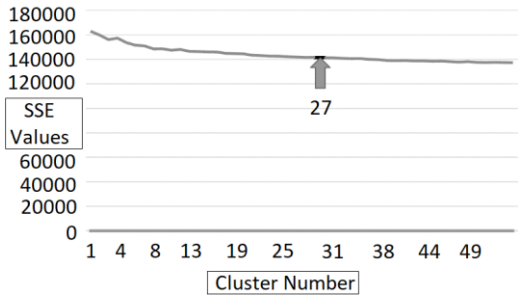

Figure 4 Graph representation of SSE values

In Figure 6, each column represents a cluster and each cluster includes attributes that are represented by 1. Thus, a data structure that can keep each cluster has been preferred and it has been possible that each instance is reachable from another instance easily. Also, another property of this structure is that the first element will be a string while the others are integers.

Function K-MEANS ($\{\overrightarrow{x_1}, \dots, \overrightarrow{x_N}\}$, K)
1: $(\overrightarrow{s_1}, \overrightarrow{s_2}, \dots, \overrightarrow{s_k}) \leftarrow$RandomCentroidSelector($\{\overrightarrow{x_1}, \dots, \overrightarrow{x_N}\}$, K)
2: **for** $k \leftarrow 1$ **to** K
3: **do** $\overrightarrow{\mu_k} \leftarrow \overrightarrow{s_k}$
4: **while** ending criteria has not met
5: **do for** $k \leftarrow 1$ **to** K
6: **do** $\overrightarrow{\propto_k} \leftarrow \{\}$
7: **for** $n \leftarrow 1$ **to** N
8: **do** $j \leftarrow argmin_{j'} \mid \overrightarrow{\mu_{j'}} - \overrightarrow{x_n} \mid$
9: $\propto_j \leftarrow \propto_j \cup \{\overrightarrow{x_N}\}$
10: **for** $k \leftarrow 1$ **to** K
11: **do** $\overrightarrow{\mu_k} \leftarrow \frac{1}{|\propto_k|} \sum_{\vec{x} \in \propto_k} \vec{x}$
12: **return** $\{\overrightarrow{\mu_1}, \dots, \overrightarrow{\mu_k}\}$

Figure 5 The pseudo-code of the KMeans algorithm

Two arrays used in the algorithm are given in Figure 6. In the next step, the data needs to be prepared as a text file. As it is expressed in the figure, there are two types of arrays. To split them into two arrays, the comma mark has been used in the data file and space characters have been cleared to transform into the substrings zeros and ones. Responses are kept in a string array as can be seen in Figure 6.

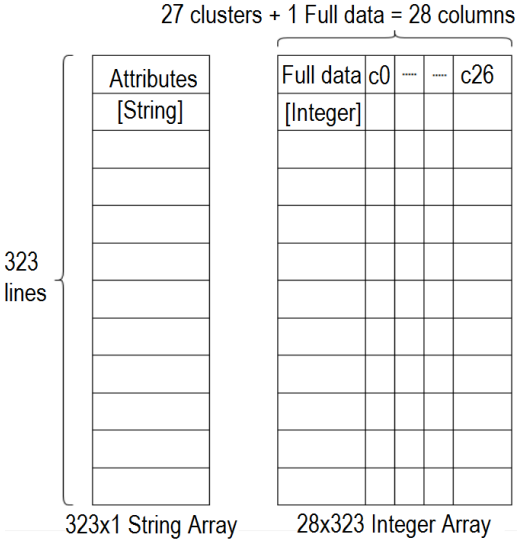

Figure 6 The data structure of the study

Each response corresponds to each cluster's attribute row. Therefore, the algorithm is developed to scan each column and its responses then write them in a text file. The algorithm finds 27 rules in a short time. The algorithm is summarized in Figure 7.

```
Function RuleFinder for K-Means ()
1:    file = readFile(example.txt)
2:    parsed = file.Split(',')
3:    foreach (string line in file)
4:        Answers[] = Parsed[0]
5:        for i←1 to 28
6:            integerArray[] = Parsed.Substring()
7:        end
8:    end
9:    iterateOver ( integerArray )
10:       if ( integerArray.element ==1 )
11:           takeCorresponding ( answers.element )
12:           StreamWrite(rules.txt)
13:       end
14:   end
```

Figure 7 The pseudo-code of the "Rule Finder" method

DBSCAN is another clustering algorithm that calculates each point's distance with its neighbors with a threshold value given and clusters the closest ones. To implement this algorithm two parameters are necessary to be checked: epsilon and minPts. Epsilon adjusts the radius of the area that will be observed and minPts designates the minimum number that will be included inside the area. DBSCAN is used to determine arbitrarily shaped data. DBSCAN is explained in detail in Figure 8 [29].

```
Function DBSCAN(K, minpts, ε)
1: for i ← 1 to K
2:    visit each point i
3:    E = ε_neighborhood of i
4:    if (E < minpts)
5:        noise += i
6:    else
7:        new cluster += i
8:        foreach ( point in E )
9:            E' = ε_neighborhood of point
10:           if size(E') >= minpts
11:               E += points
12:           end
13:       end
14:   end
15: end
```

Figure 8 The pseudo-code of DBSCAN algorithm

Table 2
Data distribution among lengths after implementing SOM algorithm

	3x3	4x4	5x5	6x6	7x7
(0,0)	10	2	1	1	2
(0,1)	8	5	9	1	0
(1,0)	3816	2	0	0	3
(1,1)	4	2	0	3	5
(2,0)	1	4	0	0	0
(2,1)	8	3792	1	0	8
(0,2)	18	2	9	9	7
(1,2)	35	10	1	2	0
(2,2)	9	2	13	1	2
(3,0)		29	0	2	3
(3,1)		2	0	0	3
(3,2)		2	5	12	0
(0,3)		13	1	5	0
(1,3)		1	1	3	0
(2,3)		13	11	1	0
(3,3)		28	0	26	0
(4,0)			5	0	0
(4,1)			15	0	4
(4,2)			0	0	0
(4,3)			1	3	2
(0,4)			25	25	0
(1,4)			3	2	1
(2,4)			3794	6	0
(3,4)			10	0	0
(4,4)			4	3779	0
(5,0)				0	0
(5,1)				2	0
(5,2)				0	0
(5,3)				3	0
(5,4)				0	8
(0,5)				5	0
(1,5)				0	0
(2,5)				1	0
(3,5)				0	25
(4,5)				13	8
(5,5)				4	3782
(6,0)					2
(6,1)					3
(6,2)					0
(6,3)					15
(6,4)					12
(6,5)					1
(0,6)					0
(1,6)					0
(2,6)					1
(3,6)					1
(4,6)					1
(5,6)					6
(6,6)					4

Results have been examined by changing parameters and DBSCAN has not fit the huge data. It has placed 3,909 data into the same

cluster, or all data have been determined as noise data, and any pattern having clusters more than one has not occurred.

The number of clusters is not asked in DBSCAN as opposed to KMeans, as it is introduced in some studies [30]. However, it does not suit datasets that have large density differences among data. So that minPts and ε cannot be determined appropriately. Additionally, SOM is a model based on a neural network that is trained by unsupervised. Usage of the SOM algorithm gives the advantage by the means of visualizing the multidimensional data with two-dimensional views. The algorithm shows similarities between the neighbors of the neurons with the distribution of neurons on the map. The steps of the algorithm are given as a pseudo-code in Figure 9 [31]. After training, each patient has been allocated by a nearby center point that is called the winner.

Algorithm SOM()

1: Initialize each node's weight
2: **for** $i \leftarrow 1$ **to** N
3: Load data from given file
3: Choose a vector from the set of training data
4: Find **winner** node (Most likely to input vector)
5: Calculate neighborhood of winner node
6: **end**

Figure 9 The pseudo-code of the SOM algorithm

In an effort to compare algorithms to choose the one that gives better results, SSE values have been calculated for the SOM algorithm for each length between 3x3 and 10x10 as square matrix maps. SSE values for the lengths of 6 and 7 are given in Table 2. The distribution of nodes between the lengths of 3 and 7 is given in Table 2.

Table 3
SSE values for two different lengths

SSE value for 6x6	SSE value for 7x7
2 739 954,39069696	2 725 156,4785282

In Figure 10, SOM maps for 3x3, 4x4, 5x5, 6x6, and 7x7 are visualized, respectively. Especially the black clusters in the middle parts of the maps represent the clusters of the pattern with high error, which have higher SSE values than the general SSE average of the patterns.

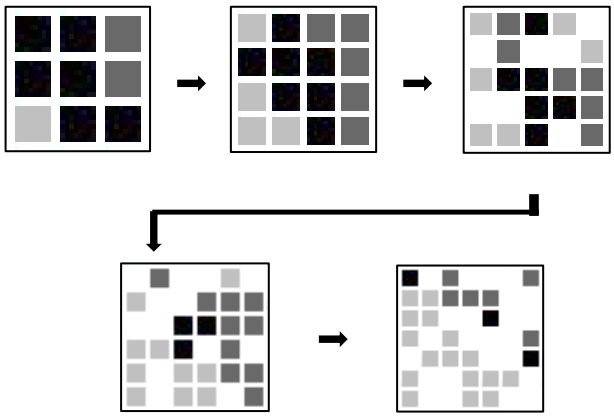

Figure 10 3x3, 4x4, 5x5, 6x6, and 7x7 SOM maps tested, respectively.

The number of these clusters increases as the map size gets smaller. Likewise, as the size of the map increases, the number of empty clusters also increases. The number of empty clusters is tolerable, but as can be seen from Table 3, high SSE values of these patterns have been obtained. Therefore, the SOM approach has been not preferred.

4. EXPERIMENTAL RESULTS AND OUTCOMES

Algorithms having different approaches have been applied for the dataset and results have been examined. DBSCAN algorithm has created only one cluster from 3,909 data. The data was excessive for efficient clustering in DBSCAN. FP-Growth and Apriori algorithms have been found incompatible for the dataset as mentioned in the previous section. Exclusion of some data like these may help extract more meaningful rules. Similarly, the SOM algorithm has given higher SSEs values than the KMeans algorithm. That is why the KMeans algorithm has been preferred to maintain the study and obtain the rules. In Figure 11, the chart of the patient number in the 27 clusters obtained as the most optimum pattern shows that the numbers among the clusters do not have any clear local density. The centroids of these 27 clusters are listed below. In other words, the outcomes discovered are given.

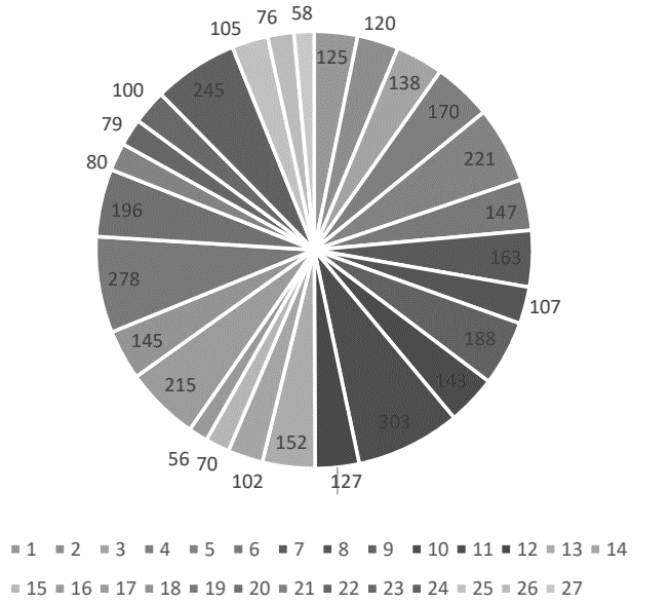

Figure 11 The chart of the patient number in the 27 clusters

- The first cluster includes men from İzmir. Those 125 patients as independent from age and level of education are limited in their daily life and work-life by complaints. They are affected by the problems given. We examined that they gave average answers to all questions. Their health status is good in general.
- The second cluster is independent of age, gender, and city, comprised of secondary and high school graduates. And they have the same complaints for one or more than one year.
- Patients' health in the third cluster deteriorates. We conclude that with the help of the high answering ratio of SF36_2 is "Almost the same". As we know, those patients come with complaints of suffering from sour water in their mouths. As they tell their health is almost the same as last year it means they keep suffering from similar problems for one year. However, other questions answered as never shows that they do not get affected badly in their life.
- The fourth cluster includes university graduates that are independent of the city, age, gender. Their answers for SF36_9 and SF36_11 display that they do not feel disturbed much from their complaints. They do not consider their health is in danger even if it remains the same for one year, this group is aware of complaints and bears it. They claim they are not badly affected by complaints in daily life.
- The fifth cluster that includes 221 people involved in the research is affected by complaints in their daily life. This group is independent of age, gender, and city, and education status. But we understand complaints spring currently because patients did not claim their health is the same as last year.
- The sixth cluster includes 147 people who are university graduates and ages between (36- 54], who are generally affected badly by the complaints. They assert that their health is worse than last year. So, it can be understood they came to the doctor after one year suffers. Complaints restrict their work and daily life for one or more than one year.
- We have observed that the health status of 163 women that are university graduates has deteriorated in the seventh cluster. Complaints restrict their daily and work life. They also stated their health is worse than last year which means they suffer for one or more than one year.
- The eighth cluster includes secondary and high school graduates independently from age, gender, and city generating a group of 107. They suffer from complaints currently and less than one year. We observe education level is affecting patients' psychology and health.
- The ninth cluster is a group of 188 that consists of primary school graduates independently from age, gender, and city. Their health is getting worse and they suffer one or more than one year with the complaints. Those patients complain because they suffer in their daily life and work life.
- In the tenth cluster it is observed that male patients who are secondary or high school graduates aged 36 to 54 years in İzmir are suffering from the restricted capability of activities such as jogging, carrying the heavy thing, etc.
- The eleventh cluster is the biggest with 303 people, is independent of age, gender, education status and city suffer from complaints currently. The group is restricted in their daily life and career. It is claimed that they cannot focus on their work.
- The twelfth cluster of 127 people that are between ages 36 and 54, is feeling tired and

angry for one month. They suffer less than one year.
- The thirteenth cluster comprises 152 women in İzmir; feel their health situation is bad in general. They are restricted in daily and business life by the complaints. They seem to be anxious and exhausted during the last month.
- 102 women from İzmir, are restricted much because of complaints in the fourteenth cluster. They claim that it is hard to walk 1-2 km. That group believes their health is bad. They seem pessimistic about their health. It is observed that they are limited in their work and social life because of complaints.
- The fifteenth cluster of patients' health, between ages 36 and 54, is observed to deteriorate. They state that their health is worse than last year. Even low effort requiring activities are restricted.
- The sixteenth cluster contains university graduates between ages 18 and 36, who are observed to be stronger than primary school graduates mentally. It is understood after analyzing their answers. Even if they suffer, they claim their health is not bad.
- The seventeenth cluster of patients between ages 18 and 36, which is independent of the city, gender, and education are mentally and socially limited by the complaints. This group consists of 215 patients.
- The eighteenth cluster comprises 145 patients that independent from the city, education status, and gender are not specified are not affected by complaints in their life. But they claim their complaints remain one or more than one year.
- The nineteenth cluster contains primary school graduates that suffer from complaints currently and they visited the doctor directly. They are not restricted in their daily or business life. City, gender, and age are independent.
- The twentieth cluster of 196 women in İzmir came with similar complaints. They claim they suffer from sour water or heartburn. But after the survey, they are found healthy. They have current effects of reflux but their daily or business life is not affected.
- 80 patients are healthy from cluster 21. They are independent of age, city, gender, and education status. They came with complaints that are similar to reflux, but they have not affected not restricted in their life.
- 79 patients that are secondary or high school graduates, answers Q12_10 as "always" in cluster 22. So, they limit themselves from eating some foods to avoid pain. They visited the doctor because their health is worse than last year. It can be understood they suffer from complaints one or more than one year and their health deteriorates. They are restricted from their daily activities. Also, their personal life is affected by complaints.
- The twenty-third cluster of 100 primary school graduates that are independent of age, gender, and city, have a huge list of complaints. Their psychology is not well because they claim they have never felt bouncy in their life and they always feel exhausted, tired, and upset. They believe they catch disease easier than others. Their daily activities, life, and business life are affected badly. They state they suffer from complaints for one or more than one year. Their answer for Q12_12 takes attention; they tell that also moving around the home is hard for them.
- The twenty-fourth cluster of 245 university graduates filled questionnaires, and their complaints are currently disturbing them, but they do not complain or feel restricted yet.
- The twenty-fifth cluster of 105 patients between ages 36 and 54, claims they have stress in their life last one month (SF36_5). Those patients are middle-aged, and the restriction of their daily activity may be related to their age. They feel very restricted by simple activities such as 1-2 km of walk.
- The twenty-sixth cluster of primary school graduates that are women and between ages 54 and 72 are restricted in their daily life. They had emotional problems during the last month.
- The twenty-seventh cluster of 58 patients that are primary school graduates are restricted and complaining from their problems in their health currently. They stated their business is affected badly. Also, their health affects their daily activities.

Dataset consists of patients from the Aegean region intensely. Among 3909 patients, there are 1338 women, 1026 men, and 1545 not specified. It shows intensities between the ages of 36 and 54.

In conclusion, we observed that education affects reflux patients' situations. It has been observed that 1114 primary school graduates participated in the questionnaires.

5. CONCLUSION

Knowledge discovery in the medical database is completed as aimed in the study. For future work, the diagnosis will be analyzed as well. The research is concluded with twenty-seven clusters. 3,909 data are clustered into 27 clusters with the KMeans algorithm that is found effective after comparing among other algorithms with their SSE values. After analyzing clusters, we end up with some results, our study will help patients to understand their pain reason if they are suffering from reflux or psychological reasons involved. As the process of the reflux center is examined, it is understood that process is painful and hard to overcome. So, the study aims to target only real patients instead of every patient suffering from unnecessary tests. The process is painful as we expressed before, so healthy patients are affected psychologically after tests and they feel weaker mentally. Already some patients cannot handle tests 24 hours and leave it in 4 hours or less. So, our aim is to decrease the number of patients who will take the test, successfully. We believe that computers and algorithms may be more efficient than doctors before examining the health status of patients. As we know it is impossible for doctors to know and remember similar cases with the relevant patient; however, for computers, it takes minutes to calculate and give a result according to previous similar occurrences. So those data will be used to determine new patients' health status without applying several tests.

Acknowledgments

This study is supported by Ege University Scientific Research Projects Coordination Unit. Project Number: 2.101.2015.0078. The authors would like to thank Prof. Dr. Serhat Bor in Ege University Faculty of Medicine Reflux Research Center. In addition, they would like to thank the reviewers for all useful and instructive comments on our manuscript.

Funding

The authors received no specific funding for this study.

The Declaration of Conflict of Interest/ Common Interest

No conflict of interest or common interest has been declared by the authors.

Authors' Contribution

All authors have contributed in experimental study and writing of the manuscript equally.

The Declaration of Ethics Committee Approval

The authors declare that this document has the ethics committee approval as Ege University Medical Faculty Ethical Committee Confirmation Number: 2017-5.1/49.

The Declaration of Research and Publication Ethics

The authors of the paper declare that they comply with the scientific, ethical and quotation rules of SAUJS in all processes of the paper and that they do not make any falsification on the data collected. In addition, they declare that Sakarya University Journal of Science and its editorial board have no responsibility for any ethical violations that may be encountered, and that this study has not been evaluated in any academic publication environment other than Sakarya University Journal of Science.

REFERENCES

[1] N. A. Farooqui, and R. Mehra, "Design of a data warehouse for medical information system using data mining techniques," Fifth International Conference on Parallel, Distributed and Grid Computing, pp. 199-203, 2018.

[2] S. Mishra, and M. Panda, "Artificial intelligence in medical science," In

Intelligent Systems for Healthcare Management and Delivery, pp. 306–330, 2019.

[3] B. Allen Jr, S. E. Seltzer, C. P. Langlotz, K. P. Dreyer, R. M. Summers, N. Petrick, D. Marinac-Dabic, M. Cruz, T. K. Alkasab, R. J. Hanisch, W. J. Nilsen, J. Burleson, K. Lyman, and K. Kandarpa, "A road map for translational research on artificial intelligence in medical imaging," Journal of the American College of Radiology, vol. 16, no. 9, pp. 1179–1189, 2019.

[4] G. Currie, K. E. Hawk, E. Rohren, A. Vial, and R. Klein, "Machine learning and deep learning in medical imaging: intelligent imaging," Journal of Medical Imaging and Radiation Sciences, vol. 50, no. 4, pp. 477–487, 2019.

[5] S. Agrawal, B. Singh, R. Kumar, and N. Dey, "Machine learning for medical diagnosis: A neural network classifier optimized via the directed bee colony optimization algorithm," U-Healthcare Monitoring Systems, vol. 1, pp. 197–215, 2019.

[6] V. Levshinskii, M. Polyakov, A. Losev, and A. V. Khoperskov, "Verification and validation of computer models for diagnosing breast cancer based on machine learning for medical data analysis," Creativity in Intelligent Technologies and Data Science, pp. 447–460, 2019.

[7] C. Le Berre, W. J. Sandborn, S. Aridhi, M. D. Devignes, L. Fournier, M. Smaïl-Tabbone, S. Danese, and L. Peyrin-Biroulet, "Application of artificial intelligence to gastroenterology and hepatology," Gastroenterology, vol. 158, no. 1, pp. 76–94, 2019.

[8] J. K. Ruffle, A. D. Farmer, and Q. Aziz, "Artificial intelligence in gastroenterology," Precision Medicine for Investigators, Practitioners and Providers, pp. 343–350, 2020.

[9] L. Q. Zhou, J. Y. Wang, S. Y. Yu, G. G. Wu, Q. Wei, Y. B. Deng, X. L. Wu, X. W. Cui, and C. F. Dietrich, "Artificial intelligence in medical imaging of the liver," World Journal of Gastroenterology, vol. 25, no. 6, pp. 672–682, 2019.

[10] M. McDonnell, R. Harris, T. Mills, L. Downey, S. Dharmasiri, R. Felwick, F. Borca, H. Phan, F. Cummings, and M. Gwiggner, "P384 High incidence of hyperglycaemia in steroid treated hospitalised inflammatory bowel disease (IBD) patients and its risk factors identified by machine learning methods," Journal of Crohn's and Colitis, vol. 13, no. 1, pp. 299–300, 2019.

[11] J. Han, and K. Micheline K. "Data Mining, Southeast Asia Edition: Concepts and Techniques," Morgan Kaufmann, pp. 30-39, 2006.

[12] U. Fayyad, G. Piatetsky-Shapiro, and S. Padhraic, "From data mining to knowledge discovery in databases," AI magazine, vol. 17, no. 3, pp. 37-54, 1996.

[13] Y. K. Jain, V. K. Yadav, and G. S. Panday, "An efficient association rule hiding algorithm for privacy preserving data mining," International Journal on Computer Science and Engineering, vol. 3, no. 7, pp. 2792-2798, 2011.

[14] O. Maimon, and R. Lior, "Data mining with decision trees: Theory and applications," World Scientific New Jersey, pp. 42-51, 2008.

[15] T. Wu, and L. Xiangyang, "Data Storage and Management, The Handbook of Data Mining," Ed. Nong Ye, New Jersey: Lawrence Erlbaum Associates, Inc., pp. 393-407, 2003.

[16] P. Giudici, and S. Figini, "Applied Data Mining for Business and Industry,Second Edition," Wiley Publicition, West Sussex, pp. 23-29, 2009.

[17] R. Nisbet, J. Elder, and G. Miner, "Handbook of Statistical Analysis and Data Mining Applications," Elsevier Inc, Burlington, pp. 18-26, 2009.

[18] M. Kantardzic, "Data Mining: Concepts, Models, Methods, and Algorithms," John Wiley & Sons J. B. Speed Scientific School, University of Louisville IEEE Computer Society, Sponser, pp. 52-66, 2003.

[19] J. Arora, N. Bhalla, and R. Sanjeev, "A review on association rule mining algorithms," International Journal of Innovative Research in Computer and Communication Engineering, vol. 1, no. 5, pp. 1246-1251, 2013.

[20] J. Nahar, T. Imam, K. S. Tickle, and Y. P. Chen, "association rule mining to detect factors which contribute to heart disease in males and females," Expert Systems with Applications, vol. 40, no. 4 pp. 1086-1093, 2013.

[21] R. Agrawal, and R. Srikant, "Fast algorithms for mining association rules," In Proceedings of the 20th International Conference on Very Large Data Bases, Santiago, Chile. Citeseer, pp. 487–499, 1994.

[22] M. Thamer, S. El-Sappagh, and T. El-Shishtawy, "A Semantic Approach for Extracting Medical Association Rules," International Journal of Intelligent Engineering Systems, vol. 13, no. 3, pp. 280-293, 2020.

[23] L. Wang, J. Li, T. H. Zhou, and W. Q. Liu, "Association Rules Extraction Method for Semantic Query Processing Over Medical Big Data," In Proceeding of Asian Conference on Intelligent Information and Database Systems, Singapore, Springer. pp. 109-120, 2020.

[24] S. Zhou, J. He, H. Yang, D. Chen, and R. Zhang, "Big Data-Driven Abnormal Behavior Detection in Healthcare Based on Association Rules," IEEE Access, vol. 8, pp. 129002-129011, 2020.

[25] S. Hançerlioğlu, Y. Yıldırım, and S. Bor, "Validity and reliability of the Quality of Life in Reflux and Dyspepsia (QoLRAD) questionnaire in patients with gastroesophageal reflux disease for the Turkish population," The Turkish Journal of Gastroenterology, pp. 511-516, 2019.

[26] S. Kodati, R. Vivekanandam, and G. Ravi, "Comparative analysis of clustering algorithms with heart disease datasets using data mining Weka tool," In Soft Computing and Signal Processing, Springer, Singapore, pp. 111-117, 2019.

[27] D. Arthur, and S. Vassilvitskii, "KMeans++: The advantages of careful seeding,". Stanford, pp. 1-11, 2006.

[28] P. Bholowalia, "EBK-Means : A clustering technique based on elbow method and KMeans in WSN," International Journal of Computer Applications, vol. 105, no. 9, pp. 17–24, 2014.

[29] E. Schubert, J. Sander, M. Ester, H. P. Kriegel, and X. Xu, "DBSCAN revisited, revisited: why and how you should (still) use DBSCAN," ACM Transactions on Database Systems (TODS), vol. 42, no. 3, pp. 1-21, 2017.

[30] T. Bilgin, and Y. Çamurcu, "Applied Comparison of DBSCAN, OPTICS and KMeans Clustering Algorithms," Journal of Polytechnic, vol. 8 no. 2, pp. 139–145, 2005.

[31] T. Kohonen, "Essentials of the self-organizing map," Neural networks, vol. 37, pp. 52-65, 2013.

SAKARYA ÜNİVERSİTESİ
FEN BİLİMLERİ ENSTİTÜSÜ DERGİSİ

Sakarya University Journal of Science
SAUJS

e-ISSN 2147-835X | Period Bimonthly | Founded: 1997 | Publisher Sakarya University |
http://www.saujs.sakarya.edu.tr/en/

Title: Mediator effect of luteolin on electrooxidation of NADH

Authors: Melike BİLGİ KAMAÇ, Gulshat GYLYJOVA

Recieved: 2020-05-30 18:00:08

Accepted: 2021-03-13 17:39:35

Article Type: Research Article

Volume: 25
Issue: 2
Month: April
Year: 2021
Pages: 453-465

How to cite
Melike BİLGİ KAMAÇ, Gulshat GYLYJOVA; (2021), Mediator effect of luteolin on electrooxidation of NADH. Sakarya University Journal of Science, 25(2), 453-465, DOI: https://doi.org/10.16984/saufenbilder.745610
Access link
http://www.saujs.sakarya.edu.tr/en/pub/issue/60672/745610

Sakarya University Journal of Science 25(2), 453-465, 2021

Mediator effect of luteolin on electrooxidation of NADH

Melike BİLGİ KAMAÇ[1*], Gulshat . GYLYJOVA[2]

Abstract

The effects of luteolin (LU) as a new mediator on the electrooxidation of the reduced nicotinamide adenine dinucleotide (NADH) were investigated and developed a new disposable NADH sensor. Firstly, screen printed carbon electrodes (SPCE) modified with gold nanoparticles (AuNP), and then, LU was deposited on SPCE modified with AuNP (SPCE/AuNP) using cyclic voltammetry. Electrochemical behavior of LU on SPCE/AuNP was investigated and, the redox proses of LU on SPCE/AuNP was found to be adsorption controlled. The number of cycles was optimized for the electrochemical deposition of LU and determined to be 15 cycles. LU modified SPCE/AuNP (SPCE/AuNP/LU) was found to show the electrocatalytic effect on electrooxidation of NADH and acts as a mediator. Working potential and pH were optimized for electrochemical detection of NADH with the proposed SPCE/AuNP/LU sensor and found to be +0.225 V and 7.25, respectively. The proposed NADH sensor showed a well linear response from 15.90 to 925 µM with a detection limit of 4.57 µM and a sensitivity of 11.19 μAmM^{-1}. The repeatability of the NADH sensor was tested +0.225 V with 50 µM NADH solution. The relative standard deviation (RSD) was calculated as 3.68% (for n=10). The operational stability studies have shown that the initial amperometric response of sensor to NADH decreased by 62.1% at the 30th day. The analysis of NADH in artificial human serum samples was successfully performed with SPCE/AuNP/LU sensor.

Keywords: NADH, luteolin, gold nanoparticles, redox mediator, human blood serum

1. INTRODUCTION

The studies on the electrooxidation of the reduced nicotinamide adenine dinucleotide (NADH) have attracted great attention because it is a vital coenzyme found in the human body [1, 2]. NADH is involved in many metabolic reactions, such as stimulating brain functions, providing energy support for the immune system [3]. In enzyme

*Corresponding author: melikesahin@karatekin.edu.tr
[1]Çankırı Karatekin University, Faculty of Science, Department of Chemistry, 18100, Çankırı, ORCID: https://orcid.org/0000-0002-3381-7522
[2] Çankırı Karatekin University, Eldivan Vocational School of Health Services, Department of Medical Laboratory Techniques, 18100, Çankırı.E-Mail: gulshatyos14@gmail.com, ORCID: https://orcid.org/0000-0002-8798-9119

experiments, analysis of NADH is usually done [4, 5]. The analysis of NADH is also important as NAD^+ coenzyme is used in dehydrogenase-based biosensors. The direct electrooxidation of NADH in bare electrodes (C, Au, Pt etc.) occurs at high overpotentials. Irreversible inactive forms of NADH are formed at high overpotential and accumulate on the electrode surface, causing electrode contamination, which results in background currents that cause interference in real samples [6, 7]. Modified electrodes with various mediators [8-11] are widely used to reduce the electooxidation potential of NADH and the interference effect.

Antioxidant that has quinone-hydroquinone (Q/QH_2) redox pairs in the structure are also used as mediators in the electrooxidation of NADH. A caffeic acid modified glassy carbon electrode (GCE) [12, 13] and screen-printed electrode modified with carbon black nanoparticle (SPCE/CB) [14] were used for determination of NADH. GCE modified with chlorogenic acid was used for electrooxidation of NADH [15]. Dilgin et al used pencil graphite electrode (PGE) modified with quercetin for electrocatalytic oxidation of NADH [16]. In recently work, SPCE modified with RA was used for amperometric determination of NADH [17]. Luteolin (LU), 3,4,5,7-tetrahydroxyflavone, is one of the most important flavonoid compounds that has an electroactive catechol group in the B ring [18, 19]. Therefore, the electrochemical behavior of LU has been widely studied and sensors have been prepared for its electrochemical determination [20-25]. The structure of the LU is given in Figure 1. In the literature, no studies have been reported that the use of modified electrode with LU used for electrooxidation of NADH. The aim of this work is to examine the mediation effects of LU for the electrooxidation of NADH and to develop a new NADH sensor.

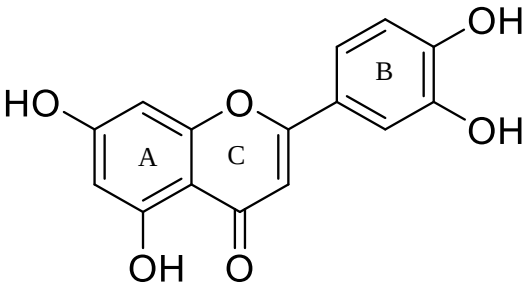

Figure 1. Chemical structure of luteolin

Screen printed carbon electrodes (SPCEs) have been reported to be widely used in the development of sensors and biosensors as they are suitable for point-of-care and are disposable [26-31]. In this study, bare SPCEs were used and modified with gold nanoparticles and LU for the preparation of a new, simple, practical, and disposable NADH sensors. Moreover, the SPCE/AuNP/LU electrode was used for the accurate determination of NADH in artificial human serum sample.

2. MATERIALS AND METHODS

2.1. Materials

LU, AuNP solution (10 nm), NADH and artificial human blood serum sample were purchased from Sigma-Aldrich. KH_2PO_4, K_2HPO_4, KCl were obtained from Merck. All solutions were prepared with deionized water supplied by a Millipore Milli-Q Direct Q-3 device. Phosphate buffer solution (PBS) were prepared using K_2HPO_4, KH_2PO_4 and KCl. NADH and LU were prepared in 50 mM PBSs (in 0.1M KCl).

2.2. Instrumentation

Screen-printed carbon electrodes (SPCEs, DRP110) were purchased from DropSens, Spain. The reference electrode is silver, while the auxiliary and working electrode are carbon, and they are deposited on a ceramic support. All electrochemical experiments were carried out using Dropsens, Bipotentiostate/Galvanostate (μSTAT 400) with DropView software. The measurements of pH were applied with a Mettler

Toledo pH-meter. Amperometric measurements were performed under stirred conditions.

2.3. Preparation of SPCEs modified with LU and AuNP

Electrochemical pretreatment to SPCEs to before use was performed by applying 1.8 V potential for 300 seconds in PBS (pH 7.5) [11, 31]. The 10 µL of AuNPs solution was deposited onto the surface of SPCE and was left to dry at 20°C. Then LU was electropolymerized on modified electrode (SPCE/AuNP) by potential cycling at a scan rate of 50 mV s^{-1}. The potential was cycled between -0.2 to +1.0 V for 15 cycles in 1 mM LU (in 50 mM pH 7.0 PBS) [32]. The electrode (SPCE/AuNP/LU) was rinsed in the PBS.

3. RESULTS AND DISCUSSION

3.1. Electrochemical behavior of LU at SPCE/AuNP

Figure 1 shows cyclic voltammogram of 1 mM LU in PBS (pH 7.0) at SPCE/AuNP electrode. It is seen that the reversible redox couple of LU at 10 mV.s^{-1} are +0.204 (Epa) and +0.168 V (Epc). While Epa corresponded to the electrooxidation of the 3',4'- dihydroxy substituent on the ring-B, Epc is corresponding reduction peak of the formed 3',4'-diquinone [20, 22, 25]. Epa values of LU reported in the literature are given in Table 1. When the literature data are examined, it is understood that the Epa value of LU observed our study was much lower. The reason for the Epa value of LU being observed at a lower potential in this study may be due to electrochemical pretreatment procedure applied to SPCEs [17]. This result is an advantage for using LU as a mediator in the electrochemical analysis of NADH.

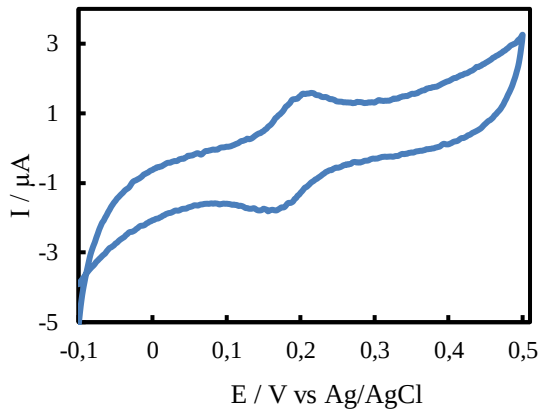

Figure 1 CV of SPCE/AuNP in 1 mM LU at 50 mM pH 7.0 PBS containing 0.1M KCl (E: from −0.1 V to +0.5V, scan rate: 10 mV s^{-1})

Table 1
Epa values of LU in the literature

Electrode formulation	Epa (V)	References
GCE	+0.410	20
MWCNT/GCE	+0.450	21
GCE	+0.336	22
PDDA-G-CNTs/β-CD/GCE	~+0.400	23
PDDA-RGO/GCE	~+0.400	24
In_2O_3NPs/GCPE	+0.459	25
SPCE/AuNP	+0.204	In this study

GCE: Glassy carbon electrode, PDDA: Poly (Diallyldimethylammonium chloride), CNT: Carbon nanotube, β-CD: β-cyclodextrin, RGO: Reduced graphene oxide, MWNCT: Multi-walled carbon nanotube, GCPE: glassy carbon paste electrode, In_2O_3NPs: Indium (III) oxide nanoparticles, SPCE: Screen-printed carbon electrode, AuNP: Gold nanoparticles

The difference between the anodic and cathodic peak potentials at scan rate of 10 mV.s^{-1} was calculated as 36 mV. ΔEp value is close to 30 mV which is reaction mechanism of a reversible two-electron [17, 20, 21, 25]. Figure 2 (a) shows CVs of 1 mM LU at SPCE/AuNP electrode with different scanning rates. The CVs show that it is apparently a well-defined redox pair and, both anodic and cathodic peak currents are linear with the scan rate (Figure 2 (b)). This indicates that the redox proses of LU on SPCE/AuNP is adsorption controlled [20, 21, 25].

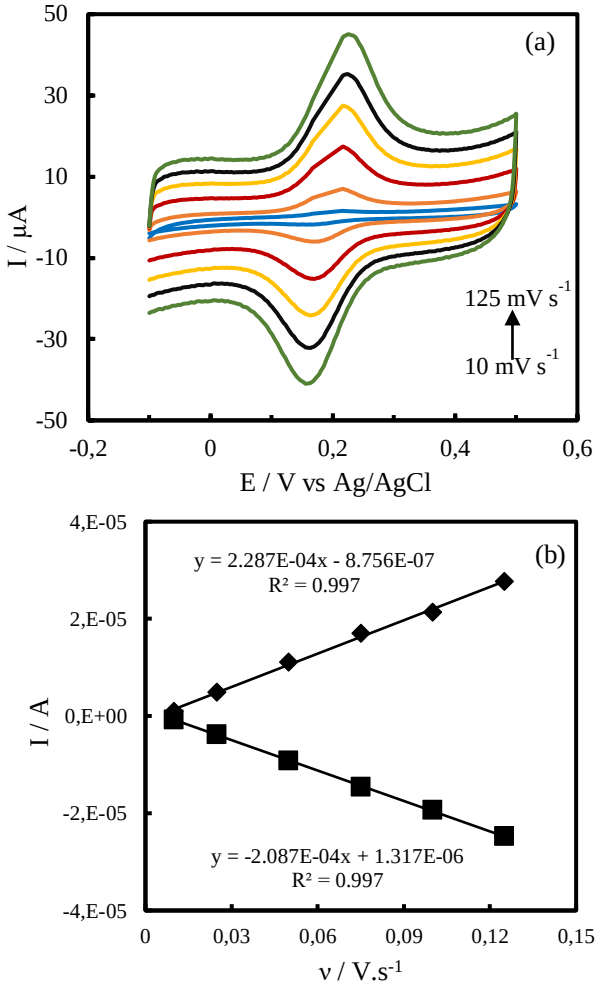

Figure 2 (a) Cyclic voltammogram of SPCE/AuNP/LU recorded in 50 mM PBS pH 7.0 (in 0.1M KCl) at different scan rates. The scan rate is 10 mV s^{-1} for the innermost CV and increases to 25, 50, 75, 100, 125 mV s^{-1} for outer CVs (b) influence of the scan rate on the peak currents

3.2. Electrochemical characterization of SPCE/AuNP/LU

In order to deposition of LU on SPCE/AuNP, the cyclic voltammetry was carried out between -0.2 to +1.0 V for 15 cycles in a solution containing 1 mM LU, 50 mM pH 7.0 PBS (0.1 M KCl). The cyclic voltammograms recorded by electropolymerization of LU on SPCE/AuNP show anodic and cathodic peaks indicating the typical Q/QH_2 redox couple (Figure 3). With the increase in the number of cycles, anodic and cathodic peak currents increased, while the relative increase rate in peak currents decreased.

Similar results were reported for the caffeic acid [12-14], chlorogenic acid [15] and rosmarinic acid [17].

To examine the effect of the number of cycles on the electrodeposition of the LU, cyclic voltammetry was applied to the SPCE/AuNP modified with LU in different cycle numbers (5, 10, 15 and 20 cycles). Figures 4 (a, b, c, d) show that the cyclic voltammograms at various scan rates in PBS (pH 7.0) for SPCE/AuNP modified with LU in different cycle numbers (5, 10, 15 and 20 cycles), respectively. The peak currents are linear with the scan rate (Figures 4 (e, f, g, h)). This indicate that the electrochemical proses is an adsorption-controlled and LU is deposited on AuNP modified SPCE.

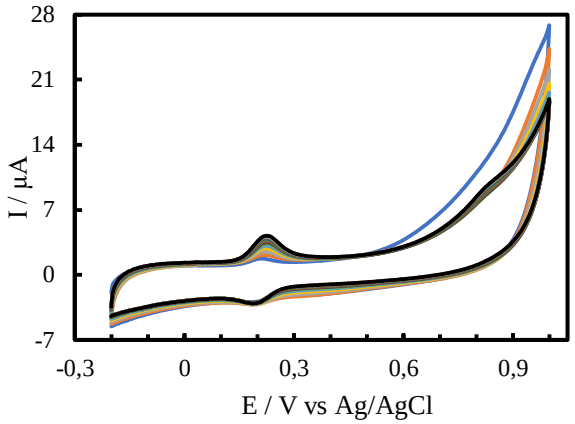

Figure 3 Cyclic voltammograms obtained during deposition of 1 mM LU on SPCE/AuNP (E: from −0.2 V to +1.0 V, scan rate: 50 mV s^{-1}, 15 cycles)

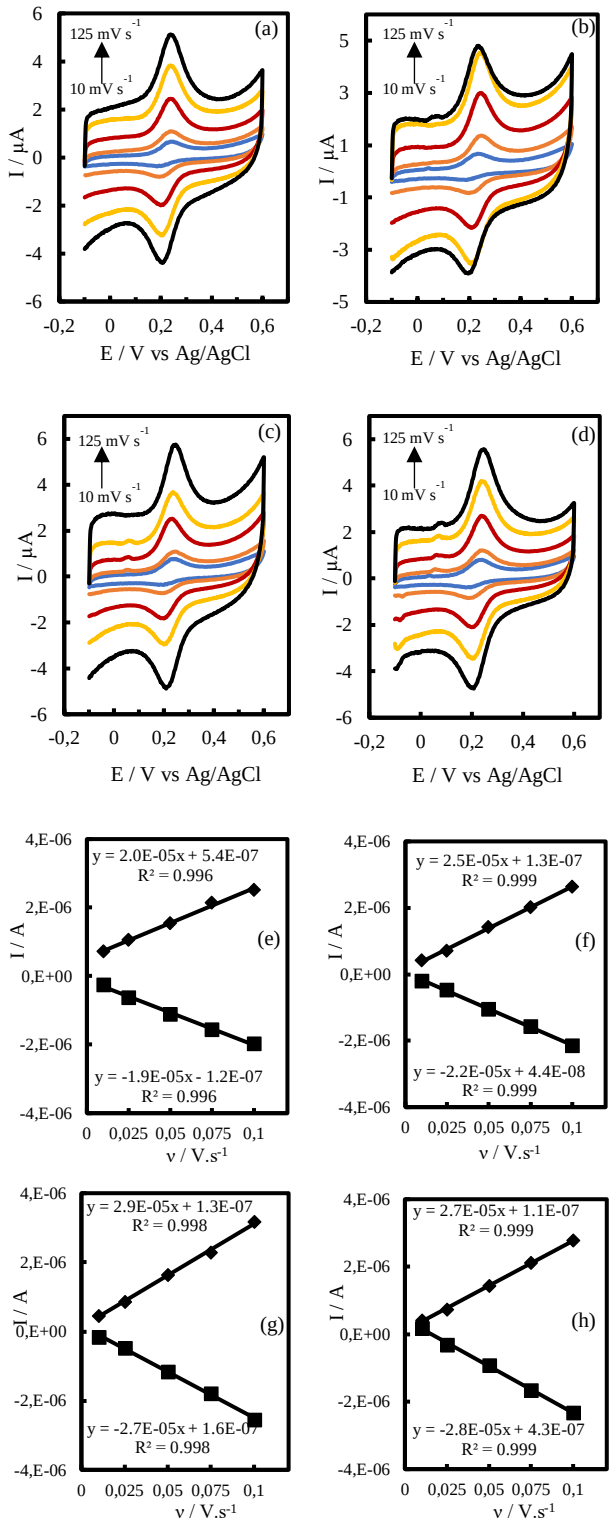

Figure 4 CVs of SPCE/AuNP modified with LU (a) 5, (b) 10, (c) 15 and (d) 20 cycles in 50 mM PBS pH 7.0 (in 0.1M KCl) at various scan rates. The scan rate is 10 mV s^{-1} for the innermost CV and increases to 25, 50, 75, 100, 125 mV s^{-1} for outer; influence of the scan rate on the peak currents (e) 5, (f) 10, (g) 15 and (h) 20 cycles

To determinate the optimization of the number of cycles on the deposition of the LU at SPCE/AuNP, the average electroactive surface concentration of LU on SPCE/AuNP, Γ, was calculated using the following equation [33]:

$$I_p = [(n^2 F^2 A\nu) / (4RT)] \Gamma \quad (1)$$

where I_p is the peak current (A), n is the number of electrons transferred, F is the Faraday constant (96485 C mol^{-1}), ν is the scan rate ($V.s^{-1}$), A is the electroactive surface area of the electrode (cm^2), R is the gas constant (8.314 J K^{-1} mol^{-1}), T is the temperature (293.15 K). To calculate the A of the SPCE/AuNP/LU electrode, the cyclic voltammetry was applied to SPCE/AuNP/LU electrode in 1 mM $K_3Fe(CN)_6$ (in 0.1MKCl) at various scan rates (10 mV s^{-1} to 125 mV s^{-1}). (Figure not shown). Using the Randless-Sevcik equation [34] and slope of I vs. $\nu^{1/2}$ plot (Figure not shown) the A of the SPCE/AuNP/LU electrode was calculated to be 0.175 cm^2. The Γ values of SPCE/AuNP modified with LU for 5, 10, 15 and 20 cycles, using values of A and the equation (1), were calculated (1.22×10^{-10}, 1.50×10^{-10}, 1.78×10^{-10} and 1.59×10^{-10}) mol cm^{-2}, respectively. The highest Γ value was obtained with the SPCE/AuNP electrode modified with LU for 15 cycles. Therefore, it was decided that 15 cycles are optimum for the deposition of LU. Further studies have been carried out to confirm the determination of optimization of the number of cycles. For this purpose, amperometric determination of NADH with these modified electrodes was performed at +0.3 V. The current vs concentration graphs of the NADH analysis are given in Figure 5. Table 2 show the sensitivities and correlation coefficient values of graphs in Figure 5. As the number of cycles increased from 5 to 15, the slope of the current concentration graphs increased, while the slope decreased in the 20th cycle due to the increase in film thickness and, as a result, decreased diffusion. The highest sensitivity and correlation coefficients are observed at SPCE/AuNP electrode modified with LU for 15 cycles. Therefore, for further studies, SPCE/AuNP electrode were modified with LU for 15 cycles.

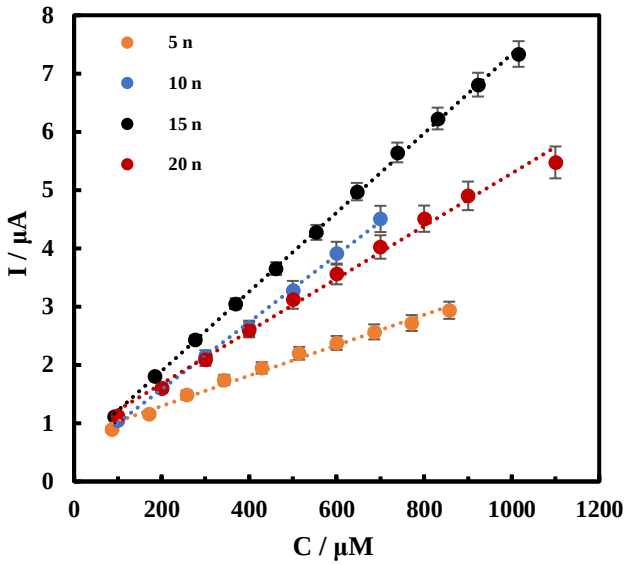

Figure 5 Current vs concentration graph for amperometric analysis of NADH at +0.30 V with SPCE/AuNP electrode modified with LU for 5, 10, 15 and 20 cycles

Table 2
Values of sensitivities and correlation coefficients of graphs in Figure 5

Number of cycles	Sensitivity/ (µA.mM-^{1})	Correlation coefficients
5	2.61± 0.009	0.9947
10	5.76 ± 0.011	0.9990
15	6.80 ± 0.006	0.9997
20	4.51 ± 0.013	0.9932

The cyclic voltammogram of bare SPCE, SPCE/AuNP and SPCE/AuNP/LU electrodes in 5 mM $K_3Fe(CN)_6/K_4Fe(CN)_6$ (in 1 M KCl) are given in Figure 6. The anodic peaks currents (Ipa) and cathodic peak currents (Ipc) increased by modification of SPCE with AuNP and, then LU. The highest values of Ipa and Ipc are obtained in SPCE/AuNP/LU electrode.

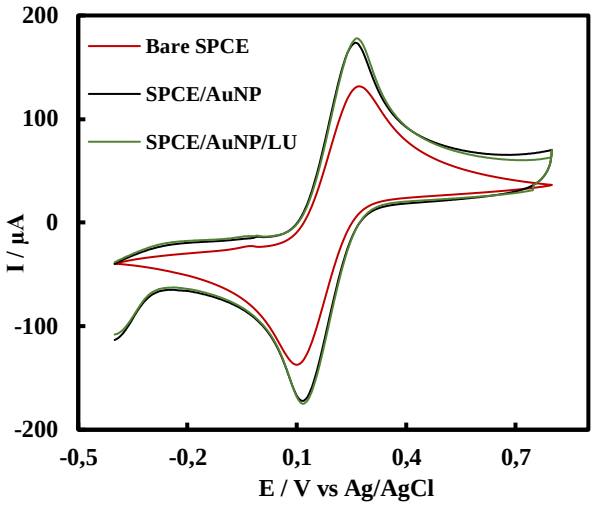

Figure 6 Cyclic voltammograms of bare SPCE, SPCE/AuNP and SPCE/AuNP/LU in 5 mM $K_3Fe(CN)_6/K_4Fe(CN)_6$ in 1 M KCl (E: from −0.4 V to +0.8V, scan rate: 50 mV s^{-1})

3.3. Electrocatalytic oxidation of NADH at SPCE/AuNP/LU

To see the electrocatalytic effect of the SPCE/AuNP/LU electrode toward electrooxidation of NADH, the CVs were performed in the absence and presence of 1 mM NADH in 50 mM pH 7.0 PBS containing 0.1 M KCl at 50 mV s^{-1} (Figure 7 (a) and (b)). With the presence of 1 mM NADH at +0.212 V, the oxidation peak current increased remarkably, from 0.92 µA to 33.35 µA, while the cathodic peak current at +0.172 V slightly increased, from 0.76 µA to 5.46 µA. The Epa of NADH at the SPCE/AuNP/LU was observed at +0.212 V, while NADH was oxidized at +0.492 V and +0.326 V at the bare SPCE and SPCE/AuNP, respectively (Figure 7 (c) and (d). According to these results, LU has an electrocatalytic effect on the oxidation of NADH and acts as a mediator [6-10]. LU was used for the first time in this study as a mediator in the electrooxidation of NADH.

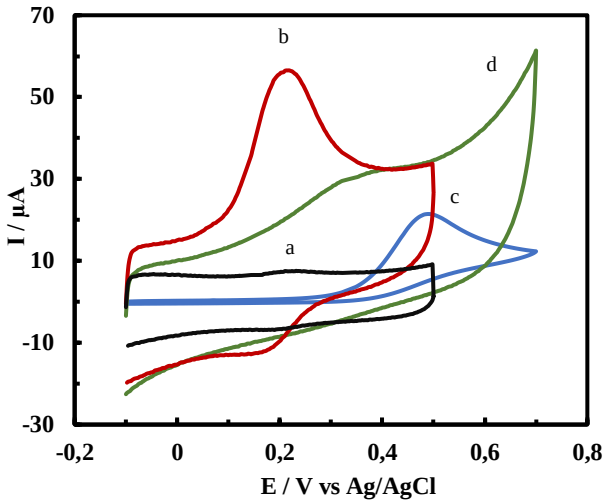

Figure 7 Cyclic voltammograms of SPCE/AuNP/LU in the absence (a) and in the presence (b) of 1 mM NADH and the CVs of 1 mM NADH at bare SPCE (c) and SPCE/AuNP (d) (50 mM pH 7.0 PBS containing in 0.1 M KCl; scan rate: 50 mV s^{-1})

The increase of anodic peak current in the presence of NADH indicates that NADH is oxidized by diffusing from the solution to the electrode surface, whereas the LU on the surface is reduced. The reaction can take place as the following reactions:

$$LU_{(red)} \rightarrow LU_{(ox)} + 2H^+ + 2e^- \quad (2)$$

$$LU_{(ox)} + NADH + H^+ \rightarrow LU_{(red)} + NAD^+ \quad (3)$$

$$NADH \rightarrow NAD^+ + H^+ + 2e^- \quad (4)$$

Figure 8 (a) shows the cyclic voltammograms recorded in 1 mM NADH at different scan rates (10 to 100 mV s^{-1}) on SPCE/AuNP/LU. The plot of the anodic peak currents obtained from these CVs against the square root of the scan rate is linear (Figure 8 (b)). This result show that electrochemical proses of the electrocatalytic oxidation of NADH at SPCE/AuNP/LU is a diffusion controlled. Using the slope of Figure 8 (b), the diffusion coefficient of 1mM NADH on SPCE/AuNP/LU was calculated to be 4.49×10^{-9} cm^2 s^{-1} using Randless-Sevcik Equation [34]. A Plot of the anodic peak potential (Epa) and the natural logarithm of scan rate (lnv) for the electrocatalytic oxidation of 1 mM NADH at SPCE/AuNP/LU is given in Figure 8 (c). The electron transfer coefficient (α) for the electrocatalytic oxidation of NADH at SPCE/AuNP/LU electrode was calculated from the following equation [35]:

$$Ep = [(RT)/(2\alpha F)] \ln \nu + \text{constant} \quad (5)$$

where Ep is the anodic or cathodic peak potential. Using the slope of Figure 8 (c), the α was calculated to be 0.654 for 1mM NADH.

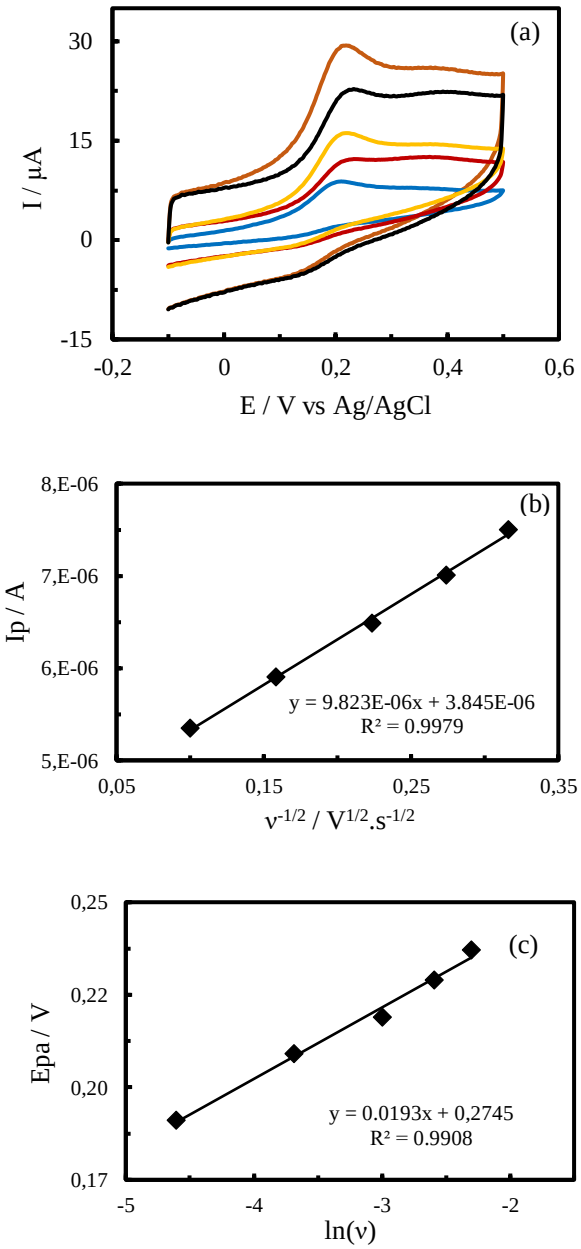

Figure 8 (a) Cyclic voltammogram of 1 mM NADH in PBS (pH 7.0) on SPCE/AuNP/LU at different scan rates from 10 to 100 mV s^{-1}, (b) Plot of anodic peak currents vs square root of scan rate, (c) The variation of anodic peak potentials vs natural logarithm of scan rate

3.4. Amperometric detection of NADH with SPCE/AuNP/LU

To obtain the best sensor performance of SPCE/AuNP/LU towards NADH, the experimental conditions which are working potential and pH were optimized. Firstly, the amperometric currents for NADH electrooxidation at a fixed concentration of 100 µM with different pH (6-8) were measured at +0.300 V. According to the current vs pH graph given in Figure 9, the highest current was observed at pH 7.25, thus the optimum pH was determined to be 7.25.

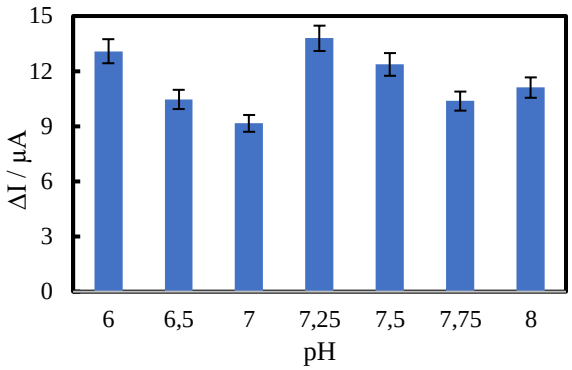

Figure 9 Current vs pH graph for the electrooxidation of 100 µM NADH at +0.300 V in PBSs of different pH

NADH analysis with SPCE/AuNP/LU were performed by amperometric detection in 50 mM phosphate buffer solution (pH 7.25) at various potentials (+0.225 V to +0.325 V) for the optimization study of the working potential. The current vs concentration graphs were obtained from the amperograms given in Figure 10. Table 3 show the sensitivities and correlation coefficient values of graphs in Figure 10. The optimum working potential is selected to be +0.225 V, due to the highest sensitivity and correlation coefficient are observed at this potential.

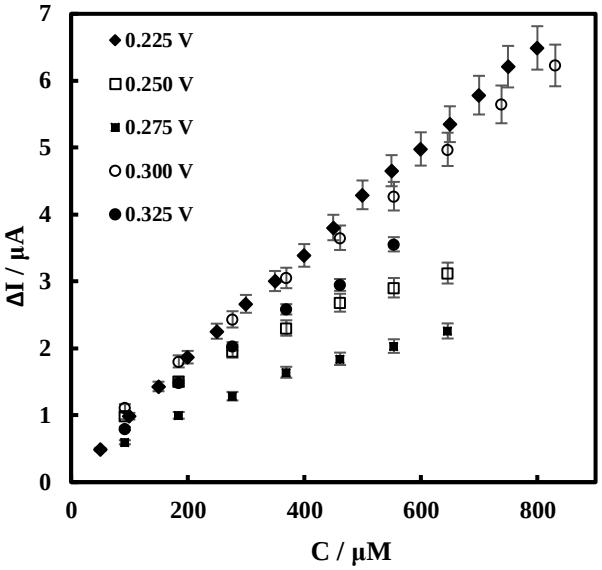

Figure 10 Current vs concentration graph for amperometric determination of NADH with SPCE/AuNP/LU sensor in PBS (pH 7.25) at various working potentials: +0.225 V (♦), +0.250V (□), +0.275 V (▲), +0.300 V (○) and +0.325 V (●)

Table 3
Values of sensitivities and correlation coefficients of graphs in Figure 10

Working potential/(V)	Sensitivity /(µA.mM^{-1})	Correlation coefficients
+0.225	7.96 ± 0.005	0.9995
+0.250	3.85 ± 0.026	0.9888
+0.275	2.95 ± 0.018	0.9910
+0.300	6.92 ± 0.006	0.9984
+0.325	5.79 ± 0.023	0.9969

Amperometric analysis of NADH was applied with SPCE/AuNP/LU sensor under stirring at +0.225 V in PBS (pH 7.25). After the stable current was reached, 25 µM NADH was injected successive to the electrochemical cell and the response of current was recorded by the potentiostat. The obtained amperogram for amperometric determination of NADH is given in Figure 11 (a). The measured current values with each injection of NADH against concentration values are plotted in Figure 11 (b). The sensitivity of the proposed NADH sensor in the range of 25 µM to 925 µM is found to be 11.19 µA.mM^{-1}. The limit of detection and quantification (3σ/m) were calculated to be 4.77 µA.mM^{-1} and 15.90 µA.mM^{-1}, respectively. For the repeatability of the SPCE/AuNP/LU sensor, NADH analysis was performed at +0.225 V with 50 µM NADH

solution. The relative standard deviation (RSD) was calculated as 3.68% (for n=10). The linear range was determined to be 25 µM - 925 µM. The comparison of the analytical performance of the proposed NADH sensor with the other recently reported NADH sensors is given in Table 4.

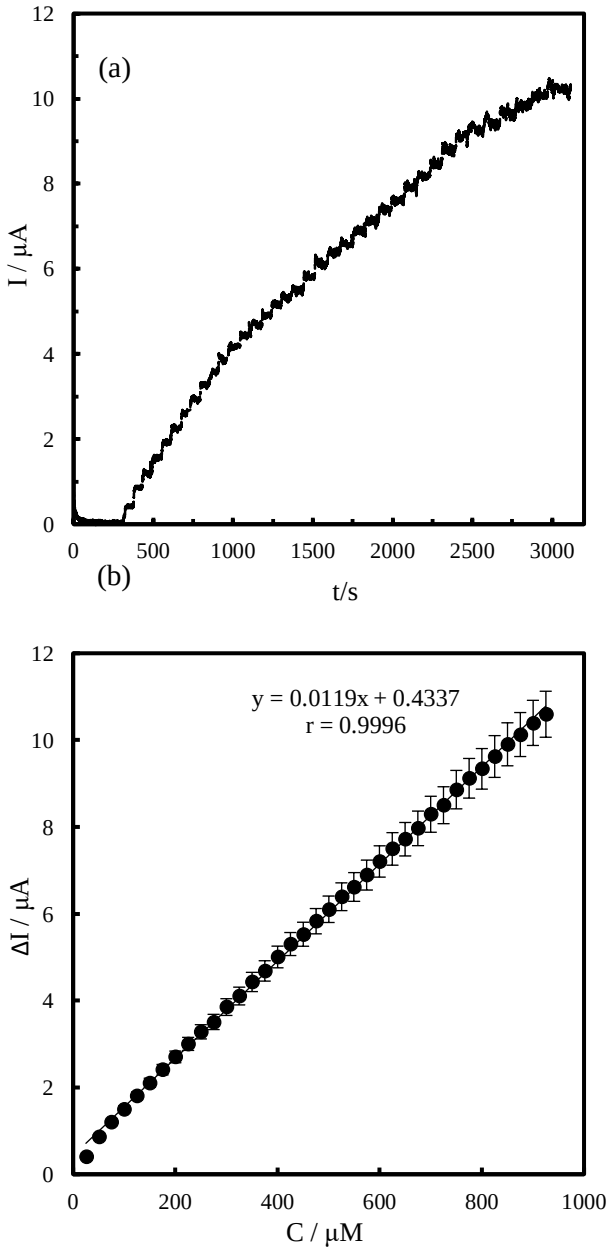

Figure 11 (a) Amperometric current response of SPCE/AuNP/LU sensor to addition of 25 µM NADH in PBS (pH 7.25) at +0.225 V, (b) Calibration curve vs NADH concentration

Table 4
Analytical performance comparison of the proposed SPCE/AuNP/LU with the other reported antioxidant mediated amperometric NADH sensors

Modified electrode	LR/ (µM)	LOD/(µM)	References
GCE/CA	50–1000	–	12
SPCE/CB/CA	–	1.6	14
GCE/CGA	100–1000	–	15
PGE/QH_2	0.5–100	0.15	16
SPCE/RA	18.7-220	5.62	17
SPCE/AuNP/LU	25-925	4.77	This work

CGA: chlorogenic acid, CA: caffeic acid, QH_2: quercetine, RA: rosmarinic acid, LU: luteolin, GCE: glassy carbon electrode, PGE: pencil graphite electrode, CB: carbon black nanoparticles, SPCE: screen-printed carbon electrode, AuNP: gold nanoparticles

To examine the operational stability of the NADH sensor, the currents of 50 µM NADH solution in PBS (pH 7.25) were measured at +0.225 V over a period of 30 days (n=3). The percent relative current values are compared as a measure of the response of SPCE/AuNP/LU sensor toward NADH for 30 days (Figure 12). The first day current response of the proposed sensor to NADH decreased by 1.50% on the 2nd day, by 13.8% on the 5th day, by 29.5% on the 10th day and by 62.1% on the 30th day. Although the operation stability of the proposed NADH sensor decreased by 62.1% on the 30th day compared to the first use, the response was received even on the 30th day with the disposable manufactured SPCEs. The presence of AuNP and natural antioxidant LU in the electrode formulation improved the operational stability of the NADH sensor.

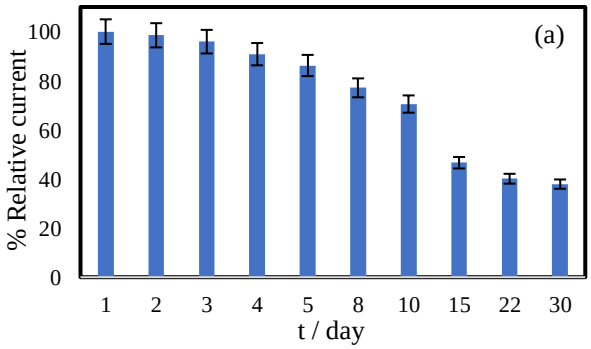

Figure 12 %Relative current responce vs time plot over 30 day for amperometric detection of NADH in PBS (pH 7.25) with SPCE/AuNP/LU sensor

3.5. Application of NADH sensor of human serum sample

The proposed NADH sensor based on SPCE/AuNP/LU is used for the analysis of NADH in artificial human serum samples. 100 μM NADH was spiked into the artificial human blood serum sample diluted 1:100 with pH 7.4 buffer solution and amperometric determination of NADH with SPCE/AuNP/LU. The experimentally calculated NADH concentration was determined to be 103.1 ± 0.18 and recovery was to be 103.1%.

4. CONCLUSION

The new disposable, simple and practical amperometric NADH sensor, easily prepared by electrodeposition of LU on the SPCE/AuNP electrode, was defined for the first time in this study. SPCE/AuNP/LU exhibits electrocatalytic effect on electrooxidation of NADH due to LU acts as a mediator. The electrooxidation potential of NADH was reduced by the effect of the LU mediator. Optimum working potential and pH of the NADH sensor were found to be +0.225 V and 7.25, respectively. The developed NADH sensor showed a good linear response in the range between 25 and 925 μM with a detection limit of 4.57 μM and sensitivity of 11.19 μAmM^{-1}. The relative standard deviation (RSD) was calculated as 3.68% (for n=10). The operational stability studies showed that the developed NADH sensor responds even on the 30th day although SPCE was produced for single use. This may be considered to be due to the presence of natural antioxidant LU and AuNP in the electrode formulation. Moreover, the developed SPCE/AuNP/LU sensor demonstrated very attractive features for the target NADH in human serum samples in terms of sensitivity (recovery was to be 103.1%). The NADH sensor mediated with LU presented a new methodology that had simplicity, disposable, practical, storage stability, and potential to perform the accurate determination of the target analyte in serum samples.

The Declaration of Conflict of Interest/ Common Interest

No conflict of interest or common interest has been declared by the authors.

Authors' Contribution

This study is the undergraduate thesis of Gulshat GYLYJOVA, and the idea of the study belongs to supervisior that is Melike BİLGİ KAMAÇ. Melike BİLGİ KAMAÇ had a great contribution in providing support for the study, preparing and developing the NADH sensor, conducting the experiments, interpreting the findings and writing the undergraduate thesis. Gulshat GYLYJOVA contributed to the experimental studies.

The Declaration of Ethics Committee Approval

The authors declare that this document does not require an ethics committee approval or any special permission.

The Declaration of Research and Publication Ethics

The authors of the paper declare that they comply with the scientific, ethical and quotation rules of SAUJS in all processes of the article and that they do not make any falsification on the data collected. In addition, they declare that Sakarya University Journal of Science and its editorial board have no responsibility for any ethical violations that may be encountered, and that this study has not been evaluated in any academic publication environment other than Sakarya University Journal of Science.

REFERENCES

[1] L. Gorton and E. Dominguez, “Electrochemistry of NAD(P)+/NAD(P)H, in: Encyclopedia of Electrochemistry,” (A.J. Bard, M. Stratmann (Eds.)), Bioelectrochemistry (G.S. Wilson (Ed.)), (Wiley-VCH, Weinheim), vol. 9, p. 67, 2002.

[2] E. Simon and P.N. Bartlett, "Biomolecular Films, Design, Function and Applications," Marcel Dekker, (New York), 2002.

[3] G. D. Birkmayer, "NADH the energizing coenzyme. Good Health Guide," Keats Publishing, Los Angeles, pp. 1-2, 1993.

[4] E. Aslan and S. Adem, "Investigation of the effects of some drugs and phenolic compounds on human dihydrofolate reductase activity," Journal of Biochemical and Molecular Toxicology, vol. 29, no. 3 pp. 135-139, 2015.

[5] S. Adem and M. Ciftci, "Purification and biochemical characterization of glucose 6-phosphate dehydrogenase, 6-phosphogluconate dehydrogenase and glutathione reductase from rat lung and inhibition effects of some antibiotics," Journal of Enzyme Inhibition and Medicinal Chemistry, vol. 31, no. 6, pp. 1342-1348, 2016.

[6] L. Gorton, "Chemically modified electrodes for the electrocatalytic oxidation of nicotinamide coenzymes," Journal of The Chemical Society-Faraday Transactions I, vol. 82, no. 4, pp. 1245-1258, 1986.

[7] S. A. Kumar and S. Chen, "Electroanalysis of NADH using conducting and redox active polymer/carbon nanotubes modified electrodes - A review," Sensors, vol. 8, no. 2, pp. 739-766, 2008.

[8] Y. Dilgin, D. Giray Dilgin, Z. Dursun, H. İ. Gökçel, D. Gligor, B. Bayrak, and B. Ertek, "Photoelectrocatalytic determination of NADH in a flow injection system with electropolymerized methylene blue," Electrochimica Acta, vol. 56, no. 3, pp. 1138-1143, 2011.

[9] M. Güneş and Y. Dilgin, "Flow injection amperometric determination of NADH at a calmagite-modified pencil graphite electrode," Monatshefte für Chemie-Chemical Monthly, vol. 150, no. 8, pp 1425-1432, 2019.

[10] M. Sahin and E. Ayranci, "Electrooxidation of NADH on modified screen-printed electrodes: effects of conducting polymer and nanomaterials," Electrochimica Acta, vol. 166, pp. 261-270, 2015.

[11] M. Bilgi Kamaç, E. Kıymaz Onat and M. Yılmaz, "A new disposable amperometric NADH sensor based on screen-printed electrode modified with reduced graphene oxide/polyneutral red/gold nanoparticle," International Journal of Environmental Analytical Chemistry, vol. 100, no. 4, pp. 419-431, 2020.

[12] H. R. Zare and S. M. Golabi, "Caffeic acid modified glassy carbon electrode for electrocatalytic oxidation of reduced nicotinamide adenine dinucleotide (NADH)," Journal of Solid-State Electrochemistry, vol. 4, no. 2, pp. 87–94, 2000.

[13] P. T. Lee and R. G. Compton, "Electrochemical detection of NADH, cysteine, or glutathione using a caffeic acid modified glassy carbon electrode," Electroanalysis, vol. 25, no. 7, pp. 1613–1620, 2013.

[14] C. Zanardi, E. Ferrari, L. Pigani, F. Arduini and R. Seeber, "Development of an Electrochemical Sensor for NADH Determination Based on a Caffeic Acid Redox Mediator Supported on Carbon Black," Chemosensors, vol. 3, no. 2, pp. 118-128, 2015.

[15] H. R. Zare and S. M. Golabi, "Electrocatalytic oxidation of reduced nicotinamide adenine dinucleotide (NADH) at a chlorogenic acid modified glassy carbon electrode," Journal of Electroanalytical Chemistry, vol. 464, no. 1, pp. 14-13, 1999.

[16] Y. Dilgin, B. Kızılkaya, D. Giray Dilgin, H. İ. Gokçel and L. Gorton, "Electrocatalytic oxidation of NADH using a pencil graphite electrode modified with quercetin," Colloids and Surfaces B-Biointerfaces, vol. 102, pp. 816-821, 2013.

[17] M. Bilgi, E. M. Sahin and E. Ayranci, "Sensor and biosensor application of a new redox mediator: Rosmarinic acid modified screen-printed carbon electrode for electrochemical determination of NADH and ethanol," Journal of Electroanalytical Chemistry, vol. 813, pp. 67-71, 2018.

[18] H. P. Hendrickson, A. D. Kaufman and C. E. Lunte, "Electrochemistry of catechol-containing flavonoids," Journal of Pharmaceutical and Biomedical Analysis, vol. 12, no. 3, pp. 325-334, 1994.

[19] L. V. Jørgensen, H. L. Madsen, M. K. Thomsen, L. O. Dragsted and L. H. Skibsted, "Regeneration of phenolic antioxidants from phenoxyl radicals: an ESR and electrochemical study of antioxidant hierarchy," Free Radical research, vol. 30, no. 3, pp. 207-220, 1999.

[20] A. Liu, S. Zhang, L. Huang, Y. Cao, H. Yao, W. Chen and X. Lin, "Electrochemical oxidation of luteolin at a glassy carbon electrode and its application in pharmaceutical analysis", Chemical and Pharmaceutical Bulletin, vol. 56, no. 6, pp. 745-748, 2008.

[21] D. Zhao, X. Zhang, L. Feng, Q. Qi and S. Wang, "Sensitive electrochemical determination of luteolin in peanut hulls using multi-walled carbon nanotubes modified electrode," Food Chemistry, vol. 127, no. 2, pp. 694-698, 2011.

[22] S. Ramešová, R. Sokolová, J. Tarábek and I. Degano, "The oxidation of luteolin, the natural flavonoid dye," Electrochimica Acta, vol. 110, pp. 646-654, 2013.

[23] D. Lu, S. Lin, L. Wang, T. Li, C. Wang and Y. Zhang, "Sensitive detection of luteolin based on poly (diallyldimethylammonium chloride)-functionalized graphene-carbon nanotubes hybrid/β-cyclodextrin composite film," Journal of Solid-State Electrochemistry, vol. 18, no. 1, pp. 269-278, 2014.

[24] L. Fu, Y. Zheng and A. Wang, "Poly (diallyldimethylammonium chloride) functionalized reduced graphene oxide based electrochemical sensing platform for luteolin determination," International Journal of Electrochemical Science, vol. 10, no. 4, pp. 3518-3529, 2015.

[25] H. Ibrahim, and Y. Temerk, "Novel sensor for sensitive electrochemical determination of luteolin based on In2O3 nanoparticles modified glassy carbon paste electrode," Sensors and Actuators B: Chemical, vol. 206, pp. 744-752, 2015.

[26] M. Bilgi and E. Ayranci, "Biosensor application of screen-printed carbon electrodes modified with nanomaterials and a conducting polymer: Ethanol biosensors based on alcohol dehydrogenase," Sensors and Actuators B: Chemical, vol. 237, pp. 849-855, 2016.

[27] M. Sayhi, O. Ouerghi, K. Belgacem, M. Arbi, Y. Tepeli, A. Ghram, Ü. Anık, L. Österlund, D. Laouini and M. F. Diouani, "Electrochemical detection of influenza virus H9N2 based on both immunomagnetic extraction and gold catalysis using an immobilization-free screen-printed carbon microelectrode," Biosensors and Bioelectronics, vol. 107, pp. 170-177, 2018.

[28] M. Bilgi and E. Ayranci, "Development of amperometric biosensors using screen-printed carbon electrodes modified with conducting polymer and nanomaterials for the analysis of ethanol, methanol and their mixtures," Journal of Electroanalytical Chemistry, vol. 823, pp. 588-592, 2018.

[29] M. Altun, M. Bilgi Kamaç, A. Bilgi and M. Yılmaz, "Dopamine biosensor based on screen-printed electrode modified with reduced graphene oxide, polyneutral red and gold nanoparticle," International Journal of Environmental Analytical Chemistry, vol. 100, no. 4, pp. 451-467, 2020.

[30] A. Merkoçi, U. Anik, S. Çevik, M. Çubukçu and M. Guix, "Bismuth film combined with screen-printed electrode as biosensing platform for phenol detection," Electroanalysis, vol. 22, no. 13, pp. 1429-1436, 2010.

[31] M. Bilgi Kamaç, E. Kıymaz Onat and M. Yılmaz, "A novel non-enzymatic amperometric H_2O_2 sensor based on screen-printed electrode modified with reduced graphene oxide, polyneutralred and gold nanoparticles," International Journal of Environmental Analytical Chemistry, vol. 100, no. 4, pp. 408-418, 2020.

[32] M. Baghayeri, and M. Namadchian, "Fabrication of a nanostructured luteolin biosensor for simultaneous determination of levodopa in the presence of acetaminophen and tyramine: application to the analysis of some real samples," Electrochimica Acta, vol. 108, pp. 22-31, 2013.

[33] S. M. Golabi and D. Nematollahi, "Electrochemical study of catechol in ethanol: Application to the electro-organic synthesis of 4, 5-diethoxy-o-benzoquinone," Bulletin of Electrochemistry, vol. 13, no. 4, pp. 156-160, 1997.

[34] C. M. A. Brett and A. M. Oliveira Brett, "Electrochemistry: principles, methods, and applications," Oxford University Press, Oxford, 1993.

[35] J. A. Harrison and Z. A. Khan, Z. A "The oxidation of hydrazine on platinum in acid solution," Journal of Electroanalytical Chemistry and Interfacial Electrochemistry, vol. 28, no. 1, pp. 131-138, 1970.

SAKARYA ÜNİVERSİTESİ
FEN BİLİMLERİ ENSTİTÜSÜ DERGİSİ

Sakarya University Journal of Science
SAUJS

e-ISSN 2147-835X | Period Bimonthly | Founded: 1997 | Publisher Sakarya University |
http://www.saujs.sakarya.edu.tr/en/

Title: Machine-Part Formation for Cellular Manufacturing in Group Technology: An Application for Furniture Company

Authors: İlker GÜVEN,Fuat ŞİMŞİR

Recieved: 2020-12-17 00:00:00

Accepted: 2021-03-14 12:52:00.995000

Article Type: Research Article

Volume: 25
Issue: 2
Month: April
Year: 2021
Pages: 466-483

How to cite
İlker GÜVEN,Fuat ŞİMŞİR; (2021), Machine-Part Formation for Cellular Manufacturing in Group Technology: An Application for Furniture Company. Sakarya University Journal of Science, 25(2), 466-483, DOI:
https://doi.org/10.16984/saufenbilder.842423
Access link
http://www.saujs.sakarya.edu.tr/en/pub/issue/60672/842423

Sakarya University Journal of Science 25(2), 466-483, 2021

Machine-Part Formation for Cellular Manufacturing in Group Technology: An Application for Furniture Company

İlker GÜVEN[1], Fuat ŞİMŞİR[*1]

Abstract

Group technology's basic logic is grouping and producing products of the same type together. An important reason behind Group Technology becoming such an important topic is that nowadays companies have quite an extensive range and workshop type production has increased. Both fuzzy clustering and rank order clustering methods use for grouping parts and machines based on a part-machine matrix created from the production flow technique in order to increase productivity and reduce cost and workmanship required. In this study, Group Technology techniques such as the rank order clustering and fuzzy clustering methods were applied in order to increase the efficiency of the production line, reduce transportation between machines, and form a machine-parts groups in the wood cutting department of a furniture company producing modular furniture in Istanbul. The TOPSIS method was used to determine which products to take into account. According to results of the study, it is shown that fuzzy clustering method has overperformed rank order clustering method based on the evaluation criteria which are group productivity with 21,36%, group efficiency with 43,21% and grouping measure with 82,33%.

Keywords: Group Technology, Fuzzy Clustering, Rank Order Clustering, TOPSIS, Cellular Manufacturing

1. INTRODUCTION

Companies have simple steps to keep themselves in business. According to most people, selling their services or products, in other words making profit, is accepted as the first stage of those steps. Typically, all production plans are designed base on this concept. However, nowadays products' life cycles have become short and variation of products has increased. Also, production times have started to become shorter along with life cycle. Therefore, companies have to react to changes of variation of products as fast as they can. Otherwise, they may not be able to meet changes of product design and customer demands [1].

Flexible production systems can allow for a shorter adaptation period and make companies

[*]Corresponding author: fuatsimsir@karabuk.edu.tr
[1]Karabuk University, Faculty of Engineering, Industrial Engineering Department, 78050, Karabük.
E-Mail: ilkerguv@gmail.com
ORCID: https://orcid.org/0000-0002-2754-6893; https://orcid.org/0000-0001-7001-5951

more responsive against those changes. "Cellular Manufacturing" or "Group Technology", one of the applications of these systems used especially in the automotive sector, is becoming a widespread concept and has been successful as demonstrated by many studies [2].

In a simple definition, group technology (GT) is a production method that groups products using their similarity within all products to increase productivity.

GT's basic logic is grouping and producing products together that are same type. One of the biggest reasons that GT is so prominent is that is nowadays companies have quite an extensive range and workshop type production has increased.

Therefore, setting up machines or renewing the assembly line during the changing groups of products has become a problem because of setup process time. Companies cannot build an assembly line for each product. That's why they are grouped products and they build the assembly line for groups as a solution [3].

The philosophy of GT suggests similarities in repetitive works should be grouped together in three ways [4].

1. When doing similar activities, collecting activities together reduces time loses when passing to independent activities.
2. Standardization of activities that have a close relationship with each other, thus avoiding unnecessary repetition by focusing attention on certain differences
3. Collecting and storing information about repetitive problems, thus shortening the time spent searching for information and preventing attempts to solve previously solved problems

This method aims to combine the productivity of the GT flow line production system, which can be used in all sectors in which the production batch size is small, and the product variety is high, allowing for the flexibility of workshop type production. Products manufactured using GT are grouped according to their similarities in terms of design, planning and production activities, thereby increasing productivity in terms of time, workmanship and cost.

In this study, GT techniques were applied in order to increase the efficiency of a production line, reduce the transportation between the machines, and form machine-parts groups in the wood cutting department in a furniture company producing modular furniture in Istanbul. In section 2, literature review on the problem has been given. In section 3, methods used in the study have been explained and in section 4, given methods have been carried out with the data obtained from the manufacturer. Finally, in section 5, results and conclusions of the study have been discussed and suggestions have been given.

2. LITERATURE REVIEW

Many methods have been developed to apply cellular production techniques in group technology, which is more important than previous years. In the early era of GT, the main goal was calculating number of part-machine groups. Nowadays, reduced non-grouped and exceptional parts, attention to process priorities or similar machineries, evaluated process times and minimized cost of workload methods have been introduced in the literature. The biggest share in the development of these methods is undoubtedly development of computer technologies and heuristics, or artificial intelligence applications [5].

These methods ensure that the commonly produced parts are processed in the same cell throughout the production period. To accomplish this, cell creation problems are summarized in three basic steps [4]:

1. Determination of part families
2. Creating of machine cells
3. Assignment of part families to cells

Depending on the technique used, the steps are applied either simultaneously or sequentially. In cellular production, classification techniques or cell formation techniques can be used to create cells. Classification techniques are techniques

which consider part constraints such as shape, size, raw material, processing and processing times. It can be used visually or with the coding systems. There is no need for coding systems or visual evaluation in cell formation techniques, unlike classification techniques. Parts and machines can be grouped based on production process. A summarized list of clustering techniques is given for creating cells in Table 1 [4].

Table 1
Clustering techniques

Array-Based Clustering Techniques	**Hierarchical Clustering Techniques**	**Non-Hierarchical Clustering Techniques**	**Mathematical Programming Techniques**	**Graphic Theory Techniques**	**Artificial Intelligence Techniques**
Production Flow Analysis	Single Link Clustering	Ideal Core Algorithm	P-Median		Artificial Neural Networks
Rank Order Clustering	Average Link Clustering	GRAFICS Technique	Goal Programming		Fuzzy Logic
Direct Clustering			Dynamic Programming		Expert Systems
Bond Energy Algorithm			Assignment Technique		Genetic Algorithm
Cluster Identification Algorithm			Quad Programming		Simulated Annealing Algorithm
Modified Rank Order Clustering					Tabu Search Algorithm

Numerous studies have been done for creating part-machine families. While many applications have been implemented, many researchers use artificial intelligence techniques such as Tabu search algorithm, genetic algorithm, k-means clustering algorithm, fuzzy set theory [1], [3], [6–31]. In addition to these researchers, a few researchers have used series-based clustering techniques such as modified rank order clustering, goal programing [4], [12], [26], [32-34], and mathematical modeling techniques [18], [35–37]. Other researchers suggest a hybrid solution consisting of a combination of two or more different methods and they created performance evaluation criteria by comparing their methods with others for methods which they suggested in their papers. Also, constraints are generally considered such as ungrouped parts, cluster number, intercell transport costs as performance criteria. One of the recent research areas that gain interest is energy efficient scheduling in cellular manufacturing[38–40].

Another point that draws attention in the literature review is that there is a lack of information in the selection of part-machine for using clustering and the way the data is obtained. Most researchers have used part-machine matrices and data provided in previous papers in the literature for testing their methods in their papers. Researchers who have prepared datasets themselves have not provided a technique or explanation of why these data were selected. The issues such as which parts will be taken into account for the formation of cells, and why these parts should be selected, are steps to be considered in companies where machine and parts numbers are too numerous. If selected part is different from the production process of other parts in general, it is inevitable that the formed cells are only efficient for a small number of parts, as the cost of transportation intercell increases and production process will become more complicated. Seifoddini and Tjahjana (1999) encountered 300.000 pieces in the Harnischfeger Company in their work. They examined the product properties and determined that there were many parts in different dimensions passing through the same production processes and managed to classify them into 22 part groups by grouping them according to their size. Because so many parts cannot be placed on the part-machine matrix [41].

According to literature review, researchers have tried different approach to overcome high variety in the products and production route. Due to overcome the challenge created by different type of products and their production routes, in this study, TOPSIS method which is one of the ordering techniques, is used to choose the best product by several criteria, thus, the efficiency of production line is expected to be increased in terms of grouping the machines according to selected product. The idea of the logic behind this approach is, if production line is arranged according to the product which is produced most then that production line would represent most of the production.

3. MATERIAL AND METHOD

The fact that there are many product varieties in the company where the application is made poses a problem in the formation of machine part families. As machine cells cannot be formed for all of the products, there may be cases in which the cells formed are not suitable for all products. The parts of the product and the products to be used during the formation of the cells should show similarities with the other products produced in the company on the basis of the production routes and products with high demand. This would mean that the cell to be formed is more efficient. In view of that fact, product to be considered when cell is forming, is a step as important as forming cells. In this respect, necessity of combining TOPSIS with clustering methods is very high.

The use of multi-criteria decision-making methods in cases in which there are many alternatives and more than one evaluation criterion will give more accurate results because it is a scientific method. In this study, the TOPSIS (Technique for Order-Preference by Similarity to Ideal Solution) method, which is one of the multi-criteria decision-making methods, has been used in the determination of machine-parts groups.

Choosing the best multi criteria decision-making techniques is a hard process since each of them have advantages and disadvantages. The reason of using TOPSIS method among other multi criteria decision-making techniques is that, TOPSIS is one of the most popular and widely used method, its algorithm reliable and simple. Another reason of using the TOPSIS is it's interpretability and applicability in various fields [42]. One of the most important advantage of TOPSIS is that regardless the number of criteria and alternatives, it has same amount of process which provide flexibility[43]. Besides that, TOPSIS has standardization step that allow to use data where data range for each criterion can be various.

Machine-part matrices were created for the selected product with TOPSIS and machine-part cells were formed by using ROC (Rank Order Clustering) algorithm and Fuzzy Clustering algorithm.

3.1. TOPSIS

When the TOPSIS method is used, cases where the ideal solution is the nearest and the negative ideal solution is far away are examined among the alternatives. In this case optimal solution point is the farthest from the negative ideal solution and the closest to the positive ideal solution [44]. Relation of alternatives with positive and negative ideal solution is given in Figure 1.

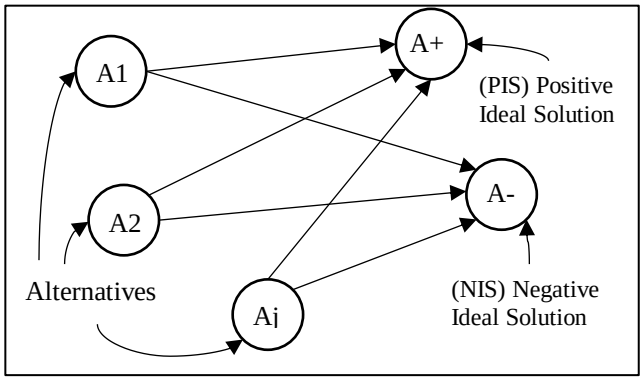

Figure 1 Distance of alternatives to ideal solutions

The general algorithm for TOPSIS is given below [45];

Step 1: The decision matrix is generated by the decision maker. The size of the matrix consists of m alternatives and n criteria. Alternatives are in rows, and criteria are in columns.

Step 2: After the decision matrix is formed, the standard matrix is formed by

using decision matrix. TOPSIS allows researchers to use different normalization techniques to form standard matrix which is important when range of values for each criterion is various. In this study vector normalization method is used to normalize decision matrix according to the equation (1). Where *i* is the alternative, *j* is the criteria.

$$r_{ij} = \frac{a_{ij}}{\sqrt{\sum_{i=1}^{m} a_{ij}^2}} (i = 1, \dots, m \; and \; j = 1, \dots, n) \quad (1)$$

Step 3: The weighted standard matrix is calculated using the equation (2). Here, the weight of *i* th criterion is expressed by *wi*. Total weights must equal one. ($\sum_{i=1}^{n} w_i = 1$).

$$V_{ij} = w_i * r_{ij} (i = 1, \dots, m \; and \; j = 1, \dots, n) \quad (2)$$

Step 4: In order to obtain a positive ideal solution, maximum values are taken for each column in the V matrix obtained by considering the structure of the problem. In order to obtain a negative ideal solution in the same way, the minimum values in each column are taken. Related equations are given at equations (3) and (4). *J* cluster is used for benefit criteria while *J'* cluster is used for cost criteria. The largest best rule in cluster *J* is valid, while the smallest best rule is in cluster *J'*.

$$A^* = \begin{cases} max_i\{v_{ij} | j \in J \\ min_i\{v_{ij} | j \in J' \end{cases} \quad (3)$$

$$A^- = \begin{cases} min_i\{v_{ij} | j \in J \\ max_i\{v_{ij} | j \in J' \end{cases} \quad (4)$$

Step 5: The distance of *i* th alternative to positive ideal solution (s_i^*) and the distance to negative ideal solution (s_i^-) are calculated using equations (5) and (6).

$$S_i^* = \sqrt{\sum_{j=1}^{n} (v_{ij} - v_j^*)^2} \quad (5)$$

$$S_i^- = \sqrt{\sum_{j=1}^{n} (v_{ij} - v_j^-)^2} \quad (6)$$

Step 6: In the calculation of the distance of the alternatives to ideal solution point, distance of alternative to positive and negative solution is used and indicated by C_i^*. The calculated ideal solution takes a value between $0 \leq C_i^* \leq 1$. It is calculated according to the equation (7).

$$C_i^* = \frac{S_i^-}{S_i^- + S_i^+} \quad (7)$$

An alternative with a higher C_i^* value is a better.

3.2. Rank Order Clustering

The Rank Order Clustering (ROC) technique is a method developed by King on the basis of a production flow technique for the formation of machine-part cells. In this technique, a machine-part matrix is formed according to the information on which machines the parts are processed.

Then, this matrix is applied to the King algorithm given in the following steps to formation machine-parts cells [46].

Step 1: After the formation of the machine-part matrix, the values in the binary system decreasing from left to right for each row are calculated. The values of 1 on each line are summed to calculate the decimal value of the line.
Step 2: Go to Step 6 if the calculated row order is the same as the current row order, otherwise go to Step 3.
Step 3: Rows of the machine-part matrix are rearranged in descending order according to the decimal values obtained in Step 1. The values are calculated for each part that has 1 value in matrix, which goes down from top to bottom decreasingly for the columns. The decimal sum of columns is calculated by the sum of those values.

Step 4: Go to Step 6 if the calculated column order is the same as the current column order, otherwise go to Step 5.
Step 5: Columns of the machine-part matrix are rearranged in descending order according to the decimal values obtained in Step 4. Go to Step 1.

Stop 6: Stop

3.3. Fuzzy Clustering

Fuzzy clustering is a clustering method which allows a single variable to be a member of multiple clusters in part by generalizing clustering methods such as K-Means or Medoid. In this method, the membership function of the clusters is distributed among all the clusters. In the fuzzification step, which is the classic fuzzy logic step, that membership function can take a value between 0 and 1, provided that sums are 1.

In the literature, there are two methods of fuzzy clustering. One of them is Fuzzy C-Means as known as FCM which follows c-partition logic. Other one is FANNY, hierarchical clustering method which based on fuzzy equality principle [47].

The algorithm used for Fuzzy Clustering, FANNY, was created by Kaufman and Rousseeuw [48]. The purpose of the algorithm is to minimize the goal function (8) consisting of cluster membership and distance.

$$C = \sum_{v=1}^{k} \frac{\sum_{i,j=1}^{n} u_{iv}^2 u_{jv}^2 d_{ij}}{2\sum_{j=1}^{n} u_{jv}^2} \quad (8)$$

d_{ij} gives the distance between *i* and *j* in the equation, while u_{iv} gives the coefficient of the unknown membership of the *i* unit to *v* cluster. Similarly, u_{jv} gives the coefficient of the unknown membership of the *j* unit to *v* cluster. Here *k* is the number of clusters and *n* is the total number of units. One of the constraints here is that the membership function cannot have a negative value and sum of membership function must be 1 in total for cluster.

In normal clustering algorithm, each object must have only one membership coefficient and this coefficient must be different from 0, in case no value other than 1 can be taken. Therefore, fuzzy objects also limited in normal clustering. Dunn's partition coefficient (9) can quantify the amount of fuzzification in the fuzzy clustering solution by measuring similarity between fuzzy clustering solution and corresponding normal clustering solution.

$$F_k(U) = \sum_{i=1}^{n} \sum_{v=1}^{k} u_{iv}^2 / n \quad (9)$$

U indicates the membership matrix and *n* indicates the number of objects in equation (9). Coefficient range is limited to between 1 and 1/k. When an object receives a value, which is 1/k, all objects get the same value. If this coefficient is to be standardized, it can be expressed as 0 (fully fuzzy) and 1 (not fuzzy). Standardized equation is given below (10). This process also known as defuzzification.

$$F'_k(U) = \frac{F_k(U) - (1/k)}{1 - (1/k)} \quad (10)$$

As a second function other than Dunn's partitioning coefficient, the mean square error can be used.

$$D_k(U) = \sum_{v=1}^{k} \sum_{i=1}^{n} (w_{iv} - u_{iv})^2 / n \quad (11)$$

The object expressed by *w* which is formed by normal clustering, is the most similar object to fuzzy object *u*. $D_k(U)$ is calculates the mean square error of fuzzy clustering in the closest way to normal clustering. Unlike Dunn's partitioning coefficient, it is expressed as 0 (not fuzzy) and 1-1/k (fully fuzzy). Standardized version of the equation is given equation (12).

$$D'_k(U) = \frac{D_k(U)}{1 - 1/k} \quad (12)$$

The general steps of algorithm are as shown below [1];

Step 1: Determine the number of clusters to be formed
Step 2: Select the membership function
Step 3: Determine the stopping criterion
Step 4: Find the starting matrix and calculate the membership value

Step 5: Calculate the initial values of cluster centers
Step 6: Updating membership functions according to initial values
Step 7: Continue until the difference between the calculated membership function and the current function is less than the stopping criterion

The biggest disadvantage of the fuzzy clustering method is that the number of clusters to be formed must be determined in advance. It is impossible to estimate it where companies with lots of parts and machines. For this reason, these algorithms experiment on various cluster numbers and calculate the results and error rates. Thus, the cluster number is determined where the error rate is lowest, the standardized version of Dunn's partition coefficient $F'_k(U)$ in equation 10 is the highest, and the standardized Kaufman coefficient $D'_k(U)$ in equation 12 is the lowest.

4. APPLICATION

In the scope of this study, a wood cutting workshop was taken into consideration in the production department of modular furniture manufacturer. The cells to be formed are evaluated according to the processes that parts undergo in the wood cutting workshop.

The study has three steps of implementation. First is determining which product parts were to be used to form machine-part matrix by TOPSIS method, then implementation of ROC method, and finally implementation of Fuzzy Clustering method. Steps of approach are illustrated in Figure 2.

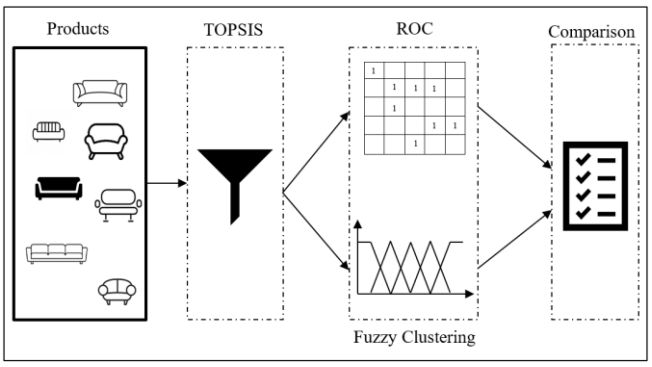

Figure 2 Proposed approach

Dataset for TOPSIS method is created based on the all products that company produce which are 277 products in total. Then, criteria are determined by the production planning team of the company considering the factors that might affect the production routes. Thus, information regarding criteria has been obtained for each product from production planning resources and dataset is finalized for TOPSIS.

After selection of the most suitable product with TOPSIS method, datasets which contains machine-part information of the product has been used to carry out grouping algorithms.

Considering 277 products that would be manufactured in the company, it is quite impossible to arrange production line for each of them. Therefore, decision makers need to choose a reference product that reflects the company's daily production route, which means that product could be the most seller one. Hence, there might be some other criteria that should be considered to choose right product. That is why TOPSIS is used to make a decision based on multi-criteria and choices.

4.1. TOPSIS Application

In the first step of the application, the selection of the product to be used is included. The TOPSIS algorithm given in section 3.1 will be used for this. The algorithm of the given TOPSIS method is coded and executed in the Microsoft Excel 2010 program using the Visual Basic for Applications (VBA) language.

A number of criteria must be assessed in order to choose which product parts to use. In order to cells to be efficient, some variables are defined as key roles, such as how many machines are used for the product to be processed, how many parts it has, size of product, production time and number of orders. Therefore, the criteria to be used in TOPSIS are as follows:

- Production time
- Number of parts
- Number of orders
- Size of product

- Number of machines

Expert opinions have been finalized to determine which of these criteria is more important by using Delphi method. Weights of the criteria are given in Table 2.

Table 2
Criteria and weights

Criteria	Weights(w)
Production Time	0,1
Number of parts	0,3
Number of orders	0,2
Size of product	0,15
Number of machines	0,25

The values of the products taken into consideration for the determined criteria and the decision matrix are given in Table 3.

Table 3
TOPSIS decision matrix

No	Product Code	Production Time (Min)	Number of Parts (PCS)	Number of Order (PCS)	Machine Number (PCS)	Size of Product (CM)
1	PKT.0001	423	45	8	7	120
2	PKT.0002	482	45	7	7	140
3	PKT.0003	312,5	31	11	10	60
4	PKT.0005	386,4	33	8	10	140
5	PKT.0006	415,5	34	10	10	180
6	PKT.0007	288	22	7	12	60
7	PKT.0009	388,9	34	6	12	140
.	.	.	.	.	.	.
56	PKT.0116	647	56	20	11	200
.	.	.	.	.	.	.
276	PKT.0966	245	55	5	10	70
277	PKT.0967	245	55	5	10	70

The results obtained after running the TOPSIS algorithm in the Microsoft Excel 2010 program are given in Table 4. According to TOPSIS algorithm each product has it's C_i^* point and products can be listed based on these points. As we mentioned in the section 3.1. higher point indicates the most suitable products.

When results were examined, the product with the highest C_i^* values, was product PRD.0116.

Table 4
*Ci** values obtained after TOPSIS application

No	Product Code	C_i^* Value	No	Product Code	C_i^* Value	No	Product Code	C_i^* Value
1	PRD.0001	0,291476	**55**	PRD.0115	0,360284	**78**	PRD.0186	0,243217
2	PRD.0002	0,286407	**56**	**PRD.0116**	**0,640292**	**79**	PRD.0187	0,249414
3	PRD.0003	0,266665	**57**	PRD.0117	0,143348	**80**	PRD.0188	0,260233
4	PRD.0005	0,240191	**58**	PRD.0119	0,441315	**81**	PRD.0189	0,325993
5	PRD.0006	0,293847	**59**	PRD.0120	0,293266	**82**	PRD.0190	0,272331
6	PRD.0007	0,172323	**60**	PRD.0121	0,112321	**83**	PRD.0191	0,33493
7	PRD.0009	0,239567	**61**	PRD.0122	0,145293	**84**	PRD.0192	0,283935

8	PRD.0010	0,258862	**62**	PRD.0123	0,166797	**85**	PRD.0193	0,34425
.	.	.	**.**	.	.	**.**	.	.
.	.	.	**.**	.	.	**.**	.	.
53	PRD.0113	0,341918	**76**	PRD.0180	0,204487	**276**	PRD.0966	0,315148
54	PRD.0114	0,146228	**77**	PRD.0185	0,237553	**277**	PRD.0967	0,315148

4.2. Rank Order Clustering (ROC) Application

In order to implement the ROC algorithm, a machine-part matrix of the product must be created. A machine-part matrix is shown in Table 5. It includes parts of PRD.0116 and the machines used for processing in the wood cutting workshop, along with the information obtained after examining bill of materials and route of product PRD.0116. In this matrix, 0 indicates that the parts are not processed in the corresponding machine, and 1 indicates that the parts are processed by the corresponding machine.

Table 5
Machine-part matrix of PRD.0116

PARTS / MACHINES	**M1**	**M2**	**M3**	**M4**	**M5**	**M6**	**M7**	**M8**	**M9**	**M10**	**M11**	**M12**
P1	0	0	1	0	0	0	0	0	0	0	0	1
P2 – P4	0	0	1	0	0	0	0	0	0	0	0	0
P5 – P8	0	0	0	0	0	0	0	1	1	0	0	0
P9	0	0	1	0	0	0	0	0	0	0	0	0
P10, P11, P13	1	1	0	0	0	0	0	0	0	0	0	0
P12, P14 –P16	0	0	1	0	0	0	0	0	0	0	0	0
P17, P39	1	1	0	0	0	0	0	0	0	0	0	0
P18 – P21	0	0	0	0	0	0	0	1	1	0	0	0
P22	0	0	0	0	1	1	1	0	0	0	1	0
P23	0	1	0	0	1	1	1	0	0	0	1	0
P24	0	0	0	0	1	1	1	0	1	0	0	0
P25	1	1	0	1	0	0	0	0	0	0	0	0
P26, P27	0	0	1	0	0	0	0	0	0	0	0	0
P28, P29	1	1	0	0	0	0	0	0	0	0	0	0
P30 – P32	0	0	1	0	0	0	0	0	0	0	0	0
P33	0	1	0	0	0	0	0	1	1	1	1	0
P34	0	1	0	0	0	0	0	1	1	0	1	0
P35	0	0	0	0	0	0	0	1	1	1	0	0
P36 – P38	0	0	0	0	0	0	0	1	1	0	0	0
P40 – P44	0	0	1	0	0	0	0	0	0	0	0	0
P45	0	0	1	0	0	0	0	0	0	1	0	0
P46	1	1	0	0	0	0	0	0	0	0	0	0
P47	0	0	1	0	0	0	0	0	0	0	0	0
P48, P49	0	0	1	0	0	0	0	0	0	0	0	1
P50	1	1	0	0	0	0	0	0	0	0	0	0
P51, P52	0	1	0	0	1	1	1	0	1	1	1	0
P53	0	0	1	1	0	0	0	0	0	0	0	0
P54	0	0	1	1	0	0	0	0	0	0	0	1
P55	0	0	0	0	1	1	1	0	1	0	1	0
P56	0	0	1	0	0	0	0	0	0	0	0	0

In implementing the ROC algorithm, the algorithm steps given in section 3.2 have been coded and executed in Microsoft Excel 2010 program using VBA. The obtained machine-part cells are given in Table 6.

Table 6
Formed machine-part cells

PARTS / MACHINES	M3	M12	M4	M10	M2	M1	M9	M11	M8	M5	M6	M7
P54	1	1	1	0	0	0	0	0	0	0	0	0
P1	1	1	0	0	0	0	0	0	0	0	0	0
P48	1	1	0	0	0	0	0	0	0	0	0	0
P49	1	1	0	0	0	0	0	0	0	0	0	0
P53	1	0	1	0	0	0	0	0	0	0	0	0
P45	1	0	0	1	0	0	0	0	0	0	0	0
P2	1	0	0	0	0	0	0	0	0	0	0	0
…	…	…	…	…	…	…	…	…	…	…	…	…
P56	1	0	0	0	0	0	0	0	0	0	0	0
P25	0	0	1	0	1	1	0	0	0	0	0	0
P33	0	0	0	1	1	0	1	1	1	0	0	0
P51	0	0	0	1	1	0	1	1	0	1	1	1
P52	0	0	0	1	1	0	1	1	0	1	1	1
P35	0	0	0	1	0	0	1	0	1	0	0	0
P10	0	0	0	0	1	1	0	0	0	0	0	0
P11	0	0	0	0	1	1	0	0	0	0	0	0
…	…	…	…	…	…	…	…	…	…	…	…	…
P50	0	0	0	0	1	1	0	0	0	0	0	0
P34	0	0	0	0	1	0	1	1	1	0	0	0
P23	0	0	0	0	1	0	0	1	0	1	1	1
P55	0	0	0	0	0	0	1	1	0	1	1	1
P5	0	0	0	0	0	0	1	0	1	0	0	0
…	…	…	…	…	…	…	…	…	…	…	…	…
P38	0	0	0	0	0	0	1	0	1	0	0	0
P24	0	0	0	0	0	0	1	0	0	1	1	1
P22	0	0	0	0	0	0	0	1	0	1	1	1

As a result of the ROC algorithm, three groups are formed. Part groups are shown in Figure 3 and machine groups are shown in Figure 4.

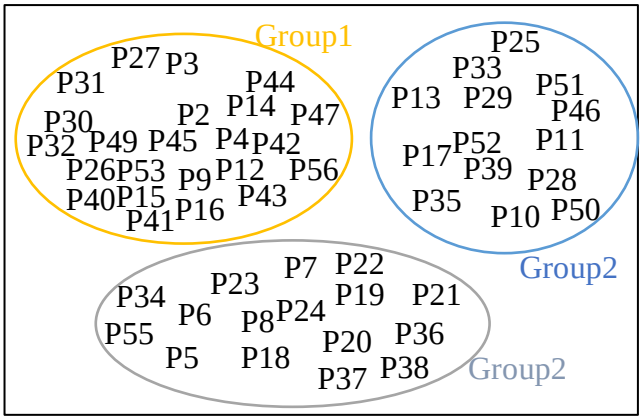

Figure 3 Part groups according to ROC results

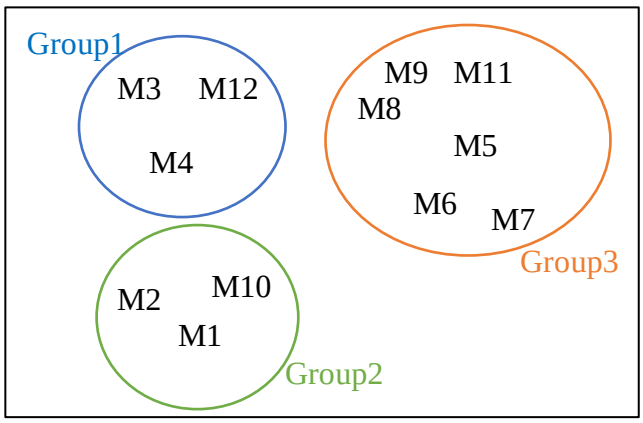

Figure 4 Machine groups according to ROC results

4.3. Fuzzy Clustering Application

In order to implement the fuzzy clustering algorithm, we need the machine-part matrix as in the ROC algorithm. For this reason, the machine-part matrix in Table 5, which is used in the application phase of the ROC algorithm, will also be used for fuzzy clustering in the same way.

For the fuzzy clustering algorithm, version 1.3.1093 of the R Studio was used free license. The steps to be followed when fuzzy clustering is applied are given below [1].

Step 1: Machine-part matrix is entered into the package program while machines are on the lines and parts are on the columns.
Step 2: Fuzzification level is determined.
Step 3: Cluster number is determined.
Step 4: Algorithm is executed for clustering
Step 5: Groups of machines and parts are written in matrix format.

The machine and part cells obtained after applying the steps are given in Table 7. Euclidean distance is used as distance criterion, and the fuzzification level is set to 2. Cluster number is set to be 4 after tried few different cluster numbers.

Table 7
Obtained machine-part cells after fuzzy clustering applied

Machine	Cluster	Part	Cluster	Part	Cluster	Part	Cluster	Part	Cluster	Part	Cluster
M1	1	**P1**	1	**P13**	3	**P25**	3	**P37**	2	**P49**	1
M2	1	**P2**	1	**P14**	1	**P26**	1	**P38**	2	**P50**	3
M3	2	**P3**	1	**P15**	1	**P27**	1	**P39**	3	**P51**	4
M4	1	**P4**	1	**P16**	1	**P28**	3	**P40**	1	**P52**	4
M5	3	**P5**	2	**P17**	3	**P29**	3	**P41**	1	**P53**	1
M6	3	**P6**	2	**P18**	2	**P30**	1	**P42**	1	**P54**	1
M7	3	**P7**	2	**P19**	2	**P31**	1	**P43**	1	**P55**	4
M8	4	**P8**	2	**P20**	2	**P32**	1	**P44**	1	**P56**	1
M9	4	**P9**	1	**P21**	2	**P33**	4	**P45**	1		
M10	1	**P10**	3	**P22**	4	**P34**	4	**P46**	3		
M11	3	**P11**	3	**P23**	4	**P35**	2	**P47**	1		
M12	1	**P12**	1	**P24**	4	**P36**	2	**P48**	1		

In order to be able to compare the formed cells with the ROC algorithm, the machines and parts are placed in the machine-part matrix in Table 8.

Table 8
Fuzzy clustering resultant machine-part matrix

PARTS / MACHINES	M3	M8	M9	M1	M2	M4	M10	M12	M5	M6	M7	M11
P1	1	0	0	0	0	0	0	1	0	0	0	0
..	..	…	…	…	…	…	…	…	…	…	…	…
P4	1	0	0	0	0	0	0	0	0	0	0	0
P9	1	0	0	0	0	0	0	0	0	0	0	0
P12	1	0	0	0	0	0	0	0	0	0	0	0
P14	1	0	0	0	0	0	0	0	0	0	0	0
P15	1	0	0	0	0	0	0	0	0	0	0	0
P16	1	0	0	0	0	0	0	0	0	0	0	0
P26	1	0	0	0	0	0	0	0	0	0	0	0
P27	1	0	0	0	0	0	0	0	0	0	0	0
P30	1	0	0	0	0	0	0	0	0	0	0	0
P31	1	0	0	0	0	0	0	0	0	0	0	0

P32	1	0	0	0	0	0	0	0	0	0	0	0
P40	1	0	0	0	0	0	0	0	0	0	0	0
…	…	…	…	…	…	…	…	…	…	…	…	…
P49	1	0	0	0	0	0	0	1	0	0	0	0
P53	1	0	0	0	0	1	0	0	0	0	0	0
P54	1	0	0	0	0	1	0	1	0	0	0	0
P56	1	0	0	0	0	0	0	0	0	0	0	0
P5	0	1	1	0	0	0	0	0	0	0	0	0
…	…	…	…	…	…	…	…	…	…	…	…	…
P8	0	1	1	0	0	0	0	0	0	0	0	0
P18	0	1	1	0	0	0	0	0	0	0	0	0
…	…	…	…	…	…	…	…	…	…	…	…	…
P21	0	1	1	0	0	0	0	0	0	0	0	0
P35	0	1	1	0	0	0	1	0	0	0	0	0
…	…	…	…	…	…	…	…	…	…	…	…	…
P38	0	1	1	0	0	0	0	0	0	0	0	0
P10	0	0	0	1	1	0	0	0	0	0	0	0
P11	0	0	0	1	1	0	0	0	0	0	0	0
P13	0	0	0	1	1	0	0	0	0	0	0	0
P17	0	0	0	1	1	0	0	0	0	0	0	0
P25	0	0	0	1	1	1	0	0	0	0	0	0
P28	0	0	0	1	1	0	0	0	0	0	0	0
P29	0	0	0	1	1	0	0	0	0	0	0	0
P39	0	0	0	1	1	0	0	0	0	0	0	0
P46	0	0	0	1	1	0	0	0	0	0	0	0
P50	0	0	0	1	1	0	0	0	0	0	0	0
P22	0	0	0	0	0	0	0	0	1	1	1	1
P23	0	0	0	0	1	0	0	0	1	1	1	1
P24	0	0	1	0	0	0	0	0	1	1	1	0
P33	0	1	1	0	1	0	1	0	0	0	0	1
P34	0	1	1	0	1	0	0	0	0	0	0	1
P51	0	0	1	0	1	0	1	0	1	1	1	1
P52	0	0	1	0	1	0	1	0	1	1	1	1
P55	0	0	1	0	0	0	0	0	1	1	1	1

Fuzzy clustering resulted in 4 groups. Part groups are shown in Figure 5 and machine groups are shown in Figure 6. Part and machine locations on the graphs are extracted from the Fuzzy Clustering algorithm.

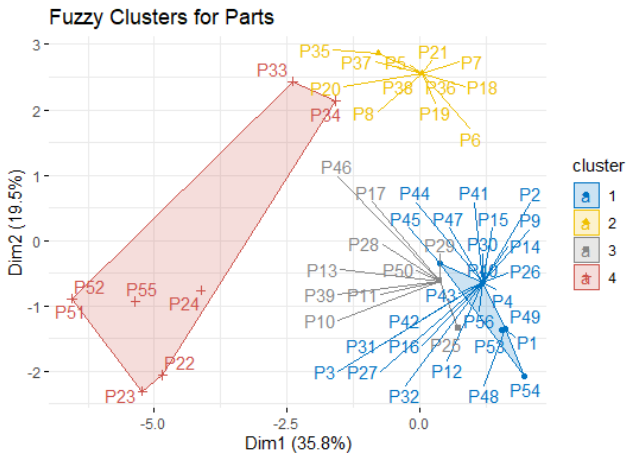

Figure 5 Part groups according to Fuzzy Clustering results

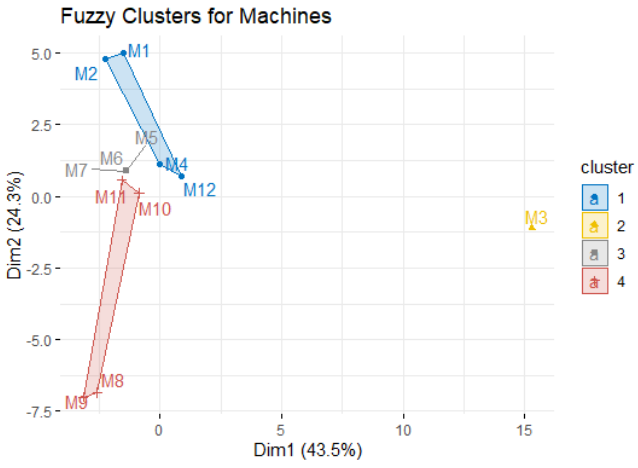

Figure 6 Machine groups according to Fuzzy Clustering results

The membership degrees of the machines to clusters are given in Table 9.

Table 9
Membership degrees of the machines

Machine	Cluster	Membership Degree
M1	1	0.5901
M2	1	0.5406
M3	2	0.9720
M4	1	0.4096
M5	3	0.9791
M6	3	0.9791
M7	3	0.9791
M8	4	0.7132
M9	4	0.6556
M10	1	0.3557
M11	3	0.3787
M12	1	0.3700

Obtained Dunn's coefficient for part clustering is 0.77 and standardized version of it is 0.69. On the other hand, Dunn's coefficient for machine clustering is 0.45 and standardized version is 0.26. Thus, fuzzy clustering for machine was successful than fuzzy clustering for parts.

4.4. Calculation of Evaluation Criteria

When the evaluation methods used for the success of the obtained machine-part matrix are examined, the three different evaluation criteria are found as stated in the literature. The most commonly used of these criteria is group productivity [1], [3], [13], [49].

- Group efficiency (%)
- Group productivity (%)
- Grouping measure (%)

The equations used to calculate these criteria are given below.

Group productivity (η);

$$\eta = q.\eta_1 + (1-q).\eta_2 \quad (13)$$

$$\eta_1 = \frac{e_d}{\sum_{r=1}^{k} M_r.N_r} \quad (14)$$

$$\eta_2 = 1 - \left[\frac{e_0}{M.N - \sum_{r=1}^{k} M_r.N_r}\right] \quad (15)$$

Group efficiency (r);

$$r = 1 - \frac{e_0 + e_v}{e + e_v} \quad (16)$$

Grouping measure (η_p);

$$\eta_p = \eta_u - \eta_m \quad (17)$$

$$\eta_u = \eta_1,\ \eta_m = \frac{e_0}{e_d} \quad (18)$$

Here;

e_d = Number of 1 in diagonal blocks

e_0 = Number of 1 out of diagonal blocks

q = Equation constant (0,5)

k = Cell number

M = Machine number

N = Part number

M_r = Machine number in r th cell, N_r = Part number in r th cell

e = Total process number

e_v = Number of 0 in diagonal blocks

The group productivity, group efficiency and grouping measure resultant from the ROC algorithm and Fuzzy Clustering are given in Table 10.

Table 10
Comparing of ROC and Fuzzy Clustering methods

Evaluation Criteria	ROC Algorithm	Fuzzy Clustering
Cell Number (k)	3	4
Group Productivity (η)	0,7129	0,8652
Group Efficiency (r)	0,4297	0,6154
Grouping Measure (η_p)	0,2875	0,5242
Number of 1 in diagonal blocks (e_d)	101	96
Number of 1 out of diagonal blocks (e_0)	19	24
Equation constant (q)	0,5	0,5
Number of 0 in diagonal blocks (e_v)	115	36
Total process number (e)	120	120

5. CONCLUSIONS AND DISCUSSION

In this study, it was realized that product selection is a multi-criteria decision-making problem. TOPSIS, one of the most effective methods used in multi-criteria decision making problems, has been used [44], [45], [50]. The products in the sofa group produced by the manufacturer have been evaluated according to the four criteria determined in the selection of the most suitable product. Thus, contrary to previous studies in the literature, a scientific approach has been adopted, as in the case of Seifoddini and Tjahjana, only differing in the process of selecting parts in the problems of forming machine-parts families [41].

Comparing the ROC algorithm and the Fuzzy Clustering method, the Fuzzy Clustering method showed better results as shown in Table 11.

Table 11
Advantages of Fuzzy Clustering Algorithm over ROC

Evaluation Criteria	Fuzzy Clustering > ROC
Group Productivity (η)	21,36%
Group Efficiency (r)	43,21%
Grouping Measure (η_p)	82,33%

Four production cells were created with the Fuzzy Clustering algorithm, while three production cells were created with the ROC algorithm. In the ROC algorithm, there are 101 operations included in the production cell, while in the Fuzzy Clustering algorithm this number decreases to 96 operations. While the success of the ROC algorithm reached 84.16%, because the grouping success covers 101 of 120 operations, the Fuzzy Clustering algorithm grouped 96 of 120 operations and remained at 80%. In evaluating of two methods group productivity, group efficiency, and grouping measure are important criteria, in addition to grouping the operations. These three criteria are taken into account in the literature. For this reason, the Fuzzy Clustering algorithm would be a better choice.

Funding

The author (s) has no received any financial support for the research, authorship or publication of this study.

The Declaration of Conflict of Interest/ Common Interest

No conflict of interest or common interest has been declared by the authors.

Authors' Contribution

The first author contributed 50%, the second author 50%.

The Declaration of Ethics Committee Approval

This study does not require ethics committee permission or any special permission

The Declaration of Research and Publication Ethics

The authors of the paper declare that they comply with the scientific, ethical and quotation rules of SAUJS in all processes of the paper and that they do not make any falsification on the data collected. In addition, they declare that Sakarya University Journal of Science and its editorial board have no responsibility for any ethical violations that may be encountered, and that this study has not been evaluated in any academic publication environment other than Sakarya University Journal of Science.

REFERENCES

[1] T. Tunacan, "Machine and Part Cell Formation Using Fuzzy and K-Means Clustering Methods," *Electron. Lett. Sci. Eng.*, vol. 1, no. 1, pp. 33–41, 2005.

[2] E. A. Demirtaş, "Hücre oluşturma yöntemlerine ilişkin bir değerlendirme," *Osmangazi Üniversitesi Müh.Mim.Fak.Dergisi*, vol. 17, no. 2, 2004.

[3] M. C. Kaplan, "Grup Teknolojilerinde Kümelendirme Yöntemlerine Sezgisel Yaklaşımlar ve Bir Uygulama," İstanbul Üniversitesi, 2008.

[4] E. Babalı, "Grup Teknolojisinde Parça Ailesi ve İmalat Hücresi Oluşturma: Bir Örnek İnceleme," Sakarya Üniversitesi, 2007.

[5] Y. Gökşen and S. Erdem, "Hücresel Üretim Sisteminde Makine-Parça Ailelerinin Oluşturulmasında Dengeli Talep-Kapasite ve Dengesiz Talep-Kapasite Durumunun Analizi," *D.E.Ü.İ.İ.B.F.Dergisi*, vol. 18, no. 2, pp. 99–111, 2003.

[6] M. Imran, C. Kang, Y. Hae Lee, J. Zaib, and H. Aziz, "Cell Formation in a Cellular Manufacturing System Using Simulation Integrated Hybrid Genetic Algorithm," *Comput. Ind. Eng.*, vol. 105, pp. 123–135, 2016, doi: 10.1016/j.cie.2016.12.028.

[7] A. Tariq, I. Hussain, and A. Ghafoor, "A hybrid genetic algorithm for machine-part grouping," *Comput. Ind. Eng.*, vol. 56, no. 1, pp. 347–356, 2009, doi: 10.1016/j.cie.2008.06.007.

[8] T. L. James, E. C. Brown, and K. B. Keeling, "A hybrid grouping genetic algorithm for the cell formation problem," *Comput. Oper. Res.*, vol. 34, no. 7, pp. 2059–2079, 2007, doi: 10.1016/j.cor.2005.08.010.

[9] I. Mahdavi, M. M. Paydar, M. Solimanpur, and A. Heidarzade, "Genetic algorithm approach for solving a cell formation problem in cellular manufacturing," *Expert Syst. Appl.*, vol. 36, no. 3 PART 2, pp. 6598–6604, 2009, doi: 10.1016/j.eswa.2008.07.054.

[10] T.-H. Wu, C.-C. Chang, and S.-H. Chung, "A simulated annealing algorithm for manufacturing cell formation problems," *Expert Syst. Appl.*, vol. 34, no. 3, pp. 1609–1617, 2008, doi: 10.1016/j.eswa.2007.01.012.

[11] A. M. Zohrevand, H. Rafiei, and A. H. Zohrevand, "Multi-objective dynamic cell formation problem: A stochastic programming approach," *Comput. Ind. Eng.*, vol. 98, pp. 323–332, 2016, doi: 10.1016/j.cie.2016.03.026.

[12] S. Karthikeyan, M. Saravanan, and K. Ganesh, "GT machine cell formation problem in scheduling for cellular manufacturing system using meta-heuristic method," *Procedia Eng.*, vol. 38, pp. 2537–2547, 2012, doi: 10.1016/j.proeng.2012.06.299.

[13] C. R. Shiyas and V. Madhusudanan Pillai, "A mathematical programming model for manufacturing cell formation to develop multiple configurations," *J. Manuf. Syst.*, vol. 33, no. 1, pp. 149–158, 2014, doi: 10.1016/j.jmsy.2013.10.002.

[14] H. Nouri and T. S. Hong, "Development of bacteria foraging optimization algorithm for cell formation in cellular manufacturing system considering cell load variations," *J. Manuf. Syst.*, vol. 32, no. 1, pp. 20–31, 2013, doi: 10.1016/j.jmsy.2012.07.014.

[15] B. Bootaki, I. Mahdavi, and M. M. Paydar, "A hybrid GA-AUGMECON method to solve a cubic cell formation problem considering different worker skills," *Comput. Ind. Eng.*, vol. 75, no. 1, pp. 31–40, 2014, doi: 10.1016/j.cie.2014.05.022.

[16] Z. Güngör and F. Arıkan, "Application of fuzzy decision making in part-machine grouping," *Int. J. Prod. Econ.*, vol. 63, pp. 181–193, 2000, doi: 10.1016/S0925-5273(99)00010-9.

[17] M. M. Paydar and M. Saidi-Mehrabad, "A hybrid genetic-variable neighborhood search algorithm for the cell formation problem based on grouping efficacy," *Comput. Oper. Res.*, vol. 40, no. 4, pp. 980–990, 2013, doi: 10.1016/j.cor.2012.10.016.

[18] I. Mahdavi, E. Teymourian, N. T. Baher, and V. Kayvanfar, "An integrated model for solving cell formation and cell layout problem simultaneously considering new situations," *J. Manuf. Syst.*, vol. 32, no. 4, pp. 655–663, 2013, doi: 10.1016/j.jmsy.2013.02.003.

[19] S. E. Cömert, S. H. Gökler, and H. R. Yazgan, "Hücresel İmalat Sistemlerinin K-Means Algoritması ve Genetik Algoritma İle Tasarlanması: Bir Uygulama," *Acad. Platf. J. Eng. Sci.*, vol. 4, no. 3, Oct. 2016, doi: 10.21541/apjes.06335.

[20] L. Jie, W. Liu, Z. Sun, and S. Teng, "Hybrid fuzzy clustering methods based on improved self-adaptive cellular genetic algorithm and optimal-selection-based fuzzy c-means," *Neurocomputing*, vol. 0, pp. 1–17, 2017, doi: 10.1016/j.neucom.2017.03.068.

[21] R. G. Özdemir, G. Gençyilmaz, and T. Aktin, "The modified fuzzy art and a two-stage clustering approach to cell design," *Inf. Sci. (Ny).*, vol. 177, no. 23, pp. 5219–5236, 2007, doi: 10.1016/j.ins.2007.06.027.

[22] A. Rostami, M. M. Paydar, and E. Asadi-Gangraj, "A hybrid genetic algorithm for integrating virtual cellular manufacturing with supply chain management considering new product development," *Comput. Ind. Eng.*, vol. 145, p. 106565, 2020, doi: https://doi.org/10.1016/j.cie.2020.106565.

[23] S. Büyüksaatçı Kiriş and F. Tüysüz, "İmalat Hücresi Oluşturulması İçin Farklı Kümeleme Yöntemlerinin Performans Karşılaştırması," *SAÜ Fen Bilim. Enstitüsü Derg.*, pp. 1–1, Oct. 2017, doi: 10.16984/saufenbilder.310267.

[24] C. Mejía-Moncayo and O. Battaia, "A hybrid optimization algorithm with genetic and bacterial operators for the design of cellular manufacturing systems," *IFAC-PapersOnLine*, vol. 52, no. 13, pp. 1409–1414, 2019, doi: https://doi.org/10.1016/j.ifacol.2019.11.396.

[25] S. Kaparthi, N. C. Suresh, and R. P. Cerveny, "An improved neural network leader algorithm for part-machine grouping in group technology," *Eur. J. Oper. Res.*, vol. 69, no. 3, pp. 342–356, 1993, doi: 10.1016/0377-2217(93)90020-N.

[26] B. Adenso-Díaz, S. Lozano, and I. Eguía, "Part-machine grouping using weighted similarity coefficients," *Comput. Ind. Eng.*, vol. 48, no. 3, pp. 553–570, May 2005, doi: 10.1016/j.cie.2003.03.008.

[27] C. Andrés and S. Lozano, "A particle swarm optimization algorithm for part-machine grouping," *Robot. Comput. Integr. Manuf.*, vol. 22, no. 5–6, pp. 468–474, 2006, doi: 10.1016/j.rcim.2005.11.013.

[28] Y. Won and K. R. Currie, "Fuzzy ART/RRR-RSS: a two-phase neural network algorithm for part-machine grouping in cellular manufacturing.," *Int. J. Prod. Res.*, vol. 45, no. 9, pp. 2073–2104, 2007, doi: 10.1080/00207540600635227.

[29] J. W. Owsiński, J. Stańczak, K. Sep, and H. Potrzebowski, "Machine-Part Grouping in Flexible Manufacturing: Formalisation and the Use of Genetic Algorithms," *IFAC Proc. Vol.*, vol. 43, no. 4, pp. 216–221, 2010, doi: 10.3182/20100701-2-PT-4011.00038.

[30] B. Shirazi, H. Fazlollahtabar, and I. Mahdavi, "A six sigma based multi-objective optimization for machine grouping control in flexible cellular manufacturing systems with guide-path flexibility," *Adv. Eng. Softw.*, vol. 41, no. 6, pp. 865–873, 2010, doi: 10.1016/j.advengsoft.2010.02.002.

[31] S. Zolfaghari and M. Liang, "A new

genetic algorithm for the machine/part grouping problem involving processing times and lot sizes," *Comput. Ind. Eng.*, vol. 45, no. 4, pp. 713–731, 2003, doi: 10.1016/j.cie.2003.09.003.

[32] E. Atmaca, "Grup Teknolojisi Hücrelerinin Tasarımı ve Amaç Programlama Yaklaşımının Uygulanması," *Süleyman Demirel Üniversitesi İktisadi ve İdari Bilim. Fakültesi Derg.*, vol. 7, no. 2, pp. 285–298, 2002.

[33] N. Amruthnath and T. Gupta, "Modified Rank Order Clustering Algorithm Approach by Including Manufacturing Data," *IFAC-PapersOnLine*, vol. 49, no. 5, pp. 138–142, 2016, doi: 10.1016/j.ifacol.2016.07.103.

[34] T. Kataoka, "A multi-period mixed integer programming model on reconfigurable manufacturing cells," *Procedia Manuf.*, vol. 43, pp. 231–238, 2020, doi: https://doi.org/10.1016/j.promfg.2020.02.147.

[35] J. R. Brown, "A capacity constrained mathematical programming model for cellular manufacturing with exceptional elements," *J. Manuf. Syst.*, vol. 37, pp. 227–232, 2015, doi: 10.1016/j.jmsy.2014.09.005.

[36] I. Mahdavi, A. Aalaei, M. M. Paydar, and M. Solimanpur, "A new mathematical model for integrating all incidence matrices in multi-dimensional cellular manufacturing system," *J. Manuf. Syst.*, vol. 31, no. 2, pp. 214–223, 2012, doi: 10.1016/j.jmsy.2011.07.007.

[37] S. Arumugam, J. Saral, and A. Somasundaram, "Minimizing the Number of Exceptional Edges in Cellular Manufacturing Problem," *Electron. Notes Discret. Math.*, vol. 53, pp. 465–472, 2016, doi: 10.1016/j.endm.2016.05.040.

[38] V. Saddikuti and V. Pesaru, "NSGA Based Algorithm for Energy Efficient Scheduling in Cellular Manufacturing," *Procedia Manuf.*, vol. 39, pp. 1002–1009, 2019, doi: https://doi.org/10.1016/j.promfg.2020.01.379.

[39] Z. Hong, Z. Zeng, and L. Gao, "Energy-efficiency scheduling of multi-cell manufacturing system considering total handling distance and eligibility constraints," *Comput. Ind. Eng.*, p. 106998, 2020, doi: https://doi.org/10.1016/j.cie.2020.106998.

[40] A. Iqbal and K. A. Al-Ghamdi, "Energy-efficient cellular manufacturing system: Eco-friendly revamping of machine shop configuration," *Energy*, vol. 163, pp. 863–872, 2018, doi: https://doi.org/10.1016/j.energy.2018.08.168.

[41] H. Seifoddini and B. Tjahjana, "Part-family formation for cellular manufacturing: A case study at Harnischfeger," *Int. J. Prod. Res.*, vol. 37, no. 14, pp. 3263–3273, 1999, doi: 10.1080/002075499190275.

[42] D. Yu and T. Pan, "Tracing knowledge diffusion of TOPSIS: A historical perspective from citation network," *Expert Syst. Appl.*, vol. 168, p. 114238, 2021, doi: https://doi.org/10.1016/j.eswa.2020.114238.

[43] F. Sari, "Forest fire susceptibility mapping via multi-criteria decision analysis techniques for Mugla, Turkey: A comparative analysis of VIKOR and TOPSIS," *For. Ecol. Manage.*, vol. 480, p. 118644, 2021, doi: https://doi.org/10.1016/j.foreco.2020.118644.

[44] M. N. Kasirian and R. M. Yusuff, "An integration of a hybrid modified TOPSIS with a PGP model for the supplier selection with interdependent criteria," *Int. J. Prod. Res.*, vol. 51, no. 4, pp. 1037–1054, 2013,

doi: 10.1080/00207543.2012.663107.

[45] M. Yurdakul and Y. T. Ic, "Development of a performance measurement model for manufacturing companies using the AHP and TOPSIS approaches," *Int. J. Prod. Res.*, vol. 43, no. 21, pp. 4609–4641, 2005, doi: 10.1080/00207540500161746.

[46] J. R. King, "Machine-component group formation in group technology," *Omega*, vol. 8, no. 2, pp. 193–199, 1980, doi: 10.1016/0305-0483(80)90023-7.

[47] H. Küçükönder, T. Ayaşan, and H. Hızlı, "Classification of Holstein Dairy Cattles in Terms of Parameters Some Milk Component Belongs by Using The Fuzzy Cluster Analysis," *Kafkas Univ. Vet. Fak. Derg.*, vol. 23, no. 4, pp. 601–606, 2015, doi: 10.9775/kvfd.2015.12987.

[48] L. Kaufman and P. J. Rousseuw, "Finding Groups in Data: An Introduction to Cluster Analysis.," *Biometrics*, vol. 47, no. 2, p. 788, Jun. 1991, [Online]. Available: https://www.jstor.org/stable/2532178?origin=crossref.

[49] C. Suresh Kumar and M. P. Chandrasekharan, "Grouping efficacy: a quantitative criterion for goodness of block diagonal forms of binary matrices in group technology," *Int. J. Prod. Res.*, vol. 28, no. 2, pp. 233–243, 1990, doi: 10.1080/00207549008942706.

[50] H. S. Shih, H. J. Shyur, and E. S. Lee, "An extension of TOPSIS for group decision making," *Math. Comput. Model.*, vol. 45, no. 7–8, pp. 801–813, 2007, doi: 10.1016/j.mcm.2006.03.023.

SAKARYA ÜNİVERSİTESİ
FEN BİLİMLERİ ENSTİTÜSÜ DERGİSİ

Sakarya University Journal of Science
SAUJS

e-ISSN 2147-835X | Period Bimonthly | Founded: 1997 | Publisher Sakarya University |
http://www.saujs.sakarya.edu.tr/en/

Title: Vehicular and industrial sources of PGEs, Au and Ce in surface soil and roadside soils and dusts from two cities of Turkey

Authors: Murat ÖZEN,Songül AKBULUT ÖZEN, Uğur ÇEVİK

Recieved: 2020-07-07 15:18:00

Accepted: 2021-03-15 12:52:00.995000

Article Type: Research Article

Volume: 25
Issue: 2
Month: April
Year: 2021
Pages: 484-497

How to cite
Murat ÖZEN,Songül AKBULUT ÖZEN, Uğur ÇEVİK; (2021), Vehicular and industrial sources of PGEs, Au and Ce in surface soil and roadside soils and dusts from two cities of Turkey. Sakarya University Journal of Science, 25(2), 484-497, DOI: https://doi.org/10.16984/saufenbilder.765677
Access link
http://www.saujs.sakarya.edu.tr/en/pub/issue/60672/765677

Sakarya University Journal of Science 25(2), 484-497, 2021

Vehicular and industrial sources of PGEs, Au and Ce in surface soil and roadside soils and dusts from two cities of Turkey

Murat ÖZEN[1], Songül AKBULUT ÖZEN[2*], Ugur CEVIK[3]

Abstract

In this study, rhodium, palladium, platinum, gold and cerium were determined by ICP-MS after trace-matrix separation in roadside dusts and soil samples along different motorways in Ankara and Bursa, and in soil samples taken from industrial locations in Nilüfer, Bursa. The clear presence of Pd and Rh was determined at different traffic locations. Platinum remained below the method's quantification limit for most of the samples. Results showed that both cities showed relatively high concentrations of; Rh and Pt in tunnels and downtowns, Pd in tunnels, bus stations and crossroads, and Au in downtowns. Consistent with the daily road traffic, relatively high concentrations of Rh, Pd and Pt were determined for Ankara. Based on the limited data available for Pt, Pt:Pd ratios varied between 0.04 and 0.25, and Pt:Rh ratios varied between 0.59 and 2.1. Measurements at the industrial location showed an average Rh and Pd concentration of 11 and 359 µg/kg, respectively. On the other hand, Au concentrations remained below the method's quantification limit except for one sampling location. The average Ce concentration was determined as 23 mg/kg. Platinum remained below the method's quantification limit for all industrial sampling locations. Overall, high average Rh and Pt concentrations were determined at the traffic sites, while higher average Pd concentration was determined at the industrial locations. Cerium remained consistently below the earth's crustal levels, which infers that no anthropogenic source can be attributed to Ce.

Keywords: platinum group elements, vehicular traffic, industrial region, surface soil, roadside dusts.

1. INTRODUCTION

Platinum group elements (PGEs) consist of six elements, namely iridium (Ir), osmium (Os), palladium (Pd), platinum (Pt), rhodium (Rh), and ruthenium (Ru). They are naturally present in the earth's crust in a few parts per billion. PGEs are categorized under precious metals together with gold (Au) due to their economic value and their rare occurrences. These precious elements are the

* Corresponding author: songul.akbulut@btu.edu.tr
[1] Bursa Technical University, Department of Chemistry, 16310 Bursa, Turkey, E-mail: murat.ozen@btu.edu.tr, ORCID: 0000-0002-3589-2059
[2] Bursa Technical University, Department of Physics, 16310 Bursa, Turkey, E-mail: songul.akbulut@btu.edu.tr, ORCID: 0000-0001-8025-2141
[3]Karadeniz Technical University, Department of Physics, TR-61080 Trabzon, Turkey E-mail: ugurcevik61@gmail.com,
ORCID: 0000-0002-7513-5175

least abundant elements in the earth's crust and are present in the environment in ultra-trace quantities. The bulk of the continental crust includes 0.38, 1.50 and 2.00 μg/kg of, respectively, Rh, Pd and Pt, while the lithosphere contains 0.10, 1 – 10.0 and 15.0 μg/kg of Rh, Pd and Pt, respectively [1]. The upper continental crust, on the other hand, contains 0.018, 0.599, 0.526 μg/kg Rh, Pd and Pt respectively [2].

Platinum group elements are applied in, e.g., fuel cells, electronics, cancer therapies, catalysts and are thus strategic elements. The automotive sector is leading on demand for PGEs (especially Pt, Pd and Rh) [3].

Emission of PGEs into the environment has been traced back to exhaust catalysts in automotive catalytic converters. Due to traffic density and industrial organizations large cities are obvious locations where the potential hazardous effects of PGEs might be observed [4]. A number of articles has been published concerning PGEs and their increasing concentrations in different environmental media such as: air and airborne particulate matter [5-6], soil [7], road dust [8–10], vegetation [11], organisms [12-13], and sewage sludge [14].

Some PGE elements and their complex salts such as Pd-, Rh- and Pt-chlorides, have been reported as potential risks, not only to the environment [15-16], but also to the human health, causing tumor, asthma, rhinoconjuctivitis and other serious health problems [16-17]. While particulate PGEs are said to be biologically inert, soluble PGEs can pose an environmental hazard due to their biological availability, which leads to accumulation in the environment [18-19]. In addition, PGEs are resistant to poisoning of sulfur oxide residues in the exhaust [17]. PGEs have the required potential for the chemical reduction of pollutants such as hydrocarbons, nitrogen oxides, and carbon monoxide.

Due to its use in automotive electronics (electronic fuel injection, anti-lock brake and ignition control) in recent years, gold (Au) was additionally measured in this study [20].

PGEs are coated onto the surface of the catalytic converter together with cerium dioxide, usually in combination with zirconium dioxide, to promote oxygen storage and thermal stability [21]. Because of this, cerium is emitted with PGE exhaust catalysts. In many countries, CeO_2 nanoparticles are added to diesel fuels to improve fuel combustion efficiency and to reduce soot emissions [22]. Several studies have reported Ce accumulation in the environment [23-25]. Potential human health implications of Ce emissions have received limited attention. In this study, PGEs, Au and Ce were investigated in the summer of 2010 at different traffic locations with varying daily traffic and driving styles in Ankara and Bursa, and at an industrial area in Nilufer, Bursa. The available publications on PGEs in Turkey are confined to ore mines, such as ophiolitic chromitite deposits [27-28]. Anthropogenic input of PGEs, Au and Ce in the environment received much less attention, and to the best of the authors' knowledge no publication has been made on the subject in Turkey. The aim of this study is to examine PGEs, Au, Ce and their enrichment in the environment especially in roadside dust and roadside soil. The concentrations of these elements will be examined as a function of proximity to roadways with high to medium traffic densities in two major Turkish cities (Bursa and Ankara). Soil samples collected at nine locations from a heavily industrialized region in Bursa was also examined.

2. MATERIAL AND METHODS

2.1. Study area

In this study, traffic-sampling locations in Ankara and Bursa with different characteristics were selected, such as parking lots, highways, bus stations, tunnels, downtown, and crossroads. Road characteristics that are believed to be of importance in this study are: start-stop frequency of vehicles, speed limits, closed environments such as tunnels, and the average daily road occupancy. All sampling locations geographical coordinates are given in Table 1. The average road occupancy for the year 2010 as given by the Road, Traffic and Safety Association can be summarized as follows: State roads were

occupied by 526.541 vehicle per day (annual average) in Bursa and 478.134 vehicle per day (annual average) in Ankara. The yearly average number of vehicles per day on motorways in Bursa was 67.727, of which 60.67% were automobiles, and 91.168 vehicle per day in Ankara, of which 71.00% were automobiles [29]. The average number of vehicles at the selected roads, their average speed and sample designations are summarized in Table 1.

Table 1
Traffic sampling locations, vehicle speed, and densities [26]

Sampling Points	Speed (km/h)		Location Bursa	Av. vehicle per day		Location Ankara	Av. vehicle per day
Parking Lot	-	B1	Uluyol (40°11'37.7"N, 29°04'12.9"E)	1500	A1	Mesrutiyet St. ($39^0$55'07.1"N, $32^0$51'39.7"E)	3000
Highway	> 120	B2	Istanbul-Ankara road ($40^0$15'59.9"N, $28^0$57'15.8"E)	28000	A2	Konya road ($39^0$53'18.8"N, $32^0$48'44.4"E)	45000
Bus Station	-	B3	Bursa bus terminal ($40^0$15'55.6", $29^0$03'12.9"E)	850	A3	Ankara bus terminal ($39^0$55'05.9"N, $32^0$48'44.4'E)	1250
Tunnel	< 90	B4	Izmir road ($40^0$12'41.9"N, $28^0$56'25.3"E)	13000	A4	M. Kemal St. ($39^0$54'49.4"N, $32^0$51'09.4"E)	30000
Downtown	< 50 – 60	B5	Heykel St. ($40^0$11'0.03"N, $29^0$03'41.5"E)	45000	A5	Akay St. ($39^0$54'48.1"N, $32^0$51'19.0"E)	58000
Cross Road	< 80	B6	Sirameseler St. ($40^0$12'49.6"N, $29^0$01'32.3"E)	35000			

Furthermore, soil samples were collected from nine different locations in Nilufer (Bursa), a heavily industrialized area. There are several types of industry in the vicinity such as; agro-based industry, iron-steel factories, petro chemistry, automotive, electronics, generator production factories, arms factories, textile, and tannery. At the same time, the area is known for agricultural activities. Bursa's soil profile has a typical aluminum enriched weathering profile and is developed on a variety of rocks such as granite, sand-shale, limestone, and basalt [30]. All sampling coordinates are shown in Figure 1.

2.2. Sampling

Samples were collected in August 2010, approximately 2 weeks after the last rainy period during dry and warm weather. Roadside soil samples from the surface layer (0-3 cm) were collected at a distance of 4 m from the sidewalk close to traffic lights from downtown areas, crossroads and highways. Soil samples from bus stations were collected at a distance of 4 m from the bus platforms.

Parking lot dust samples were collected around the edge of the parking lot at a distance of 2 m from an area of 4×0.5 m. The roadside dusts were hand-brushed along kerb stones from an area of 4×0.5 m. Wall dust from tunnels was also hand brushed from an area of 0.5×0.9 m above the ground up to 1 m. Soil samples (from nine sampling point) from the industrial area were collected from the surface of the soil (0 – 3 cm). Samples were transferred to the laboratory in plastic bags.

2.3. Sample preparation

The collected samples were dried at room temperature for a week. Afterwards, the samples were sieved through a 2 mm stainless steel sieve. A portion of the sieved samples was homogenized by grounding in a porcelain mortar and sieving again with a 63 μm sieve and stored in polypropylene bottles at room temperature.

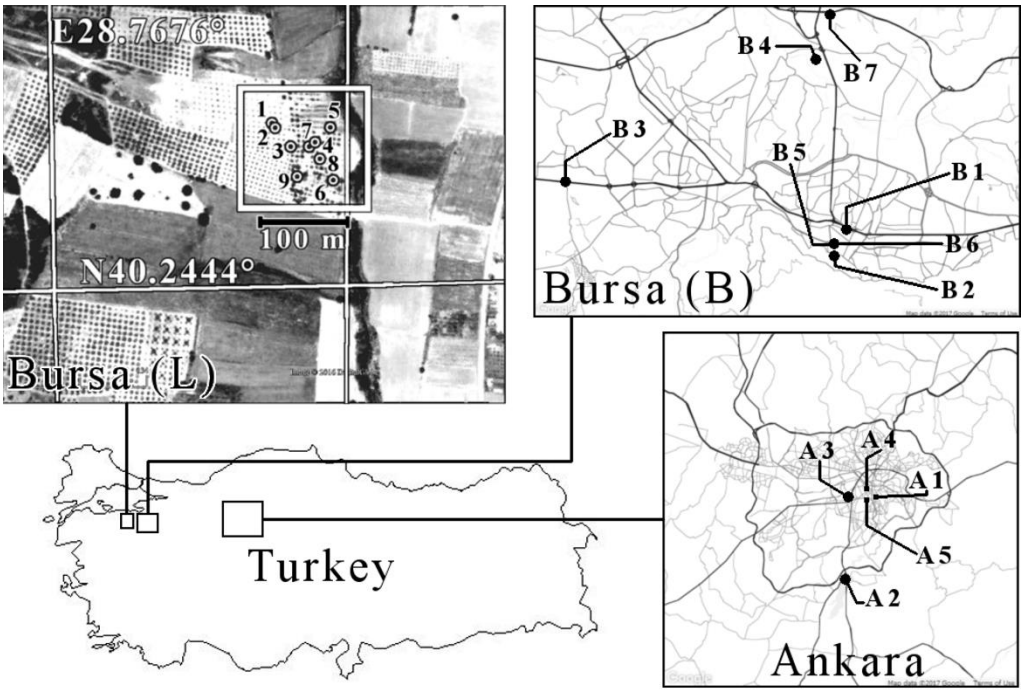

Figure 1 Sampling locations in Bursa (L: industrial area, B: traffic locations) and Ankara (A: traffic locations)

A digestion procedure was applied before analysis. Digestion of samples was conducted in a professional microwave oven (ETHOS 900, Milestone/Shelton). 0.3 g of the pre-prepared sample was transferred into a teflon digestion vessel. A mixture of 4.5 mL HNO_3 (69%) and 1.5 mL HCl (37%) was added and the vessel was closed. Each set of vessels included at least one standard reference sample (BCR-141R) with about 0.17 g and one blank that went in the microwave with a capacity of 10 samples. Five standard reference samples and five acid blank samples were prepared. The microwave digestion program was carried out in the following sequence: 5 min at 90 W, 3 min at 200 W, 5 min at 350 W, and 5 min at 500 W. All vessels were transferred to an ice-water bath when the microwave procedure was completed and kept in the water bath for a minimum of 30 min. Afterwards, the samples (solutions and any solid residues) were quantitatively transferred into 50 mL polypropylene vials with milli-Q water.

The polypropylene tubes were centrifuged at 300 rpm for 5 min. Afterwards, 50 mL of aqua regia (70%) was added. Finally, 4 mL aliquots were pipetted into polypropylene tubes and 8 mL of H_2O_2 was added before ICP-MS analysis.

2.4. Measurement of PGEs (Rh, Pd, Pt), Au and Ce

Samples were analyzed with high resolution inductively coupled plasma-mass spectroscopy equipment (HR-ICP-MS, Thermo Scientific ELEMENT XR) after a chemical digestion process. The ICP-MS ELEMENT XR equipment had a wide crossover range (> 2 orders of

magnitude) between different detector modes that allowed accurate and automated cross-calibration, with a dynamic range of 5×10^7 to 1×10^{12} cps (1 ms sample time). Any limitation on the upper level of quantification was removed due this increase in the dynamic range as the maximum measurable concentration achievable with the equipment was over 1000 µg/g. The flow rates of the instrument were as follows: 15.09 L/min for the coolant argon flow rate, 0.8 L/min for the sample argon flow rate, and 1.078 L/min for plasma argon flow rate. The plasma power was 1350 W. An external calibration was used with solutions prepared from a PGEs standard solution ın order to calibrate the HR-ICP-MS instrument [11]. The instrument's detection limit and the method's quantification limit were calculated using blank analyses and dilution factors. Detection limits and measurement results for Rh, Pd, Pt, Au and Ce were summarized in Table 2.

Table 2
Results for Rh, Pd, Pt, Au and Ce of the standard reference material, Instrument Detection Limit (IDL) and Method Quantification Limit (MQL). [BMQL: Below Method Quantification Limit)]

	Rh	**Pd**	**Pt**	**Au**	**Ce**
Average	15	336	BMQL	22	13
St. dev.	1	17	BMQL	4	1
IDL ($\times 10^{-9}$ g/kg)	< 10	< 100	< 10	< 100	< 10
MQL ($\times 10^{-6}$ g/kg)	1	1	1	1	1

3. RESULTS AND DISCUSSION

PGEs, Au and Ce concentrations of roadside soil and dust samples from Ankara and Bursa are summarized in Figure 2. The highest Rh concentration in Ankara was measured in a tunnel as 60 µg/kg, while the Rh concentration in a tunnel in Bursa was determined as 10 µg/kg. The Pd concentration was the highest in a tunnel in Ankara with 648 µg/kg, which was 307 µg/kg in a tunnel in Bursa. Tunnels are closed environments where accumulation of heavy metals was to be expected (Table 3). Hence, these relatively high values might be attributed to the daily vehicle traffic (see Table 1), but also the fact that tunnels are closed environments as opposed to open air locations. High Pd values in roadside dust are known to occur in areas of high traffic flow [9]. In urban areas where vehicle engines that are not warmed up enough to be operating at peak efficiency, precious metal concentrations are higher at roundabouts or traffic lights [31-32]. The relatively high Rh and Pd concentration found in a tunnel in Ankara can be related to the high vehicle traffic (see Figure 2 and Table 1). The Pt concentration found in dust sample in a tunnel in Ankara was 124 µg/kg, 62 µg/kg in soil sample in downtown Ankara and 10 µg/kg in soil sample from a bus station in Bursa. The Pt concentration for the remaining samples was below the method's quantification limit (see Figure 2). The relatively high Pt abundance found in tunnel dust was due to the isolated environment from ambient meteorology and from dispersion. The ratios of Pt, Pd and Rh vary depending on parameters such as engine capacity, fuel used, and vehicle mass. A logical assumption would be that the number of vehicles crossing a particular location per day and the speed of the vehicle will have an effect on the deposited PGEs in the area.

It is interesting to note that differences were observed between roadside dust samples and roadside soil samples with regard to PGEs concentrations. In this study roadside soil samples had, relatively speaking, lower PGEs contents in comparison to dust samples, except for downtown areas (higher rates of stop-start actions and stationary traffic and daily vehicle flow).

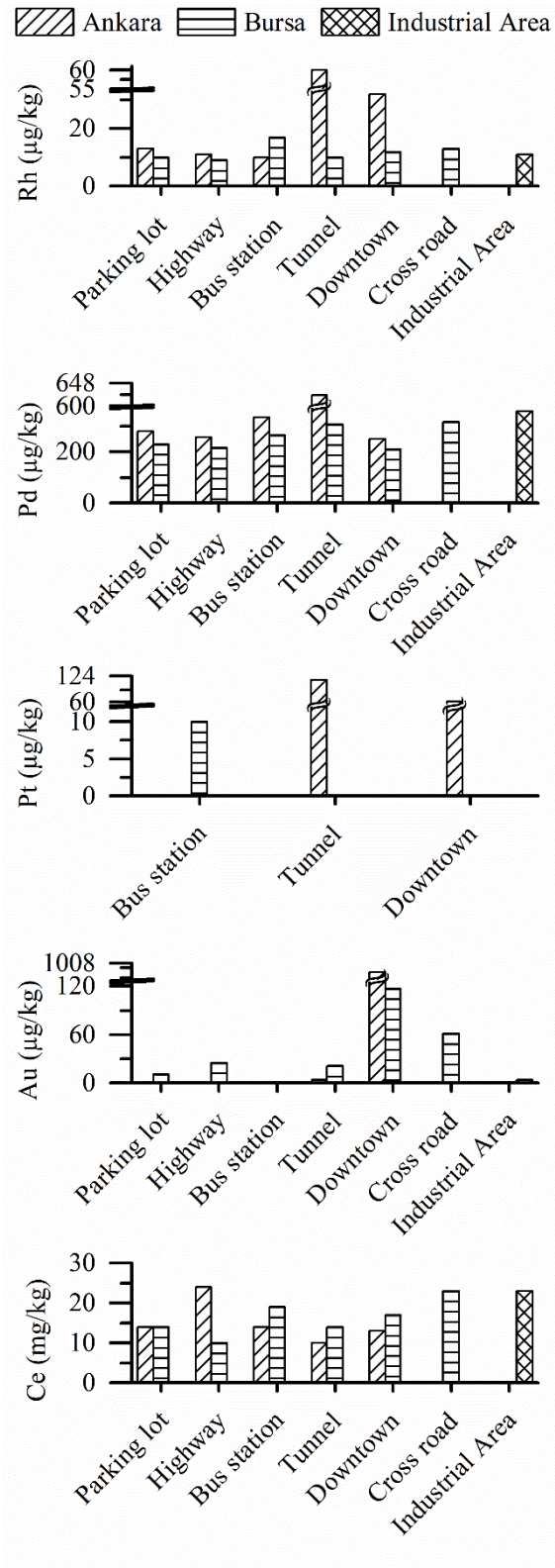

Figure 2 The concentrations of PGEs, Au and Ce measured from samples at different traffic locations and industrial area

Table 3
The concentrations for Rh, Pd, Pt and Pt:Pd, Pt:Rh, Pd:Rh ratios of samples taken at different traffic locations in Ankara (A) and Bursa (B), and *average concentrations of samples taken from the industrial area in Nilüfer, Bursa. (BMQL: Below Method Quantification Limit)

	Rh	Pd	Pt	Pt:Pd	Pt:Rh	Pd:Rh
A-1	13	279	BMQL			21.46
A-2	11	258	BMQL			23.45
A-3	10	334	BMQL			33.40
A-4	60	648	124	0.19	2.07	10.80
A-5	32	249	62	0.25	1.94	7.78
B-1	10	229	BMQL			22.90
B-2	9	216	BMQL			24.00
B-3	17	265	10	0.04	0.59	15.59
B-4	10	307	BMQL			30.70
B-5	12	210	BMQL			17.50
B-6	13	316	BMQL			24.31
Ind.*	11	359	BMQL			32.64

Compositional differences in the reported ratios for PGEs are mainly due to the differences in auto-catalyst compositions used in different countries; differences in sample matrices etc. Various sources have reported different ratios for PGEs, such as Pt:Pd between 1 and 2.5 [33-34], Pt:Rh ratios between 5 and 16 [33], [35], 5.8 [19], and 2.40 – 19.6 [19]; Pd:Rh ratios of 5 [35], 4 – 9 [33], 3.7 [19], and 1.83 – 31.3 [19]. The Pt:Pd ratios in this work were rather on the low side (see Table 3). Likewise, the Pt:Rh ratios were relatively lower than those mentioned in literature. Pt-Rh catalysts dominated the market for many years. Technological developments have stimulated the (partial) substitution of Pt and Rh by Pd. In the 1980s, Pt:Pd-catalysts were used and in the beginning of 1990 Pt was replaced by Pd giving combinations of Pt:Pd:Rh with varying ratios from 1:14:1 to 1:28:1 [35]. Finally, Pd:Rh and Pd-only catalysts were used [17]. As can be seen from Table 3, Pd:Rh ratios lie in the range given in literature, however, they vary considerably. In all cases, Pd concentrations were determined to be relatively higher than Pt and Rh. With the advent of new technologies, palladium costs were reduced. Hence, additional Pd emissions were to be expected.

Gold concentrations were also measured. A concentration of 1008 µg/kg was determined in downtown Ankara, the highest Au concentration of all samples, while a concentration of 117 µg/kg was found in a sample in downtown Bursa. A sample taken from a crossroad in Bursa had a gold concentration of 61 µg/kg and varied between 5-25 µg/kg at other locations, except for a bus station location that remained below the method's quantification limit. Gold's catalytic reaction temperature is too high, hence, it is not used in catalysts [43].

Table 4
Comparison of PGEs concentrations (µg/kg) from different countries and locations obtained from roadside dust and soil samples (***Bursa industrial area soil samples, BMQL: Below Method Quantification Limits)

Country	Location	Year	Dust	Soil	Rh	Pd	Pt	Vehicle/day	Reference
China	Hong Kong	2008	+		11	83	64	/	[36]
	Hong Kong	2007		+	11	39	62	59	[37]
	Guangzhou	2008	+		7	87	22	/	[36]
	Guangzhou	2008		+	1	13	7	/	[37]
	Beijing	2010	+		98	58	28	/	[38]
	Beijing	2007		+	10	21	40	300	[37]
Germany	Braunschweig(city)	2005	+		110	410	2	16.000	[39]
	Braunschweig(city)	2005		+	39	124	261	16.000	[39]
Greece	Athens	2003		+	/	1 - 126	2 - 141	36.510 - 48.756	[34]
Hungary	Budapest	2010	+		/	50	36	/	[40]
India	Hyderabad	2007	+		2	18	15	/	[41]
	Mumbai	2007		+	1	16	6	/	[37]
USA	Houston, Texas (tunnel)	2012	+		152	770	208	25.000	[42]
	Houston, Texas	2012	+		6 - 8	10 - 88	35 - 131	220.000	[42]
Turkey	Ankara	2010	+		36	464	62	16.500	This study
	Ankara	2010		+	18	280	21	34.750	This study
	Bursa	2010	+		10	268	BMQL	7.250	This study
	Bursa	2010		+	10	275	2	21.786	This study
	***Bursa	2010		+	11	359	BMQL	-	This study

Au behaved in a different way to PGEs, which is not surprising since it is primarily used in automotive electronics. Gold does not vary in the same way as the other precious metals. Hence, gold does not increase with higher traffic flow in any of the sample types. Heavier Au particles move by gravity to the bottom of the drain. The lack of correlation of Au with the other precious metals (Figure 3) also confirms that gold's origin are different from the platinum group elements' (jewelry, for example).

PGEs have been said to be emitted in the form of monocrystals. As a result of chemical reactions, mechanical abrasion and high temperatures wash coated particles and other components such as Ce, Al and related lanthanides are emitted from

vehicles [44]. As can be seen from Figure 2, Ce concentrations varied between 10 – 23 mg/kg. Cerium is more abundant, with an estimated concentration of 60 mg/kg in the earth's crust [10]. Hence, Ce could not be traced back to a anthropogenic source.

Figure 3 revealed a linear relation between Pd-Rh and Ce-Pd. When disregarding extremes in Figure 3, the remaining plots did not show such correlations. Also, it is interesting to note that Ce was correlated with Pd, but not Rh. This might very well be the result of technological improvements whereby catalytic converters were mainly Pd-based[17] and Ce was added to the

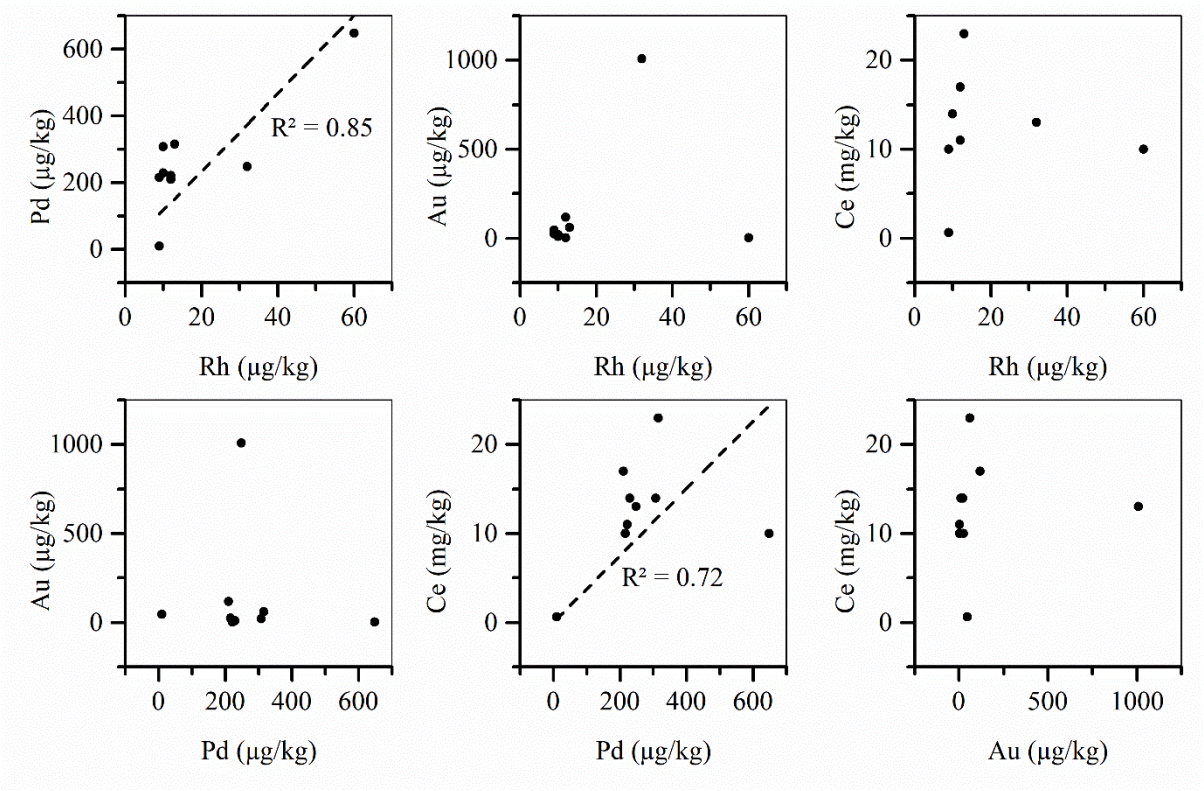

Figure 3 Correlation graphs for elements studied in this work.

Vehicle Exhaust Catalysts (VEC) for stability and for particulate matter control in diesel fuels (in the form of cerium oxide) [45]. Although Pt data was only analyzed for a small number of samples, higher Rh values tend to occur with high Pd and Pt values. The roadside samples suggest that Pt, Rh and Pd were derived from, predominantly, vehicle catalytic converters. This is in agreement with previous studies [8], [11], [46], [47].

Results obtained from samples taken from the industrial area in Nilufer showed that Pt concentrations were below the method's quantification limit. Average Rh and Pd concentrations were 11 µg/kg and 359 µg/kg, respectively. Rhodium and Pd were attributed to the industrial area in the vicinity, but the Pt was surprisingly below the method's quantification limit. Rhodium is used in electrical connections, glass production, and optical instruments. Palladium's uses are numerous and include areas such as dental alloys, chemicals (e.g., ethanol fuel production, oil refining, polyester), and the electronics sector. Only one sample of the nine sampling locations had detectable Au concentration of 38 µg/kg (i.e., above the method's quantification limit).

The average Ce concentration was 23 mg/kg. Higher Rh and Pt concentrations were found for samples taken from the traffic locations compared to the industrialized areas. Since agricultural

lands are extensively abraded by heavy vehicles such as tractors, the Pd discharge by exhaust catalysts of these heavy vehicles might have been larger than expected. Similar to the case where PGEs concentrations were more pronounced at stationary traffic locations (bus station, parking lots, tunnels), heavy vehicles on agricultural lands can also be regarded as partially stationary due to the frequency they are used in the same limited piece of land. A different explanation for the relatively high Pd concentration at the industrial and agricultural area might be related to palladium's higher solubility (relatively to Rh and Pt) when in contact with inorganic anions, such as Cl^-, NO_3^-, SO_4^{2-} and PO_4^{3-} [48].

While Rh and Pt total average concentrations were relatively higher for traffic-related locations, the total average Pd concentration was higher for the industrial locations (see Figure 4). Although Pd can be found naturally in soils and water, the relatively high Pd level, a typical traffic-related element, was surprising to observe at the industrial area. However, Pd is known to be mainly used in the manufacture of steel, steel alloys and stainless steel, which are important products fabricated in the industrial area in Nilüfer, Bursa.

Table 4 summarizes some literature values for Rh, Pd and Pt from different countries and different locations. Palladium concentrations found in literature were considerably lower compared to Pd concentrations in this study. Rhodium concentrations were comparable to results from this study. Platinum concentrations consistently remained below the method's quantification limit. Literature data and to a certain extent this study showed that accumulation of elements was higher in dust samples. Soil samples are affected by weathering conditions that speeds up the diffusion process, leading to lower concentrations detected at the upper parts of the soil.

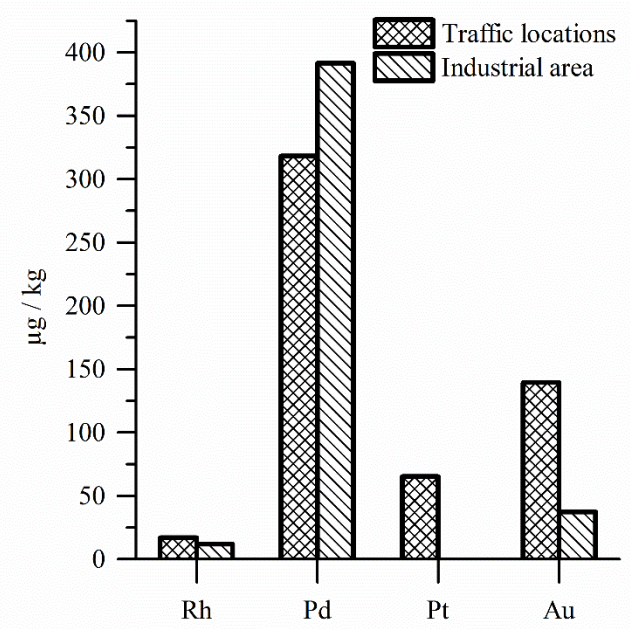

Figure 4 The overal average concentrations for PGE and heavy metals for the different traffic locations in Ankara and Bursa, and the soil surface (0 – 3 cm) at the industrial area of Nilufer, Bursa

4. CONCLUSIONS

This pilot study presents the results of Pt, Pd, Rh, Au and Ce determination in environmental samples. The concentration of the measured elements was largely concentrated at traffic locations (mainly dust samples) as opposed to industrial locations (mainly soil samples). Higher concentrations of PGEs were determined at traffic locations where vehicles remained stationary for a relatively long time, such as bus stations, downtown and tunnels. Although the number of vehicles per day that had used the highway in Ankara and Bursa was much greater than the other traffic locations, the relatively high speeds of vehicles on highways did not allow the accumulation of PGEs. Any preventive and remedial measures should begin at locations where vehicles remain stationary for a relatively long time. These are locations where people face real-time environmental and health implications of accumulated heavy metals including PGEs.

The clear presence of Pd and Rh was determined at different traffic locations. Platinum remained below the method's quantification limit for most of the samples. The relatively high Pd and Rh

levels confirmed the shift from Pt to Pd and Rh seen in modern Vehicle Exhaust Catalysts (VEC) technologies.

Cerium concentrations found in this study remained well below the earth's crustal Ce-levels. Hence, Ce could not be traced back to a anthropogenic source.

These precious elements occur in ultra-trace quantities in the environment. The fact that Rh, Pd, Pt, and Au concentrations were well above the earth's crustal concentrations, shows the necessity to further investigate the anthropogenic nature of these elements. This pilot study serves as a reference for future studies on PGEs and other precious metals in the region.

Acknowledgement

The authors would like to acknowledge Prof. Dr. Rene Van Grieken and Kayawe Valentine Mubiana from Antwerp University for their valuable contributions.

Funding

No funding has been declared by the authors.

The Declaration of Conflict of Interest/ Common Interest

No conflict of interest or common interest has been declared by the authors.

Authors' Contribution

The idea of the studies belongs to Songül AKBULUT ÖZEN. Murat ÖZEN had a great contribution in providing support for the experiments and writing & editing of the manuscript. Ugur CEVIK had a contribution in investigation and analysis of the data.

The Declaration of Ethics Committee Approval

The authors declare that this document does not require an ethics committee approval or any special permission.

The Declaration of Research and Publication Ethics

The authors of the paper declare that they comply with the scientific, ethical and quotation rules of SAUJS in all processes of the article and that they do not make any falsification on the data collected. In addition, they declare that Sakarya University Journal of Science and its editorial board have no responsibility for any ethical violations that may be encountered, and that this study has not been evaluated in any academic publication environment other than Sakarya University Journal of Science.

REFERENCES

[1] G. Schmidt and H. Palme, "Abundances of Os, Ir, Ru, Rh, Pt and Pd in the Earth's crust," in *The origin and fractionation of highly siderophile elements in the Earth's mantle*, 1997.

[2] F. R. Hartley, Ed., *Chemistry of the platinum group metals: recent developments*. Amsterdam ; New York: Elsevier, 1991.

[3] A. Fornalczyk, "Industrial catalysts as a source of valuable metals," *Journal of Achievements in Materials and Manufacturing Engineering*, vol. 55, no. 2, pp. 864–869, Dec. 2012.

[4] B. Gómez *et al.*, "Levels and risk assessment for humans and ecosystems of platinum-group elements in the airborne particles and road dust of some European cities," *Sci Total Environ*, vol. 299, no. 1–3, pp. 1–19, Nov. 2002, doi: 10.1016/S0048-9697(02)00038-4.

[5] C. L. S. Wiseman and F. Zereini, "Airborne particulate matter, platinum group elements and human health: A review of recent evidence," *Science of The Total Environment*, vol. 407, no. 8, pp. 2493–2500, Apr. 2009, doi: 10.1016/j.scitotenv.2008.12.057.

[6] O. Morton-Bermea, O. Amador-Muñoz, L. Martínez-Trejo, E. Hernández-Álvarez, L. Beramendi-Orosco, and M. E. García-Arreola, "Platinum in PM2.5 of the metropolitan area of Mexico City," *Environ Geochem Health*, vol. 36, no. 5, pp. 987–994, Oct. 2014, doi: 10.1007/s10653-014-9613-8.

[7] M. Ďuriš, "Geochemical and Ecological Survey of the Prague City Area, Czech Republic," in *Mapping the Chemical Environment of Urban Areas*, C. C. Johnson, A. Demetriades, J. Locutura, and R. T. Ottesen, Eds. Chichester, UK: John Wiley & Sons, Ltd, 2011, pp. 364–374.

[8] K. Boch and M. Schuster, "Determination of palladium in road dust and sewage sludge ashes," in *Palladium Emissions in the Environment*, F. Zereini and F. Alt, Eds. Berlin/Heidelberg: Springer-Verlag, 2006, pp. 191–201.

[9] S. J. Parry and K. E. Jarvis, "Temporal and Spatial Variation of Palladium in the Roadside Environment," in *Palladium Emissions in the Environment*, F. Zereini and F. Alt, Eds. Berlin/Heidelberg: Springer-Verlag, 2006, pp. 419–432.

[10] C. L. S. Wiseman, Z. Hassan Pour, and F. Zereini, "Platinum group element and cerium concentrations in roadside environments in Toronto, Canada," *Chemosphere*, vol. 145, pp. 61–67, Feb. 2016, doi: 10.1016/j.chemosphere.2015.11.056.

[11] B. Leniewska, B. Godlewskaykiewicz, B. Bocca, S. Caimi, S. Caroli, and A. Hulanicki, "Platinum, palladium and rhodium content in road dust, tunnel dust and common grass in Biaystok area (Poland): a pilot study," *Science of The Total Environment*, vol. 321, no. 1–3, pp. 93–104, Apr. 2004, doi: 10.1016/j.scitotenv.2003.07.004.

[12] K. H. Ek, G. M. Morrison, and S. Rauch, "Environmental routes for platinum group elements to biological materials—a review," *Science of The Total Environment*, vol. 334–335, pp. 21–38, Dec. 2004, doi: 10.1016/j.scitotenv.2004.04.027.

[13] K. H. Ek, S. Rauch, G. M. Morrison, and P. Lindberg, "Platinum group elements in raptor eggs, faeces, blood, liver and kidney," *Sci Total Environ*, vol. 334–335, pp. 149–159, Dec. 2004, doi: 10.1016/j.scitotenv.2004.04.067.

[14] M. T. Jackson, H. M. Prichard, and J. Sampson, "Platinum-group elements in sewage sludge and incinerator ash in the United Kingdom: Assessment of PGE sources and mobility in cities," *Science of The Total Environment*, vol. 408, no. 6, pp. 1276–1285, Feb. 2010, doi: 10.1016/j.scitotenv.2009.09.014.

[15] I. Bednarova *et al.*, "Study of the influence of platinum, palladium and rhodium on duckweed (Lemna minor)," *Neuroendocrinol Lett*, vol. 35, no. 2, pp. 35–42, 2014.

[16] J. Pawlak, E. Łodyga-Chruścińska, and J. Chrustowicz, "Fate of platinum metals in the environment," *J Trace Elem Med Bio*, vol. 28, no. 3, pp. 247–254, Jul. 2014, doi: 10.1016/j.jtemb.2014.03.005.

[17] F. Zereini and F. Alt, Eds., *Palladium emissions in the environment: analytical methods, environmental assessment and health effects*. Berlin ; New York: Springer, 2006.

[18] K. E. Jarvis, S. J. Parry, and J. M. Piper, "Temporal and Spatial Studies of Autocatalyst-Derived Platinum, Rhodium, and Palladium and Selected Vehicle-Derived Trace Elements in the Environment," *Environ Sci Technol*, vol. 35, no. 6, pp. 1031–1036, Mar. 2001, doi: 10.1021/es0001512.

[19] G. Nordberg, Ed., *Handbook on the toxicology of metals*, 3rd ed. Amsterdam ; Boston: Academic Press, 2007.

[20] G. Hutchings, "A golden future," *Nature Chem*, vol. 1, no. 7, pp. 584–584, Oct. 2009, doi: 10.1038/nchem.388.

[21] J. Kašpar, P. Fornasiero, and N. Hickey, "Automotive catalytic converters: current status and some perspectives," *Catalysis Today*, vol. 77, no. 4, pp. 419–449, Jan. 2003, doi: 10.1016/S0920-5861(02)00384-X.

[22] F. R. Cassee *et al.*, "Exposure, Health and Ecological Effects Review of Engineered Nanoscale Cerium and Cerium Oxide Associated with its Use as a Fuel Additive," *Critical Reviews in Toxicology*, vol. 41, no. 3, pp. 213–229, Mar. 2011, doi: 10.3109/10408444.2010.529105.

[23] J. D. Whiteley and F. Murray, "Anthropogenic platinum group element (Pt, Pd and Rh) concentrations in road dusts and roadside soils from Perth, Western Australia," *Science of The Total Environment*, vol. 317, no. 1–3, pp. 121–135, Dec. 2003, doi: 10.1016/S0048-9697(03)00359-0.

[24] F. Zereini *et al.*, "Concentration and Distribution of Heavy Metals in Urban Airborne Particulate Matter in Frankfurt am Main, Germany," *Environ. Sci. Technol.*, vol. 39, no. 9, pp. 2983–2989, May 2005, doi: 10.1021/es040040t.

[25] V. Lyubomirova, R. Djingova, and J. T. van Elteren, "Fractionation of traffic-emitted Ce, La and Zr in road dusts," *J. Environ. Monit.*, vol. 13, no. 6, p. 1823, 2011, doi: 10.1039/c1em10187k.

[26] S. Akbulut and U. Cevik, "Accumulation of Metals in Roadside Soil, Dust and Pine Needles in Different Characteristic Traffic Areas," *Fresen Environ Bull*, vol. 23, no. 2A, pp. 516–522, 2014.

[27] A. Ucurum, P. J. Lechler, G. B. Arehart, and F. Molnar, "Platinum-Group Element, Stable Isotope, and Fluid Inclusion Investigation of the Ultramafic Rock-Hosted Gunes-Sogucak Ni-Cu-Sulfide Mineralization in the Gunes Ophiolite, East-Central Turkey," *Int Geol Rev*, vol. 49, no. 2, pp. 169–192, Feb. 2007, doi: 10.2747/0020-6814.49.2.169.

[28] H. Kozlu, H. Prichard, F. Melcher, P. Fisher, C. Brough, and D. Stueben, "Platinum group element (PGE) mineralisation and chromite geochemistry in the Berit ophiolite (Elbistan/Kahramanmaraş), SE Turkey," *Ore Geol Rev*, vol. 60, pp. 97–111, Jul. 2014, doi: 10.1016/j.oregeorev.2013.12.011.

[29] M. C. Turhan, "Traffic and Transportation Survey of Highway (KGM), General Directorate of Highways, Turkey," 2010. [Online]. Available: http://www.kgm.gov.tr/SiteCollectionDocuments/KGMdocuments/Istatistikler/TrafikveUlasimBilgileri/10TrafikUlasimBilgileri%20.pdf.

[30] MTA, "General Directorate of Mineral Research and Exploration, Turkey," 2017. http://yerbilimleri.mta.gov.tr/anasayfa.aspx.

[31] N. I. Ward and L. M. Dudding, "Platinum emissions and levels in motorway dust samples: influence of traffic characteristics," *Science of The Total Environment*, vol. 334–335, pp. 457–463, Dec. 2004, doi: 10.1016/j.scitotenv.2004.04.049.

[32] D. Fliegel, Z. Berner, D. Eckhardt, and D. Stüben, "New data on the mobility of Pt emitted from catalytic converters," *Analytical and Bioanalytical Chemistry*, vol. 379, no. 1, pp. 131–136, May 2004, doi: 10.1007/s00216-004-2556-7.

[33] J. C. Ely, C. R. Neal, C. F. Kulpa, M. A. Schneegurt, J. A. Seidler, and J. C. Jain, "Implications of Platinum-Group Element Accumulation along U.S. Roads from Catalytic-Converter Attrition," *Environ Sci Technol*, vol. 35, no. 19, pp. 3816–3822, Oct. 2001, doi: 10.1021/es001989s.

[34] A. N. Riga-Karandinos, C. J. Saitanis, and G. Arapis, "First Study of Anthropogenic Platinum Group Elements in Roadside Top-Soils in Athens, Greece," *Water Air Soil Poll*, vol. 172, no. 1–4, pp. 3–20, May 2006, doi: 10.1007/s11270-005-9016-7.

[35] J. Fritsche and T. Meisel, "Determination of anthropogenic input of Ru, Rh, Pd, Re, Os, Ir and Pt in soils along Austrian motorways by isotope dilution ICP-MS," *Sci Total Environ*, vol. 325, no. 1–3, pp. 145–154, Jun. 2004, doi: 10.1016/j.scitotenv.2003.11.019.

[36] L. Qi, M.-F. Zhou, Z. Zhao, J. Hu, and Y. Huang, "The characteristics of automobile catalyst-derived platinum group elements in road dusts and roadside soils: a case study in the Pearl River Delta region, South China," *Environ Earth Sci*, vol. 64, no. 6, pp. 1683–1692, Nov. 2011, doi: 10.1007/s12665-010-0635-y.

[37] S. Pan, G. Zhang, Y. Sun, and P. Chakraborty, "Accumulating characteristics of platinum group elements (PGE) in urban environments, China," *Sci Total Environ*, vol. 407, no. 14, pp. 4248–4252, Jul. 2009, doi: 10.1016/j.scitotenv.2009.03.030.

[38] B. Gao, Y. Yu, H. Zhou, and J. Lu, "Accumulation and distribution characteristics of platinum group elements in roadside dusts in Beijing, China," *Environ Toxicol Chem*, vol. 31, no. 6, pp. 1231–1238, Jun. 2012, doi: 10.1002/etc.1833.

[39] H. Wichmann, G. A. K. Anquandah, C. Schmidt, D. Zachmann, and M. A. Bahadir, "Increase of platinum group element concentrations in soils and airborne dust in an urban area in Germany," *Sci Total Environ*, vol. 388, no. 1–3, pp. 121–127, Dec. 2007, doi: 10.1016/j.scitotenv.2007.07.064.

[40] M. Sager, H.-T. Chon, and L. Marton, "Spatial variation of contaminant elements of roadside dust samples from Budapest (Hungary) and Seoul (Republic of Korea), including Pt, Pd and Ir," *Environ Geochem Hlth*, vol. 37, no. 1, pp. 181–193, Feb. 2015, doi: 10.1007/s10653-014-9639-y.

[41] R. Mathur, V. Balaram, M. Satyanarayanan, S. S. Sawant, and S. L. Ramesh, "Anthropogenic platinum, palladium and rhodium concentrations in road dusts from Hyderabad city, India," *Environ Earth Sci*, vol. 62, no. 5, pp. 1085–1098, Mar. 2011, doi: 10.1007/s12665-010-0597-0.

[42] N. Spada, A. Bozlaker, and S. Chellam, "Multi-elemental characterization of tunnel and road dusts in Houston, Texas using dynamic reaction cell-quadrupole-inductively coupled plasma–mass spectrometry: Evidence for the release of platinum group and anthropogenic metals from motor vehicles," *Anal Chim Acta*, vol. 735, pp. 1–8, Jul. 2012, doi: 10.1016/j.aca.2012.05.026.

[43] F. Zereini, C. Wiseman, F. Alt, J. Messerschmidt, J. Müller, and H. Urban, "Platinum and Rhodium Concentrations in Airborne Particulate Matter in Germany from 1988 to 1998," *Environ. Sci. Technol.*, vol. 35, no. 10, pp. 1996–2000, May 2001, doi: 10.1021/es001126z.

[44] S. Artelt, H. Kock, H. P. König, K. Levsen, and G. Rosner, "Engine dynamometer experiments: platinum emissions from differently aged three-way catalytic converters," *Atmospheric Environment*, vol. 33, no. 21, pp. 3559–3567, Sep. 1999, doi: 10.1016/S1352-2310(99)00109-0.

[45] J. G. Dale, S. S. Cox, M. E. Vance, L. C. Marr, and M. F. Hochella, "Transformation of Cerium Oxide Nanoparticles from a Diesel Fuel Additive during Combustion in a Diesel Engine," *Environ. Sci. Technol.*, vol. 51, no. 4, pp. 1973–1980, Feb. 2017, doi: 10.1021/acs.est.6b03173.

[46] R. A. Sutherland, "A First Look at Platinum in Road-Deposited Sediments and Roadside Soils, Honolulu, Oahu, Hawaii," *Archives of Environmental Contamination and*

Toxicology, vol. 44, no. 4, pp. 430–436, May 2003, doi: 10.1007/s00244-002-2096-0.

[47] M. E. Kylander, S. Rauch, G. M. Morrison, and K. Andam, "Impact of automobile emissions on the levels of platinum and lead in Accra, Ghana," *J. Environ. Monitor.*, vol. 5, no. 1, pp. 91–95, Jan. 2003, doi: 10.1039/b211736c.

[48] F. Zereini, C. L. S. Wiseman, J. Poprizki, P. Albers, W. Schneider, and K. Leopold, "Assessing the potential of inorganic anions (Cl^-, NO_3^-, SO_4^{2-} and PO_4^{3-}) to increase the bioaccessibility of emitted palladium in the environment: Experimental studies with soils and a Pd model substance," *Environmental Pollution*, vol. 220, pp. 1050–1058, Jan. 2017, doi: 10.1016/j.envpol.2016.11.039.

SAKARYA ÜNİVERSİTESİ
FEN BİLİMLERİ ENSTİTÜSÜ DERGİSİ

Sakarya University Journal of Science
SAUJS

e-ISSN 2147-835X | Period Bimonthly | Founded: 1997 | Publisher Sakarya University |
http://www.saujs.sakarya.edu.tr/en/

Title: An experimental and comparative study of the self-loosening of bolted-joints under cyclic transverse loading

Authors: Umut İNCE, Mustafa GÜDEN

Recieved: 2020-07-07 11:35:15

Accepted: 2021-03-16 12:52:00.995000

Article Type: Research Article

Volume: 25
Issue: 2
Month: April
Year: 2021
Pages: 498-512

How to cite
Umut İNCE, Mustafa GÜDEN; (2021), An experimental and comparative study of the self-loosening of bolted-joints under cyclic transverse loading. Sakarya University Journal of Science, 25(2), 498-512, DOI: https://doi.org/10.16984/saufenbilder.765481
Access link
http://www.saujs.sakarya.edu.tr/en/pub/issue/60672/765481

Sakarya University Journal of Science 25(2), 498-512, 2021

An Experimental and Comparative Study of the Self-Loosening of Bolted-Joints Under Cyclic Transverse Loading

Umut İNCE*[1], Mustafa GÜDEN[2]

Abstract

The capabilities of analytic models in predicting the experimental critical displacements of the self-loosening of bolted-joints were investigated experimentally and numerically. The experimental loosening rates were determined in a Junker test bench at a constant transverse displacement amplitude (0.45 mm) and under varying initial clamp force and clamp length and controlled bearing and thread friction coefficients. The analytic critical displacements were then calculated using experimental parameters. In addition, a three-dimensional accompanying finite element (FE) model was developed in order to calculate the ratio of spring constants engaging the thread to spring. The results showed relatively low capabilities of present analytic model in the prediction of the critical displacements of the self-loosening of bolted-joints. The efforts to modify the nut reaction moment and the inclination compliance of bolt head portion in the investigated equations however resulted moderate increase in the appropriate predictions. On the other side, the use of the reaction moment determined by FE model increased the appropriate prediction from 58.3 to 73.4%. The accuracy of the equations was further increased by the use of an appropriate k_w value, but the increase in this case was only ~4%.

Keywords: bolted-joints, self-loosening, numerical simulation, Junker test, analytic model.

1. INTRODUCTION

Bolted-joints are widely used in engineering structures as they are relatively easy to implement, offer relatively low cost and generate comparatively high clamping forces. Nevertheless, they are prone to catastrophic failure, particularly at prolonged service durations, making them one of the most critical structural parts. The well-known failure mode of bolted-joints is self-loosening which is primarily caused by vibrational forces. The gradual decrease of preload with the increase of dynamic load on a bolt leads to the initiation of self-loosening. Self-loosening plays a pivotal role in the initiation of fatigue failure, causing not only material and financial losses but also fatal accidents. The crash of a Tupolev 154M type passenger jet in 1999, an example to fatal

* Corresponding author: umut.ince@normcivata.com
[1] Norm Cıvata San. Ve Tic A.Ş, Atatürk Organize Sanayi Bölgesi, 10007 sokak, 35620, Çiğli, İzmir ,
ORCID: https://orcid.org/0000-0002-3118-3060
[2] İzmir Institute of Technology, Department of Mechanical Engineering, Urla, İzmir
E-Mail: mustafaguden@iyte.edu.tr
ORCID : https://orcid.org/0000-0001-6397-8418

accidents, resulted in the death of 61 persons. The officially reported cause of the accident was the self-loosening of a self-locking nut connecting the pull rod and bell crank in the elevator control system [1]. A United States Air Force reconnaissance airplane caught fire in 2015 as a result of the self-loosening of a fastener, which led to damages in the aircraft control and mission-related systems. The repair cost was declared $62.4 million [2]. A high-speed train derailed in the United Kingdom in 2007, resulted from the self-loosening of a fastener according to the report published by RAIB [3]. There have been many other reports on the causalities resulted from the self-loosening of bolts. The existent analytic equations developed for the self-loosening of bolted-joints under transverse vibrational loads were reviewed in section 2. The applicability of these equations to the experimental results of the self-loosening of bolted-joints, according to authors' knowledge, has not been completely investigated so far. Hence, this study aimed at determining the capabilities of the existent self-loosening analytic models in predicting the experimental critical displacements. For that purpose, extensive transverse vibration experiments were performed under varying initial clamp force and length, controlled bearing and thread friction coefficients and a constant transverse displacement amplitude of 0.45 mm. The transverse vibration experiments were conducted in a Junker bench on the bolted-joints in conjunction with a Finite Element (FE) model. The critical transverse displacements were then calculated for each equation using the experimental parameters. Finally, the experimentally determined loosening rates were drawn as function of analytically calculated critical transverse displacements. The percentages of the correct or appropriate and wrong or inappropriate predictions of the critical displacement of self-loosening were shown in the graphs for each equation. In addition, a three-dimensional simplified accompanying FE model of the bolted-joint was used to calculate the ratio of spring constants engaging the thread to spring which was used in the equations.

2. PREVIOUS EXPERIMENTAL AND NUMERIC STUDIES ON THE SELF LOOSENING OF BOLTED-JOINTS

Early studies on the self-loosening of bolted-joints merely focused on the effect of axial dynamic loads along fastener.

Goodier and Sweeney [4] developed an equation for the loosening of nuts caused by axial vibrational forces. In the same study, the radial micro slips under axial tension, both at the bolt-nut thread interface and the bearing surface, were reported to vary with the radial contraction of bolt and the radial expansion of nut.

Sauer [5] showed that when the ratio of the amplitude of axial dynamic load to mean bolt axial tension was less than 0.7, the axial vibrational forces resulted in no loosening.

Gambrell [6] investigated the effect of fine and coarse thread size, lubrication and frequency on the loosening of fasteners under axial vibrational forces. No effect of fastener thread size and frequency was reported when the dynamic to static load ratio and frequency were less than 1 and between 3.3 and 22 Hz, respectively. When the dynamic to static load ratio was above 1, the fine threaded bolts were shown to loosen less than the coarse threaded bolts. Also, lubrication was shown to be a critical factor in the loosening of coarse threaded bolts.

Junker [7] showed experimentally that the transverse vibrational forces were much more effective than the axial vibrational forces in the self-loosening. The loosening rate expressed as the loss of clamp load per cycle (N/cycle) increased with increasing the amplitude of transverse displacement and thread pitch. An experimental testing device used in the same study, called the Junker tester, was standardized as DIN 65151 in 2002 [8]. DIN 25201 superseded DIN 65151 was published in 2010 [9].

Finkelston [10] showed that the increase of friction and preload enhanced the loosening resistance of fastener.

Yamamoto and Kasei [11, 12] introduced a parameter called the critical relative slippage (S_{cr}) which determines the upper transverse displacement limit for the initiation of loosening. The schematic of threaded fastener deformation subjected to a transverse external force is shown in Figure 1(a). In the same figure, the nut bearing surface is subjected to a shear force (F_s) and a nut reaction moment (M_t). The critical relative slip proposed by Yamamoto and Kasei [11, 12] is

$$S_{cr} = 2\delta = \frac{2l_n F\mu_b(l_n^2+3k_w l_n EI)}{3EI} - \frac{3l_n M_t(l_n+2k_w EI)}{3EI} \quad (1)$$

In Eqn. 1, δ is the critical slip distance, μ_b is the friction coefficient of bearing surface, F is the clamping force, I is the moment of the inertia of the cross-sectional area of bolt, E is the longitudinal elastic modulus of bolt, k_w, is the inclination compliance of bolt head portion and l_n is the length of bolt.

Based on an FE analysis, Izumi et. al. [13] refined the Yamamoto and Kasei's equation as

$$S_{cr} = 2F\left[\mu_b\left(\frac{l_g^3}{3EI_g}+\frac{l_s^3}{3EI_s}+\frac{l_g l_s l_n}{EI_g}+k_w l_n^2\right) - \frac{m}{4}\frac{\mu_t}{Cos^2\alpha}\left(\frac{l_g^2}{2EI_g}+\frac{l_s^2}{2EI_s}+\frac{l_g l_s}{EI_g}+k_w l_n\right)\right] \quad (2)$$

where, l_g and l_s are sequentially the length of bolt and bolt thread and I_g and I_s are the moment of inertia of cross-sectional area of bolt and bolt thread, respectively (Figure 1(b)). The reaction moment on the thread is given as

$$M_t = \left(\frac{m}{4}\right)\left(\frac{\mu_t F}{Cos^2\alpha}\right) \quad (3)$$

where, m is the height of nut, μ_t is the friction coefficient of threaded interface and α is the half-thread angle. Nakamura et. al [14] proposed an equation for the inclination compliance of bolt head portion (k_w) as

$$k_w = 0.168\left(\frac{1}{d}\right)^3 \left[\frac{1}{kN\ mm}\right] \quad (4)$$

where d is the bolt diameter.

Blume and Illgner [15] proposed the following equation for the critical slip distance based on a beam model fixed on both sides,

$$\delta = \frac{F\mu_b l_n^3}{12EI} \quad (5)$$

Friede and Lange [16] performed experiments on the critical slip distance of transversely loaded fasteners including M16 and M24. Comparison of test results with the Blume and Illgner's equation [15] showed conservative results. They proposed an equation for the critical slip distance as

$$\delta = F\mu_b\left(\frac{l_n^3}{12EI}+\frac{l_n^2}{2C_\varphi}\right) \quad (6)$$

where C_φ (kNm/rad) is rotational stiffness of bolt. Nassar and Housari [17-20] investigated the self-loosing of fasters and proposed a mathematical model for the loosening under cyclic transverse loads. The loosening rate was shown to be sensitive to the thread and bearing friction coefficients of fasteners. In the same study, the loosening rate of fine threaded fasteners decreased with the initiation of loosening; a larger clearance between bolt and pilot increased the loosening rate almost exponentially and the number of cycles for complete loosening was directly proportional to initial clamp force.

Yokoyama et. al [21] presented an analytic model for the bolts subjected to transverse loads. The model well agreed with the FE modelling results. In the same study M_t was proposed as

$$\Delta M_t = \frac{K_t}{K_b+K_t}\Delta F_s l_n \quad (7)$$

where K_t and K_b are the spring constant of engaged thread and the spring constant of bolt head, respectively. The spring constant of bolt head is given as

$$K_b = \frac{EI}{0.6d} \quad (8)$$

where d is the nominal thread diameter.

Although the use of numerical simulation method for the investigation of the loosening behavior of bolt-nut joints with the development of computer and allowing comprehensive analysis in a short time, the number of studies combining experimental - analytical and numerical simulation methods is quite few [22-25].

3. EXPERIMENTAL STUDY

M8x1.25 8.8 ISO 4017 [26] carbon steel bolts and M8x1.25 8 DIN 934 [27] carbon steel nuts were selected for the Junker tests. The thread forming and heat-treatment of bolts and nuts were performed sequentially according to ISO 898-1 [28] and ISO 898-2 [29]. Before testing, the bolts and nuts were coated with Delta Protekt® KL100 + VH301 GZ zinc flake by a dip-spin process in a single batch. Delta Protekt® KL100 + VH301 GZ zinc flake coating induces a friction coefficient between 0.09 and 0.14 and widely preferred by the automotive industry. Thread and bearing friction coefficients of five bolt/nut specimens were measured according to ISO 16047 [30] using SCHATZ® friction coefficient tester. Transverse vibration tests were performed in a Junker test bench shown in Figure 2(a) and Figure 2(c).

In a typical test, the test bench applies a transverse dynamic vibrational force with variable frequency and amplitude on a glider plate. The glider top plate is driven by an eccentric cam. The bolted joint being tested is clamped together the glider plate and fixed plate as shown in Figure 2(b). The clamp force is measured by means of load cells as function of time. The clamp force-cycle data are then exported for the analysis.

The parameters used in transverse vibration tests are tabulated in Table 1. The tests were performed at three different initial clamp forces, six different clamp lengths, four different bearing-thread friction coefficients and a constant transverse displacement amplitude of 0.45 mm and a frequency of 5 Hz. Total 360 vibration tests were performed for 72 test conditions and at least five tests were performed for each test condition. In order to improve the reliability of data, maximum allowable standard deviation of loosening rates was accepted as %20 of average loosening rate value of five test results. If the standard deviation is bigger than the allowed, additional tests performed until the allowable standard deviation value was reached.

An average value for loosening rate for each test condition was the calculated using 5 tests. The loosening rate (kN/cycle) was determined from the slope of a linear fit to the average clamping force–cycle curve. For the experimental test conditions resulting in self-loosening, the critical transverse displacements were then calculated using the analytic equations elaborated in section 2. These equations are also listed in Table 2 and numbered from 1 to 3 as equation sets numbers. The corresponding parameters and the equations (section 2) used to calculate the critical transverse displacements are also listed in the same table. For example, for the equation set number 1 (Eqn. Set Nr-1) of Table 2, the critical transverse displacement (δ) was calculated using Eqn.1 (Yamamoto and Kasei, 1977) and k_w was calculated using Eqn. 4 (Nakamura et. al, 2001) given in section 2.

Finally, the experimentally determined loosening rates were drawn as function analytically calculated critical transverse displacements for comparison.

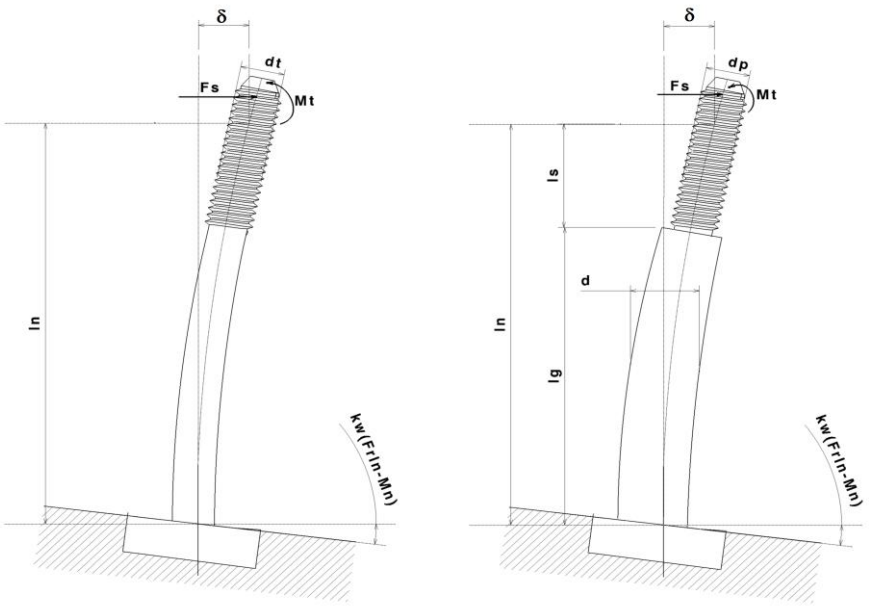

(a) (b)

Figure 1 (a) Deflection of a bolt caused by a transverse external force and (b) deflection of multi sectioned bolt caused by transverse external force

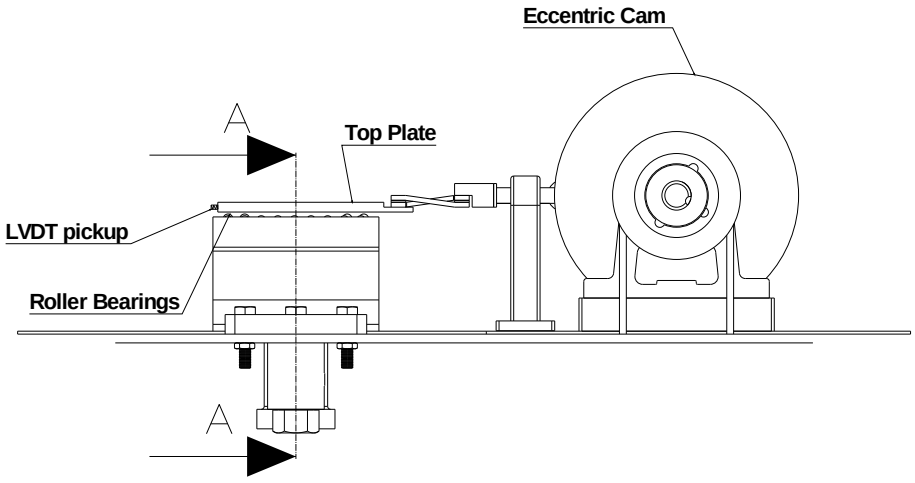

(a)

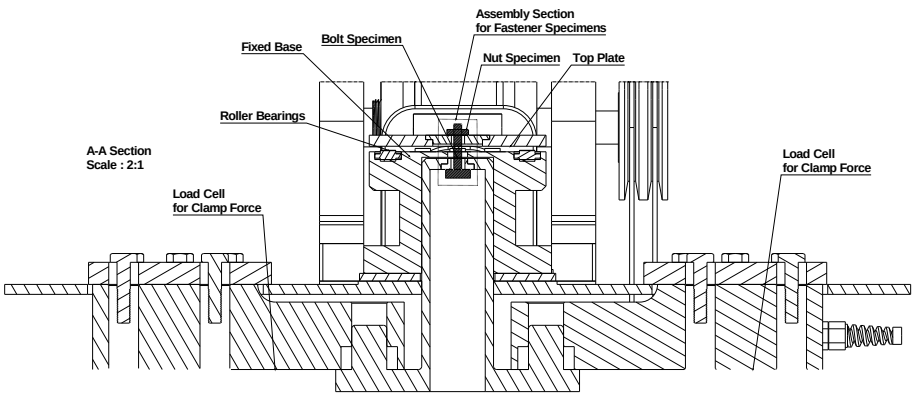

(b)

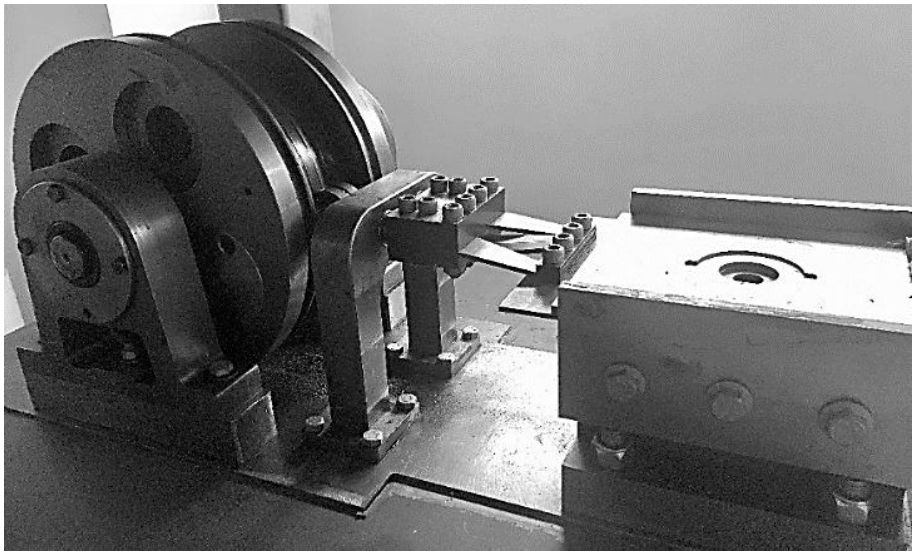

(c)

Figure 2 (a) Transverse vibration experimental set-up and (b) cross-section view of A-A showing the fixture used in the experimental setup (c) image of Junker test bench

Table 1
Parameters used in the transverse vibration tests

Initial Clamping Force (kN)	Clamp Length (mm)	Bearing Friction Coefficient	Thread Friction Coefficient	Transverse Displacement Amplitude (mm)	Frequency (Hz)
17.6	23	0.121	0.113	0.45	5
14.3	31	0.153	0.125		
10.27	44.5	0.172	0.137		
	53	0.204	0.146		
	65				
	85				

Table 2
Equation set numbers used to calculate the critical displacement (Eqn. Set Nr-1 through Eqn. Set Nr-3)

Number	δ	M_t	K_t	k_w
1	Yamamoto and Kasei [1977]			Nakamura et. al [2001]
2	Blume and Illgner [1988]	NA		NA
3	Friede and Lange[2010]	NA		NA

4. NUMERICAL STUDY

A three-dimensional simplified FE model of the bolted-joint shown in Figure 3 was used to determine the proportion of M_t to $F_s l_n$ to find the ratio of spring constant ratio in Eqn. 7. The finite element simulation was performed in commercial simulation software Simufact®. The elastic modulus and Poisson's ratio were taken 210 GPa and 0.3, respectively, for all deformable steel parts. All geometrical properties of bolt and nut joint model including helical thread (comply with DIN 13 [31]) and the tolerances given for 6h/6H, were kept the same as the experiments. The clamping force was applied by moving up "rigid nut washer" element in z-direction (Figure 3). After creating clamping force, the transverse excitation with 5 Hz frequency and 0.45 mm transverse displacement amplitude was applied to the moving "rigid nut washer" element through Y direction for 10 cycles (Figure 3). The numerical simulation was implemented with 23 mm clamp length and 17.6 kN initial clamping force. 0.121 bearing friction coefficient and 0.113 thread friction coefficient. Coulomb friction model was used and friction coefficients assigned to bearing and thread sides as 0.121 and 0.113 respectively. The numbers of tetrahedral 134 elements that are used at bolt and nut models, were 31041 and 25911 respectively. Segment to segment contact algorithm, mixed-direct iterative solver and adaptive time stepping based on automatic displacement change parameters were used.

5. RESULTS AND DISCUSSION

The variations of experimentally measured thread and bearing friction coefficient as function of the number of tightening-loosening (1st, 3rd, 5th, and 7th tightening-loosening) are shown given in Figure 4. All thread and bearing friction coefficients were measured according to ISO 16047 Fasteners-Torque/clamp force testing. At least 5 friction coefficient measurements were taken and the values were then averaged for each tightening-loosening number. The average friction coefficients of 1st, 3rd, 5th, and 7th tightening-loosening are sequentially 0.121, 0.153, 0.172 and 0.204 for bearing friction coefficient and 0.113, 0.125, 0.137 and 0.146 for friction thread coefficient. As the tightening-loosening number increases the friction coefficients increase as seen in Figure 4. Note in the same figure that the increase of bearing friction coefficient with the tightening-loosening number is higher than that of thread friction coefficient. The increase in friction coefficients with the increase of tightening-loosening number is also noted to show nearly a linear dependence. Hence, the experimental bearing and threat friction coefficients tabulated in Table 1 were average values of these measurements and determined by applying tightening-loosening prior to the transverse vibration experiments.

The critical transverse displacement prediction was taken correct or appropriate if the calculated critical transverse displacement of the equation sets numbered from 1 to 3 in Table 2 was less than 0.45 mm in the experimentally self-loosened bolts or if the calculated critical transverse displacement was higher than 0.45 mm in the experimentally no self-loosened bolts. Otherwise, the prediction was taken wrong or inappropriate. Figures 5(a-c) show the experimentally measured loosening rates as function of calculated critical displacement of the equation sets listed in Table 2. The experimental displacement amplitude (0.45 mm) is also shown as a vertical dotted line in Figures 5(a-c). As noted in Figures 5(a) and (c), the appropriate predictions of critical displacements of the Eqn. Set Nr-1 and Eqn. Set Nr-3 of Table 2 are 50 and 36.1%, respectively. The highest appropriate predictions of critical displacements are found in the Eqn Set Nr-2 of Table 2 as seen in Figures 5(b). This equation set predicts appropriately 58.3% of the critical displacements. The value of k_w is reduced from 3.28×10^{-4} to 1×10^{-8} in order to determine its effect on the correctness of the critical displacement prediction of Eqn. Set Nr-1. Note that Eqn. Set Nr-2 and Eqn. Set Nr-3 do not use the inclination

compliance of bolt head portion. The results of the calculations are shown in Figure 6 as the appropriate prediction percentage versus log k_w curve. As seen in Figure 6, the reduction of k_W is effective in increasing the appropriate prediction of the critical displacements down to $1x10^{-5}$ and further reduction is noted to have no significant effect on the appropriate prediction percentages of the equations investigated. Until this critical k_w value, $1x10^{-5}$, the appropriate prediction percentages increase to ~57% for the Eqn. Set Nr-1 (Figure 6). This critical value of k_w ,$1x10^{-5}$, is noted to be much smaller than *kw* values specified by Nishumira [32]. The finite element model variations of M_t and F_s with transverse displacement are shown in Figures 7(a) and (b), respectively. The ratio of spring constant $(\frac{K_t}{K_b+K_t})$ in Eqn. 7 was then calculated using numerical M_t and F_s values revealing pure bolt bending behavior during transverse loading. The ratio was determined 0.628. In order to compare the loosening rate of numerical simulation with those of experiments, the loosening rate of numerical simulation was numerically extended to higher cycles. Initially a linear fit lto the FE model clamp force-cycle curve was applied within 100 cycles; then, using the slope of this linear fitting the FE model clamp force-cycle curve was extended to 850 cycles. Figure 7(c) shows the variation of the extended FE model clamp force with the number of cycle at an initial clamp force of 17.6 kN. In the same figure, the variations of experimental clamp forces of five tests with the number of cycle at an initial clamp force of 17.6 kN are shown together with the variation of the experimental average clamp force. Note that the average experimental clamp force-cycle curve shows well agreements with the FE model clamp force-cycle curve especially at low cycles. The slope of the experimental average clamp force-cycle curve shown in Figure 7(c) yields a loosening rate of approximately 0.01256 kN/cycle. Finally, a new set of equations was developed using the FE model M_t values. This new equation is coded as Eqn. Set Nr-4 and tabulated in Table 3. Using the numerically calculated spring constant ratio and reaction moment, the critical transverse displacement amplitude was calculated for Eqn. Set Nr-4. Initially, the effect of value of k_w on the critical transverse displacement predictions of Eqn. Set Nr-4 was determined. The variation of the appropriate prediction percentage of Eqn. Set Nr-4 of Table 3 with the value of k_w is shown in Figure 8(a). The appropriate prediction percentage increases from 73.4 to 77.7% with the increase of k_w from $7.5x10^{-5}$ to $5x10^{-5}$ thereafter the appropriate percentage values saturate. Figure 8(b) shows the experimentally measured loosening rate as function of calculated critical displacement amplitudes with k_w value of $5x10^{-5}$. The use of FE model determined reaction moment increases the accuracy from 50.0 to 73.4%. The accuracy of the equations further increased with the use of appropriate k_w value, while the increase is only ~4%. The total increase in the appropriate prediction percentage is 27.7%.

6. CONCLUSIONS

The capabilities of the analytic models in predicting experimental self-loosening of bolted-joints was investigated both experimentally and numerically. The experimental loosening rates were determined in a Junker test bench at a constant transverse displacement amplitude (0.45 mm) and under controlled thread and bearing friction coefficient. The experimental test parameters were then used to calculate the critical displacement for self-loosening for each equation investigated. In addition, a three-dimensional accompanying FE model of bolted-joint was developed to calculate the ratio of spring constants engaging the thread to spring. The results indicated relative low capabilities of present analytical models in the prediction of the critical displacements of bolted-joint for self-loosening. The efforts to modify the nut reaction moment and the inclination compliance of bolt head portion in the equations investigated however resulted in moderate increase in the predictions of the critical displacements for self-loosening. On the other side, the use of the

reaction moment determined through the FE model was found to increase the prediction capabilities of the equations significantly.

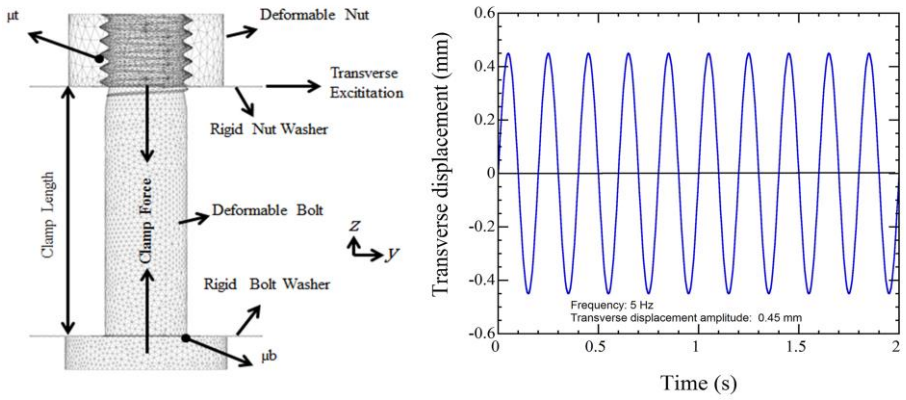

Figure 3 Finite element model of bolted-joint and applied transverse displacement versus time curve

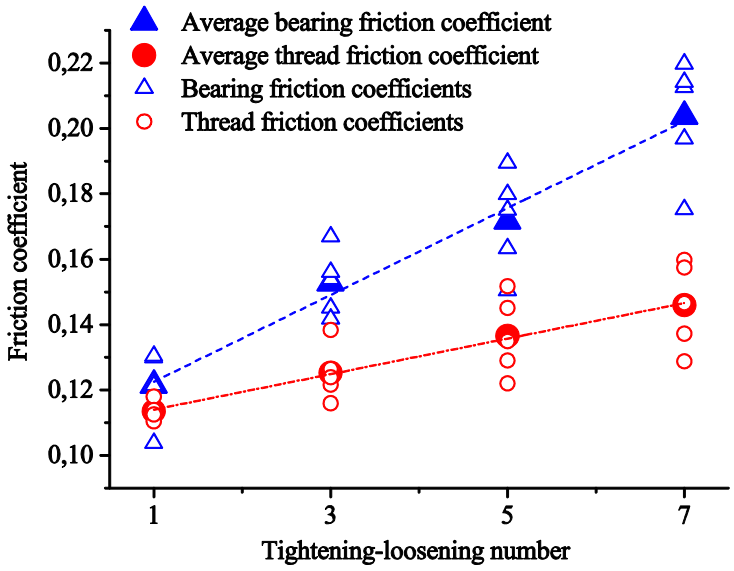

Figure 4 The variations of the thread and bearing friction coefficients with the number of tightening-loosening

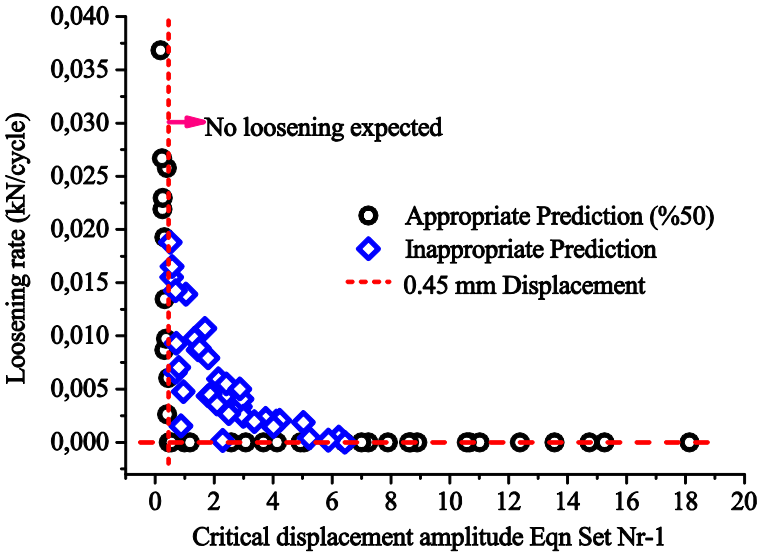
Loosening rate (kN/cycle)
0,040
0,035
0,030
0,025
0,020
0,015
0,010
0,005
0,000
No loosening expected
Appropriate Prediction (%50)
Inappropriate Prediction
0.45 mm Displacement
0
2
4
6
8
10
12
14
16
18
20
Critical displacement amplitude Eqn Set Nr-1

(a)

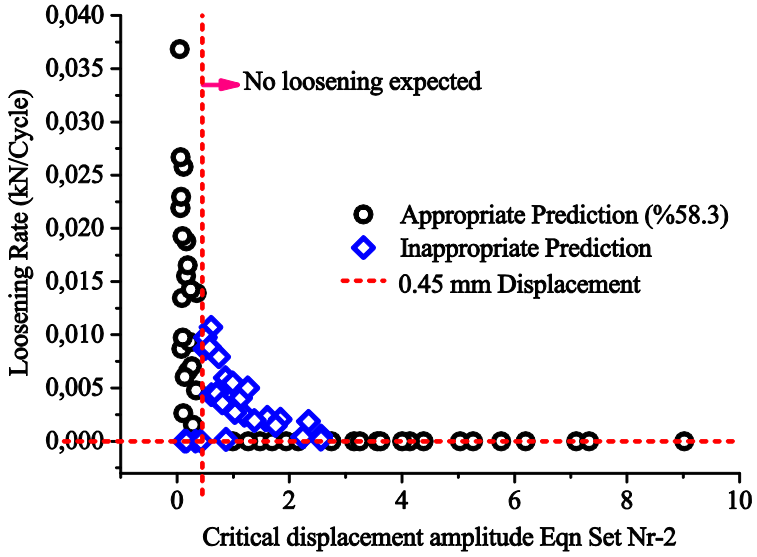
Loosening Rate (kN/Cycle)
0,040
0,035
0,030
0,025
0,020
0,015
0,010
0,005
0,000
No loosening expected
Appropriate Prediction (%58.3)
Inappropriate Prediction
0.45 mm Displacement
0
2
4
6
8
10
Critical displacement amplitude Eqn Set Nr-2

(b)

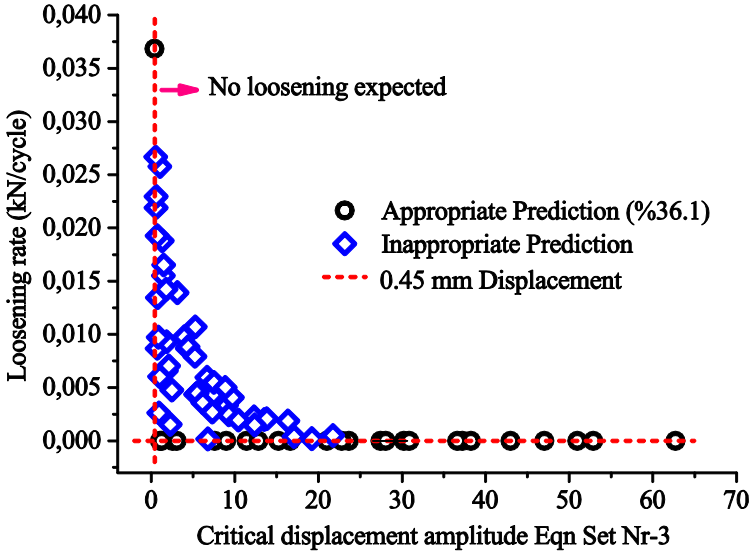

(c)

Figure 5 Comparison of experimental and analytical results of Eqn. Set Nr (a) 1, (b) 2, (c) 3 of Table 2

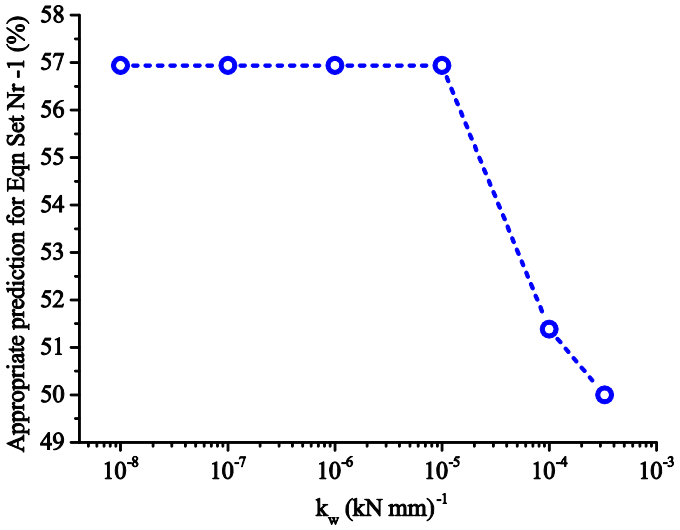

Figure 6 Change of appropriate prediction percentage with k_w for Eqn. Set Nr-1 of Table 2

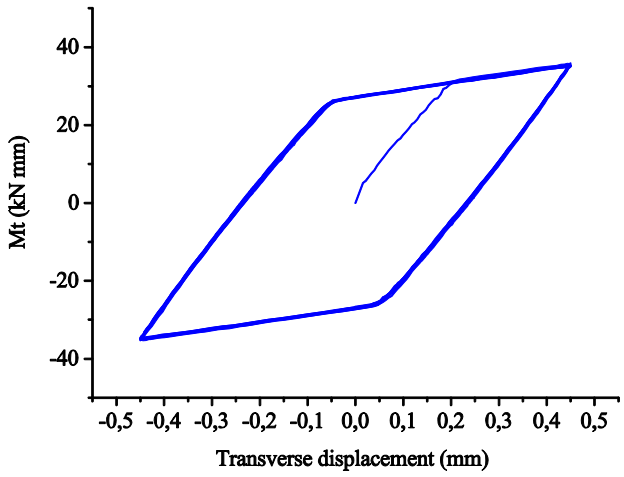

(a)

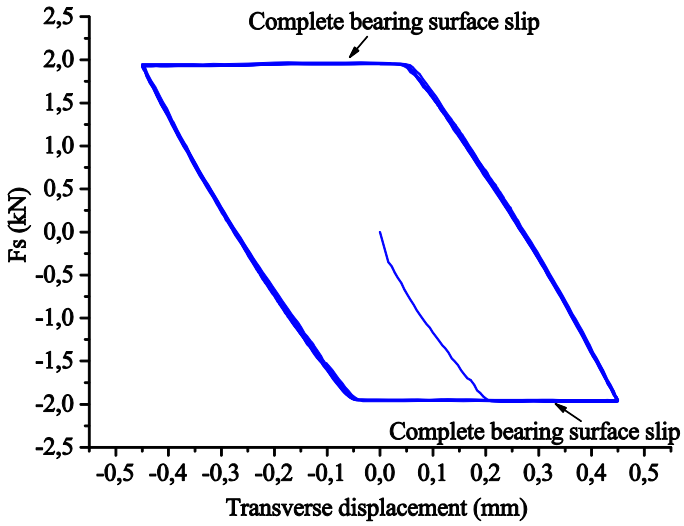

(b)

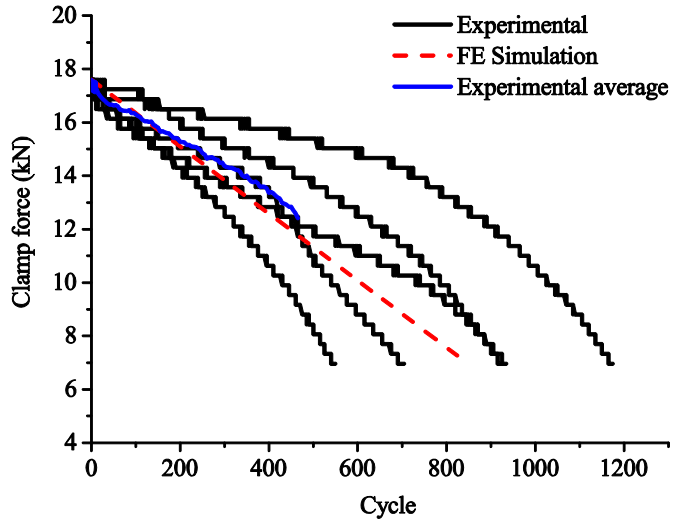

(c)

Figure 7 The curves of numerical simulation results of (a) M_t versus transverse displacement and (b) F_s versus transverse displacement and (c) the experimental and FE model clamp force versus cycle

Table 3
Equation set for Eqn Set Nr-4 for the critical displacement

Number	δ	M_t	$Kt/(Kb+Kt)$	k_w
4	Yamamoto and Kasei [1977]	Yokoyama et. al [2010]	Using Yokoyama et. al [2010] equation, derived from simulation : 0.628	Various

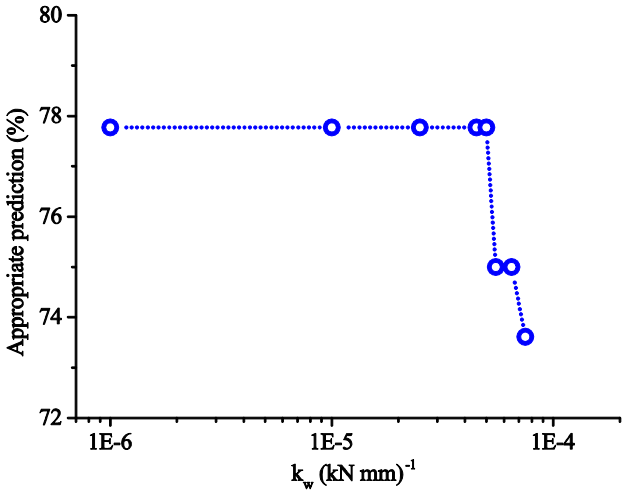

(a)

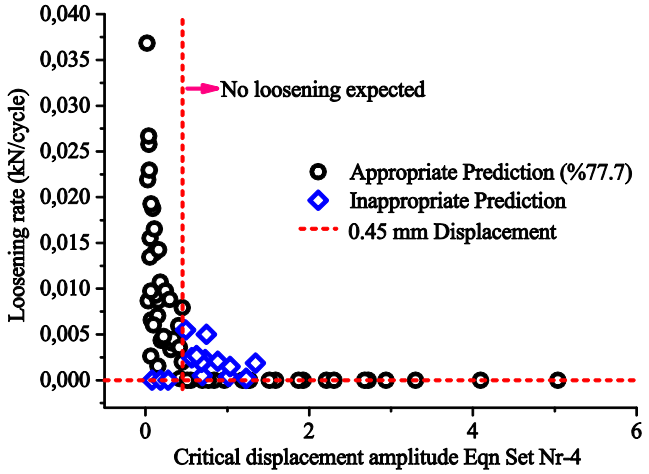

(b)

Figure 8 (a) variation of appropriate prediction percentage with k_w and (b) comparison of experimental and analytical results of Eqn. Set Nr-4 of Table 3

Acknowledgements

No acknowledgements has been declared by the authors.

Funding

The authors received no financial support for the research, authorship or publication of this work.

The Declaration of Conflict of Interest/ Common Interest

No conflict of interest or common interest has been declared by the authors.

Authors' Contribution

Umut İnce : Literature research, data collection, data processing, organize the execution of the study, contribution to article writing and study.

Mustafa Güden : Contribution to article writing and study, literature research

The Declaration of Ethics Committee Approval

The authors declare that this document does not require an ethics committee approval or any special permission.

The Declaration of Research and Publication Ethics

The authors of the paper declare that they comply with the scientific, ethical and quotation rules of SAUJS in all processes of the article and that they do not make any falsification on the data collected. In addition, they declare that Sakarya University Journal of Science and its editorial board have no responsibility for any ethical violations that may be encountered, and that this study has not been evaluated in any academic publication environment other than Sakarya University Journal of Science.

REFERENCES

[1] (1999, March of 3rd). *Aviation Safety Network - Accident Description*. Available: https://aviation-safety.net/database/record.php?id=19990224-0

[2] W. M. Evans, "United States Air Force Aircraft Accident Investigation Board Report," 2015.

[3] R. A. I. Branch, "Rail Accident Report - Derailment at Grayrigg," 2011.

[4] J. Goodier and R. Sweeney, "Loosening by vibration of threaded fastenings," *Mechanical Engineering*, vol. 67, pp. 798-802, 1945.

[5] J. Sauer, D. Lemmon, and E. Lynn, "Bolts: How to prevent their loosening," *Machine Design*, vol. 22, pp. 133-139, 1950.

[6] S. C. Gambrell, "Why bolts loosen?," *Machine Design*, vol. 40, pp. 163-167, 1968.

[7] G. H. Junker, "New Criteria for Self-Loosening of Fasteners Under Vibration," *SAE Transactions*, vol. 78, pp. 314-335, 1969.

[8] "DIN 65151:2002-08 Aerospace series - Dynamic testing of the locking characteristics of fasteners under transverse loading conditions (vibration test)," ed. 2002-08, 2002.

[9] "DIN 25201-1:2015-12 Design guide for railway vehicles and their components " in *Bolted joints - Part 4: Securing of bolted joints* ed, 2015.

[10] R. J. Finkelston, "How much shake can bolted joints take," *Machine Design*, vol. 44, pp. 122-128, 1972.

[11] A. Yamamoto and S. Kasei, "Investigation on the self loosening of threaded fasteners under transverse vibration - A solution for self-loosening mechanism," *Journal of the Japan Society of Precision Engineering*, vol. 43, pp. 470-475, 1977.

[12] A. Yamamoto and S. Kasei, "A solution for self-loosening mechanism of threaded fasteners under transverse vibration," *Journal of the Japan Society of Precision Engineering*, vol. 18, pp. 261-266, 1984.

[13] S. Izumi, T. Yokoyama, A. Iwasaki, and S. Sakai, "Three-dimensional finite element analysis of tightening and loosening mechanism of threaded fastener," *Engineering Failure Analysis*, vol. 12, pp. 604-615, Aug 2005.

[14] M. Nakamura, T. Hattori, S. Tsujimoto, and T. Umeki, "Estimation of back-off loosening limit for bolted joints under transverse cyclic loading," *Transactions of the Japan Society of Mechanical Engineers*, vol. 67, pp. 2976-3056, 2001.

[15] Araki.H and Pereyra.J., "Safely Secure Fasteners in Critical Applications," presented at the 2014 FAA Worldwide Airport Technology Transfer Conference, Galloway, New Jersey, USA, 2014.

[16] R. Friede and J. Lange, "Loss of Preload in Bolted Connections Due to Embedding

and Self Loosening," presented at the Stability and Ductility of Steel Structures, Rio, Brazil., 2010.

[17] S. A. Nassar and B. A. Housari, "Study of the effect of hole clearance and thread fit on the self-loosening of threaded fasteners," *Journal of Mechanical Design*, vol. 129, pp. 586-594, Jun 2007.

[18] B. A. Housari and S. A. Nassar, "Effect of thread and bearing friction coefficients on the vibration-induced loosening of threaded fasteners," *Journal of Vibration and Acoustics-Transactions of the Asme*, vol. 129, pp. 484-494, Aug 2007.

[19] S. A. Nassar and B. A. Housari, "Effect of thread pitch and initial tension on the self-loosening of threaded fasteners," *Journal of Pressure Vessel Technology-Transactions of the Asme*, vol. 128, pp. 590-598, Nov 2006.

[20] S. A. Nassar, B. A. Housari, and Asme, *Self-loosening of threaded fasteners due to cyclic transverse loads* vol. 2. New York: Amer Soc Mechanical Engineers, 2005.

[21] T. Yokoyama, S. Izumi, S. Sakai, and Asme, *Analytical Modeling Of The Transverse Load-Displacement Relation Of A Bolted Joint With Consideration Of The Mechanical Behavior On Contact Surfaces*. New York: Amer Soc Mechanical Engineers, 2009.

[22] D. Yasui, T. Fukuoka, and M. Nomura, "Finite Element Analysis of Loosening Phenomena of Bolted Joints with Washers," *The Proceedings of Conference of Kansai Branch*, vol. 2018.93, p. 417, 09/25 2018.

[23] S. Borawake and S. Naik, "An Investigation of Loosening Phenomenon in Bolted Joint by Finite Element Method," *SSRN Electronic Journal*, 01/01 2018.

[24] M. Zhang, D. Zeng, L. Lu, Y. Zhang, and J. Xu, "Finite element modeling and experimental validation of bolt loosening due to thread wear under transverse cyclic loading," *Engineering Failure Analysis*, vol. 104, 05/01 2019.

[25] V. Rafik, C. Bertrand, A. Daidié, and C. Chirol, *Experimental and Numerical Study of the Self-loosening of a Bolted Assembly*. Advances on Mechanics, Design Engineering and Manufacturing II, 2019.

[26] "DIN EN ISO 4017 "Fasteners – Hexagon head screws – Product grades A and B", 2015/05," ed, 2015.

[27] "DIN 934 "Hexagon nuts ,with metric coarse and fine pitch thread ,product grades A and B", 1987/10.," ed, 1987.

[28] "ISO 898-1 "Mechanical properties of fasteners made of carbon steel and alloy steel Part 1:Bolts, screws and studs with specified property classes — Coarse thread and fine pitch thread", 2013/01.," ed, 2013.

[29] "ISO 898-2 “Mechanische Eigenschaften von Verbindungselementen aus Kohlenstoffstahl und legiertem Stahl – Teil 2: Muttern mit festgelegten Festigkeitsklassen – Regelgewinde und Feingewinde”, 2012/08.," ed, 2012.

[30] "DIN EN ISO 16047:2013-01 Fasteners - Torque/clamp force testing ", ed, 2013.

[31] "DIN 13-1:1999-11 ISO general purpose metric screw threads - Part 1: Nominal sizes for coarse pitch threads; nominal diameter from 1 mm to 68 mm " 1999.

[32] N. Nishimura, T. Hattori, M. Yamashita, and N. Hayakawa, "Self loosening behavior of metal thread joints under transverse cyclic loading," in *Engineering Plasticity and Its Applications from Nanoscale to Macroscale, Pts 1 and 2*. vol. 340-341, N. Ohno and T. Uehara, Eds., ed Stafa-Zurich: Trans Tech Publications Ltd, 2007, pp. 1467-1472.

SAKARYA ÜNİVERSİTESİ
FEN BİLİMLERİ ENSTİTÜSÜ DERGİSİ

Sakarya University Journal of Science
SAUJS

e-ISSN 2147-835X | Period Bimonthly | Founded: 1997 | Publisher Sakarya University |
http://www.saujs.sakarya.edu.tr/en/

Title: A Novel Hybrid Algorithm: Sine Cosine Harmony Search Algorithm for Global Optimization

Authors: Bahadur ALIZADA

Recieved: 2020-07-16 14:16:12

Accepted: 2021-03-17 12:44:43

Article Type: Research Article

Volume: 25
Issue: 2
Month: April
Year: 2021
Pages: 513-529

How to cite
Bahadur ALIZADA; (2021), A Novel Hybrid Algorithm: Sine Cosine Harmony Search Algorithm for Global Optimization. Sakarya University Journal of Science, 25(2), 513-529, DOI: https://doi.org/10.16984/saufenbilder.770367
Access link
http://www.saujs.sakarya.edu.tr/en/pub/issue/60672/770367

Sakarya University Journal of Science 25(2), 513-529, 2021

A Novel Hybrid Algorithm: Sine Cosine Harmony Search Algorithm for Global Optimization

Bahadur ALIZADA*[1]

Abstract

The study is about the new hybrid optimization algorithm called Sine Cosine Harmony Search (SCHS). SCHS was created by combining the features of Sine Cosine Algorithm (SCA) and Harmony Search (HS) meta-heuristic algorithms. In the research, the stage of creating the model was confirmed by experiments. For this, it has been tested using global optimization techniques. Benchmark Functions (BF) with different parametric properties were used for testing time. For performance measurement, comparisons were made with various optimization algorithms. The improvement of SCHS on the basis of exploitation and exploration shows that the algorithm is competitive.

Keywords: Sine Cosine Algorithm, Harmony Search, Benchmark Functions, Meta-heuristic algorithms

1. INTRODUCTION

Meta-heuristic optimization algorithms are too many to follow. A single algorithm may not always be successful in various problems [1]. Therefore, new optimization algorithms are derived. Apart from this, sometimes hybrid techniques are obtained by combining existing algorithms. Hybrids show more successful results compared to the algorithms they derive from. They achieve this by improving their exploration and exploitation phases. Meta-heuristics are inspired by nature, it has a simple and useful structure, and it can be adapted to real life problems, increasing the interest of scientists in this field.

Some of the most common meta-heuristic optimization techniques and hybrid studies related to them are shown in Table 1.

Table 1
Some popular meta-heuristic optimization algorithms and their hybrids

Algorithms	Hybrids
Genetic Algorithm (GA) [2]	Taguchi – GA [3] GA – Particle Swarm Optimization [4] Grouping – GA [5]
Artificial Bee Colony (ABC) [6]	ABC – Levenberq Marquardt Algorithm [7] ABC – GA [8]

* Corresponding Author: bahadur_alizade@yahoo.com
[1] Erciyes University, Department of Computer Engineering, Kayseri, Turkey, ORCID: https://orcid.org/0000-0001-6587-4057

	Simplex – ABC [9]
Harmony Search (HS) [10]	Bat Algorithm – HS [11] Taguchi – HS [12] HS – ABC [13]
Sine Cosine Algorithm (SCA) [14]	SCA – Crow Search Algorithm [15] SCA – Whale Optimization Algorithm [16] Grey Wolf Optimizer – SCA [17]
Multi-Verse Optimizer (MVO) [18]	PSO –MVO [19] Electricity Generation System – MVO [20] Self-Adaptive – MVO [21]

In this study, 7 different models were first created based on the SCA's position update and based on HS. By comparing these models, final models were decided. Then, hybrid models were evaluated by making comparison with some known optimization problems. Benchmark

Functions (BF) [22-27], which are the most frequently encountered in the literature at the time of comparison, were used. BF are listed in Table 2. In the table, functions, dimension (Dim), range (Lower Bound (LB) - Upper Bound (UB)), the smallest value (f_{min}) that the function takes.

Information about the algorithms inspired by the work done and the models created are shown in part 2. Comparison in various aspects is given in section 3. General interpretation is given in section 4 (conclusion).

Table 2
Benchmark functions list

Function	**Dim**	**[LB UB]**	f_{min}
Unimodal Benchmark Functions			
$BF_1=\sum_{i=1}^{n} x_i^2$	30	[-100,100]	0
$BF_2=\sum_{i=1}^{n}\|x_i\| + \prod_{i=1}^{n}\|x_i\|$	30	[-10,10]	0
$BF_3=\sum_{i=1}^{n}(\sum_{j-1}^{i} x_j)^2$	30	[-100,100]	0
$BF_4=max_i\{\|x_i\|, 1 \le i \le n\}$	30	[-100,100]	0
$BF_5= \sum_{i=1}^{n-1}[100(x_{i+1} - x_i^2)^2 + (x_i - 1)^2]$	30	[-30,30]	0
$BF_6=\sum_{i=1}^{n}([x_i + 0.5])^2$	30	[-100,100]	0
$BF_7=\sum_{i=1}^{n} ix_i^4 + random[0,1)$	30	[-1.28,1.28]	0
Multimodal Benchmark Functions			
$BF_8=\sum_{i=1}^{n} -x_i \sin(\sqrt{\|x_i\|})$	30	[-500,500]	-418.9829× 30
$BF_9=\sum_{i=1}^{n}[x_i^2 - 10\cos(2\pi x_i) + 10]$	30	[-5.12,5.12]	0
BF_{10}=-20exp(-0.2$\sqrt{\frac{1}{n}\sum_{i=1}^{n} x_i^2}$)exp($\frac{1}{n}\sum_{i=1}^{n}\cos(2\pi x_i)$)+20+e	30	[-32,32]	0
$BF_{11}=\frac{1}{4000}\sum_{i=1}^{n} x_i^2 - \prod_{i=1}^{n}\cos\left(\frac{x_i}{\sqrt{i}}\right) + 1$	30	[-600,600]	0
$BF_{12}=\frac{\pi}{n}\{10\sin(\pi y_1) + \sum_{i=1}^{n-1}(y_i - 1)^2[1 + 10\sin^2(\pi y_{i+1})] + (y_n - 1)^2\} + \sum_{i=1}^{n} u(x_i, 10,100,4)$ $y_i = 1 + \frac{x_i + 1}{4}$ $u(x_i, a, k, m) = \begin{cases} k(x_i - a)^m & x_i > a \\ 0 & -a < x_i < a \\ k(-x_i - a)^m & x_i < -a \end{cases}$	30	[-50,50]	0
$BF_{13}= 0.1\{sin^2(3\pi x_1) + \sum_{i=1}^{n}(x_i - 1)^2[1 + sin^2(3\pi x_i + 1)] + (x_n - 1)^2[1 + sin^2(2\pi x_n)]\} + \sum_{i=1}^{n} u(x_i, 5,100,4)$	30	[-50,50]	0
Fixed-dimension Multimodal Benchmark Functions			

$BF_{14}= (\frac{1}{500}+\sum_{j=1}^{25}\frac{1}{j+\sum_{i=1}^{2}(x_i-a_{ij})^6})^{-1}$	2	[-65,65]	1
$BF_{15}= \sum_{i=1}^{11}\left[a_i-\frac{x_1(b_i^2+b_ix_2)}{b_i^2+b_ix_3+x_4}\right]^2$	4	[-5,5]	0.00030
$BF_{16}=4x_1^2-2.1x_1^4+\frac{1}{3}x_1^6+x_1x_2-4x_2^2+4x_2^4$	2	[-5,5]	-1.0316
$BF_{17}=(x_2-\frac{5.1}{4\pi^2}x_1^2+\frac{5}{\pi}x_1-6)^2+10(1-\frac{1}{8\pi})\cos x_1+10$	2	[-5,5]	0.398
$BF_{18}=[1+(x_1+x_2+1)^2(19-14x_1+6x_1x_2+3x_2^2)]\times[30+(2x_1-3x_2)^2\times(18-32x_1+12x_1^2+48x_2-36x_1x_2+27x_2^2)]$	2	[-2,2]	3
$BF_{19}=-\sum_{i=1}^{4}c_i\exp(-\sum_{j=1}^{3}a_{ij}(x_j-p_{ij})^2)$	3	[1,3]	-3.86
$BF_{20}=-\sum_{i=1}^{4}c_i\exp(-\sum_{j=1}^{6}a_{ij}(x_j-p_{ij})^2)$	6	[0,1]	-3.32
$BF_{21}=-\sum_{i=1}^{5}[(X-a_i)(X-a_i)^T+c_i]^{-1}$	4	[0,10]	-10.1532
$BF_{22}=-\sum_{i=1}^{7}[(X-a_i)(X-a_i)^T+c_i]^{-1}$	4	[0,10]	-10.4028
$BF_{23}=-\sum_{i=1}^{10}[(X-a_i)(X-a_i)^T+c_i]^{-1}$	4	[0,10]	-10.5363

2. RELATED WORKS

2.1. Harmony search algorithm

HS is a human-based algorithm inspired by the improvised music stage. Musicians improvise the sounds of the instruments seeking the most appropriate fit [10].

The properties of the algorithm are represented by its control parameters. Proper adjustment of these control parameters affects the results of the algorithm. Control parameters are described in Table 3.

Table 3
HS control parameters

Name of Control Parameter	Definition
Maximum Number of Iteration (**MaxIt**)	It shows the number of loops and is often the stopping criterion [28].
Harmony Memory Size (**HMS**)	The number of solution vectors represents the population size [28].
Harmony Memory Consideration Rate (**HMCR**)	It represents the probability of choosing one of the old values in the population [28].
Pitch Adjustment Rate (**PAR**)	It helps to produce different solutions and corresponds to changing pitch adjustment frequencies in music. [10].
Fret Width (**FW**) or Bandwidth (**BW**)	It is a design variable affecting exploration and exploitation [26].

The steps of the algorithm are shown as below with pseudocode.

Step 1: Assign values of control parameters.

Step 2: Create random population (HM) and calculate objective function.

Step 3: Improvise a new harmony ($x_{new}(j)$)

REPEAT

Step 4:

if_1 rand_1 < HMCR

$x_{new}(j)= x_{\propto}(j)$

If_2 rand_2 < PAR

$x_{new}(j)= x_{new}(j) \pm rand() \times BW$

end_if_2

else

$x_{new}(j)= LB(j) + rand() \times (UB(j) - LB(j))$

end_if_1

Where $\alpha \in (1,2,\dots,HMS)$, $x_\alpha(j)$ is selected from HM

Step 5: Update the HM

UNTIL the stop criterion is satisfied (MaxIt).

j represents the instant iteration. Here ±rand() shows uniform distribution and this shows that it changes in the range of [-1,1].

2.2. Sine cosine algorithm

SCA is a meta-heuristic optimization technique graphically inspired by sine and cosine motions. The algorithm creates random solutions first, then determines the best solution with the fitness function [14]. According to this solution, other elements in the population update their position. The update is done with the following function:

$$X_i^{t+1} = \begin{cases} X_i^T + r_1 \times \sin(r_2) \times \left| r_3 P_i^t - X_i^T \right|, r_4 < 0.5 \\ X_i^T + r_1 \times \cos(r_2) \times \left| r_3 P_i^t - X_i^T \right|, r_4 \geq 0.5 \end{cases} \quad (1)$$

X_i^T is the current position. P_i^t represents the best solution at the moment. r_1 is the random number that represents the direction of the update calculated by the equation $r_1 = a - t\frac{a}{T}$. Here, a represents the constant in the range [0.2], t is the beginning, and T is the maximum iteration. r_2, r_3, r_4 are random numbers that define the update distance in the range [0, 2π], the weight of the target in the range [0, 2], the balance between the sine and cosine movements ranging from [0, 1].

2.3. The proposed hybrid models

While performing hybridization, the following formulas were obtained by inspiring the position update model in SCA:

$$x_{new}(j) = \begin{cases} r_1 \times \sin(r_2) \times r_3 \times x_\alpha(j), r_4 < 0.5 \\ r_1 \times \cos(r_2) \times r_3 \times x_\alpha(j), \ \ r_4 \geq 0.5 \end{cases} \quad (2)$$

$$x_{new}(j) = \begin{cases} x_{new}(j) \pm r_1 \times \sin(r_2) \times r_3 \times rand() \times BW, \\ r_4 < 0.5 \\ x_{new}(j) \pm r_1 \times \cos(r_2) \times r_3 \times rand() \times BW, \\ r_4 \geq 0.5 \end{cases} \quad (3)$$

$$x_{new}(j) = \begin{cases} LB(j) + r_1 \times \sin(r_2) \times |r_3 \times LB(J) - UB(J)|, \\ r_4 < 0.5 \\ LB(j) + r_1 \times \cos(r_2) \times |r_3 \times LB(J) - UB(J)|, \\ r_4 \geq 0.5 \end{cases} \quad (4)$$

Details about whether the formulas are applied to the models are shown in Table 4 in an explanatory way. In the table, Sine Cosine Harmony Search (SCHS) hybrid models are numbered respectively according to the above formulas.

Table 4
Using formulas in hybrid models

Used Formulas	SCHS1	SCHS2	SCHS3	SCHS4	SCHS5	SCHS6	SCHS7
(2)	+	-	-	+	+	-	+
(3)	-	+	-	+	-	+	+
(4)	-	-	+	-	+	+	+

SCHS4 and SCHS7 have been chosen as the final models since they have had close success. These comparisons are more clearly stated in the results section.

2.3.1. SCHS4 pseudocode

r_5 in the model are random numbers in the range [0,1] equal to r_4.

Step 1: Assign values of control parameters.

Step 2: Create random population (HM) and calculate objective function.

Step 3: Improvise a new harmony ($x_{new}(j)$)

REPEAT

Step 4:

if_1 rand_1 < HMCR

if_2 $r_4 < 0.5$

$x_{new}(j) = r_1 \times \sin(r_2) \times r_3 \times x_\alpha(j)$

else

$x_{new}(j) = r_1 \times \cos(r_2) \times r_3 \times x_\alpha(j)$

end_if_2

If_3 rand_2 < PAR

if_4 $r_5 < 0.5$

$x_{new}(j) = x_{new}(j) \pm r_1 \times \sin(r_2) \times r_3 \times rand() \times BW$

else

$x_{new}(j) = x_{new}(j) \pm r_1 \times \cos(r_2) \times r_3 \times rand() \times BW$

end_if_4

end_if_3

else

$x_{new}(j) = LB(j) + rand() \times (UB(j) - LB(j))$

end_if_1

Where $\alpha \in (1,2,\dots,HMS), x_\alpha(j)$ is selected from HM

Step 5: Update the HM

UNTIL the stop criterion is satisfied (MaxIt).

2.3.2. SCHS7 pseudocode

r_5 and r_6 in the model are random numbers in the range [0,1] equal to r_4.

Step 1: Assign values of control parameters.

Step 2: Create random population (HM) and calculate objective function.

Step 3: Improvise a new harmony ($x_{new}(j)$)

REPEAT

Step 4:

if_1 rand_1 < HMCR

if_2 $r_4 < 0.5$

$x_{new}(j) = r_1 \times \sin(r_2) \times r_3 \times x_\alpha(j)$

else

$x_{new}(j) = r_1 \times \cos(r_2) \times r_3 \times x_\alpha(j)$

end_if_2

If_3 rand_2 < PAR

if_4 $r_5 < 0.5$

$x_{new}(j) = x_{new}(j) \pm r_1 \times \sin(r_2) \times r_3 \times rand() \times BW$

else

$x_{new}(j) = x_{new}(j) \pm r_1 \times \cos(r_2) \times r_3 \times rand() \times BW$

end_if_4

end_if_3

else

if_5 $r_6 < 0.5$

$x_{new}(j) = LB(j) + r_1 \times \sin(r_2) \times |r_3 \times LB(J) - UB(J)|$

else

$x_{new}(j) = LB(j) + r_1 \times \cos(r_2) \times |r_3 \times LB(J) - UB(J)|$

end_if_5

end_if_1

Where $\alpha \in (1,2,\dots,HMS), x_\alpha(j)$ is selected from HM

Step 5: Update the HM

UNTIL the stop criterion is satisfied (MaxIt).

3. RESULTS AND DISCUSSIONS

Several test cases should be used to demonstrate the performance of optimization algorithms. In this way, various tests are performed to prove that satisfactory results are not accidental. The high number of tests makes the performance of the algorithm more evident.

In the study, seven different models were created first. These models were adapted to 23 familiar BF and compared. These BFs are chosen from two kinds of test functions: unimodal and multimodal functions. Unimodal is locally optimistic and has only one global optima, which tests the speed of convergence and exploitation capability. Multimodal has one global and more than one local solution. This evaluates exploration abilities and avoidance of local consequences.

To solve the specified test functions, the population size, which is the common parameter values in all algorithms, is accepted as 30 and Maxit 500. The codes were run 30 times for each problem. The reason for the high number of run is chosen because the algorithms have a stochastic structure, so the results obtained at once are not very reliable. According to the results, best min, best max, average, standard deviation (S.D.) values were compared. Special control parameters in HS and hybrid models are set as HMCR 0.9, PAR 0.25, and BW 0.01. These specific parametric values are recommended in many studies [28,30]. Comparisons are given in Table 5. In the table, the minimum values were bold by making a comparison over the average.

Table 5
Comparison for the selection of hybrid models

BF1

Algorithms	Best min	Best Max	Average	S.D.
HS	3892,989	12803,9546	7322,6655	2191,8977
SCA	0,097509	308,8207	28,0842	58,0673
SCHS1	5,477E-07	4,1891E-05	1,5360E-05	1,0416E-05
SCHS2	4452,6873	11122,7397	7753,1206	1529,0288
SCHS3	19,1734	417,0179	124,0915	94,7923
SCHS4	**0**	**7,5319E-11**	**2,8383E-12**	**1,3496E-11**
SCHS5	3,9349E-10	5,0071E-05	1,6579E-05	1,3394E-05
SCHS6	24,3369	377,591	111,3353	75,6256
SCHS7	0	3,5452E-10	2,1837E-11	6,8979E-11

BF2

Algorithms	Best min	Best Max	Average	S.D.
HS	16,7249	38,1766	27,9543	5,362864
SCA	6,6656E-05	0,23871	0,030136	0,046223
SCHS1	0,001001	0,012557	0,006608	0,002498
SCHS2	19,1466	35,484	25,8691	4,109259
SCHS3	0,76331	7,0095	3,1899	1,649256
SCHS4	**0**	**1,715E-05**	**1,0579E-06**	**3,2487E-06**
SCHS5	3,9566E-05	0,013136	0,006604969	0,003462
SCHS6	0,58747	5,5668	3,030047	1,227704
SCHS7	0	3,7155E-05	4,3374E-06	9,7959E-06

BF3

Algorithms	Best min	Best Max	Average	S.D.
HS	42778,3951	72911,4585	54844,2568	8007,6166
SCA	1,098E-08	0,10377	0,011794	0,030333
SCHS1	1,5754E-06	0,00017371	7,9154E-05	4,5904E-05
SCHS2	41108,2485	72675,6962	56656,2683	7128,3273
SCHS3	4798,9901	44242,8833	25287,4192	9630,3654

SCHS4	**0**	**1,084E-09**	**4,0015E-11**	**1,9413E-10**
SCHS5	4,951E-09	0,00021399	6,7319E-05	4,8057E-05
SCHS6	9647,2455	41720,7357	23295,7146	8338,3719
SCHS7	0	1,0988E-09	1,1542E-10	2,9091E-10

BF4

Algorithms	Best min	Best Max	Average	S.D.
HS	46,8093	82,3186	66,8731	7,547957
SCA	5,1109E-06	0,01669	0,001494	0,003454
SCHS1	0,00068455	0,0045149	0,002688	0,001014
SCHS2	52,8333	78,3761	66,9844	5,742987
SCHS3	10,3387	23,0841	15,9445	2,717738
SCHS4	**0**	**6,5301E-06**	**3,9403E-07**	**1,2145E-06**
SCHS5	9,6349E-06	0,004835	0,002554	0,001107
SCHS6	10,6076	24,1984	15,9419	3,495881
SCHS7	0	9,7551E-06	1,0691E-06	2,3018E-06

BF5

Algorithms	Best min	Best Max	Average	S.D.
HS	2217460,2225	15905922,3856	7231848,7423	3145552,1831
SCA	**6,3911**	**8,8004**	**7,56233**	**0,531098**
SCHS1	28,717	28,9404	28,8872	0,063852
SCHS2	2788243,1984	19547082,5754	9945070,8493	4155608,2303
SCHS3	529,1656	18757,2572	4904,4418	4503,9617
SCHS4	28,7464	28,9529	28,9279	0,036041
SCHS5	28,7108	28,9453	28,8919	0,050414
SCHS6	498,4125	35196,7695	6035,5670	7178,0631
SCHS7	28,7476	28,9496	28,9103	0,040447

BF6

Algorithms	Best min	Best Max	Average	S.D.
HS	2518,511	11747,9984	7380,9895	2148,0398
SCA	**0,16086**	**0,79996**	**0,437673**	**0,154097**
SCHS1	5,5267	6,8412	6,247517	0,305211
SCHS2	4149,0916	12571,9666	8319,6886	2215,7416
SCHS3	15,2097	407,4046	119,2951	100,9400
SCHS4	5,7956	6,7532	6,34424	0,224476
SCHS5	5,1286	6,5285	6,02554	0,340724
SCHS6	17,7998	463,9078	120,0234	100,8902
SCHS7	4,7331	6,5591	5,984907	0,397911

BF7

Algorithms	Best min	Best Max	Average	S.D.
HS	1,2254	10,5976	5,466523	2,268252
SCA	0,00016383	0,012511	0,003751	0,003455
SCHS1	3,1223E-05	0,0086856	0,002243	0,001928
SCHS2	1,5591	9,804	5,294937	2,064621
SCHS3	0,030193	0,19244	0,089510	0,034497
SCHS4	**3,1062E-05**	**0,0058526**	**0,001664**	**0,001558**
SCHS5	0,00041785	0,0064498	0,002067	0,001534
SCHS6	0,058142	0,23677	0,097752	0,039159
SCHS7	0,00036513	0,0051217	0,001989	0,001330

BF8

Algorithms	Best min	Best Max	Average	S.D.
HS	-10153,2716	-7913,6101	-9075,1808	487,9375
SCA	-2444,2061	-1854,9322	-2144,9223	148,0728
SCHS1	-7182,2703	-4692,1159	-5937,4085	694,3250
SCHS2	-10099,8634	-8485,8737	-9186,2638	400,7526
SCHS3	-12555,5763	-11930,8468	-12461,5521	129,2061

SCHS4	-6972,4301	-4555,3865	-5851,5905	651,2755
SCHS5	-8035,435	-5686,84	-6762,1025	738,6810
SCHS6	**-12559,8936**	**-12258,4787**	**-12481,0026**	**66,2260**
SCHS7	-9277,3491	-5261,9817	-6943,4675	996,4264

BF9

Algorithms	Best min	Best Max	Average	S.D.
HS	64,1678	152,0628	102,0298	18,1078
SCA	0,1658	143,3196	41,9869	30,6500
SCHS1	0,00010829	0,0079029	0,00303246	0,00199915
SCHS2	78,3988	145,3067	106,1607	14,2405
SCHS3	2,6974	42,5112	15,6449	9,53840557
SCHS4	**0**	**1,5035E-08**	**5,6241E-10**	**2,6942E-09**
SCHS5	6,5127E-08	0,0066272	0,00270065	0,00202066
SCHS6	1,8938	30,9549	13,8947	7,67023005
SCHS7	0	3,1922E-08	2,7743E-09	7,22261E-09

BF10

Algorithms	Best min	Best Max	Average	S.D.
HS	15,3455	19,913	19,4762	0,82737886
SCA	5,1076E-10	0,0099231	0,00039209	0,00179942
SCHS1	0,00054147	0,0046738	0,00268940	0,00102041
SCHS2	15,7277	19,9079	19,3959	0,80679996
SCHS3	1,8132	6,3888	3,87572667	1,19379534
SCHS4	**8,8818E-16**	**6,4032E-06**	**3,6103E-07**	**1,1853E-06**
SCHS5	7,4968E-06	0,004716	0,00266100	0,00131918
SCHS6	1,346	7,5954	3,80907667	1,23364947
SCHS7	8,8818E-16	1,3753E-05	1,3807E-06	3,1348E-06

BF11

Algorithms	Best min	Best Max	Average	S.D.
HS	41,6513	117,2951	69,6358	21,4391
SCA	0,51441	3,7794	1,170392	0,575652
SCHS1	1,2188E-08	1,519E-06	6,0945E-07	4,2816E-07
SCHS2	51,6759	103,0083	70,4829	13,0294
SCHS3	1,1777	4,3834	2,112377	0,864032
SCHS4	**0**	**3,1213E-12**	**1,4386E-13**	**5,6899E-13**
SCHS5	3,6235E-11	2,2418E-06	6,8218E-07	5,2416E-07
SCHS6	1,2281	6,2853	2,054643	0,955177
SCHS7	0	1,4267E-11	9,1580E-13	2,8707E-12

BF12

Algorithms	Best min	Best Max	Average	S.D.
HS	446715,7721	42139487,8243	7772057,7222	8393477,1462
SCA	**0,04303**	**0,24875**	**0,116879**	**0,050462**
SCHS1	0,68974	1,3094	0,931589	0,122832
SCHS2	235897,5488	56501724,1297	10991804,1448	11364757,8560
SCHS3	0,054152	9,4979	1,969113	2,056264
SCHS4	0,66057	1,3758	0,990964	0,195818
SCHS5	0,53711	1,0901	0,808253	0,137141
SCHS6	0,07123	9,4034	2,014328	2,181666
SCHS7	0,48584	1,1154	0,749709	0,158297

BF13

Algorithms	Best min	Best Max	Average	S.D.
HS	**0,10684**	**0,45856**	**0,306805**	**20940012,2331**
SCA	4333950,6429	110214270,9505	27811430,3828	0,078630
SCHS1	2,7701	2,9933	2,93936	0,051508
SCHS2	3578600,3414	169144889,1309	37779172,4047	35286497,9803
SCHS3	2,2758	42,0018	11,1463	9,580429

SCHS4	2,76	2,9945	2,920243	0,057321
SCHS5	2,0926	2,9937	2,51881	0,184007
SCHS6	1,1087	39,6832	13,2758	9,432823
SCHS7	1,8001	2,9204	2,42839	0,249008

BF14

Algorithms	Best min	Best Max	Average	S.D.
HS	0,998	18,3043	7,360953	6,025582
SCA	0,998	2,9821	1,595877	0,907521
SCHS1	0,99801	12,6705	6,494600	5,213908
SCHS2	0,998	25,6947	8,959773	7,330919
SCHS3	**0,998**	**6,9033**	**1,479651**	**1,369136**
SCHS4	0,99803	12,6705	7,527455	5,173333
SCHS5	0,998	12,6705	2,328715	3,002079
SCHS6	0,998	12,6705	2,167169	2,970434
SCHS7	0,998	3,008	1,73453	0,874200

BF15

Algorithms	Best min	Best Max	Average	S.D.
HS	0,00080187	0,028963	0,00853507	0,00899296
SCA	0,00031894	0,0016633	0,00098219	0,00040097
SCHS1	0,00040062	0,0011645	0,00079686	0,00015385
SCHS2	0,00080366	0,051455	0,00935059	0,01276088
SCHS3	0,00072934	0,020974	0,00404222	0,00649864
SCHS4	0,00035644	0,00087938	0,00075387	0,00012224
SCHS5	0,00034061	0,0010246	0,00072536	0,00013144
SCHS6	0,00077058	0,020916	0,00535980	0,00740826
SCHS7	**0,00034967**	**0,0015024**	**0,00071505**	**0,00022873**

BF16

Algorithms	Best min	Best Max	Average	S.D.
HS	**-1,0316**	**-1,0316**	**-1,0316**	**6,6614E-16**
SCA	-1,0316	-1,0313	-1,0316	7,1802E-05
SCHS1	-1,0316	-1,0248	-1,0310	0,001586
SCHS2	-1,0316	-0.21546	-0.9772	0.203581
SCHS3	**-1,0316**	**-1,0316**	**-1,0316**	**6,6614E-16**
SCHS4	-1,0316	-1,0124	-1,0305	0,003563
SCHS5	-1,0316	-1,0269	-1,0312	0,000987
SCHS6	**-1,0316**	**-1,0316**	**-1,0316**	**6,6614E-16**
SCHS7	-1,0316	-1,0258	-1,0312	0,001244

BF17

Algorithms	Best min	Best Max	Average	S.D.
HS	0,39789	0,53847	0,40274	0,02522
SCA	0,39792	0,40201	0,39881	0,00075
SCHS1	0,39789	0,40179	0,39872	0,00091
SCHS2	0,39789	0,40264	0,39805	0,00085
SCHS3	**0,39789**	**0,39789**	**0,39789**	**1,6653E-16**
SCHS4	0,39791	0,40695	0,39929	0,00201
SCHS5	0,3979	0,41079	0,39972	0,00302
SCHS6	**0,39789**	**0,39789**	**0,39789**	**1,6653E-16**
SCHS7	0,39791	0,40462	0,39911	0,00132

BF18

Algorithms	Best min	Best Max	Average	S.D.
HS	3	84,0105	33,7297	35,4572
SCA	**3**	**3,001**	**3,0001**	**0,00025**
SCHS1	3,0003	30,005	6,21685	7,69182
SCHS2	3	30	6.6	9.17824
SCHS3	3	30	11,1	12,3730

SCHS4	3,0002	30,0267	5,89671	6,79378
SCHS5	3	3,3301	3,03977	0,07827
SCHS6	3	30	9,3	11,4197
SCHS7	3,0001	3,6531	3,08564	0,14505

BF19

Algorithms	Best min	Best Max	Average	S.D.
HS	**-0,30048**	**-0,30048**	**-0,30048**	**1,1102E-16**
SCA	**-0,30048**	**-0,30048**	**-0,30048**	**1,1102E-16**
SCHS1	**-0,30048**	**-0,30048**	**-0,30048**	**1,1102-16**
SCHS2	-0,30048	-0,25323	-0,29736	0,00888
SCHS3	**-0,30048**	**-0,30048**	**-0,30048**	**1,1102E-16**
SCHS4	**-0,30048**	**-0,30048**	**-0,30048**	**1,1102E-16**
SCHS5	**-0,30048**	**-0,30048**	**-0,30048**	**1,1102E-16**
SCHS6	**-0,30048**	**-0,30048**	**-0,30048**	**1,1102E-16**
SCHS7	**-0,30048**	**-0,30048**	**-0,30048**	**1,1102E-16**

BF20

Algorithms	Best min	Best Max	Average	S.D.
HS	-3,322	-3,2031	-3,2744	0,058249
SCA	-3,2205	-1,7941	-2,8824	0,358220
SCHS1	-3,3154	-3,1521	-3,2762	0,035434
SCHS2	-3,322	-3,2031	-3,2824	0,056050
SCHS3	**-3,322**	**-3,2031**	**-3,2982**	**0,04756**
SCHS4	-3,3163	-3,1625	-3,2658	0,047893
SCHS5	-3,3174	-3,1374	-3,2608	0,048837
SCHS6	-3,322	-3,2031	-3,2903	0,052580
SCHS7	-3,3144	-2,929	-3,2525	0,082241

BF21

Algorithms	Best min	Best Max	Average	S.D.
HS	-10,1532	-2,4593	-3,99803	2,789443
SCA	-6,0306	-0,49726	-2,45088	1,936642
SCHS1	-5,0489	-4,9267	-5,00425	0,031241
SCHS2	-10,1532	-1,2646	-5,03592	3,674335
SCHS3	**-10,1532**	**-2,6305**	**-5,07905**	**3,364213**
SCHS4	-5,0507	-3,7408	-4,96542	0,231392
SCHS5	-5,0533	-4,9385	-5,01395	0,028906
SCHS6	-10,1532	-2,6305	-4,42073	3,162511
SCHS7	-5,051	-2,8328	-4,93240	0,395816

BF22

Algorithms	Best min	Best Max	Average	S.D.
HS	-10,4029	-2,7519	-6,20212	3,686260
SCA	-6,0837	-0,90396	-3,61791	1,606093
SCHS1	-5,0832	-4,8636	-5,04436	0,039995
SCHS2	**-10,4029**	**-2,6548**	**-6,49577**	**3,705835**
SCHS3	-10,4029	-1,8376	-5,57897	3,547183
SCHS4	-5,0831	-4,978	-5,04532	0,026063
SCHS5	-5,0857	-4,9767	-5,04650	0,024022
SCHS6	-10,4029	-2,7519	-4,94047	3,152824
SCHS7	-5,0755	-4,8795	-5,02789	0,056975

BF23

Algorithms	Best min	Best Max	Average	S.D.
HS	-10,5364	-2,3558	-5,21524	3,264729
SCA	-7,0357	-0,94159	-4,26876	1,577655
SCHS1	-5,1259	-5,0391	-5,08894	0,025244
SCHS2	-10,5364	-2,4217	-6,89508	3,532485
SCHS3	**-10,5364**	**-2,8066**	**-7,33870**	**3,668120**

SCHS4	-5,1166	-4,9047	-5,08352	0,042022
SCHS5	-5,1251	-4,9137	-5,08013	0,050410
SCHS6	-10,5364	-2,4273	-6,71929	3,583871
SCHS7	-5,1226	-4,9277	-5,07796	0,046998

3.1. Exploitation and Exploration analysis

Looking at the results, whether the unimodal or multimodal benchmarks, SCHS4 and SCHS7 hybrid models have been successful. When viewed on the basis of unimodal, the success of hybrids shows that the exploitation phase is developing. Similarly, the results in terms of multimodal show that hybrid algorithms are also successful in the discovery phase. Hybrids are developed on the basis of HS. Therefore, it is seen that hybrids provide improvement when compared with HS.

According to the results in Table 5, a general ranking table (Table 6) was created. This is because SCHS3 shows first place in some problems. But the hybrid has a lot of bad results. Table 6 shows how many times the Algorithms won. Thus, the ranking that each algorithm earns the most shows its order among all algorithms. In the rankings given, the hybrid algorithms that win the 1st and 2nd places the most are chosen as the final models.

Table 6
Scoring of hybrid models

Algorithms	**Ranks**									**Ranking**
	I	**II**	**III**	**IV**	**V**	**VI**	**VII**	**VIII**	**IX**	**Won**
HS	3	1	-	2	1	-	1	10	5	VIII
SCA	5	2	2	1	6	-	1	1	5	V
SCHS1	1	1	3	9	6	2	1	-	-	IV
SCHS2	1	4	2	-	-	1	1	4	10	IX
SCHS3	7	1	1	-	-	8	5	1	-	VI
SCHS4	9	-	1	2	5	4	-	2	-	I
SCHS5	1	2	9	5	1	1	4	-	-	III
SCHS6	4	1	1	1	1	5	9	1	-	VII
SCHS7	2	11	3	1	2	1	1	2	-	II

According to the results in Table 6, SCHS4 and SCHS7 were compared with well-known algorithms (Ant Lion Optimizer (ALO) [31], Particle Swarm Optimization (PSO) [32], States of Matter Search (SMS) [33,34], Bat Algorithm (BA) [35], Flower Pollination Algorithm (FPA) [36], Cuckoo Search (CS) [37,38], Firefly Algorithm (FA) [39,40], GA [2]) due to their success. Comparison time has been changed to iteration 1000 only. The reason for this is to adapt to the parameters of the ready data used for comparison [31]. Comparison time was compared only through average. The results are discussed in Table 7 over 13 BF.

Table 7
General comparison

F	f_{min}	SCHS4	SCHS7	ALO	PSO	SMS
				Average		
BF1	0	**7,53E-13**	1,65E-12	2.59E-10	2.70E-09	0.056987
BF2	0	**7,21E-07**	1,07E-06	1.84241E-06	7.15E-05	0.006848
BF3	0	**1,03E-11**	1,09E-11	6.06847E-10	4.71E-06	0.959865
BF4	0	2,19E-07	2,51E-07	**1.36061E-08**	3.25E-07	0.276594
BF5	0	28,817207	28,82529	0.346772393	0.123401	0.085348
BF6	0	5,1356	4,877317	**2.56183E-10**	5.23E-07	0.125323
BF7	0	0,000748	0,000739	0.004292492	0.001398	**0.000304**
BF8	-12569.487	-6869,62732	**-7789,52884**	-1606.27643	-1367.01	-4.20735
BF9	0	**1,36E-10**	3,99E-10	7.71411E-06	0.278588	1.32512
BF10	0	2,73E-07	3,34E-07	**3.73035E-15**	1.11E-09	8.88E-06
BF11	0	**3,19E-14**	9,45E-14	0.018604494	0.273674	0.70609
BF12	0	0,716598	0,532728	**9.74645E-12**	9.42E-09	0.12334
BF13	0	2,88286	2,367167	**2.00222E-11**	1.35E-07	1.35E-02

F	f_{min}	BA	FPA	CS	FA	GA
				Average		
BF1	0	0.773622	1.06346E-07	6.50E-03	0.039615	0.118842
BF2	0	0.334583	0.000624246	2.12E-01	0.050346	0.145224
BF3	0	0.115303	5.6682E-08	2.47E-01	0.049273	0.13902
BF4	0	0.192185	0.003837885	1.12E-05	0.145513	0.157951
BF5	0	0.334077	0.781200043	**0.007197**	2.175892	0.714157
BF6	0	0.778849	1.08459E-07	5.95E-05	0.05873	0.167918
BF7	0	0.137483	0.003105276	0.001321	0.000853	0.010073
BF8	-12569.487	-1065.88	-1842.42621	-2094.91	-1245.59	-2091.64
BF9	0	1.233748	0.273294621	0.127328	0.263458	0.659271
BF10	0	0.129359	0.007398721	8.16E-09	0.168306	0.956111
BF11	0	1.451575	0.085021659	0.122678	0.099815	0.487809
BF12	0	0.395977	0.000265711	5.60E-09	0.126076	0.110769
BF13	0	0.386631	3.67E-06	4.88E-06	0.00213	1.29E-01

Looking at the results, both hybrid models were observed to exhibit competitive results. Table 8 has been created to show the comparison more comfortably. Thus, the comparison score of each algorithm was determined. Likewise, the results here show that the hybrid has successful exploitation and exploration features compared to other algorithms.

3.2. Convergence behavior analysis

Although the balance provided by the hybrid algorithm in exploitation and exploration phases is exhibited with the above results, the observations of the convergence behavior are not specified. Therefore, the algorithm was inspected from another perspective by preparing the convergence curves.

Table 8
Scoring of the compared algorithms

Algorithms	Ranks										Best Score
	I	II	III	IV	V	VI	VII	VIII	IX	X	
SCHS4	5	3	-	1	-	-	-	-	1	3	I
SCHS7	1	5	2	-	1	-	-	-	3	1	II
ALO	5	-	5	-	1	1	-	1	-	-	I, III
PSO	-	2	3	3	1	1	3	-	-	-	III, IV, VII
SMS	1	1	-	-	1	4	-	1	1	4	VI, X
BA	-	-	-	1	-	-	1	4	3	4	VII, X
FPA	-	1	1	3	3	2	3	-	-	-	IV, V, VII
CS	1	1	2	3	2	2	-	-	2	-	IV
FA	-	-	-	1	3	2	4	2	1	-	VII
GA	-	-	-	1	1	1	2	5	2	1	VIII

Comparison of selected hybrid algorithms in terms of convergence rate was made. For this, comparison was made with HS, ALO and SCA over BF1, BF2, BF3, BF8, BF9 and BF11. The results are shown in Figure 1. The results are compared with the results obtained over 500 iterations. It was run 30 times independently for each problem. The average was calculated as 30 different results were obtained for each iteration. Convergence graphs were created over these 500 average results.

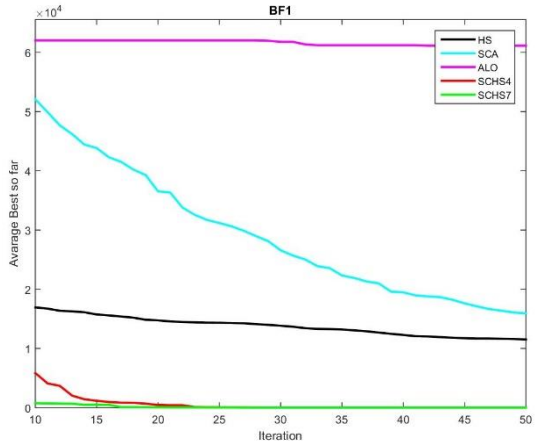

a) BF1

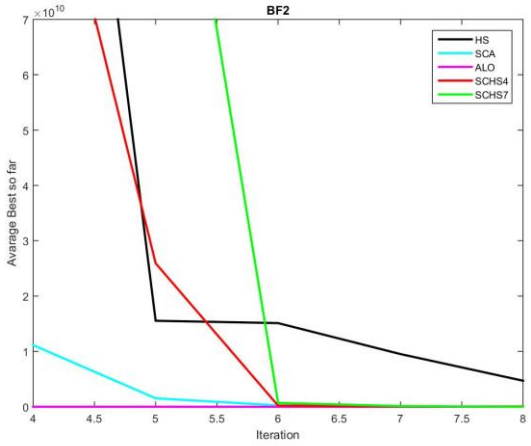

b) BF2

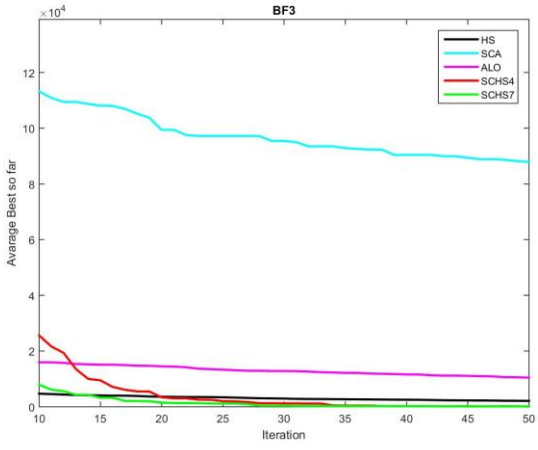

c) BF3

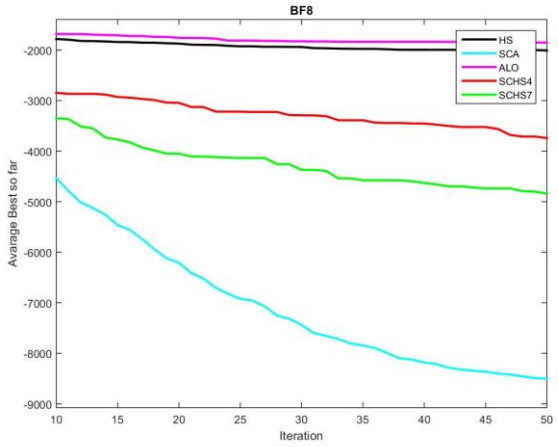

d) BF8

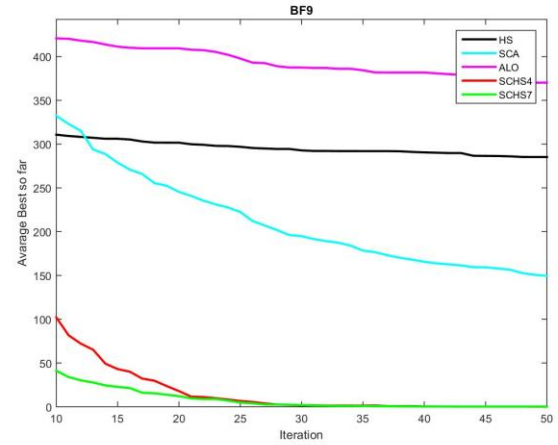

e) BF9

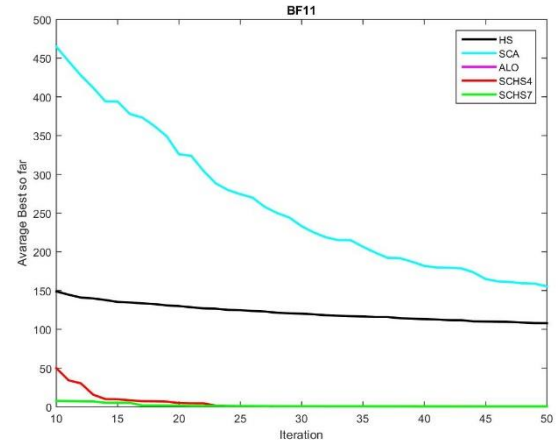

f) BF11

Figure 1 Convergence curves

Looking at the figures, it is observed that SCHS4 and SCHS7 have similar speeds. The iteration interval was kept short in the graphs to notice the comparison between speeds.

In summary, hybrid algorithms show that they are competitive in terms of improvements on the basis of HS, in comparison with other optimization algorithms and in terms of their convergence rate.

4. CONCLUSION

In this study, the new hybrid technique SCHS is presented. BF was used to test the algorithms. Experiments were made to decide on the final models and the optimization algorithms they derive were compared. It has been compared with the known optimization algorithms to demonstrate the performance of the algorithm that has improved. By comparison, it has been observed that the algorithm can compete with other optimization algorithms. In addition, the time of convergence curve comparisons also showed successful performance.

The study is thought to be motivating other researchers to use this algorithm. In future studies, binary and similar models of SCHS can be created. In addition, the performance map can be expanded by adapting the model to various engineering problems.

Acknowledgments

I would like to thank Dr. Seyedali Mirjalili and Seyed Mostapha Kalami Heris for their work in the field and for making them open to us.

Funding

The author received no financial support for the research, authorship or publication of this study.

The Declaration of Conflict of Interest/ Common Interest

No conflict of interest or common interest has been declared by the authors.

The Declaration of Ethics Committee Approval

Ethics Committee Approval is not required.

The Declaration of Research and Publication Ethics

The author of the paper declare that he comply with the scientific, ethical and quotation rules of SAUJS in all processes of the paper and that he does not make any falsification on the data collected. In addition, he declares that Sakarya University Journal of Science and its editorial board have no responsibility for any ethical violations that may be encountered, and that this study has not been evaluated in any academic publication environment other than Sakarya University Journal of Science.

REFERENCES

[1] Wolpert, D. and Macready, W., 1997. No free lunch theorems for optimization. *IEEE Transactions on Evolutionary Computation*, 1(1), pp.67-82.

[2] J. H. Holland, "Genetic Algorithms," Scientific American, vol. 267, no. 1, pp. 66–72, 1992.

[3] J.-T. Tsai, T.-K. Liu, and J.-H. Chou, "Hybrid Taguchi-Genetic Algorithm for Global Numerical Optimization," IEEE Transactions on Evolutionary Computation, vol. 8, no. 4, pp. 365–377, 2004.

[4] C.-F. Juang, "A Hybrid of Genetic Algorithm and Particle Swarm Optimization for Recurrent Network Design," IEEE Transactions on Systems, Man and Cybernetics, Part B (Cybernetics), vol. 34, no. 2, pp. 997–1006, 2004.

[5] E. Falkenauer, "A hybrid grouping genetic algorithm for bin packing," Journal of Heuristics, vol. 2, no. 1, pp. 5–30, 1996.

[6] D. Karaboga and B. Basturk, "A powerful and efficient algorithm for numerical function optimization: artificial bee colony (ABC) algorithm," Journal of Global Optimization, vol. 39, no. 3, pp. 459–471, 2007.

[7] C. Ozturk and D. Karaboga, "Hybrid Artificial Bee Colony algorithm for neural network training," 2011 IEEE Congress of Evolutionary Computation (CEC), 2011.

[8] X. Yan, Y. Zhu, W. Zou, and L. Wang, "A new approach for data clustering using hybrid artificial bee colony algorithm," Neurocomputing, vol. 97, pp. 241–250, 2012.

[9] F. Kang, J. Li, and Q. Xu, "Structural inverse analysis by hybrid simplex artificial bee colony algorithms," Computers & Structures, vol. 87, no. 13-14, pp. 861–870, 2009.

[10] Z. W. Geem, J. H. Kim, and G. Loganathan, "A New Heuristic Optimization Algorithm: Harmony Search," Simulation, vol. 76, no. 2, pp. 60–68, 2001.

[11] G. Wang and L. Guo, "A Novel Hybrid Bat Algorithm with Harmony Search for Global Numerical Optimization," Journal of Applied Mathematics, vol. 2013, pp. 1–21, 2013.

[12] A. R. Yıldız, «Hybrid Taguchi-Harmony Search Algorithm for Solving,» International Journal of Industrial Engineering Theory, Applications and Practice, cilt 15, no. 3, pp. 286-93, 2008.

[13] B. Wu, C. Qian, W. Ni, and S. Fan, "Hybrid harmony search and artificial bee colony algorithm for global optimization problems," Computers & Mathematics with Applications, vol. 64, no. 8, pp. 2621–2634, 2012.

[14] S. Mirjalili, "SCA: A Sine Cosine Algorithm for solving optimization problems," Knowledge-Based Systems, vol. 96, pp. 120–133, 2016.

[15] S. H. R. Pasandideh və S. Khalilpourazari, "SINE COSINE CROW SEARCH ALGORITHM: A POWERFUL HYBRID META HEURISTIC FOR GLOBAL OPTIMIZATION," arXiv preprint arXiv:1801.08485, 2018.

[16] S. Khalilpourazari and S. Khalilpourazary, "SCWOA: an efficient hybrid algorithm for parameter optimization of multi-pass milling process," Journal of Industrial and Production Engineering, vol. 35, no. 3, pp. 135–147, 2018.

[17] N. Singh and S. Singh, "A novel hybrid GWO-SCA approach for optimization problems," Engineering Science and Technology, an International Journal, vol. 20, no. 6, pp. 1586–1601, 2017.

[18] S. Mirjalili, S. M. Mirjalili, and A. Hatamlou, "Multi-Verse Optimizer: a nature-inspired algorithm for global optimization," Neural

Computing and Applications, vol. 27, no. 2, pp. 495–513, 2015.
[19] P. Jangir, S. A. Parmar, I. N. Trivedi, and R. Bhesdadiya, "A novel hybrid Particle Swarm Optimizer with multi verse optimizer for global numerical optimization and Optimal Reactive Power Dispatch problem," Engineering Science and Technology, an International Journal, vol. 20, no. 2, pp. 570–586, 2017.
[20] M. Sulaiman, S. Ahmad, J. Iqbal, A. Khan, and R. Khan, "Optimal Operation of the Hybrid Electricity Generation System Using Multiverse Optimization Algorithm," Computational Intelligence and Neuroscience, vol. 2019, pp. 1–12, 2019.
[21] X. Wang, D. Luo, X. Zhao, and Z. Sun, "Estimates of energy consumption in China using a self-adaptive multi-verse optimizer-based support vector machine with rolling cross-validation," Energy, vol. 152, pp. 539–548, 2018.
[22] M. Jamil and X. S. Yang, "A literature survey of benchmark functions for global optimisation problems," International Journal of Mathematical Modelling and Numerical Optimisation, vol. 4, no. 2, p. 150, 2013.
[23] B. Alizada, «Improved Whale Optimization Algorithm Based On Π Number,» International Scientific And Vocational Journal (Isvos Journal), Cilt 4, No. 1, Pp. 21-30, 2020.
[24] S. Mirjalili Ve A. Lewis, «The Whale Optimization Algorithm,» Advances In Engineering Software, Cilt 95, Pp. 51-67, 2016.
[25] M. Danacı And M. A. Dıallo, "A New Hybrid Fruit Fly Optimization Algorithm For Solving Benchmark Problems," Euroasia Journal Of Mathematics-Engineering Natural & Medical Sciences , Vol.2, Pp.23-27, 2019
[26] M. Danacı And Z. Akhdır, "A Novel Hybrid Bat Crow Search Algorithm For Solving Optimization Problems," Euroasia Journal Of Mathematics-Engineering Natural & Medical Sciences , vol.2, pp.40-45, 2019
[27] M. Danacı And B. Alızada, "An Improvement Of Hybrid Whale Optimization Algorithm," Euroasia Journal Of Mathematics-Engineering Natural & Medical Sciences , vol.2, pp.60-68, 2019
[28] P. Chakraborty, G. G. Roy, S. Das, D. Jain, and A. Abraham, "An Improved Harmony Search Algorithm with Differential Mutation Operator," Fundamenta Informaticae, vol. 95, no. 4, pp. 401–426, 2009.
[29] Q.-K. Pan, P. Suganthan, M. F. Tasgetiren, and J. Liang, "A self-adaptive global best harmony search algorithm for continuous optimization problems," Applied Mathematics and Computation, vol. 216, no. 3, pp. 830–848, 2010.
[30] X. Gan, E. Jiang, Y. Peng, S. Geng, and M. Kustudic, "Research Optimization on Logistic Distribution Center Location Based on Improved Harmony Search Algorithm," Lecture Notes in Computer Science Advances in Swarm Intelligence, pp. 410–420, 2018.
[31] S. Mirjalili, "The Ant Lion Optimizer," Advances in Engineering Software, vol. 83, pp. 80–98, 2015.
[32] R. Eberhart and J. Kennedy, "A new optimizer using particle swarm theory," MHS'95. Proceedings of the Sixth International Symposium on Micro Machine and Human Science.
[33] E. Cuevas, A. Echavarría, and M. A. Ramírez-Ortegón, "An optimization algorithm inspired by the States of Matter that improves the balance between exploration and exploitation," Applied Intelligence, vol. 40, no. 2, pp. 256–272, 2013.
[34] E. Cuevas, A. Echavarría, D. Zaldívar, and M. Pérez-Cisneros, "A novel evolutionary algorithm inspired by the states of matter for template matching," Expert Systems with Applications, vol. 40, no. 16, pp. 6359–6373, 2013.
[35] X. S. Yang, "A New Metaheuristic Bat-Inspired Algorithm," Nature Inspired Cooperative Strategies for Optimization (NICSO 2010), pp. 65–74, 2010.
[36] X. S. Yang, "Flower Pollination Algorithm for Global Optimization," Unconventional Computation and Natural Computation, pp. 240–249, 2012.

[37] X. S. Yang and S. Deb, "Cuckoo Search via Lévy flights," 2009 World Congress on Nature & Biologically Inspired Computing (NaBIC), pp. 210–4, 2009.
[38] X. S. Yang and S. Deb, "Engineering optimisation by cuckoo search," International Journal of Mathematical Modelling and Numerical Optimisation, vol. 1, no. 4, p. 330, 2010.
[39] X. S. Yang, "Firefly Algorithm, Lévy Flights and Global Optimization," Research and Development in Intelligent Systems XXVI, pp. 209–218, 2009.
[40] X. S. Yang, "Firefly algorithm, stochastic test functions and design optimisation," International Journal of Bio-Inspired Computation, vol. 2, no. 2, p. 78, 2010.

SAKARYA ÜNİVERSİTESİ
FEN BİLİMLERİ ENSTİTÜSÜ DERGİSİ

Sakarya University Journal of Science
SAUJS

e-ISSN 2147-835X | Period Bimonthly | Founded: 1997 | Publisher Sakarya University |
http://www.saujs.sakarya.edu.tr/en/

Title: Evaluation of Urban Images: The Case of Adana

Authors: Özlem ŞENYİĞİT, Gamze ATAY

Recieved: 2020-08-28 16:16:16

Accepted: 2021-03-17 12:52:00.995000

Article Type: Research Article

Volume: 25
Issue: 2
Month: April
Year: 2021
Pages: 530-546

How to cite
Özlem ŞENYİĞİT, Gamze ATAY; (2021), Evaluation of Urban Images: The Case of Adana. Sakarya University Journal of Science, 25(2), 530-546, DOI: https://doi.org/10.16984/saufenbilder.787051
Access link
http://www.saujs.sakarya.edu.tr/en/pub/issue/60672/787051

Sakarya University Journal of Science 25(2), 530-546, 2021

Evaluation of Urban Images: The Case of Adana

Özlem ŞENYİĞİT*[1], Gamze ATAY[1]

Abstract

The need of people, who began to form the artificial environment while shaping nature, to understand, shape, and interact with the environment has increased with the process of visual perception-interpretation-definition. Objective information perceived from the environment creates different effects on people. Mental schemas shared by cultural group members lead to the emergence of visible patterns and orders in culture. This situation occasionally causes intersections in the visual elements, which common meanings are attributed to, in the perceptual cognition of the individuals using the physical environment. The image taking shape as a result of intersections is a formation of momentary perceptions, past experiences, and memories. From this point of view, the perception of images is not merely visual; it has sociological and historical aspects that it represents. In this context, the city of Adana, which has a multicultural history of 8000 years, hosts a wide variety of elements in terms of architectural imagery. In the study, the historical and new architectural images on the banks of the Seyhan River were interpreted by the public. In line with this objective, the data obtained by using photo archives, the statistical results obtained from surveys were analyzed in order to question the architectural image components. Within this framework, with the survey conducted of 60 people, the followings were questioned and answers were sought for the city users:
- Primary images of the city,
- The reasons that have created the images, in other words, the values that have been effective in transforming these buildings into images,
- The reasons for the differentiation of the selected historical and new images in their imagery values. The results of the statistical analyses revealed that the urban element/building that has not been utilized actively could not establish the relationship of belonging with urbanites, therefore, the building's imaginative effect has been weakened, and particularly the historical buildings that make up their traces in urban memory have been the most influential factors. In this context, the present study and similar studies in order to protect on retaining urbanites' relationship with the residential areas are considered valuable in terms of both shedding light on future studies and using them as data in the practices.

Keywords: Visual perception, meaning, image, Adana

*Corresponding author: osenyigit@cu.edu.tr
[1]Çukurova University, Faculty of Architecture, Department of Architecture, 01250, Adana.
E-Mail: osenyigit@cu.edu.tr; gatay@cu.edu.tr
ORCID: https://orcid.org/ 0000-0003-0086-1647; https://orcid.org/0000-0002-7740-1641

1. INTRODUCTION

It is becoming even more important to evaluate the effects of architecture, which form the physical, intellectual, and visual world of humans, on individuals. It is known that producing meaning in interpersonal relations, especially in communication forms including visuality, is more successful than words. For most people, visual symbols are stronger and more effective than verbal symbols [1]. Therefore, in today's world where architecture is accepted as a language transmitting meaning, the interaction of an individual with his/her environment is provided through the organic integrity between the form and meaning of the architectural product. Images formed as a result of the past experiences, perceptions, and interpretations of people undoubtedly change according to time and environment and differ according to people and groups. People adapt themselves to the new indicators brought by the period they live to a certain extent and attribute meanings to them.

With its 8000 years of multicultural history (Hittites, Persians, Ancient Greek, Cilicia, Rome, Seljuk, Ottoman), Adana hosts a wide range of elements in terms of architectural imagery. In the study, the values of the images on the banks of the Seyhan River in Adana and how they were interpreted were tried to be analyzed. Also, the following issues were questioned for the urbanites: "What are the primary images of the city?", "What are the reasons that created these images, in other words, what values had an impact on these buildings to become images?", "What are the reasons for the differentiation in the imaginative values of the selected historical and new images?". Therefore, the city's language was tried to be understood in the context of the data obtained from the images.

A total of sixty urbanites, consisting of architects who add formal and semantic values to the city and non-architects who make sense of these values, participated in this study, in which the survey technique was used to measure the urbanites' degree of being impressed by the image buildings on the riverside of the Seyhan River in Adana, as well as their reasons. The data obtained as a result of the survey, which was also conducted to determine the factors (name value, historical value, functional value, aesthetic value, sociological value, location) causing the participants to be affected by the urban images, were evaluated with Thurstone and Mann-Whitney Technique.

2. CONCEPTS INCLUDED IN THE STUDY

An architectural product is a cultural object and also has a symbolic function in addition to many functions. Regardless of its value, the architectural product is included as an icon in the environment and culture stock by giving right or wrong messages. Since perceived meaning gains an expression in both cognitive and affective areas in architectural products, it is expressed as knowing, understanding, liking/disliking. In this context, meaning gains an expression not only on a plane resulting from the physical characteristics of architecture but also depending on the cognitive area capacity determined by phenomena, ideas, opinions, and impressions [2]. Accordingly, a city has a meaning beyond agglomeration or accumulation.

Yücel states that "an architectural space is not only a reality existing on its own but also a conceptual tool to be applied for comprehending its own reality" [3]. In this context, space gives information regarding the discourse of a city. Like the real meanings that we attribute to words, spaces are also the reflection of the reality visualized in the mind with the meaning that individual attributes to that space. In this context, as Rapaport also states, the question to be asked is: "*Since meanings are specific to the culture and change culturally like the environments shaping them, what does the built environment mean for residents, users, or society?"* [4].

2.1. The Image Concept

The word image is originated from the Latin word "image" or "imago," which means "to make something visible" [5]. According to lexical

meaning, it is defined as “what is designed in mind and long-awaited to happen”, “general view, impression”, and “reflection of an external object perceived by the sense organs in the consciousness” [6].

The environment offers certain differences and connections, and the observer selects, organizes, and makes sense of what he/she sees in the light of his/her own objectives. In this way, limiting and emphasizing what is seen forms the image [7]. In this regard, the perception of the images, which is formed by the instantaneous perceptions and experiences, is not merely visual; however, they become images due to factors such as the sociological definitions they represent, their functionalities, histories, and names.

The image was used as a key concept on subjects such as the readability, sustainability, and cognitive mapping of the city for reading the architectural product or the city by various researchers. Several study fields examine the image concept and try to analyze it. In this study, the image concept, which has been discussed in an extensive range of disciplines from literature to philosophy, from psychology to architecture, has been discussed in terms of imaginative evaluation and analysis in the city.

2.2. The Urban Architecture Images

The city is a heterogeneous socio-cultural structure that represents all kinds of ideas and beliefs. On the other hand, a city image is the mental reflection of an urban view resulting from these differences in the perspectives. Therefore, the perceptions about the city and the meanings attached to them differ for each urbanite. Since the image of a city has been formed over time, it does not have just an individual value, it also has historical and cultural values. It can perform this function by use of its urban image elements. Urban image elements, which make a mark on the urbanites, are signs, spaces, or regions that make sense for the urbanites. These elements, which cause mood changes and contribute to awareness, are also effective in perceiving the city.

Many architectural works have formed the characteristic lines of the cities, and they established the urban silhouette. Ensuring that the details that make up the city such as color, texture, size, occupancy, and availability ratios are perceived in a hierarchy is valuable in terms of a meaningful, identifiable, open, and readable creation for the communities living in it, as well as, gaining importance in creating a healthy environment [8]. The buildings, which are regarded as the sign element images, provide the environment with the features of being readable and understandable. Images, which have a meaning for the urbanites, facilitates understanding and perceiving the city. In this case, the city becomes an open work that can be read and interpreted by its image.

2.3. Urbanite's Image Acquisition

Architectural products are not only physical objects, but they also bear imaginative and semantics values. Because the object and its image are different. While the object exists independently of the viewer, the image inevitably depends on the subjective view and space of the interaction [9]. Hence, the urbanites (subject) perceives the city in line with their experiences and thoughts, and they create and have their images.

On the other hand, there may be more or fewer consistencies and similarities among the individuals included in the same cluster (such as age, education, occupation, nature, or family) as the social image. These are the common images that the majority of the residents of a city carry in their minds. Mental schemas shared by cultural group members lead to the emergence of visible patterns and orders in the culture. This situation can occur without being designed or images can be provided by creating intersections on objects by forming successful orientation in the physical environment to be established with future studies on certain visual elements with observer/user activity and perceptions.

Consequently, the city image is a picture in which the individual generalizes the external world in

his/her mind. The city image, which is used to interpret the acquired knowledge and direct the movement, is a product of instant emotions and past experiences [10]. In this context, which characteristics of urbanites and buildings in the study area have an impact and the extents of their impacts will be evaluated using data based on the assumption that the imaginative values of city image buildings show similarities and differences for the urbanites.

3. SCOPE AND METHOD OF THE STUDY

Architectural products and architectural discourses find an expression in the minds of city users. The buildings experienced in the study establish a bond with the intuitive and subjective reactions -*sociological meanings, functions, histories, names, aesthetic values, locations*- of the users and are expressed with imagery values. The purpose of this study is to find out people's differentiating and resembling images, to reveal their reasons and to determine the images' reason for changing depending on especially design education/knowledge (occupational difference) in the study area where different socio-cultural groups were used.

The riverside of the Seyhan River in the city of Adana, which has retained its importance in history in terms of historical, economic, sociological, etc. contexts, has been selected as the study area to conduct the experimental part of the study. In the study;

1. What are the imagery rankings of users?
2. What are the factors that were effective in turning these buildings into images? (name value, historical value, functional value, aesthetic value, sociological meaning, location)
3. What are the imagery values of the defined images and the reasons for differentiation?

were the questions whose answers were questioned through the suggested model in Figure 1.

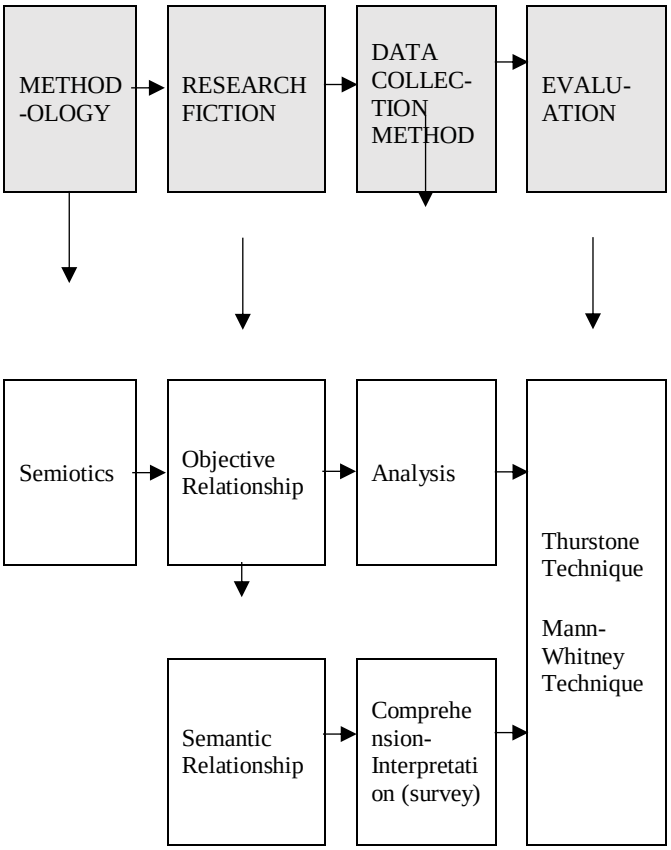

Figure 1 Subjective evaluation model of image

Based on the definition that architecture is a language and architectural product is a sign, "Semiotics" was used as the methodology in the suggested model in Figure 2 to determine the communication relationship of the images.

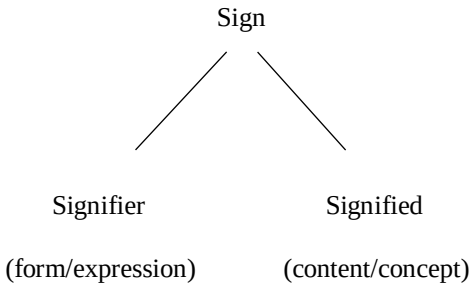

Figure 2 The most commonly used sign schema in semiotics [11]

In its shortest definition, Barthes defines semiotics as "*solving the meanings behind everything that seems ordinary and seeing the secondary meanings that they return*" [12]. According to Max Bense, signs should create the

conceptual equivalents of the particular forms they express, represent something, meet a certain function, that is, have a meaning beyond the specific form of the perceived image [13]. Figure 3 shows three elements of the sign in Peirce's understanding of semiotics: **Object** which replaces semiotics; **Medium** on which the sign is based; **Interpretant** of the sign [3].

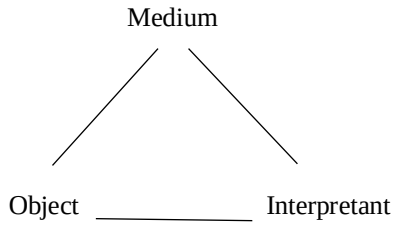

Figure 3 Three-element sign relationship [3]

In the present study, the architectural images, which are parts of the city, and the perceptual data of the users who are interacting with them are evaluated in the context of the subject-object relationship in the semiotics method. The perception of the images is not merely visual, they have the name, historical, functional, aesthetic, sociological, locational, and personal experience values that they represent. In this context, factor groups were used in the analysis of the semantic dimensions in the subjective evaluation of images to measure the emotional reactions of the user. Therefore, in the beginning, the factor groups extracted and/or used by researchers [14-19] studying on this subject were analyzed. In line with the purpose of the research, a survey study was conducted to seek answers to the questions of "What is the effective factor(s) for the building to become an image?", "What are the image values of the building?", and "Why does it differentiate from others?"

The factor groups extracted and/or used by researchers were evaluated in a preliminary test (a survey conducted with the participation of an academic group of 10 people who knew the region) to find the suitable ones for the purpose of the study. In the survey study, the factor groups that were found suitable were divided into the following six groups: ***name value, historical value, functional value, aesthetic value, sociological value, and location*** (Figure 4). Therefore, these six factor groups, which were determined to analyze subjective evaluations on the formation of architectural imagination, were used in the survey study. Thurstone Scaling and the Mann-Whitney U Test were used to analyze the data collected by the survey study. The method of this study is shown in Figure 4.

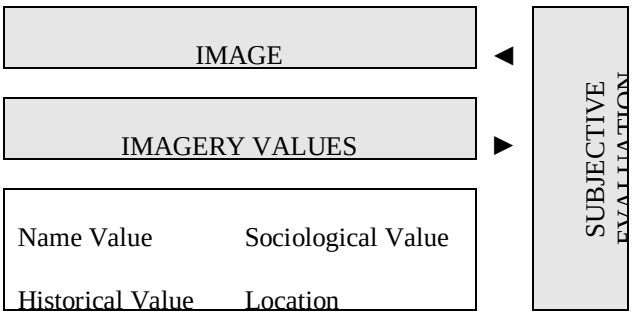

Figure 4 The method of the study

4. FIELD STUDY ON THE IMAGERY VALUES OF THE BUILDINGS IN THE ADANA SEYHAN RIVER COASTAL REGION

The images chosen within the scope of the purpose and scope of the study were examined in the context of subjective evaluations of the participant groups. In the data collection phase of the study, the followings constitute the research tools;

- Image buildings determined on the bank of Adana Seyhan River,
- Survey forms where subjective evaluations will be questioned.

The process of the study is detailed in Table 1.

Table 1
Field study diagram

Determination of Architectural Images
▼
Determination of Observation Groups
▼
Preparation of Survey Questions to Determine Subjective Evaluations in the Context of Architectural Images
▼
Implementation of the Subjective Evaluation

▼

Analysis and Interpretation of the Data
*Thurstone Technique
**Mann-Whitney Test

4.1. The Study Area: Adana Seyhan River Coastal Region

Adana, which has a multicultural history of 8000 years particularly Hittites, Persians, Ancient Greek, Cilicia, Rome, Seljuk, Ottoman, hosts a wide variety of elements in terms of architectural imagery depending on its historical background, industrialization, and development process. Accordingly, Seyhan River coastal region in Figure 5, which has an imagery value historically and socio-culturally and where the residents intensely engage in shopping-recreation activities, was selected as the study area.

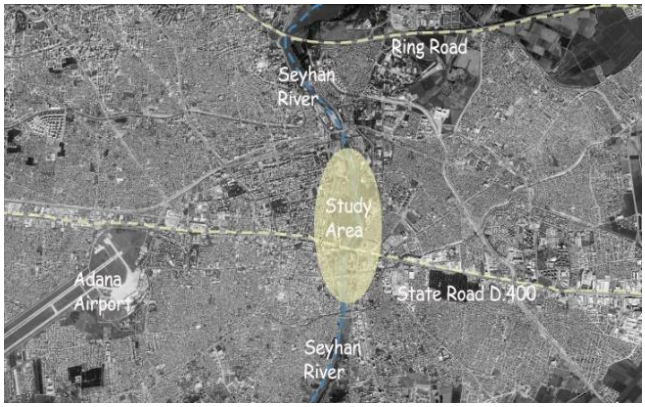

Figure 5 Location of the region on Adana map

Adana is located on the banks of Seyhan River and Seyhan Lake formed by the accumulation of this river's water. The mansions located on the riverbank were in close relationship with the river from the end of the 19th century to the beginning of the 20th century and create an impressive silhouette. However, with the filling of the riverbank in the 1950s, the silhouette of the coastline changed dramatically and the road called “Seyhan Street” was opened through the magnificent mansions and the river. As of the 1980s, the region began to lose its attraction in terms of commerce and social life. Today, the coastal region of Seyhan River, which is an important part of the city, is tried to be revived by recreation and restoration works (Figure 6).

4.2. Architectural Images in the Coastal Region of Seyhan River

The image buildings that were selected from the riverside of the Seyhan River for evaluation in the study were not determined considering their functionalities and styles. They were selected because of their imaginative values (sociological meanings, functions, dates, names, aesthetic values, locations) for the urbanites in Adana. The location of the determined imagery buildings were shown in Figure 7 and Table 2 in detail. In this context, a pilot study was first conducted with a group of academicians competent in expressing their opinions on the subject to determine the buildings to be used in the study. The sample group of the study consists of the buildings which are located in the coastal region of Seyhan River and include at least three of the factors of name, history, function, aesthetics, sociological meaning, and position.

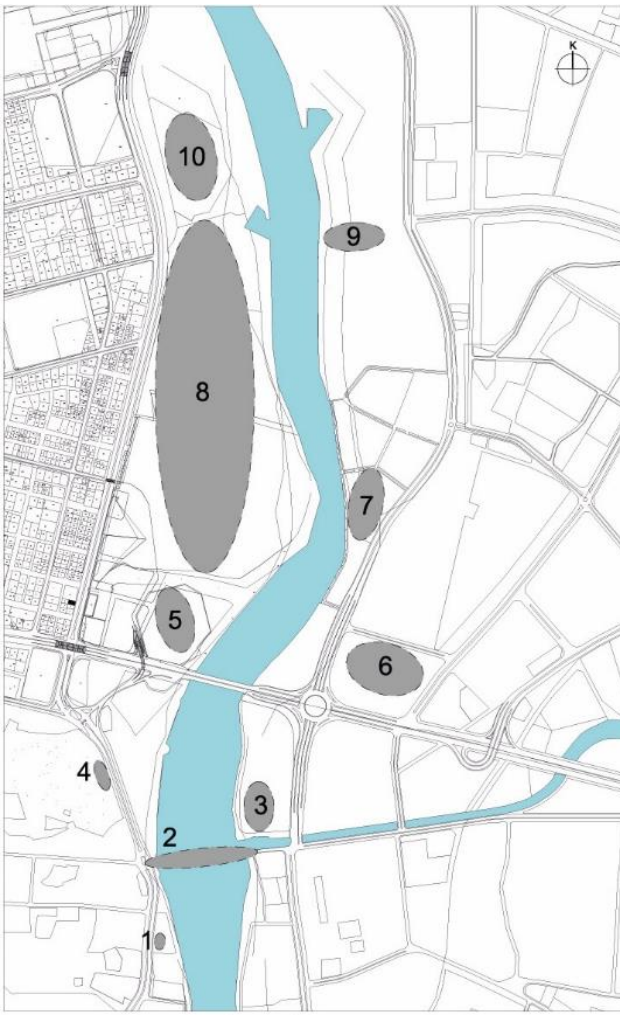

1. Girls' High School	6. Optimum Mall
2. Stone Bridge	7. Sheraton Hotel
3. Hilton Hotel	8. Central Park
4. Row Houses	9. Blue Water Aqualand
5. Sabancı Central Mosque	10. Galleria Mall

Figure 7 Location of the determined imagery buildings on region map

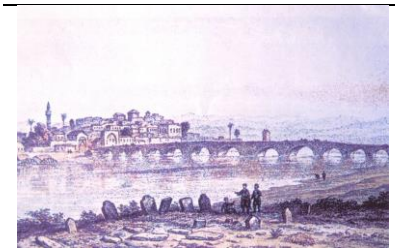

Stone Bridge, engraving belonging to the 1850s (AFAD).

The banks of Seyhan River at the beginning of the 20th century (AFAD).

The banks of the Seyhan River in 2020 [20].

Figure 6 Transformation of the Seyhan River in the historical process

Table 2
Image buildings studied

	**IMAGE 1**	**Girls' High School, 1883**
	It was built as a Military High School during the Ottoman period and opened in 1885 as a high school. It was used as Sultan and Boys' High School and Girls' High School in 1934, respectively. In the past, it was located on the banks of the Seyhan River. Today, it is located in inner parts due to land reclamation [21]. It is the oldest educational building of the city, and it is an image-building in terms of its use as a museum today.	
	**IMAGE 2**	**Stone Bridge, 117-138 AD**
	Stone Bridge belongs to the Roman period and has the title of "the oldest bridge still used in the world". 7 arches of the bridge having originally 21 arches remained under Abidin Pasha Street as a result of the filling of the riverside [22]. The building, which has survived from the Roman period to the present day, is a significant image building in terms of the city's historical value.	
	**IMAGE 3**	**Hilton Hotel, 2001**
	The Hilton Hotel is one of the city's image buildings since it is the first 5-star hotel in the city. Having views of the Stone Bridge and Seyhan River, this hotel is a social center for the city with its outward-oriented functions as well as accommodation.	
	**IMAGE 4**	**Row Houses, late 19th century-early 20th century**
	From the historical silhouette on the riverbank, only 5 mansions have remained. These houses which are called "Row Houses" are a row of attached dwellings and their connection with the river has been decreased due to Seyhan Street. With their successful restoration, they are significant image building examples that could convey Adana's traditional building design until today. The buildings serve different functions such as Atatürk House, Cinema Museum, Bosnian Hotel, and meet the residents of the city.	
	**IMAGE 5**	**Sabancı Central Mosque, 1988-1998**
	The mosque covers a large area in terms of its location and size and is easily perceived from many areas of the city. Sabancı Central Mosque is similar to the Selimiye Mosque in Edirne in terms of its architecture and Sultan Ahmed Mosque in Istanbul in terms of its silhouette. With its feature of being the largest mosque in Turkey and the Middle East, it is an image-building as a notable place of worship and a benchmark for the urbanites.	
	**IMAGE 6**	**Optimum Mall, 2011**
	Adana Optimum, which is a popular shopping mall located at the intersection of important axes on the riverside of the Seyhan River, has an imaginative value in this respect. The mall, which was positioned with the idea of transforming the region it is located in, offers a multi-choice social living space for the region.	
	**IMAGE 7**	**Sheraton Hotel, 2014**
	The 5-star Sheraton Hotel has many outward-oriented functions as well as being used for accommodation. With its striking architecture that symbolizes the flow of the Seyhan River, it is an image-building that looks at the Seyhan River.	
	**IMAGE 8**	**Central Park, 2004**
	The park, which is an urban-scaled recreation area, starts from the Sabancı Central Mosque on the banks of the Seyhan River and ends at Galleria. Merkez Park, which is mainly used on weekends, is an imaginative element of the city that soothes the urbanites on the riverside.	
	**IMAGE 9**	**Blue Water Aqualand, 2006**
	Mavi Su Aqualand, which is an amusement park with water playgrounds, has a large area. The image, which is used by the urbanites for entertainment, is an entertainment space that hosts several activities on the water and eating and drinking spaces.	

Table 2 Continue

	**IMAGE 10** **Galleria Mall, 1992**
	Galeria AVM is a significant imaginative building in the urbanites' memory in terms of being the first indoor shopping center in the city. Although the mall is located on the banks of the river, it has enclosed planning that does not view the river. This mall, which has lost its popularity today, still offers service with its small shops, markets, and restaurants.

4.3. Participant Groups

Within the scope of the study, a group of 60 participants as architects (30 individuals) and non-architects (30 individuals) was formed in order to make subjective evaluations of urban images. The purpose is to determine whether receiving design education creates awareness of imagery evaluation.

The survey questions were answered through a one-to-one interview in the Chamber of Architects Adana Branch for the group consisting of architects and in the study area for the group consisting of non-architects.

4.4. Approach to Survey Design and Preparation of Question Form

Within the scope of the study, how the subjective evaluation of the selected imagery buildings in the region was perceived by the users was questioned through the survey technique. The questions designed for the survey were collected in 3 groups:

1. Group Questions: Obtaining demographic information (Demographic data except for the occupational status was not used in this study.),
2. Group Questions: Ranking images,
3. Group Questions: Determining the factors that enable imagery.

In the context of these questions, the participants were asked to sort the 10 imagery buildings according to their preferences and then evaluate the images and indicate the characteristics for which they chose those images.

Microsoft Office Excel and SPSS programs were used for statistical evaluation and the data obtained through the Thurstone and Mann-Whitney techniques (regressions, correlations, line and radar graphs, factor analyses) were evaluated. Through the data obtained from the survey results, preference rankings of the images, frequency analyses, and hypothesis tests were performed. The elements which have a significant relationship between the two observer groups were determined and the differences between the two groups were revealed with the Mann-Whitney U test. In this way, the preference and perception level and image value of each building were determined depending on user groups.

4.5. Analysis and Interpretation of Data

The survey data obtained within the scope of the study were evaluated based on the Thurstone scale/technique. Thurstone's comparative evaluation technique is a method developed by the psychologist Louis L. Thurstone in 1927 and used to analyze the data of paired comparison and ranking decisions [23]. In order to evaluate the imagery effect of the buildings subjectively, 10 imagery buildings were selected in the study area and the observation groups were asked to rank these images in order of importance (1 'More preferred' and 10 'Less preferred'). As can be seen from the Table 3, the data were analyzed in five phases by using Thurstone's comparative evaluation technique.

Table 3
V steps in Thurstone technique

1- Ranking Data Table Tabulating survey data for analysis.
▼
2- Structure of Frequency Matrix (F) Determining the frequency of the preference of an image more than other images.
▼
3- Construction of Proportioning Matrix (P) Converting the frequency matrix value to % values in this study.
▼
4- Construction of the Normal Deviation Matrix (N) Converting the proportion matrix values to Z values by using the standard total distribution table.
▼
5- Creating the Score Table Ranking of the Z values through total, mean, and absoluteness of the least mean value and forming the score table through the mean value points.

4.3.1. Ranking Urban Images (Thurstone Technique)

The architectural value ranking of the architect participants was determined as follows: "***Stone Bridge***" was on the first rank, "***Row Houses, Girls' High School, Central Park, Sheraton Hotel, Sabancı Central Mosque, Hilton Hotel, Optimum Mall and Galleria Mall***" followed it, respectively. According to Table 4 and Figure 8, the least preferred urban image was "**Aqualand**".

The architectural value ranking of the non-architect participants was determined as follows: "***Stone Bridge***" was on the first rank, "***Girls' High School, Sabancı Central Mosque, Row Houses, Sheraton Hotel, Central Park, Hilton Hotel, Optimum Mall and Aqualand***" followed it, respectively. According to Table 4 and Figure 8, the least preferred urban image was "***Galleria Mall***".

Table 4
Average Z+ min value table of urban images

	Urban Images	Scores
For Architect	Stone Bridge	4,125
	Row Houses	2,391
	Girls' High School	2,241
	Central Park	1,054
	Sheraton Hotel	0,925
	Sabancı Central Mosque	0,791
	Hilton Hotel	0,783
	Optimum Mall	0,572
	Galleria Mall	0,213
	Blue Water Aqualand	0,000
For Non-Architects	Urban Images	Scores
	Stone Bridge	2,460
	Girls' High School	1,581
	Sabancı Central Mosque	1,575
	Row Houses	1,451
	Sheraton Hotel	1,149
	Central Park	1,149
	Hilton Hotel	0,763
	Optimum Mall	0,475
	Blue Water Aqualand	0,343
	Galleria Mall	0,000

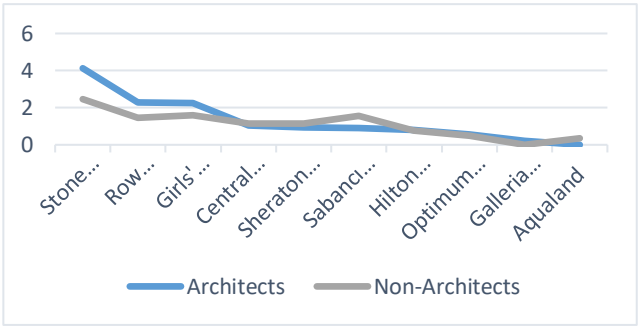

Figure 8 Comparison of ranking preferences and scores of the participants

According to the data, the historical Stone Bridge on the Seyhan River was chosen as the 1st urban image by both participant groups. The weakest urban image was chosen as "Galleria Mall" and "Aquapark".

On the other hand, the ranking preferences of the two groups show great similarity in general. In both groups, historical imagery buildings are on the first ranks. However, there are semantic differences in preference ranking in Sabancı Central Mosque. For non-architects, the mosque is on the third rank even though it is not a historical image (Table 4). Besides, while Merkez Park comes the fourth according to architects in terms of its imaginative value, it is in the sixth place according to non-architects; thus, it causes a semantic difference between the groups.

4.3.2. Factor Analyses of The Urban Images

In the study, in order to question the imagery values of the buildings, the participant groups were asked what is and/or what are the imagery values of the buildings. As a result of the survey conducted, factor analysis of imagery value judgments of the participant groups was performed in Table 5.

Table 5
Factor Analysis of imagery value judgments of participant groups

			Imagery Values					
			Name Value	Historical Value	Functional Value	Aesthetic Value	Sociological Value	Location
Girls'High School	Architects	n	17	27	11	12	10	10
		%	56,7	90	36,7	40	33,3	33,3
	Non-Architects	n	12	28	8	12	12	4
		%	40,0	***93,3***	26,7	40,0	40,0	13,3
Stone Bridge	Architects	n	19	30	13	18	18	20
		%	63,3	***100,0***	43,3	60,0	60,0	66,7
	Non-Architects	n	18	29	11	18	13	13
		%	60,0	***96,7***	36,7	60,0	43,3	43,3
Hilton Hotel	Architects	n	15	0	15	1	2	18
		%	50,0	0,0	50,0	3,3	6,7	60,0
	Non-Architects	n	21	0	16	7	3	5
		%	70,0	0,0	53,3	23,3	10,0	16,7
Row Houses	Architects	n	5	28	7	21	13	10
		%	16,7	***93,3***	23,3	70	43,3	33,3
	Non-Architects	n	5	30	2	18	11	5
		%	16,7	***100***	6,7	60	36,7	16,7
Central Mosque	Architects	n	12	3	16	5	10	15
		%	40,0	10,0	53,3	16,7	33,3	50,0
	Non-Architects	n	14	7	20	11	17	13
		%	46,7	23,3	66,7	36,7	56,7	43,3
Optimum Mall	Architects	n	7	0	22	3	9	9
		%	23,3	0,0	73,3	10,0	30,0	30,0
	Non-Architects	n	8	0	20	5	2	6
		%	26,7	0,0	66,7	16,7	6,7	20,0
Sheraton Hotel	Architects	n	17	0	19	17	5	16
		%	56,7	0,0	63,3	56,7	16,7	53,3
	Non-Architects	n	18	0	16	18	1	9
		%	60,0	0,0	53,3	60,0	3,3	30,0
		n	4	0	23	4	11	21

Central Park	Architects	%	13,3	0,0	76,7	13,3	36,7	70,0
	Non-Architects	n	7	1	21	21	7	16
		%	23,3	3,3	70,0	70,0	23,3	53,3
Aqualand	Architects	n	2	1	16	3	4	8
		%	6,7	3,3	53,3	10,0	13,3	26,7
	Non-Architects	n	4	0	17	2	4	6
		%	13,3	0,0	56,7	6,7	13,3	20,0
Galleria Mall	Architects	n	6	0	9	3	2	14
		%	20,0	0,0	30,0	10,0	6,7	46,7
	Non-Architects	n	8	0	9	0	3	11
		%	26,7	0,0	30,0	0,0	10,0	36,7
	Average		0,38	0,32	0,47	0,37	0,24	0,29
	Standard Deviation		0,487	0,466	0,50	0,485	0,43	0,456

As a result of the survey data, factor analyses of the imagery buildings on the first four ranks of the participants were evaluated in Table 6 in detail.

Table 6
Comparative analysis of participants' imagery value judgments

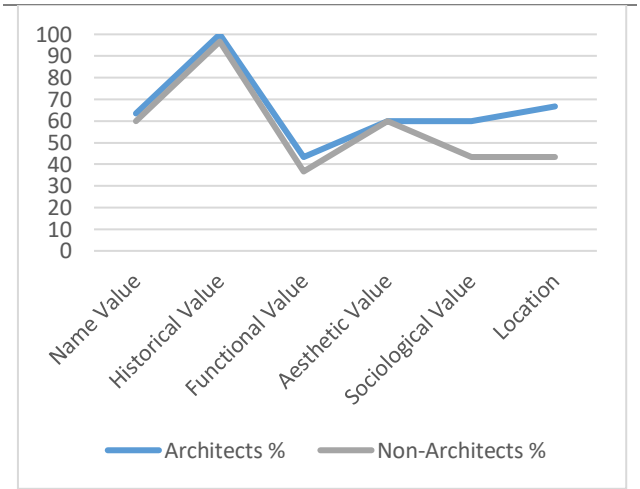

The Stone Bridge has the highest imagery value in terms of historical value according to both participant groups. The architects made the highest evaluation for the Stone Bridge in all defined imagery values.

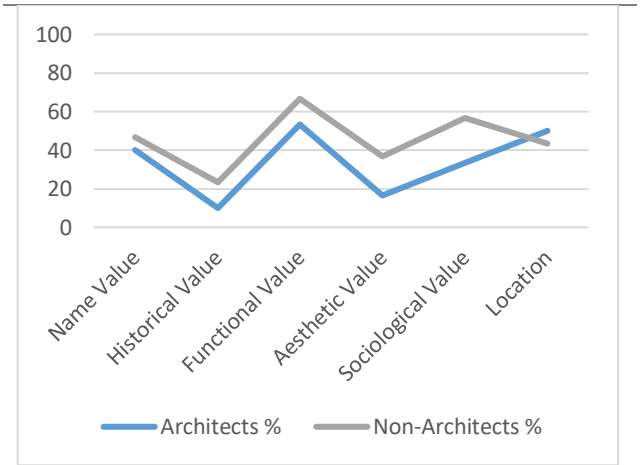

For the Central Mosque, both participant groups give priority to the functional value.
Furthermore, the location is another important factor for architects while the sociological meaning for non-architects.
The fact that the image building has a low profile in terms of its name, functionality, and location is due to its low or no frequency of being experienced/used.

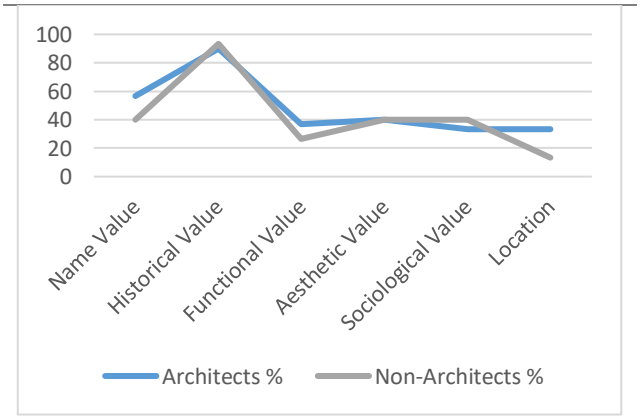

For Girls' High School, the historical value was given priority for both participant groups. In addition, for

architects, the name value of the building is a significant factor.
According to participants from the non-architect group, the building's functional and locational values are the least important factors due to the scarcity of experiencing the building.

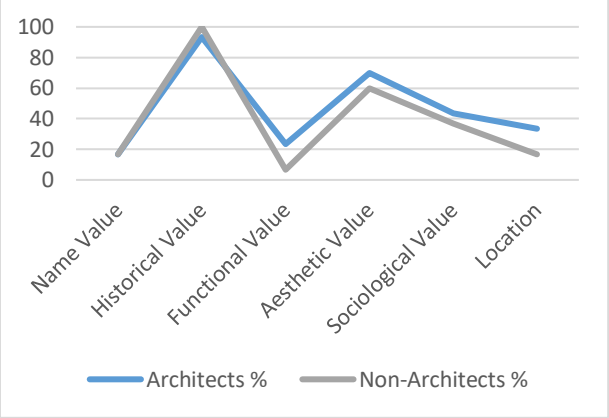

For Row Houses, first the historical value, then the aesthetic value was determined as important factors in imagery preference ranking.
There are semantic differences between the groups of architects and non-architects in terms of aesthetics features.

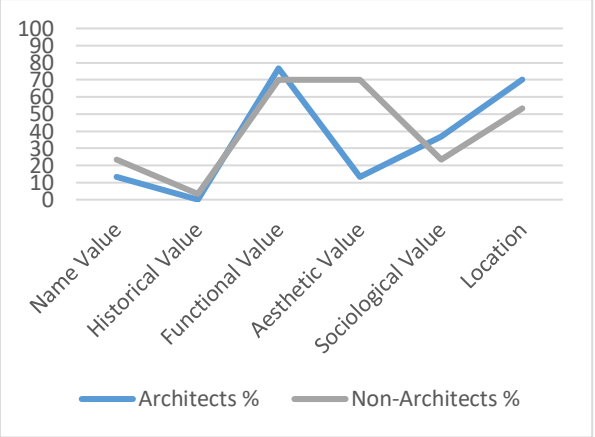

Merkez Park has been defined as the top architectural image in terms of its functional and locational values by both participant groups.
There was a significant difference between the groups of architects and non-architects in terms of aesthetic value.

Hilton, Sheraton, and Optimum Mall, Central Park, and Aqualand are imagery buildings that have a high value in terms of functional value. The name values of Hilton and Sheraton hotels come to the forefront and the aesthetic value of Sheraton is seen as an important factor.

On the other hand, while Aqualand, which is the last preferred in the ranking, has a functionally significant value, there is no prominent factor in imagery value judgments in Galleria Mall.

4.3.3. Comparison of Participant Groups (Mann-Whitney Technique)

This method, which is also known as the Mann-Whitney U test, is used to test the differences between two independent groups measured continuously [24]. This test was used to examine/question whether there was a difference between imagery perceptions/interpretations of the architect and non-architect participant groups. The results of test is given Table 7.

Table 7
Mann-Whitney test results

	Z	Significance	Explanation
Name	-,932	,351	Acceptance
Historical	-,531	,596	Acceptance
Functional	-,898	,369	Acceptance
Aesthetic	-2,196	,028	Rejection
Sociological	-1,021	,307	Acceptance
Location	-4,450	,000	Rejection

As a result of the analysis, in the cases that the probability value (p) is less than or equal to 0.05, the result is statistically significant. Accordingly, it is possible to state that there is a statistically significant difference between the evaluations of the two groups regarding image-related **aesthetics and location**.

From this point of view, depending on the observation groups, the buildings having significant differences related to ***aesthetic value*** are; ***Central Park, Hilton Hotel,*** *and* ***Central Mosque***. While non-architects find these buildings aesthetic, the aesthetic value of these buildings is very low for architects (Table 5).

In ***Hilton Hotel***, ***Girls' High School,*** and ***Row Houses***, there are significant differences in terms of ***location*** depending on observation groups. While the architects give importance to the location of these buildings, location is the last factor as imagery value judgment for the non-architects.

Moreover, there are evaluation differences between the groups in terms of "**sociological**" for Optimum Mall and "**functional**" for the Sheraton Hotel.

Analysis of architects' and non-architects' imagery value judgments are given in Table 8. While the architects gave priority to functionality, historical value, and location, the non-architect participant group determined functionality, historical value, and name value as the primary factors. In this context, while the recognition of the building is related to its function and history for the non-architect participants, the architects attach more importance to the functional and historical values as well as the location of the building in the city.

Table 8
Analysis of participants' imagery value judgments

Architects

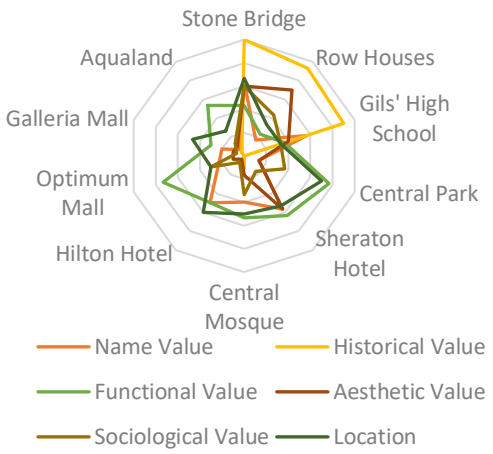

Non-Architects

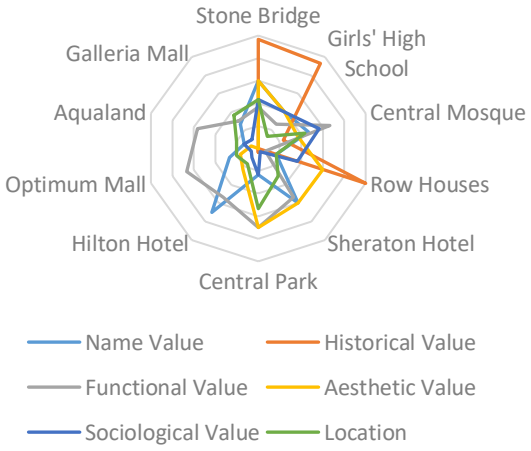

Architect and non-architect urban users associate the image with its functional value. This situation is observed particularly in Optimum, Central Park, Hilton, Sheraton, and Central Mosque. In this context, it can be stated that both participant groups have common values in terms of functional values except for the historical buildings.

It is seen that the most powerful criterion in the imagery preference of urban users is the historical value. On the other hand, while the historical buildings in the study area are found to be aesthetic, the functional value of these buildings is thought to be weak due to the fact that they are not used by the city users.

Although both groups have common values for historical buildings in terms of their aesthetic values, only the group of non-architects attaches high importance to Merkez Mosque and Merkez Park in terms of their aesthetic values. This case suggests that the functional values and cultural codes have an impact on creating imaginative values for the group of non-architect urbanites.

5. CONCLUSION

In the use of the physical environment, people's perceptual cognition intersects in visual elements, which common meanings are attributed to, albeit different reasons. What reveals the consensus among urban planners/designers/architects/groups, who desire to form an environment to be used by many people, is to engage in such images.

Especially in the cities whose historical background dates back to old times, the urban change accelerated by globalization has brought to the agenda whether the architectural symbols of the cities protect their meanings and whether the images related to the city have changed. For this purpose, in order to ensure continuity in the city, it is necessary to get to the root of the repertoire of concepts and images that have been formed for centuries.

Every architectural form contains a definition, meaning, and interpretation regarding human life. For this reason, it is one of the reliable witnesses of the period to which it belongs. Buildings convey information about that society. The buildings on the banks of Adana Seyhan River, whose historical background dates back to old times and whose cultural continuity should be ensured in this context, were examined and their imagery values were revealed. As a result of the study conducted;

Since the concept of belonging is not formed between the user and urban building that is not actively and functionally used, its imagery effect is weakened. The traces of the historical buildings in urban memory are the most important factors forming the imagery value. However, the functionality weakness of historical buildings causes the location and name value of buildings to remain in the background. In this context, the following conclusions were obtained in the study:

- The images coming from the past should be protected for the continuity of the urban memory,
- The images functionally weakened or changed within the urban texture should be revived,
- In order to ensure urban integrity, the right steps should be taken at the urban scale in order to provide the coexistence of the past and present images.
- Urban planners/designers should read the city from the perspective of society's sociological and cultural values and they should create contemporary imaginative values in this context,
- An in-depth analysis should be made on the difference between the city planners and urbanites in terms of the imaginative values about the past and present architectural images,
- In particular, functional values should be strengthened to enable urbanites to establish strong links with the architectural images,
- It has been concluded that correct steps should be taken on the city-scale of Adana to ensure urban integrity, and thus the unity of the past and present images.

To retain the urbanites' sense of belonging to the residential areas, to ensure the continuity of the city, and also to ensure that urban planners can read the expectations of the urbanites, the present study, and similar studies are considered valuable both in terms of shedding light on future studies and being used as data in practices.

Funding

The authors received any financial support for the research, authorship or publication of this study.

The Declaration of Conflict of Interest/ Common Interest

No conflict of interest or common interest has been declared by the authors.

Authors' Contribution

All authors have contributed to the theory and the writing of the article, collection and evaluation of data equally.

The Declaration of Ethics Committee Approval

The authors declare that this document does not require an ethics committee approval or any special permission.

The Declaration of Research and Publication Ethics

The authors of the paper declare that they comply with the scientific, ethical and quotation rules of SAUJS in all processes of the article and that they do not make any falsification on the data collected. In addition, they declare that Sakarya University Journal of Science and its editorial board have no responsibility for any ethical violations that may be encountered, and that this study has not been evaluated in any academic publication environment other than Sakarya University Journal of Science.

REFERENCES

[1] N. B. Winters, "Architecture is Elementary: Visual Thinking Through Architectural Concepts," Gibbs M. Smith. Inc., 1986.

[2] S. Aydınlı, "Mimarlıkta Estetik Değerler," Birinci Baskı, İ.T.Ü. Mimarlık Fakültesi, pp. 4, 9, 6, 28-29, 71-73, 1993.

[3] A. Yücel, "Mimarlıkta Biçim Ve Mekânın Dilsel Yorumu Üzerine," İ.T.Ü. Mimarlık Fakültesi, pp. VIII, 3-4, 8, 75, 79, 86, 92, 96-97, 100, 102, 116-117, 129, 136-137,154, 1981.

[4] A. Rapoport, "The Meanıng Of The Built Envıronment: A Nonverbal Communication Approach," Sage Publications, pp. 9-24, 1982.

[5] J. A. Cuddon, "Imagery, Dictionary of Literary Terms and Literary Theory", Penguin Books, pp. 413, 1999.

[6] Türk Dil Kurumu Sözlüğü, 2020. [Online]. Available: https://sozluk.gov.tr/. [Accessed:03-July-2020].

[7] K. Lynch, "The Image Of The City," Massachusetts Institute Of Technology, pp. 157-158, 1975.

[8] A. Köksal, "Anlamanın Sınırı," Arkeoloji ve Sanat Yayınları, 2009.

[9] R. Burnet, "İmgeler Nasıl Düşünür?," (Çev: Güçsal Pusar), 2. baskı, Metis Yayınları, pp. 336, 2007.

[10] K. Lynch, "Kent İmgesi," İrem Başaran (Çev.), Türkiye İş Bankası Yayınları, 2017.

[11] F. Erkman, "Göstergebilimine Giriş," Alan, pp. 31, 63, 70-72, 1987.

[12] R. Barthess, "Göstergebilim İlkeleri," Berke Vardar, Mehmet Rifat (Çev.), Kültür Bakanlığı Yayınları, pp. 89, 337, 1979.

[13] V. Özek, "Mimarlıkta Gösterge Ve Simge Eşik Analizinin Belirlenmesi," Karadeniz Gazetecilik Ve Matbaacılık A.Ş. pp. 3, 63, 1980.

[14] J. A. Russell, "Environmental Aesthetics, Theory, Research and Applications," Jack L. Nasar (Ed.), Affective Appraisals of Environments, pp. 122-123, Cambridge University, 1988.

[15] J. V. Kasmar, "Environmental Aesthetics, Theory, Research and Applications," Jack L. Nasar (Ed.), The Development of a Usable Lexicon of Environmental Descriptors, pp. 153-155, Cambridge University, 1988.

[16] R. G. Hershberger, "Environmental Aesthetics, Theory, Research and Applications," Jack L. Nasar (Ed.), A Study Of Meaning And Architecture, pp. 180, Cambridge University, 1988.

[17] R. Küller, "A Semantic Test for Use in Cross-Cultural Studies," Man-Environment Systems, 9 (4-5), 253, 1979.

[18] M. Krampen "Psychology and The Built Environment," David Canter& Lee Terence (Ed.), A Possible Analogy Between (Psycho-Linguistic and Architectural Measurement- The Type- Token Ratio (TTR), pp. 87-95, New York: Architectural, 1974.

[19] H. Sanoff, "Designing For Human Behavior: Architecture and the Behavioral Sciences," Jon Lang (Ed.), Measuring Attributes Of The Visual Environment, University of Pennsylvania, 1974.

[20] H. Tanak, "Adana aerial cityscape," Shutterstock.com, https://www.shutterstock.com/video/clip-1018310188-adana-aerial-city-scape-sabanci-central-mosque [Accessed:23-April-2020].

[21] G. Ramazanoğlu, "Adana'da Tarih Tarihte Adana," (2. Baskı). Etik, pp. 216-217, 2012.

[22] S. H. Uygur, "Tarihi, Adana The Center of Çukurova with Historycal, Touristic places and City Tissue," (I. Baskı). Koza Kültür Sanat turizm Hizmetleri A.Ş., pp. 22, 2003.

[23] T. G. Vavra, "Improving Your Measurement of Customer Satisfaction," ASQ Quality, 1997.

[24] Ş. Kalaycı, "SPSS Uygulamalı Çok Değişkenli İstatistik Teknikleri," (6. Baskı), Asil, pp. 99-101, 2014.

SAKARYA ÜNİVERSİTESİ
FEN BİLİMLERİ ENSTİTÜSÜ DERGİSİ

Sakarya University Journal of Science
SAUJS

e-ISSN 2147-835X | Period Bimonthly | Founded: 1997 | Publisher Sakarya University |
http://www.saujs.sakarya.edu.tr/en/

Title: Smart Touch Voltage Limitation

Authors: Mahmut TURHAN

Recieved: 2020-10-19 12:54:21

Accepted: 2021-03-18 12:52:00.995000

Article Type: Research Article

Volume: 25
Issue: 2
Month: April
Year: 2021
Pages: 547-553

How to cite
Mahmut TURHAN; (2021), Smart Touch Voltage Limitation. Sakarya University Journal of Science, 25(2), 547-553, DOI:
https://doi.org/10.16984/saufenbilder.812423
Access link
http://www.saujs.sakarya.edu.tr/en/pub/issue/60672/812423

Sakarya University Journal of Science 25(2), 547-553, 2021

Smart Touch Voltage Limitation

Mahmut TURHAN*[1]

Abstract

In modern railway electric infrastructure design there are two major concerns that should be considered as touch voltage and stray current. The first problem is touch and step voltage which endangers human safety even to deathly situations. Second problem is stray current which leads to corrosion of metallic infrastructure. Since human safety has higher priority early on railway systems has grounded the rail voltage to the earth but this caused stray current problem. Thus these two problems should be handled together. In this paper we present a touch voltage control and stray current monitoring solution to handle both problems. Our solution presented here uses thyristor based grounding to limit touch voltage and monitor and report stray current

Keywords: touch voltage, stray current, railway electric infrastructure, thyristor

1. INTRODUCTION

Subway and railway systems running with DC power are supplied with AC power which is converted by redressors in traction power substations and carried over dedicated catenary to the train. Running rails are used for returning current back to traction power substation since a second catenary is not cost effective.

Although the rails are insulated from earth voltage and current happens on the running rails which can be high levels because of trains and faults like lightening. Touch voltage is the voltage potential difference between an energized object and other object some distance away. When voltage over the rails, reaches dangerous levels negative circuit must be grounded. This is a requirement both for personnel / public safety and protection of equipment. Stray current comes into existence where electricity flows unintentionally from materials other than regular electric circuit elements. Stray current leads to corrosion of buried metallic infrastructure. So, touch voltage mitigation and stray current protection are needed to be considered together when applied to infrastructure, equipment and personnel safety [1-7].

There are different types of mitigating touch voltage stated in [1] such as;
Solidly grounding: In this case leaking current leads to corrosion of infrastructure. This method is used in older railway systems.

Ungrounding: Ungrounding is dangerous for public safety since running rails can have higher voltage than ground.

Diode grounding: Diodes act as a one way controller which allows current to negative but disallows from negative to earth. This method solely does not give a solution to stray current to

*Corresponding author: mahmutturhan@medelelektronik.com
[1]Medel Mühendislik ve Elektronik San.Tic. A.Ş.,34956 , Tuzla/İSTANBUL
ORCID: https://orcid.org/000-0001-7633-4830

earth. Two alternative methods of this kind are auto-grounding and thyristor-grounding.

Stray current collection systems: By using mats underground stray current is collected and maintained either fully insulated earthling or drainage systems.

To achieve this protection, our implementation steps in at times determined by the standard curve to empty the load.

Our solution presented here uses thyristor based grounding to limit touch voltage and monitor and report stray current. The limiter has a high resistance until the voltage of running rail is below the pre-defined value. Whenever the voltage of running rail exceeds the pre-defined value the limiter step in and thyristor releases the transmission until the voltage of running rail drops down the pre-defined value. The limiter satisfies the time constraint (300 ms) indicated by the standard EN 50121. Moreover the standard it is possible to adjust the time constraint to decrease the voltage also to adjust voltage value to step in. [8-12].

2. ASPECTS OF AC/DC CURRENTS

Today's Aspects of ac/dc Currents Rail electrification schemes are either dc or ac. Usually, dc current is used for low voltages (up to 3 kV) and ac is used for higher voltages (15 or 25 kV). The grounding approach for both schemes is different. Historically, dc current was used for the good control characteristics of dc motors and electromagnetic compatibility characteristics, because dc currents do not induce voltages or currents in the surrounding metallic elements [13]. The main drawback of dc electrification is that it must be well managed, designed, and maintained throughout the whole life cycle of the line due to stray currents. Stray currents are inevitable because part of the return currents flows away from the rails. These stray currents provoke corrosion where they depart from the metallic material with a positive voltage potential [for example, when they leave the rail or any other underground material (pipes, conduits, or cables) to go back to the substation]. Several effective mitigation strategies can be employed, and the basis for each is the adequate isolation of the dc rails to Earth. The first strategy is to increase the isolation of the rails, but we need to ensure that no unsafe voltages are present between the rails and the ground. Additional mitigations consist of facilitating a return path to dc currents and, in doing so, returning them in mostly controlled ways by lowering the rail's equivalent impedance and using higher-quality materials with low resistivity. Another option commonly applied is the installation of a cable in parallel to the rails, which offers an additional path so that the current returns beside the rails rather than beside the ground. Other options also applied to mitigate the effects of dc currents (but not so effective in principle) include collectors or mats that attract dc currents to limit the corrosion effects. The problem that arises from strategies of this nature comes from the negative effects that may occur as a result of the increase in the amount of current that leaves the rail by facilitating an alternative return path. Leakage currents must be controlled, and we must ensure that collectors are properly designed; otherwise, they could have the opposite effect. On the contrary, ac-electrified lines do not generate stray currents because the time-varying characteristics of this electrification mode prevent a steady flow of currents in one direction. As ac voltages are relatively high, the best way to have a safe touch voltage between the rail and grounded elements is to ground the rails and connect them to all surroundings conductive elements, such as OCS poles, metallic walkways, signaling boxes or huts, and so on. For mixed environments where both dc and ac trains run over the same line, the mitigations are aimed at the ac elements that are already grounded and may include not grounding certain elements that reduce the stray current paths. The success of this strategy lies in determining the minimum grounding connections required to decrease corrosion and remaining within limits of touch potential, according to EN 50122-1. Other trackside elements, such as cables or fences, must be considered in terms of both effects (ac and dc) and provide a tradeoff solution to prevent dangerous ac voltages and dc corrosion. The European standard concerned with stray currents and contact voltages is EN 50122. The first part

[14], “Electrical Safety, Earthing and the Return Circuit— Part 1: Protective Provisions Against Electric Shock,” establishes the maximum admissible touch voltages of both ac- and dc-electrified lines. Part two [15] addresses the provisions for the effects of stray currents caused by dc traction systems, and part three [16] discusses the mutual interaction of ac and dc traction systems. There are mixed dc and ac environments where both types of electrification coexist, sometimes using the same tracks (for example, dc third rail and ac OCSs for mixed-use lines and terminal stations). In these areas, there is a risk of corrosion to the grounded metallic elements of the ac grounding system because they provide a low resistance path to the ground. This problem could be solved by not mixing ac and dc systems; however, sometimes that is not possible. In many cases, lines are not greenfield but, rather, overhauled over time. Additionally, rolling stock has a long life cycle, which makes it difficult to completely upgrade one system from one day to the next. Elements, such as ac/dc changeovers or neutral or transition zones, can be implemented, thus hindering the passage of dc current into the ac area. Reducing the elements that are grounded in the ac area and hence susceptible to corrosion is a better way of managing the mixed-current scenario. Doing so decreases the number of areas where corrosion must be monitored and protects an increased number of assets against corrosion. Once the elements subject to corrosion are identified, they can be managed, and mitigation strategies, such as protective cathodic or anodic approaches, can be applied.

3. TOUCHVOLTAGE MITIGATION

As stated in [16], efficiency of rail voltage reduction is correlated with the grounding system quality. Mainly dependant on the grounding systems resistance reducing the rail voltage below the required level can be achieved in required time interval wrt0.1 ohm grounding is possible only above 55 V as simulated in [17-19] and depicted in Figure 2.

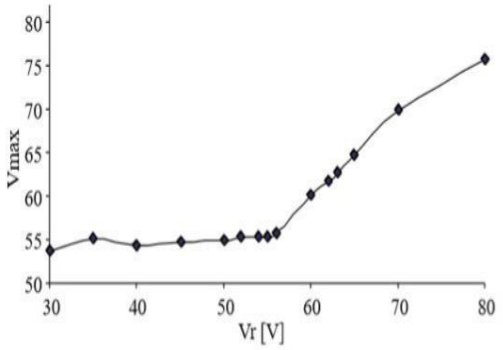

Figure 2 Reducible Rail Voltage wrt0.1 ohm Grounding

A simplified circuit schema of stray current and touch voltage is given in [1] in Figure 3 with equations in equations (1) and (2):

$$I = \frac{R_R R_T}{R_T+R_R+R_S} \quad (1)$$

$$V_T=R_R X I_R \quad (2)$$

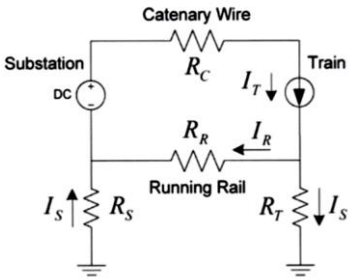

Figure 3 Circuit schema of stray current and touch voltage

In Figure 4, you can the prototype solution front view. The solution monitors the voltage difference between the running rail and the ground. Whenever this DC voltage difference is abovethan the preset value; it smartly discharges within time limitations of EN50122 standard.

Figure 4 Front view of prototype solution.

Although the EN50122 standard requires the discharge of voltage by means of 300 sec. our solution has the capability to do this in 0.2 sec and this time requirement can be adjustable. The comparison of the standard and the capability can be better seen in Figure 5. Purple line depicts the standard requirement red line depicts the performance our solution.

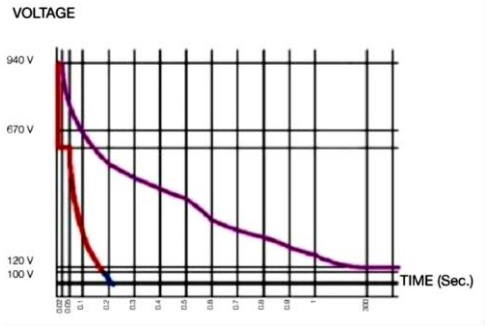

Figure 5 Comparison of the standard and the capability. (Red line: PresentedSolution, Purple Line: Standard).

Block diagram of the solution is given in Figure 6.

Figure 6 Block diagram of the solution.

4. TEST RESULTS

To prove that the solution is working properly, activates whenever the voltage is higher than the preset value and discharges the voltage, it is tested under simulated laboratory. To simulate the voltage difference between the device and the ground a potential generator is used giving different voltages. By charging the condansator at the beginning of the circuit the activity of the device has been inspected. Condansator is charged over a variac by a tri-phase rectifier diode and an appropriate resistance. The preset values to become active are set to 70,80,90,100,110,120 V one by one and the current and voltage values of activation times are recorded by an oscilloscope. Results can be seen
in Figure 7-12.
A sample references list is given below;

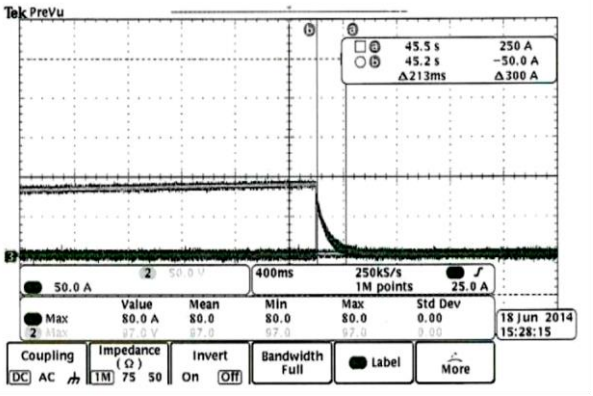

Figure 7 Test result with 70 V

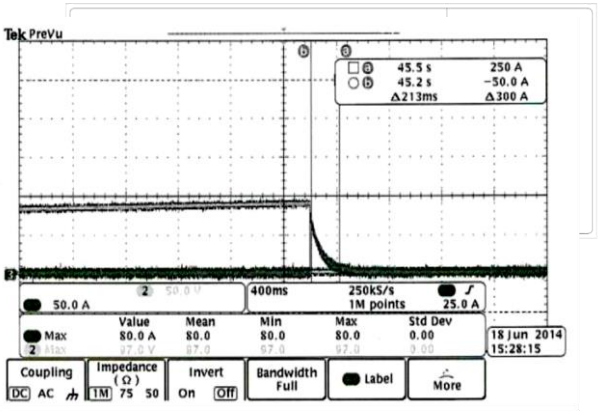

Figure 8 Test result with 80 V.

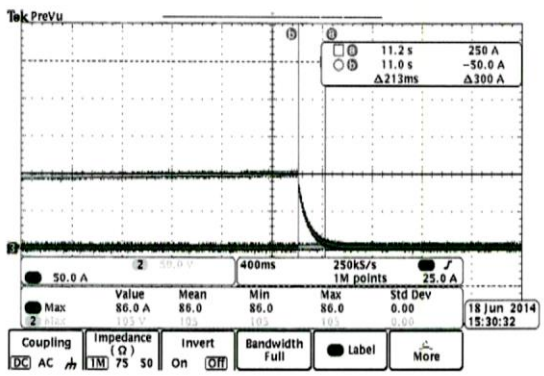

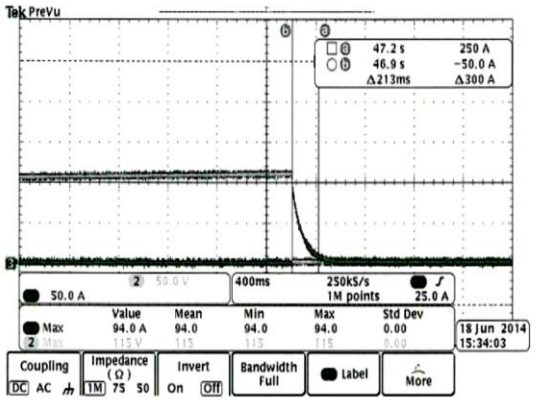

Figure 9 Test result with 90 V.

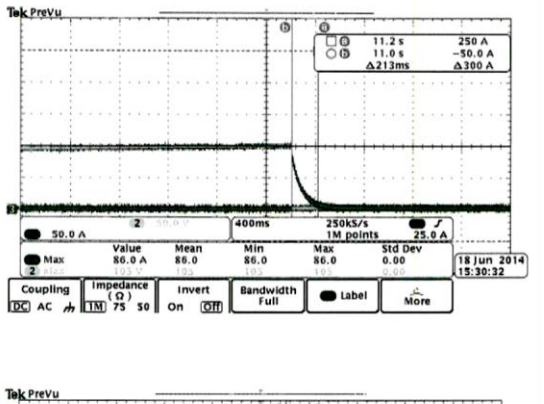

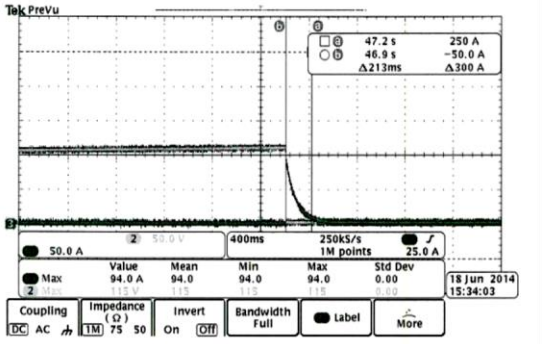

Figure 10.Test result with 100 V.

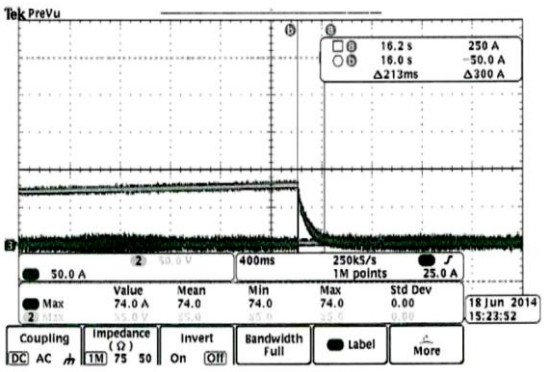

Figure 11 Test result with 110 V.

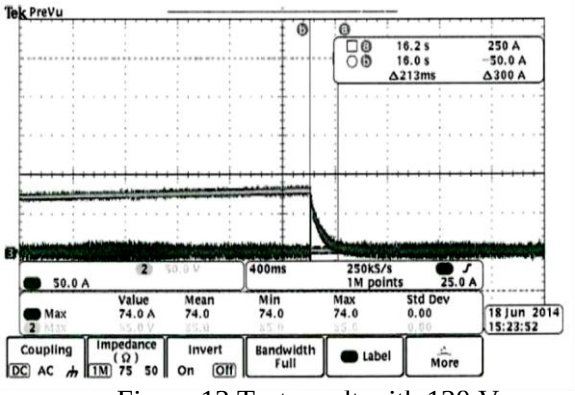

Figure 12 Test result with 120 V.

As seen above the device achieves the desired discharging by times between 213 ms-277 ms which satisfies the EN50122 standard. In test setup a 2 Ω resistance has been used torepresent ground resistance. When the grounding resistance gets smaller, higher current can pass through the device and time to discharge decreases.

5. CONCLUSION

The presented solution for touch mitigation satisfies EN50122 standard approved by laboratory tests. Although the EN50122 standard requires the discharge of voltage by means of 300 sec. our solution has the capability to do this in 0.2 sec and this time requirement can be adjustable. Adding a wireless communication capability and monitoring over web platform is a future work.

The Declaration of Conflict of Interest/ Common Interest

No conflict of interest or common interest has been declared by the authors.

Authors' Contribution

The author contributed equally to the study.

The Declaration of Ethics Committee Approval

The authors declare that this document does not require an ethics committee approval or any special permission.

The Declaration of Research and Publication Ethics

The authors of the paper declare that they comply with the scientific, ethical and quotation rules of SAUJS in all processes of the article and that they do not make any falsification on the data collected. In addition, they declare that Sakarya University Journal of Science and its editorial board have no responsibility for any ethical violations that may be encountered, and that this study has not been evaluated in any academic publication environment other than Sakarya University Journal of Science.

REFERENCES

[1] M.Niasati, A.Gholami, "Overview of Stray Current Control in DC Railway Systems" April 2008

[2] S.Acıkbas, M.T.Soylemez, "Catenary System Paralleling and its Effect on Power Consumption and Regenerated Energy Recuperation", 4th International Conference on Electrical and Electronics Engineering (ELECO 2005), Bursa, Turkey, pp 17-21, 2005.

[3] IEEE Std 81-1983, IEEE Guide for Measuring Earth Resistivity, Ground Impedance, and Earth Surface Potentials of a Ground System.

[4] K.S. Bahra, R.B. Catlow. "Control of Stray Currents for D.C. Traction Power Systems", Electrical Railways in a United Europe, pp. 136-142, 1995.

[5] D. Paul. "DC Traction Power System Grounding", IEEE Transactions on Industry Applications, vol. 38, no 3, 2002

[6] IEEE-SA Standard Boards 2000, IEEE Guide for Safety in AC Substation Grounding, IEEE Std 80-2000, IEEE Incorporate

[7] Sakis Meliopoulos, A. P., Patel Shashi, Cokkinides, G. J., "A New Method and Instrument for Touch and Step Voltage Measurements", IEEE Transactions on Power Delivery, vol. 9, No. 4, October 1994, pp. 1850-1860

[8] IEEE Incorporate. . Romulad K., Mukhedar D., "Field Measurement of Touc h and Step Voltages", IEEE Transaction on Power Apparatus and System Voltages,vol.PAS-103, No.11, November 1984, pp.3286-3294

[9] Spuntunpong K., Chartratana S., "Design of Groundin g System for GIS indoor Substation", IEEE Region 10 th Conference, volume C ,21-24 Nov.2004, pp.413-416.

[10]Ghoneim Sherif, Hirsch Holger, Elmorshedy Ahdab, Amer Rabah, "Optimum Grounding Grid Design by using an Evolut ionary Algorithm", IEEE Power Enginerering Society General Meeting 2007, 24-28 June 2007, pp1-7.

[11]C.-H. Lee, H.-M. Wang. "Effects of Grounding Schemes on Rail Potential and Stray Currents in Taipei Rail Transit Systems", IEE Proc.-Electr. Power Appl., vol. 148, No 2, pp. 148-154, 2001.

[12] Chow, Y.L., Salama, M.M.A., Djogo, G., "Thevenin Source Resistances of the Touch,Transferred and Step Voltages of a Grounding System" IEE Proceedings Gener. Transin. D istrib., vol. 146, No. 2, March 1999, pp. 107-114

[13]A. Ogunsola and A. Mariscotti, Electromagnetic Compatibility in Railways: Analysis and Management. Berlin, Germany: Springer-Verlag, 2013, p. 23.

[14] Railway Applications. Fixed Installations. Electrical Safety, Earthing and the Return Circuit. Protective Provisions Against Electric Shock, BS EN 50122-1:2011+A4:2017, 2011.

[15] Railway Applications. Fixed Installations. Electrical Safety, Earthing and the Return Circuit. Provisions Against the Effects of Stray Currents Caused by D.C. Traction Systems, BS EN 50122-2:2010.

[16] Railway Applications. Fixed Installations. Electrical Safety, Earthing and the Return Circuit. Mutual Interaction of A.C. and D.C. Traction Systems, BS EN 50122-3:2010.

[17] Cotton I, Charalambous C, Aylott P, Ernst P. Stray current control in DC mass transit systems. IEEE Trans Veh Technol 2005; 54: 722– 730.

[18] Z. Chen, D.Koleva , K.Breugel, "A review on straycurrent-induced steel corrosion in infrastructure", https://www.researchgate.net/publication/320969257

[19] M.T. Söylemez, S. Açıkbaş. A.Kaypmaz, Controlling Rail Potential of DC Supplied Rail Traction Systems, Turk J Elec Engin, VOL.14, NO.3 2006

SAKARYA ÜNİVERSİTESİ
FEN BİLİMLERİ ENSTİTÜSÜ DERGİSİ

Sakarya University Journal of Science
SAUJS

e-ISSN 2147-835X | Period Bimonthly | Founded: 1997 | Publisher Sakarya University |
http://www.saujs.sakarya.edu.tr/en/

Title: Shielding Performance of Composite Materials Used in Air Vehicles

Authors: Baha KANBEROĞLU, Ahmet Yahya TEŞNELİ

Recieved: 2021-01-28 00:00:00

Accepted: 2021-03-19 12:52:00.995000

Article Type: Research Article

Volume: 25
Issue: 2
Month: April
Year: 2021
Pages: 554-562

How to cite
Baha KANBEROĞLU, Ahmet Yahya TEŞNELİ; (2021), Shielding Performance of Composite Materials Used in Air Vehicles. Sakarya University Journal of Science, 25(2), 554-562, DOI: https://doi.org/10.16984/saufenbilder.869674
Access link
http://www.saujs.sakarya.edu.tr/en/pub/issue/60672/869674

Sakarya University Journal of Science 25(2), 554-562, 2021

Shielding Performance of Composite Materials Used in Air Vehicles

Baha KANBEROĞLU*[1], Ahmet Yahya TEŞNELİ[1]

Abstract

The metal skin of air vehicles provides an important shielding effectiveness against the effects of high amplitude electromagnetic waves. In recent years, the composite materials with the advantages such as being lighter, causing lower fuel consumption, are used as a replacement of metals. In this paper, electromagnetic shielding performance of composite materials in air vehicle manufacturing industry is investigated. A panel model is used to obtain the shielding performance of these composite materials. Due to the geometrical similarity of air vehicles with a cylinder, a cylindrical shell model is also considered. Analytical calculations for the interaction of an electromagnetic pulse(EMP) with composite materials are carried out for both panel and cylindrical models. Also, the panel and cylindrical models are constructed via Computer Software Technology(CST) program and analytical and simulation results are compared. There is a good agreement with the results.

Keywords: Composite materials, shielding effectiveness, electromagnetic pulse, analytical calculation, simulation

1. INTRODUCTION

Involuntary electromagnetic interference(EMI) is an important issue for the protection of electronic equipment of aircraft from the effects of external sources like High-Intensity Radiated Fields(HIRF), Lighting(LEMP) and Electromagnetic Pulse(EMP)[1–10]. The aluminum skin of air vehicles provides important level of shielding effectiveness(SE) performance against external EMI sources[1]. With the development of the technology, various studies have been carried out on composite material design that can be used in the manufacture of air vehicles such as aircraft, spacecraft and unmanned aerial vehicle(UAV). In these studies, it has been an important issue to reduce the production cost by reducing the weight of the air vehicles and to prevent the increase of electromagnetic interference [3], [9], [11–16]. With the advantages like lower weight, good mechanical and thermal characteristics, lower maintenance costs, lower corrosion and higher hardness, the use of composite materials such as Composite material skin(CMS)[2], Carbon fiber reinforced polymer(CFRP)[9], [16-17], Carbon fiber reinforced composites(CFRC)[15], [18] and Graphite-epoxy(GrEp)[19] as a replacement of

*Corresponding author: bkanberoglu@sakarya.edu.tr
[1]Sakarya University, Faculty of Engineering, Electrical and Electronic Engineering Department, 54187, Sakarya.
E-Mail: bkanberoglu@sakarya.edu.tr; atesneli@sakarya.edu.tr
ORCID: https://orcid.org/0000-0003-1938-3470; https://orcid.org/0000-0003-0534-5473

metals on aircraft manufacturing industry increases rapidly. Multilayered composite materials show good shielding performance as surface the aircraft (> 20 dB) and can provide protection against EMP and electromagnetic interference [20]. Instead of the advantages of these materials, the electrical conductivity of the composite materials is much lower than metals[21].

The purpose of this paper is to investigate the shielding performance of the composite materials (CFRP, CMS etc.). Firstly, a panel model is considered to calculate the shielding performance of these composite materials. The panel model results are also compared with the model established at CST[22].

Most of the air vehicles such as airplane, UAV can be considered as a cylindrical shell due to their geometry and the surface of the air vehicle is considered to be made of composite materials. Mathematical model of electromagnetic wave interaction with aircraft is carried out at cylindrical coordinates. The electric field on the axis of the cylinder is used to obtain the SE level. Also, a cylindrical shell model is constructed at CST program to validate the analytical results. To reduce the simulation time and mesh number, CST simulations are performed up to 2 GHz for cylindrical model.

2. MODELLING AND ANALYSIS OF COMPOSITE MATERIALS

The electromagnetic SE of the panel can be described as the ratio of the magnitude of the transmitted field to incident field. SE and given as:

$$SE_E = -20\log\left|\frac{E_t}{E_i}\right| \qquad (1)$$

E_i and E_t are the incident and transmitted electric field strengths. SE performance is evaluated for a plane wave interaction. EMP is described by a double-exponential equation given by[23], [24]

$$E(t) = E_0 \times (e^{-\alpha t} - e^{-\beta t}), \qquad t > 0 \qquad (2)$$

where the parameters E_0=5x10^4 V/m, α=4x10^7 s^{-1}, β=6x10^8 s^{-1}. The waveforms of EMP are shown in Fig. 1 for both time and frequency domains.

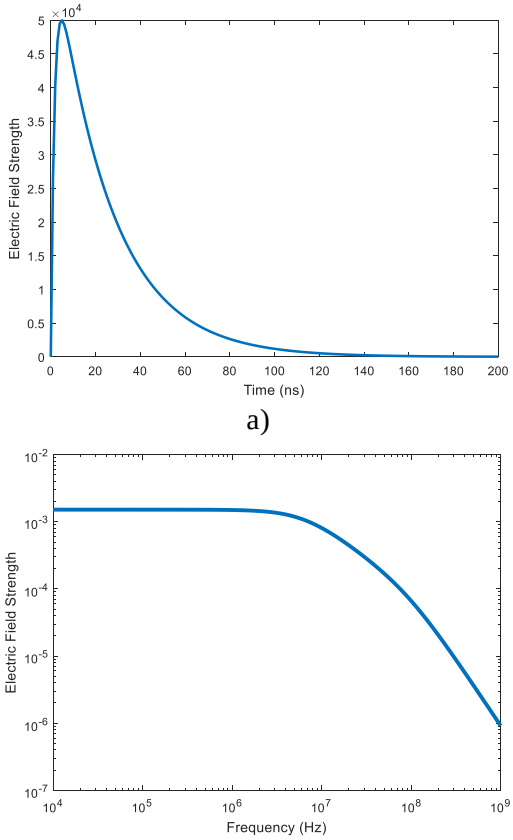

Figure 1 EMP waveform at a) time and b) frequency domains

Two cases are considered for analytical calculations and simulations. SE is calculated for a panel model in case 1 and for a cylindrical shell model in case 2.

2.1. Case 1: Panel Model Interaction

A three-layer model(Air/Panel/Air) is considered for the SE simulation as shown in Figure 2.

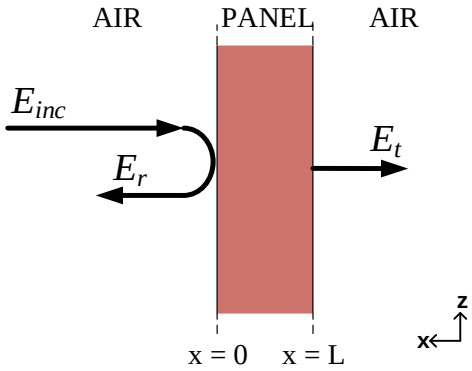

Figure 2 Interaction model of homogeneous panel

x polarized TM electromagnetic pulse interacts with the cable channel placed in the ground. Interaction mechanism is shown at Figure 1. A transfer matrix is used to determine the transmitted and reflected electromagnetic waves[25-26]. The matrix model defines the linear connection of electromagnetic field vectors at layer boundaries.

$$\begin{bmatrix} E_x \\ H_y \end{bmatrix}_{tr} = [T] \begin{bmatrix} E_x \\ H_y \end{bmatrix}_{inc} \tag{3}$$

Transfer matrix T is a 2x2 matrix [25].

$$[T] = \begin{bmatrix} \cos(k_i \cdot d) & jZ\sin(k_i \cdot d) \\ \frac{j}{Z}\sin(k_i \cdot d) & \cos(k_i \cdot d) \end{bmatrix} \tag{4}$$

where the thickness of the layer

$$d = y_{l+1} - y_l \tag{5}$$

Wave impedance and wave number of the layers used in transfer matrix are given below, respectively[27].

$$Z = \sqrt{\frac{jw\mu}{\sigma + jw\varepsilon}} \tag{6}$$

$$k_i = \sqrt{-jw\mu(\sigma + jw\varepsilon)} \tag{7}$$

w=2πf is the angular frequency, $\boldsymbol{\sigma}$ is the electrical conductivity, $\boldsymbol{\varepsilon_0}$ and $\boldsymbol{\mu_0}$ are the electric permittivity and magnetic permeability of free space, respectively.

2.2. Case 2: Cylindrical interaction

TM_Z polarized EMP is considered to interact with a shielded cylinder as shown in Figure 3.

The electric and magnetic fields in cylindrical coordinates are given as[28]

$$\begin{aligned} E^{inc}(r,\phi,z) &= E_z^{inc}(r,\phi)\overrightarrow{a_z} = E_0^{inc} e^{-jk_0 r\cos\phi}\overrightarrow{a_z} \\ H^{inc}(r,\phi,z) &= H_r^{inc}(r,\phi)\overrightarrow{a_r} + H_\phi^{inc}(r,\phi)\overrightarrow{a_\phi} \\ &= -\frac{E_0^{inc}}{\eta_0}(\overrightarrow{a_r}\sin\phi + \overrightarrow{a_\phi}\cos\phi)e^{-jk_0 r\cos\phi} \end{aligned} \tag{8}$$

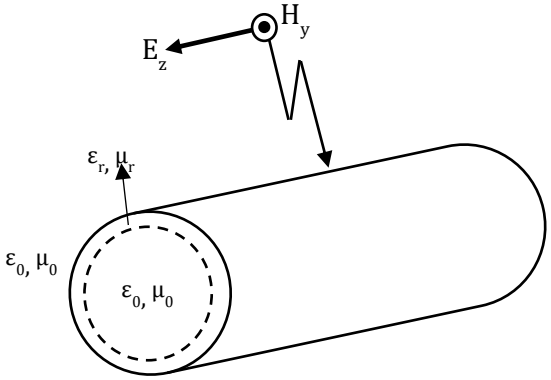

Figure 3 Cylindrical shell interaction model

The tangential fields to the cylindrical surface can be shown as

$$\begin{aligned} E_z^{inc}(r,\phi) &= E_0^{inc}\sum_{n=-\infty}^{\infty} j^{-n} J_n(k_0 r) e^{jn\phi} \\ H_\phi^{inc}(r,\phi) &= \frac{1}{jw\varepsilon_0}\frac{\partial E_z^{inc}}{\partial r} \\ &= -j\frac{E_0^{inc}}{\eta_0}\sum_{n=-\infty}^{\infty} j^{-n} J_n'(k_0 r) e^{jn\phi} \end{aligned} \tag{9}$$

$J_n(\cdot)$ is the nth order Bessel function of the first kind and $J_n'(\cdot)$ is the derivate of $J_n(\cdot)$. η_0 and k_0 are the characteristic impedance and the wavenumber of the air, respectively[27].

$$\begin{aligned} \eta_0 &= \sqrt{\frac{\mu_0}{\varepsilon_0}} \\ k_0 &= w\sqrt{\varepsilon_0\mu_0} \end{aligned} \tag{10}$$

For TM wave incidence, the relation between the tangential electric and magnetic fields can be characterized by given equation at the boundaries of the layers[29].

$$\begin{bmatrix} E_{z,n} \\ H_{\phi,n} \end{bmatrix}_b = \sum_{n=-\infty}^{\infty} [Z_n]_{TM} \begin{bmatrix} E_{z,n} \\ H_{\phi,n} \end{bmatrix}_a \tag{11}$$

$[Z_n]_{TM}$ is the transfer impedance matrix and expressed as

$$[Z_{TM}] = \frac{\pi k_p r_b}{2}\begin{bmatrix} A & B \\ C & D \end{bmatrix} \quad (12)$$

where the related expansion terms are formulated by Wronskian's results on J_n and Y_n [30]

$$\begin{aligned} A &= J_n(k_p \cdot r_b)\cdot Y_n'(k_p \cdot r_a) - J_n'(k_p \cdot r_a)\cdot Y_n(k_p \cdot r_b) \\ B &= -i\eta_s (J_n(k_p \cdot r_a)\cdot Y_n(k_p \cdot r_b) - J_n(k_p \cdot r_b)\cdot Y_n(k_p \cdot r_a)) \\ C &= \frac{1}{i\eta_s}(J_n'(k_p \cdot r_a)\cdot Y_n'(k_p \cdot r_b) - J_n'(k_p \cdot r_b)\cdot Y_n'(k_p \cdot r_a)) \\ D &= J_n(k_p \cdot r_a)\cdot Y_n'(k_p \cdot r_b) - J_n'(k_p \cdot r_b)\cdot Y_n(k_p \cdot r_a) \end{aligned} \quad (13)$$

$Y_n(\cdot)$ is nth order Neumann function of the first kind and $Y_n'(\cdot)$ is the derivate of $Y_n(\cdot)$. η_s is the characteristic impedance and k_p is the wavenumber of the surface[31].

$$\eta_s = \sqrt{\frac{jw\mu_s}{\sigma_s + jw\varepsilon_s}} \quad (14)$$
$$k_p = \sqrt{-jw\mu_s(\sigma_s + jw\varepsilon_s)}$$

where ε_s is the relative permittivity, μ_s is the relative permeability and σ_s is the conductivity of the surface layer of cylinder.

3. RESULTS

Firstly, SE of composite panel exposed to EMP is investigated. Electrical parameters of the composite materials used in air vehicles manufacturing are given in Table 1. These parameters are used at analytical calculations and construction of a panel model at CST program.

Table 1 Electrical Properties of Composite Materials

Material	Relative Permittivity	Electrical conductivity(S/m)
CMS[1]	14.5	500
CFC[8]	1	10^4
CFRP[6]	6.4	$1.5x10^4$
GrEp[19]	1	$4x10^4$

Analytical calculation results are given in Figure 4. Simulations performed for 0.5 mm thickness panel at frequency range between 1 MHz to 10 GHz.

It is clear from Figure 4 that GrEp shows the best shielding performance among 4 composite materials. 0.5 mm thick GrEp panel provides SE between 70 and 220 dB at selected frequency spectrum. CFC and CFRP have similar shielding performances and a notable increase occurs with frequency. SE performance of all composite materials remain constant up to 100 MHz and shielding efficiency in the range of 40–80 dB up to material. With increasing frequency, SE performance of composite materials increase dramatically.

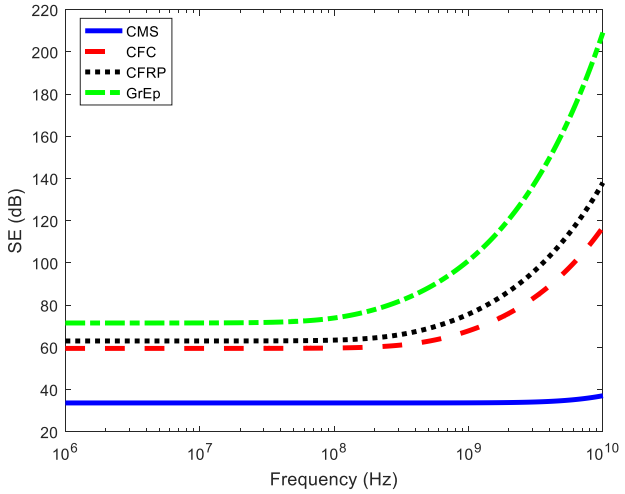

Figure 4 SE Comparison of Composite Materials

The panel is constructed for CMS and CFC materials at CST and simulation results are compared with analytical results in Figure 5. Frequency Domain Solver is preferred for CST simulations. According to Figure 5, there is an excellent agreement between analytical and simulation results.

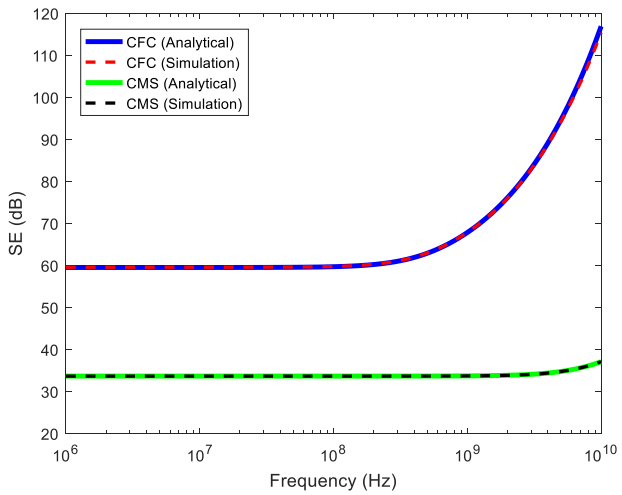

Figure 5 SE Comparison of Composite Materials

A cylinder can be considered as a small model of aircrafts. A cylindrical shell model is considered to analyze the cylindrical SE performance of composite materials against EMP. The shell of the cylinder is assumed to be constructed by composite materials and electric field along the axis of cylinder and cylindrical SE performance of materials is analyzed.

As in the panel model, the analytical calculations and CST simulations are performed for a cylindrical shell model. To reduce the simulation time and mesh number in CST simulations, the highest frequency is limited to 2 GHz, the radius of cylinder is selected as R=20 cm and the thickness of composite panel d= 0.5 mm. The analytical results are given in Figure 6.

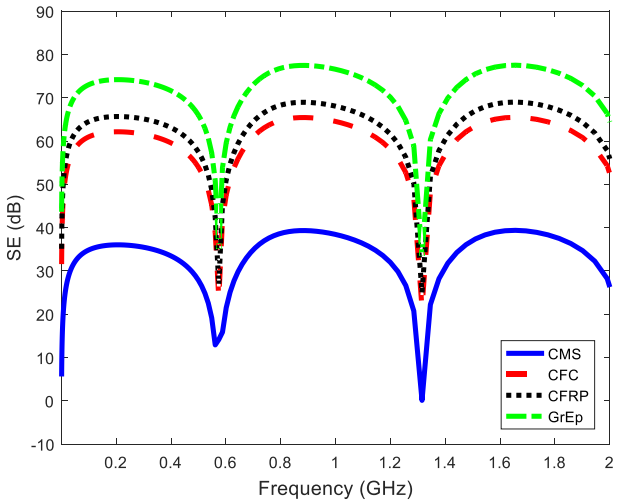

Figure 6 SE Comparison of Composite Materials

All composite materials show the same characteristics except the SE magnitudes. There is a significant increase at SE values up to 100 MHz. After 100 MHz, resonances occur, and SE values decrease sharply at resonance frequencies. GrEp material provides the highest SE performance about 80 dB and the CMS the lowest about 30 dB.

Except resonance frequencies, there isn't a notable change at SE values with increasing frequency. It is clear from the Figure 6 that the electrical properties of the materials don't have a significant effect on resonance frequencies. First resonance frequency is 574.65 MHz and second is 1.315 GHz. These frequency values are related to the radius of the cylinder and roots of the Bessel function.

$$f_{rez} = \frac{c}{2\pi\sqrt{\varepsilon_r \mu_r}} \sqrt{\left(\frac{x_{mn}}{R}\right)^2 + \left(\frac{p\pi}{l}\right)^2} \qquad (15)$$

where mth root of nth order of Bessel function is denoted by x_{mn}. R is the radius, l is the length, ε_r is the relative permittivity and μ_r is the relative permeability of the cylinder. Due to Figure 6 and Equation 9, the radius of the cylinder is more decisive on resonance frequencies than electrical parameters of composite materials.

Then, the cylindrical shell model is constructed in the CST program. GrEp material is selected as the shell of the cylinder. Time domain solver is used for simulation. The result of the model is compared with analytical results in Figure 7.

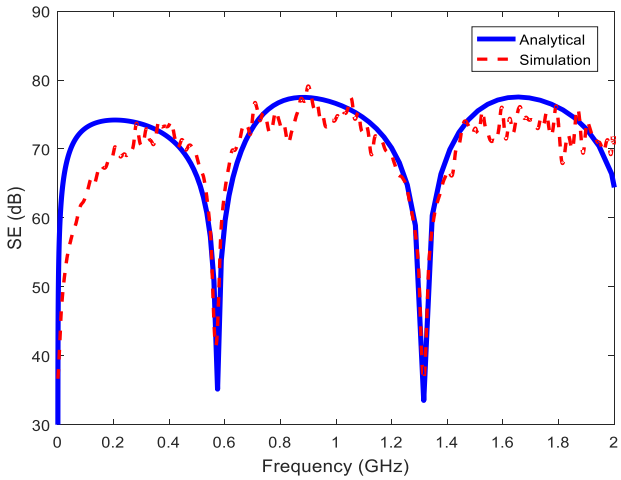

Figure 7 SE performance of cylindrical shell with single layer AML (d=0.5 mm, r= 20 cm)

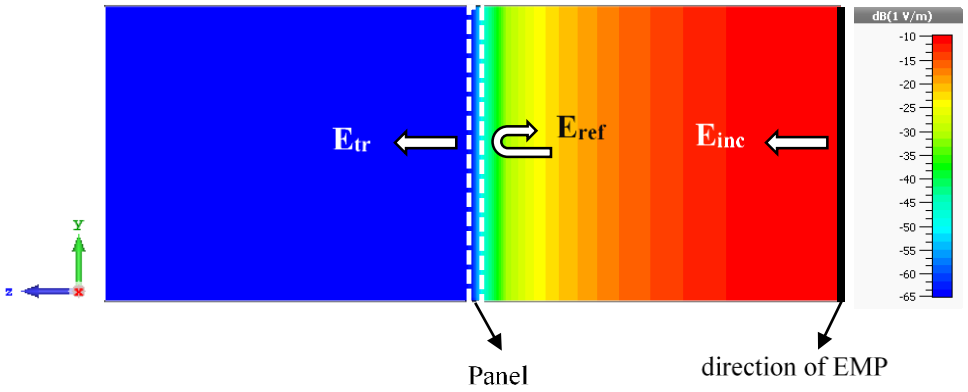

Figure 8 E-Field distribution of panel model interaction

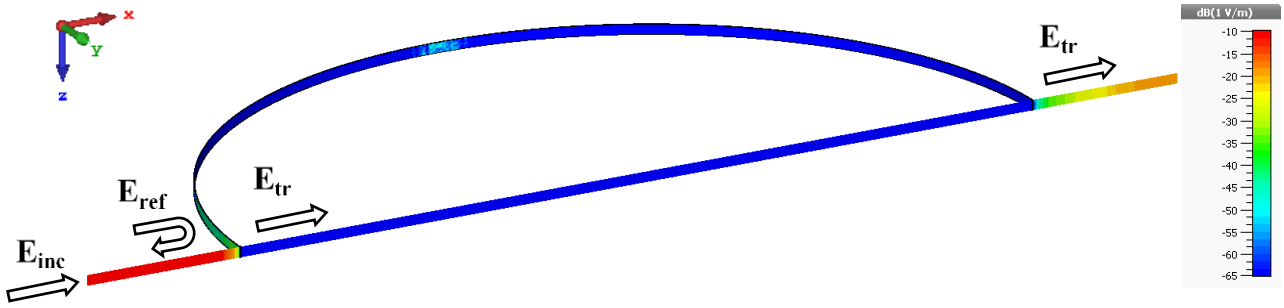

Figure 9 E-Field distribution of cylindrical model interaction

Analytical and simulation results show the same characteristics and there is a good agreement between the resonance frequencies and magnitude values.

Due to the good agreement between analytical and simulation results, it is considered to perform some additional simulations to obtain E-field distributions at 935 MHz that is the central frequency of resonances of cylindrical interaction given in Figures 6 and 7. Field monitors are used to evaluate E-field distributions. E-field distribution for plane wave interaction with CFC material is given in Figure 8.

It is clear from Figure 8 that the E-field distribution behind the panel has similar results as given in Figure 5. The majority of incident E-field is reflected through the CFC panel and CFC panel provides a notable SE.

E-field distribution for plane wave interaction with cylindrical shell model is also given in Figure 9. Simulations are performed for GrEp material as in Figure 7. Incident, transmitted and reflected E-fields are given in Figure 9. Due to inner reflections, the major part of the incident E-field is reflected and transmitted from the cylindrical shell model. A good SE performance is achieved.

4. CONCLUSIONS

In this paper, the composite materials used in air vehicle manufacturing industry are investigated. The analytical calculations and simulations are performed for composite materials. A panel model is considered to obtain the SE level of materials. Due to geometric similarity of air vehicles and cylinder except the wings, a cylindrical shell model is constructed and SE level on the axis of the cylinder is calculated. CST models are constructed for both panel and cylindrical model. There is a good agreement between analytical results and simulations for panel and cylindrical shell models. CFC, CFRP and GrEp materials obtain 60dB shielding

performance at least for 0.5 mm thickness. GrEp provides the highest shielding effect for panel and cylindrical models. Except resonance frequencies, 75 dB shielding is achieved by GrEp for cylindrical shell application. Based on the agreement, E-field distributions are evaluated at central frequency of resonances at 935 MHz for planar and cylindrical models. The results are compatible with analytical and simulation results. Also, it is noticed that the analytical model has an advantage of solving the problem in a brief, simple and fast way.

Funding

"This study is supported by Sakarya University Scientific Research Projects Coordination Unit. Project Number: 2011-50-02-028."

The Declaration of Conflict of Interest/ Common Interest

This study was produced from the Baha KANBEROĞLU's PhD thesis entitled "Electromagnetic pulse shielding effectiveness analysis of multilayered cylindrical structures", which was accepted in 2020.

Authors' Contribution

The authors contributed equally to the study.

The Declaration of Ethics Committee Approval

This study does not require ethics committee permission or any special permission.

The Declaration of Research and Publication Ethics

The authors of the paper declare that they comply with the scientific, ethical and quotation rules of SAUJS in all processes of the paper and that they do not make any falsification on the data collected. In addition, they declare that Sakarya University Journal of Science and its editorial board have no responsibility for any ethical violations that may be encountered, and that this study has not been evaluated in any academic publication environment other than Sakarya University Journal of Science.

REFERENCES

[1] B. D. Cordill, S. A. Seguin, and M. S. Ewing, "Shielding effectiveness of composite and aluminum aircraft, model and measurement comparison," *Conf. Rec. - IEEE Instrum. Meas. Technol. Conf.*, pp. 1408–1413, 2011.

[2] M. A. Aziz *et al.*, "Shielding effectiveness of composite aircraft: A reverberation chamber and virtual measurement study," *2012 IEEE I2MTC - Int. Instrum. Meas. Technol. Conf. Proc.*, pp. 2775–2779, 2012.

[3] G. G. Gutiérrez *et al.*, "HIRF virtual testing on the C-295 aircraft: On the application of a pass/fail criterion and the FSV method," *IEEE Trans. Electromagn. Compat.*, vol. 56, no. 4, pp. 854–863, 2014.

[4] M. H. Vogel, "Impact of lightning and high-intensity radiated fields on cables in aircraft," *IEEE Electromagn. Compat. Mag.*, vol. 3, no. 2, pp. 56–61, 2014.

[5] A. Jazzar, E. Clavel, G. Meunier, and E. Vialardi, "Study of lightning effects on aircraft with predominately composite structures," *IEEE Trans. Electromagn. Compat.*, vol. 56, no. 3, pp. 675–682, 2014.

[6] L. Huang, C. Gao, F. Guo, and C. Sun, "Lightning Indirect Effects on Helicopter: Numerical Simulation and Experiment Validation," *IEEE Trans. Electromagn. Compat.*, vol. 59, no. 4, pp. 1171–1179, 2017.

[7] R. R. Nunes and J. Schuur, "Investigation on the propagation and coupling in aircraft using absorbing films," *IEEE Int. Symp. Electromagn. Compat.*, vol. 2015-Septm, pp. 322–327, 2015.

[8] M. R. Cabello *et al.*, "SIVA UAV: A Case Study for the EMC Analysis of Composite Air Vehicles," *IEEE Trans. Electromagn. Compat.*, vol. 59, no. 4, pp. 1103–1113, 2017.

[9] V. P. Bui, W. Thitsartarn, E. X. Liu, J. Y. C. Chuan, and E. K. Chua, "EM Performance of Conductive Composite Laminate Made of Nanostructured Materials for Aerospace Application," *IEEE Trans. Electromagn. Compat.*, vol. 57, no. 5, pp. 1139–1148, 2015.

[10] B. Kanberoglu, M. . Hilmi Nişanci, and A. Şükran Demirkiran, "Electromagnetic characterization of ceramic material produced with natural zeolite," *Mater. Sci. Semicond. Process.*, vol. 38, pp. 352–356, 2015.

[11] M. D'Amore, D. A. Lampasi, M. S. Sarto, A. Tamburrano, V. De Santis, and M. Feliziani, "Optimal design of multifunctional transparent shields against radio frequency electromagnetic fields," *Electromagn. Compat. Symp. Adelaide 2009, EMCSA 2009 - Symp. Proc.*, pp. 81–86, 2009.

[12] Y. Corredores, P. Besnier, X. Castel, J. Sol, C. Dupeyrat, and P. Foutrel, "Adjustment of Shielding Effectiveness, Optical Transmission, and Sheet Resistance of Conducting Films Deposited on Glass Substrates," *IEEE Trans. Electromagn. Compat.*, vol. 59, no. 4, pp. 1070–1078, 2017.

[13] L. Guadagno *et al.*, "Development of epoxy mixtures for application in aeronautics and aerospace," *RSC Adv.*, vol. 4, no. 30, pp. 15474–15488, 2014.

[14] I. M. De Rosa, F. Sarasini, M. S. Sarto, and S. Member, "EMC Impact of Advanced Carbon Fiber / Carbon Nanotube Reinforced Composites for Next-Generation Aerospace Applications," vol. 50, no. 3, pp. 556–563, 2008.

[15] S. Greco, A. Tamburrano, A. D'Aloia, R. Mufatti, and M. S. Sarto, "Shielding effectiveness properties of carbon-fiber reinforced composite for HIRF applications," *IEEE Int. Symp. Electromagn. Compat.*, pp. 1–6, 2012.

[16] N. Abdelal, "Electromagnetic interference shielding of stitched carbon fiber composites," *J. Ind. Text.*, pp. 1–18, 2018.

[17] D. Munalli, G. Dimitrakis, D. Chronopoulos, S. Greedy, and A. Long, "Electromagnetic shielding effectiveness of carbon fibre reinforced composites," *Compos. Part B Eng.*, vol. 173, no. December 2018, p. 106906, 2019.

[18] I. M. De Rosa, R. Mancinelli, F. Sarasini, M. S. Sarto, and A. Tamburrano, "Electromagnetic Design and Realization of Innovative Fiber-Reinforced Broad-Band Absorbing Screens," *IEEE Trans. Electromagn. Compat.*, vol. 51, no. 3, pp. 700–707, Aug. 2009.

[19] A. L. Bogorad, M. P. Deeter, K. A. August, G. Doorley, J. J. Likar, and R. Herschitz, "Shielding Effectiveness and Closeout Methods for Composite Spacecraft Structural Panels," *IEEE Trans. Electromagn. Compat.*, vol. 50, no. 3, pp. 547–555, Aug. 2008.

[20] J. Wang, B. Zhou, L. Shi, C. Gao, and B. Chen, "Analyzing the electromagnetic performances of composite materials with the FDTD method," *IEEE Trans. Antennas Propag.*, vol. 61, no. 5, pp. 2646–2654, 2013.

[21] R. W. Evans, "Design Guidelines for Shielding Effectiveness, Current Carrying Capability, and the Enhancement of Conductivity of Composite Materials," *NASA Contract. Rep.*, no. 4784, 1997.

[22] CST, "Computer Simulation Technology, CST Studio Suite 2015, User Guide," Darmstadt, Germany, 2019.

[23] US Department Of Defence, "MIL-STD-464C Electromagnetic environmental effects requirements for systems," Washington, 2010.

[24] IEC 61000-2-9, "IEC 61000-2-9 Electromagnetic compatibility (EMC) –

Part 2: Environment – Section 9: Description of HEMP environment – Radiated disturbance Basic EMC publication Compatibilité," *International Organization*. 2009.

[25] H. Oraizi and A. Abdolali, "Several theorems for reflection and transmission coefficients of plane wave incidence on planar multilayer metamaterial structures," *IET Microwaves, Antennas Propag.*, vol. 4, no. 11, pp. 1870–1879, 2010.

[26] B. Kanberoğlu and A. Şükran Demirkıran, "Shielding Effectiveness of Ceramic Bodies Produced with Natural Zeolite," *Acta Phys. Pol. A*, vol. 125, no. 2, pp. 642–644, Jan. 2014.

[27] K. Zhang and D. Li, *Electromagnetic Theory for Microwaves and Optoelectronics*. Berlin, Heidelberg: Springer Berlin Heidelberg, 2008.

[28] S. Celozzi, R. Araneo, and G. Lovat, *Electromagnetic Shielding*. 2008.

[29] P. R. Renaud and J. J. Laurin, "Shielding and scattering analysis of lossy cylindrical shells using an extended multifilament current approach," *IEEE Trans. Electromagn. Compat.*, vol. 41, no. 4 PART 1, pp. 320–334, 1999.

[30] M. Abramowitz and I. A. Stegun, *Handbook of Mathematical Functions*. New York: Dover, 2003.

[31] F. M. Tesche, M. Ianoz, and T. Karlsson, *EMC Analysis Methods and Computational Models*. Canada: John Wiley & Sons, 1997.

SAKARYA ÜNİVERSİTESİ
FEN BİLİMLERİ ENSTİTÜSÜ DERGİSİ

Sakarya University Journal of Science
SAUJS

e-ISSN 2147-835X | Period Bimonthly | Founded: 1997 | Publisher Sakarya University |
http://www.saujs.sakarya.edu.tr/en/

Title: Noise Emission from Building Integrated Wind Turbines: A Case Study of a Tall Building

Authors: İlker KARADAĞ, Emre KURUÇAY

Recieved: 2021-02-21 00:00:00

Accepted: 2021-03-20 12:52:00.995000

Article Type: Research Article

Volume: 25
Issue: 2
Month: April
Year: 2021
Pages: 563-570

How to cite
İlker KARADAĞ, Emre KURUÇAY; (2021), Noise Emission from Building Integrated Wind Turbines: A Case Study of a Tall Building. Sakarya University Journal of Science, 25(2), 563-570, DOI: https://doi.org/10.16984/saufenbilder.884517
Access link
http://www.saujs.sakarya.edu.tr/en/pub/issue/60672/884517

Sakarya University Journal of Science 25(2), 563-570, 2021

Noise Emission from Building Integrated Wind Turbines: A Case Study of a Tall Building

İlker KARADAĞ*[1], Emre KURUÇAY[2]

Abstract

Tall buildings have the ability to produce wind energy, having been exposed to relatively high airflow speeds at a far distance from ground levels. However, with the introduction of wind energy into urban areas, there are many concerns. These include especially environmental noise impacts since the wind turbines will be located in dense urban areas where tall buildings are mostly located. Therefore, this increasing use of wind energy in the built environment has led to the publication of up-to-date regulations that limit noise levels for wind farms in many European countries. At this point, the following three aspects should be considered for noise emission: the noise source, the distance from the source, and the sound pressure level of the noise source. The choice of wind turbines for urban environments should, therefore, be compatible with low noise levels. In addition, careful positioning of turbines is also important (avoid locations where wind conditions are unfavorable, avoid sensitive places, i.e. areas at which noise levels must be low). It was necessary to calculate the noise in strong winds because the noise from a wind turbine rises with wind velocity. For the measurement of noise emitted from the wind turbine, two potential solutions were proposed until now; either it could be measured in a wind tunnel or it could be measured in the natural wind outside. However, in the early design stage, these types of measurement methods are mostly not preferable due to high financial requirements and long measurement processes. Hence, in this study, wind turbine noise is simulated via software. A case study of a tall mixed-use tower is chosen and the environmental noise distribution due to the wind turbine located on the roof of the tower is simulated. The results may provide an important guideline for architects looking for an acoustically comfortable way to integrate wind turbines into their buildings in the early design stage.

Keywords: building-integrated wind turbines, environmental noise, tall buildings

1. INTRODUCTION

Due to the increasing need for energy and the negative impact of existing fossil fuels on the environment, the use of alternative energy sources is gradually increasing. Active use of wind is the fastest-growing alternative among sustainable energy sources. Despite the global economic

*Corresponding author: ilker.karadag@cbu.edu.tr
[1]Manisa Celal Bayar University, Faculty of Fine Arts, Design and Architecture, Architecture Department, 45010, Manisa.,ORCID: https://orcid.org/0000-0001-7534-2839
[2]Sakarya University, E-Mail: kurucay@sakarya.edu.tr.
ORCID: https://orcid.org/0000-0002-5239-7084

crisis of 2009, wind turbine investments continued to increase in the world and our country [1].

In our country, there are many wind turbine farms with a total capacity of 801 MW and the construction of the farm with a total capacity of approximately 500 MW continues.

Increasing active use of wind has led to the creation of up-to-date regulations that set noise limits for wind farms in many European countries where its use is widespread (England, Germany, the Netherlands) and explains how to measure and evaluate noise.

The sound emitted from the wind turbines is significantly different in structure and level from the one emitted by large-scale power plants that categorized as industrial sound sources. Wind turbines with their unique ambient sound character are mostly located in rural areas or the fields far from the urban areas. Although noise can be a problem for the population living near wind turbines, as the distance increases, the ambient or background noise arising from the nature of the wind is able to mask the sound produced from the turbine [2]. However, this distance cannot be secured easily in a dense urban environment.

Tall buildings are widely seen forms of urban areas which require too many activities with plenty of spaces on a low base area and too many floors being useful to use. In addition, they have major effects on local wind characteristics across the urban area near the site. In the urban environment surrounding tall buildings, winds are usually strengthened at the roof level given the complex aerodynamic structures generally associated with this type of building [3].

Acceleration of the local air flow at the roof level due to the separated flow makes it feasible to integrate small-scale wind turbines that are capable of harnessing wind energy. These wind turbines can be integrated into the building design. But in most cases, it is not easy to integrate the turbine into an existing building. Therefore, mounting the turbine to the roof when structural requirements are fulfilled is the most viable and common option [4].

2. SOURCES OF WIND TURBIN NOISE

Sources of sounds emitted from the wind turbines are classified into two headings: mechanical sound (1) and environmental sound (2).

2.1. Mechanical Sound

The relative interaction of mechanical components with each other is a result of sounds and dynamic responses between components. The mechanisms that cause these noises can be listed as follows: gearbox, generator, yaw mechanism (the system that directs the turbine in the direction of the wind), auxiliary equipment (such as hydraulics) and cooling fans [5].

Because the sound emitted is correlated with the mechanical and electrical component rotation, it appears to be tonal (at a common frequency), but a broadband component may also be available for the sound. For instance, the rotational frequencies of shafts and generators and the network frequencies of gears may convey pure tones.

Additionally, rotor, the hub and tower can function as loudspeakers that transmit and subsequently emit mechanical sound. This permeation can take place through the structure as well as through the air gap. Air-borne transmission indicates the sound is directly dispersed from the element's surface or from the interior [5]. On the other hand, in structural transmission (structure-borne) sound first passes through the structural elements and then spreads in the air. For example, Figure 1 comprehensively shows the transmission path for a 2 MW wind turbine and the sound power levels for each component. When examined in detail, it is seen that the main source of mechanical sounds is the gearbox. This component emits sound from the nacelle surfaces and the component surrounding the mechanical parts.

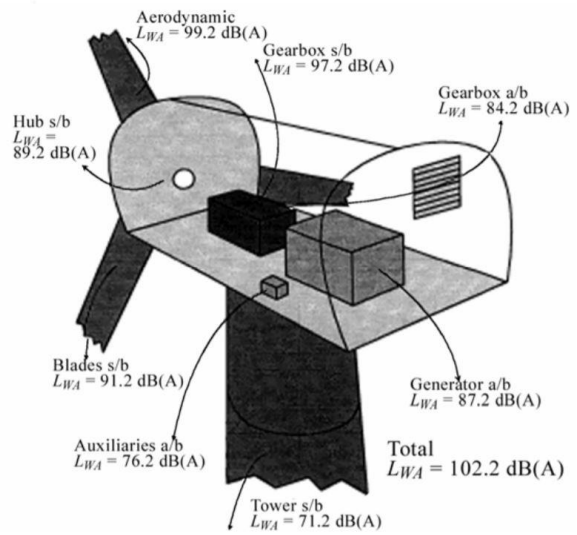

Figure 1 Parts and total sound power level of a wind turbine, indicating transmission paths of structure-borne (s/b) and airborne (a/b) [5].

2.2. Aerodynamics Sound

The largest component of wind turbine acoustic emission is usually aerodynamic broadband sound. The airflow around the blades creates it. As seen in Figure 2, many complex flow phenomena arise, each of them can produce a certain amount of sound.

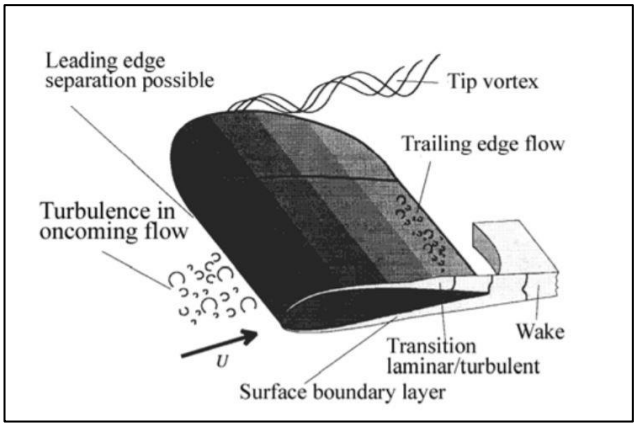

Figure 2 Schematic of Flow around a Rotor Blade [5].

With rotor velocity, aerodynamic noise typically increases. Table 1 indicates some aerodynamic sound generation mechanisms that should be noticed [5]. These mechanisms are grouped under 3 separate headings:

II.I. Low-Frequency Sound: In the low-frequency section of the sound spectrum, sounds encounter local flow disconnections due to reasons such as the flow around the rotating turbine blade turbine tower, the change in wind speed, or the fall of the track left by other blades.

II.II. Sound from Incoming Flow Turbulence: Varies depending on the size of atmospheric turbulence which induces local variations in force and local pressure across the blade.

II.III. Wing Section Originated Sound: The sound created by the air flow which continues across the full surface of the wing is included in this group. This sound type is characteristic of a broadband nature, but tonal components could also be seen owing to the choice of cut-out trailing fins (figure 3) or gaps or tears that could cause infiltration.

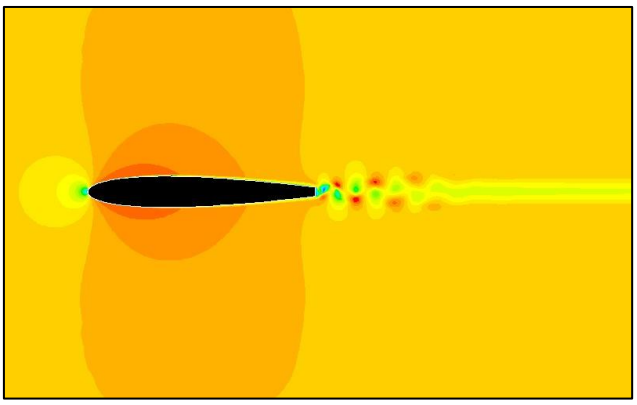

Figure 3 Eddies that cause noise originated from the blunt end of the wing trailing edge [6].

Table 1
Aerodynamic Sound Mechanisms of a Wind Turbine [5]

Type or indication	**Mechanism**	**Main characteristics & importance**
Low-frequency sound		
Steady loading noise; dteady thickness noise;	Rotation of lifting surfaces or Rotation of blades	Frequency is correlated to blade passing frequency which is not significant at current rotational velocities

Table 2 Continue

Unsteady loading noise	Passage of blades through tower speed	Frequency is correlated to blade

	deficit or wakes	passing frequency, low in cases of upwind rotors, though possibly contributing in case of wind farms
Inflow turbulence sound	Blades interacting with atmospheric turbulence	Contributing to broadband noise; not yet fully quantified
Airfoil self-noise		
Trailing-edge noise	Boundary layer turbulence interacting with blade trailing edge	Broadband, main source of high frequency noise (770 Hz < f < 2 kHz)
Tip noise	Tip turbulence interacting with blade tip surface	Broadband; not fully understood
Stall, separation noise	Turbulence interacting with blade surface	Broadband
Laminar boundary layer noise	Interaction of Non-linear boundary layer instabilities with the blade surface	Tonal, can be prevented
Blunt trailing edge noise	Vortex shedding at blunt trailing edge	Tonal, can be prevented
Noise from flow over holes, slits and intrusions	Unstable shear flows over holes and slits, vortex shedding from intrusions	Tonal, can be prevented

3. SIMULATING THE SOUND PROPOGATION

Since sound is measurable, limits can be drawn in establishing planning criteria related to noise. The emission and propagation of wind turbine-induced noise can be simulated. In this simulation, surrounding structures, landscape and roads are also taken into account. (Asphalt and concrete are known to be highly reflective materials in terms of acoustics).

In a study conducted by the National Renewable Energy Laboratory [7], noise emission measurements were made for a turbine with a diameter of 7m and a capacity of 10 kW, and a distance of 54 m was taken between the microphone and the rotor. As a result of the study, it has been observed that the noise generated by the turbine is almost not perceived with increasing distance and does not exceed the rural background noise level at most different wind speeds. Urban background noise is much higher than the background noise considered in the study, even at low wind speeds.

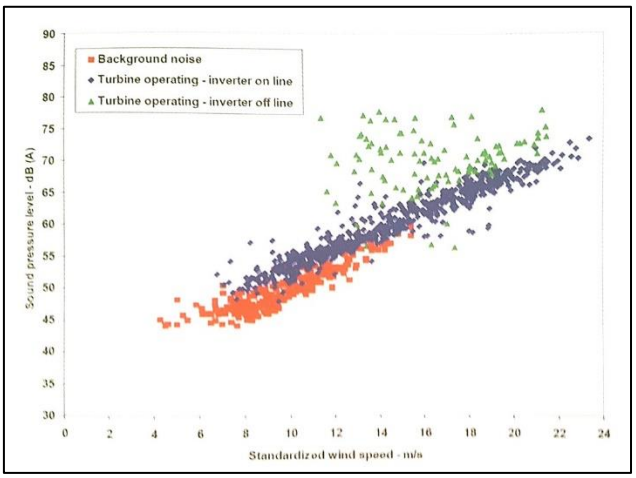

Figure 4 Noise emission measurements for a turbine with a diameter of 7m and a capacity of 10 kW, data taken at a distance of 54 m from the microphone [7].

If the wind speed is low, the noise level from the wind turbine remains minimal. However, if the turbine is exposed to wind speeds between 4m / s and 30m / s at the body height, the sound power level increases monotonously, the noise specifications of the Vestas 3MW turbine can be seen in Figure 5.

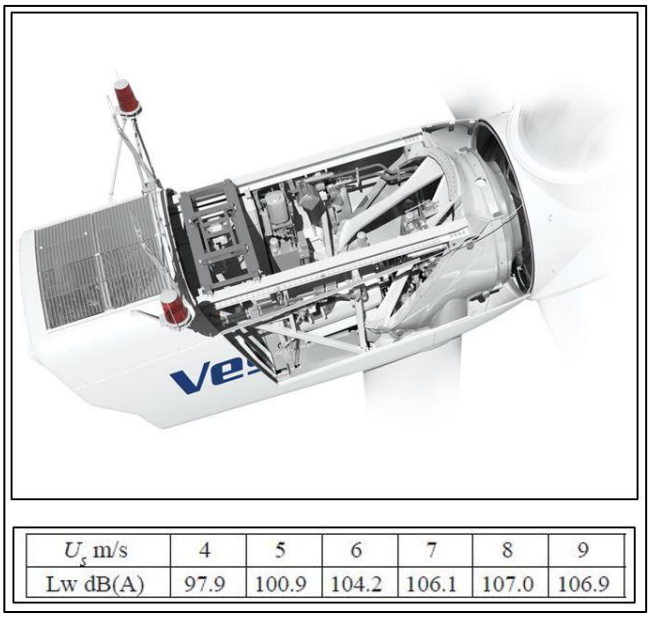

U_s m/s	4	5	6	7	8	9
Lw dB(A)	97.9	100.9	104.2	106.1	107.0	106.9

Figure 5 Sound power levels of the Vestas 3 MW wind turbine at different wind speeds [8].

When any turbine runs freely, that is, when the Inverter is off, it creates much more aerodynamic

noise. While the inverter is on, that is, while generating energy, a resistance occurs between the rotor (rotating part) and the stator (fixed part) that prevents the rotor from rotating in an uncontrolled manner.

Different wind turbines produce sound of significantly varying quality and level. In the past, noise was a serious issue for wind farms, and the cumulative impact of many turbines was causing serious problems. But technological advances and better analysis of the mechanisms that cause noise have paved the way for new production processes and quieter turbines. The best known of these are turbines that can operate at different speeds without gearbox, improvements in blade design, and low wing-tip speed ratios.

4. SIMULATION OF SOUND PROPAGATION AND DISTRIBUTION OF THE CASE STUDY

The 238m high Sapphire Tower was chosen for the case study to assess the noise emission and distribution of the building integrated wind turbine. In fact, this choice represents a possible situation because the structure to be integrated with the wind turbine must have a certain height and be free from turbulence caused by surrounding structures and topographic effects. A prototype wind turbine with a horizontal axis of 20m in diameter and 49m of hub height was selected for this study. Predictor Lima v.9 software was used during the analyzes, this software takes into account the frequency-dependent behavior and the scattering of the sound around the obstacles, which are of great importance in sound dispersion models (Figure 6).

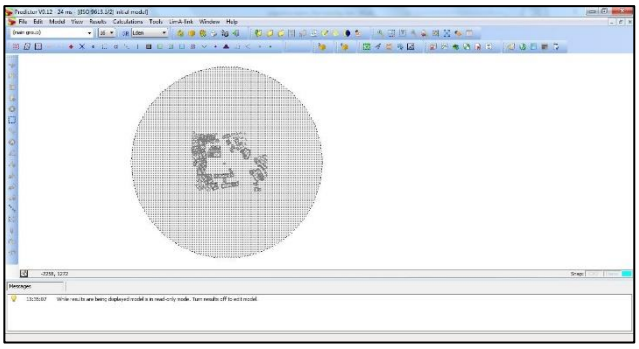

Figure 6 Graphical User Interface of the Predictor Lima v9.2 software.

In this study, the "wind turbine" object defined in the software based on the center point of the circle forming the turbine blade sweep area was used as the sound source. In this way, the availability of such an object made it possible to define a much more detailed sound source instead of the standard point source.

In order to create a consistent simulation of wind turbine noise, the "wind turbine catalog" tool, which contains values taken from manufacturers, was used. Data on turbine selection and sound power levels are shown in Figure 7. The Lw_{min} value for the selected turbine is 99.9 dB (A), and the Lw_{max} value is 103.2.

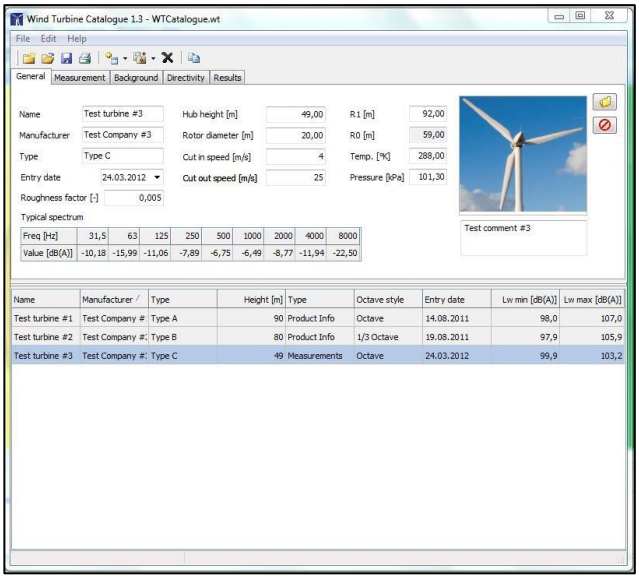

Figure 7 Predictor Lima v9.2 wind turbine catalog-turbine selection and sound power levels.

In the second phase of the study, the selected vertical axis wind turbine was integrated into the

roof of the building and primary estimates were obtained. Subsequently, two different grid options in the program were used to determine the buyers and to create a calculation grid. The first of the grids was taken in the horizontal plane using the "grid tool" and at a height of 4m from the ground. The second grid was created using the vertical grid tool on the fronts of the surrounding structures, which were considered critical.

Since it was predicted that the near-field perceptions of sound would not be affected much by the wind regime in the urban scale, the effect of wind speed and direction was not determined from climate data. Instead, 5 different possible scenarios were discussed. In these scenarios, wind speed played a role as the determining factor. Simulations were conducted for wind speeds of 4 m/s, 8 m/s, 12 m/s, 16 m/s, 20 m/s, respectively. These speeds were determined by reference to the operating range of the selected wind turbine, 4 m / s (cut in speed) and 25 m / s (cut out speed). As a result of the simulation, facade noise maps were drawn on the surrounding buildings (4. Levent - Büyükdere Boulevard). The graphs where sound pressure levels are obtained for 5 different scenarios are given below.

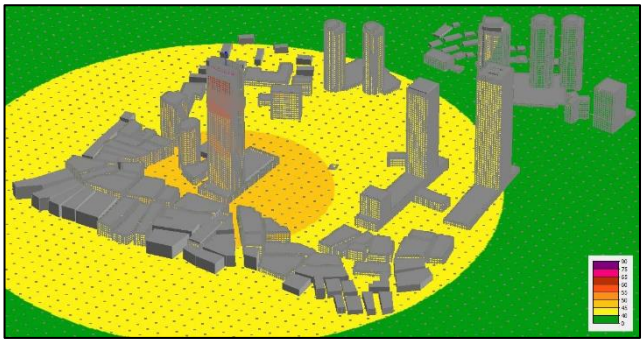

Figure 8 Axonometric view of sound pressure levels on façades (wind speed: 4 m/s).

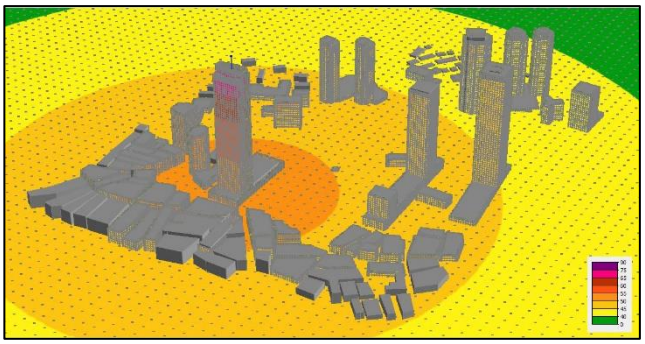

Figure 9 Axonometric view of sound pressure levels on façades (wind speed: 8 m/s).

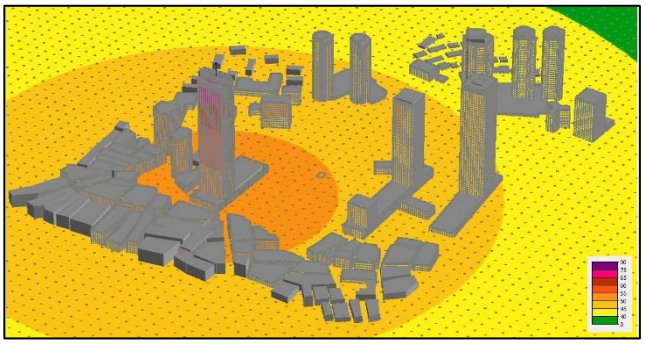

Figure 10 Axonometric view of sound pressure levels on façades (wind speed: 12 m/s).

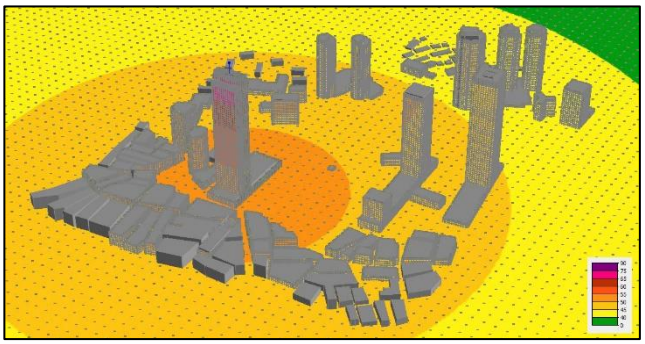

Figure 11 Axonometric view of sound pressure levels on façades (wind speed: 16 m/s).

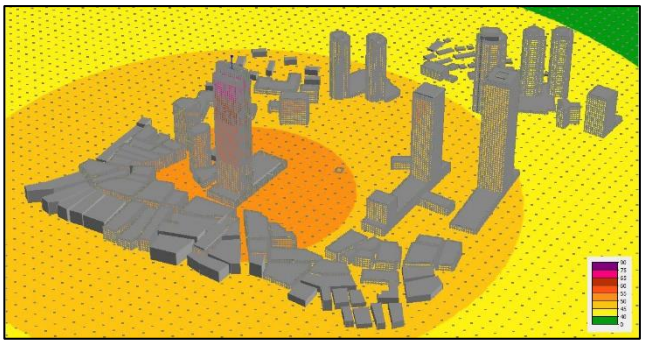

Figure 12 Axonometric view of sound pressure levels on façades (wind speed: 20 m/s).

5. RESULTS & CONCLUSION

A wide spectrum of conclusions can be drawn from numerical analysis:

- A structure can act in a number of different ways in terms of emitting noise: it can focus sound waves close to the structure: it can reflect sound waves away from the building surface: it can act as a noise barrier for structures in the vicinity: and it can absorb sound energy.
- For a structure with an aerodynamic form: the highest sound pressure levels will likely occur perpendicular to the spin plane of the horizontal axis wind turbine. In the case study discussed, critical sound pressure levels were observed in the floors just below the turbine (65-75 dB).
- Even for a completely reinforced concrete structure, the maximum sound pressure levels measured at 4 m above ground plane for the selected turbine will not exceed 50 dB (A), which complies with even the strictest noise standards and does not pose a problem in terms of planning criteria.

For interior receivers (e.g., within an aerodynamic building), the problem of focusing sound waves requires a special numerical analysis for acoustic improvements, and possibly also for turbine façades. Sound absorbing materials such as acoustic plaster (acoustic plaster), eps (expanded polyurethane foam) and fiber panels (fiberboard) can be used and additional layers can be specified for glass surfaces. This improvement will also minimize problems with sound propagation, as it will reduce sound pressure levels by approximately 3 dB (A) in areas close to the ground plane.

For the selected urban location, the distance to the closest buildings varies between 15m and 25m. The maximum sound pressure levels on the surrounding buildings were measured at the level of 50-55 dB (A) and on the building facades just behind the turbine. This value is below the frequently determined 55 dB (A) upper limit value for buildings located on commercial axes.

It is concluded that a special acoustic improvement is often necessary for facades and wind turbine integrated structures, especially in urban areas where commercial and residential areas are located.

In future studies, the acoustic properties of the mesh surfaces designed for security purposes that can be placed on the normal axis of the turbine rotor plane can be examined: the effect of sound absorption or screening can be analyzed. These surfaces may not match the integrity of the architectural design as it breaks transparency; however, this situation can be overcome by determining detailed design criteria and energy efficient aerodynamic design.

A combination of approaches that accommodate all of these improvements will ensure that the cumulative noise impact generated by building integrated turbine projects alone or combined with background sound levels remains within acceptable limits in terms of planning.

Acknowledgments

We wish to thank the reviewers, editor, and Prof. Dr. Sevtap Yılmaz Demirkale for the contributions to this research.

The Declaration of Conflict of Interest/ Common Interest

"No conflict of interest or common interest has been declared by the authors".

Authors' Contribution

The authors contributed equally to the study.

The Declaration of Ethics Committee Approval

This study does not require ethics committee permission or any special permission.

The Declaration of Research and Publication Ethics

The authors of the paper declare that they comply with the scientific, ethical and quotation rules of SAUJS in all processes of the paper and that they do not make any falsification on the data

collected. In addition, they declare that Sakarya University Journal of Science and its editorial board have no responsibility for any ethical violations that may be encountered, and that this study has not been evaluated in any academic publication environment other than Sakarya University Journal of Science.

REFERENCES

[1] "GWEC Global Wind Report 9 April 2014," www.gwec.net. [Online]. Available: http://www.gwec.net/publications/global-wind-report-2/global-wind-report-2014-annual-market-update. [Accessed: 20-Feb-2021].

[2] T. Stathopoulos and B. Blocken, "Pedestrian Wind Environment Around Tall Buildings," Advanced Environmental Wind Engineering, pp. 101–127, 2016.

[3] J. F. Manwell, J. G. McGowan, and A. L. Rogers, Wind energy explained: theory, design and application. Chichester: John Wiley & Sons, 2011.

[4] S. Stankovic, N. Campbell, and A. Harries, Urban wind energy. London: Routledge, 2015.

[5] S. Wagner, R. Bareiss, and G. Guidati, Wind turbine noise. Berlin: Springer, 2012.

[6] "Keel profiles, blunt trailing edge and xfoil/XFLR5," Boat Design Net. [Online]. Available: http://www.boatdesign.net/forums/hydrodynamics-aerodynamics/keel-profiles-blunt-trailing-edge-xfoil-xflr5-40889.html. [Accessed: 20-Feb-2021].

[7] "NREL Collaborates to Improve Wind Turbine Technology (Fact Sheet)," 2012.

[8] "Catalogs," V90-3.0 MW® - Vestas - Page - PDF Catalogs | Documentation | Brochures. [Online]. Available: https://pdf.archiexpo.com/pdf/vestas/v90-30-mw/88087-281441-_7.html. [Accessed: 20-Feb-2021].

SAKARYA ÜNİVERSİTESİ
FEN BİLİMLERİ ENSTİTÜSÜ DERGİSİ

Sakarya University Journal of Science
SAUJS

e-ISSN 2147-835X | Period Bimonthly | Founded: 1997 | Publisher Sakarya University |
http://www.saujs.sakarya.edu.tr/en/

Title: A GIS Based Comparison of Statistical Methods for Identifying Quality of Life Index in The Provinces of Turkey

Authors: Cem KIRLANGIÇOĞLU

Recieved: 2021-01-25 00:00:00

Accepted: 2021-03-21 12:52:00.995000

Article Type: Research Article

Volume: 25
Issue: 2
Month: April
Year: 2021
Pages: 571-583

How to cite
Cem KIRLANGIÇOĞLU; (2021), A GIS Based Comparison of Statistical Methods for Identifying Quality of Life Index in The Provinces of Turkey. Sakarya University Journal of Science, 25(2), 571-583, DOI:
https://doi.org/10.16984/saufenbilder.867361
Access link
http://www.saujs.sakarya.edu.tr/en/pub/issue/60672/867361

Sakarya University Journal of Science 25(2), 571-583, 2021

A GIS-Based Comparison of Statistical Methods for Identifying Quality of Life Index in The Provinces of Turkey

Cem KIRLANGIÇOĞLU*[1]

Abstract

Throughout history, human beings have lived to survive, have struggled to have a job and have enough income for a better life. But at the point we have reached today, people's quality of life not only depends on wealth and employment but also on many subjective factors, including the conditions of the environment in which they live, physical and mental health, education, recreation, security, leisure, freedom, human rights, social belonging and happiness level. Although this situation is related to the individuals at the micro scale, it is one of the important focal points of central and local governments on the macro scale. For administrators, revealing regional differences in well-being is an important criterion for eliminating social inequalities. There are many different multi-criteria decision making based studies that calculated the index of quality of life in 81 provinces of Turkey following 11 dimensions and 41 indicators determined by Turkstat. This study aims to compare the quality of life studies and rankings of cities based on six different statistical methods. GIS-based IDW interpolation technique was used to understand the spatial distribution of the well-being index and make an accurate comparison of the calculation methodologies. As a result of the study, it was seen that different methods performed on the same data gave very different results from each other.

Keywords: Quality of Life Index, Statistics, GIS, MCDM, IDW

1. INTRODUCTION

Today, one of the most significant problems of countries is to ensure the equal distribution of resources to citizens, thus to regions. However, this is not always possible due to geographical, political, or economic reasons. The ability of decision-makers and policy-makers to see inequalities in the regions and to determine the source and even the amount of inequalities are important steps in the solution of the problems. As a result, the living conditions of individuals play a decisive role in revealing regional inequalities. Therefore, the quality of life in the regions should be measured by objective and subjective indicators [1].

The World Health Organization (WHO) defines the quality of life as individuals' perception of their position in life concerning their goals,

*Corresponding author: kirlangicoglu@sakarya.edu.tr
[1]Sakarya University, Faculty of Art, Design and Architecture, Department of Architecture, 54187, Sakarya.
ORCID: https://orcid.org/0000-0002-5998-9496

expectations, standards, and concerns within the context of the culture and value systems they live in. Quality of life is a comprehensive concept that is complexly affected by a person's physical health, psychological status, level of independence, social relationships, personal beliefs, and relationships with his environment [1].

Şeker [2] supports this view and says that; quality of life is the sum of quantitative and qualitative values of an individual's lifestyle, health and relationship with society. Besides, Geray [3] claims that quality of life is related to the opportunities of people to live in a healthy environment, to meet their nutrition, protection and shelter needs, to find opportunities suitable for their physical and spiritual development, to use their creative power, to reflect the balanced harmony of natural and artificial living environments.

The definition of quality of life varies from person to person and from time to time. For instance; while the growth rate of national income was accepted as an indicator of welfare in the 1950s, per capita income was accepted as an indicator of development in the 1960s. The approach of Meeting Basic Needs developed by Simon Kuznets in the 1970s diversified the welfare criteria in development, and starting from this period, there was a lot of variability in the measurement of social welfare. In the 1980s, for measuring development or underdevelopment, meeting social and individual basic needs was taken into account and monetary and non-monetary indicators were used together in the measurement of quality of life [4]. In this study, indicators of the Turkish Statistical Institute (Turkstat) has been used to determine the geographical distribution of quality of life in Turkey.

This study aims to compare the results of different statistical methods using the same indicators and measuring the quality of life indexes in 81 provinces of Turkey in a GIS (Geographic Information Systems) based environment. The statistical methods compared in this study are VIKOR, TOPSIS, Data Envelopment Analysis, EDAS, WASPAS, and Min.-Max. method which is used by Turkstat for calculating the well-being index of the provinces.

2. DATA

Turkstat conducted a quality of life index study in the year 2015 to measure, compare and monitor the lives of individuals and households at the local level in terms of life dimensions by using objective and subjective criteria. The main purpose of the study is to develop an indicator system that will form a basis for monitoring and increasing life quality in the provinces with 11 basic dimensions which are; housing, health, income and wealth, social life, work-life, education, safety, environment, civic engagement, life satisfaction and access to infrastructure services [5].

These 11 basic dimensions have 41 indicators in total. While there are indicators that affect life positively in the study, there are also indicators that have a negative contribution to the index. The dimension, indicator, and contribution direction of the indicators are given in Table 1.

Table 1
The Dimensions and Indicators used in Turkstat Quality of Life Index

DIMENSIONS	INDICATORS	DIRECTION
CIVIC ENGAGEMENT	Participation rate in local government elections	Positive
	Membership rate of political parties	Positive
	Percentage of those involved in union / association activities	Positive
ACCESS TO INFRASTR. SERVICES	Internet subscribers (per hundred people)	Positive
	Access rate to sewerage and mains water	Positive
	Access rate to the airport	Positive
	Satisfaction rate of the municipality with public transport services	Positive
SOCIAL LIFE	Cinema and theater audience number	Positive
	Shopping center area per thousand people	Positive
	Social relations satisfaction rate	Positive
	Social life satisfaction rate	Positive

Source: TURKSTAT (2020)

Turkstat [5] says that each dimension has a critical and unique role in affecting the quality of life degrees of people. Housing is a basic life dimension used by people as a shelter and living space, where individuals meet their vital needs and enter into social relationships. The residence must have the minimum qualifications in terms of the basic needs of an individual and household. Ownership of toilets in the house, an independent room or sufficient living space for the privacy of the individual, physical characteristics of the house, adequate heating, being protected against external influences, and being able to receive sufficient daylight are some of these features. Work-Life has significant effects on people's mental, physical and financial life.

The factors that improve the working life enable people to live a life in which they have access to more financial resources, more opportunities to improve their lives by improving their skills, realizing their goals, feeling useful in society, and increasing their self-confidence. The Income and Wealth dimension is another important determinant in meeting the needs and desires of individuals and providing protection against economic and personal risks. Better health and education, higher satisfaction with life, and the likelihood of living in cleaner and safer places will increase in parallel with the rise in income and wealth.

Health is one of the most important dimensions that is directly proportional to the quality of life of individuals. Health opportunities, longevity, subjective health status, satisfaction with health services received, a life without disease, and disability are important values for individuals. These values are also of great importance for issues such as education, social life, social relations, the participation of the individual in the workforce, and raising healthy generations.

Education plays a key role in providing people with the knowledge, skills, and competencies needed to participate effectively in society and the economy. Studies show that educated people live longer, participate more effectively in politics and society where they live, commit fewer crimes, and are less dependent on social assistance. Environment, in which people live directly, affects their current and future health and sustainable life. Air and water quality is a source of satisfaction for the environment and provides opportunities to improve mental health, relieve the stress of daily life and perform physical activities.

The Security dimension is of great importance when examining the social development of an administrative unit or a region. Individuals need to feel safe to continue their other vital activities. Murder rate, number of fatal and injured traffic accidents, percentage of those who feel safe walking alone at night, etc. factors affect the lives of individuals directly. Civic Engagement is another important social issue that concerns all segments of society. For the individuals; being involved in the management system and contributing to the issues that concern their life are important factors to make them feel better. People’s demands, desires, and voices are heard only if they contribute to management. Access to Infrastructure dimension may be measured by the prevalence and accessibility of municipalities and the general infrastructure services in the province. Factors such as rate of internet subscribers, access rate to sewerage and mains water, access rate to

the airport, and satisfaction rate of the municipality with public transport services may severely affect the quality of daily life in a city. Social Life is an important part of human life that includes activities such as cultural, artistic, sports, and entertaining activities. Having strong social relations, rich and diverse social life offers positive effects on the quality of life. Life Satisfaction is the last dimension of Turkstat to measure the quality of indexes of different provinces in Turkey. Life satisfaction arises from having the needs and desires of people at different times and areas of their lives. Subjective well-being reflects the concept of how people experience their living conditions in terms of their assessment of health, education, income, personal integrity, and social conditions. Besides, life satisfaction surveys, in particular, provide a measure of satisfaction and happiness. Life satisfaction means that a person evaluates his / her life as a whole.

3. METHODOLOGY

In literature, Multi-Criteria Decision Making (MCDM) methods are available to be used for determining the livability of cities based on many different factors. MCDM provides support to decision makers in evaluating decision options based on multiple criteria that affect each other, hence affecting the final decision to be applied. There are many particular MCDM based statistical methods to calculate the quality of life levels in different cities. MULTIMOORA (The Multi-Objective Optimization by Ratio Analysis), DEA (Data Envelopment Analysis), TOPSIS (The Technique for Order of Preference by Similarity to Ideal Solution), SAW (Simple Additive Weighting), Min.-Max. Method, EDAS (Evaluation based on Distance from Average Solution), WASPAS (Weighted Aggregated Sum Product Assessment), GRA (Grey Relational Analysis), VIKOR (Vlse Kirterijumska Optimizacija I Kompromisno Resenje), and COPRAS (COmplex PRoportional ASsessment) are generally used by researchers in quality of life related studies. Just six of them will be used and compared to each other in this study because the others do not have detailed results and index values prepared for all 81 provinces of Turkey.

3.1. TURKSTAT (Min. – Max.) Method

Turkstat use a composite index application to calculate the quality of life index for different cities in Turkey. Composite indices are generally used in the comparison of cities, regions, and countries. It consists of different stages such as a selection of indicators, normalization, weighting, and aggregation of indicator values. The indicator values should be normalized to make the data set comparable to each other.

The Min-Max method was used to normalize the Quality of Life Index indicators in the provinces [5]. Min-Max is a method that normalizes indicators in the range of 0 and 1. Indicators with a negative contribution to the index (such as unemployment rate, homicide rate) are included in the index calculation as reverse coded.

$$I_i = (x_i - x_{min}) / (x_{max} - x_{min}) \quad (1)$$

$$\hat{I}_i = 1 - (x_i - x_{min}) / (x_{max} - x_{min}) \quad (2)$$

x_i : Indicator Value

x_{min} : The minimum value of an indicator

x_{max} : The maximum value of an indicator

Composite index calculation has been made according to the hierarchical equal weighting method in which dimensions and indicators under the same dimension are equally weighted. According to this method, dimension and indicator weights are as follows;

$$\text{Dimension Number (N)} \rightarrow w_D = 1/N \quad (3)$$
$$\text{Indicator Number (n)} \rightarrow w_I = 1/n \quad (4)$$

Dimension score value was obtained by multiplying each normalized indicator value by the indicator weight in the dimension and aggregating these multiplications. The aggregation method used in obtaining the

dimension score value can be expressed as follows;

$$\text{Dimension Score Value} = \Sigma (w_{Ii} * I_i) \quad (5)$$

w_{Ii} = Weight of Indicator

Ii = Normalized Indicator Value

The overall score value was obtained by multiplying each normalized indicator value by the dimension weight and the indicator weight and by aggregating these results together. The aggregation method used in obtaining the general score value can be expressed as follows;

$$\text{General Score Value} = \Sigma (w_{Di} * w_{Ii} * I_i) \quad (6)$$

w_{Di} = Weight of Dimension

w_{Ii} =Weight of Indicator

Ii = Normalized Indicator Value

Geographic Information Systems (GIS) based maps have been prepared to see the spatial distribution of each dimension Turkstat uses to define the quality of life indexes all around Turkey. Figure 1 shows the spatial distribution of 11 dimensions and overall index score as compared to each other.

GIS, which was used to prepare these thematic maps, is a decision support system that allows operations such as collecting geographic information for a specific purpose, storing, updating, controlling, analyzing, and displaying in a computer environment [6]. It is a geographical database that expresses the world in geographical terms and helps to understand and transform data into information and knowledge. GIS enables the integration of tabular and geographical data and allows both thematic visualizations and detailed analyses. By using GIS, it is possible to make geographically weighted analyses instead of just numerical based statistical calculations.

IDW (Inverse Distance Weighted) interpolation method is widely used in GIS studies. Both the ease of calculation and the solution accuracy are the most important factors in the widespread use of the method. The point value to be estimated is a function of the distance and size of the neighboring points around this point, and the effect of neighboring points on the estimated value depends on the change in distance. In the IDW method, as the distance to the anchor points increases, the effect of the far point on the value to be estimated decreases.

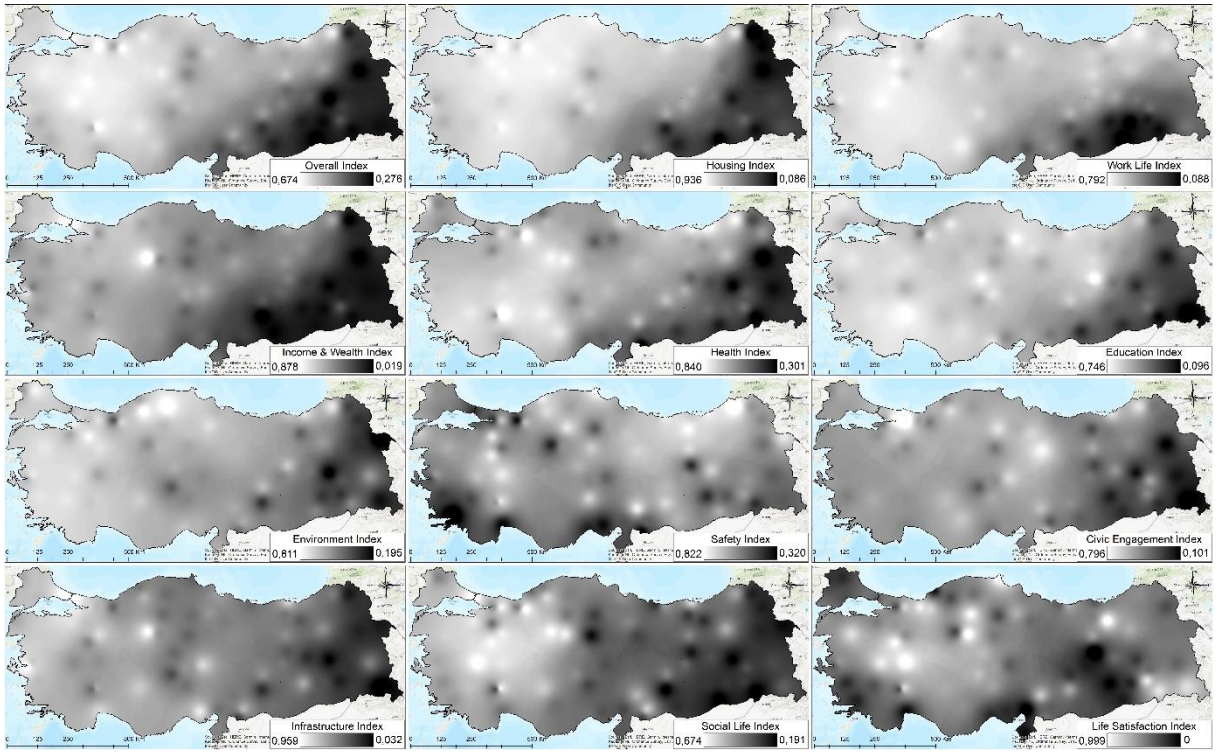

Figure 1 Spatial Distribution of Quality of Life Dimensions in Turkey

Alpaykut [4] says that; the well-being index ranking of Turkstat is based on the assumption that the dimensions affecting the overall quality of life index score have equal weight. Although the assumption that all dimensions have equal weight is a relevant method, all dimensions can have different weights at the same time. Therefore, he suggests using the idea that the factors affecting the quality of life index should have different weights and TOPSIS Method should be used to calculate the quality of life index of each province in Turkey.

3.2. TOPSIS Method

The Technique for Order of Preference by Similarity to Ideal Solution (TOPSIS) is a Multi-Criteria Decision Making (MCDM) method applied in many different areas. The evaluation of alternatives (decision options) is based on two basic points: positive ideal solution and negative ideal solution. In the TOPSIS method, it is aimed to determine the decision option at the shortest distance from the positive ideal solution and the furthest distance from the negative ideal solution [7]. The application process of the TOPSIS process is given below.

The first step is to create a decision matrix having n*m dimensions. In this matrix; the rows are decision options while the columns show the criteria.

$$D = \begin{bmatrix} d_{11} & d_{12} & \cdots & d_{1m} \\ d_{21} & d_{22} & \cdots & d_{2m} \\ . & . & . & . \\ . & . & . & . \\ . & . & . & . \\ d_{n1} & d_{n2} & \cdots & d_{nm} \end{bmatrix} \quad (7)$$

n = Number of Decision Options

m = Number of Evaluation Criteria

The second step is to create a normalized decision matrix (R matrix). The standard decision matrix is obtained by taking the square root of the sum of squares (sum of squares of column values) of the

values belonging to each criterion of the decision matrix and dividing the related element of the column by the resulting value.

Then the remaining steps are calculating the criteria weighted matrix, finding the weighted normalized decision matrix, determining the positive ideal and negative ideal solution, finding the separation of each alternative from a positive and negative ideal solution, and finally calculating the relative closeness to the ideal solution [8]. The greatest relative closeness to the ideal solution gives us the best alternative. In this study, it gives us the highest and lowest quality of life indexes in Turkish provinces.

Alpaykut [4] used Principal Components Method (PCM) for giving weights of variables in the TOPSIS method to rank the cities following their quality of life degrees. All 41 indicators, previously determined by Turkstat, have been weighted by PCM to be used in TOPSIS calculations in the study. GIS-based results of this study are given in Figure 2 as compared to the results of the other statistical methods.

3.3. DEA Method

Turkstat uses the min.-max. method and gives equal weight to each indicator under each dimension while calculating the quality of life index of the provinces. TOPSIS method gives weight to each indicator in accordance with their importance degree. Çağlar [9] used a Data Envelopment Analysis (DEA) based statistical model to find out the quality of life index of each province in Turkey.

In the model, it is aimed to present an approach that both evaluates the cities relatively and eliminates the problem of determining the weights of the indicators used in the index calculation. In the proposed method, there is no need to determine the indicator weights, it is possible to use the indicators without normalization.

Charnes, Cooper, & Rhodes [10] propose Data Envelopment Analysis (DEA), which measures the relative efficiency of decision-making units in case of many inputs and multiple outputs. DEA is a linear programming based non-parametric method that does not need any pre-assumptions. In DEA, the efficiency criterion is obtained by dividing the weighted sums of the outputs by the weighted sums of the inputs. Figure 2 gives a GIS-based comparison of DEA model results produced by Çağlar [9] and five different methods.

3.4. VIKOR Method

VIKOR (Vlse Kirterijumska Optimizacija I Kompromisno Resenje in Serbian) is a Multi-Criteria Decision Making (MCDM) method first introduced by Opricovic in 1998 and it means multicriteria optimization and compromise solution. Also, it was firstly used by Opricovic and Tzeng [11] in solving multi-criteria decision-making problems [12]. VIKOR is a popular statistical model because of its computational simplicity and solution accuracy. The basis of the method is to create a compromise solution within the framework of alternatives and within the scope of evaluation criteria.

This compromise solution is the closest one to the ideal solution [13]. In the method, it is possible to make the closest decision to the ideal solution under certain conditions by creating a multi-criteria ranking index for alternatives. The consensual ranking is achieved by comparing the values of proximity to the ideal alternative [14].

Yüce [15] used the VIKOR method to define a sorting index for the provinces of Turkey in terms of livability. In the ranking; Well-Being Index in Turkey (2015) data are used. He has weighted all 11 dimensions separately and prepared a ranking table sorting all 81 provinces from best to worst in terms of livability.

Each province has a VIKOR based score in the table. These scores have been transferred to a GIS-based mapping algorithm and given in Figure 2 as compared to the other methodologies.

3.5. EDAS Method

EDAS (Evaluation based on Distance from Average Solution) method was introduced to the literature by Ghorabaee, Zavadskas, Olfat and Turskis [16] in 2015. EDAS method is similar to some other MCDM methods such as MOORA,

TOPSIS, and VIKOR in terms of trying to find solutions based on distance. However, it is not necessary to calculate the best and worst values in the EDAS method. The best alternative in the method is found by calculating the average solution distances of the alternatives according to each criterion [17]. Besides, there are two measures in the method regarding the acceptability of alternatives.

The first one is the positive distance from the average (PDA) and the second one is the negative distance from the average (NDA). The alternative evaluation process is made according to higher values of PDA and lower values of NDA [18]. Thus, higher values of PDA and/or lower NDA values indicate that the alternative solution is better than the average solution.

3.6. WASPAS Method

WASPAS (Weighted Aggregated Sum Product Assessment) is an MCDM method based on Weighted Sum Model (WSM) and Weighted Product Model (WPM) methods [19]. The WASPAS method, developed by Zavadskas et al. [20] in 2012, gives the performance values of the options according to the criteria by using the criterion weights in the solution of MCDM problems. As a result of the solution, the options are ranked from best to worst. Also, the method tries to achieve high consistency in estimation by optimizing the weighted integrated function [21].

Özbek [22] used EDAS and WASPAS methods to evaluate the quality of life in the Turkish provinces within the framework of the determined criteria. In this way; the central government, local governments, and relevant institutions may improve the quality of life in all the provinces with low quality of life. The results of his study are mapped for 81 provinces and given in Figure 2 as compared to GIS-based maps of the other statistical methods used in this study.

Quality of Life Index distribution in Turkey is mapped on ArcGIS software-based on six different statistical methods compared in this study. In Figure 2, the red-colored areas have higher rates, yellow areas have medium rates and blue areas have lower rates than the other areas.

All statistical methods show that the Eastern and Southeastern regions of Turkey have a lower quality of life indexes than the Western regions. In GIS-based maps, the TOPSIS method gives significantly different results than the others while DEA method has slightly particular results. Figure 3 shows the five best cities and five lowest rated cities for living in accordance with each statistical method.

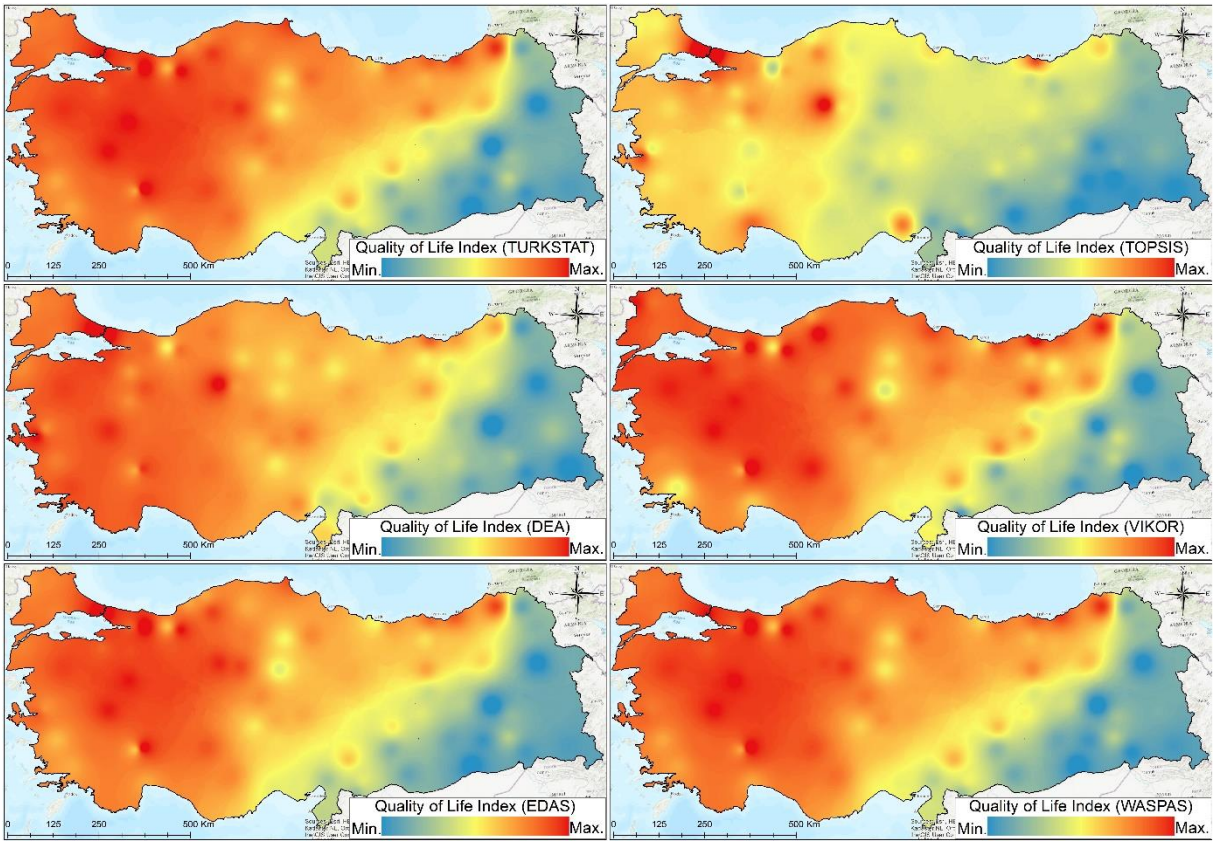

Figure 2 GIS-Based Comparison of Statistical Methods Identifying Quality of Life Distribution in Turkey

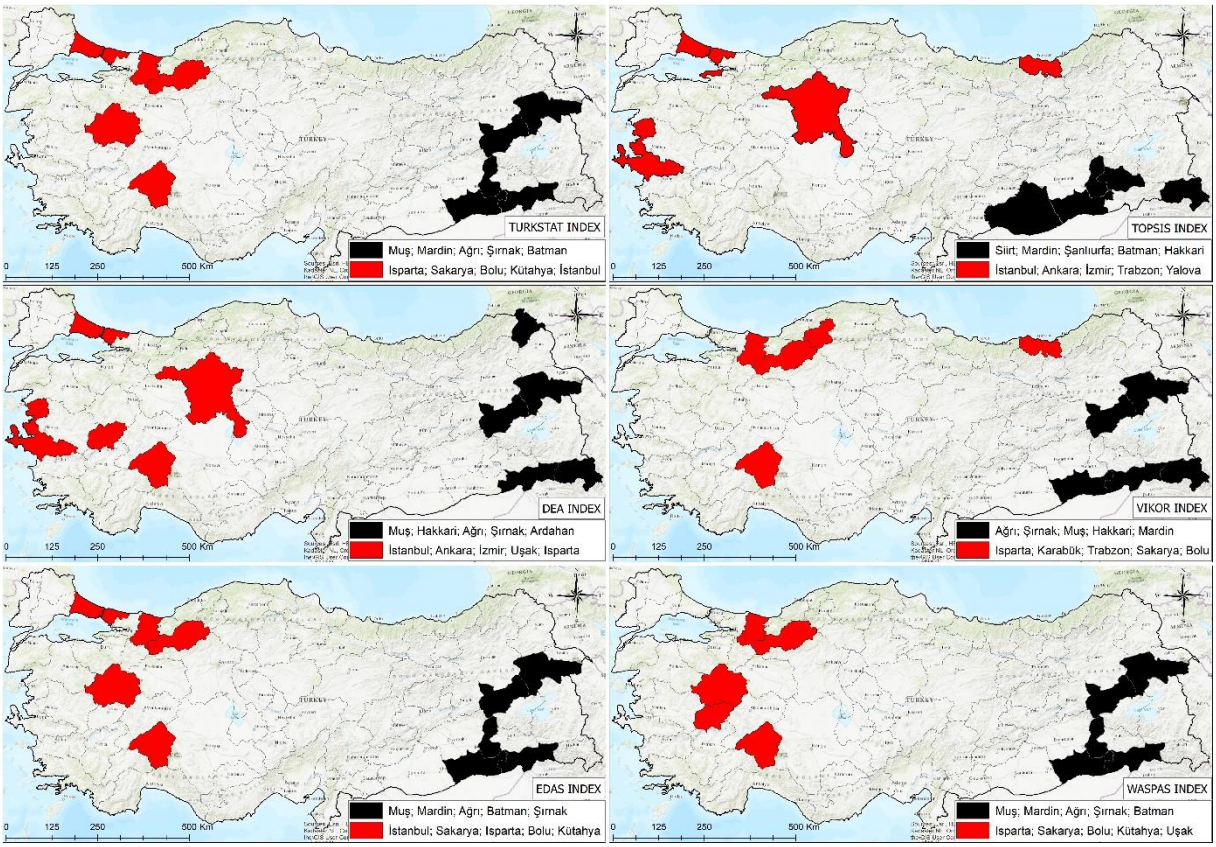

Figure 3 Comparison of Statistical Methods Based on the Highest and Lowest Rated Cities

As it is seen in Figure 2 and Figure 3, different methods give different results. Today, Turkey uses the Min.-Max. method applied by Turkstat. The other ones have been applied by different researchers based on the same data, same dimensions, and same indicators. Alpaykut [4] applied the TOPSIS method, Yüce [15] applied the VIKOR method, Çağlar [9] applied the DEA method, Özbek [22] applied the EDAS and WASPAS methods. Table 2 shows the ranking of each province following the statistical method applied.

Quality of Life Rankings of Provinces by Applied Statistical Methods (Top 10 Cities)

Province Name & Rank	TURKSTAT (Min.-Max.)	TOPSIS	DEA	VIKOR	EDAS	WASPAS
Isparta	1	19	5	1	3	1
Sakarya	2	11	14	4	2	2
Bolu	3	12	17	5	4	3
Kütahya	4	30	28	8	5	4
İstanbul	5	1	1	30	1	6
Uşak	6	22	4	6	6	5
Balıkesir	7	20	7	12	8	9
Artvin	8	18	42	9	12	7
Kırıkkale	9	27	37	14	11	10
Afyonkrhsr	10	40	15	15	14	11

Table 2

Same data, same dimensions, same indicators but different results. While Turkstat claims that Isparta is the best city in Turkey in terms of quality of life; according to the TOPSIS method it is 19th and according to DEA it is 5th city to live. While TOPSIS method shows that İstanbul is the 1st city to live, VIKOR method shows it as the 30th one. Kütahya is 4th city in Turkstat ranking, while it is 30th in TOPSIS and 28th in DEA methods. EDAS and WASPAS give the closest results to Turkstat method but they also have slightly different results than each other. While the EDAS method shows İstanbul as the best city to live, the WASPAS method shows it as the 6th one. As it can be seen in Table 2, especially for top cities the results of statistical methods severely different from each other in general. Table 3 shows the lowest rated 10 cities according to Turkstat statistics and their ranks under other statistical methods.

Table 3
Quality of Life Rankings of Provinces by Applied Statistical Methods (Lowest Rated 10 Cities)

Province Name & Rank	TURKSTAT (Min.-Max.)	TOPSIS	DEA	VIKOR	EDAS	WASPAS
Iğdır	72	70	72	72	71	72
Şanlıurfa	73	79	74	71	73	74
Ardahan	74	66	77	70	74	73
Diyarbakır	75	64	65	68	75	75
Hakkari	76	77	80	78	76	76
Batman	77	78	69	74	78	77
Şırnak	78	76	78	80	77	78
Ağrı	79	73	79	**81**	79	79
Mardin	80	80	76	77	80	80
Muş	**81**	75	**81**	79	**81**	**81**

Table 3 shows that different statistical methods give results similar to each other for the lowest-rated cities. There are slightly different results among the methodologies. For example; while Muş is the lowest-rated city in Turkstat, DEA, EDAS, and WASPAS rankings; it is 75th in TOPSIS and 79th in VIKOR methods. Diyarbakır is the 75th city in Turkstat ranking but it is 64th in TOPSIS and 65th in DEA rankings.

4. CONCLUSION

As a result of the study, it is seen that the ranking of the provinces in terms of quality of life dramatically changes by the applied weights, chosen statistical methods, and the pre-assumptions of the decision-makers. It is clear that, for quality of life studies, the statistical method must be independent of these factors as much as possible. It should be suitable for determining dimensions and sub-indices by combining the information of different indicators. No guesswork should be required for indicators. The model should allow for a relative assessment of the best when evaluating the provinces. Prior information should not be needed in determining the weight for indicators and if there is definite prior information, it should be allowed to be added to the model. Therefore, Data Envelopment Analysis (DEA) seems like the best statistical method to calculate the quality of life index of the provinces.

Besides, all the statistical methods show that the lowest-rated cities are located in the Eastern Anatolia and the Southeastern Anatolia Regions of Turkey. That means; while the quality of life degree is higher in Western cities, it is lower in Eastern cities in Turkey. There are many different factors such as economic, political, and demographic factors at the root of this situation. Central and local governments should take the necessary steps to eliminate this inequality between provinces.

Funding

The author has not received any financial support for the research, authorship, or publication of this study.

The Declaration of Conflict of Interest/ Common Interest

No conflict of interest or common interest has been declared by the author.

The Declaration of Ethics Committee Approval

This study does not require ethics committee permission or any special permission.

The Declaration of Research and Publication Ethics

The author of the paper declares that he complies with the scientific, ethical and quotation rules of SAUJS in all processes of the paper and that he does not make any falsification on the data collected. Also, he declares that Sakarya University Journal of Science and its editorial board have no responsibility for any ethical violations that may be encountered and that this study has not been evaluated in any academic publication environment other than Sakarya University Journal of Science.

REFERENCES

[1] A. Çağlar, "İllerin Yaşam Kalitesi: Türkiye İstatistik Kurumu Verileriyle Veri Zarflama Analizi'ne Dayalı Bir Endeks," Eskişehir Osmangazi Üniversitesi İİBF Dergisi, vol. 15, no. 3, pp. 875-902, 2020.

[2] WHO, "WHOQOL Measuring Quality of Life," World Health Organization Division of Mental Health and Prevention of Substance Abuse, Geneva, Switzerland, 1997.

[3] M. Şeker, "Quality of Life Index: A Case Study of Istanbul," Ekonometri ve İstatistik, no. 23, pp. 1-15, 2015.

[4] C. Geray, "Kentsel Yaşam Kalitesi ve Belediyeler," Türk İdare Dergisi, no. 421, p. 323–345, Aralık 1998.

[5] S. Alpaykut, Journal of Süleyman Demirel University Institute of Social Sciences, vol. 4, no. 29, pp. 367-395, 2017.

[6] TURKSTAT, "Well-Being Index for Provinces," 2020. [Online]. Available: https://turkstatweb.tuik.gov.tr/PreTablo.do?alt_id=1106.

[7] Başarsoft, "Coğrafi Bilgi Sistemleri (CBS) Nedir?," Ankara, 2020.

[8] A. Apaydın and Ö. Türkşen, "ÇOK ÖLÇÜTLÜ KARAR VERME YÖNTEMLERİ - II," 2020. [Online]. Available: https://acikders.ankara.edu.tr/course/view.php?id=5704.

[9] M. Monjezi, H. Dehghani, T. N. Singh, A. R. Sayadi and A. Gholinejad, "Application of TOPSIS method for selecting the most appropriate blast design," Arabian Journal of Geosciences, vol. 5, pp. 95-101, 2012.

[10] A. Charnes, W. Cooper and E. Rhodes, "Measuring the efficiency of decision making units," European Journal of Operational Research, vol. 2, no. 6, pp. 429-444, 1978.

[11] S. Opricovic and G. H. Tzeng, "Compromise Solution by MCDM Methods: A Comparative Analysis of VIKOR and TOPSIS," European Journal of Operational Research, vol. 106, no. 2, pp. 445-455, 2004.

[12] H. Dinçer and A. Görener, "Performance Evaluation Using AHP-VIKOR and AHP-TOPSIS Approaches: The Case of Service Sector," Journal of Engineering and Natural Sciences, pp. 244-260, 2011.

[13] M. T. Chu, J. Shyu, G. H. Tzeng and R. Khosla, "Comparison Among Three Analytical Methods for Knowledge Communities Group Decision Analysis," Expert Systems with Applications, vol. 33, no. 4, pp. 1011-1024, 2007.

[14] S. Opricovic and G. H. Tzeng, "Extended VIKOR Method in Comparison with Other Outranking Methods," European Journal of Operational Research, vol. 178, no. 2, pp. 514-529, 2007.

[15] H. U. Yüce, "Türkiye'deki Yaşanılabilir İller Sıralaması," Dış Ticaret Enstitüsü, 2018.

[16] M. K. Ghorabaee, E. K. Zavadskas, L. Olfat and Z. Turskis, "Multi-Criteria Inventory Classification Using A New Method of Evaluation Based on Distance From Average Solution (EDAS)," Informatica, vol. 26, no. 3, pp. 435-451, 2015.

[17] E. Çakır, "Elektronik Belge Yönetim Sistemi (Ebys) Yazılımı Seçiminde Çok Kriterli Karar Verme Yöntemleri: Bir Belediye Örneği," Business, Economics and Management Research Journal, vol. 1, no. 1, pp. 15-30, 2018.

[18] C. Kahraman, M. K. Ghorabaee, E. K. Zavadskas, S. C. Onar, M. Yazdani and B. Oztaysi, "Intuitionistic fuzzy EDAS method: An application to solid waste disposal site selection," Journal of Environmental Engineering and Landscape Management, vol. 25, no. 1, pp. 1-12, 2017.

[19] S. H. Zolfani, M. H. Aghdaie, A. Derakhti, E. K. Zavadskas and M. H. M. Varzandeh, "Decision making on business issues with foresight perspective: An application of new hybrid MCDM model in shopping mall locating," Expert systems with applications, vol. 40, no. 17, pp. 7111-7121, 2013.

[20] E. K. Zavadskas, Z. Turskis, J. Antucheviciene and A. Zakarevicius, "Optimization of weighted aggregated sum product assessment," Elektronika ir elektrotechnika, vol. 122, no. 6, pp. 3-6, 2012.

[21] S. Lashgari, J. Antuchevičienė, A. Delavari and O. Kheirkhah, "Using QSPM and WASPAS methods for determining outsourcing strategies," Journal of Business Economics and Management, vol. 15, no. 4, pp. 729-743, 2014.

[22] A. Özbek, "Türkiye'deki İllerin EDAS ve WASPAS Yöntemleri ile Yaşanabilirlik Kriterlerine Göre Sıralanması," Kırıkkale University Journal of Social Sciences, vol. 9, no. 1, pp. 177-200, 2019.

SAKARYA ÜNİVERSİTESİ
FEN BİLİMLERİ ENSTİTÜSÜ DERGİSİ

Sakarya University Journal of Science
SAUJS

e-ISSN 2147-835X | Period Bimonthly | Founded: 1997 | Publisher Sakarya University |
http://www.saujs.sakarya.edu.tr/en/

Title: Dispersion of Graphene Using cetyltrimethylammonium bromide (CTAB): Dye Removal and Characterization Studies

Authors: Ferda MİNDİVAN, Meryem GÖKTAŞ, Ülküye Dudu GÜL

Recieved: 2020-05-07 00:00:00

Accepted: 2021-03-22 12:52:01

Article Type: Research Article

Volume: 25
Issue: 2
Month: April
Year: 2021
Pages: 584-593

How to cite
Ferda MİNDİVAN, Meryem GÖKTAŞ, Ülküye Dudu GÜL; (2021), Dispersion of Graphene Using cetyltrimethylammonium bromide (CTAB): Dye Removal and Characterization Studies. Sakarya University Journal of Science, 25(2), 584-593, DOI: https://doi.org/10.16984/saufenbilder.732643
Access link
http://www.saujs.sakarya.edu.tr/en/pub/issue/60672/732643

Sakarya University Journal of Science 25(2), 584-593, 2021

Dispersion of Graphene Using cetyltrimethylammonium bromide (CTAB): Dye Removal and Characterization Studies

Ferda MİNDİVAN*[1], Meryem GÖKTAŞ[2], Ülküye Dudu GÜL[3]

Abstract

The aim of this study to determine the usability of cetyltrimethylammonium bromide **(**CTAB)-reduced graphene oxide (RGO) composites in the removal of methylene blue (MB) from aqueous solutions and to investigate the stability of composites in the aqueous dispersions. And also, we compared the effects of three different CTAB concentrations on the decolorization of MB. The CTAB-RGO composites performed increasing decolorization activity, decreasing average particle size and resulting individual graphene layers with the increasing CTAB concentration. CTAB-RGO with 40 and 80 mg/L composites were unstable, RGO and CTAB-RGO with 120 mg/L had good stability in the aqueous solutions. Effective repulsive forces of CTAB-RGO-120 composite prevented to forming graphene aggregates. The highest decolorization rate of CTAB-RGO-120 composite at neutral pH can result from both the electrostatic interaction and π-π interaction.

Keywords: reduced graphene oxide, cetyltrimethylammonium bromide, decolorization, methylene blue

1. INTRODUCTION

Surfactants are the surface-active agents which are commonly used in industrial applications [1]. Most studies emphasized that surfactants were used in coloring the products to improve color quality [2, 3]. It is known that the effluents of coloring industries include both surfactants and dyes together [4]. The treatment of industrial effluents is an ongoing problem and most of the studies continuously aim to solve this problem. The most concerning issue is the dye-containing

*Corresponding author: ferda.mindivan@bilecik.edu.tr
[1]Bilecik Seyh Edebali University, Faculty of Engineering, Bioengineering Department, 11230, Bilecik.
E-Mail: ferda.mindivan@bilecik.edu.tr
ORCID: https://orcid.org/0000-0002-6046-2456
[2]Bilecik Seyh Edebali University, Vocational College, Department of Metallurgy, 11230, Bilecik.
E-Mail: meryem.goktas@bilecik.edu.tr
ORCID: https://orcid.org/0000-0003-1583-8300
[3]Bilecik Seyh Edebali University, Vocational School of Health Services, 11230, Bilecik.
E-Mail: ulkuyedudu.gul@bilecik.edu.tr
ORCID: https://orcid.org/0000-0001-6443-1633

effluents due to their toxic effects on the health of living organisms and also the environment [5]. Recently, inexpensive and environmentally friendly treatment technologies are searched for the treatment of industrial effluents [6]. Some of the studies are shown the positive effect of surfactants on the removal of dyes from aqueous solutions [7, 8]. The recent studies focused on the use of graphene as an adsorbent in the treatment of wastewaters with the adsorption process. Because of the excellent properties of graphene, it has attracted much attention for various applications [9]. Graphene derivatives (Graphene oxide (GO), Reduced graphene oxide (RGO)) were used for in the treatment of Methylene Blue (MB) dye contaminated wastewater [10-14]. However, there is limited study that shows the MB removal properties of CTAB-graphene composites [15-17]. For example, Sankar et al. [17] reported that the chemical reduction of graphene oxide by hydrazine hydrate in the presence of CTAB and was obtained a highly stable aqueous dispersion. Yusuf et al. [16] synthesized GO, reduced to graphene (GN) by ascorbic acid and intercalated with CTAB. Then, prepared GN-CTAB was used for the adsorptive removal of acid red 265 (AR265) and acid orange 7 (AO7) dyes from water. Mahmoodi et al. [15] manufactured rGO/CTAB nanomaterial and characterized in detail. They used the rGO/CTAB to remove anionic dyes (direct red 80 and direct red 23) from wastewater. Therefore, the decolorization of MB with CTAB-RGO composite has never been explored and thus requires investigation.

The objectives of this study are the following: (1) to prepare CTAB-RGO composites with three different CTAB concentrations, to analyses the structures of CTAB-RGO composites and to investigate the stability of composites in the aqueous dispersions, (2) to use the composites as sorbents to remove MB from aqueous solutions and to examine the effects of pH.

2. MATERIALS AND METHOD

2.1. Preparation of Composites

GO was prepared by the modified Hummers method; the details of the process were described by Mindivan [18]. For each experiment, 0,1 g of GO was mixed with 25 ml each of the aqueous solutions of CTAB at different concentrations under ultrasonic agitation. Accordingly, concentrations of 40, 80 and 120 ppm were used for the CTAB aqueous solution. Then 0,1 g ascorbic acid was added into the mixture. The amount of ascorbic acid was determined according to optimum values obtained from previous reports [19]. Then, the mixture was heated to 98 °C for 12 h. After that, the mixture was centrifuged to remove excess ascorbic acid and CTAB. By changing the various concentrations of CTAB in the resulting composites, a series of CTAB-RGO composites were prepared and coded as CTAB-RGO-40, CTAB-RGO-80, and CTAB-RGO-120. The synthesis process of RGO as a control sample was presented in our previous reports [19].

2.2. Characterization of Composites

X-ray diffraction (XRD) analyses were carried out by an X-ray diffractometer in the range of $2\theta = 5°$ to 40° (PAN analytical Empyrean). The zeta-potential and particle size of dispersions were measured by a Zetasizer Nano ZS (Malvern Instruments, Malvern, UK). The surface morphology of CTAB-RGO-120 composite was examined by a field emission scanning electron microscopy (FESEM, Supra 40VP, Zeiss).

2.3. Preparation of Dye Solution

MB, which was a cationic dye, used in this study. The stock dye solution was prepared by dissolving in distilled water at a concentration of 2% (w/v). Experiments were carried out with the desired amounts of these stock solutions.

2.4. Decolorization Experiments

Decolorization experiments were done via the batch technique using 50 ml flasks contained solutions with MB. The experimental flasks were continuously agitated on a shaker with a constant shaking rate of 100 rpm for 24 hours. To examine the effect of adsorbent type on MB adsorption, the different types of graphene-based composites (Dry weight: 1 g/L) were added into flasks contained 50 ml distilled water with 50 mg/L MB at pH 7,05 for 0 to 1440 minutes. The 50 ml distilled water flask containing only MB without adsorbent was used as a control. The experiments were repeated four times and the averages were used and also, the standard deviations were calculated.

2.5. Decolorization Analysis

The 1 ml samples were taken at certain times and centrifuged at 10000 rpm for 7 minutes. The supernatants were analyzed with a spectrophotometer (Thermo scientific, Genesys 150) at 665 nm. The control group contained only distilled water was used in the spectrophotometric method. Equation 1 was used to calculate the percentage of decolorization;

Equation 1: $D\ (\%) = (C_o - C_f)/C_o \times 100$ (1)

Equation 2 was used to calculate the dye uptake capacity of adsorbent;

Equation 2: $q_m = (C_o - C_f) / X_m$ (2)

In these equations; D (%) is the percentage of dye removal rate, q_m is the maximum specific dye uptake (mg/g), X_m is the maximum dried cell mass (g/L), C_o is the initial dye concentration (mg/L), C_f is the final dye concentration (mg/L).

3. RESULTS AND DISCUSSION

3.1. XRD Analysis

The diffraction patterns of RGO and CTAB-RGO composites were shown in Figure 1. As shown in Figure 1, the typical diffraction peak of RGO appeared at about 2θ=25,31°. This broad peak indicated that the successful synthesis of RGO by ascorbic acid [20]. The location of the diffraction peaks of CTAB-RGO composites was the same as that of the RGO sample. But the increase in the interlayer distance from 3,52 °A to 3,90 °A was due to CTAB intercalated for CTAB-RGO-120 composite compared to RGO. At the same time, the diffraction peak of the composite shifted leftward. Hu et al. [21] found similar results and reported that interlayer π-π van der Waals bond was broken after the intercalation of surfactants.

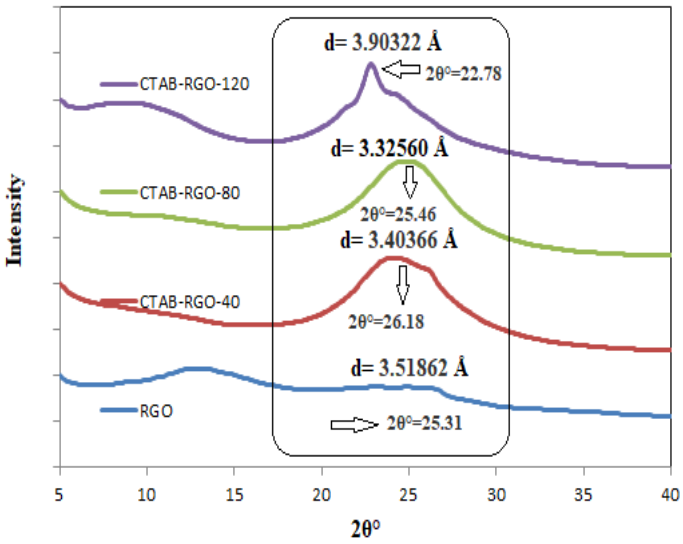

Figure 1 The diffraction patterns of RGO and CTAB-RGO composites

3.2. ZP Analysis

The zeta potential values of the RGO and CTAB-RGO composites are presented in Figure 2a. The zeta potential exhibits surface charges of colloidal particles and the colloidal stability of the solution. Particles with zeta potentials between |-31| mV |-40| mV and |-41| mV |-50| mV are known that they exhibited moderate stability (no agglomeration) and good stability, respectively [22]. Zeta

potential in Figure 2a was -41,0 mV for RGO due to oxygen-containing functional groups and had good stable dispersion. As the CTAB concentrations were increased, the surface charge became more positive, the highest value of zeta potential (42,4 mV) was shown for the CTAB-RGO-120 composite, which was the most stable composite [23]. Particles with zeta potential between |- 41| mV and |−50| mV were considered to form good stable dispersion due to electrostatic repulsion between the charged particles. While the CTAB-RGO-40 and CTAB-RGO-80 remaining composites showed the absolute value of zeta potential less than 30 mV. These ZP values of CTAB-RGO-40 and CTAB-RGO-80 composites could be caused unstable aggregations of graphene in the aqueous solutions because lower repulsive forces did not overcome the attractive van der Waals forces [24]. As a result, the highest CTAB concentration played a role better than the other two CTAB concentrations and RGO, due to high surface coverage of CTAB-RGO-120 could be enough for an effective dispersion process [24]. Figure 2b showed the average particle sizes of RGO and CTAB-RGO composites. It could be seen that the average particle size of composites decreased by increasing the CTAB concentration. Increasing the concentration from 40 ppm to 120 ppm resulted in an average particle size decrement from 2028 nm to 554,0 nm. And also, RGO resulted in large particle size in the range of 2468 nm. Sarsam et al. [23] reported that low average particle size indicates high stability of the colloidal suspension. Average particle size results confirmed with the ZP values because zeta potential value linked directly to the stability of a colloidal suspension.

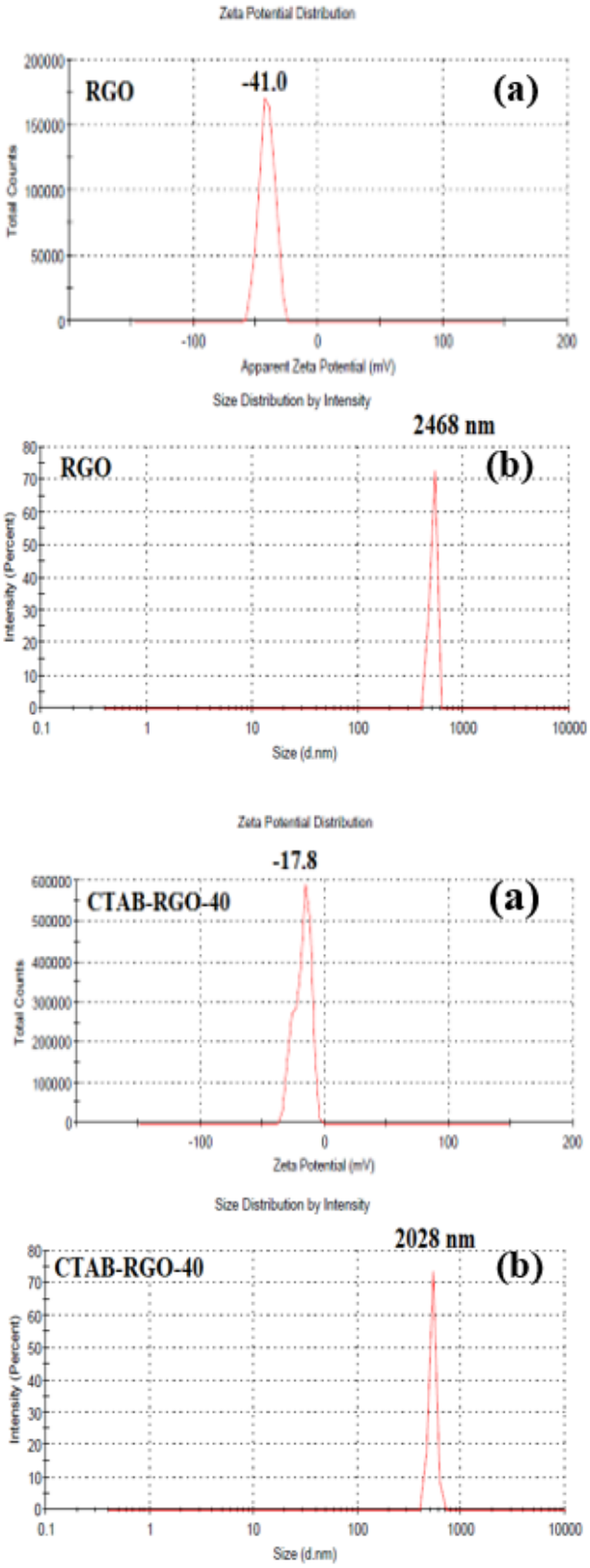

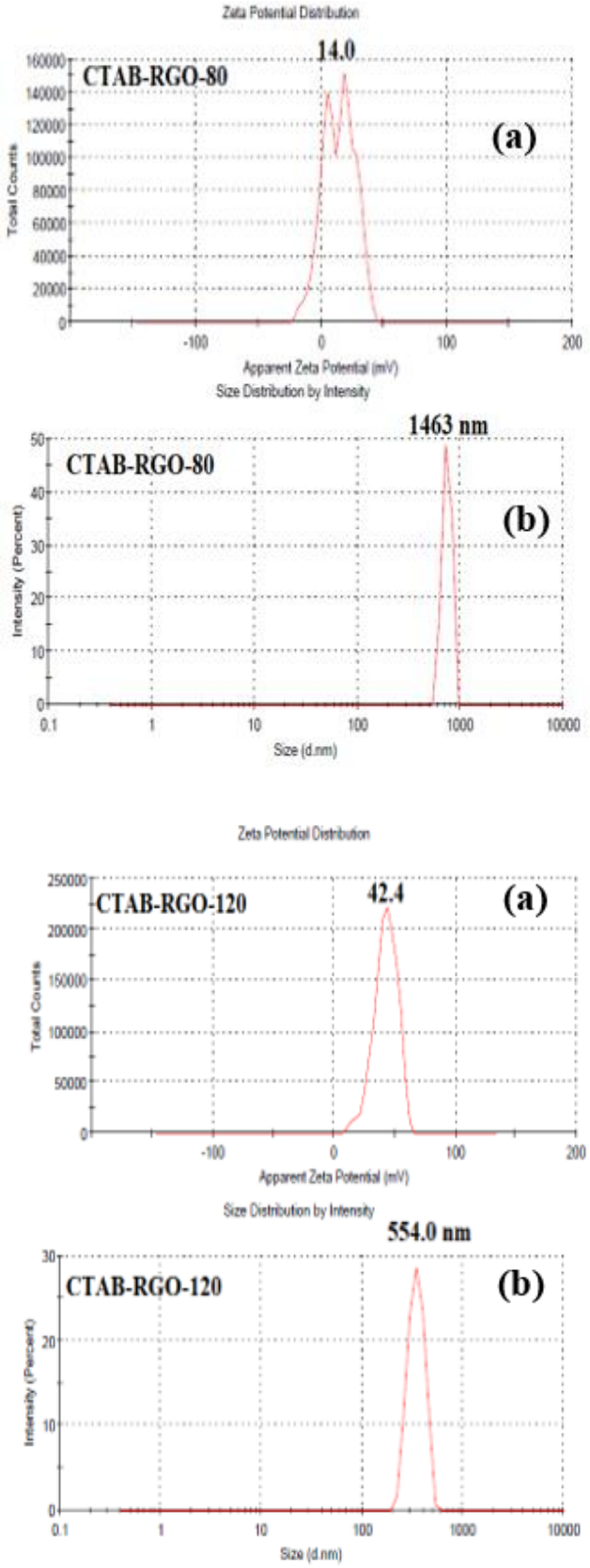

Figure 2 The zeta potential values (a) and average particle sizes (b) of the RGO and CTAB-RGO composites

3.3. FESEM Analysis

Figure 3 displayed the FESEM images of three different magnification of the highest stability composite (CTAB-RGO-120) that were prepared in this study. It could be seen that the CTAB-RGO-120 exhibited smooth structures and the individual graphene layers showing the effect of concentration of CTAB (Figure 3(a)). These layers were seen more obvious in enlarging the FESEM images (Figure 3. (b) and (c)). These images are compatible with the literature. For example; Wu et al. [25] reported that the graphene layers were become thinner and more obvious by the CTAB and this situation was increased the adsorption surface area. Nazari et al. [24] reported that the aggregation of graphene flakes was seen before adding CTAB but the image of the sample with CTAB showed that graphene flakes were stacked flat on top of each other.

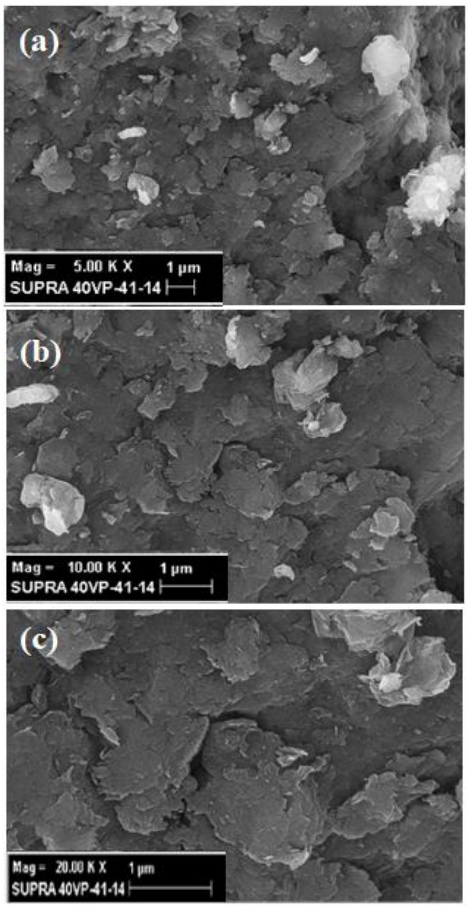

Figure 3 FESEM images of three different magnification of the highest stability composite (CTAB-RGO-120)

3.4. Decolorization Experiments

Decolorization of MB dye by RGO and CTAB-RGO composites such as were examined in this study. As seen in Figure 4, the composites performed increasing decolorization activity with the increasing CTAB concentration. Previously, most of the studies reported that surfactants could enhance the decolorization capacity of some adsorbents such as fungal biosorbent [26], active carbon [27] and gold graphene composite [28]. A similar pattern was observed in this study and the maximum decolorization rate was occurred by using the CTAB-RGO-120 composite. The electrostatic interaction between the positively charged headgroup of CTAB and the negatively charged surface of RGO was the highest at CTAB-RGO-120 composite. At the same composite, the excellent intercalation of CTAB succeeded in reducing the Van der Waals forces between the graphene layers. Effective dispersion forces between the charged particles due to good stable dispersion of composite prevented graphene aggregates. As a result, the dominant mechanism in CTAB-RGO-40 and CTAB-RGO-80 composites were Van der Walls forces, but the effective mechanism in CTAB-RGO-120 composite was electrostatic interactions.

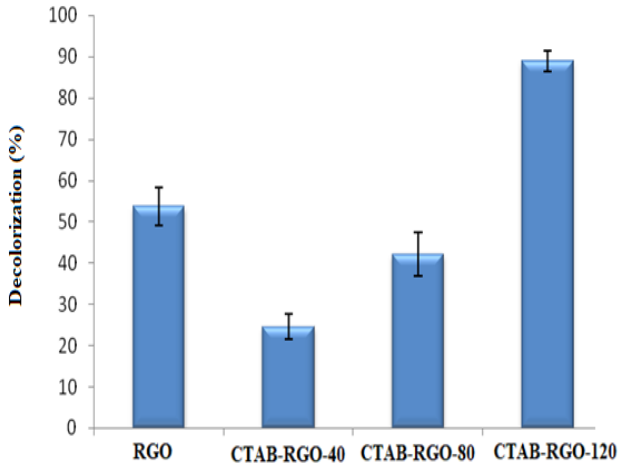

Figure 4 Decolorization of MB dye by RGO and CTAB-RGO composites

The effect of pH on decolorization was also tested and the results were given in Figure 5. The initial pH of the solution affected the decolorization rate by RGO and the decolorization rates were 4,98% and 53,76% at pH 5 and 7, respectively. It was reported that the carboxyl groups found on the surface of RGO were protonated at low pH values [29]. The dye used in this study MB was also a cationic dye with a positively charged. So, it was expected that the affinity of dye molecules to the adsorbent surface was reduced at acidic conditions such as pH 5. The maximum decolorization rate was reached at pH 7 for CTAB-RGO adsorbents in this study (Figure 5). Maximum dye uptake by CTAB-RGO-120 was calculated as 4,33 mg/g. MB was not favorable under acidic conditions as the CTAB-RGO surface was highly protonated. As pH increased above 5, the deprotonation of the CTAB-RGO surface resulted in electrostatic forces between CTAB-RGO surface and cationic dyes, meaning an increase of decolorization rate. CTAB-RGO-120 exhibited a much higher decolorization rate rather than RGO and other composites. This high decolorization rate was due to л-л interactions between the aromatic rings of MB dyes and delocalized л electrons of CTAB-RGO-120 [16]. Three forces such as electrostatic interaction, π-π stacking interaction and Van der Waals forces are very important at the adsorption of dyes onto graphene-based materials [30, 31]. The highest decolorization rate of CTAB-RGO-120 composite at neutral pH may have resulted from both the electrostatic interaction and π-π interaction. The driving forces were Van der Walls forces and π-π interaction for CTAB-RGO-40 and CTAB-RGO-80 composites. The Schematic representation for the interactions between of RGO-CTAB and RGO-MB were shown in Figure 6.

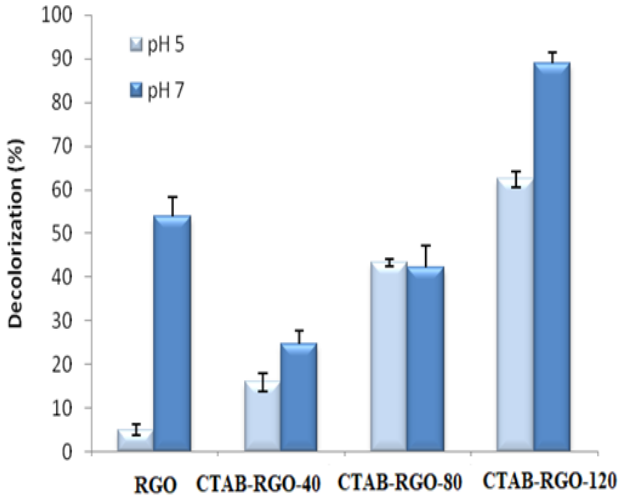

Figure 5 The effect of pH on decolorization

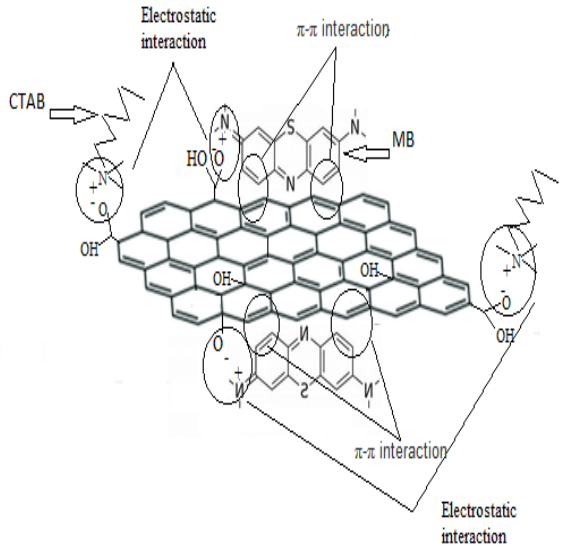

Figure 6 Schematic representation for the interactions between of RGO-CTAB and RGO-MB

4. CONCLUSION

In this study, the effect of CTAB concentration ability to produce optimal dispersion of graphene and on the decolorization of methylene blue (MB) dye was also examined. We determined that the optimal concentration of CTAB was 120 ppm. According to ZP analysis results were found that CTAB-RGO-120 composite was both the most stable composite and average particle size was the lowest. The individual graphene layers of the composite were seen thin and obvious at SEM images and it exhibited maximum decolorization rate. Unstable aggregations of graphene in the aqueous solutions of CTAB-RGO-40 and CTAB-RGO-80 composites had lower repulsive forces and they did not overcome the attractive van der Waals forces. In CTAB-RGO-120 composite, a good stable dispersion was created; compared to the other composites and an effective dispersion forces prevented to forming graphene aggregates. CTAB-RGO-120 exhibited the highest decolorization rate at pH 7 due to л-л interactions between the aromatic rings of MB dyes and delocalized л electrons of it.

Acknowledgements

The authors acknowledge the Biotechnology Application and Research Center of Bilecik S. E. University for providing the laboratory facility.

Funding

The authors have not received financial support for the research, authorship and publication of this study.

The Declaration of Conflict of Interest/ Common Interest

The authors declare that they have no conflict of interest.

The Declaration of Ethics Committee Approval

This study does not require ethics committee approval or any special permission.

Authors' Contribution

The authors contributed equally to the study.

The Declaration of Research and Publication Ethics

The authors of this study followed the scientific, ethical and quotation rules of Sakarya University

Journal of Science in all processes of the paper and that they did not make any falsification on the collected data. The authors declare that Sakarya University Journal of Science and its editorial board have no responsibility for all ethical violations. All responsibility belongs to the responsible author and this study has not been evaluated in any academic publication environment other than Sakarya University Journal of Science.

REFERENCES

[1] Ü. D. Gül, "A green approach for the treatment of dye and surfactant contaminated industrial wastewater," Brazilian Journal of Biology, Ahead of Print, pp. 1-6, 2019.

[2] H. Liu, S. K. Obendorf, M. J. Leonard, T. J. Young and M. J. Incorvıa, "Adsorption of aroma chemicals on cotton fabric from aqueous systems," Journal of Surfactants and Detergents, vol.8, 4, pp. 311-317, 2005.

[3] S. Alehyen, F. Bensejjay, M. El Achourı, L. Pérez and M. R. Infante, "Study of the interaction between methyl orange and mono and bis-quaternary ammonium surfactants," Journal of Surfactants and Detergents, vol. 13, no. 2, pp. 225-231, 2010.

[4] Ü. D. Gül and G. Dönmez, "Influence of surfactants on dye removal and growth of Aspergillus versicolor: an effective way to decolorize textile dye," Clean Soil Air Water, vol.42, no. 7, pp. 917-922, 2014.

[5] I. Mnif, R. Fendri and D. Ghribi, "Biosorption of Congo Red from aqueous solution by Bacillus weihenstephanensis RI12: effect of SPB1 biosurfactant addition on biodecolorization potency," Water Science and Technology, vol.72, no. 6, pp. 865-874, 2015.

[6] M. E. Ramírez, Y. H. Vélez, L. Rendón and E. Alzate, "Potential of microalgae in the bioremediation of water with chloride content," Brazilian Journal of Biology = Revista Brasileira de Biologia, vol. 78, no. 3, pp. 472-476, 2018.

[7] H. Ouni, A. Hafiane and M. Dhahbi, "The effect of surfactant on dye removal by polyelectrolyte enhanced ultrafiltration," Desalination and Water Treatment, vol.56, no. 6, pp. 1526-1535, 2015.

[8] Ü. D. Gül, S. İlhan and C. Filik İşçen, "Optimization of Biosorption Conditions for Surfactant Induced Decolorization by Anaerobic Sludge Granules," Tenside Surfactants and Detergents, vol.56, pp. 188-196, 2019.

[9] M. Poorsargola, M. Alimohammadiana, B. Sohrabia and M. Dehestani, "Dispersion of graphene using surfactant mixtures: Experimental and molecular dynamics simulation studies," Applied Surface Science, no. 464, pp. 440–450, 2019.

[10] W. Zhang, C. Zhou, W. Zhou, A. Lei, Q. Zhang, Q. Wan and B. Zou, "Fast and Considerable Adsorption of Methylene Blue Dye onto Graphene Oxide," Bull. Environ. Contam. Toxicol., vol. 87, no. 86, 2011.

[11] P. Sharma, N. Hussain, D. J. Borah and M. R. Das, "Kinetics and Adsorption Behavior of the Methyl Blue at the Graphene Oxide/Reduced Graphene Oxide Nanosheet-Water Interface: A Comparative Study," J. Chem. Eng. Data., vol. 58, pp. 3477–3488, 2013.

[12] P. Sharma and R. Manash, "Das Removal of a Cationic Dye from Aqueous Solution Using Graphene Oxide Nanosheets: Investigation of Adsorption Parameters," J. Chem. Eng. Data., vol. 58, pp. 151−158, 2013.

[13] R. K. S. Rathour, J. Bhattacharya and A. Mukherjee, "β-Cyclodextrin Conjugated Graphene Oxide: A Regenerative Adsorbent for Cadmium and Methylene

Blue,"J. Mol. Liq., no. 282, pp. 606–616, 2019.

[14] N. H. Othman, N. H. Alias, M. Z. Shahruddinn, N. F. Abu Bakar, N. R. N. Him and W. J. Lau, "Adsorption Kinetics of Methylene Blue Dyes onto Magnetic Graphene Oxide," J. Environ. Chem. Eng., vol. 6, pp. 2803–2811, 2018.

[15] N. M. Mahmoodi, M. Maroofi Seyyed, M. Mazarji and G. Nabi-Bidhendi, "Preparation of modified reduced graphene oxide nanosheet with cationic surfactant and its dye adsorption ability from colored wastewater," J. Sufactants Deterg., vol. 20, pp. 1085–1093, 2017.

[16] M. Yusuf, M. A. Khan, M. Otero, E. C. Abdullah, M. Hosomi, A. Terada and S. Riya, "Synthesis of CTAB intercalated graphene and its application for the adsorption of AR265 and AO7 dyes from water," J. Colloid Interface Sci., no. 493 pp. 51–61, 2017.

[17] K. N. Amba Sankar, C. Sathish Kumar and K. Mohanta, "Highly Stable Aqueous Dispersion of CTAB- Intercalated Reduced Graphene Oxide," Materials Today: Proceedings, vol. 18, no. 3, pp. 759–764, 2019.

[18] F. Mindivan, "Effect of various initial concentrations of CTAB on the noncovalent modified graphene oxide (MGNO) structure and thermal stability," Materials Testing, vol. 59, no. 9, 729-734, 2017.

[19] F. Mindivan and M. Göktaş, "Effects of various vitamin C amounts on the green synthesis of reduced graphene oxide," Materials Testing, vol.61, no.10, 2019.

[20] F. Mindivan and M. Göktas, "Green synthesis of Reduced Graphene Oxide (RGNO) /Polyvinylchloride (PVC) composites and their structural Characterization," Materials Research Proceedings, (Powder Metallurgy and Advanced Materials– RoPM&AM 2017), vol. 8, pp. 143-151, 2018.

[21] Y. Hu, M. Su, X. Xie, C. Sun and J. Kou, "Few-layer graphene oxide with high yield via efficient surfactant-assisted exfoliation of mildly-oxidized graphite," Applied Surface Science, vol. 494, pp. 1100–1108, 2019.

[22] B. White, S. Banerjee, S. O'Brien, J. N. Turro and I. P. Herman, "Zeta-Potential Measurements of Surfactant-Wrapped Individual Single-Walled Carbon Nanotubes," J. Phys. Chem C., no. 111, pp. 13684-13690, 2007.

[23] W. S. Sarsam, A. Amiri, S. N. Kazi and A. Badarudin, "Stability and thermophysical properties of non-covalently functionalized graphene nanoplatelets nanofluids," Energy Conversion and Management, no. 116, pp. 101–111, 2016.

[24] B. Nazaria, Z. Ranjbara, R. R. Hashjina, A.R. Moghaddama, G. Momenc and B. Ranjbard, "Dispersing graphene in aqueous media: Investigating the effect of different Surfactants," Colloids and Surfaces A, vol.58, no.123870, 2019.

[25] Y. Wu, H. Luo, H. Wang, C. Wang, J. Zhang and Z. Zhang, "Adsorption of hexavalent chromium from aqueous solutions by graphene modified with cetyltrimethylammonium bromide," Journal of Colloid and Interface Science, no. 394, pp. 183–191, 2013.

[26] Ü. D. Gül and G. Dönmez, "Effects of Dodecyl Trimethyl Ammonium Bromide Surfactant on Decolorization of Remazol Blue by a Living Aspergillus versicolor Strain," J Surfact Deterg, vol.15, pp. 797-803, 2012.

[27] G. M. Nabil, N. M. El-Mallah and M. E. Mahmoud, "Enhanced decolorization of reactive black 5 dye by active carbon sorbent-immobilized-cationic surfactant (AC-CS)," Journal of Industrial and

Engineering Chemistry, vol.20, no.3, pp. 994-1002, 2014.

[28] R. S. S. Siddhardha, V. L. Kumar, A. Kaniyoor, V. S. Muthukumar, S. Ramaprabhu, R. Podila, A. M. Rao and S. S. Ramamurthy, "Synthesis and characterization of gold graphene composite with dyes as model substrates for decolorization: A surfactant free laser ablation approach," Spectrochimica Acta Part A: Molecular and Biomolecular Spectroscopy, no. 133, pp. 365-371, 2014.

[29] C.-J. Shih, S. Lin, R. Sharma, M. S. Strano and D. Blankschtein, "Understanding the pH-Dependent Behavior of Graphene Oxide Aqueous Solutions: A Comparative Experimental and Molecular Dynamics Simulation Study," Langmuir, vol. 28, no. 1, pp. 235-241, 2012.

[30] J. Su, S. He, Z. Zhao, X. Liu and H. Li "Efficient preparation of cetyltrimethylammonium bromide-graphene oxide composite and its adsorption of Congo red from aqueous solutions," Colloids and Surfaces A, no. 554, pp. 227–236, 2018.

[31] A. Y. W. Sham and S. M. Notley, "Adsorption of organic dyes from aqueous solutions using surfactant exfoliated graphene," Journal of Environmental Chemical Engineering, no. 6, pp. 495–504, 2018.

SAKARYA ÜNİVERSİTESİ
FEN BİLİMLERİ ENSTİTÜSÜ DERGİSİ

Sakarya University Journal of Science
SAUJS

e-ISSN 2147-835X | Period Bimonthly | Founded: 1997 | Publisher Sakarya University |
http://www.saujs.sakarya.edu.tr/en/

Title: Species of Cixiidae and Issidae (Hemiptera: Auchenorrhyncha: Fulgoromorpha) Distributed in Sinop and Kastamonu (North Turkey)

Authors: Rukiye TANYERİ, Ünal ZEYBEKOĞLU

Recieved: 2021-01-27 00:00:00

Accepted: 2021-03-22 13:44:09

Article Type: Research Article

Volume: 25
Issue: 2
Month: April
Year: 2021
Pages: 594-600

How to cite
Rukiye TANYERİ, Ünal ZEYBEKOĞLU; (2021), Species of Cixiidae and Issidae (Hemiptera: Auchenorrhyncha: Fulgoromorpha) Distributed in Sinop and Kastamonu (North Turkey). Sakarya University Journal of Science, 25(2), 594-600, DOI: https://doi.org/10.16984/saufenbilder.869438
Access link
http://www.saujs.sakarya.edu.tr/en/pub/issue/60672/869438

Sakarya University Journal of Science 25(2), 594-600, 2021

Species of Cixiidae and Issidae (Hemiptera: Auchenorrhyncha: Fulgoromorpha) Distributed in Sinop and Kastamonu (North Turkey)

Rukiye TANYERİ*[21], Ünal ZEYBEKOĞLU[2]

Abstract

In this study, Cixiidae and Issidae (Hemiptera: Auchenorrhyncha) species collected from various localities in Sinop and Kastamonu between the years 2016-2018 were evaluated. 12 species belonging to 7 genera from Issidae and 4 species belonging to 4 genera from Cixiidae were determined. In addition, distributional data of the species in Turkey and in the world, and collection localities were given. Among the identified species, *Kervillea placophora*, *Mycterodus confusus* (Issidae) and *Reptalus panzeri* (Cixiidae) were recorded for the first time from the Black Sea Region of Turkey.

Keywords: Issidae, Cixiidae, Black Sea Region, Turkey

1. INTRODUCTION

According to Demir [1], Turkey Fulgoromorpha fauna is represented by 219 species belonging to 12 families. Families from Fulgoromorpha group located in Turkey are: Achilidae, Caliscelidae, Cixiidae, Delphacidae, Derbidae, Dictyopharidae, Flatidae, Issidae, Meenoplidae, Ricaniidae, Tettigometridae ve Tropiduchidae [2, 3].

Cixiidae Spinola, 1839 is represented worldwide with 2416 species belonging to 221 genera [4]. 22 genera and 212 species in the Palearctic Region [5, 6]. According to Kalkandelen [7], Cixiidae fauna of Turkey consist of 48 species belonging to 12 genus. In the following years, this number increased to 51 with new records [8, 9, 10]

Issidae Spinola, 1839 is a large family of the Fulgoromorpha group, with more than 1000 species identified throughout the world [4]. Issidae family is examined under 3 tribus in modern classification: Issini, Haemisphaeriini and Parahiraciini. Issini forms the largest group with 755 species and subspecies belonging to 129 genera. It is a rich group that includes economically harmful species that distributed in all zoogeographical areas [11] Issidae has 445 species in the Palearctic Region and 102 species in Turkey. With this number, Turkey is the most rich country in the Palearctic Region [12].

* Corresponding author: rtanyeri@sinop.edu.tr
[1] Sinop University,Faculty of Art of Science,ORCID: https://orcid.org/0000-0001-9994-8783
[2] Ondokuz Mayıs University, Faculty of Art of Science, unalz@omu.edu.tr, ORCID: https://orcid.org/0000-0003-1646-5999

This study is carried out to determine the species of Cixiidae and Issidae which are known as potential vectors of phytopathogens in Sinop and Kastamonu. And also in order to contribute to Turkey's insect fauna and taxonomic status of detected species from the region.

2. MATERIAL AND METHODS

The specimens were collected by sweeping net and a hand aspirator over the plants during the daytime between May 2016 and October 2018 from different localities in Sinop and Kastamonu provinces. The collected samples were taken in insect killing jars, labeled and brought to the laboratory and placed in insect storage packages. The material to be prepared was taken from the insect storage packages and put in 5% acetic acid and softened a few hours. The genital capsule of males were separated from the body with the help of a dissecting needle. The remaining body part of the insects was attached to the rectangular insect preparation label with a needle attached to one end, from the ventral with the help of cellulosic adhesive. In the genital capsule, genital structures which have taxonomically reliable characteristics, aedeagus, stylus, connective, pygofer, genital plate, anal tube in males and pregenital sternite VII in females, were separated. From the materials prepared, shape, size, structure, color, patterning and features of the genital structures were examined under the microscope and they were identified by being compared with diagnosed museum materials and current literature.

Examples are stored at Sinop University, Faculty of Arts and Sciences, Department of Biology, Invertebrata Laboratory.

3. RESULTS

3.1. Familya: Cixiidae Spinola, 1839

Genus: *Hyalesthes* Signoret, 1865

***Hyalesthes obsoletus* Signoret, 1865**

Material examined: Sinop: 13.06.2017, 41° 45' 40.7" N 34° 58' 32.4" E (7 ♀♀), 06.08.2017, 41° 49' 54.0" N 35° 05' 21.1" E (6 ♂♂, 1 ♀), 12.08.2017, 41° 25' 13.1" N 34° 58' 44.2 E (2 ♂♂, 5 ♀♀), 17.08.2017, 41° 46' 17.8" N 35° 12' 20.4" E (1 ♀), 42° 01' 04.8" N 35° 05' 30.0" E (1 ♀); Kastamonu: 19.07.2018, 41° 46' 38.3" N 33° 43' 05.8" E (2 ♂♂, 2 ♀♀)

Distribution in Turkey: Adana, Adapazarı, Adıyaman, Afyon, Ağrı, Ankara, Antalya, Aydın, Balıkesir, Bolu, Burdur, Bursa, Çanakkale, Çankırı, Çorum, Diyarbakır, Düzce, Edirne, Erzincan, Elazığ, Erzurum, Eskişehir, Gaziantep, Giresun, Hakkâri, Iğdır, Isparta, İstanbul, Kahramanmaraş, Kars, Konya, Malatya, Mardin, Manisa, Mardin, Mersin, Muğla, Nevşehir, Ordu, Rize, Sakarya, Sinop, Sivas, Şanlıurfa, Tokat, Trabzon, Van [1, 2, 3]

Zoogeographic distribution: Albania, Austria, Balearic Islands, Bosnia and Herzegovina, Bulgaria, Corsica, Crete Croatia, Cyprus, Czech Republic, Dodakenes Islands, East Palearctic, France, Germany, Greece, Hungary, Italy, Kiklades Islands, Macedonia, Malta, Near East, North Aegean Islands, North Africa, Portugal, Romania, Russia (Central Europe), Russia (Southern Europe), Sardinia, Sicily, Slovakia, Slovenia, Spain, Switzerland, Turkey, Ukraine, Yugoslavia [13]

Genus: *Reptalus* Emeljanov, 1971

***Reptalus (Reptalus) panzeri* (Löw, 1883)**

Material examined: Sinop: 17.08.2017, 41° 46' 02.5" N 35° 12' 11.0" E (1 ♂, 1 ♀)

Distribution in Turkey: Ankara, Çankırı [3]

Zoogeographic distribution: Algeria, Armenia, Austria, Azerbaijan, Belgium, Bulgaria, Czechoslovakia, England, France, Germany, Georgia, Italy, Kazakhstan, Poland, Romania, Spain, Tunisia, Turkey, Ukraine, Yugoslavia [13]

Genus: *Setapius* Dlabola, 1988

***Setapius barajus* (Dlabola, 1957)**

Material examined: Sinop: 17.08.2017, 41° 46' 02.5" N 35° 12' 11.0" E (1 ♂)

Distribution in Turkey: Adana, Ağrı, Ankara, Bursa, Denizli, Diyarbakır, Elazığ, Erzincan, Erzurum, Gümüşhane, İzmir, Iğdır, Kars, Malatya, Mardin, Muş, Nevşehir, Samsun, Sinop, Siirt, Sivas, Uşak [14].

Zoogeographic distribution: Afghanistan, Armenia, Iran, Russia, Turkey [3, 15]

Genus: *Tachycixius* Wagner, 1939

***Tachycixius (Eupalame) desertorum* (Fieber, 1876)**

Material examined: Sinop: 12.08.2017, 41° 36' 03.5" N 34° 51' 28.3" E (1 ♀), 17.08.2017 42° 01' 04.8" N 35° 05' 30.0" E (2 ♂♂)

Distribution in Turkey: Ankara, Adıyaman, Antalya, Artvin, Diyarbakır, Edirne, Eskişehir, Gaziantep, Hakkari, İstanbul, İzmir, Kastamonu, Konya, Mersin, Manisa, Mardin, Muğla, Nevşehir, Sakarya, Sinop, Uşak [3]

Zoogeographic distribution: Albania, Bulgaria, Cyprus, Czech Republic, Greece, Hungary, Italy, Near East, Romania, Russia (Southern Europe), Sicily, Slovakia, Turkey, Ukraine, Yugoslavia [13]

3.2. Familya: Issidae Spinola, 1839

Genus: *Agalmatium* Emeljenov, 1971

***Agalmatium bilobum* (Fieber, 1877)**

Material examined: Sinop: 12.08.2016 41° 45' 40.7" N 34° 58' 32.6" E (4 ♂, 1 ♀)

Distribution in Turkey: Adapazarı, Adıyaman, Afyon, Ankara, Antalya, Alanya, Aydın, Balıkesir, Bilecik, Burdur, Bursa, Çanakkale, Çorum, Denizli, Eskişehir, Gaziantep, Gümüşhane, İzmir, Kütahya, Konya, Malatya, Manisa, Muğla, Tekirdağ, Tokat, Uşak [1, 3]

Zoogeographic distribution: Bulgaria, France, Germany, Greece, Italy, Moldova, Near East, North Africa, Portugal, Russia (Southern Europe), Sardinia, Spain, Turkey, Yugoslavia [13]

***Agalmatium flavescens* (Olivier, 1791)**

Material examined: Sinop: 12.08.2016, 41° 45' 40.7" N 34° 58' 32.6" E (1 ♂, 1 ♀); 30.07.2017, 41° 38' 30.8" N 34° 36' 42.7" E (18 ♂♂, 12 ♀♀); 06.08.2017, 41° 49' 54.0" N 35° 05' 21.1" E (25 ♂♂, 24 ♀♀); Kastamonu: 19.07.2017, 41° 37' 07.0" N 34° 37' 32.0" E (34 ♂♂, 37 ♀♀).

Distribution in Turkey: Ankara, Bursa, Çorum, Edirne, İstanbul, Kastamonu, Konya, Tekirdağ, Van, Zonguldak [1, 3]

Zoogeographic distribution: Africa, Albania, Austria, Bulgaria, Canary Islands, Cyprus Czech Republic, France, Greece, Hungary, Italy, Moldova, Near East, Northern Poland, Portugal, Romania, Sardinia, Sicily, Spain, Switzerland, Turkey,Yugoslavia [13]

Genus: *Kervillea* de Bergevin, 1918

***Kervillea (Kervillea) placophora* Horváth, 1905**

Material examined: Kastamonu: 12.08.2016, 41° 40' 27.6" N 33° 55' 48" E (1 ♂, 1 ♀)

Distribution in Turkey: Eskişehir- Ilgın arası, Yozgat [16]

Zoogeographic distribution: Israel, Russia, Turkey [3]

Genus: *Latilica* Emelyanov, 1971

***Latilica antalyica* (Dlabola, 1986)**

Material examined: Sinop: 17.08.2017, 41° 46' 02.5" N 35° 12' 11.0" E (17 ♂♂, 21 ♀♀)

Distribution in Turkey: Amasya, Antalya, Hatay, Muğla, Samsun [9, 17]

Zoogeographic distribution: Greece, Turkey [12]

Genus: *Mycterodus* Spinola, 1839

***Mycterodus (Mycterodus) confusus* Stal, 1861**

Material examined: Sinop: 27.05.2017, 41° 44' 52.0" N 34° 57' 40.9" E (16 ♂♂, 20♀♀), 41° 47'

38.7" N 35° 09' 46.8" E (14 ♂♂, 18 ♀♀); 01.06.2017, 41° 52' 31.3" N 34°51'0.95"E (10 ♂♂, 10 ♀♀); 18.06.2017, 42° 00' 505" N 34° 56' 906" E (12 ♂♂, 6 ♀♀); 07.06.2017, 42° 03' 22.8" N 34°59'32.2" E (2 ♂♂, 2 ♀♀); Kastamonu: 20.05.2017, 41° 52' 48.9" N 33° 42' 38.0" E (24 ♂♂, 14 ♀♀); 16.06.2017, 41° 39' 33.3" N 33° 08' 01.9" E (12 ♂♂, 5 ♀♀); 15.06.2017, 41° 52' 49.0" N 33° 42' 38.1" E (8 ♂♂, 10 ♀♀)

Distribution in Turkey: İstanbul, Karaman [18]

Zoogeographic distribution: Near East, Turkey, Ukraine, Yugoslavia [13]

***Mycterodus (Mycterodus) rostratulus* Emelyanov, 1964**

Material examined: Sinop: 01.06.2016, 41° 84' 42.6" N 35° 09' 06.68" E (1 ♂, 1 ♀); 08.06.2017, 42° 01' 21.6" N 35° 12' 06.8" E (26 ♂♂, 29 ♀♀); Kastamonu: 20.05.2017, 41° 58' 10.7" N 34° 05' 22.7" E (22 ♂♂, 12 ♀♀); 16.06.2017, 41° 38' 29.7" N 33° 07' 05.1" E (11 ♂♂, 6 ♀♀); 15.06.2017, 41° 46' 38.3" N 33° 43' 05.8" E (9 ♂♂, 10 ♀♀)

Distribution in Turkey: Ankara, Samsun, Ordu [9, 17]

Zoogeographic distribution: Caucasia, Russia (Southern Europe) [13, 17]

Genus: *Scorlupella* Emelyanov, 1971

***Scorlupella assimilis* (Horvath, 1905)**

Material examined: Kastamonu: 19.05.2017, 41° 38' 35.8" N 33° 07' 13.9" E (10 ♂♂)

Distribution in Turkey: Manisa, Konya-Kayseri arası, Tokat [3, 19]

Zoogeographic distribution: Turkey [3]

***Scorlupella discolor* Germar, 1821**

Material examined: Sinop: 13.06.2017, 41° 36' 10.0" N 34° 51' 12.5" E (6 ♂♂, 2 ♀♀); Kastamonu: 19.05.2017, 41° 36' 45.4" N 33° 07' 02.9" E (25 ♂♂, 20 ♀♀), 41° 38' 35.8" N 33° 07' 13.9" E (6 ♂♂, 2 ♀♀); 20.05.2017, 41° 52' 48.9" N 33° 42' 38.0" E (24 ♂♂, 20 ♀♀), 14.06.2017, 41° 14' 03.9" N 34° 00' 45.6" E (12 ♂♂, 20 ♀♀); 16.06.2017, 41° 42' 09.1" N 33° 26' 41.9" E (6 ♂♂, 2 ♀♀)

Distribution in Turkey: Ankara, Amasya, Edirne, Erzincan, Samsun, Yozgat [14, 17, 19, 20]

Zoogeographic distribution: Bulgaria, İtalian, Near East, Romania, Turkey, Ukraine [13]

***Scorlupella montana* (Becker, 1865)**

Material examined: Sinop: 27.05.2017, 41° 32' 45.1" N 34° 47' 0.01" E (6 ♂♂)

Distribution in Turkey: Ankara, Amasya, Erzincan, Kars, Konya, Samsun, Tokat [1, 3, 19]

Zoogeographic distribution: Azerbaijan, Armenia, Georgia (?), Greece Iran, Kazakhistan, Kyrgyzstan, Moldavia, Romania, Russia, Tajikistan, Turkmenistan, Ukraine, Uzbekistan [12]

Genus: *Tshurtshurnella* Kusnezov, 1927

***Tshurtshurnella extrema* (Dlabola, 1980)**

Material examined: Sinop: 12.08.2017, 41° 36' 03.5" N 34° 51' 28.3" E (1 ♂, 1 ♀)

Distribution in Turkey: Ankara, Çorum [17, 21]

Zoogeographic distribution: Turkey

***Tshurtshurnella yozgatica* Kartal, 1985**

Material examined: Kastamonu: 19.07.2017, 41° 37' 07.0" N 34° 37' 32.0" E (4 ♂♂, 5 ♀♀)

Distribution in Turkey: Amasya**,** Çorum, Samsun, Yozgat [17, 19]

Zoogeographic distribution: Turkey

Genus: *Issus* Fabricius, 1803

***Issus muscaeriformes* (Von Schrank, 1781)**

Material examined: Sinop: 12.08.2016, 41° 45' 40.7" N 34° 58' 32.6" E (1♂)

Distribution in Turkey: Samsun, Giresun [17]

Zoogeographic distribution: Austria, Bulgaria, Czech Republic, Denmark, France, Germany, Greece, Hungary, Italy, Netherlands, Norway, Poland, Romania, Slovakia, Sweden, Switzerland, Yugoslavia [13]

4. DISCUSSION

Turkey is considered as one of the main centres for diversification of Issidae taxa, with 102 species and 4 subspecies recorded so far [12].

In the study, 12 species of Issidae were determined: *Agalmatium flavescens*, *A. bilobum*, *Issus muscaeriformis*, *Kervillea placophora*, *Latilica antalyica*, *Mycterodus confusus*, *M. rostratulus*, *Scorlupella assimilis*, *S. discolor*, *S. montana*, *Tshurtshurnella extrema* and *T. yozgatica* from research area. It has been found that they are generally found in thorny plants and vegetation in bush form. Among the identified species, *K. placophora* and *M. confusus* were recorded for the first time from the Black Sea Region of Turkey.

Agalmatium flavescens has a wide distribution area and it is one of the best known Issidae species that has no taxonomic problems. Highest population density was determined in the research area. Lodos and Kalkandelen [22] reported that *A. flavescens* caused damage by feeding and laying eggs on young branches and shoots of *Olea europea* L. and *Ficus cerica* L., and the damage was not economically significant.

The type locality of *K. placophora* is between Eskişehir and Ilgın. And also recorded from Yozgat [16]. The specimens examined in this study were collected from Kastamonu.

L. antalyica is a species of Mediterranean origin. It was collected from a single locality from Sinop.

3 species belonging to the genus *Scorlupella* were identified in the study area. It has been determined that there is variation the structure of light colored membranized structure with small teeth on the tip of the aedeagus. In addition, a high rate of variation in wing veins was detected in *S. discolor* specimens. In some individuals of the same taxon, the wing veins are light and distinct, while in others the veins are less pronounced and pale.

Scorlupella assimilis, *Tshurtshurnella extrema* and *Tshurtshurnella yozgatica* are endemic species known from Turkey. *Mycterodus rostratulus*, *Kervillea placophora*, *Latilica antalyica* and *Scorlupella discolor* species are species with narrow zoogeographic range. The region is important for endemism and more detailed studies are needed.

In the study, 4 species of Cixiidae: *Hyalesthes obsoletus*, *Reptalus panzeri*, *Setapius barajus* and *Tachycixius desertorum* were determined. It was observed that the number of individuals evaluated in this study belonging to Cixiidae was quite low. This is thought to be due to the specialization of host plants. It was concluded that more comprehensive studies focusing only on the species of this family should be conducted in order to determine the distribution, population density and host plants of the Cixiidae species distributed in the region. It is known that *R. panzeri* causes infection in the maize [23]. At the end of the study, specimens of *R. panzeri* which is distributed in Ankara and Çankırı were collected from Sinop. This record is the first from the Black Sea Region of Turkey for this taxon.

Acknowledgments

This study is prepared from part of first author' phd thesis approved by the Graduate School of Sciences of Ondokuz Mayıs University on August 2019.

Funding

"This study is supported by Ondokuz Mayıs University Scientific Research Projects Coordination Unit. Project Number: PYO.FEN.1904.16.013

The Declaration of Conflict of Interest/ Common Interest

"No conflict of interest or common interest has been declared by the authors".

Authors' Contribution

"The authors contributed equally to the study"

The Declaration of Research and Publication Ethics

"The authors of the paper declare that they comply with the scientific, ethical and quotation rules of SAUJS in all processes of the paper and that they do not make any falsification on the data collected. In addition, they declare that Sakarya University Journal of Science and its editorial board have no responsibility for any ethical violations that may be encountered, and that this study has not been evaluated in any academic publication environment other than Sakarya University Journal of Science."

REFERENCES

[1] E. Demir, "Fulgoromorpha (Hemiptera) records from Southwestern Turkey," Entomologia Hellenica, vol. 26, no. 2, pp. 17-28, 2017.

[2] E. Demir, "Antalya ilinin Auchenorrhyncha (Homoptera) fauna ve taksonomisi üzerine araştırmalar," Doktora Tezi, Gazi Üniversitesi Fen Bilimleri Enstitüsü Biyoloji Anabilim Dalı, 235, Ankara, 2005.

[3] F. Önder, S. Tezcan ve Ü. Zeybekoğlu, "*Türkiye Cicadomorpha*, Fulgoromorpha ve Sternorrhyncha Kataloğu," Meta Basım, 157, İzmir, 2011.

[4] Bourgoin T. 2021. FLOW (Fulgoromorpha Lists on The Web): a world knowledge base dedicated to Fulgoromorpha. Version 8, updated [19.02.2021]. https://hemiptera-databases.org/flow/

[5] J. Nast, "Palaearctic Auchenorrhyncha (Homoptera) an Annotated Check List," Polish Academy of Sciences, Institute of Zoology, 550, Warszawa, 1972.

[6] J. Nast, "Palaearctic Auchenorrhyncha (Homoptera) Part 3. New taxa and replacement names introduced till 1980," Annales Zoologici, vol. 36, no. 1, pp. 289-362, 1982.

[7] A. Kalkandelen, "Türkiye Cixiidae (Homoptera) türleri üzerinde taksonomik çalışmalar, I- Familyanın morfolojik özellikleri ve teşhis anahtarı," Bitki Koruma Bülteni, vol. 27, pp. 119-146, 1987.

[8] E. Demir, "Contributions to the knowledge of Turkish Auchenorrhyncha (Homoptera) with a new record, *Pentastiridius nanus* (Ivanoff, 1885)," Munis Entomology and Zoology, vol. 1, pp. 97-122, 2006.

[9] E. Demir, "Contributions to the knowledge of Turkish Auchenorrhyncha (Homoptera, Fulgoromorpha and Cicadomorpha, excl. Cicadellidae) with a new record, *Setapius klapperichianus* Dlabola, 1988," Munis Entomology and Zoology, vol. 2, no:1, pp. 39-58, 2007.

[10] E. Demirel and A. Hasbenli "Contributions to the Bolkar Mountains Cixiidae fauna with a new record and an identification key for Turkey's *Tachycixius* (Hemiptera: Auchenorrhyncha)," Pakistan Journal of Zoology, vol. 47, pp. 1341-1346, 2015.

[11] V.M. Gnezdilov, "Modern classification and distribution of the family Issidae Spinola (Homoptera: Auchenorrhyncha: Fulgoroidea)." Entomological Review, vol. 94, pp. 687-697, 2014.

[12] V.M. Gnezdilov, W.E. Holzinger and M.R. Wilson, "The Western Palaearctic Issidae (Hemiptera, Fulgoroidea): An Illustrated Checklist and Key to Genera and Subgenera," Proceedings of the Zoological Instıtute, RAS, 318, 1-124, 2014.

[13] https://www.fauna-eu.org

[14] E. Demir and A. Demirsoy, "Preliminary report on the Fulgoromorpha (Hemiptera) fauna of Kemaliye (Erzincan) with a new record for Turkey" Munis Entomology and Zoology, vol. 4, No: 1, pp. 280-286, 2009.

[15] E. Demir, "The Fulgoromorpha and Cicadomorpha of Turkey. Part I: Mediterranean region (Hemiptera)," Munis Entomology & Zoology, vol.3, No:1, pp.447-522, 2008.

[16] V. Kartal, and A. Miroğlu, "Systematic position of *Kervillea (Kervillea) ancyrana* Bergevin, 1918 (Hemiptera, Fulgoromorpha, Issidae) from Turkey, with a new synonym of the species," Turkish Journal of Zoology, vol. 35, No: 1, pp. 57-62, 2011.

[17] D. Karadeniz, "Orta Karadeniz Bölgesi Issidae (Homoptera) familyası üzerine faunistik bir araştırma," Yüksek Lisans Tezi, Ondokuz Mayıs Üniversitesi Fen Bilimleri Enstitüsü Biyoloji Anabilim Dalı, 31, Samsun, 2008.

[18] E. Demirel, "Bolkar Dağları'nın Auchenorrhynchaları," Doktora Tezi, Gazi Üniversitesi Fen Bilimleri Enstitüsü Biyoloji Anabilim Dalı, 566, Ankara, 2010.

[19] V. Kartal, "Türkiye Yukarı Kızılırmak Havzası'ndaki Issidae (Homoptera, Auchenorrhyncha) familyasi türlerinin taksonomik yönden incelenmesi," Doga Bilim Dergisi, vol. 9, no: 1, pp. 64-77, 1985a.

[20] A. Dursun and M. Fent, "Contributions to the Cicadomorpha and Fulgoromorpha (Hemiptera) fauna of Turkish Thrace Region," Trakya University Journal of Natural Sciences, vol. 17, no: 2, pp. 123-128, 2016.

[21] V. Kartal, "Türkiye'den az bilinen *Tshurtshurnella extrema* Dlabola, 1980 (Homoptera, Auchenorrhyncha, Issidae) türü," Doga Bilim Dergisi, vol. 10, no: 2, pp. 99-103, 1985.

[22] N. Lodos and A. Kalkandelen, "Preliminary list of Auchenorrhyncha with notes on distribution and importance of species in Turkey IV. Family Issidae Spinola," Türkiye Bitki Koruma Dergisi, vol. 5, no: 1, pp. 5-21, 1981.

[23] S. Bertin, L. Picciau, Z. Acs, A. Alma, and D. Bosco, "Molecular differentiation of four *Reptalus* species (Hemiptera: Cixiidae)," Entomological Research, vol. 100, pp. 551-558, 2010.

SAKARYA ÜNİVERSİTESİ
FEN BİLİMLERİ ENSTİTÜSÜ DERGİSİ

Sakarya University Journal of Science
SAUJS

e-ISSN 2147-835X | Period Bimonthly | Founded: 1997 | Publisher Sakarya University |
http://www.saujs.sakarya.edu.tr/en/

Title: Utilization of Cheese Whey for Production of Azurin by Pseudomonas aeruginosa

Authors: Yağmur ÜNVER

Recieved: 2021-01-12 00:00:00

Accepted: 2021-03-23 20:23:12

Article Type: Research Article

Volume: 25
Issue: 2
Month: April
Year: 2021
Pages: 601-609

How to cite
Yağmur ÜNVER; (2021), Utilization of Cheese Whey for Production of Azurin by Pseudomonas aeruginosa . Sakarya University Journal of Science, 25(2), 601-609,
DOI: https://doi.org/10.16984/saufenbilder.853961
Access link
http://www.saujs.sakarya.edu.tr/en/pub/issue/60672/853961

Sakarya University Journal of Science 25(2), 601-609, 2021

Utilization of Cheese Whey for Production of Azurin by *Pseudomonas aeruginosa*

Yağmur ÜNVER[*1]

Abstract

Azurin which has attracted much attention as potential anticancer agent in recent years is a bacterial secondary metabolite. This copper-containing redox protein secreted by *Pseudomonas aeruginosa* has capability of preferentially entering into many human cancer cells and inducing apoptosis. In this study, whey which is the considerable by-product of the casein or cheese manufacture was used as azurin production medium by *P. aeruginosa*. Also, effects of copper (II) sulphate ($CuSO_4$) and potassium nitrate (KNO_3) on the azurin production were determined. At the end of the studies, optimum azurin expression level was reached during the incubation of 18 hours. The best $CuSO_4$ concentration was 2.5 mg/L while the best KNO_3 concentration was 45 mg/L according to Western blot analysis. This process can be used to obtain high levels of azurin using *P. aeruginosa* in whey medium. Also, using whey for azurin production can reduce many processing industrial whey waste management problems.

Keywords: azurin, *Pseudomonas aeruginosa*, secondary metabolite, expression, whey

1. INTRODUCTION

Natural products which are also referred to as specialized metabolites or secondary metabolites are produced by microorganisms and plants. These are a group of complex bioactive compounds which have unusual chemical properties and low-molecular weight structurally diverse [1, 2]. Antibiotics, growth hormones, pigments, antitumor agents, organic acids, nutraceuticals and others, are known as microbial secondary metabolites and not essential for the growth of microorganism. But, they have useful effects for human and animal health. Up to now, microbial secondary metabolites with their great potential have been used for other applications apart from antiviral, antibacterial and antifungal infections [3, 4].

Natural products and their derivatives are of great importance as they make up more than 40% of the therapeutic drugs such as antitumour, antibiotics and cholesterol-lowering agents [3, 5]. Cancers which are a great threat to humans are the second leading cause of death after cardiovascular disease [6]. Currently, a complete cancer remission often fails to achieve with the conventional cancer treatments such as chemotherapy, surgery and radiotherapy. Also, significant side effects have been recognized by radiotherapy and/or chemotherapy. Therefore, lots of new approaches for the treatment of cancer

[*] Corresponding author: yagmurunver@yahoo.com
[1] Ataturk University, Department of Genetic Engineering, Erzurum,ORCID:0000-0003-1497-081X

have been improved. Some of them, use of live, attenuated bacteria or their native purified [7] and recombinant products [8, 9]. Cancer targeted drugs, which provide to treat tumour and reduce side effects have shown rapid progress in recent year [7, 10, 11]. Azurin, one of them, is a redox protein containing copper and secreted by *Pseudomonas aeruginosa* which is a Gram-negative bacterium and can cause disease in certain sensible individuals [12]. Azurin has attracted much attention in the last two decades, because it preferentially enters into many human cancer cells and induce apoptosis [8,13–15]. This protein and its derived peptide p28 have anticancer activity that has been confirmed in mouse-based tumor models and various cancer cells [16, 17].

Whey which is the considerable by-product of the casein or cheese manufacture composes of 80% to 90% of the processed milk and contains about 55% of milk nutrients. Several factors such as milk quality, feed and animal breed are effect on whey composition and whey has about 6-10 g/L of proteins and a high lactose concentration (about 45 g/L) [18–20]. It is also rich in mineral salts (0.5-0.7 w/v), lipids (0.4-0.5 w/v) and minor components such as citric and lactic acids and B group vitamins, etc. [21]. Worldwide, around 190 $x10^6$ ton/year of whey production is estimated and it is known that about 9 liter of whey is produced in every 1 kg of cheese made [22, 23]. So, serious environmental problems arise due to high lactose content and discharging of whey in water systems without pre-treatments can not be possible [19]. Biotechnology, medical, agri-food and related industries exploit the whey because it is an ideal source of functional proteins and peptides, vitamins, lipids, lactose and minerals [24]. In this study, cheese whey was used as an alternative material for azurin production medium to defined media. Also, effects of copper (II) sulphate ($CuSO_4$) and potassium nitrate (KNO_3) on the azurin expression were determined. This is the first report on the production of azurin in whey medium.

2. MATERIAL and METHODS

2.1. Strain and Medium

P. aeruginosa ATCC9027 was obtained from Ataturk University, Department of Food Engineering, Microbiology Research Laboratory. Bacterial cells were incubated on LB (Luria-Bertani) agar plate to maintain the culture. Whey was obtained from a cheese plant in Erzurum. It was autoclaved at 121°C for 15 minutes and after being kept at +4 °C for a night, yellow whey was used as production medium. The production medium composed of whey (50 mL), 5 g/L $(NH_4)_2SO_4$, 2.5 g/L KH_2PO_4, 2,5 g/L Na_2HPO_4, 0.2 g/L $MgSO_4.7H_2O$, 0.01 g/L $MnSO_4.7H_2O$, 5 mg/L $CuSO_4$ and 30 mg/L KNO_3. Initial pH value of the medium was adjusted to 6.5.

2.2. Azurin production in whey medium

Bacteria were streaked on LB agar and incubated for a night. Then, one colony was transferred into 10 mL LB medium and grown at 37 °C and 150 rpm during a night. After incubation, 1 mL of inoculum (OD_{600} ~1.6) was transferred to 50 mL production medium in a shaking flask. Then, it was closed by a cotton and an aluminum foil. To determine optimum azurin production time, culture medium was incubated at 37 °C and 150 rpm for 6 h, 12 h, 18 h and 24 h. At the end of each incubation times, culture liquids were collected and centrifuged at 9000 rpm and +4 °C for 10 minutes. After centrifugation, supernatants were discarded and cells were used for both preparing cell lysates and determination of wet cell weight as g/L.

2.3. Effect of copper (II) sulphate ($CuSO_4$) and potassium nitrate (KNO_3) on the production of azurin in whey medium

To obtain the highest azurin production, the influence of different concentrations of $CuSO_4$ (2.5 mg/L, 5 mg/L, 7.5 mg/L and 10 mg/L) and KNO_3 (15 mg/L, 30 mg/L, 45 mg/L, 60 mg/L and 75 mg/L) were studied at shaking-flask level, separately. Culture liquids were collected and centrifuged at 9000 rpm and +4 °C for 10 minutes.

After centrifugation, supernatants were discarded and cells were used for both preparing cell lysates and determination of wet cell weight as g/L.

2.4. Extraction of cellular protein

Extraction of proteins from bacterial cells was modified from Ramachandran et al. (2012). After cultivations, 2 ml of culture liquid obtained from each culture was centrifuged as described above. Cell pellets were washed with sterile distilled water and centrifuged again. Then, the cells were suspended in 500 µL, 0.02 M potassium phosphate buffer (pH 7) containing 1mM PMSF (phenylmethylsulfonyl fluoride) as protease inhibitor. The cell suspensions were sonicated by keeping in the ice basket using eighteen 10 second bursts at high intensity and a 10 second cooling period between each burst was performed. Then, sonicated suspensions were stirred vigorously and centrifuged at 9000 rpm and +4 °C for 10 minutes. After centrifugation, the supernatants were transferred to fresh tubes and stored on ice [25].

2.5. Western blot analysis

To determine the optimal values of incubation time, concentration of copper sulphate and potassium nitrate for azurin expression, Western blot analysis was used. For this purpose, obtained cell lysates were used and total protein amounts of the lysates were determined by Bradford method [26]. Then, the cell lysates which included equal amount of total protein (for determination of optimum incubation time, $CuSO_4$ and KNO_3 concentrations, total protein amount was used as 60 µg, 50 µg and 40 µg, respectively) and 2X SDS-PAGE sample buffer were mixed together and boiled for 5 minutes to run on SDS-PAGE gel. After gel electrophoresis, proteins were blotted to a PVDF (polyvinylidene difluoride) membrane from the gel by transfer at 25 V and 2.5 A for 7 min. PBST (Phosphate Buffered Saline with Tween 20; 1.8 mM KH_2PO_4, 137 mM NaCl, 10 mM Na_2HPO_4, 2.7 mM KCl and 0.05% Tween 20) containing 5% skim milk powder were used for blocking the membrane for 1h. The membrane was incubated with anti-azurin antibody (Sicgen) for overnight after it was washed with PBST three times. At the end of the incubation, the membrane was incubated with peroxidase conjugated rabbit anti-goat immunoglobulin G (Anti-Goat IgG H&L (HRP), Abcam) as the secondary antibody for 1 h, after it was washed with PBST six times. Then, the membrane was washed with PBST. Supersignal® West Femto and Pico chemiluminescent substrate (Pierce Biotechnology, Rockford, IL) were used for visualization of the protein bands by ChemiDoc™ Touch Imaging System (Bio-Rad). Based on this analysis results, the relative expression levels of azurin were quantified with ImageJ software and compared to each other. Tukey Test (One-way ANOVA) was used for statistical analysis and $P<0.05$ was regarded as significant using GraphPad Prism 5.

3. RESULTS and DISCUSSION

3.1. Determination of incubation time for optimum azurin production

Yamada *et al*. (2002) reported that azurin enters into the cytosol of the human melanoma cell line (UISO-Mel-2), transports to the nucleus and stabilizes the protein by forming a complex with p53 [27]. Punj *et al*. (2004) also found that azurin shows strong cytotoxic activity in MCF-7 breast cancer cell line and increases apoptosis density by more than 50%, while reported that it increases apoptosis density by 15-18 %, in MDA-MB-231 and MDA-MB-157 cells [28]. Similarly, Choi *et al*. (2011) observed a decrease in the viability of oral squamous cancer cells treated with azurin, DNA breakage, morphological changes and an increase in cyclin B1 and p53 protein levels [29]. Therefore, novel methods have been searching by researchers to enhance the production of azurin which has been known to be a potential anticancer protein [30]. In this regard, this study aimed to enhance the expression of azurin in *P. aeruginosa* in low-cost whey medium. Since the existence of a copper ion in the polypeptide chain of azurin is known to contribute to stability of azurin [31], copper sulphate was also added to the culture medium. On the other hand, a comparatively high concentration of $(NH_4)_2SO_4$ (5 g/L) was added to the medium so that KNO_3 was used only for denitrification and not as a source of nitrogen

[32]. To determine optimum incubation time for azurin production in whey medium, bacterial cells were incubated during 24 hours. 2 ml of culture liquids were taken in 6th, 12th, 18th and 24th hours. Because azurin protein with the secretion signal peptide is located in the periplasm [33], the cells were lysed by sonication and obtained lysates were analysed by Western blotting. According to this analysis result, azurin was observed in expected size (14 kDa). Maximum azurin expression was obtained in 18th hour and a decrease of azurin expression was observed after this time. On the other hand, it was shown that cells had the lowest azurin expression in 6th hour (Figure 1a and 1b). Because azurin is a secondary metabolite, it is produced by *P. aeruginosa* in stationary phase of growth. Similarly, Vijgenboom *et al.* (1997) reported that there was an increase in azurin expression when shifting from exponential to stationary phase. Also, as described these researchers, the upper band of azurin in the lanes may not associated with azurin and is a cross-reaction of the anti-azurin antibody [34]. On the other hand, an increase in cell biomass was observed up to the 18th hour while no significant difference was observed between cell weights belong to 18th and 24th hours (Figure 1 c).

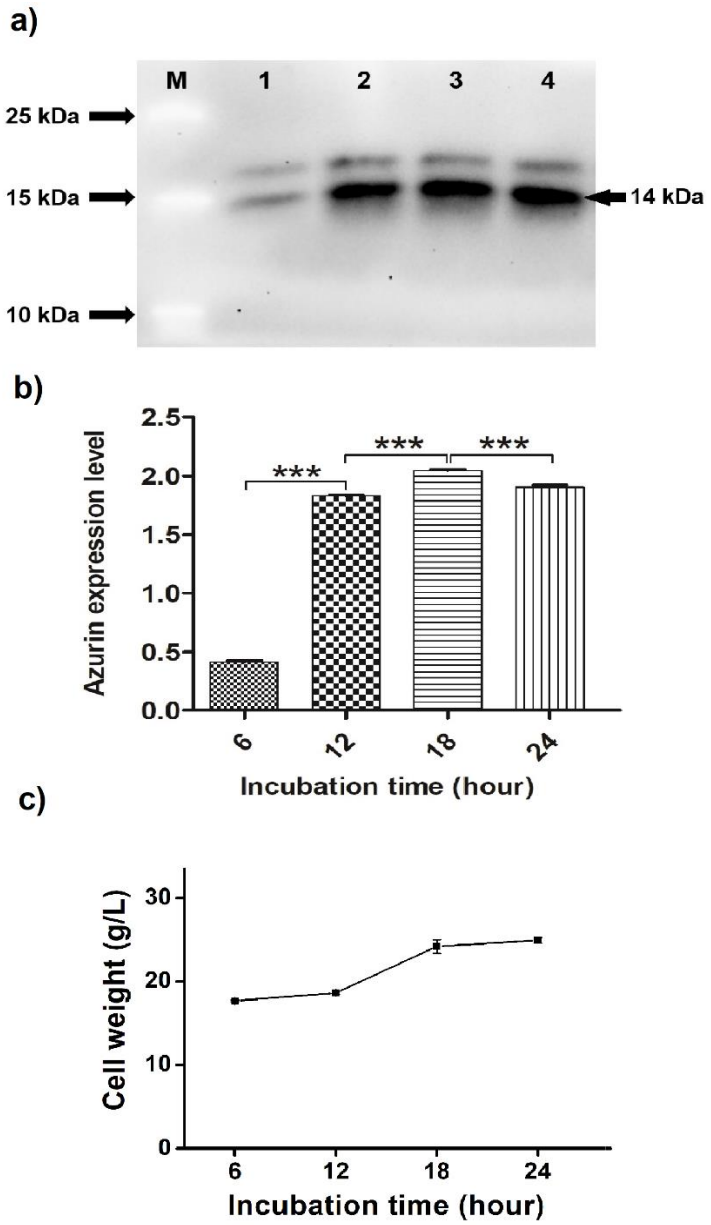

Figure 1 Effect of incubation time on expression level of azurin and cell growth, a) Western blot analysis result of samples from cell lysates (M: Marker, 1: 6 h, 2:12 h, 3:18 h and 4:24 h) b) The relative expression levels of azurin, c) Wet cell weight for incubation time.

3.2. Effect of copper (II) sulphate ($CuSO_4$) on azurin production in whey medium

Sutherland (1966) reported that the copper content of the culture medium affect azurin content of the cells and azurin was nearly absent in the cells when the copper content was lower

than 0.5 mg/L in the medium. On the other hand, it was reported that while the azurin content of cells grown in a medium containing 0.5-5 mg/L copper increased, the copper content above this range did not lead to increase of azurin content [35]. Therefore, in this study, different $CuSO_4$ concentrations (2.5 mg/L, 5 mg/L, 7.5 mg/L and 10 mg/L) were added to the culture media to determine the optimum $CuSO_4$ concentration used as the source of copper ions. After 18 h incubation, obtained cell lysates were analyzed by Western blotting. According to the results (Figure 2a and 2b), 2.5 mg/L $CuSO_4$ was lead to maximum azurin expression. Namely, presence of copper ion in whey medium was lead to enhance azurin synthesis. Over this concentration, as concentration of $CuSO_4$ increase, a decrease of expression level of the protein was observed. Similarly, Ramachandran *et al*. (2012) reported that adding copper in the culture medium was lead to both enhance azurin synthesis and reveal the differences of secondary structure stability of azurin expressed in *P. aeruginosa* [25].

3.3. Effect of copper sulphate on cell growth in whey medium

After 18h incubation, cells were harvested from culture media which contain different concentrations of $CuSO_4$ and wet cell weight of the cells were calculated. According to the results, a decrease in biomass yield was observed over 7.5 mg/L $CuSO_4$ concentration (Figure 2c). This situation might be attributed to toxicity of copper ions to *P. aeruginosa* cells over this concentration.

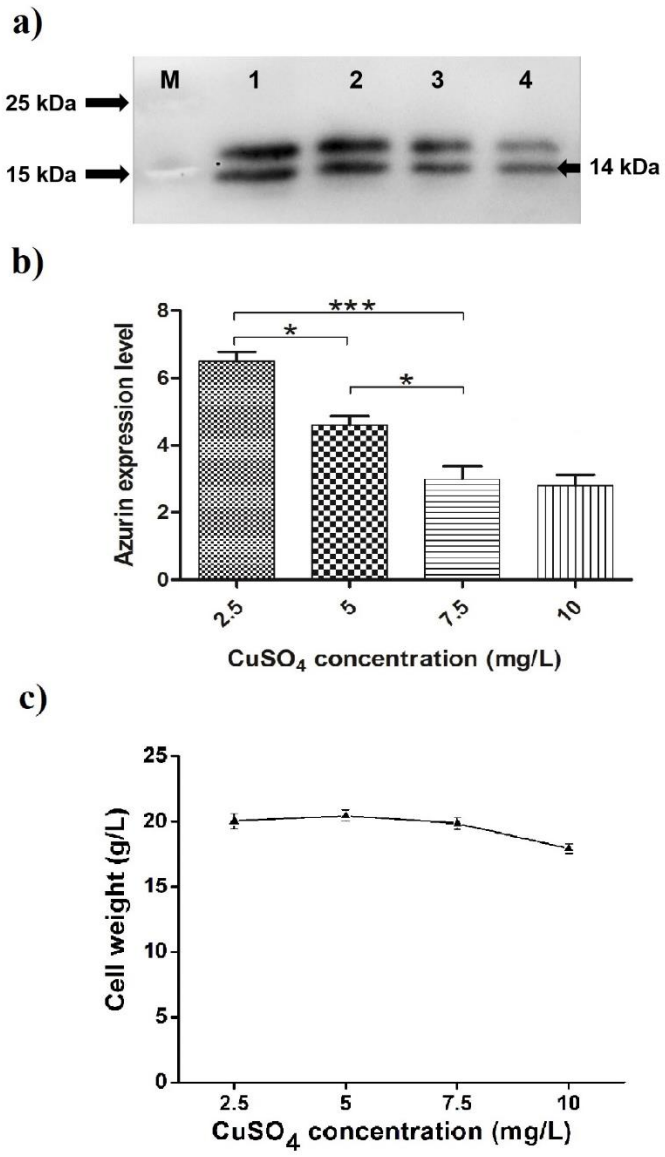

Figure 2 Effect of $CuSO_4$ concentration on expression level of azurin and cell growth, a) Western blot analysis result of samples from cell lysates (M: Marker, 1: 2.5 mg/L, 2: 5 mg/L, 3: 7.5 mg/L and 4: 10 mg/L), b) The relative expression levels of azurin, c) Wet cell weight for different $CuSO_4$ concentrations.

3.4. Effect of KNO_3 on azurin production in whey medium

P. aeruginosa can perform denitrification in the presence of nitrate and under anaerobic conditions. In this respiratory process, nitrate is reduced to nitrogen gas via nitrite (NO_2), nitric oxide (NO) and nitrous oxide (N_2O). In this way, produced nitric oxide by nitrite reductase causes

intracellular damage, whether nitric oxide reductase does not immediately convert nitric oxide to nitrous oxide. To avoid this damage, a stress response can be induced with a higher expression of azurin as potential electron donor [31]. So, in this study, the optimum KNO_3 concentration used only for denitrification was determined to achieve a high level of azurin expression in whey medium. For this purpose, different concentrations of KNO_3 (15 mg/L, 30 mg/L, 45 mg/L, 60 mg/L and 75 mg/L) were added to the culture media. After 18 h incubation, obtained cell lysates were analyzed by Western blotting. According to the results, expression level of azurin was increased related to increasing of KNO_3 and 45 mg/L KNO_3 was lead to maximum azurin expression (Figure 3a and 3b). When using KNO_3 concentrations of 60 mg/L and 75 mg/L above this concentration, a significant decrease in the level of protein expression was observed. This situation might be related to increasing nitric oxide level in the cells. In the respiratory process of these cells high level of nitrate in the medium caused high level of nitric oxide (NO) by reduced and nitric oxide reductase amount in the cells was not enough for immediately convertion of all nitric oxide to nitrous oxide. Therefore, increased nitric oxide level in the cells induced intracellular damage that caused decreasing of azurin expression level.

3.5. Effect of KNO_3 on cell growth in whey medium

After 18h incubation, cells were harvested from culture media which contain different concentrations of KNO_3 and wet cell weight of the cells were calculated. According to the results, biomass yield was increased related to increasing of KNO_3 and maximum wet cell weight was observed in the concentration of 45 mg/L KNO_3. Above this concentration, a decrease in the biomass yield was observed. This might be related to increasing nitric oxide level induced intracellular damage in the cells as seen in the decreasing level of azurin expression after the same KNO_3 concentration. An occured intracellular damage might cause a decrease of cell biomass (Figure 3c).

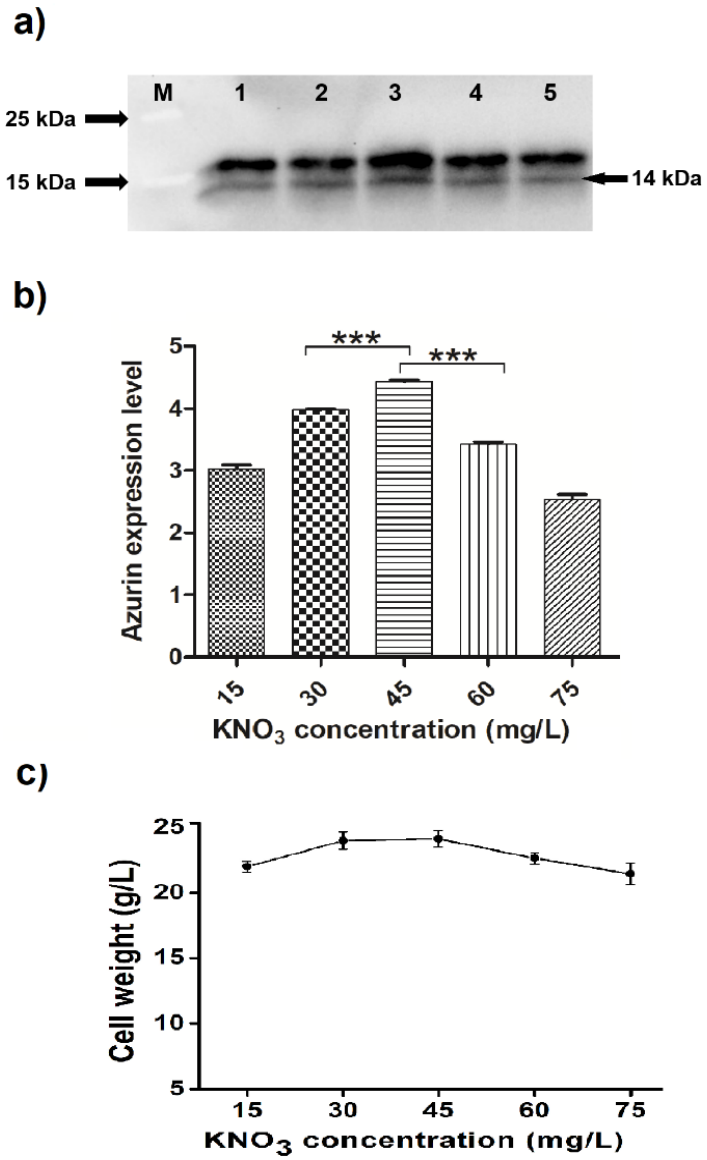

Figure 3 Effect of KNO_3 concentration on expression level of azurin and cell growth, a) Western blot analysis result of samples from cell lysates (M: Marker, 1: 15 mg/L, 2: 30 mg/L, 3: 45 mg/L, 4: 60 mg/L and 5: 75 mg/L), b) The relative expression levels of azurin, c) Wet cell weight for different KNO_3 concentrations.

4. CONCLUSION

The secondary metabolites are used for development of new chemotherapeutics and drugs. Azurin, which is a bacteriocin, has a cytostatic property with its penetration to breast cancer cells. So, it can be used as a potential anticancer agent. In this study, the production of the azurin protein was carried out for the first time in whey medium by *Pseudomonas aeruginosa*. Furthermore, the effective expression of this therapeutic protein was obtained with the addition of $CuSO_4$ and KNO_3 in whey medium. So, the high-level azurin production was achieved in a cost-effective medium and also, using whey for azurin production can reduce many processing industrial whey waste management problems.

Acknowledgments

The author would like to acknowledge East Anatolia High Technology Application and Research Center (DAYTAM, Erzurum, Turkey) and Prof. Dr. Bülent Çetin for providing *P. aeruginosa* ATCC9027.

Funding

The author has no received any financial support for the research, authorship or publication of this study.

The Declaration of Conflict of Interest/ Common Interest

No conflict of interest or common interest has been declared by the author.

The Declaration of Ethics Committee Approval

The author declares that this document does not require an ethics committee approval or any special permission.

The Declaration of Research and Publication Ethics

The author of the paper declares that she comply with the scientific, ethical and quotation rules of SAUJS in all processes of the paper and that they do not make any falsification on the data collected. In addition, she declares that Sakarya University Journal of Science and its editorial board have no responsibility for any ethical violations that may be encountered, and that this study has not been evaluated in any academic publication environment other than Sakarya University Journal of Science.

REFERENCES

[1] A.R. Awan, W.M. Shaw, T. Ellis, "Biosynthesis of therapeutic natural products using synthetic biology", Advanced Drug Delivery Reviews, vol. 105, Part A, pp. 96–106, 2016.

[2] S.B. Singh, Confronting the challenges of discovery of novel antibacterial agents, Bioorganic & Medicinal Chemistry Letters, vol. 24, no. 6, pp. 3683-3689, 2014.

[3] D.J. Newman, G.M. Cragg, Natural products as sources of new drugs over the last 25 years, Journal of Natural Products, vol. 70, pp. 461-477, 2007.

[4] B. Ruiz, A. Chávez, A. Forero, Y. García-Huante, A. Romero, M. Snchez, D. Rocha, B. Snchez, R. Rodríguez-Sanoja, S. Sánchez, E. Langley, Production of microbial secondary metabolites: Regulation by the carbon source, Critical Reviews in Microbiology, vol. 36, no. 2, pp. 146-167, 2010.

[5] G.M. Cragg, D.J. Newman, Natural products: A continuing source of novel drug leads, Biochimica et Biophysica Acta (BBA) - General Subjects, vol. 1830, no. 6, pp. 3670-3695, 2013.

[6] F. Huang, Q. Shu, Z. Qin, J. Tian, Z. Su, Y. Huang, M. Gao, Anticancer Actions of Azurin and Its Derived Peptide p28, The Protein Journal, vol. 39, no.2 pp. 182-189, 2020.

[7] S. Biswas, P. Kumari, P.M. Lakhani, B. Ghosh, Recent advances in polymeric micelles for anti-cancer drug delivery, European Journal of Pharmaceutical Sciences, vol. 83, pp. 184-202, 2016.

[8] N. Bernardes, R. Seruca, a M. Chakrabarty, a M. Fialho, Microbial-based therapy of cancer: current progress and future prospects, Bioengineered Bugs. vol. 1, no. 3, pp. 178-190, 2010.

[9] A. Sharma, N. Kumari, E. Menghani, Bioactive Secondary Metabolites: an Overview, International Journal of Scientific & Engineering Research, vol. 5, no. 4, pp. 1395-1407, 2014.

[10] T. Chatzisideri, G. Leonidis, V. Sarli, Cancer-targeted delivery systems based on peptides, Future Medicinal Chemistry, vol. 10, no. 18, pp. 2201-2226, 2018.

[11] R. Soudy, N. Byeon, Y. Raghuwanshi, S. Ahmed, A. Lavasanifar, K. Kaur, Engineered Peptides for Applications in Cancer-Targeted Drug Delivery and Tumor Detection, Mini-Reviews Medicinal Chemistry, vol. 17, no. 18, pp.1696-1712, 2016.

[12] M. Sánchez, F.J. Aranda, M.J. Espuny, A. Marqués, J.A. Teruel, Á. Manresa, A. Ortiz, Aggregation behaviour of a dirhamnolipid biosurfactant secreted by Pseudomonas aeruginosa in aqueous media, Journal of Colloid and Interface Science, vol. 307, no. 1, pp.246-253, 2007.

[13] A.M. Chakrabarty, N. Bernardes, A.M. Fialho, Bacterial proteins and peptides in cancer therapy: Today and tomorrow, Bioengineered, vol. 5 pp. 234-242, 2014.

[14] A. Fialho, T. Das Gupta, A. Chakrabarty, Designing Promiscuous Drugs? Look at What Nature Made!, Letters in Drug Design & Discovery, vol. 4, no. 1, pp.40-43, 2007.

[15] D. Raucher, J.S. Ryu, Cell-penetrating peptides: Strategies for anticancer treatment, Trends in Molecular Medicine, vol. 21, no. 9, pp.560-570, 2015.

[16] Y. Zhang, Y. Zhang, L. Xia, X. Zhang, X. Ding, F. Yan, F. Wu, Escherichia coli Nissle 1917 targets and restrains mouse B16 melanoma and 4T1 breast tumors through expression of azurin protein, Applied Environmental Microbiology, vol. 78, no. 271, pp.7603-7610, 2012.

[17] P. Ghasemi-Dehkordi, A. Doosti, M.S. Jami, The concurrent effects of azurin and Mammaglobin-A genes in inhibition of breast cancer progression and immune system stimulation in cancerous BALB/c mice, 3 Biotechnology, vol. 9, no. 27, pp.1-15, 2019.

[18] P.M.R. Guimarães, J.A. Teixeira, L. Domingues, Fermentation of lactose to bio-ethanol by yeasts as part of integrated solutions for the valorisation of cheese whey, Biotechnology Advances, vol. 28, no. 3, pp.375-384, 2010.

[19] M.I. González Siso, The biotechnological utilization of cheese whey: A review, Bioresource Technology, vol. 57, no. 1, pp.1-11, 1996.

[20] A.R. Prazeres, F. Carvalho, J. Rivas, Cheese whey management: A review, Journal of Environmental Management, vol. 110, pp.48-68, 2012.

[21] M. Pescuma, G.F. de Valdez, F. Mozzi, Whey-derived valuable products obtained by microbial fermentation, Applied Microbiology and Biotechnology, vol. 99, pp.6183-6196, 2015.

[22] M.P. Ryan, G. Walsh, The biotechnological potential of whey, Reviews in Environmental Science and Bio/Technology, vol. 15, no. 3, pp.479-498, 2016.

[23] F. V Kosikowski, V. V Mistry, Cheese and Fermented Milk Foods, Cheese Fermented Milk Foods ,1997.

[24] G.W. Smithers, Whey and whey proteins-From "gutter-to-gold," International Dairy Journal, vol. 18, no. 7, pp.695-704, 2008.

[25] S. Ramachandran, M. Singh, M. Mandal, Purification of Azurin from Pseudomonas aeuroginosa, in: Chromatogr. - Most Versatile Method, Analytical Chemistry, 2012.

[26] M. Bradford, A Rapid and Sensitive Method for the Quantitation of Microgram Quantities of Protein Utilizing the Principle of Protein-Dye Binding, Analytical Biochemistry, vol. 72, pp.248-254, 1976.

[27] T. Yamada, M. Goto, V. Punj, O. Zaborina, M.L. Chen, K. Kimbara, D. Majumdar, E. Cunningham, T.K. Das Gupta, A.M. Chakrabarty, Bacterial redox protein azurin, tumor suppressor protein p53, and regression of cancer, Proceedings of the National Academy of Science, vol. 99, pp.14098-14103, 2002.

[28] V. Punj, S. Bhattacharyya, D. Saint-Dic, C. Vasu, E.A. Cunningham, J. Graves, T. Yamada, Bacterial cupredoxin azurin as an inducer of apoptosis and regression in human breast cancer, Oncogene, vol. 23, no. 13, pp.2367-2378, 2004.

[29] J.H. Choi, M.H. Lee, Y.J. Cho, B.S., Park, S. Kim, G.C. Kim, The bacterial protein Azurin enhances sensitivity of oral squamous carcinoma cells to anticancer drugs, Yonsei Medical Journal, vol. 52, 773-78, 2011.

[30] M. Goto, T. Yamada, K. Kimbara, J. Horner, M. Newcomb, T.K. Das Gupta, A.M. Chakrabarty, Induction of apoptosis in macrophages by Pseudomonas aeruginosa azurin: Tumour-suppressor protein p53 and reactive oxygen species, but not redox activity, as critical elements in cytotoxicity, Molecular Microbiology, vol. 47, no. 2, pp.549-559, 2003.

[31] I. Pozdnyakova, J. Guidry, P. Wittung-Stafshede, Copper stabilizes azurin by decreasing the unfolding rate, Archieves of Biochemistry and Biophysics, vol. 390, no. 1, pp.146-148, 2001.

[32] R. Knowles, Denitrification, Microbiology Reviews, vol. 46, no. 1, pp.43-70, 1982.

[33] Y. Han, T. Wang, G. Chen, Q. Pu, Q. Liu, Y. Zhang, L. Xu, M. Wu, H. Liang, A Pseudomonas aeruginosa type VI secretion system regulated by CueR facilitates copper acquisition, PLoS Pathogens, vol. 15, no. 12, pp.1-25, 2019.

[34] E. Vijgenboom, J.E. Busch, G.W. Canters, In vivo studies disprove an obligatory role of azurin in denitrification in Pseudomonas aeruginosa and show that azu expression is under control of RpoS and ANR, Microbiology. vol. 143, no. 9, pp.2853-2863, 1997.

[35] I. W. Sutherland, The Production of Azurin and Similar Proteins, Archiv für Mikrobiologie, vol. 54, pp.350-357, 1966.

SAKARYA ÜNİVERSİTESİ
FEN BİLİMLERİ ENSTİTÜSÜ DERGİSİ

Sakarya University Journal of Science
SAUJS

e-ISSN 2147-835X | Period Bimonthly | Founded: 1997 | Publisher Sakarya University |
http://www.saujs.sakarya.edu.tr/en/

Title: The Essentials of Clifford Algebras with Maple Programming

Authors: Mutlu AKAR

Recieved: 2021-01-27 15:12:41

Accepted: 2021-03-31 14:39:52

Article Type: Research Article

Volume: 25
Issue: 2
Month: April
Year: 2021
Pages: 610-618

How to cite
Mutlu AKAR; (2021), The Essentials of Clifford Algebras with Maple Programming. Sakarya University Journal of Science, 25(2), 610-618, DOI: https://doi.org/10.16984/saufenbilder.869402
Access link
http://www.saujs.sakarya.edu.tr/en/pub/issue/60672/869402

Sakarya University Journal of Science 25(2), 610-618, 2021

The Essentials of Clifford Algebras with Maple Programming

Mutlu AKAR*[1]

Abstract

Clifford algebra (geometric algebra) which has many applications in physics, robotics, Computer-Aided Manufacture, computer graphics, image processing, Computer-Aided Design etc. is one of the important subjects in mathematics. In this paper, after we give the definition of Clifford algebras, introduce their subspaces. Firstly, we develop an algorithm which obtains some concepts of Clifford algebras using Maple programming. Secondly, another algorithm calculates the norm of the multivector obtained by finding the Clifford product of any two vectors of the same finite dimension.

Keywords: Clifford algebras, Clifford product, multivector, Maple

1. INTRODUCTION

Quaternions, a generalization of complex numbers, were discovered by William Hamilton in 1843. After Hamilton's discovery of quaternions, J. T. Graves invented octonion algebra in 1843. However, Graves did not publish the article. Octonions were rediscovered by Cayley in 1845 and octonions are also known as Cayley numbers. Clifford algebras were first found in 1878 by the British mathematician W. K. Clifford and published in his article titled "Application of Grasmann's Extensive Algebra" in the journal "American Journal of Mathematics Pure and Applied". Clifford's geometric algebras; Grasmann defined it as a generalization of algebras, complex numbers and quaternions. W. K. Clifford used hyperbolic numbers to represent the sum of spins in 1882. Corrado Segre dealt with algebras called bicomplex numbers in his work with these algebras in 1892 [1].

Clifford algebra is increasingly used in almost every field. In recent years, Clifford algebras have applications in many fields such as robot vision, neural computing, computer vision, image and signal processing, control problems, electromagnetism, physics [2].

Clifford support vector machines were characterized as a speculation of real and complex valued support vector machines using Clifford algebras. By including the Clifford product in the core function in nonlinear support vector machines, more precise results have been obtained in classifications by improving multiple data input and data output. Thus, satellite control,

* Corresponding Author: makar@yildiz.edu.tr
[1] Yildiz Technical University, College of Arts & Sciences, ORCID: 0000-0003-3718-7449

neural computing, pattern recognition, etc. areas have been contributed [3].

In this study, after giving the basic concepts in Clifford algebras, for a number n inputting with the help of Maple programming, we give how to make the Clifford product in $C\ell_{n,0}$, which prints the basis of $C\ell_{n,0}$ (or $C\ell_{0,n}$) Clifford algebras by grouping their dimensions, the bases of their subspaces and the dimensions of their subspaces.

2. CLIFFORD ALGEBRAS

In this section, some basic concepts of Clifford algebras are given.

Definition 1. Let us consider bilinear form for $x, y \in \mathbb{R}^n$ and $r+s=n$

$$\langle x,y\rangle_{r,s} = x_1y_1+\cdots+x_ry_r - x_{r+1}y_{r+1}-\cdots-x_{r+s}y_{r+s}. \quad (1)$$

If $\mathbb{R}^{r,s}=\mathbb{R}^n$ has the following quadratic form for $x\in\mathbb{R}^n$,

$$\langle x,x\rangle_{r,s} = x_1^2+\cdots+x_r^2-x_{r+1}^2-\cdots-x_{r+s}^2 \quad (2)$$

$\left(\mathbb{R}^{r,s},\langle .\rangle_{r,s}\right)$ is called a real quadratic space.

$\langle x,y\rangle_{n,0}$ an dot product for $x,y\in\mathbb{R}^{n,0}$ and $\langle x,x\rangle_{n,0}=|x|^2$. That is, Euclidean dot product is a special case of quadratic form [4].

Definition 2: For $r+s=n$

$$e_i^2=1,\ i=1,\ldots,r,\quad e_i^2=-1,\ i=r+1,\ldots,n \quad (3)$$

and for

$$e_ie_j=-e_je_i,\qquad i,j=1,\ldots,n,\quad i\neq j\ , \quad (4)$$

The algebra produced by the standard orthonormal basis of the $\{e_1,e_2,\ldots,e_n\}$ in $\mathbb{R}^n$ is called the real Clifford algebra $C\ell_{r,s}$ [4].

Example 1: Some known sets of numbers are actually examples of Clifford algebra. The algebra $C\ell_{0,1}$ is the usual algebra of complex numbers $\mathbb{C}$. The algebra $C\ell_{0,2}$ is the algebra of quaternions $\mathbb{H}$. Whereas the algebra $C\ell_{1,0}$ is often called the split complex numbers (or hyperbolic numbers).

An element $\zeta\in C\ell_{0,1}$ has the form $x_0+x_1e_1$ where $x_0,x_1\in\mathbb{R}$ and $e_1^2=-1$. We identify ζ with the point (x_0,x_1) in $\mathbb{R}^2$. In this way we view $\mathbb{C}$ as the plane $\mathbb{R}^2$ with an additional algebraic structure. Its conjugate by definition is $\overline{\zeta}=x_0-x_1e_1$. Notice that $\zeta\overline{\zeta}=x_0^2+x_1^2=\langle x,x\rangle_{2,0}$. Therefore, the complex numbers are associated with the quadratic space $\mathbb{R}^{2,0}$.

Similarly, an element $\zeta\in C\ell_{1,0}$ has the form $x_0+x_1e_1$ where $x_0,x_1\in\mathbb{R}$ and $e_1^2=1$. The conjugate again by definition is $x_0-x_1e_1$. In this case $\zeta\overline{\zeta}=x_0^2-x_1^2=\langle x,x\rangle_{1,1}$. So the split complex numbers are associated with the quadratic space $\mathbb{R}^{1,1}$.

A quaternion $\zeta\in\mathbb{H}$ has the form $\zeta=x_0+x_1e_1+x_2e_2+x_3e_3$. The conjugate of ζ is now $\overline{\zeta}=x_0-x_1e_1-x_2e_2-x_3e_3$ so that $\zeta\overline{\zeta}=x_0^2+x_1^2+x_2^2+x_3^2$. Hence the quaternions are associated with the quadratic space $\mathbb{R}^{4,0}$ [4].

The Clifford algebra $C\ell_{r,s}$ is a $\sum_{p=0}^{n}\binom{n}{p}=2^n$ dimensional vector space with a basis

$$\{1, e_1, e_2, \ldots, e_n, e_1e_2, \ldots, e_{n-1}e_n, \ldots, e_1e_2\ldots e_n\}. \quad (5)$$

The vector space $C\ell_{r,s}$ can be written as the direct sum of subspaces

$$C\ell_{r,s} = \Lambda^0\mathbb{R}^n \oplus \Lambda^1\mathbb{R}^n \oplus \cdots \oplus \Lambda^n\mathbb{R}^n. \quad (6)$$

The dimension of each subspace is $\binom{n}{p}$ for $p = 0, \ldots, n$. The element $\mathcal{A}$ of Clifford algebra $C\ell_{r,s}$ is called a multivector. The element of subspaces $\Lambda^p\mathbb{R}^n$, $(p = 0, \ldots, n)$ is a $p-$vector. For instance, the subspace $\Lambda^0\mathbb{R}^n = \mathbb{R}$ of dimension is 1 and its element is $0-$vector, that is a real number. The subspace $\Lambda^1\mathbb{R}^n = \mathbb{R}^n$, has the basis $\{e_1, e_2, \ldots, e_n\}$, its element is $1-$vector, that is a vector and the dimension of subspace $\Lambda^1\mathbb{R}^n$ is n. $\{e_1e_2, e_1e_3, \ldots, e_{n-1}e_n\}$ is a basis of subspace $\Lambda^2\mathbb{R}^n$ whose element is bivector ($2-$vector). $\{e_1e_2\ldots e_n\}$ is a basis of subspace $\Lambda^n\mathbb{R}^n$ whose element is called pseudoscalar ($n-$vector). The multivector $\mathcal{A}$, which is the element of the vector space $C\ell_{r,s}$ given as direct sums of subspaces $\Lambda^p\mathbb{R}^p$, $(0 \le p \le n)$ given by Eq. (6) equation, can be written as in [5,6]

$$\mathcal{A} = \langle\mathcal{A}\rangle_0 + \langle\mathcal{A}\rangle_1 + \cdots + \langle\mathcal{A}\rangle_n. \quad (7)$$

In Eq. (7) $\langle\mathcal{A}\rangle_p$ is the $p-$vector of the multivector $\mathcal{A}$ and denotes the projection of multivector $\mathcal{A} \in C\ell_{r,s}$ onto the subspace $\Lambda^p\mathbb{R}^p$. The notation $\langle\ \rangle$ represents the elements of each subspace with respect to the subscript [6,7].

Definition 3: $\mathbf{fg}$ is called the Clifford product or geometric product of two vectors $\mathbf{f}$ and $\mathbf{g}$ if

$$\mathbf{fg} = \mathbf{f}\bullet\mathbf{g} + \mathbf{f}\wedge\mathbf{g} \quad (8)$$

where $\mathbf{f}\bullet\mathbf{g}$ is the inner or dot product while $\mathbf{f}\wedge\mathbf{g}$ is the wedge or outer (or exterior) product. Hence [3,5]

$$\mathbf{f}\bullet\mathbf{g} = \frac{1}{2}(\mathbf{fg} + \mathbf{gf}) \quad (9)$$

$$\mathbf{f}\wedge\mathbf{g} = \frac{1}{2}(\mathbf{fg} - \mathbf{gf}). \quad (10)$$

$\mathbf{f}\wedge\mathbf{g}$ is a bivector. The generalized form $\mathbf{f}\wedge\mathbf{g}\wedge\mathbf{h}$ of the wedge product is the trivector ($3-$vector). The most generalized form is pseudoscalar ($n-$vector). Clifford algebras are non-commutative, but is associative and distributive over addition [3].

For $\mathbf{f} = (f_1, f_2, \ldots, f_n) \in \mathbb{R}^n$,
$\mathbf{g} = (g_1, g_2, \ldots, g_n) \in \mathbb{R}^n$ [5,8]

$$\begin{aligned}\mathbf{fg} &= (f_1e_1 + f_2e_2 + \cdots + f_ne_n)(g_1e_1 + g_2e_2 + \cdots + g_ne_n)\\ &= \sum_{i=1}^{n} f_ig_i + \sum_{j=1}^{n}\sum_{i=j+1}^{n}(f_jg_i - f_ig_j)e_je_i \quad (11)\\ &= \mathbf{f}\bullet\mathbf{g} + \mathbf{f}\wedge\mathbf{g}.\end{aligned}$$

For example, we get the following equation for $\mathbf{f} = (f_1, f_2, f_3) \in \mathbb{R}^3$, $\mathbf{g} = (g_1, g_2, g_3) \in \mathbb{R}^3$

$$\begin{aligned}\mathbf{f}\wedge\mathbf{g} = \mathbf{f}\times\mathbf{g} &= \begin{vmatrix} e_1 & e_2 & e_3 \\ f_1 & f_2 & f_3 \\ g_1 & g_2 & g_3 \end{vmatrix}\\ &= (f_2g_3 - f_3g_2, f_3g_1 - f_1g_3, f_1g_2 - f_2g_1) \in \mathbb{R}^3.\end{aligned}$$

That is, in $\mathbb{R}^3$ wedge product is vector product.

Definition 4. Positive definite norm of a multivector $\mathcal{A}$ is defined as below [3,4]:

$$\|\mathcal{A}\|^2 = \mathcal{A}.\mathcal{A} \quad (12)$$

where $\|\mathcal{A}\| = 0$ if and only if $\mathcal{A} = \mathbf{0}$.

We will use the notation $e_ie_je_ke_t = e_{ijkt}$ in the rest of our work [4].

2.1. Clifford Algebra $C\ell_2$

The Clifford algebra $C\ell_{2,0} = C\ell_2$ generated by the orthonormal basis $\{e_1, e_2\}$ of the real vector space $\mathbb{R}^2$ is a $2^{2+0} = 4$ dimensional space. For every $u \in C\ell_2$ since $\{1, e_1, e_2, e_{12}\}$ is the basis of $C\ell_2$

$$u = u_0 + u_1 e_1 + u_2 e_2 + u_{12} e_{12}$$

can be written where u_0 is a scalar, $u_1 e_1$, $u_2 e_2$ are vectors, and $u_{12} e_{12}$ is a bivector.

For every $\mathbf{f}, \mathbf{g} \in \mathbb{R}^2$,

$$\mathbf{f} = f_1 e_1 + f_2 e_2, \qquad \mathbf{g} = g_1 e_1 + g_2 e_2$$

can be written, where $\{e_1, e_2\}$ of $\mathbb{R}^2$ is the standard orthonormal basis.

The Clifford products of the vectors **f** and **g** are as follows:

$$\begin{aligned}\mathbf{fg} &= (f_1 e_1 + f_2 e_2)(g_1 e_1 + g_2 e_2) \\ &= f_1 g_1 e_1 e_1 + f_1 g_2 e_1 e_2 + f_2 g_1 e_2 e_1 + f_2 g_2 e_2 e_2 .\end{aligned} \tag{13}$$

Since $e_1 e_1 = e_2 e_2 = 1$ and $e_2 e_1 = -e_1 e_2$, Eq. (13) is obtained as the sum of dot product and wedge product as below [9]:

$$\mathbf{fg} = (f_1 g_1 + f_2 g_2) + (f_1 g_2 - f_2 g_1) e_1 e_2 \tag{14}$$

where the wedge product $\mathbf{f} \wedge \mathbf{g}$ is a bivector and it means the area of the parallelogram built on the vectors **f** and **g**. The value of this area is $|\mathbf{f} \wedge \mathbf{g}| = |f_1 g_2 - f_2 g_1|$ [8].

2.2. Clifford Algebra $C\ell_3$

The Clifford algebra $C\ell_{3,0} = C\ell_3$ generated by the orthonormal basis $\{e_1, e_2, e_3\}$ of the real vector space $\mathbb{R}^3$ is a $2^{3+0} = 8$ dimensional space.

For every $u \in C\ell_3$ since $\{1, e_1, e_2, e_3, e_{12}, e_{13}, e_{23}, e_{123}\}$ is the basis of $C\ell_3$

$$\begin{aligned}u = {} & u_0 + u_1 e_1 + u_2 e_2 + u_3 e_3 + u_{12} e_{12} \\ & + u_{13} e_{13} + u_{23} e_{23} + u_{123} e_{123}\end{aligned}$$

can be written where u_0 is a scalar, $u_1 e_1$, $u_2 e_2$, $u_3 e_3$ are vectors, $u_{12} e_{12}$, $u_{13} e_{13}$, $u_{23} e_{23}$ are bivectors, and $u_{123} e_{123}$ is a trivector.

For every $\mathbf{f}, \mathbf{g} \in \mathbb{R}^3$,

$$\mathbf{f} = f_1 e_1 + f_2 e_2 + f_3 e_3, \qquad \mathbf{g} = g_1 e_1 + g_2 e_2 + g_3 e_3$$

can be written, where $\{e_1, e_2, e_3\}$ of $\mathbb{R}^3$ is the standard orthonormal basis.

The Clifford products of the vectors **f** and **g** are as follows:

$$\begin{aligned}\mathbf{fg} &= (f_1 e_1 + f_2 e_2 + f_3 e_3)(g_1 e_1 + g_2 e_2 + g_3 e_3) \\ &= f_1 g_1 e_1 e_1 + f_1 g_2 e_1 e_2 + f_1 g_3 e_1 e_3 + f_2 g_1 e_2 e_1 \\ &\quad + f_2 g_2 e_2 e_2 + f_2 g_3 e_2 e_3 + f_3 g_1 e_3 e_1 + f_3 g_2 e_3 e_2 \\ &\quad + f_3 g_3 e_3 e_3 .\end{aligned} \tag{15}$$

Since $e_1 e_1 = e_2 e_2 = e_3 e_3 = 1$, $e_2 e_1 = -e_1 e_2$, $e_3 e_1 = -e_1 e_3$, $e_3 e_2 = -e_2 e_3$, Eq. (15) is obtained as the sum of dot product and wedge product as below [9]:

$$\begin{aligned}\mathbf{fg} = {} & (f_1 g_1 + f_2 g_2 + f_3 g_3) + (f_1 g_2 - f_2 g_1) e_1 e_2 \\ & + (f_1 g_3 - f_3 g_1) e_1 e_3 + (f_2 g_3 - f_3 g_2) e_2 e_3 .\end{aligned} \tag{16}$$

The terms $e_1 e_2$, $e_1 e_3$, and $e_2 e_3$ in Eq. (16) are bivectors and are interpreted as the oriented area element lying on the planes defined by the vectors (e_1, e_2), (e_1, e_3), and (e_2, e_3), respectively. $e_1 e_2 e_3$ represents the directed volume element in $\mathbb{R}^3$ and is the trivector [9].

Since $\mathbf{f} \wedge \mathbf{g} = -\mathbf{g} \wedge \mathbf{f}$ for every $\mathbf{f}, \mathbf{g} \in \mathbb{R}^n$ we get $\mathbf{gf} = \mathbf{f} \bullet \mathbf{g} - \mathbf{f} \wedge \mathbf{g}$. Hence [4]

$$\mathbf{fg}=\mathbf{gf}\Leftrightarrow\mathbf{f}\|\mathbf{g}\Leftrightarrow\mathbf{f}\wedge\mathbf{g}=\mathbf{0}\Leftrightarrow\mathbf{fg}=\mathbf{f}\bullet\mathbf{g},$$

$$\mathbf{fg}=-\mathbf{gf}\Leftrightarrow\mathbf{f}\perp\mathbf{g}\Leftrightarrow\mathbf{f}\bullet\mathbf{g}=0\Leftrightarrow\mathbf{fg}=\mathbf{f}\wedge\mathbf{g}.$$

Let's summarize the Clifford algebras in the following tables:

Table 1. Clifford algebras and their subspaces and dimensions

Clifford Algebras	Subspaces	Dimensions
$C\ell_0$	$\mathbb{R}$	$2^0=1$
$C\ell_1$	$\Lambda^0\mathbb{R}^1\oplus\Lambda^1\mathbb{R}^1$	$2^1=2$
$C\ell_2$	$\Lambda^0\mathbb{R}^2\oplus\Lambda^1\mathbb{R}^2\oplus\Lambda^2\mathbb{R}^2$	$2^2=4$
$C\ell_3$	$\Lambda^0\mathbb{R}^3\oplus\Lambda^1\mathbb{R}^3\oplus\Lambda^2\mathbb{R}^3\oplus\Lambda^3\mathbb{R}^3$	$2^3=8$
$C\ell_4$	$\Lambda^0\mathbb{R}^4\oplus\Lambda^1\mathbb{R}^4\oplus\Lambda^2\mathbb{R}^4\oplus\Lambda^3\mathbb{R}^4\oplus\Lambda^4\mathbb{R}^4$	$2^4=16$
$C\ell_5$	$\Lambda^0\mathbb{R}^5\oplus\Lambda^1\mathbb{R}^5\oplus\Lambda^2\mathbb{R}^5\oplus\Lambda^3\mathbb{R}^5\oplus\Lambda^4\mathbb{R}^5\oplus\Lambda^5\mathbb{R}^5$	$2^5=32$
$\vdots$	$\vdots$	$\vdots$
$C\ell_n$	$\Lambda^0\mathbb{R}^n\oplus\Lambda^1\mathbb{R}^n\oplus\Lambda^2\mathbb{R}^n\oplus\Lambda^3\mathbb{R}^n\oplus\Lambda^4\mathbb{R}^n\cdots\oplus\Lambda^n\mathbb{R}^n$	2^n

Table 2. The bases of Clifford algebras and the dimensions of their subspaces

Clifford Algebras	Bases	The numbers of elements of Bases (Pascal Triangle)
$C\ell_0$	$\{1\}$	1
$C\ell_1$	$\{1,e_1\}$	1 1
$C\ell_2$	$\{1,e_1,e_2,e_{12}\}$	1 2 1
$C\ell_3$	$\{1,e_1,e_2,e_3,e_{12},e_{13},e_{23},e_{123}\}$	1 3 3 1
$C\ell_4$	$\{1,$ $e_1,e_2,e_3,e_4,$ $e_{12},e_{13},e_{14},e_{23},e_{24},e_{34},$ $e_{123},e_{124},e_{134},e_{234},$ $e_{1234}\}$	1 4 6 4 1

$C\ell_5$	$\{1,$ $e_1,e_2,e_3,e_4,e_5,$ $e_{12},e_{13},e_{14},e_{15},e_{23},e_{24},e_{25},e_{34},e_{35},e_{45},$ $e_{123},e_{124},e_{125},e_{134},e_{135},e_{145},e_{234},e_{235},e_{245},e_{345},$ $e_{1234},e_{1235},e_{1245},e_{1345},e_{2345},$ $e_{12345}\}$	1 5 10 10 5 1
⋮	⋮	⋮
$C\ell_n$	$\{1,$ $e_1,e_2,\ldots,e_n,$ $e_1e_2,e_1e_3,\ldots,e_{n-1}e_n,\ldots,e_1e_2\ldots e_n\}$	$\binom{n}{0}$ $\binom{n}{1}$ $\binom{n}{2}\cdots\binom{n}{n}$

3. MAPLE APPLICATIONS

In this section, how to calculate some basic concepts of Clifford algebras with the help of Maple programming is given. Then, a program that calculates the norm of the multivector obtained by finding the Clifford product of any two vectors of the same finite dimension in $\mathbb{R}^n$ $\left(n\in\mathbb{Z}^+\right)$ is mentioned.

3.1. Clifford Algebras in Maple

In Maple programming, an algorithm has been developed that prints $C\ell_{n,0}$ (or $C\ell_{0,n}$) the basis and size of Clifford algebras by grouping the bases of the subspaces (multivector types) and subspaces according to the pascal triangle for any number n $\left(0\le n\le 12\right)$ inputted.

```
> restart:
> c:=proc(n) local b,d;
> b[1]:=seq(e[i1],i1=1..n):
>
b[2]:=seq(seq(e[i1]*e[i2],i2=i1+
1..n),i1=1..n):
>
b[3]:=seq(seq(seq(e[i1]*e[i2]*e[
i3],i3=i2+1..n),i2=i1+1..n),i1=1
..n):
>
b[4]:=seq(seq(seq(seq(e[i1]*e[i2
]*e[i3]*e[i4],i4=i3+1..n),i3=i2+
1..n),i2=i1+1..n),i1=1..n):
>
b[5]:=seq(seq(seq(seq(seq(e[i1]*
e[i2]*e[i3]*e[i4]*e[i5],i5=i4+1.
.n),i4=i3+1..n),i3=i2+1..n),i2=i
1+1..n),i1=1..n):
>
b[6]:=seq(seq(seq(seq(seq(seq(e[
i1]*e[i2]*e[i3]*e[i4]*e[i5]*e[i6
],i6=i5+1..n),i5=i4+1..n),i4=i3+
1..n),i3=i2+1..n),i2=i1+1..n),i1
=1..n):
>
b[7]:=seq(seq(seq(seq(seq(seq(se
q(e[i1]*e[i2]*e[i3]*e[i4]*e[i5]*
e[i6]*e[i7],i7=i6+1..n),i6=i5+1.
.n),i5=i4+1..n),i4=i3+1..n),i3=i
2+1..n),i2=i1+1..n),i1=1..n):
>
b[8]:=seq(seq(seq(seq(seq(seq(se
q(seq(e[i1]*e[i2]*e[i3]*e[i4]*e[
i5]*e[i6]*e[i7]*e[i8],i8=i7+1..n
),i7=i6+1..n),i6=i5+1..n),i5=i4+
1..n),i4=i3+1..n),i3=i2+1..n),i2
=i1+1..n),i1=1..n):
>
b[9]:=seq(seq(seq(seq(seq(seq(se
q(seq(seq(e[i1]*e[i2]*e[i3]*e[i4
]*e[i5]*e[i6]*e[i7]*e[i8]*e[i9],
i9=i8+1..n),i8=i7+1..n),i7=i6+1.
.n),i6=i5+1..n),i5=i4+1..n),i4=i
3+1..n),i3=i2+1..n),i2=i1+1..n),
i1=1..n):
```

```
>
b[10]:=seq(seq(seq(seq(seq(seq(s
eq(seq(seq(seq(e[i1]*e[i2]*e[i3]
*e[i4]*e[i5]*e[i6]*e[i7]*e[i8]*e
[i9]*e[i10],i10=i9+1..n),i9=i8+1
..n),i8=i7+1..n),i7=i6+1..n),i6=
i5+1..n),i5=i4+1..n),i4=i3+1..n)
,i3=i2+1..n),i2=i1+1..n),i1=1..n
):
>
b[11]:=seq(seq(seq(seq(seq(seq(s
eq(seq(seq(seq(seq(e[i1]*e[i2]*e
[i3]*e[i4]*e[i5]*e[i6]*e[i7]*e[i
8]*e[i9]*e[i10]*e[i11],i11=i10+1
..n),i10=i9+1..n),i9=i8+1..n),i8
=i7+1..n),i7=i6+1..n),i6=i5+1..n
),i5=i4+1..n),i4=i3+1..n),i3=i2+
1..n),i2=i1+1..n),i1=1..n):
>
b[12]:=seq(seq(seq(seq(seq(seq(s
eq(seq(seq(seq(seq(seq(e[i1]*e[i
2]*e[i3]*e[i4]*e[i5]*e[i6]*e[i7]
*e[i8]*e[i9]*e[i10]*e[i11]*e[i12
],i12=i11+1..n),i11=i10+1..n),i1
0=i9+1..n),i9=i8+1..n),i8=i7+1..
n),i7=i6+1..n),i6=i5+1..n),i5=i4
+1..n),i4=i3+1..n),i3=i2+1..n),i
2=i1+1..n),i1=1..n):
>
print(The_basis_of_Clifford_alge
bra,[1,b[1],b[2],b[3],b[4],b[5],
b[6],b[7],b[8],b[9],b[10],b[11],
b[12]]);
```

$$\mathit{The\_basis\_of\_Clifford\_algebra}, [1, e_1, e_2, e_3, e_4, e_1\,e_2, e_1\,e_3, e_1\,e_4, e_2\,e_3, e_2\,e_4, e_3\,e_4, e_1\,e_2\,e_3, e_1\,e_2\,e_4, e_1\,e_3\,e_4, e_2\,e_3\,e_4, e_1\,e_2\,e_3\,e_4]$$

```
>
print(The_dimension_of_Clifford_
algebra,2**n);
>
print(This_Clifford_algebra_has,
n+1,subspaces_and_their_dimensio
n_respectively,seq(binomial(n,d)
,d=0..n));
> for d from 1 to n do
>print(d-
vectors_and_their_numbers,b[d],b
inomial(n,d));
> od;
> end:
```

$$\mathit{The\_dimension\_of\_Clifford\_algebra}, 16$$

$$\mathit{This\_Clifford\_algebra\_has}, 5, \mathit{subspaces\_and\_their\_dimension\_respectively}, 1, 4, 6, 4, 1$$

$$1 - \mathit{vectors\_and\_their\_numbers}, e_1, e_2, e_3, e_4, 4$$

$$2 - \mathit{vectors\_and\_their\_numbers}, e_1\,e_2, e_1\,e_3, e_1\,e_4, e_2\,e_3, e_2\,e_4, e_3\,e_4, 6$$

$$3 - \mathit{vectors\_and\_their\_numbers}, e_1\,e_2\,e_3, e_1\,e_2\,e_4, e_1\,e_3\,e_4, e_2\,e_3\,e_4, 4$$

$$4 - \mathit{vectors\_and\_their\_numbers}, e_1\,e_2\,e_3\,e_4, 1$$

Let's get the information we mentioned above for Clifford algebra $C\ell_{4,0}$ by inputting 4:

```
> c(4);
```

3.2. Clifford Product and Norm in Maple

In this subsection, we develop the following algorithm that finds the Clifford product in $C\ell_{n,0}$

of any two vectors of the same finite dimension inputted and the norm of the multivector we have obtained.

```
> restart:
> P:=proc(x,y) local P,l,N,A,R;
> if nops(x)=nops(y) then
> l:=sum(x[i]*y[i],i=1..nops(x)):
>
 N:=l+sum(sum((x[j]*y[i]-
x[i]*y[j])*e[j]*e[i],i=j+1..nops
(x)),j=1..nops(x)):
>
A:=seq(seq((x[j]*y[i]-
x[i]*y[j]),i=j+1..nops(x)),j=1..
nops(x)):
>
R:=(sqrt(l**2+sum(A[k]**2,k=1..b
inomial(nops(x),2))));
> else print("The dimensions of
the vectors inputted must be the
same.")
> fi;
> end:
```

Let's calculate the norm of the resulting multivector by finding the Clifford product of the vectors $\mathbf{x}=(-1,1,2,4,-0.4)\in\mathbb{R}^5$ and $\mathbf{y}=(1,-3,-0.7,5,2)\in\mathbb{R}^5$ in $C\ell_{5,0}$:

```
> x:=[-1,1,2,4,-0.4]:
> y:=[1,-3,-0.7,5,2]:
>
> P(x,y);
```

```
> print(N);print([l,A]);
```

$$13.8 + 2\,e_1\,e_2 - 1.3\,e_1\,e_3 - 9\,e_1\,e_4 - 1.6\,e_1\,e_5 + 5.3\,e_2\,e_3 + 17\,e_2\,e_4 + 0.8\,e_2\,e_5 + 12.80000000\,e_3\,e_4 + 3.720000000\,e_3\,e_5 + 10.0\,e_4\,e_5$$

$$[13.8, 2, -1.3, -9, -1.6, 5.3, 17, 0.8, 12.8, 3.72, 10.0]$$

$$29.58206213$$

4. CONCLUSION

Clifford algebras, a topic that is getting popular day by day, are more involved especially in technological developments. It is often difficult to operate with multidimensional vectors. For this reason, these algorithms written in Maple will contribute to faster progress by facilitating the operations in the applications of Clifford algebras such as computer graphics, physics, robotics, computer-aided manufacturing, image processing, machine learning, computer-aided design, etc.

Acknowledgments

The author would like to thank the SAUJS editors and reviewers who reviewed the study.

Funding

The author received no financial support for the research, authorship, and/or publication of this paper.

The Declaration of Conflict of Interest/ Common Interest

No conflict of interest or common interest has been declared by the author.

The Declaration of Ethics Committee Approval

The author declares that this document does not require an ethics committee approval or any special permission.

The Declaration of Research and Publication Ethics

The author of the paper declares that he complies with the scientific, ethical and quotation rules of SAUJS in all processes of the article and that he does not make any falsification on the data collected. In addition, he declares that Sakarya University Journal of Science and its editorial board have no responsibility for any ethical violations that may be encountered, and that this study has not been evaluated in any academic publication environment other than Sakarya University Journal of Science.

REFERENCES

[1] J. Jr. Vaz and R. Jr. Da Rocha, "An introduction to Clifford algebras and spinors," Oxford University Press, 2016.

[2] E. Hitzer, T. Nitta and Y. Kuroe, "Applications of Clifford's geometric algebra," arXiv:1305.5663v1 [math.RA] 24 May 2013.

[3] E. J. Bayro-Corrochano and N. Arana-Daniel, "Clifford support vector machines for classification, regression, and recurrence," IEEE Transactions on Neural Networks, vol. 21, no. 11, pp. 1731-1746, 2010.

[4] P. Lounesto, "Clifford algebras and spinors," 2nd edition, Cambridge University Press, 2001.

[5] M. Akar and N. M. Sirakov, "Support vector machine skin lesion classification in Clifford algebra subspaces," Applications of Mathematics, vol. 64, no. 5, pp. 581-598, 2019.

[6] J. L. Aragon, G. Aragon-Camarasa, G. Aragon-Gonzalez and M. A. Rodriguez-Andrade, "Clifford algebra with mathematica," arXiv:0810.2412v2 [math-ph] 22 January, 2018.

[7] S. Roy, A. Mitra and S. K. Setua, "Color image representation using multivector," 2014 Fifth International Conference on Intelligent Systems, Modelling and Simulation, Langkawi, Malaysia, IEEE Xplore, pp. 357-363, 27-29 January 2014.

[8] F. Brackx, N. De Schepper and F. Sommen, "Clifford-Hermite and two-dimensional Clifford-Gabor filters for early vision," 17th International Conference on the Application of Computer Science and Mathematics in Architecture and Civil Engineering K. Gürlebeck and C. Könke (eds.) Weimar, Germany, 12-14 July 2006.

[9] S. Franchini, G. Vassallo and F. Sorbello, "A brief introduction to Clifford algebra," University of Palermo, Department of Computer Engineering, Technical Report N. 2/2010.